Simulation, optimisation, and control of multirate dynamics

Yana Lishkova

St. Hugh's College
University of Oxford

A thesis submitted for the degree of
Doctor of Philosophy

Trinity 2024

Abstract

Multirate systems, which exhibit dynamics across various time scales, are common in both scientific and real-world applications. Predicting and prescribing their behaviour, however, is challenging, as resolving fast dynamics requires fine-grid treatment, affecting the accuracy and efficiency of computational methods. This thesis comprehensively tackles this challenge, focusing on simulation, open-loop control, and robust feedback strategies. The proposed methods build upon each other, leveraging the properties of the system's model to design bespoke methods for high-fidelity simulation and optimal control at reduced computational cost.

We begin by employing a multirate variational approach for uncontrolled simulations of multirate systems, achieving great reductions in the number of intermediate variables for negligible penalties in accuracy. We prove that the resulting discrete model is structure-preserving and derive its order of accuracy for a class of dissipative systems. Implementing this model for optimal control, we demonstrate the adjoint system inherits the structure-preservation and accuracy of the variational model, while the multirate formulation significantly reduces the number of optimisation variables and constraints. These findings are showcased through two theoretical and two practical aerospace examples: simultaneous slewing and vibration control of flexible satellites, and control of satellites in three-body gravitational environment using a six degree-of-freedom model.

This variational open-loop control strategy can not account for modelling errors or disturbances and often results in an intractible nonconvex problem. Therefore, we formulate a novel linearisation strategy for variational models and implement the multirate variational approach within a tube-based nonlinear receding horizon (RH) strategy. This results in a successive convex approximation approach that reduces the size of the optimal control problem, and without loss of feasibility or stability guarantees, increases the receding horizon time step compared to the time step used to discretise the fast dynamics.

Although providing feedback, this technique does not account for disturbances and does not provide guarantees for obtaining a local optimum of the original nonlinear problem. For this purpose, we develop a novel successive linearisation RH strategy for systems with explicit and implicit models. We prove that unless terminated early, the technique obtains a local optimum of the original nonlinear problem and demonstrate how variational models can be used to reduce the size of the resulting convex problems while preserving some structures and the convexity of the continuous model. For systems with explicit models, this technique is extended to consider the presence of additive disturbances. Recursive feasibility and stability are proved and demonstrated through examples.

Simulation, optimisation, and control of multirate dynamics



Yana Lishkova

St. Hugh's College

University of Oxford

A thesis submitted for the degree of

Doctor of Philosophy

Trinity 2024

to my Mum and Dad

на Мама и Тате

Acknowledgements

I would like to express my deepest gratitude to my co-supervisors, Prof. Mark Cannon and Prof. Sina Ober-Blöbaum. Prof. Cannon, thank you for taking a chance on me when I needed it most. Your calm and steady support over the last few years has been invaluable. Through your example— in how you work and treat others— you've shown me the kind of researcher I aspire to be. To Prof. Sina Ober-Blöbaum, I have no words to describe how deeply you've shaped my life. Thank you for your trust, guidance, and the opportunities you've given me. You made me feel like a true apprentice — someone you believed in, supported, and generously welcomed into your craft.

I also thank Prof. Paul Goulart and Asst. Prof. Konstantinos Gatsis for their thoughtful support and assessment throughout my DPhil milestones. A sincere thanks again to Prof. Goulart and Prof. Moritz Diehl from the University of Freiburg for examining my thesis and oral defence. Your insightful feedback and our engaging discussions were both thought-provoking and deeply motivating.

I am also incredibly grateful to my funder — the Engineering and Physical Sciences Research Council (EPSRC) — for making this journey possible and for continuing to support me with a Postdoctoral Award. A thank you as well to Zonta International for my Amelia Earhart Fellowship and the inspiring community it brought me into. Many thanks also go to the Engineering Science department — especially the graduate studies team — and to the college offices and library staff at St Edmund Hall and St Hugh's College for their support throughout my time there.

To the Oxford Control Group — professors, postdocs, students, and visitors — thank you for fostering such a welcoming, collaborative environment. I've always felt valued as both a colleague and a friend, and I'm grateful for the community I've found among you.

To the Numerical Mathematics and Control Group at Paderborn University — though I was only ever a virtual presence, your warmth, openness, and curiosity made me feel like part of the team. I'm truly grateful for your support and encouragement.

I'd also like to thank my collaborators who believed in my crazy ideas enough to join in. A big thank you to Prof. Mai Bando from Kyushu University for her guidance, support, and the opportunities our collaboration brought. Many thanks also to Dr. Paul Scherer and Dr. Christian Offen for the challenging yet rewarding journey we shared in the world of machine learning. Thank you to Dr. Avishai Weiss, Dr. Abraham P. Vinod, and their colleagues at Mitsubishi Electric Research Laboratories (MERL) for an unforgettable summer filled with inspiring challenges

and stimulating discussions. A special thank you to Dr. Weiss for this opportunity, his invaluable mentorship, and ongoing support.

Apart from research I also ventured into what feels like a million part-time jobs with the different departments and colleges — be it teaching, admissions, or supervision, I truly enjoyed them all. Thank you to St Hugh's College, St Edmund Hall, St John's College, and the Department of Engineering Science for letting me choose and shape the next generation. I'm especially grateful to my students, who taught me more than I could teach them. To the St Hugh's Dean and Assistant Dean — Dr. Damian Jenkins and Dr. Eri Ichijo — thank you for entrusting me as Junior Dean for the last four years. Living in the library flat, working on-call, and supporting students taught me responsibility and self-care. An enormous thank you to the porters, catering staff, and my teammates who made the role easier.

To the societies that entrusted me with helping shape their future and reach wide audiences — the Graduate Joint Consultative Committee (GJCC), the Oxford University Aeronautical Society (AerOx), the Royal Aeronautical Society (RAeS) Oxford Branch, the Oxford Women in Computer Science Society (OxWoCS), and the Cambridge University Spaceflight (CUSF) — thank you for the teamwork, laughter, and shared purpose. A heartfelt thanks to the Oxford Gliding Club (OGC) and the Oxford University Gliding Club (OUGC) — especially the instructors and support team — for teaching me to fly and giving me a community I will always cherish. On the airfield, I found space to breathe and to challenge myself.

And as they say, it's the people you meet along the way that make it all worthwhile. My deepest thanks to Eva Angelova, Alexandra Bednarczyk, Natasha Pourkarimi and Dr. Yurim Park. I met these incredible ladies at different stages in my life and they have been my dear friends and supporters ever since. You four bring sunshine to my days and I love you dearly.

Thank you also to Dr. Matthew Newton, Dr. Han Wang, and Dr. Yuwen Chen — not only brilliant colleagues, but cherished friends. Thank you for sharing this DPhil journey with me. To my friends in the Control Group — Dr. Fernando Jiménez, Dr. Idris Kempf, Sebastian Steffen, Allan André do Nascimento, Andre Bertolace, Asst. Prof. Filippo Fabiani, Dr. Ross Drummond, Dr. Georgios Pantazis, Kristin Funke, Dr. Marta Fochesato, Dr. Nikolaus Vertovec, Dr. Emmanouil (Manos) Alexis, Steffen Ridderbusch, Zuxun Xiong, Dominik Frej, Janani Venkatasubramanian, Mathilde Leuridan, and Kirill Sechkar — thank you for your camaraderie and support. To my brilliant Oxford ladies — Dr. Barbora Schonfeldova, Dr. Katie Mellor, Yao Yao, Dr. Misha Patel, Dr. Linde Hesse, and Laura Zeng — thank you for your friendship and the joy of our girl nights. To Gregory Brooks, Natalia Narożańska, and Dr. Michael Hutchinson for standing by me all those years, and to

Diana Korkina, Daniela Nesheva, and Veronika Dimitrova for always giving me a refuge. And to the wonderful friends I made at MERL — thank you for making that summer unforgettable and for friendships I will cherish forever.

Coming to Oxford wouldn't have been possible without the incredible support I received at every stage. My deep gratitude goes to my teachers back home in Bulgaria — especially Mrs. Silvia Lazova, Mrs. Helga Uzunova, and Mrs. Nina Kavaldzhieva — and to my tutors and professors at the University of Cambridge, especially Prof. Matthew Juniper, Dr. Elena Punskaya, Prof. Gareth Rees, and Dr. Graham Spelman. I am also deeply grateful to Dr. H. Martin Reekie and Prof. Filipe Teixeira-Dias from the University of Edinburgh, who helped me find the courage and means to change my path.

And lastly, to the person I admire deeply — Dr. Paul Scherer. You saw how hard my academic journey was and stood by me, even when it came at a cost to you. Your belief in me and my dreams kept me going when I needed it most. I'll always be grateful for your strength, kindness, and unwavering companionship.

Of course, the biggest thank you goes to my family.

To my Mum, Katya Miteva, and Dad, Valentin Lishkov, to whom this thesis is dedicated — thank you for being the kind of people I aspire to become, while always letting me choose my own path. You gave me every chance to succeed, never wavering in your support, no matter the cost. I wouldn't be here without you. Thank you. I love you. To my Grandma Veneta, my closest friend in childhood — your love and dedication have shaped so much of who I am. To my Uncle Alexandar (Vuicho) and Kaka Veni — who I have always been able to rely on and who have wholeheartedly believed in me, often asking for souvenirs from Mars. Vuicho, thank you for all you have taught and inspired me to do. Kakich, thank you for teaching me to follow my own path and live colourfully. And to my Grandma Stefka, my Aunt Dimka (Vuina), and Grandma Stoyna, who I miss dearly and whose gestures of love and support I will always remember.

Finally, to the girl who arrived in Scotland all those years ago — scared but unyielding. If only you knew what you'd achieve and the extraordinary people you'd meet.

University of Oxford — it has been an honour.

Yana Valentinova Lishkova

Abstract

Multirate systems, which exhibit dynamics across various time scales, are common in both scientific and real-world applications. Predicting and prescribing their behaviour, however, is challenging, as resolving fast dynamics requires fine-grid treatment, affecting the accuracy and efficiency of computational methods. This thesis comprehensively tackles this challenge, focusing on simulation, open-loop control, and robust feedback strategies. The proposed methods build upon each other, leveraging the properties of the system's model to design bespoke methods for high-fidelity simulation and optimal control at reduced computational cost.

We begin by employing a multirate variational approach for uncontrolled simulations of multirate systems, achieving great reductions in the number of intermediate variables for negligible penalties in accuracy. We prove that the resulting discrete model is structure-preserving and derive its order of accuracy for a class of dissipative systems. Implementing this model for optimal control, we demonstrate the adjoint system inherits the structure-preservation and accuracy of the variational model, while the multirate formulation significantly reduces the number of optimisation variables and constraints. These findings are showcased through two theoretical and two practical aerospace examples: simultaneous slewing and vibration control of flexible satellites, and control of satellites in three-body gravitational environment using a six degree-of-freedom model.

This variational open-loop control strategy can not account for modelling errors or disturbances and often results in an intractible nonconvex problem. Therefore, we formulate a novel linearisation strategy for variational models and implement the multirate variational approach within a tube-based nonlinear receding horizon (RH) strategy. This results in a successive convex approximation approach that reduces the size of the optimal control problem, and without loss of feasibility or stability guarantees, increases the receding horizon time step compared to the time step used to discretise the fast dynamics.

Although providing feedback, this technique does not account for disturbances and does not provide guarantees for obtaining a local optimum of the original nonlinear problem. For this purpose, we develop a novel successive linearisation RH strategy for systems with explicit and implicit models. We prove that unless terminated early, the technique obtains a local optimum of the original nonlinear problem and demonstrate how variational models can be used to reduce the size of the resulting convex problems while preserving some structures and the convexity of the continuous model. For systems with explicit models, this technique is extended to consider the presence of additive disturbances. Recursive feasibility and stability are proved and demonstrated through examples.

Notation

Acronyms

cMPC . . . Convex Model Predictive Control

CR3BP . . . the circular restricted three-body problem

DMOC . . . Discrete Mechanics and Optimal Control

DOF . . . . degrees of freedom

EcMPC . . cMPC with explicit system model

EnMPC . . nonlinear model predictive control with explicit system model

FE . . . . . Forward Euler (integrator)

HF . . . . . Hamiltonian formulation

IcMPC . . . cMPC with implicit system model

InMPC . . . nonlinear model predictive control with implicit system model

KKT . . . . Karush-Kuhn-Tucker (conditions)

LF . . . . . Lagrangian formulation

MPC . . . . Model Predictive Control

MVI . . . . Multirate variational integrator

NLP . . . . nonlinear program

NMPC . . . Nonlinear Model Predictive Control

OCP . . . . optimal control problem

RcMPC . . Robust Convex Model Predictive Control

REcMPC . RcMPC with explicit system model

RHOCP . . receding horizon optimal control problem

RIcMPC . . RcMPC with implicit system model

RK . . . . . Runge- Kutta (integrator)

SDP . . . . semidefinite program

SOCP . . . second-order cone program

SVI . . . . . singlerate variational integrator

VcMPC . . cMPC with variational system model

Sets

$\mathbb{R}$ . . . . . the set of real numbers

$\mathbb{R}^n$ . . . . . the set of real $n-$ dimensional vectors

$\mathbb{R}^{m\times n}$ . . . . the set of real $m \times n$ real matrices

$\{x^1, ..., x^m\}$ a set of elements $x^1, ..., x^m$

$\text{co}\{x^1, ..., x^m\}$ denotes the convex hull of a set of vertices $\{x^1, ..., x^m\}$

Operators

$[\cdot]_i$ . . . . . the i-th row of the respective vector or matrix

$[\cdot]_{i,j}$ . . . . . the (i, j)-th element of the respective matrix

$D_n(\cdot, \ldots, \cdot)$. denotes the gradient operator with respect to the n-th argument

$\nabla_x f(x, \ldots, z)$ gradient operator of $f(x, \ldots, z)$ with respect to x

$A \succ 0$ . . . positive definite matrix A

$A \succeq 0$ . . . positive semi-definite matrix A

$\text{diag}(x)$ . . . transforming vector $x \in \mathbb{R}^n$ into a diagonal matrix $\text{diag}(x) \in \mathbb{R}^{n\times n}$

$\langle x, y\rangle$ . . . . the inner product of vectors x, y

Norms

$|a|$ . . . . . absolute value of a

$\|x\|_2$ . . . . Euclidean norm of vector x: $\|x\|_2 := \sqrt{\langle x, x\rangle}$

$\|x\|_\infty$ . . . . supremum norm of vector $x \in \mathbb{R}^n$: $\|x\|_\infty := \max\{|\,[x]_1\,|, \ldots, |\,[x]_n\,|\}$

$\|x\|_Q^2$ . . . . norm of the form $x^\intercal Q x$

Common symbols

Q . . . . . real configration manifold

TQ . . . . . tangent bundle (state space)

T^*Q . . . . cotangent bundle (phase space)

$\mathcal{U}$ . . . . . control manifold

$\mathcal{C}$ . . . . . path space

q . . . . . configuration vector (generalised coordinates)

$\dot{q}$ . . . . . velocity vector (generalised coordinates)

p . . . . . conjugate momentum vector

u . . . . . control vector

q^{s} . . . . . slow varying generalised coordinates

q^{f} . . . . . fast varying generalised coordinates

$x_{k|i}$ . . . . . indicates the prediction at horizon time $i\Delta t_{\mathrm{horizon}}$ for the value of x at time $i\Delta t_{\mathrm{horizon}} + k\Delta t_{\mathrm{simulation}}$

Δt . . . . . discrete time step for singlerate schemes, micro discrete time step for multirate schemes

ΔT . . . . . macro discrete time step for multirate schemes

$\mathbb{p}$ . . . . . macro-micro proportionality $\mathbb{p} := \Delta T / \Delta t$

$\mathfrak{L}(q, \dot{q})$ . . . Lagrangian of the considered system in a singlerate coordinate system

$\mathcal{L}(q^{\mathrm{s}}, q^{\mathrm{f}}, \dot{q}^{\mathrm{s}}, \dot{q}^{\mathrm{f}})$ Lagrangian of the considered mechanical system in a multirate coordinate system

$H(q, p)$ . . . Hamiltonian of the considered mechanical system in a singlerate coordinate system

$\mathcal{H}(q^{\mathrm{s}}, p^{\mathrm{s}}, q^{\mathrm{f}}, p^{\mathrm{f}})$ Hamiltonian of the considered mechanical system in a multirate coordinate system

f_{L} . . . . . Lagrangian force

f_{LC} . . . . . Lagrangian control force

f^{s}_{LC} . . . . . Lagrangian control forces resolved along the slow generalised coordinates

$f^{\mathrm{f}}_{\mathrm{LC}}$ . . . . . Lagrangian control forces resolved along the fast generalised coordinates

t_k . . . . . discrete time node- in singlerate setting $t_k = k\Delta t$, in multirate setting $t_k = k\Delta T$

t^m_k . . . . . discrete time node- in multirate setting $t^m_k = k\Delta T + m\Delta t$

q_k^{s} . . . . . discrete approximation of $q^{\mathrm{s}}(t)$ at $t = t_k$

$q_k^{\mathrm{f},m}$ . . . . . discrete approximation of $q^{\mathrm{f}}(t)$ at $t = t_k^m$

p_k^{s} . . . . . discrete approximation of $p^{\mathrm{s}}(t)$ at $t = t_k$

$p_k^{\mathrm{f},m}$ . . . . . discrete approximation of $p^{\mathrm{f}}(t)$ at $t = t_k^m$

$f_k^{\pm}$ . . . . . left and right discrete force approximation of f_{LC} at $t = t_k$

$F_k^{s,\pm}$ . . . . left and right discrete approximations of $f_{\mathrm{LC}}^{\mathrm{s}}$ at $t = t_k$

$f_k^{\mathrm{f},m,\pm}$ . . . . left and right discrete approximations of $f_{\mathrm{LC}}^{\mathrm{f}}$ at $t = t_k^m$

$\mathfrak{L}_{\mathrm{d},k}$ . . . . . discrete Lagrangian in the singlerate coordinate system approximating the action integral for the time period $[t_k, t_{k+1}]$

L_{d}^k . . . . . discrete Lagrangian in the multirate coordinate system approximating the action integral for the time period $[t_k, t_{k+1}]$

$L_{\mathrm{d}}^{k,m}$ . . . . discrete Lagrangian in the multirate coordinate system approximating the action integral for the time period $\left[t_k^m, t_k^{m+1}\right]$

Notation **vii**

1 Introduction **1**

1.1 Motivation 1

1.2 Thesis outline and contributions 2

1.3 Publications 7

2 Background **9**

2.1 Introduction 9

2.2 System modelling using variational mechanics 10

2.2.1 Lagrangian formalism 10

2.2.2 Hamiltonian formalism 12

2.2.3 Constrained systems 13

2.3 Simulation through discretisation 14

2.3.1 Quantative measures of accuracy 14

2.3.2 Qualitative measures of accuracy 16

2.3.3 Variational integrators 19

2.4 Optimal control 22

2.4.1 Problem statement 22

2.4.2 Solution methods 23

2.5 Model Predictive Control 28

2.5.1 Feasibility and stability guarantees 29

2.5.2 Uncertainty considerations 31

3 Multirate variational simulation **33**

3.1 Introduction 33

3.2 Background 34

3.3 Multirate variational mechanics for forced systems 37

3.3.1 Lagrangian viewpoint 37

3.3.2 Hamiltonian viewpoint 38
3.3.3 Properties of the Lagrangian flow for forced systems 41
3.4 Multirate discrete variational mechanics for forced systems 43
3.4.1 Lagrangian viewpoint 43
3.4.2 Multirate discrete Legendre transform and Hamiltonian viewpoint 48
3.4.3 Properties of the time-stepping scheme 53
3.4.4 Order of accuracy 57
3.5 Discrete variational mechanics for forced constrained systems 70

4 Examples of multirate variational modelling and simulation 73
4.1 Introduction 74
4.1.1 Choice of approximation rules 74
4.1.2 Experimental set-up 76
4.2 Example 1: Fermi–Pasta–Ulam–Tsingou system with quadratic potentials 76
4.2.1 Mathematical model 76
4.2.2 Computational results 79
4.3 Example 2: Fermi–Pasta–Ulam–Tsingou system with quartic potential 85
4.3.1 Computational results 86
4.4 Example 3: Flexible spacecraft dynamics 87
4.4.1 Background 87
4.4.2 Mathematical model 88
4.4.3 Multirate configuration description and discretisation 92
4.4.4 Computational results 93
4.5 Example 4: Electrodynamic tether motion 96
4.5.1 Introduction 97
4.5.2 Variational model of 6DOF tethered spacecraft dynamics . . 98
4.5.3 Numerical results 103

5 Open-Loop Control **107**

5.1 Introduction 107

5.2 Background 107

5.3 Optimal control of multirate mechanics 110

5.3.1 Lagrangian viewpoint 110

5.3.2 Hamiltonian viewpoint 112

5.3.3 Necessary optimality conditions 114

5.4 Multirate Discrete Mechanics and Optimal Control (Multirate DMOC) 117

5.4.1 Lagrangian viewpoint 120

5.4.2 Hamiltonian viewpoint 120

5.4.3 Necessary optimality conditions 121

5.5 Examples 127

5.5.1 Example 2: FPUT system with quartic potential 127

5.5.2 Example 3: Flexible spacecraft control 128

6 Variational linearisation and multirate MPC **135**

6.1 Introduction 135

6.2 Background 136

6.3 System representation 139

6.3.1 Singlerate variational linearisation and error bounds 140

6.3.2 Multirate variational linearisation and error bounds 144

6.4 Receding horizon control strategy 146

6.5 Multirate receding horizon control 149

6.6 Examples 150

7 A successive convexification approach for robust receding horizon control **154**

7.1 Introduction 154

7.2 Background 155

7.3 Technique for explicit system models 162
7.3.1 Problem formulation 162
7.3.2 Proposed nominal control law 164
7.3.3 Nominal feasibility and stability guarantees 170
7.3.4 Problem formulation with additive disturbances 173
7.3.5 Proposed robust control law 174
7.3.6 Robust feasibility and stability guarantees 177
7.3.7 Numerical examples 181
7.4 Technique for implicit system models 186
7.4.1 Problem formulation 187
7.4.2 Proposed nominal control law 188
7.4.3 Nominal feasibility and stability guarantees 191
7.4.4 Proposed variational reformulation 194
7.4.5 Numerical examples 198

8 Conclusion **201**
8.1 Contributions of this dissertation 201
8.2 Directions for future research 204

Appendices

A Appendix: MVI derivation for forced systems **208**

B Appendix: MVI formulation for Demonstration problem 2 **210**

C Appendix: Simplified MVI for constrained forced systems **213**

D Appendix: Proofs of the non-conservativeness of cMPC **216**
D.1 Proof of the non-conservativeness of EcMPC 216
D.2 Proof of the non-conservativeness of IcMPC 220

1 Introduction

1.1 Motivation

Systems which exhibit dynamics on different time scales are often referred to as multirate systems and examples of such can be found in all areas of life and science– from the laws behind the motion of molecules to those describing planetary dynamics. One illustrative example is a satellite with flexible solar panels performing a rotational manoeuvre. Even when this rotational motion evolves slowly, it can induce vibrations in the flexible appendages which include very fast modes, thus demonstrating dynamics across different time scales. Similarly, such multirate behavior arises in technological systems composed of rigid and elastic parts with varying, and often high, stiffness, such as in vehicle dynamics or biomechanics.

Despite the abundant presence of multirate systems, we still face great numerical challenges when attempting to predict and prescribe their behaviour. The presence of fast and slow dynamics leads to great difficulties in their simulation, control, and optimisation. For this reason, many works have developed bespoke multirate numerical techniques, however, most of them focus on a specific application or restrict the discussion to one or two aspects of the problem – be it the development of a mathematical model, simulation strategy, open-loop control law, feedback control law or a bespoke optimisation algorithm. Furthermore, the numerical methods

chosen often fail to preserve key properties and structures of the mathematical model vital for the in-depth understanding of the physical system and its accurate long-term simulation.

The thesis aims to approach all these aspects of the problem in a structured manner. We plan to address, in turn, the simulation, open-loop control, and nominal and robust feedback control strategies, extending each method from the previous one. Each method is developed to exploit the characteristics of the mathematical model and the physical system in order to design bespoke approaches capable of high-fidelity simulation and optimal control of multirate systems at a reduced computational cost. These methods are tested for several theoretical examples and two practical examples from the aerospace domain.

1.2 Thesis outline and contributions

This thesis aims to develop novel high-fidelity, computationally efficient methods for simulation, optimisation and control. We begin with a detailed description of each chapter, highlighting its main contributions toward this goal.

In **Chapter 2 (Background)**, we introduce the mathematical background used throughout this thesis and discuss the related literature. The chapter is divided into three sections:

- Simulation: We introduce the Lagrangian and Hamiltonian formalisms for modelling system behaviour in the presence of forces and constraints. We describe the challenges of simulating these dynamics numerically and discuss quantitative measures of the simulation accuracy. We then present geometric integrators, which are numerical discretisation techniques for system simulation which focus on preserving qualitative features of the model during simulations in order to reduce the long-term quantitative error of the simulation. We discuss important qualitative features such as symmetries and symplecticity and introduce the primary method for discrete system representation, which is used throughout this thesis: variational integrators [1].

- Optimal control: Next, we explain how system models can be used to control the system optimally and present a general form of an optimal control problem. We discuss the direct and indirect methods for its solution and their necessary optimality conditions. We note that these problems can result in nonconvex optimisation problems, for which there are no guarantees for successful and efficient solution. Thus, we present ideas from the literature on how these can be addressed using convex programming.
- Feedback control: Lastly, we discuss the importance of feedback in controlling the system's behaviour and introduce the receding horizon strategy for optimisation-based closed-loop control [2], summarising some of the main milestones in its development for nominal and robust systems.

In **Chapter 3 (Simulation)**, we delve into the core theoretical aspect of this thesis. The focus lies on introducing the multirate formulation of variational integrators, a concept initially proposed by [3]. While existing literature on multirate variational integrators (MVI) primarily addresses their application in non-dissipative systems, showcasing their ability to accurately preserve symplecticity, energy, or momenta, this chapter takes a step further. Following the approach of [4, 5], we incorporate external forces and rigorously derive their mathematical representation within the scheme. Moreover, we extend prior research by establishing the integrator's accuracy in the presence of external forces for a specific class of systems and demonstrating its structure-preserving properties even in the presence of external forcing through the formulation and proof of the multirate discrete forced Noether's theorem. The chapter concludes with the development of a multirate variational integrator for constrained dissipative systems in both Lagrangian and Hamiltonian formulations.

In **Chapter 4 (Examples)**, we introduce two theoretical and two practical examples to showcase the capabilities of multirate variational integrators, as established in Chapter 3 and elaborated on in subsequent chapters. We begin with the Fermi-Pasta-Ulam-Tsingou (FPUT) system, employing a linear dynamics configuration to showcase the order and structure-preserving properties of MVI through direct

comparison with the analytic solution and several alternative methods. Additionally, we conduct tests to demonstrate MVI's capacity to reduce computational costs in simulating multirate systems without sacrificing accuracy. Order and conservation tests are also conducted for a nonlinear configuration of the FPUT system, confirming the integrator's performance without the need to decouple the equations of motion, as required by some competing schemes.

These findings are reinforced by a second example focusing on a practical application: simulating flexible satellite dynamics. By developing a linear system model, we discuss the benefits of utilising an MVI to achieve high-fidelity simulations with reduced computational overhead. This is particularly crucial for safety-critical simulations on resource-constrained hardware, such as spacecraft control systems.

Finally, we delve into the example of a satellite with a tether in a three-body gravitational environment. Introducing a novel variational six-dimensional system model, we implement the constrained forced MVI to demonstrate the trade-off between efficiency and accuracy achievable for this example with this approach.

Chapter 5 (Open-loop control) focuses on a detailed description of the implementation of multirate variational integrators for open-loop optimal control. Initially introduced as Multirate Discrete Mechanics and Optimal Control (Multirate DMOC) by [4], this approach demonstrated great potential but was never further analysed theoretically or extended. While Gail's thesis [5] provided a more detailed description of the method, it offered limited new insights. In Chapter 5, we present a detailed mathematical development of the method, which cannot be currently found in the literature and we expand on prior works by investigating the order of the optimal control solution. To showcase the capabilities of Multirate DMOC, we apply it to the control of the FPUT system and the simultaneous slewing and vibration control of the flexible satellites introduced in Chapter 4. We assess the fidelity of the approach by highlighting the conservation properties and the order of accuracy of the resulting solutions. We further showcase the computational savings achievable with Multirate DMOC by examining how the size of the optimal control problem

can be significantly reduced and exploring the favourable trade-off between accuracy and computational cost that the approach offers.

Based on the multirate variation approach, **Chapter 6 (Multirate receding horizon control)** focuses on the development of a receding horizon strategy for multirate systems, which allows for accurate control of both slow and fast subsystems while obeying the constraints placed on the system and its controls. Previous works in this direction, such as non-uniform grid approaches and move blocking strategies, often face issues with discretisation error, computational load, and feasibility guarantees [6–8]. Building upon the theory from Chapters 3 and 5 and a tube-based successive linearisation approach by [9], we formulate an alternative tube-based approach for multirate systems with coupled nonlinear dynamics. The use of the multirate variational approach enables the increase of the receding horizon time step beyond the discretisation step used for the fast system dynamics. Additionally, it reduces the size of the receding horizon optimal control problem (RHOCP) by reducing the number of degrees of freedom and model constraints. Consequently, it necessitates the solution of the RHOCP less frequently than alternative singlerate approaches, with negligible penalties in accuracy and without loss of feasibility or stability guarantees. Furthermore, we develop a novel linearisation technique, which maintains the structure-preserving nature of a variational model and facilitates new methods of computing linearisation error bounds. The superior qualitative properties of variational models and the run-time savings achievable with this approach compared to singlerate methods are demonstrated using the FPUT example from Chapter 4 and a planar quadcopter model.

Despite the introduction of a novel method for bounding the linearisation error, obtaining these bounds remains a challenge for many problems and can affect the performance of the scheme, potentially leading to conservativeness, slow convergence or infeasibility even when the original nonconvex problem is feasible. Furthermore, the proposed scheme cannot straightforwardly be expanded to account for the presence of external disturbances.

To this end, **Chapter 7 (Robust receding horizon control)** introduces a novel successive convexification receding horizon approach for system with convex state and control constraints, and with nonlinear dynamics that can be expressed as a difference of convex functions. The scheme uses both the nonconvex model and its linearisation to construct a tube containing all possible future system trajectories without the need to compute linearisation bounds. The tube is used to predict performance and ensure constraint satisfaction, and is optimised online alongside the control sequence in a sequence of convex programs.

We begin by introducing the scheme for explicit models in the absence of disturbances and prove that the proposed approach is non-conservative, with solutions of the successive convex programs converging to a locally optimal solution of the original nonconvex optimal control problem. Furthermore, we prove that a sequence of convex programs can be terminated early without affecting the stability or feasibility guarantees. We extend the approach to the case of additive disturbances using a novel strategy for selecting the linearisation points. As a result, we formulate a robust receding horizon strategy that guarantees recursive feasibility and closed-loop system stability. As in the disturbance-free case, the robust approach solves the sequence of programming problems at each discrete time step without the need for pre-computed error bounds or heuristics and can also be terminated early without loss of feasibility guarantees. We illustrate these properties through two examples, including the FPUT system. The results showcase the runtime reductions attained with the new RH strategy compared to directly solving the original nonconvex problem and demonstrate the tube's convergence to one of its optima.

The nominal scheme is then reformulated for the more general case of implicit system models. It is established through formal proofs and supported by numerical examples that this reformulated scheme ensures the same guarantees as the one for explicit models. We demonstrate, for a broad class of mechanical systems, that by using a variational integrator, the convexity of the continuous model can be preserved while achieving a better qualitative system representation and reduced

size of the RHOCP. These claims are supported by the results from applying the variational approach to the same examples used for the explicit-model scheme, showing the convergence of the successive convex problems and the impact of the structure-preserving model on the resulting trajectory and the RHOCP size.

In **Chapter 8 (Conclusion)** summarises the contributions made by this thesis and outlines future research directions.

1.3 Publications

The work presented in these chapters has been submitted to several conferences, journals and a magazine article. In all the articles included, the author of this thesis conducted the research, performed the numerical analysis, and prepared the manuscripts. The author's supervisors provided guidance throughout the process, while the collaborators contributed by reviewing the manuscript and offering occasional feedback or direction.

Chapters 3, 4, and 5:

- Journal paper under preparation:

  Y. Lishkova and S.Ober-Blöbaum, " Multirate Discrete Mechanics and Optimal Control: review and extension ;" To be submitted in October 2024.

- Journal paper under preparation:

  Y. Lishkova, S. Ober-Blöbaum, M. Cannon, and S. Leyendecker, "A multirate variational approach to simulation and optimal control for flexible spacecraft;" To be submitted in October 2024.

- Conference paper:

  Y. Lishkova, S. Ober-Blöbaum, M. Cannon, and S. Leyendecker, "A multirate variational approach to simulation and optimal control for flexible spacecraft," Advances in the Astronautical Sciences, vol. 175; Presented at the 2020 AAS/AIAA Astrodynamics Specialist Conference.

- Conference paper:

  Y. Lishkova, M. Bando, and S. Ober-Blöbaum, "Variational approach for

modelling and optimal control of electrodynamic tether motion," in 2023 International Astronautical Congress (IAC).

- Magazine article:

  Y. Lishkova, S. Ober-Blöbaum, and S. Leyendecker, "Multirate discrete mechanics and optimal control for a flexible satellite model," in GAMM Rundbrief 2023.

Chapter 6:

- Conference paper:

  Y. Lishkova, M. Cannon, and S. Ober-Blöbaum, "A multirate variational approach to nonlinear MPC," in 2022 European Control Conference (ECC), IEEE, 2022, pp. 729–735.

Chapter 7:

- Journal paper under review:

  Y. Lishkova and M. Cannon, "Robust receding horizon control for convex dynamics and bounded disturbances," arXiv preprint:2302.07744, 2023; Submitted for Transactions on Automatic Control (TAC).

- Conference paper:

  Y. Lishkova and M. Cannon, "Optimization-based trajectory generation and receding horizon control for systems with convex dynamics," in 62nd IEEE Conference on Decision and Control (CDC), IEEE, 2023, pp. 3262–3269.

Additional papers produced during this degree, but not covered in this thesis include:

- Conference paper:

  Y. Lishkova, P. Scherer, S. Ridderbusch, M. Jamnik, P. Liò, S. Ober-Blöbaum, and C. Offen, "Discrete lagrangian neural networks with automatic symmetry discovery," IFAC-PapersOnLine, vol. 56, 2023; Presented at IFAC 2023.

- Conference paper:

  Y. Lishkova, A. Vinod, S. Di Cairano, and A. Weiss, "Divert-feasible lunar landing under navigational uncertainty," in 63rd IEEE Conference on Decision and Control (CDC), IEEE, 2024.

2

Background

Contents

2.1 Introduction 9
2.2 System modelling using variational mechanics 10
2.2.1 Lagrangian formalism 10
2.2.2 Hamiltonian formalism 12
2.2.3 Constrained systems 13
2.3 Simulation through discretisation 14
2.3.1 Quantative measures of accuracy 14
2.3.2 Qualitative measures of accuracy 16
2.3.3 Variational integrators 19
2.4 Optimal control 22
2.4.1 Problem statement 22
2.4.2 Solution methods 23
2.5 Model Predictive Control 28
2.5.1 Feasibility and stability guarantees 29
2.5.2 Uncertainty considerations 31

2.1 Introduction

In this chapter, we present the mathematical formulation that will be used throughout the thesis and introduce the main results from the literature that underpin the developments of this thesis. In turn, we delve into system modelling, simulation methodologies, optimal control strategies, and the pivotal role of feedback

mechanisms in controlling the system's behaviour.

2.2 System modelling using variational mechanics

To predict and prescribe the behaviour of a dynamical system, we first need to derive its mathematical model. Consider a mechanical system whose path evolves on a configuration manifold Q with associated tangent bundle TQ and let the system be described by a Lagrangian $\mathfrak{L} : TQ \to \mathbb{R}$. The change in the system's state in time can be described by the evolution of its configuration vector $q(t) \in Q$ and its associated velocity vector $\dot{q}(t)$ such that $(q(t), \dot{q}(t)) \in TQ$, with the tangent bundle being the state space. Thus, the space of all possible paths for the system in the time interval $[0, T]$ can be expressed as

$$\mathcal{C}([0,T], Q) = \{q : [0,T] \to Q \mid q \text{ is a } C^2 \text{ curve}\}. \tag{2.1}$$

2.2.1 Lagrangian formalism

To derive the equations of motion, we consider the action integral $S : \mathcal{C}([0,T], Q) \to \mathbb{R}$ as

$$S(q) = \int_0^T \mathfrak{L}(q(t), \dot{q}(t))\, dt \tag{2.2a}$$

and assume the Lagrangian is regular, thus its derivative with respect to the velocity vector is full rank. Since we consider dissipative and controlled motions, external (control) forces have to be taken into account. As suggested by [1], *time independent* external inputs can be interpreted as fiber-preserving maps $f_L : TQ \to T^*Q$ over the identity id_Q[1], where T^*Q is the cotangent bundle associated with the configuration manifold Q. In coordinate form these maps can be expressed as

$$f_{\mathrm{L}} : (q, \dot{q}) \mapsto (q, f_{\mathrm{L}}(q, \dot{q})),$$

and are termed *Lagrangian forces*. Such are, for example, friction forces, and, in general, those forces dependent on the velocity and configuration but not explicitly on time.

[1] i.e. it holds that $\pi_Q \circ f_{\mathrm{L}} = \tau_Q$ with $\pi_Q : T^*Q \to Q$ and $\tau_Q : TQ \to Q$ being the canonical projections (for definition see [18])

On the other hand, to define and interpret *time-dependent* control inputs in the Lagrangian formalism, we need to extend this definition and define the *Lagrangian control forces* similarly to [19]. Given a control manifold $\mathcal{U}$ with control parameter $u(t) \in \mathcal{U}$ and control path space

$$\mathcal{C}([0,T],\mathcal{U}) = \{u:\ [0,T] \to \mathcal{U} \mid u \in L^\infty\} \tag{2.3}$$

we define the *Lagrangian control forces* as maps $f_{\mathrm{LC}} : TQ \times \mathcal{U} \to T^*Q$, which in coordinate form can be written as

$$f_{\mathrm{LC}} : (q, \dot{q}, u) \mapsto (q, f_{\mathrm{LC}}(q, \dot{q}, u)).$$

Here L^∞ denotes the space of essentially bounded, measurable functions equipped with the essential supremum norm [18]. In fact, as [18] and [19] note, the *Lagrangian control force* f_{LC} can be interpreted as a family of Lagrangian forces f_L for a fixed control path u. Consequently, a Lagrangian control force f_{LC} can be interpreted as a parameter-dependent Lagrangian force f_{L} in the following manner

$$f_{\mathrm{LC}}(q, \dot{q}, u) = f_L(u)(q, \dot{q}).$$

Here $f_L(u) : TQ \to T^*Q$ are fiber-preserving maps over the identity id_Q, which in coordinates take the form

$$f_L(u) : (q, \dot{q}) \mapsto (q, f_{\mathrm{L}}(u)(q, \dot{q})). \tag{2.4}$$

For this reason, the Lagrangian control forces will be utilised in the rest of this thesis to represent both time-dependent and independent external forces. Systems under their influence will be referred to as forced systems or dissipative systems and the use of $f_{\mathrm{LC}}(q, \dot{q}, u)$ as one-form on TQ would refer to a family of horizontal one-forms $f_{\mathrm{L}}(u)(q, \dot{q})$ on TQ induced by the family of fiber-preserving maps $f_{\mathrm{L}}(u)$. With this in mind, for dissipative systems, the virtual work $W : \mathcal{C}([0,T], Q) \times \mathcal{C}([0,T],\mathcal{U}) \to \mathbb{R}$ of the external forces can be defined as

$$W(q,u) = \int_0^T f_{\mathrm{LC}}(q(t), \dot{q}(t), u(t)) \cdot \delta q(t)\ dt. \tag{2.5}$$

For these systems, it is then known that the path of the system $q \in \mathcal{C}([0,T], Q)$ must satisfy the Lagrange-d'Alembert principle, which requires that

$$\delta \int_0^T \mathfrak{L}(q(t), \dot{q}(t))\, dt + \int_0^T f_{\mathrm{LC}}(q(t), \dot{q}(t), u(t)) \cdot \delta q(t) dt = 0 \tag{2.6}$$

for all variations of δq vanishing at the endpoints $t = 0$ and $t = T$ (see [19, 20]). This is a standard modification of Hamilton's principle used to obtain stationary points of the action in the case of unforced systems (see [1, 18, 19]). Based on (2.5), the equations of motion for a dissipative system can thus be shown as:

$$\frac{\partial \mathfrak{L}(q(t), \dot{q}(t))}{\partial q(t)} - \frac{d}{dt}\Big(\frac{\partial \mathfrak{L}(q(t), \dot{q}(t))}{\partial \dot{q}(t)}\Big) + f_{\mathrm{LC}}(q(t), \dot{q}(t), u) = 0. \tag{2.7}$$

These equations implicitly define a family of forced Lagrangian vector fields $X_{\mathfrak{L}}(u) : TQ \times [0, T] \to T(TQ)$ and associated forced Lagrangian flow $F_{\mathfrak{L}}(u) : TQ \times [0, T] \to TQ$ for a fixed $u \in \mathcal{C}([0, T], \mathcal{U})$ (see [19] for more details). The forced Lagrangian flow at fixed time t is denoted as $F^t_{\mathfrak{L}}(u) : TQ \to TQ$.

This method of obtaining the equation is known as the *Lagrangian formalism*, describing the system's motion through the evolution of its configuration and velocity in state space, i.e., on the tangent bundle TQ. Using Hamiltonian mechanics, the evolution of the system can equivalently be described in the phase space using the configuration vectors $q(t)$ and conjugate momenta $p(t)$ which belong to the cotangent bundle T^*Q associated with the configuration manifold Q.

2.2.2 Hamiltonian formalism

To derive the equations of motion within the *Hamiltonian formalism*, the Legendre transform can be defined for unforced systems. It is a map $\mathbb{F}L : TQ \to T^*Q$, which in coordinate form can be written as

$$\mathbb{F}L : (q, \dot{q}) \mapsto \left(q, \left(\frac{\partial \mathfrak{L}}{\partial \dot{q}}(q, \dot{q})\right)^{\intercal}\right) = (q, p) \tag{2.8}$$

where p denotes the conjugate momenta of the system, and the time dependence has been omitted to simplify the notation. For a regular Lagrangian, the Legendre transform is a unique mapping. To model the behaviour of forced systems the *Hamiltonian control forces* can be defined $f_{\mathrm{H}}(q, p, u) : T^*Q \times \mathcal{U} \to T^*Q$ and considered as parameter-dependent *Hamiltonian forces* $f_{\mathrm{H}}(u)$ where

$$f_{\mathrm{L}}(u) = f_{\mathrm{H}}(u) \circ \mathbb{F}L.$$

similarly to the Lagrangian counterpart in (2.4). Based on these definitions, the Hamiltonian H is defined as

$$H(q,p) = \mathbb{F}L(q,\dot{q}) \cdot \dot{q} - \mathfrak{L}(q,\dot{q})$$

and the equations describing the motion within the phase space in the presence of external forcing become

$$\dot{q} = \frac{\partial H}{\partial p}, \qquad \dot{p} = -\frac{\partial H}{\partial q} + f_{\mathrm{HC}}, \tag{2.9}$$

where $f_{\mathrm{HC}}(q,p,u) = f_{\mathrm{H}}(u)(q,p)$ and the time dependency has been dropped to simplify the exposition. The Hamiltonian flow of the Hamiltonian vector field X_H defined by (2.9) can be defined as a map $F_H(u) : T^*Q \times \mathbb{R} \to T^*Q$ [1].

2.2.3 Constrained systems

Constraints on the system dynamics, such as, for example, those present in multibody dynamics, can be accommodated using a Lagrange multiplier as described by [1, 3]. This is interpreted in a similar way as using Lagrange multipliers to place equality constraints in the cost in an optimal control problem.

Consider a holonomic scleronomic constraint $\mathfrak{g}(q(t))=0$, where $\mathfrak{g}:Q\to\mathbb{R}^m$, with a regular value of 0. Consequently, a $(n–m)$-dimensional submanifold can be defined as $\mathfrak{C}=\mathfrak{g}^{-1}(0)=\{q \mid q \in Q, \mathfrak{g}(q)=0\}\subset Q$, known as the constraint manifold. Following the approach proposed by [1], an augmented Lagrangian $\mathfrak{L}^c(q(t),\dot{q}(t),\lambda(t)) = \mathfrak{L}(q(t),\dot{q}(t))–\mathfrak{h}(q,\lambda)$ can be formulated, where the Lagrange multiplier $\lambda(t)\in\mathbb{R}^m$ and $\mathfrak{h}(q,\lambda) = \lambda(t)^T\mathfrak{g}(q(t))$. Employing the continuous Lagrange-d'Alembert principle with this augmented Lagrangian, the equations of motion become:

$$\frac{\partial \mathfrak{L}(q,\dot{q})}{\partial q} - \frac{d}{dt}\frac{\partial \mathfrak{L}(q,\dot{q})}{\partial \dot{q}} - \frac{\partial \mathfrak{h}(q,\lambda)}{\partial q} + f_{\mathrm{LC}}(q,\dot{q},u) = 0 \tag{2.10a}$$

$$\mathfrak{g}(q) = 0 \tag{2.10b}$$

which is now a system of differential-algebraic equations (DAE). In fact, the term $(-\frac{\partial \mathfrak{h}(q,\lambda)}{\partial q})$ can be viewed as a force exerted from the constraints to keep the system trajectory on $T\mathfrak{C}$, the induced tangent space to the constraint manifold $\mathfrak{C}$.

2.3 Simulation through discretisation

So far, we have seen that Equations (2.7) and (2.9) represent the evolution of the system in state space and phase space, respectively. Ideally, these equations would be solved analytically, providing the solution trajectory at any point in time starting from an initial configuration. The nonlinear nature of most problems, however, does not allow for an analytical solution to be found, and thus, the solution must be approximated. Many numerical methods exist to achieve this, and for an introduction to the topic, we refer the reader to books such as [21] and [22].

Most classical methods rely on direct discretisation of the equations of motion. This is achieved by discretising the time domain to a finite number of time nodes $t_k = k\Delta t, k = 0, 1, \ldots$, on which the differential equations are approximated using difference equations. Such schemes are known as integrators and are solved a step at a time to integrate the dynamics numerically.

For a continuous-time system with a continuous trajectory represented by $x(t) = [q(t)^\intercal, \dot{q}(t)^\intercal]^\intercal$ or $x(t) = [q(t)^\intercal, p(t)^\intercal]^\intercal$ and a control sequence $u(t)$, we classify the system model as *explicit* when the state update equations are of the form $\dot{x} = f(x, u)$, and *implicit* when they adhere to the form $0 = z(x, \dot{x}, u)$. Similarly, in discrete time, with trajectory approximation $x_k \approx x(t_k)$ and discrete control sequence $u_k \approx u(t_k)$, state update equations of the form $x_{k+1} = f_\mathrm{d}(x_k, u_k)$ are referred to as explicit models, while those of the form $0 = z_\mathrm{d}(x_{k+1}, x_k, u_k)$ are termed implicit. Implicit formulations inherently pose greater numerical challenges. Root-finding schemes often become necessary in such cases, aiming to obtain a solution up to a user-defined accuracy. One such scheme is the Newton-Raphson method, an iterative procedure outlined in Algorithm 1 for a system of equations $f(x) = 0$, where $\mathbb{J}(x)$ denotes its Jacobian [23].

2.3.1 Quantative measures of accuracy

One measure of the accuracy of an integrator is its *order*, which measures the quantitative difference between the continuous trajectory and its discrete-time

Algorithm 1: Multidimenstional Newton's Method for finding a root of a system of equations

Given :

A system of equations $f(x) = 0$, initial solution guess x^0, solution tolerance *tol*, maximum iteration *maxiter* and $iter = 0$;

Main :

while $\|x^0\| \geq tol$ and $iter < maxiter$ **do**
  $\Delta x \leftarrow (-\mathbb{J}(x^0))^{-1} f(x^0)$;
  $x^0 \leftarrow x^0 + \Delta x$;
  $iter \leftarrow iter + 1$

approximation. Given a numerical integrator $F : T^*Q \times \mathbb{R} \to T^*Q$, which approximates the Hamiltonian flow F_H, the local error at time Δt and the global error at time T of the approximation can be defined respectively as [20]:

$$e_{\mathrm{l}}(q, p, \Delta t) = \|F(q, p, \Delta t) - F_H(q, p, \Delta t)\|$$
$$e_{\mathrm{g}}(q, p, \Delta t, T) = \|F^N(q, p, \Delta t) - F_H(q, p, T)\|$$

where N is an integer with $\Delta t = T/N$ and $F^N(q, p, \Delta t)$ refers to the consecutive application of the F integrator N times (i.e. for N steps). The integrator is said to be of *order* r if there exist constants $c_{\mathrm{l}} >, h_{\mathrm{l}} > 0$ and an open set $U \subset T^*Q$ such that for all $(q, p) \in U$ and $\Delta t \leq h_{\mathrm{l}}$

$$e_{\mathrm{l}}(q, p, \Delta t) \leq c_{\mathrm{l}} \Delta t^{r+1}. \tag{2.11}$$

It is said to be *convergent of order* r if there exist constants $c_{\mathrm{g}} > 0$, $h_{\mathrm{g}} > 0$, $T_{\mathrm{g}} > 0$ and an open set $S \subset T^*Q$ such that for all $(q, p) \in S$, $\Delta t \leq h_{\mathrm{g}}$, and $T \leq T_{\mathrm{g}}$

$$e_{\mathrm{g}}(q, p, \Delta t, T) \leq c_{\mathrm{g}} \Delta t^r \tag{2.12}$$

[1]. Often, the error is described by its limiting behaviour. This can be mathematically expressed using big $\mathcal{O}$ notation (Bachmann–Landau notation) as will be demonstrated in Chapter 3. Let $h, r : \mathbb{R}^n \to \mathbb{R}$ and $h(x) = \mathcal{O}(r(x))$ for $x \to x_0$ then

$$\exists c > 0,\ \exists \epsilon > 0 \text{ such that } |h(x)| \leq c|r(x)| \text{ for } \forall x \in \{x : \|x - x_0\| < \epsilon\}. \tag{2.13}$$

In other words, r describes the asymptotic upper bound on h.

2.3.2 Qualitative measures of accuracy

Although many of the standard numerical integrators focus on reducing the quantitative error of the approximation, they often fail to preserve important properties of the mathematical model.

One such property, particularly relevant in practice, is the convexity of the model.

Definition 2.3.1. *A set $S \subseteq \mathbb{R}^n$ is convex if for any two points $s_1, s_2 \in S$ and any $\theta \in [0,1]$, the set includes the line between them, i.e. it holds that $\theta s_1 + (1-\theta)s_2 \in S$ [24]. A function $f : \mathbb{R}^{n_s} \to \mathbb{R}^{n_f}$ is said to be (componentwise) convex if its domain* $\mathrm{dom} f$ *is a convex set and for all $s_1, s_2 \in \mathrm{dom} f$, $i = 1, \ldots, n_f$, and $\theta \in [0,1]$*

$$[f(\theta s_1 + (1-\theta)s_2)]_i \leq \theta[f(s_1)]_i + (1-\theta)[f(s_2)]_i.$$

We define a system as having a convex model or convex dynamics if the right-hand side of its state update equation is componentwise convex. For systems with convex continuous models, preserving this property in the discretisation allows for improvement in the computational cost of simulating and optimally controlling the system, as we will discuss shortly.

Apart from convexity, the equations of motion hide additional information about the system, such as conservation laws and other (time) invariants of the mathematical model. This additional information regarding the behaviour of the system is encoded within the geometric structure of the equations, and many standard integrators fail to preserve it from the continuous to the discrete-time domain [21]. Thus, they often fail to accurately represent the system's long-term behaviour even when using very fine time grids [25].

In contrast, a class of numerical integrators, referred to as geometric integrators (see for example [26]) adopts a different strategy and prioritises the preservation of specific structures in the discrete-time model. These integrators are thus tailored to the problems at hand (unforced systems, constrained systems, stochastic systems, etc.), yielding improved qualitative behaviour and enhanced accuracy in long-term

integration [25–27]. We will now list some of the main structures typically preserved by these integrators.

Symplecticity

Of particular importance for Lagrangian systems is the conservation of their symplectic structure, which provides important mathematical insight into the system's behaviour. This structure can be defined as the preservation of a differential two-form

$$w = dp \wedge dq = \sum_{i=1}^{n^q} d[p]_i \wedge d[q]_i, \tag{2.14}$$

where $\wedge$ is the wedge product, and has several consequences [28]. For example, it restricts the system to evolve on trajectories which, in the case for $n^q = 1$, preserve the oriented area of the parallelogram spanned by dq and dp in the phase space, or in the case of $n^q > 1$ conserve the sum of the oriented areas of the projections of the parallelogram onto the coordinate planes $([p]_i; [q]_i)$ [21, 25, 26]. The preservation of the symplectic structure by numerical integration methods allows for qualitatively more accurate long-term simulation which can often be understood through backward error analysis tools [26, 29].

Lagrangian symmetries

If the Lagrangian exhibits symmetries, then the system's dynamics may also fulfil conservation laws, such as conservation of energy (time invariance), momentum (translation invariance), or angular momentum (rotational invariance). These invariances can be defined mathematically in several ways. Simply, as [20] outlines, consider a system with Lagrangian $\mathfrak{L}$ which is invariant under the translation $q^\eta(t) = q(t) + \eta\,\zeta$ or rotation $q^\eta(t) = \exp(\eta\Omega)q(t)$ where ζ is a vector and Ω is a skew-symmetric matrix. These examples can be generalised as a one-parameter group of curves $q^\eta(t)$ with $q^0(t) = q(t)$ for which $\mathfrak{L}(q^\eta(t), \dot{q}^\eta(t)) = \mathfrak{L}(q(t), \dot{q}(t))$ thus

$$\int_0^T \mathfrak{L}(q(t), \dot{q}(t))dt = \int_0^T \mathfrak{L}(q^\eta(t), \dot{q}^\eta(t))dt. \tag{2.15}$$

Considering the solution curve $q(t)$ and a variation in an infinitesimal symmetry direction $\xi(t) = \frac{\partial q^\eta(t)}{\delta \eta}\Big|_{\eta=0}$, due to the invariance (2.15) applying the Lagrange-d'Alembert principle in the absence of forces and integration by parts leads to

$$0 = \frac{\partial}{\partial \eta}\int_0^T \mathfrak{L}(q(t), \dot{q}(t))dt =$$
$$\int_0^T \Big(\frac{\partial \mathfrak{L}}{\partial q} - \frac{d}{dt}\Big(\frac{\mathfrak{L}}{\partial \dot{q}}\Big)\Big) \cdot \xi \, dt + \Big[\frac{\partial \mathfrak{L}}{\partial q} \cdot \xi\Big]_0^T = \frac{\partial \mathfrak{L}}{\partial q}\Big|_{t=T} \cdot \xi(T) - \frac{\partial \mathfrak{L}}{\partial q}\Big|_{t=0} \cdot \xi(0). \quad (2.16)$$

Here $\frac{\partial \mathfrak{L}}{\partial q}\Big|_{t=0} \cdot \xi(0)$ and $\frac{\partial \mathfrak{L}}{\partial q}\Big|_{t=T} \cdot \xi(T)$ represent the momentum in the direction $\xi(t)$ at the times $t = 0$ and $t = T$ and their equality signifies that under the considered translation or rotation, the momentum is preserved as T can be arbitrarily chosen.

More generally, [20] consider the action of a multidimensional Lie group G with Lie algebra $\mathfrak{g}$ and an action $\xi \in \mathfrak{g}$ of G on Q whose lift to TQ leaves $\mathfrak{L}$ invariant. The momentum map $J_{\mathfrak{L}} : TQ \to \mathfrak{g}^*$ can then be defined as $J_{\mathfrak{L}}(q, \dot{q}) \cdot \xi = (\partial \mathfrak{L}/\partial \dot{q}) \cdot \xi_Q(q)$ where $\xi_Q : Q \mapsto TQ$ is the infinitesimal generator. Taking a variation $\delta q = \xi_Q$, equation (2.16) becomes

$$\Big(\frac{\partial \mathfrak{L}}{\partial q} \cdot \xi_Q(q)\Big)|_{t=T} - \Big(\frac{\partial \mathfrak{L}}{\partial q} \cdot \xi_Q(q)\Big)|_{t=0}$$

signifying preservation of the momentum map due to the invariance of $\mathfrak{L}$ on the lifted action. This can formally be stated as a theorem ([20], Theorem 2.3):

Theorem 2.3.1. ***(Noether's theorem)*** *Consider a Lagrangian system $\mathfrak{L} : TQ \to \mathbb{R}$ which is invariant under the lift of the (left or right) action $\Phi : G \times Q \to Q$. Then the corresponding Lagrangian momentum map $J_{\mathfrak{L}} : TQ \to \mathfrak{g}^*$ is a conserved quantity of the flow so that $J_{\mathfrak{L}} \circ F_{\mathfrak{L}}^t = J_{\mathfrak{L}}$ for all times t.*

A proof can be found in [20].

Adiabatic invariance

Another useful mathematical structure which the dynamics of the system might possess is adiabatic invariance. Consider again the equations of motion

$$\dot{p} = -\frac{\partial H}{\partial q}, \quad \dot{q} = \frac{\partial H}{\partial p}, \quad (2.17)$$

for a Hamiltonian of the form $H(p, q, \xi t)$ where ξ is a small parameter. Then [30] defines the quantity $\mathcal{I}(p(t), q(t), \xi t)$ as an adiabatic invariant of this system if for every $k > 0$ there $\exists\, \xi$ such that $|\mathcal{I}(p(t), q(t), t) - \mathcal{I}(p(0), q(0), 0)| < k$ if $0 < \xi < \xi_0$, $0 < t < 1/\xi$. In other words, this is a quantity which changes very little under slow changes of the parameter even if other functions of the system, such as the Hamiltonian, vary significantly. For more rigorous definitions see [26, 30].

Dissipative systems

When the system is dissipative or under the action of external control, then the symplectic form and the system's energy are no longer preserved by the flow. In such cases, however, Noether's theorem can be adjusted to account for the presence of forces [18, 20] and establish modified momentum conservation laws.

2.3.3 Variational integrators

The work of Ge and Marsden [31] proved that a geometric integrator can simultaneously preserve energy and momenta or symplecticity and momenta, but not all three at once. Thus, the work on structure-preserving integration schemes advanced in two main directions: energy-momentum methods and symplectic-momentum methods [20]. We will not attempt to systematically review these methods, as the literature is too vast to allow for a comprehensive review within this thesis. We refer the reader to [26] for references and overview. Instead, we focus on a subgroup of symplectic-momentum methods, known as variational integrators, as it is an important development on which our work relies.

Variational integrators are based on the theory of discrete variational mechanics (see [1]). This mathematical framework provides a discrete parallel to the continuous variational principles. It formulates discrete analogues to Hamilton's principle of stationary action, Lagrange-d'Alembert principle, Noether's theorem and Legendre's transform. Using this discrete framework, one can derive the discrete equations of motion by discretising the underlying variational principle rather than directly discretising the continuous equations of motion as standard methods. This leads

to the formulation of time-stepping equations, which are symplectic and momenta preserving [3]. By the choice of variational formulation one can derive an integrator tailored to the physics and goals of the specific problem. For example, for conservative systems, one uses Hamilton's variational principle [1], while for forced or controlled systems, one can use the Lagrange-d'Alembert principles [19, 32–34]. Other examples include work focused on holonomically [3, 35–37] and non-holonomically [38] constrained systems, stochastic systems [39, 40], multibody systems [37, 41], dissipative systems [42] and many more. As these integrators fall in the group of symplectic-momentum methods, they are not capable of exactly preserving the energy of the system. Nevertheless, they accurately represent it up to small fluctuations around the true value, resulting in a bounded error over long-term simulation [20]. For a detailed review of the theory of discrete variational mechanics and variational integrators, we refer the reader to [1], [20] and [43].

As an example to which we will often refer, we now consider the dissipative unconstrained system defined in Section 2.2 and focus on the variational integrator presented by [1]. To represent the system dynamics in discrete time, the discrete configuration path is defined as

$$q_d = \{q_k\}_{k=0}^{N} \quad \text{with } q_k \approx q(t_k).$$

Similarly, we define the discrete control path

$$u_\mathrm{d} = \{u_{k+1/2}\}_{k=0}^{N-1} \quad \text{with } u_{k+1/2} \approx u(t_{k+1/2}).$$

The action integral on each discrete time step is approximated as

$$\mathfrak{L}_{\mathrm{d},k} = \mathfrak{L}_d(q_k, q_{k+1}) \approx \int_{t_i}^{t_{k+1}} \mathfrak{L}(q, \dot{q})\, dt$$

where $\mathfrak{L}_\mathrm{d}$ is often called the discrete Lagrangian [1]. The virtual work can similarly be approximated as

$$f_k^- \cdot \delta q_k + f_k^+ \cdot \delta q_{k+1} \approx \int_{t_k}^{t_{k+1}} (f(q, \dot{q}, u) \cdot \delta q)\, dt.$$

Here f_k^-, f_k^+ are left and right discrete forces [19], with f_{k-1}^+ (f_k^-) representing the effects of continuous Lagrangian control forces acting over $[t_{k-1}, t_k]$ ($[t_k, t_{k+1}]$ respectively) on configuration node q_k. These approximations can be combined to formulate the discrete version of the Lagrange-d'Alembert principle:

$$\delta \sum_{k=0}^{N-1} \mathfrak{L}_\mathrm{d}(q_k, q_{k+1}) + \sum_{k=0}^{N-1} (f_k^- \cdot \delta q_k + f_k^+ \cdot \delta q_{k+1}) = 0$$

for all variations $\{\delta q_k\}_{k=0}^N$ vanishing at the endpoints ($\delta q_0 = \delta q_N = 0$). The resulting discrete equations of motion are [19]

$$D_2\mathfrak{L}_\mathrm{d}(q_{k-1}, q_k) + D_1\mathfrak{L}_\mathrm{d}(q_k, q_{k+1}) + f_{k-1}^+ + f_k^- = 0 \tag{2.18}$$

for $k = 1, \ldots, N-1$, where D_n denotes the gradient operator with respect to the n-th argument. These equations define the evolution of the discrete path in configuration space.

This method of obtaining the equations, analogously to the continuous formulation, can again be interpreted as the Lagrangian formalism. Alternatively, using the Hamiltonian formalism, we can describe the discrete-time system dynamics using an equivalent set of equations

$$p_k + D_1\mathfrak{L}_\mathrm{d}(q_k, q_{k+1}) + f_k^- = 0 \tag{2.19a}$$

$$p_{k+1} - D_2\mathfrak{L}_\mathrm{d}(q_k, q_{k+1}) - f_k^+ = 0 \tag{2.19b}$$

where $\{p_k\}_{i=0}^N$ are the discrete conjugate momenta defined by the *discrete forced Legendre transform* as follows [19]:

$$\mathbb{F}^{f^+} L_\mathrm{d}(u_{k+1/2}) : (q_k, q_{k+1}) \mapsto (q_{k+1}, p_{k+1}) = (q_{k+1}, D_2\mathfrak{L}_\mathrm{d}(q_k, q_{k+1}) + f_k^+)$$

$$\mathbb{F}^{f^-} L_\mathrm{d}(u_{k+1/2}) : (q_k, q_{k+1}) \mapsto (q_{k+1}, p_k) = (q_{k+1}, -D_1\mathfrak{L}_\mathrm{d}(q_k, q_{k+1}) - f_k^-)$$

Both models (2.18), (2.19) have been shown to preserve momenta using a discrete version of the Forced Noether's Theorem [1, 3]. In this thesis, we will collectively refer to these formulations as singlerate variational integrators (SVI). It should be noted that throughout the remainder of this thesis, the term "Hamiltonian formalism"

will be used loosely to describe the formulation of time-stepping equations that govern the evolution of both the configuration and conjugate momentum in discrete time. However, it's important to clarify that this approach actually employs discrete Lagrangians instead of discrete Hamiltonians.

2.4 Optimal control

Given an initial state of the system, the methods presented so far allow us to predict its subsequent motion numerically, even in the presence of external inputs. These external forces are often designed to influence the behaviour of the system to achieve a task, and in many cases, to do so in the fastest or most efficient way with respect to some criteria. In such cases, the theory of optimal control allows for the computation of a control sequence $u(t)$, which will optimise the performance while complying with system or control constraints.

2.4.1 Problem statement

A generic example of an optimal control problem (OCP) can take the form

Problem 1.

$$\min_{x,u} J(x,u) = \int_0^T C(x(t),u(t)) \tag{2.20a}$$

$$\textit{subject to: for } 0 \leq t \leq T \tag{2.20b}$$

$$x(0) = x^0 \tag{2.20c}$$

$$z(\dot{x}(t),x(t),u(t)) = 0 \tag{2.20d}$$

$$h(x(t),u(t)) \geq 0 \tag{2.20e}$$

where $t \in [0,T]$, $x(t) = [q(t)^\intercal, \dot{q}(t)^\intercal]^\intercal$, x^0 *is a given initial state and* $C : TQ \times \mathcal{U} \to \mathbb{R}^1$ *is the objective function representing the performance index being minimised. Here* z *and* h *are vector functions which denote the constraints placed on the system state and the controls (including the model of the system motion) and are assumed to be differentiable. This formulation can trivially be rewritten for a state in the phase space* $x(t) = [q(t)^\intercal, p(t)^\intercal]^\intercal$.

Definition 2.4.1. *A feasible trajectory* $(x, \dot{x}, u)$ *is a trajectory from the feasible set* $\Omega := \{\dot{x}(t), x(t), u(t)|\ x(0) = x^0,\ h(x(t), u(t)) \geq 0,\ z(\dot{x}, x, u) = 0$ *for* $\forall t[0, T]\}$. *A feasible trajectory is a local solution (optimum) of Problem 1 if there exists a neighbourhood* $\mathcal{N}$ *of* $(\dot{x}^*, x^*, u^*)$ *such that* $J(x, u) \geq J(x^*, u^*)$ *for all* $(x, \dot{x}, u) \in \mathcal{N} \cap \Omega$. *It is a global solution (optimum) if* $J(x, u) \geq J(x^*, u^*)$ *holds for* $\forall(\dot{x}, x, u) \in \Omega$.

2.4.2 Solution methods

Obtaining an optimum of Problem 1 is not a trivial task and has received significant attention from the research community over the years. For a comprehensive overview of the available approaches, we refer the reader to [44–47].

One possible numerical scheme is based on dynamic programming developed initially by R. E. Bellman in the 1950s [48, 49]. This approach divides the problem into smaller subproblems and computes an optimal policy (control law) for every point in the state space. From these candidates, a final optimal trajectory and control sequence is chosen. Although this method guarantees global optimality, the computational time depends on the number of feasible trajectories and the discretisation of the continuous state. It further scales exponentially with the dimensionality of the state and control vectors of the system in general [47]. As an alternative, one could use, iterative dynamic programming [50] or differential dynamic programming [51], in both of which the control law is iteratively approximated in a neighbourhood of a nominal, non-optimal trajectory.

Another large class of solution methods focuses on directly obtaining the optimal trajectory starting from a particular initial system state rather than computing the optimal policy for every point in the state space. This is achieved by computing a sequence of controls under whose action a single optimal trajectory is defined starting from the given initial state [47].

Overall the solution methods for OCPs can be split broadly into two groups: direct and indirect.

Indirect methods

Indirect methods first optimise and then discretise. They employ Pontryagin's Maximum Principle to analytically derive the necessary optimality conditions, which are then discretised and solved numerically. These methods suffer from several disadvantages. They require the introduction and numerical integration of adjoint variables, thus increasing the system's dimensionality by a factor of two. Additionally, incorporating constraints and terminal conditions can be challenging [44, 46, 47]. This difficulty is especially evident for inequality-constrained problems, where additional information of the structure of the solution is needed to solve the resulting two-point boundary value problem [52, 53]. Thus the practical application of indirect methods often requires an in-depth understanding of the problem and good initial guesses of the state and the adjoints.

Direct methods

On the other hand, direct methods, also known as transcription methods, first discretise and then optimise [18, 54]. These methods transcribe the continuous OCP into a parameter optimisation problem by the finite-dimensional parametrisation of the controls or of both the controls and the states. This results in a finite-dimensional optimal control problem, in which the discretised equations of motion serve as equality constraints and the necessary optimality conditions for Problem 2 are derived through the Karush-Kuhn-Tucker (KKT) conditions [23].

Consider a discretisation of Problem 1:

Problem 2.

$$\min_{\mathbf{x}_\mathrm{d},\mathbf{u}_\mathrm{d}} J_\mathrm{d}(\mathbf{x}_d,\mathbf{u}_d) = \sum_{k=0}^{N-1} C_\mathrm{d}(x_k,u_k) \tag{2.21a}$$

$$\text{subject to : } x_0 = x^0 \tag{2.21b}$$

$$z_\mathrm{d}(x_{k+1},x_k,u_k) = 0 \quad \textit{for } k=0,\dots,N-1 \tag{2.21c}$$

$$h_\mathrm{d}(x_k,u_k) \geq 0 \qquad \textit{for } k=0,\dots,N-1 \tag{2.21d}$$

for a chosen discrete time step Δt, $N = T/\Delta t$, $\mathbf{x}_\mathrm{d} = \{x_0,\dots,x_N\}$, $\mathbf{u}_\mathrm{d} = \{u_0,\dots,u_{N-1}\}$, $z_\mathrm{d} : TQ \times TQ \times \mathcal{U} \to \mathbb{R}^{n^z}$, $h_\mathrm{d} : TQ \times \mathcal{U} \to \mathbb{R}^{n^h}$, $C_\mathrm{d} : TQ \times \mathcal{U} \to \mathbb{R}^1$.

In this case, Definition 2.4.1 defines a trajectory $(\mathbf{x}_\mathrm{d}, \mathbf{u}_\mathrm{d})$ from a feasible set $\Omega_\mathrm{d} := \{(\mathbf{x}_\mathrm{d}, \mathbf{u}_\mathrm{d}) | x_0 = x^0, h_\mathrm{d}(x_k, u_k) \geq 0, z_\mathrm{d}(x_{k+1}, x_k, u_k) = 0 \text{ for } k = 0, \ldots, N-1\}$ and global and local optimality defined based on the overall discrete cost $J_\mathrm{d}(\mathbf{x}_\mathrm{d}, \mathbf{u}_\mathrm{d})$.

Let the Lagrangian for Problem 2 be defined as

$$\mathcal{L}_\mathrm{OCP}(x_d, u_d, \lambda_d, \mu_d) = J_\mathrm{d}(\mathbf{x}_\mathrm{d}, \mathbf{u}_\mathrm{d}) - \sum_{k=0}^{N-1} \Big(\lambda_k \cdot z_\mathrm{d}(x_{k+1}, x_k, u_k) - \mu_k \cdot h_\mathrm{d}(x_k, u_k) \Big) \quad (2.22)$$

where λ_k, μ_k are Lagrange multipliers, $\mathbf{x}_\mathrm{d} = \{x_0, \ldots, x_N\}$, $\lambda_\mathrm{d} = \{\lambda_0, \ldots, \lambda_{N-1}\}$ and $\mu_\mathrm{d} = \{\mu_0, \ldots, \mu_{N-1}\}$. We define the active set $\mathcal{A}(\mathbf{x}_\mathrm{d}, \mathbf{u}_\mathrm{d})$ for a feasible trajectory $(\mathbf{x}_\mathrm{d}, \mathbf{u}_\mathrm{d})$ as the set of all equality constraints $z(x_{k+1}, x_k, u_k) = 0$ and all inequality constraints $[h]_i(x_k, u_k) = 0$ which are active (satisfied with equality) at (x_{k+1}, x_k, u_k) for $k = 0, \ldots, N-1$.

Definition 2.4.2. ***(LICQ)*** *Given a trajectory $(\mathbf{x}_\mathrm{d}, \mathbf{u}_\mathrm{d})$ with active set $\mathcal{A}(\mathbf{x}_\mathrm{d}, \mathbf{u}_\mathrm{d})$ a linear independence constraint qualification (LICQ) holds if the gradients of all constraints in the active set $\mathcal{A}(\mathbf{x}_\mathrm{d}, \mathbf{u}_\mathrm{d})$ are linearly independent.*

Theorem 2.4.1. ***(KKT conditions)*** *Given a local solution $(\mathbf{x}_\mathrm{d}^*, \mathbf{u}_\mathrm{d}^*)$ at which LICQ holds, there exist Lagrange multipliers $\lambda_k^* \in \mathbb{R}^{n^z}$ and $\mu_k^* \in \mathbb{R}^{n^h}$ for $k = 0, \ldots, N-1$ such that for $k = 0, \ldots, N$:*

$$\nabla_{x_k} \mathcal{L}_\mathrm{OCP}(\mathbf{x}_\mathrm{d}^*, \mathbf{u}_\mathrm{d}^*, \lambda_\mathrm{d}^*, \mu_\mathrm{d}^*) = 0 \quad (2.23a)$$

and for $k = 0, \ldots, N-1$:

$$\nabla_{u_k} \mathcal{L}_\mathrm{OCP}(\mathbf{x}_\mathrm{d}^*, \mathbf{u}_\mathrm{d}^*, \lambda_\mathrm{d}^*, \mu_\mathrm{d}^*) = 0, \quad (2.23b)$$

$$z_\mathrm{d}(x_{k+1}^*, x_k^*, u_k^*) = 0, \quad (2.23c)$$

$$h_\mathrm{d}(x_k^*, u_k^*) \geq 0, \quad \langle \mu_k^*, h_\mathrm{d}(x_k^*, u_k^*) \rangle = 0, \quad \mu_k^* \geq 0. \quad (2.23d)$$

The problem can thus be solved using standard nonlinear programming (NLP) solvers. Direct methods offer improved robustness concerning the initial guess. However, careful initialisation is still crucial when seeking the global optimum. One of the main drawbacks of direct methods is that they involve the solution of large NLP problems, characterised by a high number of optimization variables and

constraints. Thus they can require significant computational resources without guaranteeing successful termination.

Convex programming

To address these problems, a group of methods focus on approximating the optimisation problem using a convex formulation, which can be solved efficiently and reliably [23]. A convex program is an optimisation problem in which the objective function is convex and the feasible set defined by 2.4.1 is a convex set as outlined by Definition 2.3.1. In the case of Problem 1 (or 2) that would require for $C(x(t), u(t))$ and $h(x(t), u(t))$ (or $h_{\mathrm{d}}(x_k, u_k), C_{\mathrm{d}}(x_k, u_k)$) to be convex and $z(x(t), \dot{x}(t), u(t))$ ($z_{\mathrm{d}}(x_{k+1}, x_k, u_k)$) to take the form of affine transformations (i.e. of the form $Ax_k + Bu_k + c$ where $A \in \mathbb{R}^{n^z \times 2n^q}$, $B \in \mathbb{R}^{n^z \times n^u}$, $c \in \mathbb{R}^{n^h \times 1}$) [23]. Convex quadratic programs are a subclass of convex programs in which both the equality and inequality constraints are affine transformations and the objective function is for example of the form $\sum_{i=0}^{N-1}(\|x_k - x^{\mathrm{r}}\|_Q^2 + \|u_k - u^{\mathrm{r}}\|_R^2)$ where Q,R are positive semidefinite matrices and $(x^{\mathrm{r}}, u^{\mathrm{r}})$ is a pre-calculated reference trajectory.

Several approaches can be taken to approximate the optimal control problem as a convex program. Some approximate it using a sequence of quadratic programs. For systems with nonconvex models but otherwise convex constraints, others approximate the original OCP with a sequence of convex programs using linearisation of the model around a pre-computed trajectory. These are often known as *iterative linearisation approaches* or *tube approaches*. Rather than focusing on a single trajectory from the nonconvex model, a tube strategy optimises future control sequences by considering a tube containing all possible trajectories derived from the combination of the linearised model and all the possible linearisation errors. It aims to ensure that the state and control constraints are satisfied for all trajectories within the tube. The nonconvex problem is replaced with a sequence of convex programs. During the iterations, the goal is to reduce the linearisation error and shrink the tube to a single solution which is a solution of the original OCP problem or at least a good approximation to it as shown in Figure 2.1.

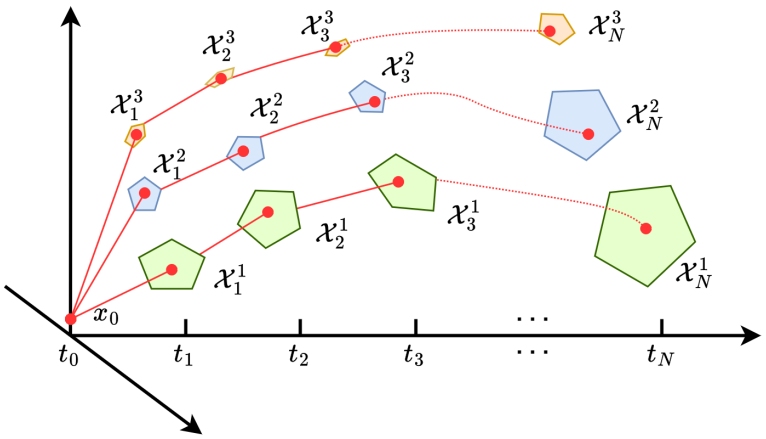


Figure 2.1: Illustration of a successive linearisation approach depicting the shrinkage of the tube during the convex program iterations. Here x_0 denotes the initial state and $\mathcal{X}_k^j$ denotes the cross-section of the trajectory tube at discrete time step k and iteration j. The red lines represent a trajectory within the tube.

More detail on iterative linearisation approaches and alternative schemes for convex approximation of the NLP will be will be provided in Chapter 6 and 7.

Discrete Mechanics and Optimal Control

A central part of our research is a direct transcription method known as Discrete Mechanics and Optimal Control (DMOC), developed by Junge et al. [34] based on the utilisation of variational integrators within the optimal control problem. In DMOC, the discrete description of the mechanical system is derived through a discrete version of the Lagrange-d'Alembert principle. The resulting structure-preserving time-stepping equations serve as equality constraints for the optimisation problem and allow for a discrete OCP formulation, which inherits the conservation properties of the continuous-time model and provides a sparse structure for the Jacobian of the constraint function. In many cases, the use of discrete Legendre transform allows for the time-stepping equations to be formulated in terms of configuration vector and controls only, making the optimal control problem smaller and thus more computationally feasible and efficient. The conservation properties, the convergence behaviour of DMOC and the order of approximation of the discrete solution were examined by [19] and [18]. Similarly to other approaches, the method often results in a nonconvex optimisation problem, and thus, convex approximation

techniques might be needed for its quick and reliable solution. In Chapter 6, we propose schemes of this nature, which maintain the structure-preserving properties of the problem formulation.

Since its creation DMOC has been applied to several aerospace applications [34, 55–63], autonomous vehicles control [64], trajectory optimisation for mobile robots [65], locomotion of an articulated body through shape changes [66] and others.

Using a discrete null space method the DMOC formulation has been extended to accommodate systems with holonomic constraints (DMOCC) and applied to multibody systems subject to joint constraints by [36, 67, 68] such as the optimal control of an upright humanoid gait [69–71]. Other variations of the method include adaptive time step formulation [72], provision for integer-valued control functions [73], multiphase implementation [74, 75], two-layered optimisation approach for simple hybrid systems [76] and multiobjective formulation [77]. Feedback policies and real-time trajectory optimisation have also been incorporated and investigated [78]. It must also be noted that other optimal control problem formulations have also been devised based on the theory of discrete mechanics underlying variational integrators (for example [79]) , but we focus on DMOC due to its multirate formulation [4, 5], which will be developed further in this thesis.

2.5 Model Predictive Control

The optimal control approaches mentioned so far provide an open-loop control strategy not capable of dealing with modelling errors or disturbances. Consequently, the resulting trajectory might vary from the prediction. A related control strategy, which is capable of providing closed-loop stability guarantees while respecting hard constraints on the admissible controls and states, is model predictive control (MPC), also known as receding-horizon control (RHC) [2, 80, 81]. In this scheme, a finite-horizon open-loop optimal control problem is solved at each sampling instant using the current state of the plant as the initial state. The result is an optimal control sequence of which only the first element is applied to the plant. At the next

sampling instant, the current plant state is again measured or estimated and taken as the new initial state to compute a new optimal control sequence over the same length horizon. Of this sequence, only the first element is again applied, and the process is repeated.

2.5.1 Feasibility and stability guarantees

Due to the use of a finite horizon, special considerations are needed to guarantee closed-loop stability even for the nominal system (meaning the system in the absence of modelling error or unknown disturbance). This is due to the fact that looking only at a finite horizon ahead could underestimate the amount of effort needed beyond that horizon to drive the trajectory to the desired state. This problem would not be present if the performance were evaluated over an infinite prediction horizon. Initial MPC strategies addressed this issue by incorporating terminal constraints on the predictive states, which guaranteed that a steady state would be achieved over this initial finite horizon. This requirement, however, was too stringent and led to computational challenges when using nonlinear system models [2, 82]. Due to these shortcomings of the original methods and the need for using a finite horizon to make the problem computationally feasible, later MPC formulations incorporated dual mode prediction strategies. In these schemes, the control law is split into two modes. The first mode refers to the control sequence over the chosen finite horizon and represents the optimisation variables in the MPC formulation. The second mode is a sequence of controls which extends the Mode 1 sequence beyond the initial finite horizon. These controls are typically based on a feedback control law, usually chosen to be the optimal control law for the unconstrained actual model of the dynamics or its linearisation about the desired steady state again in the absence of constraints [2, 82] For example, when the feedback is of the linear form $u_k = Kx_k$, the two modes can be written in the form:

$$u_k = Kx_k + c_k \quad \text{for } k = 0, \ldots, N-1$$

$$u_k = Kx_k \quad \text{for } k \geq N.$$

where the c_k sequence is a degree of freedom subject to optimisation. This formulation of the control sequence for $k < N$, known as the closed-loop paradigm additionally allows for pre-stabilisation of the system and an illustration of how far the control sequence is from the optimal due to the presence of constraints [83].

The use of an appropriate cost formulation equivalent to the infinite horizon cost can guarantee closed-loop stability and optimal performance in the absence of uncertainty. Furthermore, the inclusion of terminal constraints can ensure that the control and state predictions respect the system constraints over an infinite horizon and thus provide recursive feasibility of the receding horizon strategy. This is typically achieved by driving the state at the end of the chosen finite horizon to a subset of the state space, which is positively invariant, meaning that once the state of the system enters it, it will never be able to escape it [2, 82].

Definition 2.5.1. ***(Positively invariant set):*** *A set $\mathcal{X} \subseteq \mathbb{R}^{2n^q}$ is positively invariant for $u = Kx$ and the given system dynamics and constraints z_d, h_d if and only if $z_d(x^+, x, u) = 0$ and $x^+ \in \mathcal{X}$ for all $x \in \mathcal{X}$ [2].*

The mathematical formulation of the optimal control problem takes the form:

Problem 3.

$$(\mathbf{x}_i, \mathbf{c}_\mathrm{i}) \in \arg\min_{\mathbf{x}_i, \mathbf{c}_i} \sum_{k=0}^{N-1} C_\mathrm{d}(x_{k|i}, Kx_{k|i} + c_{k|i}) + \Phi(x_{N|i}) \tag{2.24a}$$

$$\text{subject to :} \quad x_{0|i} = x_i^0 \tag{2.24b}$$

$$z_\mathrm{d}(x_{k+1|i}, x_{k|i}, Kx_{k|i} + c_{k|i}) = 0 \qquad \text{for } k = 0, \ldots, N-1 \tag{2.24c}$$

$$h_\mathrm{d}(x_{k|i}, Kx_{k|i} + c_{k|i}) \geq 0 \qquad \text{for } k = 0, \ldots, N-1 \tag{2.24d}$$

$$x_{N|i} \in \mathcal{X}_N \tag{2.24e}$$

where $\mathbf{c}_i = \{c_{0|i}, \ldots, c_{N-1|i}\}$, $\mathbf{x}_i = \{x_{0|i}, \ldots, x_{N|i}\}$, x_i^0 is a known initial condition, $\Phi(x_{N|i}) : TQ \to \mathbb{R}$ is the terminal cost and $\mathcal{X}_N$ is the terminal invariant set. Here $x_{k|i}$ and $u_{k|i}$ denote respectively the state and input at time $i+k$, predicted at time i.

In the MPC strategy, at each discrete time step i Problem 3 is solved to obtain an optimal control sequence $\mathbf{c}_i^* = \{c_{0|i}^*, \ldots, c_{N-1|i}^*\}$ and only the first element of this

sequence is applied to the system as $u_{0|i} = Kx^*_{0|i} + c^*_{0|i}$. Based on this control action, at time $i+1$, the new state of the system x_{i+1} is obtained (measured or estimated from measurements at time $i+1$), and Problem 3 is reformulated and solved based on x_{i+1}. The process is repeated until the target state reaches a desired tolerance.

The success of this method relies on the successful solution of Problem 3 within a single horizon time step. As mentioned in Section 2.4.2, the resulting optimal problem is often nonconvex (often due to nonlinear dynamics). Thus, there are no guarantees for its successful solution within the available time. The iterative approximation techniques using quadratic or, more generally, convex programs can again be employed within the MPC strategy at each horizon time step. The forthcoming Chapters 6 and 7 will concentrate on developing innovative techniques of this nature.

2.5.2 Uncertainty considerations

Overall, one can show that for both linear and nonlinear systems, in the absence of any uncertainty, the MPC strategies described so far can provide certain guarantees for the nominal performance of the system, such as stable operation, constraints satisfaction and convergence of the actual state to the desired steady state. However, consideration of modelling errors and disturbances raises the question of robustness and how one can provide the same performance guarantees in the presence of uncertainty in the system. Several approaches have been considered in the past and can be viewed as part of three generalisations– Robust MPC, Stochastic MPC and Adaptive MPC.

Robust MPC schemes can be divided into two main groups [80]. The first focuses on deriving the nominal MPC control strategy and then examining its performance in the presence of uncertainty. The second group of approaches looks at all possible realisations of the uncertainty and, by accounting for them, explicitly devises robust MPC schemes with certain performance guarantees. One such approach is the min-max strategy, in which the constraints are respected for all possible perturbations

while the cost is minimised for their worst realisation. In the context of MPC, however, this strategy leads to a significant computational burden, which can be limiting for problems of large dimensionality (see [2] and [84] and the references within). Other more computationally efficient approaches are based on the idea of tightening the constraints of the underlying nominal receding horizon optimal control problem (RHOCP) in order to guarantee that they are respected for all possible perturbations. This theory was extended to the concept of "tube computation", i.e., computation of a sequence of sets in which the constraints are satisfied, and the future states can be guided through to guarantee that the system's final state lies in a prescribed target set. Although computationally attractive, the open-loop nature of these approaches leads to conservative solutions or even infeasible problem formulations [2, 84, 85]. As a result, research on a closed-loop strategy for Tube MPC was developed and has received significant attention from the Robust MPC community since [86–88].

Robust MPC approaches focus on respecting the constraints for all possible realisations of the uncertainty and, as such, can be more conservative than Stochastic MPC approaches, which take into account random uncertainty with a known probability distribution and incorporate probabilistic constraints and statistical information to allow for a trade-off between performance and constraint satisfaction systematically [2, 89]. A third group of approaches, known as Adaptive MPC, focuses on improving the system model by tuning the unknown parameters online while controlling the system. The combination of these approaches with robust or stochastic strategies allows the adaptive MPC schemes to provide certain robust performance guarantees and deal with stochastic constraints (see, for example, [90–92]).

3

Multirate variational simulation

Contents

3.1 Introduction 33
3.2 Background 34
3.3 Multirate variational mechanics for forced systems . . 37
3.3.1 Lagrangian viewpoint 37
3.3.2 Hamiltonian viewpoint 38
3.3.3 Properties of the Lagrangian flow for forced systems . . 41
3.4 Multirate discrete variational mechanics for forced systems 43
3.4.1 Lagrangian viewpoint 43
3.4.2 Multirate discrete Legendre transform and Hamiltonian viewpoint 48
3.4.3 Properties of the time-stepping scheme 53
3.4.4 Order of accuracy 57
3.5 Discrete variational mechanics for forced constrained systems 70

3.1 Introduction

This chapter presents a variational integrator tailored for systems exhibiting dynamics on different time scales. This multirate variational integrator (MVI) was first developed by [3], based on the singlerate variational integrator (SVI) presented in Chapter 2. In this chapter, we provide a detailed mathematical examination and justification of the multirate variational scheme in two alternative

formulations. We also extend previous literature by proving its structure-preserving properties and order of accuracy in the presence of time-dependent controls.

3.2 Background

In Chapter 2, we discussed how geometric integrators provide a new approach to system modelling capable of better qualitative behaviour and long-term accuracy. Despite their advantages, special care must still be taken when modelling multirate systems. These are systems which exhibit dynamics on different time scales, thus presenting additional challenges for numerical integrators. Such are for example multi-body systems composed of rigid and elastic parts with varying stiffness. The use of small time steps allows for the accurate integration of the fast dynamics but results in unnecessary large computational cost for the resolution of the slow ones.

The abundance of multirate systems in various fields has motivated the formulation of multiple methods capable of exploiting their multirate behaviour to reduce the computational cost associated with their simulation. In terms of geometrical integrators, one possibility is the use of the variational integrator introduced by [93], which utilises both explicit and implicit quadrature with the aim of decreasing the computational cost. This method represents a larger group of multirate methods, known as IMEX (implicit-explicit) integrators, which include various geometric and non-geometric numerical schemes. In these methods, the potential forces are split into fast and slow and integrated using implicit and explicit rules respectively. The explicit treatment reduces the computational cost of the integration [93].

Another group of methods approaches the problem by first identifying the macro and micro processes and then focusing on the simulation of either the micro- or macroscale model while using only limited information from the other. One example are equation-free methods [94, 95], which avoid the explicit closed-form derivation of a macroscopic model using suitably initialised short-time/space microscopic simulations. Another example is methods which avoid the exact resolution of the fast dynamics by using averaging techniques. For instance the heterogeneous multiscale methods ([43, 96, 97]) focus on the creation of an accurate macroscale

model while using the microscale information only locally where the macroscale model is invalid over parts of the domain or lacking vital information [43].

Another group of methods which relies on splitting based on fast and slow degrees of freedom is multiple time-stepping methods. These methods use two different time scales to resolve the slow and fast dynamics, with fewer evaluations needed for the slower subsystems due to the use of a coarser grid. One difficulty in the use of these methods is the identification of the two subsystems. Additionally, special care must be taken to ensure the stability of the scheme as resonance phenomena can lead to instability and large errors [3, 26]. For the underlying theory and examples of such schemes, we direct the reader to [26, 93, 98] and to the literature on multirate Runge-Kutta methods [98–100] and the reference therein. It is worth mentioning that once the slow and fast motions were identified, some authors have utilised singular perturbation theory [101, 102] to decouple the equations of motion into slow and fast subsystems for easier simulation and control scheme implementation (see for example [103]). However, this approach could sacrifice important information regarding the interaction between the two subsystems, which could significantly impact the accuracy of the simulation, the understanding of system behaviour, and the ability to control one subsystem through the manipulation of the other (see, for example, [11, 104] and Section 4.5 of this thesis).

Of central importance for our work is the multirate variational approach, which does not require decoupling the equations of motion. The approach was developed by [3] based on the theory of discrete mechanics and singlerate variational integrators discussed in Chapter 2. In this multirate scheme, the equations of motion are derived based on a multirate approximation of the action integral and a discerete variational principle. This leads to the formulation of symplectic and momentum-preserving time-stepping equations, which integrate the slow and fast variables on a macro and micro grid, respectively. This reduces the number of variables computed during simulation and, combined with the ability to use both explicit or implicit quadrature for the approximation of potential forces, significantly lowers

computational costs compared to singlerate methods. Investigations of the scheme's convergence behaviour, conservation properties and computational cost were carried out by [3, 105–108] for a variety of macro-micro time step proportionality and quadrature rules for both constrained and unconstrained multirate systems in the absence of forces. These works demonstrate that the scheme successfully combines the advantages of symplectic-momentum integrators with the exploitation of the multirate behaviour to provide high-fidelity simulation for multirate systems at a reduced computational cost. Furthermore, these integrators have been successfully implemented in optimal control schemes, as we will discuss in detail and extend in Chapter 5. This is in contrast to multirate Runge-Kutta methods [98, 99], whose utilisation for optimal control, to our knowledge, has not yet been explored, and thus no result exists on the order and properties of the respective solution.

In this chapter, we extend previous developments on MVI by:

1. Providing a detailed mathematical description of the scheme in the presence of external time-dependent controls.
2. Providing proof of the order of the scheme in the presence of external forcing.
3. Providing proof of Noether's theorem for multirate forced systems in both continuous and discrete time and thus proving the structure-preserving capabilities of MVI for forced systems.

Subsequent work in Chapter 4 extends this work by demonstrating the capabilities of the MVI in both Lagrangian and Hamiltonian form through several examples, whereas Chapter 6 presents a variational linearisation scheme for singlerate and multirate systems which preserves the conservational properties of SVI and MVI during the linearisation. Chapters 5, 6, and 7 delve into the implementation of these schemes for optimal control and receding horizon control, respectively. Throughout this thesis, we will develop the discussion in the broader context of systems evolving on a manifold Q, providing a general mathematical formulation. However, for the examples presented here and for many practical systems, a simplification based on replacing Q, T_qQ, T_q^*Q with $\mathbb{R}^n$ is sufficient.[1]

[1]For more rigorous definitions we refer the reader to [18, Appendix A] among other texts.

3.3 Multirate variational mechanics for forced systems

3.3.1 Lagrangian viewpoint

We assume the system presented in Section 2.2 exhibits dynamics on different time scales and assume that the vector of generalised coordinates can be transformed to a coordinate system such that $q(t) = \begin{bmatrix} q^{\mathrm{s}}(t) \\ q^{\mathrm{f}}(t) \end{bmatrix}$ where $q^{\mathrm{s}} \in \mathbb{R}^{n_{\mathrm{s}}}$ are the slow evolving variables, $q^{\mathrm{f}} \in \mathbb{R}^{n_{\mathrm{f}}}$ are the fast ones and $n^{\mathrm{s}} + n^{\mathrm{f}} = n$. Thus the slow and fast configuration vectors can be described on the submanifolds Q^{s} and Q^{f} with associated tangent bundles TQ^{s} and TQ^{f} such that $Q^{\mathrm{s}} \times Q^{\mathrm{f}} = Q$, $TQ^{\mathrm{s}} \times TQ^{\mathrm{f}} = TQ$. For multirate systems, because the configuration vector can be written as $q(t) = \begin{bmatrix} q^{\mathrm{s}}(t) \\ q^{\mathrm{f}}(t) \end{bmatrix}$, the forces can also be resolved in the direction of the virtual displacements as

$$f_{\mathrm{LC}}(q, \dot{q}, u) \cdot (\delta q^{\mathrm{s}}, \delta q^{\mathrm{f}}) = f_L(u)(q, \dot{q}) \cdot (\delta q^{\mathrm{s}}, \delta q^{\mathrm{f}}) = f^{\mathrm{s}}_{\mathrm{LC}} \cdot \delta q^{\mathrm{s}} + f^{\mathrm{f}}_{\mathrm{LC}} \cdot \delta q^{\mathrm{f}}. \tag{3.1}$$

Thus, we can define the slow and fast Lagrange control forces $f^{\mathrm{s}}_{\mathrm{LC}} : TQ \times \mathcal{U} \to T^*Q^{\mathrm{s}}$ and $f^{\mathrm{f}}_{\mathrm{LC}} : TQ \times \mathcal{U} \to T^*Q^{\mathrm{f}}$ as

$$f^{\mathrm{s}}_{\mathrm{LC}} : (q^{\mathrm{s}}, q^{\mathrm{f}}, \dot{q}^{\mathrm{s}}, \dot{q}^{\mathrm{f}}, u) \mapsto (q^{\mathrm{s}}, f^{\mathrm{s}}_{\mathrm{LC}}(q^{\mathrm{s}}, q^{\mathrm{f}}, \dot{q}^{\mathrm{s}}, \dot{q}^{\mathrm{f}}, u))$$

$$f^{\mathrm{f}}_{\mathrm{LC}} : (q^{\mathrm{s}}, q^{\mathrm{f}}, \dot{q}^{\mathrm{s}}, \dot{q}^{\mathrm{f}}, u) \mapsto (q^{\mathrm{f}}, f^{\mathrm{f}}_{\mathrm{LC}}(q^{\mathrm{s}}, q^{\mathrm{f}}, \dot{q}^{\mathrm{s}}, \dot{q}^{\mathrm{f}}, u))$$

and rewrite the virtual work expression in slow and fast components as

$$W(q, u) = W^{\mathrm{s}}(q^{\mathrm{s}}, q^{\mathrm{f}}, u) + W^{\mathrm{f}}(q^{\mathrm{s}}, q^{\mathrm{f}}, u)$$

$$W^{\mathrm{s}}(q^{\mathrm{s}}, q^{\mathrm{f}}, u) = \int_0^T f^{\mathrm{s}}_{\mathrm{LC}}\Big(q^{\mathrm{s}}(t), q^{\mathrm{f}}(t), \dot{q}^{\mathrm{s}}(t), \dot{q}^{\mathrm{f}}(t), u(t)\Big) \cdot \delta q^{\mathrm{s}}(t)\ dt,$$

$$W^{\mathrm{f}}(q^{\mathrm{s}}, q^{\mathrm{f}}, u) = \int_0^T f^{\mathrm{f}}_{\mathrm{LC}}\Big(q^{\mathrm{s}}(t), q^{\mathrm{f}}(t), \dot{q}^{\mathrm{s}}(t), \dot{q}^{\mathrm{f}}(t), u(t)\Big) \cdot \delta q^{\mathrm{f}}(t)\ dt.$$

This leads to the multirate formulation of the Lagrange-d'Alembert principle, which requires that

$$\begin{aligned} &\delta \int_0^T \mathcal{L}(q^{\mathrm{s}}(t), q^{\mathrm{f}}(t), \dot{q}^{\mathrm{s}}(t), \dot{q}^{\mathrm{f}}(t))\ dt + \int_0^T f^{\mathrm{s}}_{\mathrm{LC}}\Big(q^{\mathrm{s}}(t), q^{\mathrm{f}}(t), \dot{q}^{\mathrm{s}}(t), \dot{q}^{\mathrm{f}}(t), u(t)\Big) \cdot \delta q^{\mathrm{s}}(t) dt \\ &+ \int_0^T f^{\mathrm{f}}_{\mathrm{LC}}\Big(q^{\mathrm{s}}(t), q^{\mathrm{f}}(t), \dot{q}^{\mathrm{s}}(t), \dot{q}^{\mathrm{f}}(t), u(t)\Big) \cdot \delta q^{\mathrm{f}}(t) dt = 0 \end{aligned} \tag{3.2}$$

for all variations of δq^{s} and δq^{f} vanishing at the endpoints $t = 0$ and $t = T$ where $\mathfrak{L}(q, \dot{q}) = \mathcal{L}(q^{\mathrm{s}}, q^{\mathrm{f}}, \dot{q}^{\mathrm{s}}, \dot{q}^{\mathrm{f}})$. Using integration by parts shows that this principle is equivalent to the forced Euler-Lagrange equations [4], which take the following coordinate expression

$$\frac{\partial \mathcal{L}(q^{\mathrm{s}}, q^{\mathrm{f}}, \dot{q}^{\mathrm{s}}, \dot{q}^{\mathrm{f}})}{\partial q^{\mathrm{s}}} - \frac{d}{dt}\Big(\frac{\partial \mathcal{L}(q^{\mathrm{s}}, q^{\mathrm{f}}, \dot{q}^{\mathrm{s}}, \dot{q}^{\mathrm{f}})}{\partial \dot{q}^{\mathrm{s}}}\Big) + f^{\mathrm{s}}_{\mathrm{LC}}(q^{\mathrm{s}}, q^{\mathrm{f}}, \dot{q}^{\mathrm{s}}, \dot{q}^{\mathrm{f}}, u) = 0, \tag{3.3a}$$

$$\frac{\partial \mathcal{L}(q^{\mathrm{s}}, q^{\mathrm{f}}, \dot{q}^{\mathrm{s}}, \dot{q}^{\mathrm{f}})}{\partial q^{\mathrm{f}}} - \frac{d}{dt}\Big(\frac{\partial \mathcal{L}(q^{\mathrm{s}}, q^{\mathrm{f}}, \dot{q}^{\mathrm{s}}, \dot{q}^{\mathrm{f}})}{\partial \dot{q}^{\mathrm{f}}}\Big) + f^{\mathrm{f}}_{\mathrm{LC}}(q^{\mathrm{s}}, q^{\mathrm{f}}, \dot{q}^{\mathrm{s}}, \dot{q}^{\mathrm{f}}, u) = 0. \tag{3.3b}$$

Here the dependencies on time have not been denoted to simplify the notation. These equations implicitly define a family of forced Lagrangian vector fields $X_{\mathcal{L}}(u) : TQ \times [0, T] \to T(TQ)$ and associated forced Lagrangian flow $F_{\mathcal{L}}(u) : TQ \times [0, T] \to TQ$ with fixed $u \in \mathcal{C}([0, T], \mathcal{U})$ (see [19] for more details). By $F^t_{\mathcal{L}}(u) : TQ \to TQ$ we will denote the forced Lagrangian flow at fixed time t.

Remark 3.3.1. *In the cases where $f_{\mathrm{LC}}(q, \dot{q}, u) = u$, the control can be resolved in a similar manner*

$$f_{\mathrm{LC}}(q, \dot{q}, u) \cdot \delta q = u^{\mathrm{s}} \cdot \delta q^{\mathrm{s}} + u^{\mathrm{f}} \cdot \delta q^{\mathrm{f}} \tag{3.4}$$

leading to $f^{\mathrm{s}}_{\mathrm{LC}} = u^{\mathrm{s}}$, $f^{\mathrm{f}}_{\mathrm{LC}} = u^{\mathrm{f}}$.

3.3.2 Hamiltonian viewpoint

In the previous section, we described the motion of the system by describing the evolution of its configuration and velocity in state space, i.e. on the tangent bundle TQ. Using Hamiltonian mechanics, the evolution of the system can equivalently be described in the phase space using the configuration vectors $q^{\mathrm{s}}(t), q^{\mathrm{f}}(t)$ and conjugate momenta $p^{\mathrm{s}}(t), p^{\mathrm{f}}(t)$ which belong to the cotangent bundle T^*Q associated with the previously defined configuration manifold Q:

$$(q^{\mathrm{s}}(t), p^{\mathrm{s}}(t)) \in T^*Q^{\mathrm{s}}, \;\; (q^{\mathrm{f}}(t), p^{\mathrm{f}}(t)) \in T^*Q^{\mathrm{f}} \text{ and } \; T^*Q^{\mathrm{s}} \times T^*Q^{\mathrm{f}} = T^*Q.$$

To derive the equations of motion within the Hamiltonian formalism, we follow [109] and define the slow and fast Legendre transforms for unforced systems, which relate the Lagrangian and Hamiltonian formulations. These transformations are

defined as maps $\mathbb{F}L^{\mathrm{s}} : TQ^{\mathrm{s}} \to T^*Q^{\mathrm{s}}$ and $\mathbb{F}L^{\mathrm{f}} : TQ^{\mathrm{f}} \to T^*Q^{\mathrm{f}}$ with $\mathbb{F}L = (\mathbb{F}L^{\mathrm{s}}, \mathbb{F}L^{\mathrm{f}})$ from the Lagrangian state space TQ to the Hamiltonian phase space T^*Q and in coordinate form can be written as

$$\mathbb{F}^{\mathrm{s}}L : (q^{\mathrm{s}}, \dot{q}^{\mathrm{s}}) \mapsto \left(q^{\mathrm{s}}, \frac{\partial \mathcal{L}(q^{\mathrm{s}}, q^{\mathrm{f}}, \dot{q}^{\mathrm{s}}, \dot{q}^{\mathrm{f}})}{\partial \dot{q}^{\mathrm{s}}}\right) = (q^{\mathrm{s}}, p^{\mathrm{s}}) \tag{3.5a}$$

$$\mathbb{F}^{\mathrm{f}}L : (q^{\mathrm{f}}, \dot{q}^{\mathrm{f}}) \mapsto \left(q^{\mathrm{f}}, \frac{\partial \mathcal{L}(q^{\mathrm{s}}, q^{\mathrm{f}}, \dot{q}^{\mathrm{s}}, \dot{q}^{\mathrm{f}})}{\partial \dot{q}^{\mathrm{f}}}\right) = (q^{\mathrm{f}}, p^{\mathrm{f}}) \tag{3.5b}$$

where p^{s} and p^{f} are *the slow and fast conjugate momenta* and the time dependence has been omitted to simplify the notation. To expand this theory to the case of multirate systems under external forcing, we define the *Hamiltonian control* forces $f^{\mathrm{s}}_{\mathrm{HC}}(q,p,u) : T^*Q \times \mathcal{U} \to T^*Q^{\mathrm{s}}$, $f^{\mathrm{f}}_{\mathrm{HC}}(q,p,u) : T^*Q \times \mathcal{U} \to T^*Q^{\mathrm{f}}$ and consider them as parameter-dependent *Hamiltonian forces* $f^{\mathrm{s}}_H(u), f^{\mathrm{f}}_H(u)$ similarly to the Lagrangian counterpart in (2.4). We follow the example of [20] and relate the *Hamiltonian control* forces $(f^{\mathrm{s}}_{\mathrm{HC}}, f^{\mathrm{f}}_{\mathrm{HC}})$ and *Lagrangian control* forces $(f^{\mathrm{s}}_{\mathrm{LC}}, f^{\mathrm{f}}_{\mathrm{LC}})$ by

$$f^{\mathrm{s}}_L(u) = f^{\mathrm{s}}_H(u) \circ \mathbb{F}L, \quad f^{\mathrm{f}}_L(u) = f^{\mathrm{f}}_H(u) \circ \mathbb{F}L. \tag{3.6a}$$

Based on these definitions, the Hamiltonian H is defined as

$$\mathcal{H}(q^{\mathrm{s}}, p^{\mathrm{s}}, q^{\mathrm{f}}, p^{\mathrm{f}}) = \mathbb{F}^{\mathrm{s}}L(q^{\mathrm{s}}, \dot{q}^{\mathrm{s}}) \cdot \dot{q}^{\mathrm{s}} + \mathbb{F}^{\mathrm{f}}L(q^{\mathrm{f}}, \dot{q}^{\mathrm{f}}) \cdot \dot{q}^{\mathrm{f}} - \mathcal{L}(q^{\mathrm{s}}, \dot{q}^{\mathrm{s}}, q^{\mathrm{f}}, \dot{q}^{\mathrm{f}}). \tag{3.7}$$

and the equations describing the motion within the phase space in the presence of external forcing become

$$\dot{q}^{\mathrm{s}} = \frac{\partial \mathcal{H}}{\partial p^{\mathrm{s}}}, \qquad \dot{p}^{\mathrm{s}} = -\frac{\partial \mathcal{H}}{\partial q^{\mathrm{s}}} + f^{\mathrm{s}}_{\mathrm{HC}}, \tag{3.8a}$$

$$\dot{q}^{\mathrm{f}} = \frac{\partial \mathcal{H}}{\partial p^{\mathrm{f}}}, \qquad \dot{p}^{\mathrm{f}} = -\frac{\partial \mathcal{H}}{\partial q^{\mathrm{f}}} + f^{\mathrm{f}}_{\mathrm{HC}}. \tag{3.8b}$$

Demonstration problem 1.

As an example problem that will be used for demonstration purposes in later sections, we consider a Lagrangian system with a potential energy $V(q)$, kinetic energy

$$T(\dot{q}^{\mathrm{s}}, \dot{q}^{\mathrm{f}}) = \frac{1}{2}(\dot{q}^{\mathrm{s}})^{\intercal} M^{\mathrm{s}} \dot{q}^{\mathrm{s}} + \frac{1}{2}(\dot{q}^{\mathrm{f}})^{\intercal} M^{\mathrm{f}} \dot{q}^{\mathrm{f}}$$

and external forcing $f^{\mathrm{s}}_{\mathrm{HC}}, f^{\mathrm{f}}_{\mathrm{HC}}$. Here $M^{\mathrm{s}} \in \mathbb{R}^{n_{\mathrm{s}} \times n_{\mathrm{s}}}, M^{\mathrm{f}} \in \mathbb{R}^{n_{\mathrm{f}} \times n_{\mathrm{f}}}$ are symmetric positive definite matrices, and the time dependence has been dropped to simplify

the notation. The multirate behaviour of the system is characterised by an additive split of the potential energy $V(q) = U(q^{\mathrm{s}}, q^{\mathrm{f}}) + P(q^{\mathrm{f}})$ *in terms of a slow potential* U *and a fast potential* P*. Here* $P(q^{\mathrm{f}})$ *can be, for example, of the form* $P(q^{\mathrm{f}}) = 1/\varepsilon\, \tilde{P}(q^{\mathrm{f}})$, $\varepsilon << 1$*. Such splits can be the result of, for example, stiffness, nonlinearity, dynamical behaviour, and evaluation cost [99].The Lagrangian of the system takes the form*

$$\begin{aligned}\mathcal{L}(q^{\mathrm{s}}, q^{\mathrm{f}}, \dot{q}^{\mathrm{s}}, \dot{q}^{\mathrm{f}}) &= T(\dot{q}^{\mathrm{s}}, \dot{q}^{\mathrm{f}}) - U(q^{\mathrm{s}}, q^{\mathrm{f}}) - P(q^{\mathrm{f}}) \\ &= \frac{1}{2}(\dot{q}^{\mathrm{s}})^{\intercal} M^{\mathrm{s}} \dot{q}^{\mathrm{s}} + \frac{1}{2}(\dot{q}^{\mathrm{f}})^{\intercal} M^{\mathrm{f}} \dot{q}^{\mathrm{f}} - U(q^{\mathrm{s}}, q^{\mathrm{f}}) - P(q^{\mathrm{f}}) \end{aligned} \tag{3.9}$$

leading to the definition of the multirate discrete Legendre transforms as

$$\mathbb{F}^{\mathrm{s}}L : (q^{\mathrm{s}}, \dot{q}^{\mathrm{s}}) \mapsto (q^{\mathrm{s}}, p^{\mathrm{s}}) = \left(q^{\mathrm{s}}, \left(\frac{\partial \mathcal{L}(q^{\mathrm{s}}, q^{\mathrm{f}}, \dot{q}^{\mathrm{s}}, \dot{q}^{\mathrm{f}})}{\partial \dot{q}^{\mathrm{s}}}\right)^{\intercal}\right) = (q^{\mathrm{s}}, M^{\mathrm{s}}\dot{q}^{\mathrm{s}}),$$

$$\mathbb{F}^{\mathrm{f}}L : (q^{\mathrm{f}}, \dot{q}^{\mathrm{f}}) \mapsto (q^{\mathrm{f}}, p^{\mathrm{f}}) = \left(q^{\mathrm{f}}, \left(\frac{\partial \mathcal{L}(q^{\mathrm{s}}, q^{\mathrm{f}}, \dot{q}^{\mathrm{s}}, \dot{q}^{\mathrm{f}})}{\partial \dot{q}^{\mathrm{f}}}\right)^{\intercal}\right) = (q^{\mathrm{f}}, M^{\mathrm{f}}\dot{q}^{\mathrm{f}}).$$

Using the definitions of the conjugate momenta (3.5*a*)–(3.5*b*) *and the Hamiltonian of the system* (3.7) *one obtains*

$$p^{\mathrm{s}} = M^{\mathrm{s}}\dot{q}^{\mathrm{s}}, \quad p^{\mathrm{f}} = M^{\mathrm{f}}\dot{q}^{\mathrm{f}},$$

$$\mathcal{H} = (p^{\mathrm{s}})^{\intercal}\dot{q}^{\mathrm{s}} + (p^{\mathrm{f}})^{\intercal}\dot{q}^{\mathrm{f}} - \frac{1}{2}(\dot{q}^{\mathrm{s}})^{\intercal} M^{\mathrm{s}} \dot{q}^{\mathrm{s}} - \frac{1}{2}(\dot{q}^{\mathrm{f}})^{\intercal} M^{\mathrm{f}} \dot{q}^{\mathrm{f}} + U(q^{\mathrm{s}}, q^{\mathrm{f}}) + P(q^{\mathrm{f}}).$$

Lastly, using the equations of motion in the Hamiltonian formalism (3.8*a*), (3.8*b*) *we can derive the following equations of motion*

$$\dot{q}^{\mathrm{s}} = (M^{\mathrm{s}})^{-1}p^{\mathrm{s}}, \quad \dot{p}^{\mathrm{s}} = -\frac{\partial U(q^{\mathrm{s}}, q^{\mathrm{f}})}{\partial q^{\mathrm{s}}} + f^{\mathrm{s}}_{\mathrm{HC}}, \tag{3.10a}$$

$$\dot{q}^{\mathrm{f}} = (M^{\mathrm{f}})^{-1}p^{\mathrm{f}}, \quad \dot{p}^{\mathrm{f}} = -\frac{\partial U(q^{\mathrm{s}}, q^{\mathrm{f}})}{\partial q^{\mathrm{f}}} - \frac{\partial P(q^{\mathrm{f}})}{\partial q^{\mathrm{f}}} + f^{\mathrm{f}}_{\mathrm{HC}}. \tag{3.10b}$$

For quadratic potential energy expressions

$$U(q^{\mathrm{s}}(t), q^{\mathrm{f}}(t)) = \frac{1}{2}(q^{\mathrm{s}}(t))^{\intercal} K^{\mathrm{s}} q^{\mathrm{s}}(t), \quad P(q^{\mathrm{f}}(t)) = \frac{1}{2}(q^{\mathrm{f}})^{\intercal} K^{\mathrm{f}} q^{\mathrm{f}} \tag{3.11}$$

these equations further simplify to

$$\dot{q}^{\mathrm{s}} = (M^{\mathrm{s}})^{-1}p^{\mathrm{s}}, \quad \dot{p}^{\mathrm{s}} = -K^{\mathrm{s}}q^{\mathrm{s}} + f^{\mathrm{s}}_{\mathrm{HC}}, \tag{3.12a}$$

$$\dot{q}^{\mathrm{f}} = (M^{\mathrm{f}})^{-1}p^{\mathrm{f}}, \quad \dot{p}^{\mathrm{f}} = -K^{\mathrm{f}}q^{\mathrm{f}} + f^{\mathrm{f}}_{\mathrm{HC}}. \tag{3.12b}$$

3.3.3 Properties of the Lagrangian flow for forced systems

Several conservation laws are associated with Lagrangian and Hamiltonian systems in the absence of external forcing, such as conservation of energy, symplecticity, certain momentum maps, and adiabatic invariance (see [1, 20, 30] among many others). In instances of forced singlerate systems with symmetries of the Lagrangian (i.e. invariance with respect to the action of a given Lie Group), the conservation of momentum maps can similarly be proven by the *Forced Noether's theorem* [1, Theorem 3.1.1]. For forced multirate systems, we now introduce the *Multirate Forced Noether's theorem*. The proof of this theorem follows the method used in the proof for the singlerate case as outlined by [1, Theorem 3.1.1].

Given a Lie group G with Lie algebra g acting on Q by the left and right action $\phi : G \times Q \to Q$ we let $\xi_Q : Q \to TQ$ and $\xi_{TQ} : TQ \to T(TQ)$ denote the infinitesimal generators for $\xi \in g$ and $\phi^{TQ} : G \times TQ \times TQ$ as the tangent lifted action

$$\phi^{TQ}(g,(q,\dot{q})) = \Big(\phi^i(g,q), \frac{\partial \phi^i}{\partial q^j}(g,q)\dot{q}^j\Big),$$
$$\xi_Q(q) = \frac{d}{dg}(\phi_g(q)) \cdot \xi, \quad \xi_{TQ}(q) = \frac{d}{dg}(\phi_g^{TQ}(v_q)) \cdot \xi.$$

We define the Lagrangian momentum map $\mathbf{J}_\mathcal{L} : TQ \to g^*$ as

$$\mathbf{J}_\mathcal{L}(v_q) \cdot \xi = \Theta_\mathcal{L} \cdot \xi_{TQ}(v_q)$$

where Θ_L is the Lagrangian one-form given in coordinates by $\Theta_\mathcal{L} = \frac{\partial \mathcal{L}}{\partial \dot{q}^i} \mathrm{d}q^i$. For more details on these definitions, one can see [18, 20]. With this definition, we now state the Forced Noether's Theorem for multirate systems:

Theorem 3.3.1. ***(Forced Multirate Noether's Theorem)*** *Consider a Lagrangian system $\mathcal{L}(q^\mathrm{s}, q^\mathrm{f}, \dot{q}^\mathrm{s}, \dot{q}^\mathrm{f}) : TQ^\mathrm{s} \times TQ^\mathrm{f} \to \mathbb{R}$ with control forcing $f^\mathrm{f}_\mathrm{LC}, f^\mathrm{s}_\mathrm{LC} : TQ^\mathrm{s} \times TQ^\mathrm{f} \times \mathcal{U} \to T^*Q^\mathrm{s} \times T^*Q^\mathrm{f}$ and a symmetry action $\phi : G \times Q \to Q$ such that $\mathcal{L} \circ \phi_g^{TQ} = \mathcal{L}$ and $\langle \begin{bmatrix} f^\mathrm{s}_\mathrm{LC} \\ f^\mathrm{f}_\mathrm{LC} \end{bmatrix}, \xi_Q(q) \rangle = 0$ for all $(q,\dot{q}) \in TQ$, $u \in U$ and all $\xi \in g$ where $(q,\dot{q}) = \Big(\begin{bmatrix} q^\mathrm{s} \\ q^\mathrm{f} \end{bmatrix}, \begin{bmatrix} \dot{q}^\mathrm{s} \\ \dot{q}^\mathrm{f} \end{bmatrix} \Big)$, $Q = Q^\mathrm{s} \times Q^\mathrm{f}, TQ = TQ^\mathrm{s} \times TQ^\mathrm{f}$. Then the Lagrangian momentum map $\mathbf{J}_\mathcal{L} : TQ \to g^*$ will be preserved by the flow, such that $\mathbf{J}_\mathcal{L} \circ F^t_\mathcal{L}(u) = \mathbf{J}_\mathcal{L}$ for all t.*

Proof. The proof follows a similar approach to the proof in the singlerate case by [1]. The condition $\mathcal{L} \circ \phi_g^{TQ} = \mathcal{L}$ for all $g \in G$ means that the Lagrangian is invariant under the tangent lifted action ϕ^{TQ}. Such property is known as a *symmetry* of the Lagrangian and can be differentiated to obtain $\mathrm{d}\mathcal{L} \cdot \xi_g^{TQ} = 0$ for all $g \in G$. Writing Equation (3.2) for a variation $\delta q(t) = \begin{bmatrix} \delta q^{\mathrm{s}}(t) \\ \delta q^{\mathrm{f}}(t) \end{bmatrix} = \xi_Q(q(t))$ leads to

$$\int_0^T \mathrm{d}\mathcal{L} \cdot \xi_{TQ} dt + \int_0^T f_{\mathrm{LC}} \cdot \xi_Q dt = \int_0^T \begin{bmatrix} f_{\mathrm{LC}}^{\mathrm{s}} \\ f_{\mathrm{LC}}^{\mathrm{f}} \end{bmatrix} \cdot \xi_Q dt. \tag{3.13}$$

Using integration by parts the left-hand side is equivalent to

$$\int_0^T \begin{bmatrix} \frac{\partial \mathcal{L}(q^{\mathrm{s}},q^{\mathrm{f}},\dot{q}^{\mathrm{s}},\dot{q}^{\mathrm{f}})}{\partial q^{\mathrm{s}}} - \frac{d}{dt}\left(\frac{\partial \mathcal{L}(q^{\mathrm{s}},q^{\mathrm{f}},\dot{q}^{\mathrm{s}},\dot{q}^{\mathrm{f}})}{\partial \dot{q}^{\mathrm{s}}}\right) + f_{\mathrm{LC}}^{\mathrm{s}}(q^{\mathrm{s}}, q^{\mathrm{f}}, \dot{q}^{\mathrm{s}}, \dot{q}^{\mathrm{f}}, u) \\ \frac{\partial \mathcal{L}(q^{\mathrm{s}},q^{\mathrm{f}},\dot{q}^{\mathrm{s}},\dot{q}^{\mathrm{f}})}{\partial q^{\mathrm{f}}} - \frac{d}{dt}\left(\frac{\partial \mathcal{L}(q^{\mathrm{s}},q^{\mathrm{f}},\dot{q}^{\mathrm{s}},\dot{q}^{\mathrm{f}})}{\partial \dot{q}^{\mathrm{f}}}\right) + f_{\mathrm{LC}}^{\mathrm{f}}(q^{\mathrm{s}}, q^{\mathrm{f}}, \dot{q}^{\mathrm{s}}, \dot{q}^{\mathrm{f}}, u) \end{bmatrix} \cdot \xi_{TQ} dt + \Theta_{\mathcal{L}} \cdot \xi_{TQ}|_0^T =$$
$$(\mathbf{J}_{\mathcal{L}} \circ F_{\mathcal{L}}^t(u))(q(0), \dot{q}(0)) \cdot \xi - \mathbf{J}_{\mathcal{L}}(q(0), \dot{q}(0)) \cdot \xi.$$

Substituting this expression in Equation (3.13), we have

$$(\mathbf{J}_{\mathcal{L}} \circ F_{\mathcal{L}}^t(u))(q(0), \dot{q}(0)) \cdot \xi - \mathbf{J}_{\mathcal{L}}(q(0), \dot{q}(0)) \cdot \xi = \int_0^T \begin{bmatrix} f_{\mathrm{LC}}^{\mathrm{s}} \\ f_{\mathrm{LC}}^{\mathrm{f}} \end{bmatrix} \cdot \xi_Q dt.$$

From this equation, it is clear that in cases where the forcing is orthogonal to the group acting, the momentum map is not altered, thus proving Theorem 3.3.1. □

In a less abstract view, the forced Noether's theorem essentially states a conservation law for momentum maps stemming from Lagrangian symmetries, even in the presence of forcing. Ideally, these properties will be preserved in all system simulations. In Section 3.4.3, we will prove this is true for the proposed discretisation method by formulating a discrete version of the Forced Multirate Discrete Noether theorem for the presented discrete multirate variational system models.

3.4 Multirate discrete variational mechanics for forced systems

3.4.1 Lagrangian viewpoint

To derive a discrete-time formulation, we introduce two time grids: a macro time grid with the macro time step ΔT and a micro time grid, which is obtained by subdividing each macro step into $\mathbb{p}$ equally spaced micro time steps of size Δt as depicted in Figure 3.1. Given a final time T we define the macro time grid $\{t_k = k\Delta T \,|\, k = 0, ..., N\}$ on which we approximate the slow variables as follows:

$$q_d^{\mathrm{s}} = \{q_k^{\mathrm{s}}\}_{k=0}^{N} \quad \text{with } q_k^{\mathrm{s}} \approx q^{\mathrm{s}}(t_k) \tag{3.14}$$

where $N = T/\Delta T$ is the number of macro time steps. Similarly, the micro time grid is defined as $\{t_k^m = k\Delta T + m\Delta t \,|\, k = 0, \ldots, N-1, m = 0, \ldots, \mathbb{p}\}$ and used for the approximation of the fast variables

$$q_d^{\mathrm{f}} = \{\{q_k^{\mathrm{f},m}\}_{m=0}^{\mathbb{p}}\}_{k=0}^{N-1} \quad \text{with } q_k^{\mathrm{f},m} \approx q^{\mathrm{f}}(t_k^m) \tag{3.15}$$

with $\Delta T = \mathbb{p}\Delta t$. Additionally, we define $q_k^{\mathrm{f}} = \{q_k^{\mathrm{f},m}\}_{m=0}^{\mathbb{p}}$. For the interpolation of the slow variables on the micro time grid, we set

$$q_k^{\mathrm{s},m} = a^m \, q_k^{\mathrm{s}} + b^m \, q_{k+1}^{\mathrm{s}} \quad . \tag{3.16}$$

For the example of linear interpolation $a^m = \frac{\mathbb{p}-m}{\mathbb{p}}$, $b^m = \frac{m}{\mathbb{p}}$. It is important to note that two different micro time nodes are defined on each macro time node as shown in Figure 3.1. Thus $t_{k-1}^{\mathbb{p}} = t_k^0$ and thus $q_{k-1}^{\mathrm{f},\mathbb{p}} = q_k^{\mathrm{f},0}$ for $k = 1, ..., N$ and analogously to the continuous case $q_k = \begin{bmatrix} q_k^{\mathrm{s}} \\ q_k^{\mathrm{f},0} \end{bmatrix}$, $q_{k+1} = \begin{bmatrix} q_{k+1}^{\mathrm{s}} \\ q_k^{\mathrm{f},\mathbb{p}} \end{bmatrix}$.

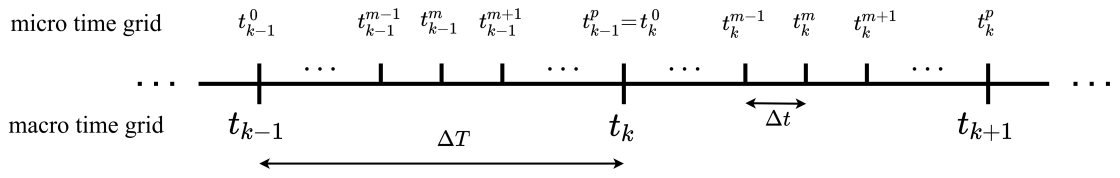


Figure 3.1: Micro and macro time grid schematic

Based on the described multirate discretisation we define the discrete Lagrangian $L_{\mathrm{d}}^{k,m} : Q^{\mathrm{s}} \times Q^{\mathrm{s}} \times Q^{\mathrm{f}} \times Q^{\mathrm{f}} \to \mathbb{R}$ on a micro time grid as

$$L_{\mathrm{d}}^{k,m}(q_k^{\mathrm{s},m}, q_k^{\mathrm{s},m+1}, q_k^{\mathrm{f},m}, q_k^{\mathrm{f},m+1}) \approx \int_{t_k^m}^{t_k^{m+1}} \mathcal{L}(q^{\mathrm{s}}, \dot{q}^{\mathrm{s}}, q^{\mathrm{f}}, \dot{q}^{\mathrm{f}}) dt$$

and the discrete Lagrangian $L_{\mathrm{d}}^{k} : Q^{\mathrm{s}} \times Q^{\mathrm{s}} \times (Q^{\mathrm{f}})^{\mathbb{p}+1} \to \mathbb{R}$ on the macro time grid as

$$L_{\mathrm{d}}^{k}(q_k^{\mathrm{s}}, q_{k+1}^{\mathrm{s}}, q_k^{\mathrm{f}}) = \sum_{m=0}^{\mathbb{p}-1} L_{\mathrm{d}}^{k,m}(q_k^{\mathrm{s},m}, q_k^{\mathrm{s},m+1}, q_k^{\mathrm{f},m}, q_k^{\mathrm{f},m+1}) \approx \int_{t_k}^{t_{k+1}} \mathcal{L}(q^{\mathrm{s}}, \dot{q}^{\mathrm{s}}, q^{\mathrm{f}}, \dot{q}^{\mathrm{f}}) dt.$$

The action integral can then be approximated as

$$S_{\mathrm{d}}(q_{\mathrm{d}}^{\mathrm{s}}, q_{\mathrm{d}}^{\mathrm{f}}) = \sum_{k=0}^{N-1} L_{\mathrm{d}}^{k}(q_k^{\mathrm{s}}, q_{k+1}^{\mathrm{s}}, q_k^{\mathrm{f}}) = \sum_{k=0}^{N-1} \sum_{m=0}^{\mathbb{p}-1} L_{\mathrm{d}}^{k,m}(q_k^{\mathrm{s},m}, q_k^{\mathrm{s},m+1}, q_k^{\mathrm{f},m}, q_k^{\mathrm{f},m+1}).$$

In the case of an externally forced or controlled system, we introduce discrete forces based on approximations of their slow $f_{\mathrm{LC}}^{\mathrm{s}}$ and fast components $f_{\mathrm{LC}}^{\mathrm{f}}$ introduced in Section 3.3.1. As mentioned in Section 3.3.1 for the continuous scenario, these forces can exhibit dependence on the configuration, velocity, and external control signals. Thus, we introduce the discrete control path u_{d} and define it by piecewise-constant values defined at the midpoints of the micro time grids as follows:

$$u_{\mathrm{d}} = \{\{u_k^{m+1/2}\}_{m=0}^{\mathbb{p}-1}\}_{k=0}^{N-1} \quad \text{where } \; u_k^{m+1/2} \approx u(t_k^{m+1/2}), \;\; u_k = \{u_k^{m+1/2}\}_{m=0}^{\mathbb{p}-1}. \tag{3.17}$$

Based on this definition, we can define the *discrete left and right slow and fast Lagrangian control forces* similarly to the continuous section as maps of the form

$$\begin{aligned}
f_{\mathrm{LC,d}}^{s-} &: \left(q_k^{\mathrm{s},m}, q_k^{\mathrm{s},m+1}, q_k^{\mathrm{f},m}, q_k^{\mathrm{f},m+1}, u_k^{m+\frac{1}{2}}\right) \mapsto \left(q_k^{\mathrm{s},m}, f_{\mathrm{LC,d}}^{s-}\left(q_k^{\mathrm{s},m}, q_k^{\mathrm{s},m+1}, q_k^{\mathrm{f},m}, q_k^{\mathrm{f},m+1}, u_k^{m+\frac{1}{2}}\right)\right) \\
f_{\mathrm{LC,d}}^{s+} &: \left(q_k^{\mathrm{s},m}, q_k^{\mathrm{s},m+1}, q_k^{\mathrm{f},m}, q_k^{\mathrm{f},m+1}, u_k^{m+\frac{1}{2}}\right) \mapsto \left(q_k^{\mathrm{s},m+1}, f_{\mathrm{LC,d}}^{s+}\left(q_k^{\mathrm{s},m}, q_k^{\mathrm{s},m+1}, q_k^{\mathrm{f},m}, q_k^{\mathrm{f},m+1}, u_k^{m+\frac{1}{2}}\right)\right) \\
f_{\mathrm{LC,d}}^{f-} &: \left(q_k^{\mathrm{s},m}, q_k^{\mathrm{s},m+1}, q_k^{\mathrm{f},m}, q_k^{\mathrm{f},m+1}, u_k^{m+\frac{1}{2}}\right) \mapsto \left(q_k^{\mathrm{f},m}, f_{\mathrm{LC,d}}^{f-}\left(q_k^{\mathrm{s},m}, q_k^{\mathrm{s},m+1}, q_k^{\mathrm{f},m}, q_k^{\mathrm{f},m+1}, u_k^{m+\frac{1}{2}}\right)\right) \\
f_{\mathrm{LC,d}}^{f+} &: \left(q_k^{\mathrm{s},m}, q_k^{\mathrm{s},m+1}, q_k^{\mathrm{f},m}, q_k^{\mathrm{f},m+1}, u_k^{m+\frac{1}{2}}\right) \mapsto \left(q_k^{\mathrm{f},m+1}, f_{\mathrm{LC,d}}^{f+}\left(q_k^{\mathrm{s},m}, q_k^{\mathrm{s},m+1}, q_k^{\mathrm{f},m}, q_k^{\mathrm{f},m+1}, u_k^{m+\frac{1}{2}}\right)\right)
\end{aligned} \tag{3.18}$$

where the dependencies on time have been dropped to simplify the notation. For convenience, we will use the following simplified notation:

$$\begin{aligned}
f_k^{\mathrm{s,m},\pm} &:= f_{\mathrm{LC,d}}^{s\pm}\left(q_k^{\mathrm{s},m}, q_k^{\mathrm{s},m+1}, q_k^{\mathrm{f},m}, q_k^{\mathrm{f},m+1}, u_k^{m+1/2}\right), \\
f_k^{\mathrm{f,m},\pm} &:= f_{\mathrm{LC,d}}^{f\pm}\left(q_k^{\mathrm{s},m}, q_k^{\mathrm{s},m+1}, q_k^{\mathrm{f},m}, q_k^{\mathrm{f},m+1}, u_k^{m+1/2}\right).
\end{aligned} \tag{3.19}$$

Together with the approximated discrete curves $\{\{q_k^{\mathrm{s},m}\}_{m=0}^{\mathbb{p}}\}_{k=0}^{N-1}$, $\{\{q_k^{\mathrm{f},m}\}_{m=0}^{\mathbb{p}}\}_{k=0}^{N-1}$ with $q_k^{s/f,\mathbb{p}} = q_{k+1}^{s/f,0}, k = 0,\dots,N-1$ and $\{\{u_k^{m+1/2}\}_{m=0}^{\mathbb{p}-1}\}_{k=0}^{N-1}$ these forces can be combined for an approximation of the virtual work in equations (2.5) and (2.6) on the discrete-time grids by the discrete virtual work as follows:

$$W_{\mathrm{d}}(q_{\mathrm{d}}^{\mathrm{s}}, q_{\mathrm{d}}^{\mathrm{f}}, u_{\mathrm{d}}) = \sum_{k=0}^{N-1} (W_{\mathrm{d},k}^{\mathrm{s}}(q_k^{\mathrm{s}}, q_{k+1}^{\mathrm{s}}, q_k^{\mathrm{f}}, u_k) + W_{\mathrm{d},k}^{\mathrm{f}}(q_k^{\mathrm{s}}, q_{k+1}^{\mathrm{s}}, q_k^{\mathrm{f}}, u_k)) \approx W(q,u).$$

Here, the virtual work associated with the fast generalised forces is

$$\begin{aligned} W_{\mathrm{d},k}^{\mathrm{f}}(q_k^{\mathrm{s}}, q_{k+1}^{\mathrm{s}}, q_k^{\mathrm{f}}, u_k) &= \sum_{m=0}^{\mathbb{p}-1} (f_k^{\mathrm{f},m,-} \cdot \delta q_k^{\mathrm{f},m} + f_k^{\mathrm{f},m,+} \cdot \delta q_k^{\mathrm{s},m+1}) \\ &\approx \int_{t_k}^{t_{k+1}} f_{\mathrm{LC}}^{\mathrm{f}}(q^{\mathrm{s}}(t), \dot{q}^{\mathrm{s}}(t), q^{\mathrm{f}}(t), \dot{q}^{\mathrm{f}}(t), u(t)) \cdot \delta q^{\mathrm{f}}(t) dt \end{aligned}$$

and the virtual work associated with the slow generalised forces is

$$\begin{aligned} W_{\mathrm{d},k}^{\mathrm{s}}(q_k^{\mathrm{s}}, q_{k+1}^{\mathrm{s}}, q_k^{\mathrm{f}}, u_k) &= \sum_{m=0}^{\mathbb{p}-1} (f_k^{\mathrm{s,m},-} \cdot \delta q_k^{\mathrm{s},m} + f_k^{\mathrm{s,m},+} \cdot \delta q_k^{\mathrm{s},m+1}) \\ &\approx \int_{t_k}^{t_{k+1}} f_{\mathrm{LC}}^{\mathrm{s}}(q^{\mathrm{s}}(t), \dot{q}^{\mathrm{s}}(t), q^{\mathrm{f}}(t), \dot{q}^{\mathrm{f}}(t), u(t)) \cdot \delta q^{\mathrm{s}}(t) dt. \end{aligned}$$

Based on equation (3.16) the virtual work associated with the slow generalised forces can be rewritten as

$$W_{\mathrm{d},k}^{\mathrm{s}}(q_k^{\mathrm{s}}, q_{k+1}^{\mathrm{s}}, q_k^{\mathrm{f}}, u_k) = F_k^{\mathrm{s}-} \cdot \delta q_k^{\mathrm{s}} + F_k^{\mathrm{s}+} \cdot \delta q_{k+1}^{\mathrm{s}}$$

where

$$\begin{aligned} F_k^{\mathrm{s},+} &:= F_{\mathrm{LC,d}}^{\mathrm{s},+}\Big(q_k^{\mathrm{s}}, q_{k+1}^{\mathrm{s}}, q_k^{\mathrm{f}}, u_k\Big) = \textstyle\sum_{m=0}^{\mathbb{p}-1}(b^m f_k^{\mathrm{s,m}-} + b^{m+1} f_k^{\mathrm{s,m}+}), \\ F_k^{\mathrm{s},-} &:= F_{\mathrm{LC,d}}^{\mathrm{s},-}\Big(q_k^{\mathrm{s}}, q_{k+1}^{\mathrm{s}}, q_k^{\mathrm{f}}, u_k\Big) = \textstyle\sum_{m=0}^{\mathbb{p}-1}(a^m f_k^{\mathrm{s,m}-} + a^{m+1} f_k^{\mathrm{s,m}+}), \end{aligned} \tag{3.20}$$

with

$$\begin{aligned} F_{\mathrm{LC,d}}^{\mathrm{s},+} &: \Big(q_k^{\mathrm{s}}, q_{k+1}^{\mathrm{s}}, q_k^{\mathrm{f}}, u_k\Big) \mapsto \Big(q_{k+1}^{\mathrm{s}}, F_{\mathrm{LC,d}}^{s-}\Big(q_k^{\mathrm{s}}, q_{k+1}^{\mathrm{s}}, q_k^{\mathrm{f}}, u_k\Big)\Big), \\ F_{\mathrm{LC,d}}^{\mathrm{s},-} &: \Big(q_k^{\mathrm{s}}, q_{k+1}^{\mathrm{s}}, q_k^{\mathrm{f}}, u_k\Big) \mapsto \Big(q_k^{\mathrm{s}}, F_{\mathrm{LC,d}}^{s+}\Big(q_k^{\mathrm{s}}, q_{k+1}^{\mathrm{s}}, q_k^{\mathrm{f}}, u_k\Big)\Big). \end{aligned} \tag{3.21}$$

Thus, the maps $F_k^{\mathrm{s},\pm}$ and $f_k^{\mathrm{s},\pm}$ can be interpreted as a resolution of a discrete Lagrangian control force along the direction of the discrete multirate coordinates. Their left and right formulations can be interpreted as presented in Figure 3.2. The left discrete forces $F_k^{\mathrm{s},-}$ can be interpreted as the forces resulting from the

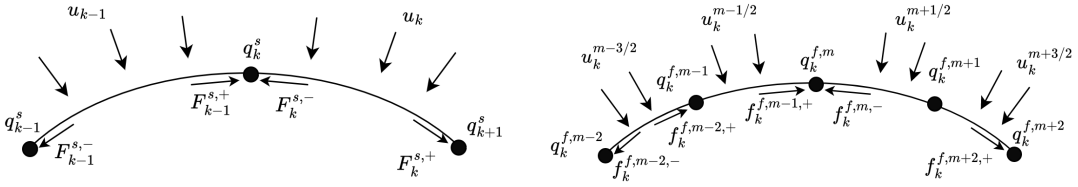


Figure 3.2: Left and right discrete forces visualisation

continuous control force acting at q_k^{s} during the time spans $[t_k, t_{k+1}]$ respectively. Analogously the right hand forces $F_k^{\mathrm{s},+}$ are resulting from the continuous control force acting at q_{k+1}^{s} during the time span $[t_k, t_{k+1}]$. Similarly $f_k^{\mathrm{f},-}$ and $f_k^{\mathrm{f},+}$ can be interpreted as the force resulting from the continuous control force acting at q_k^m and q_k^{m+1}, respectively, during the time period $[t_k^{\mathrm{f},m}, t_k^{\mathrm{f},m+1}]$.

Similarly to the singlerate case in [19], these discrete forces can again be interpreted as parameter-dependent discrete Lagrangian forces $F_{\mathrm{d}}^{\mathrm{s},\pm} : Q^{\mathrm{s}} \times Q^{\mathrm{s}} \times (Q^{\mathrm{f}})^{\mathbb{p}+1} \to T^*Q^{\mathrm{s}}$ and $f_{\mathrm{d}}^{\mathrm{f},\pm} : Q^{\mathrm{s}} \times Q^{\mathrm{s}} \times Q^{\mathrm{f}} \times Q^{\mathrm{f}} \to T^*Q^{\mathrm{f}}$:

$$F_{\mathrm{d}}^{\mathrm{s},\pm}(u_k)(q_k^{\mathrm{s}}, q_{k+1}^{\mathrm{s}}, q_k^{\mathrm{f}}) = F_{\mathrm{LC,d}}^{\mathrm{s},\pm}(q_k^{\mathrm{s}}, q_{k+1}^{\mathrm{s}}, q_k^{\mathrm{f},m}, q_k^{\mathrm{f},m+1}, u_k)$$

$$f_{\mathrm{d}}^{\mathrm{f},\pm}(u_k^{m+1/2})(q_k^{\mathrm{s},m}, q_k^{\mathrm{s},m+1}, q_k^{\mathrm{f},m}, q_k^{\mathrm{f},m+1}) = f_{\mathrm{LC,d}}^{\mathrm{f},\pm}(q_k^{\mathrm{s},m}, q_k^{\mathrm{s},m+1}, q_k^{\mathrm{f},m}, q_k^{\mathrm{f},m+1}, u_k^{m+1/2})$$

and combined to define the single one-form $f_{\mathrm{d}}(u_k)(q_k^{\mathrm{s}}, q_{k+1}^{\mathrm{s}}, q_k^{\mathrm{f}}) : Q^{\mathrm{s}} \times Q^{\mathrm{s}} \times (Q^{\mathrm{f}})^{\mathbb{p}+1} \to T^*(Q^{\mathrm{s}} \times Q^{\mathrm{s}} \times (Q^{\mathrm{f}})^{\mathbb{p}+1})$ with fixed $u_k \in \mathcal{U}^{\mathbb{p}}$ as

$$\begin{aligned} &f_{\mathrm{d}}(u_k)(q_k^{\mathrm{s}}, q_{k+1}^{\mathrm{s}}, q_k^{\mathrm{f}}) \cdot (\delta q_k^{\mathrm{s}}, \delta q_{k+1}^{\mathrm{s}}, q_k^{\mathrm{f}}) = \\ &\quad F_{\mathrm{d}}^{\mathrm{s},-}(u_k)(q_k^{\mathrm{s}}, q_{k+1}^{\mathrm{s}}, q_k^{\mathrm{f}}) \cdot \delta q_k^{\mathrm{s}} + F_{\mathrm{d}}^{\mathrm{s},+}(u_k)(q_k^{\mathrm{s}}, q_{k+1}^{\mathrm{s}}, q_k^{\mathrm{f}}) \cdot \delta q_{k+1}^{\mathrm{s}} \\ &\quad + \sum_{m=0}^{\mathbb{p}-1} \left(f_{\mathrm{d}}^{\mathrm{f},-}(u_k^{m+1/2})(q_k^{\mathrm{s}}, q_{k+1}^{\mathrm{s}}, q_k^{\mathrm{f}}) \cdot \delta q_k^{\mathrm{f},m} + f_{\mathrm{d}}^{\mathrm{f},+}(u_k^{m+1/2})(q_k^{\mathrm{s}}, q_{k+1}^{\mathrm{s}}, q_k^{\mathrm{f}}) \cdot \delta q_k^{\mathrm{f},m+1} \right) \end{aligned}$$

Remark 3.4.1. *In certain cases, the control parameters can contain components which are slowly evolving or can be altered only at the macro time grid. In such cases, we could define their separate discrete representations again using piecewise-constant values as follows:*

$$u_{\mathrm{d}}^{\mathrm{slow}} = \{u_{k+1/2}^{\mathrm{slow}}\}_{k=0}^{N-1} \qquad \text{where } u_{k+1/2}^{\mathrm{slow}} \approx u^{\mathrm{slow}}(t_{k+1/2}), \tag{3.22a}$$

$$u_{\mathrm{d}}^{\mathrm{fast}} = \{\{u_k^{\mathrm{fast},m+1/2}\}_{m=0}^{\mathbb{p}-1}\}_{k=0}^{N-1} \quad \text{where } u_k^{\mathrm{fast},m+1/2} \approx u^{\mathrm{fast}}(t_k^{m+1/2}), \tag{3.22b}$$

$$u_k^{\text{fast}} = \{u_k^{\text{fast},m+1/2}\}_{m=0}^{\mathbb{p}-1}. \tag{3.22c}$$

The multirate formulation, in general, reduces the number of nodes on which the slow variables are computed, allowing for significant computational savings as we will demonstrate in Chapters 4, 5, and 6. In the cases described by 3.22, these savings are increased due to the coarser computation of the slow control forces u^{slow}.

It must be noted that for a general problem, it is not the case that $u_{\text{d}}^{\text{slow}}$ *and* $u_{\text{d}}^{\text{fast}}$ *are discrete approximations of* $u^{\text{s}}(t)$ *and* $u^{\text{f}}(t)$*, respectively. As defined in Remark 3.3.1,* $u^{\text{s}}(t)$ *and* $u^{\text{f}}(t)$ *are the result of force resolution along the multirate coordinates, whereas* u^{slow} *and* u^{fast} *are user-defined depending on the available actuators. Of course, it can be the case that these coincide as, for example, the FPUT example introduced in Section 4.2.*

In the case of discrete forced systems the discrete Lagrange-d'Alembert principle [1] can be applied to obtain the discrete trajectory of the system as the discrete paths $\{q_k^{\text{s}}\}_{k=0}^N$ and $\{\{q_k^{\text{f}}\}_{k=0}^N\}_{m=0}^{\mathbb{p}}$. In the multirate case, this takes the form

$$0 = \delta S_{\text{d}}(q_{\text{d}}^{\text{s}}, q_{\text{d}}^{\text{f}}) \cdot (\delta q_{\text{d}}^{\text{s}}, \delta q_{\text{d}}^{\text{f}}) + W_{\text{d}}(q_{\text{d}}^{\text{s}}, q_{\text{d}}^{\text{f}}, u_{\text{d}}) = \delta \sum_{k=0}^{N-1} L_{\text{d}}^k(q_k^{\text{s}}, q_{k+1}^{\text{s}}, q_k^{\text{f}}) \tag{3.23a}$$

$$+ \sum_{k=0}^{N-1} \left(F_k^{\text{s}-} \cdot \delta q_k^{\text{s}} + F_k^{\text{s}+} \cdot \delta q_{k+1}^{\text{s}} + \sum_{m=0}^{\mathbb{p}-1} (f_k^{\text{f},m,-} \cdot \, \delta q_k^{\text{f},m} + f_k^{\text{f},m,+} \cdot \, \delta q_k^{\text{f},m+1}) \right) \tag{3.23b}$$

for all variations $(\delta q_{\text{d}}^{\text{s}}, \delta q_{\text{d}}^{\text{f}})$ vanishing at the endpoints. Based on this principle, the following theorem can be stated:

Theorem 3.4.1. *The multirate discrete forced Euler-Lagrange equations of motion for the discrete multirate Lagrangian* L_{d}^k *and* $F_k^{\text{s},\pm}, f_k^{\text{f,m},\pm}$ *take the form:*

$$D_{q_k^{\text{s}}}(L_{\text{d}}^k + L_{\text{d}}^{k-1}) + F_k^{\text{s}-} + F_{k-1}^{\text{s},+} = 0 \text{ for } k = 1, \ldots, N-1 \tag{3.24a}$$

$$D_{q_k^{\text{f},0}}(L_{\text{d}}^k + L_{\text{d}}^{k-1}) + f_k^{\text{f},0,-} + f_{k-1}^{\text{f},\mathbb{p}-1,+} = 0 \text{ for } k = 1, \ldots, N-1 \tag{3.24b}$$

$$D_{q_k^{\text{f},m}} L_{\text{d}}^k + f_k^{\text{f},m,-} + f_k^{\text{f,m}-1,+} = 0 \text{ for } k = 0, \ldots, N-1, \; m = 1, \ldots, \mathbb{p}-1 \tag{3.24c}$$

where D_i *is the partial derivative operator with respect to the* i*-th argument.*

Proof. These equations are in fact equivalent to the discrete Lagrange-d'Alembert principle (3.23). This is shown in Appendix A. □

3.4.2 Multirate discrete Legendre transform and Hamiltonian viewpoint

While the standard Legendre transform can be used for systems with forcing in the continuous case, in the discrete setting the transform needs to be redefined as noted by [20] and [1]. Building upon their derivation for the singlerate case and incorporating time-dependent controls similar to those in the singlerate scenario described in [18], in the multirate case we define the forced discrete Legendre transform as maps $\mathbb{F}^{F^{\mathrm{s},\pm}}L_{\mathrm{d}}(u_k) : Q^{\mathrm{s}} \times Q^{\mathrm{s}} \to T^*Q^{\mathrm{s}}$, $\mathbb{F}^{F^{\mathrm{f},\pm}}L_{\mathrm{d}}(u_k) : Q^{\mathrm{f}} \times Q^{\mathrm{f}} \to T^*Q^{\mathrm{f}}$ or in coordinate form:

$$\mathbb{F}^{F^{\mathrm{s},-}}L_{\mathrm{d}}(u_k)\colon (q_k^{\mathrm{s}}, q_{k+1}^{\mathrm{s}}) \mapsto (q_k^{\mathrm{s}}, -D_{q_k^{\mathrm{s}}}L_{\mathrm{d}}^k - F_k^{\mathrm{s},-}) =: (q_k^{\mathrm{s}}, p_{k,k+1}^{\mathrm{s},-}) \tag{3.25a}$$

$$\mathbb{F}^{F^{\mathrm{s},+}}L_{\mathrm{d}}(u_k)\colon (q_k^{\mathrm{s}}, q_{k+1}^{\mathrm{s}}) \mapsto (q_{k+1}^{\mathrm{s}}, D_{q_{k+1}^{\mathrm{s}}}L_{\mathrm{d}}^k + F_k^{\mathrm{s},+}) =: (q_{k+1}^{\mathrm{s}}, p_{k,k+1}^{\mathrm{s},+}) \tag{3.25b}$$

$$\mathbb{F}^{F^{\mathrm{f},-}}L_{\mathrm{d}}(u_k^{m+\frac{1}{2}})\colon (q_k^{\mathrm{f},m}, q_k^{\mathrm{f},m+1}) \mapsto (q_k^{\mathrm{f},m}, -D_{q_k^{\mathrm{f},m}}L_{\mathrm{d}}^{k,m} - f_k^{\mathrm{f},m,-}) =: (q_k^{\mathrm{f},m}, p_k^{\mathrm{f},-,\mathrm{m},\mathrm{m}+1}) \tag{3.25c}$$

$$\mathbb{F}^{F^{\mathrm{f},+}}L_{\mathrm{d}}(u_k^{m+\frac{1}{2}})\colon (q_k^{\mathrm{f},m}, q_k^{\mathrm{f},m+1}) \mapsto (q_k^{\mathrm{f},m+1}, D_{q_k^{\mathrm{f},m+1}}L_{\mathrm{d}}^{k,m} + f_k^{\mathrm{f},m,+}) =: (q_k^{\mathrm{f},m+1}, p_k^{\mathrm{f},+,\mathrm{m},\mathrm{m}+1}) \tag{3.25d}$$

for $k = 0, \ldots, N-1$, $m = 0, \ldots, \mathbb{p}-1$. Here we have defined the left and right slow discrete conjugate momenta $p_{k,k+1}^{\mathrm{s},-}, p_{k,k+1}^{\mathrm{s},+}$ to represent the slow momentum at the boundaries of each macro interval $[t_k, t_{k+1}]$, with the left one at t_k and the right one at t_{k+1}. Similarly, the left and right fast discrete conjugate momenta $p_k^{\mathrm{f},-,\mathrm{m},\mathrm{m}+1}, p_k^{\mathrm{f},+,\mathrm{m},\mathrm{m}+1}$have been respectively defined to represent the momentum at the two endpoints of each micro time interval $[t_k^m, t_k^{m+1}]$ (with the left one at t_k^m and the right one at t_k^{m+1}). Using our definition of the *discrete multirate forced Legendre transform*, Equations (3.24) can be alternatively expressed as

$$\mathbb{F}^{F^{\mathrm{s},-}}L_{\mathrm{d}}(u_k)(q_k^{\mathrm{s}}, q_{k+1}^{\mathrm{s}}) = \mathbb{F}^{F^{\mathrm{s},+}}L_{\mathrm{d}}(u_{k-1})(q_{k-1}^{\mathrm{s}}, q_k^{\mathrm{s}}), \tag{3.26a}$$

$$\mathbb{F}^{F^{\mathrm{f},-}}L_{\mathrm{d}}(u_k^{m+1/2})(q_k^{\mathrm{f},m}, q_k^{\mathrm{f},m+1}) = \mathbb{F}^{F^{\mathrm{f},+}}L_{\mathrm{d}}(u_k^{m-1/2})(q_k^{\mathrm{f},\mathrm{m}-1}, q_k^{\mathrm{f},m}). \tag{3.26b}$$

Using (3.25) and (3.26) in equations (3.24), it follows that the multirate discrete forced Euler-Lagrange equations (3.24) guarantee momentum matching:

$$p_k^{\mathrm{s}} = p_{k-1,k}^{\mathrm{s},+} = p_{k,k+1}^{\mathrm{s},-} \tag{3.27a}$$

$$p_k^{\mathrm{f},m} = p_k^{\mathrm{f},-,\mathrm{m}-1,\mathrm{m}} = p_k^{\mathrm{f},+,\mathrm{m},\mathrm{m}+1} \quad m = 0, ...\mathbb{p}-1 \quad \text{with} \quad p_{k-1}^{\mathrm{f},\mathbb{p}} = p_k^{\mathrm{f},0} \tag{3.27b}$$

for $k = 0, \ldots, N-1$. Thus, it is guaranteed that the slow conjugate momenta at time t_k are the same computed from the lower interval $[t_k, t_{k-1}]$ or the upper interval $[t_k, t_{k+1}]$. Similarly, they enforce that the fast momenta at time t_k^m are consistent when computed from $[t_k^{m-1}, t_k^m]$ or $[t_k^m, t_k^{m+1}]$ and that at each macro time node the two fast momenta stemming from $[t_{k-1}^{\mathbb{p}-1}, t_{k-1}^{\mathbb{p}}]$ and $[t_k^0, t_k^1]$ agree. Finally, it follows that along a solution curve, there is a unique slow/fast momentum at each considered discrete time node, which we denote by p_k^{s} for $k = 0, \ldots, N-1$ and $p_k^{\mathrm{f},m}$ for $k = 0, \ldots, N-1, m = 0, \ldots, \mathbb{p}-1$ with $p_{k-1}^{\mathrm{f},\mathbb{p}} = p_k^{\mathrm{f},0}$.

Remark 3.4.2. ***Initial conditions:*** *A closer look at the Lagrangian formulation of the discrete time-stepping equations* (3.24) *reveals that to begin the integration one must provide values for* q_0^{s}, q_1^{s} *and* $q_0^{\mathrm{f},0}, ..., q_0^{\mathrm{f},\mathbb{p}-1}$. *Given initial values for the velocity and configuration* $(q^{\mathrm{s}}(0), \dot{q}^{\mathrm{s}}(0), q^{\mathrm{f}}(0), \dot{q}^{\mathrm{f}}(0))$ *this can be achieved using Equation* (3.24c) *in combination with Equations* (3.25b), (3.25c), (3.27) *to find the unknowns* $q_1^{\mathrm{s}}, \{q_0^{\mathrm{f},m}\}_{m=1}^{\mathbb{p}}$ *in the following manner*

$$p_0^{\mathrm{s}} = -D_{q_0^{\mathrm{s}}} L_{\mathrm{d}}^0(q_0^{\mathrm{s}}, q_1^{\mathrm{s}}, q_0^{\mathrm{f}}) - F_0^{\mathrm{s},-} \tag{3.28a}$$

$$p_0^{\mathrm{f},0} = -D_{q_0^{\mathrm{f},0}} L_{\mathrm{d}}^{0,0}(q_0^{\mathrm{s},0}, q_0^{\mathrm{s},1}, q_0^{\mathrm{f},0}, q_0^{\mathrm{f},1}) - f_0^{\mathrm{f},0,-} \tag{3.28b}$$

$$D_{q_0^{\mathrm{f},m}} L_{\mathrm{d}}^0(q_0^{\mathrm{s}}, q_1^{\mathrm{s}}, q_0^{\mathrm{f}}) + f_0^{\mathrm{f},m,-} + f_0^{\mathrm{f},\mathrm{m}-1,+} = 0 \qquad \textit{for } m = 1, \ldots, \mathbb{p}-1 \tag{3.28c}$$

where $q_0^{\mathrm{s},1}$ *is obtained using* (3.16) *and*

$$(q_0^{\mathrm{s}}, p_0^{\mathrm{s}}) = (q^{\mathrm{s}}(0), p^{\mathrm{s}}(0)) = \mathbb{F}^{\mathrm{s}} L(q^{\mathrm{s}}(0), \dot{q}^{\mathrm{s}}(0)) \tag{3.29a}$$

$$(q_0^{\mathrm{f},0}, p_0^{\mathrm{f},0}) = (q^{\mathrm{f}}(0), p^{\mathrm{f}}(0)) = \mathbb{F}^{\mathrm{f}} L(q^{\mathrm{f}}(0), \dot{q}^{\mathrm{f}}(0)). \tag{3.29b}$$

Thus given $q^{\mathrm{s}}(0), \dot{q}^{\mathrm{s}}(0), q^{\mathrm{f}}(0), \dot{q}^{\mathrm{f}}(0)$ *and using the Equations* (3.28), *one can initiate the integration while satisfying the initial conditions at* $k = 0$ *and proceed using the multirate Equations* (3.24) *for* $k > 0$.

The approach of calculating the conjugate momentum could be extended for time steps $k > 0$. Thus, as mentioned at the end of Section 3.3.2, with the help of the Multirate Forced Discrete Legendre Transform, the evolution of the trajectory can

be described equivalently in the phase space using both the configuration and the conjugate momentum as follows:

$$p_k^{\mathrm{s}} = -D_{q_k^{\mathrm{s}}} L_{\mathrm{d}}^k - F_k^{\mathrm{s},-} \qquad \text{for } k = 0, \dots, N-1 \quad (3.30a)$$

$$p_{k+1}^{\mathrm{s}} = D_{q_k^{\mathrm{s}}} L_{\mathrm{d}}^k + F_k^{\mathrm{s},+} \qquad \text{for } k = 0, \dots, N-1 \quad (3.30b)$$

$$p_k^{\mathrm{f},m} = -D_{q_k^{\mathrm{f},m}} L_{\mathrm{d}}^{k,m} - f_k^{\mathrm{f},m,-} \qquad \text{for } k = 0, \dots, N-1,\ m = 0, \dots, \mathbb{p}-1 \quad (3.30c)$$

$$p_k^{\mathrm{f},m+1} = D_{q_k^{\mathrm{f},m+1}} L_{\mathrm{d}}^{k,m} + f_k^{\mathrm{f},m,+} \quad \text{for } k = 0, \dots, N-1,\ m = 0, \dots, \mathbb{p}-1. \quad (3.30d)$$

Given $q_k^{\mathrm{s}}, p_k^{\mathrm{s}}, q_k^{\mathrm{f},0}, p_k^{\mathrm{f},0}$ these equations can be solved to obtain the values over the next macro time step: $q_{k+1}^{\mathrm{s}}, p_{k+1}^{\mathrm{s}}$, $q_k^{\mathrm{f},1}, ..., q_k^{\mathrm{f},\mathbb{p}}$, $p_k^{\mathrm{f},1}, ..., p_k^{\mathrm{f},\mathbb{p}}$.

Remark 3.4.3. *From the two models* (3.30), (3.24)*, derived in the Lagrange and Hamiltonian formalism, respectively, it follows that in the discrete multirate setting, the trajectory of the slow variables can be described based only on discrete configurations by the evolution of* $\{(q_k^{\mathrm{s}}, q_{k+1}^{\mathrm{s}})\}_{k=0}^{N-1}$ *in* $Q^{\mathrm{s}} \times Q^{\mathrm{s}}$ *using the discrete Lagrangian formalism we defined in Section 3.4 or equivalently in phase space by the evolution of* $\{(q_k^{\mathrm{s}}, p_k^{\mathrm{s}})\}_{k=0}^{N}$ *in* T^*Q^{s} *based on the theory presented above. Similarly, the discrete trajectory of the fast variables can be defined based on configurations only using* $\{\{(q_k^{\mathrm{f},m}, q_k^{\mathrm{f},m+1})\}_{m=0}^{\mathbb{p}-1}\}_{k=0}^{N}$ *in* $Q^{\mathrm{f}} \times Q^{\mathrm{f}}$ *or, equivalently, in phase space using* $\{\{(q_k^{\mathrm{f},m}, p_k^{\mathrm{f},m})\}_{m=0}^{\mathbb{p}-1}\}_{k=0}^{N}$ *in* T^*Q^{f}*. Thus, it is clear that, to describe the system, the Lagrangian formulation requires approximately half the variable computations compared to the Hamiltonian formulation.*

Demonstration problem 2.

To provide an example, we reconsider Demonstration problem 1 with linear interpolation for the approximation of $q_k^{\mathrm{s},m}$ *and midpoint quadrature with forward difference velocity approximations for the slow and fast potential energy, the slow and fast kinetic energy and the virtual work. With these choices the equations of motion in the Hamiltonian formalism (Section 3.4.2),* (3.30a)–(3.30d) *can be simplified to:*

$$q_{k+1}^{\mathrm{s}} = q_k^{\mathrm{s}} + \Delta T (M^{\mathrm{s}})^{-1} \Big[\frac{p_k^{\mathrm{s}} + p_{k+1}^{\mathrm{s}}}{2} - \frac{\Delta t}{2} \sum_{m=0}^{\mathbb{p}-1} \frac{\mathbb{p}-(2m+1)}{\mathbb{p}} \frac{\partial U(\bar{q}_k^{\mathrm{s},m}, \bar{q}_k^{\mathrm{f},m})}{\partial \bar{q}_k^{\mathrm{s},m}} - F_k^{\mathrm{s},-} + F_k^{\mathrm{s},+} \Big] \quad (3.31a)$$

$$p^{\mathrm{s}}_{k+1} = p^{\mathrm{s}}_k - \Delta t \sum_{m=0}^{\mathbb{p}-1} \frac{\partial U(\bar{q}^{\mathrm{s},m}_k, \bar{q}^{\mathrm{f},m}_k)}{\partial \bar{q}^{\mathrm{s},m}_k} + \frac{1}{2}(F^{\mathrm{s},-}_k + F^{\mathrm{s},+}_k) \tag{3.31b}$$

$$q^{\mathrm{f},m+1}_k = q^{\mathrm{f},m}_k + \Delta t (M^{\mathrm{f}})^{-1} \Big(\frac{p^{\mathrm{f},m}_k + p^{\mathrm{f},m+1}_k}{2} - f^{\mathrm{f},m,-}_k + f^{\mathrm{f},m,+}_k \Big) \tag{3.31c}$$

$$p^{\mathrm{f},m+1}_k = p^{\mathrm{f},m}_k - \Delta t \frac{\partial (U(\bar{q}^{\mathrm{s},m}_k, \bar{q}^{\mathrm{f},m}_k) + P(\bar{q}^{\mathrm{s},m}_k))}{\partial \bar{q}^{\mathrm{f},m}_k} + \frac{1}{2}(f^{\mathrm{f},m,-}_k + f^{\mathrm{f},m,+}_k) \tag{3.31d}$$

as shown in Appendix B for $q^{\mathrm{s},m}_k$ *as defined in* (3.16) *with* $a^m = \frac{\mathbb{p}-m}{\mathbb{p}}$, $b^m = \frac{m}{\mathbb{p}}$,

$$\alpha_m = \frac{2\mathbb{p} - (2m+1)}{\mathbb{p}}, \qquad \beta_m = \frac{(2m+1)}{\mathbb{p}}, \tag{3.32a}$$

$$\bar{q}^{\mathrm{s},m}_k = \frac{q^{\mathrm{s},m}_k + q^{\mathrm{s},m+1}_k}{2} = \frac{\alpha_m q^{\mathrm{s}}_k + \beta_m q^{\mathrm{s}}_{k+1}}{2}, \qquad \bar{q}^{\mathrm{f},m}_k = \frac{q^{\mathrm{f},m}_k + q^{\mathrm{f},m+1}_k}{2} \tag{3.32b}$$

$$U^m_k = U(\bar{q}^{\mathrm{s},m}_k, \bar{q}^{\mathrm{f},m}_k), \quad P^m_k = P(\bar{q}^{\mathrm{f},m}_k), \quad \partial_{\mathrm{s}} U^m_k = \frac{\partial U^m_k}{\partial \bar{q}^{\mathrm{s},m}_k}, \quad \partial_{\mathrm{f}} U^m_k = \frac{\partial U^m_k}{\partial \bar{q}^{\mathrm{f},m}_k}, \quad \nabla P^m_k = \frac{\partial P^m_k}{\partial \bar{q}^{\mathrm{f},m}_k}. \tag{3.32c}$$

For discrete approximations of the forces such that $f^{\mathrm{f},m,+}_k = f^{\mathrm{f},m,-}_k$ *and* $F^{\mathrm{s},+}_k = F^{\mathrm{s},-}_k$ *these equations are clearly a discrete approximation of the continuous equations of motion* (3.10)*. As shown in the following section, for particular systems this time-stepping scheme is of order two on the macro time scale. Furthermore, it is easy to see that for* $\mathbb{p} = 1$ *it reduces to the standard singlerate midpoint rule formulation. Of course, other choices of interpolation rules, velocity approximation, and explicit or implicit quadrature approximations can lead to alternative time-stepping schemes of different orders of approximation (see for example [109]). Thus, the general multirate formulation presented in this chapter provides freedom in the choice of approximations and can readily be tailored to the requirements of the specific application and the trade-off between computational cost and accuracy.*

The equations of motion can also be expressed in Lagrangian formulation as:

$$q^{\mathrm{s}}_{k+1} = 2q^{\mathrm{s}}_k - q^{\mathrm{s}}_{k-1} - \Delta T (M^{\mathrm{s}})^{-1} \Big(\sum_{m=0}^{\mathbb{p}-1} \tfrac{\Delta t}{2} (\, \alpha_m \partial_s U^m_k + \beta_m \partial_{\mathrm{s}} U^m_{k-1}) + F^{\mathrm{s},-}_k + F^{\mathrm{s},+}_{k-1} \Big) \tag{3.33a}$$

$$q^{\mathrm{f},1}_k = 2q^{\mathrm{f},\mathbb{p}}_{k-1} - q^{\mathrm{f},\mathbb{p}-1}_{k-1} + \Delta t (M^{\mathrm{f}})^{-1} \Big(- \tfrac{\Delta t}{2} (\partial_{\mathrm{f}} U^{\mathbb{p}}_{k-1} + \partial_{\mathrm{f}} U^{\mathbb{p}-1}_{k-1}) \tag{3.33b}$$

$$- \tfrac{\Delta t}{2} (\nabla P^{\mathbb{p}}_{k-1} + \nabla P^{\mathbb{p}-1}_{k-1}) + f^{\mathrm{f},0,-}_k + f^{\mathrm{f},\mathbb{p}-1,+}_{k-1} \Big)$$

$$q^{\mathrm{f},m+1}_k = 2q^{\mathrm{f},m}_k - q^{\mathrm{f},m-1}_k + \Delta t (M^{\mathrm{f}})^{-1} \Big(- \tfrac{\Delta t}{2} (\partial_{\mathrm{f}} U^m_k + \partial_{\mathrm{f}} U^{m-1}_k) \tag{3.33c}$$

$$- \tfrac{\Delta t}{2}(\nabla P_k^m + \nabla P_k^{m-1}) + f_k^{\mathrm{f},m,-} + f_k^{\mathrm{f},m-1,+}\Big)$$

with (3.33c) *for* $k = 0, \dots, N-1, \quad m = 1, \dots, \mathbb{p}-1$ *and* (3.33a), (3.33b) *for* $k = 1, \dots, N-1$. *This formulation is also a second order structure-preserving scheme due to its equivalence to the Hamiltonian version.*

Specifying the potential as (3.11), *approximating it as*

$$V_{\mathrm{d}}(q_{\mathrm{d}}^{\mathrm{s}}, q_{\mathrm{d}}^{\mathrm{f}}) = \frac{1}{2}\sum_{k=0}^{N-1}\left(\left(\frac{q_k^{\mathrm{s}}+q_{k+1}^{\mathrm{s}}}{2}\right)^{\intercal} K^{\mathrm{s}} \frac{q_k^{\mathrm{s}}+q_{k+1}^{\mathrm{s}}}{2} + \sum_{m=0}^{\mathbb{p}-1}\left(\frac{q_k^{\mathrm{f},m}+q_k^{\mathrm{f},m+1}}{2}\right)^{\intercal} K^{\mathrm{f}} \frac{q_k^{\mathrm{f},m}+q_k^{\mathrm{f},m+1}}{2}\right).$$

and using the forces approximation $f_k^{\mathrm{f},m,-} = f_k^{\mathrm{f},m,+}$, $F_k^{\mathrm{s},-} = F_k^{\mathrm{s},+}$ *leads to the following discrete equations of motion in Hamiltonian formulation:*

$$q_{k+1}^{\mathrm{s}} = q_k^{\mathrm{s}} + \Delta T (M^{\mathrm{s}})^{-1}\Big(\frac{p_k^{\mathrm{s}} + p_{k+1}^{\mathrm{s}}}{2} + \frac{\Delta t}{2}\sum_{m=0}^{\mathbb{p}-1}\alpha_m K^{\mathrm{s}} \frac{\alpha_m q_k^{\mathrm{s}} + \beta_m q_{k+1}^{\mathrm{s}}}{2}\Big) \tag{3.34a}$$

$$p_{k+1}^{\mathrm{s}} = p_k^{\mathrm{s}} - \frac{\Delta T}{2} K^{\mathrm{s}}(q_k^{\mathrm{s}} + q_{k+1}^{\mathrm{s}}) + \frac{1}{2}(F_k^{\mathrm{s},-} + F_k^{\mathrm{s},+}) \tag{3.34b}$$

$$q_k^{\mathrm{f},m+1} = q_k^{\mathrm{f},m} + \frac{\Delta t (M^{\mathrm{f}})^{-1}}{2}(p_k^{\mathrm{f},m} + p_k^{\mathrm{f},m+1}) \tag{3.34c}$$

$$p_k^{\mathrm{f},m+1} = p_k^{\mathrm{f},m} - \frac{\Delta t}{2} K^{\mathrm{f}}(q_k^{\mathrm{f,m}} + q_k^{\mathrm{f,m+1}}) + \frac{1}{2}(f_k^{\mathrm{f},m,-} + f_k^{\mathrm{f},m,+}) \tag{3.34d}$$

or in Lagrangian formulation:

$$0 = M^{\mathrm{s}}\frac{q_k^{\mathrm{s}} - q_{k-1}^{\mathrm{s}}}{\Delta T} - M^{\mathrm{s}}\frac{q_{k+1}^{\mathrm{s}} - q_k^{\mathrm{s}}}{\Delta T} - \frac{\Delta t}{2}\sum_{m=0}^{\mathbb{p}-1}\Big(\alpha_m K^{\mathrm{s}}\frac{\alpha_m q_k^{\mathrm{s}} + \beta_m q_{k+1}^{\mathrm{s}}}{2} + \beta_m K^{\mathrm{s}}\frac{\alpha_m q_{k-1}^{\mathrm{s}} + \beta_m q_k^{\mathrm{s}}}{2}\Big) \tag{3.35a}$$

$$0 = M^{\mathrm{f}}\frac{q_{k-1}^{\mathrm{f},\mathbb{p}} - q_{k-1}^{\mathrm{f},\mathbb{p}-1}}{\Delta t} - M^{\mathrm{f}}\frac{q_k^{\mathrm{f},1} - q_k^{\mathrm{f},0}}{\Delta t} - \frac{\Delta t}{2}K^{\mathrm{f}}\frac{q_k^{\mathrm{f},0} + q_k^{\mathrm{f},1}}{2} - \frac{\Delta t}{2}K^{\mathrm{f}}\frac{q_{k-1}^{\mathrm{f},\mathbb{p}-1} + q_{k-1}^{\mathrm{f},\mathbb{p}}}{2} \tag{3.35b}$$

$$0 = M^{\mathrm{f}}\frac{q_k^{\mathrm{f},m} - q_k^{\mathrm{f},m-1}}{\Delta t} - M^{\mathrm{f}}\frac{q_k^{\mathrm{f},m+1} - q_k^{\mathrm{f},m}}{\Delta t} - \frac{\Delta t}{2}K^{\mathrm{f}}\frac{q_k^{\mathrm{f},m+1} + q_k^{\mathrm{f},m}}{2} - \frac{\Delta t}{2}K^{\mathrm{f}}\frac{q_k^{\mathrm{f},m-1} + q_k^{\mathrm{f},m}}{2}. \tag{3.35c}$$

For $\mathbb{p} = 1$ *both formulations are clearly equivalent to a direct midpoint discretisation of* (3.12).

Remark 3.4.4. *Comparing* (3.33) *and* (3.31) *we can see that, although the the Hamiltonian (phase-space) formulation* (3.30) *is equivalent to Lagrangian formulation* (3.28), (3.24), *the former has approximately twice as many unknowns due to the computation of the momentum not only at the boundary conditions but for*

all macro and micro time nodes. For the same reason, in an optimal control problem the Hamiltonian formulation leads to a much higher number of optimisation variables and constraints. However, the Lagrangian formulation may yield less sparse Jacobians of the model equality constraints, increasing its associated computational cost.

The computational efficiency is also influenced by the value of $\mathbb{p}$*. Although increasing* $\mathbb{p}$ *reduces the number of slow variable computations, it increases the number of fast variables being obtained using the Newton-Raphson Method at each macro time node. This can lead to slower computations and thus diminishing returns in increasing* $\mathbb{p}$*. These trade-offs are demonstrated with examples in the following chapters.*

3.4.3 Properties of the time-stepping scheme

To be able to use existing results on the discrete Noether's theorem and the order of accuracy of an SVI, we now establish an alternative formulation of the multirate scheme based on variations only at the boundaries of the macro time nodes. By defining a new Lagrangian based on critical values on the micro time nodes, we assume that the equations of motion at the micro time grid are satisfied. Then assuming the forces depend only on the configuration at macro time nodes, we demonstrate that this new multirate formulation is equivalent to the one presented previously in this chapter and, therefore, can be used to establish its structure-preserving properties and order of accuracy.

We define the *extreme discrete Lagrangian*, which depends only on the macro-step values of the slow and fast configuration variables $(q_k^{\mathrm{s}}, q_k^{\mathrm{f},0}, q_{k+1}^{\mathrm{s}}, q_k^{\mathrm{f},\mathbb{p}})$:

$$\hat{L}_{\mathrm{d}}^k = \hat{L}_{\mathrm{d}}^k(q_k, q_{k+1}) = \underset{(q_k^{\mathrm{f},1},\dots,q_k^{\mathrm{f},\mathbb{p}-1})}{\mathrm{ext}} L_{\mathrm{d}}^k(q_k^{\mathrm{s}}, q_{k+1}^{\mathrm{s}}, q_k^{\mathrm{f}}) \tag{3.36}$$

where "ext" means evaluated at the critical values of $q_k^{\mathrm{f},1}, \dots, q_k^{\mathrm{f},\mathbb{p}-1}$ such that Equation (3.24c) is satisfied and as before $q_k = \begin{bmatrix} q_k^{\mathrm{s}} \\ q_k^{\mathrm{f},0} \end{bmatrix}, q_{k+1} = \begin{bmatrix} q_{k+1}^{\mathrm{s}} \\ q_k^{\mathrm{f},\mathbb{p}} \end{bmatrix}$. Similarly we define the *extreme left and right discrete forces* $F_{\mathrm{d}}^{\mathrm{s}}, F_{\mathrm{d}}^{\mathrm{f}}$ as the one-forms

$$F_{\mathrm{d}}^{\mathrm{s}}(u_k)(q_k, q_{k+1}) \cdot (\delta q_k^{\mathrm{s}}, \delta q_{k+1}^{\mathrm{s}}) = F_k^{\mathrm{s},-} \cdot \delta q_k^{\mathrm{s}} + F_k^{\mathrm{s},+} \cdot \delta q_{k+1}^{\mathrm{s}} \tag{3.37a}$$

$$F_{\mathrm{d}}^{\mathrm{f}}(u_k)(q_k, q_{k+1}) \cdot (\delta q_k^{\mathrm{f},0}, \delta q_k^{\mathrm{f},\mathbb{p}}) = F_k^{\mathrm{f},-} \cdot \delta q_k^{\mathrm{f},0} + F_k^{\mathrm{f},+} \cdot \delta q_k^{\mathrm{f},\mathbb{p}} \tag{3.37b}$$

where $F_k^{\mathrm{s},+}, F_k^{\mathrm{s},-}$ are defined in Equation (3.20) as

$$F_k^{\mathrm{s},+} := F_{\mathrm{LC,d}}^{\mathrm{s},+}\Big(q_k^{\mathrm{s}}, q_{k+1}^{\mathrm{s}}, q_k^{\mathrm{f}}, u_k\Big), \quad F_k^{\mathrm{s},-} = F_{\mathrm{LC,d}}^{\mathrm{s},-}\Big(q_k^{\mathrm{s}}, q_{k+1}^{\mathrm{s}}, q_k^{\mathrm{f}}, u_k\Big),$$

and

$$F_k^{\mathrm{f},+} := F_{\mathrm{LC,d}}^{\mathrm{f},+}\Big(q_k^{\mathrm{s}}, q_{k+1}^{\mathrm{s}}, q_k^{\mathrm{f}}, u_k\Big) = f_k^{\mathrm{f},\mathbb{p}-1,+} + \sum_{m=1}^{\mathbb{p}-1}(f_k^{\mathrm{f},m,-} + f_k^{\mathrm{f,m-1,+}})\frac{\partial q_k^{\mathrm{f},m}}{\partial q_k^{\mathrm{f},\mathbb{p}}} \tag{3.38a}$$

$$F_k^{\mathrm{f},-} := F_{\mathrm{LC,d}}^{\mathrm{f},-}\Big(q_k^{\mathrm{s}}, q_{k+1}^{\mathrm{s}}, q_k^{\mathrm{f}}, u_k\Big) = f_k^{\mathrm{f},0,-} + \sum_{m=1}^{\mathbb{p}-1}(f_k^{\mathrm{f},m,-} + f_k^{\mathrm{f,m-1,+}})\frac{\partial q_k^{\mathrm{f},m}}{\partial q_k^{\mathrm{f},0}}. \tag{3.38b}$$

with

$$F_{\mathrm{LC,d}}^{\mathrm{f},+} : \Big(q_k^{\mathrm{s}}, q_{k+1}^{\mathrm{s}}, q_k^{\mathrm{f}}, u_k\Big) \mapsto \Big(q_k^{\mathrm{f},\mathbb{p}}, F_{\mathrm{LC,d}}^{f-}\Big(q_k^{\mathrm{s}}, q_{k+1}^{\mathrm{s}}, q_k^{\mathrm{f}}, u_k\Big)\Big)$$
$$F_{\mathrm{LC,d}}^{\mathrm{f},-} : \Big(q_k^{\mathrm{s}}, q_{k+1}^{\mathrm{s}}, q_k^{\mathrm{f}}, u_k\Big) \mapsto \Big(q_k^{\mathrm{f},0}, F_{\mathrm{LC,d}}^{f+}\Big(q_k^{\mathrm{s}}, q_{k+1}^{\mathrm{s}}, q_k^{\mathrm{f}}, u_k\Big)\Big).$$

Proposition 3.4.1. *Using the extreme Lagrangian and the force one-forms we apply the discrete Lagrange-d'Alembert principle to obtain*

$$\begin{aligned}
0 &= \Big(D_{q_k^{\mathrm{s}}}(\hat{L}_{\mathrm{d}}^k + \hat{L}_{\mathrm{d}}^{k-1}) + F_k^{\mathrm{s},-} + F_{k-1}^{\mathrm{s},+}\Big)\cdot\delta q_k^{\mathrm{s}} + \Big(D_{q_k^{\mathrm{f},0}}(\hat{L}_{\mathrm{d}}^k + \hat{L}_{\mathrm{d}}^{k-1}) + F_k^{\mathrm{f},-} + F_{k-1}^{\mathrm{f},+}\Big)\cdot\delta q_k^{\mathrm{f},0} \\
&= \Big(D_{q_k^{\mathrm{s}}}(L_{\mathrm{d}}^k + L_{\mathrm{d}}^{k-1}) + F_k^{\mathrm{s},-} + F_{k-1}^{\mathrm{s},+}\Big)\cdot\delta q_k^{\mathrm{s}} + \Big(D_{q_k^{\mathrm{f},0}}(L_{\mathrm{d}}^k + L_{\mathrm{d}}^{k-1}) + f_k^{\mathrm{f},0,-} + f_{k-1}^{\mathrm{f},\mathbb{p}-1,+}\Big)\cdot\delta q_k^{\mathrm{f},0} + \\
&\quad \sum_{m=1}^{\mathbb{p}-1}\Big((D_{q_k^{\mathrm{f},m}} L_{\mathrm{d}}^k + f_k^{\mathrm{f},m,-} + f_k^{\mathrm{f,m-1,+}})\frac{\partial q_k^{\mathrm{f},m}}{\partial q_k^{\mathrm{f},0}}\cdot\delta q_k^{\mathrm{f},0} + \\
&\quad \sum_{m=1}^{\mathbb{p}-1}\Big((D_{q_{k-1}^{\mathrm{f},m}} L_{\mathrm{d}}^{k-1} + f_{k-1}^{\mathrm{f},m,-} + f_{k-1}^{\mathrm{f,m-1,+}})\frac{\partial q_{k-1}^{\mathrm{f},m}}{\partial q_{k-1}^{\mathrm{f},\mathbb{p}}}\cdot\delta q_{k-1}^{\mathrm{f},\mathbb{p}}\Big)
\end{aligned} \tag{3.39}$$

in a similar way to that described in Appendix A. Since the discrete Euler-Lagrange equations (more specifically (3.24c)*) are satisfied at the inner micro nodes for the extreme Lagrangian and forces (by the definition of* $\hat{L}_{\mathrm{d}}^k$, $F_k^{\mathrm{s},\pm}$, $F_k^{\mathrm{f},\pm}$*), taking independent variations* δq_k^{s} *and* $\delta q_k^{\mathrm{f},0}$ *for* $k = 0, \ldots, N-1$*, we receive the original forced Euler-Lagrange equations* (3.24a)-(3.24b)*. Thus, the Lagrange-d'Alembert principle based on the extreme Lagrangian and forces results in the same set of equations of motion as the main formulation presented in Section 3.4.1.*

Based on this new formulation, we can define *the forced discrete Lagrangian flow map* $F_{\hat{L}_{\mathrm{d}}}^{u_{k-1},u_k} : Q \times Q \to Q \times Q$ for fixed controls $u_{k-1}, u_k \in \mathcal{U}^{\mathbb{p}}$ such that for example

$F_{L_\mathrm{d}}^{u_0,u_1} : (q_0, q_1) \to (q_1, q_2)$ (for more details, see [18, 20]). It is important to note that, as desired, this Lagrangian flow has the form $Q \times Q$ to $Q \times Q$ and, due to the equivalence to our multirate formulation, allows us to use existing results on conservation and approximation properties for classical Lagrangian defined on $Q \times Q$.

Lastly, for this formulation, we define the Legendre transform analogously to (3.25):

$$\begin{aligned}
\mathbb{F}^{F^{\mathrm{s},-}}\hat{L}_\mathrm{d}(u_k) &: (q_k^\mathrm{s}, q_{k+1}^\mathrm{s}) \mapsto (q_k^\mathrm{s}, -D_{q_k^\mathrm{s}}\hat{L}_\mathrm{d}^k - F_k^{\mathrm{s},-}) = (q_k^\mathrm{s}, p_k^s) \\
\mathbb{F}^{F^{\mathrm{s},+}}\hat{L}_\mathrm{d}(u_k) &: (q_k^\mathrm{s}, q_{k+1}^\mathrm{s}) \mapsto (q_{k+1}^\mathrm{s}, D_{q_{k+1}^\mathrm{s}}\hat{L}_\mathrm{d}^k + F_k^{\mathrm{s},+}) = (q_{k+1}^\mathrm{s}, p_{k+1}^s) \\
\mathbb{F}^{F^{\mathrm{f},-}}\hat{L}_\mathrm{d}(u_k) &: (q_k^{\mathrm{f},0}, q_k^{\mathrm{f},\mathbb{p}}) \mapsto (q_k^{\mathrm{f},0}, -D_{q_k^{\mathrm{f},0}}\hat{L}_\mathrm{d}^k - F_k^{\mathrm{f},-}) = (q_k^{f,0}, p_k^{f,0}) \\
\mathbb{F}^{F^{\mathrm{f},+}}\hat{L}_\mathrm{d}(u_k) &: (q_k^{\mathrm{f},0}, q_k^{\mathrm{f},\mathbb{p}}) \mapsto (q_k^{\mathrm{f},\mathbb{p}}, D_{q_k^{\mathrm{f},\mathbb{p}}}\hat{L}_\mathrm{d}^k + F_k^{\mathrm{f},+}) = (q_k^{f,\mathbb{p}}, p_k^{f,\mathbb{p}})
\end{aligned}$$

Note that with the definition of the extreme Lagrangian and forces, the discrete Legendre transforms for $\hat{L}_d$ correspond to those for L_d^k at the macro nodes.

Structure-preserving properties

In the absence of forces, similarly to the continuous case, one can show that discrete multirate variational models lead to the conservation of symplecticity and certain momentum maps (for details, see [20]). Energy would also be conserved up to small oscillations around a constant value [20]. However, as mentioned in Section 3.3.3, under the action of forces, preservation of the symplectic form and conservation of energy (up to bounded oscillations) does not generally hold. In those cases, the preservation of momentum maps can again be demonstrated using a discrete forced Noether's theorem as formulated by [20, Theorem 4.2].

Following the example of [20] and [19], we introduce the discrete momentum maps $\mathbf{J}^+_{\hat{L}_\mathrm{d}}, \mathbf{J}^-_{\hat{L}_\mathrm{d}}$ defined as

$$\begin{aligned}
\mathbf{J}^+_{\hat{L}_\mathrm{d}}(q_0, q_1) \cdot \xi &= \left\langle \begin{bmatrix} \mathbb{F}^{F^{\mathrm{s},+}}\hat{L}_\mathrm{d}(u_0)(q_0^\mathrm{s}, q_1^\mathrm{s}) \\ \mathbb{F}^{F^{\mathrm{f},+}}\hat{L}_\mathrm{d}(u_0)(q_0^{\mathrm{f},0}, q_0^{\mathrm{f},\mathbb{p}}) \end{bmatrix}, \xi_Q(q_1) \right\rangle, \\
\mathbf{J}^-_{\hat{L}_\mathrm{d}}(q_0, q_1) \cdot \xi &= \left\langle \begin{bmatrix} \mathbb{F}^{F^{\mathrm{s},-}}\hat{L}_\mathrm{d}(u_0)(q_0^\mathrm{s}, q_1^\mathrm{s}) \\ \mathbb{F}^{F^{\mathrm{f},-}}\hat{L}_\mathrm{d}(u_0)(q_0^{\mathrm{f},0}, q_0^{\mathrm{f},\mathbb{p}}) \end{bmatrix}, \xi_Q(q_0) \right\rangle.
\end{aligned}$$

Additionally, given an action with infinitesimal generator $\xi_Q : Q \to TQ$ we introduce the action lift to $Q \times Q$ by the product $\phi_g^{Q\times Q}(q_0, q_1) = (\phi_g(q_0), \phi_g(q_1))$ and its infinitesimal generator $\xi_{Q\times Q} : Q \times Q \to T(Q \times Q)$ given by $\xi_{Q\times Q}(q_0, q_1) = (\xi_Q(q_0), \xi_Q(q_1))$. Following the example of [20, Theorem 4.2] and using the extremised reformulation of the Lagrangian and the forces from Section 3.4.3, we now present the forced Noether's theorem for multirate system representations.

Theorem 3.4.2. ***(Forced Multirate Discrete Noether's theorem)*** *Consider a discrete Lagrangian system $\hat{L}_{\mathrm{d}}^k : Q \times Q \to \mathbb{R}$ with discrete control forces $F_k^{\mathrm{s},+}, F_k^{\mathrm{s},-}, F_k^{\mathrm{f},+}, F_k^{\mathrm{f},-} : Q \times Q \times U \to T^*Q$ and a symmetry action $\phi : G \times Q \to Q$ such that $\hat{L}_{\mathrm{d}}^k \circ \phi_g^{Q\times Q} = \hat{L}_{\mathrm{d}}^k$ and $\left\langle \begin{bmatrix} F_{\mathrm{d}}^{\mathrm{s}}(u_k) \\ F_{\mathrm{d}}^{\mathrm{f}}(u_k) \end{bmatrix}, \xi_{Q\times Q} \right\rangle = 0$ for all $\xi \in g$. Then the discrete Lagrangian momentum map $\mathbf{J}_{\hat{L}_{\mathrm{d}}}^{\mathrm{f}} : Q \times Q \to g^*$ will be preserved by the discrete Lagrangian evolution map, such that $\mathbf{J}_{\hat{L}_{\mathrm{d}}}^{\mathrm{f}} \circ F_{\hat{L}_{\mathrm{d}}}^{u_{k-1},u_k} = \mathbf{J}_{\hat{L}_{\mathrm{d}}}^{\mathrm{f}}$.*

Proof. Applying the Lagrange-d'Alembert principle in Equation (3.23a) similarly to Equation (3.39) but with $\delta q_k = \xi_Q(q_k)$ we have

$$\sum_{k=0}^{N-1} \mathrm{d}\hat{L}_{\mathrm{d}}^k(q_k, q_{k+1}) \cdot \xi_{Q\times Q}(q_k, q_{k+1}) + \sum_{k=0}^{N-1} \begin{bmatrix} F_{\mathrm{d}}^{\mathrm{s}}(u_k)(q_k, q_{k+1}) \\ F_{\mathrm{d}}^{\mathrm{f}}(u_k)(q_k, q_{k+1}) \end{bmatrix} \cdot \xi_{Q\times Q}(q_k, q_{k+1}) = \sum_{k=0}^{N-1} \begin{bmatrix} F_{\mathrm{d}}^{\mathrm{s}}(u_k)(q_k, q_{k+1}) \\ F_{\mathrm{d}}^{\mathrm{f}}(u_k)(q_k, q_{k+1}) \end{bmatrix} \cdot \xi_{Q\times Q}(q_k, q_{k+1}) \tag{3.40}$$

as $\hat{L}_d^k$ is assumed to be invariant. Using integration by parts, the left-hand side becomes

$$\sum_{k=1}^{N-1} \begin{bmatrix} D_{q_k^{\mathrm{s}}}(\hat{L}_{\mathrm{d}}^k + \hat{L}_{\mathrm{d}}^{k-1}) + F_k^{\mathrm{s}-} + F_{k-1}^{\mathrm{s},+} \\ D_{q_k^{\mathrm{f},0}}(\hat{L}_{\mathrm{d}}^k + \hat{L}_{\mathrm{d}}^{k-1}) + F_k^{\mathrm{f},-} + F_k^{\mathrm{f},+} \end{bmatrix} \cdot \xi_Q(q_k) + \begin{bmatrix} D_{q_0^{\mathrm{s}}} \hat{L}_{\mathrm{d}}^0 + F_0^{\mathrm{s},-} \\ D_{q_0^{\mathrm{f},0}} \hat{L}_{\mathrm{d}}^0 + F_0^{\mathrm{f},-} \end{bmatrix} \cdot \xi_Q(q_0)$$
$$+ \begin{bmatrix} D_{q_N^{\mathrm{s}}} \hat{L}_{\mathrm{d}}^{N-1} + F_{N-1}^{\mathrm{s},+} \\ D_{q_{N-1}^{\mathrm{f},\mathrm{p}}} \hat{L}_{\mathrm{d}}^{N-1} + F_{N-1}^{\mathrm{f},+} \end{bmatrix} \cdot \xi_Q(q_N) = \begin{bmatrix} \mathbb{F}^{F^{\mathrm{s},+}} \hat{L}_{\mathrm{d}}(u_0) \\ \mathbb{F}^{F^{\mathrm{f},+}} \hat{L}_{\mathrm{d}}(u_0) \end{bmatrix} \cdot \xi_Q(q_N) - \begin{bmatrix} \mathbb{F}^{F^{\mathrm{s},-}} \hat{L}_{\mathrm{d}}(u_{N-1}) \\ \mathbb{F}^{F^{\mathrm{f},-}} \hat{L}_{\mathrm{d}}(u_{N-1}) \end{bmatrix} \cdot \xi_Q(q_0).$$

Thus Equation (3.40) becomes

$$[\mathbf{J}_{\hat{L}_{\mathrm{d}}}^{\mathrm{f},+} \circ (F_{\hat{L}_{\mathrm{d}}}^{u_{\mathrm{d}}})^{N-1} - \mathbf{J}_{\hat{L}_{\mathrm{d}}}^{\mathrm{f}-}] \cdot \xi = \sum_{k=0}^{N-1} \begin{bmatrix} F_{\mathrm{d}}^{\mathrm{s}}(u_k)(q_k, q_{k+1}) \\ F_{\mathrm{d}}^{\mathrm{f}}(u_k)(q_k, q_{k+1}) \end{bmatrix} \cdot \xi_{Q\times Q}(q_k, q_{k+1})$$

describing the evolution of the momentum map. For all discrete forces orthogonal to the group action, so that $\left\langle \begin{bmatrix} F_{\mathrm{d}}^{\mathrm{s}}(u_k) \\ F_{\mathrm{d}}^{\mathrm{f}}(u_k) \end{bmatrix}, \xi_{Q\times Q} \right\rangle = 0$ for $\forall \xi \in g$, it holds that $[\mathbf{J}_{\hat{L}_{\mathrm{d}}}^{\mathrm{f},+} \circ (F_{\hat{L}_{\mathrm{d}}}^{u_{\mathrm{d}}})^{N-1} - J_{\hat{L}_{\mathrm{d}}}^{\mathrm{f}-}] = 0$ thus proving the theorem statement. □

3.4.4 Order of accuracy

Choice of approximation rules

The multirate formulations we have presented allow the use of different polynomial approximations for the discrete paths $q_{\mathrm{d}}^{\mathrm{s}}$ and $q_{\mathrm{d}}^{\mathrm{f}}$. One possibility is to approximate the slow and fast configuration variables using piecewise-linear polynomials as

$$q_{\mathrm{d}}^{\mathrm{s}}(t) = q_k^{\mathrm{s}} + \frac{q_{k+1}^{\mathrm{s}} - q_k^{\mathrm{s}}}{\Delta T}(t - t_k), \qquad \dot{q}_{\mathrm{d}}^{\mathrm{s}}(t) = \frac{q_{k+1}^{\mathrm{s}} - q_k^{\mathrm{s}}}{\Delta T}, \qquad \text{for } \; t \in [t_k, t_{k+1}]$$

$$q_{\mathrm{d}}^{\mathrm{f}}(t) = q_k^{\mathrm{f},m} + \frac{q_k^{\mathrm{f},m+1} - q_k^{\mathrm{f},m}}{\Delta t}(t - t_k^m), \quad \dot{q}_{\mathrm{d}}^{\mathrm{f}}(t) = \frac{q_k^{\mathrm{f},m+1} - q_k^{\mathrm{f},m}}{\Delta t}, \;\; \text{for } \; t \in [t_k^m, t_k^{m+1}]$$

for $k = 0, \ldots, N-1$, $m = 0, \ldots, \mathbb{p}-1$, but other approximations are also compliant with the multirate formulation. The choice depends on the application, the required accuracy, or the available computational resources. Moreover, the multirate scheme offers flexibility in selecting the approximation rules used for the Lagrangian, the virtual work, and later the cost of the optimisation. Most importantly, the quadrature rules can be chosen differently for different parts of the Lagrangian. In particular, if we consider systems for which the potential term in the Lagrangian can be split as $V = U(q^{\mathrm{s}}, q^{\mathrm{f}}) + P(q^{\mathrm{f}})$ then the integral of the potential energy can be approximated as

$$\Delta t V_{\mathrm{d}}(q_k^{\mathrm{s},m}, q_k^{\mathrm{s},m+1} q_k^{\mathrm{f},m}, q_k^{\mathrm{f},m+1}) \tag{3.41}$$

$$= \Delta t U_{\mathrm{d}}(q_k^{\mathrm{s},m}, q_k^{\mathrm{s},m+1}, q_k^{\mathrm{f},m}, q_k^{\mathrm{f},m+1}) + \Delta t P_{\mathrm{d}}(q_k^{\mathrm{f},m}, q_k^{\mathrm{f},m+1}) \approx \int_{t_k^m}^{t_k^{m+1}} \Big(U(q^{\mathrm{s}}, q^{\mathrm{f}}) + P(q^{\mathrm{f}}) \Big) dt$$

and one can choose the quadrature rule for the approximation of U and P separately. For example, in many highly oscillatory systems, one can split the the potential energy into a fast linear component and a slow nonlinear one. Using a combination of explicit and implicit quadrature in such problems can lead to a reduction in the computational burden as shown by the use of IMEX integrators [93].

To explore the use of different quadrature combinations in MVI, one can write the following very general expressions for the kinetic and potential energies:

$$\mathbb{T}_{\mathrm{d},k} = \Delta t \sum_{m=0}^{\mathbb{p}-1} \left(T\Big(\frac{q_k^{\mathrm{s},m+1} - q_k^{\mathrm{s},m}}{\Delta t}, \frac{q_k^{\mathrm{f},m+1} - q_k^{\mathrm{f},m}}{\Delta t} \Big) \right) \tag{3.42a}$$

$$= \frac{\Delta T}{2}\Big(\frac{q^{\mathrm{s}}_{k+1}-q^{\mathrm{s}}_{k}}{\Delta T}\Big)^{\intercal} M^{\mathrm{s}}\Big(\frac{q^{\mathrm{s}}_{k+1}-q^{\mathrm{s}}_{k}}{\Delta T}\Big) + \sum_{m=0}^{\mathbb{p}-1}\frac{\Delta t}{2}\Big(\frac{q^{\mathrm{f},m+1}_{k}-q^{\mathrm{f},m}_{k}}{\Delta t}\Big)^{\intercal} M^{\mathrm{f}}\Big(\frac{q^{\mathrm{f},m+1}_{k}-q^{\mathrm{f},m}_{k}}{\Delta t}\Big)$$

$$\mathbb{U}_{\mathrm{d},k} = \Delta t \sum_{m=0}^{\mathbb{p}-1}\Big(\alpha U(\gamma q^{\mathrm{s},m}_{k} + (1-\gamma)q^{\mathrm{s},m+1}_{k}, \gamma q^{\mathrm{f},m}_{k} + (1-\gamma)q^{\mathrm{f},m+1}_{k}) + \tag{3.42b}$$
$$(1-\alpha)U((1-\gamma)q^{\mathrm{s},m}_{k} + \gamma q^{\mathrm{s},m+1}_{k}, (1-\gamma)q^{\mathrm{f},m}_{k} + \gamma q^{\mathrm{f},m+1}_{k})\Big)$$

$$\mathbb{P}_{\mathrm{d},k} = \Delta t \sum_{m=0}^{\mathbb{p}-1}\Big(\beta P(\mu q^{\mathrm{f},m}_{k} + (1-\mu)q^{\mathrm{f},m+1}_{k}) + (1-\beta)P((1-\mu)q^{\mathrm{f},m}_{k} + \mu q^{\mathrm{f},m+1}_{k})\Big) \tag{3.42c}$$

where the kinetic energy has been simplified as shown in Appendix B, Equations (B.1c) and (B.1d). For example, the midpoint quadrature can be implemented in these approximations by using $\gamma = \mu = \frac{1}{2}$ and arbitrary values for α, β. Similarly the trapezoidal approximation corresponds to $(\alpha, \gamma) = (\frac{1}{2}, 1)$ and $(\beta, \mu) = (\frac{1}{2}, 1)$ and the rectangle rule using $\alpha \in \{0, 1\}, \gamma = 1$ and $\beta \in \{0, 1\}, \mu = 1$.

Variational error analysis

As we discussed in Section 2.3.1, given an ordinary differential equation $\dot{x}(t) = f(x(t))$, a numerical integrator $F(x, \Delta T)$ of the form $F(x, \Delta T) : x_k \mapsto x_{k+1}$ for $k = 0, 1, 2, \ldots$ with $x_0 = x(0)$ is of order r if the local truncation error $x_1 - x(\Delta T)$ is $\mathcal{O}((\Delta T)^{r+1})$ as $\Delta T \to 0$. For Hamiltonian or Lagrangian systems the state $x = (q, p)$ consists of configuration q and momentum p and the one-step scheme $F(x, \Delta T)$ plays the role of the discrete Lagrangian flow. For the variational integrators proposed by [1, 109] one can alternatively consider how close a discrete Lagrangian can approximate the exact discrete Lagrangian defined in the multirate case as

$$L^{\mathrm{E}}_{\mathrm{d}}(q^{\mathrm{s}}(0), q^{\mathrm{f}}(0), q^{\mathrm{s}}(\Delta T), q^{\mathrm{f}}(\Delta T)) = \int_0^{\Delta T} \mathcal{L}(q^{\mathrm{s}}(t), q^{\mathrm{f}}(t), \dot{q}^{\mathrm{s}}(t), \dot{q}^{\mathrm{f}}(t))dt \tag{3.43}$$

for sufficiently small ΔT. Here $q^{\mathrm{s}}(\cdot), q^{\mathrm{f}}(\cdot), \dot{q}^{\mathrm{s}}(\cdot), \dot{q}^{\mathrm{f}}(\cdot)$ are the unique solution of the Euler-Lagrange equations (3.3) with the given boundary conditions. In Theorem 6 of [109] it is stated that the if

$$\hat{L}^{k}_{\mathrm{d}}(q^{\mathrm{s}}(0), q^{\mathrm{s}}(\Delta T), q^{\mathrm{f}}(0), q^{\mathrm{f}}(\Delta T)) = L^{\mathrm{E}}_{\mathrm{d}}(q^{\mathrm{s}}(0), q^{\mathrm{s}}(\Delta T), q^{\mathrm{f}}(0), q(\Delta T)) + \mathcal{O}((\Delta T)^{r+1}) \tag{3.44}$$

then the resulting time-stepping scheme following (3.24) or equivalently, (3.30) in the absence of forces, is of order r. For forced systems, external forces have to be taken into account when computing an error estimate. Thus, we have the following statement (cf. [19]):

Statement 3.4.1. *If*

- *the discrete Lagrangian approximates the exact discrete Lagrangian to order r*
- *and the discrete forces approximate the exact discrete forces to order r*

then the resulting variational integration scheme is of order r.

More concretely, in addition to the estimate (3.44), the estimate for the forces

$$\begin{aligned}
&F^{s,\pm}_{\mathrm{LC,d}}(q^{\mathrm{s}}(0), q^{\mathrm{s}}(\Delta T), q^{\mathrm{f}}(0), q^{\mathrm{f}}(\Delta T), \{u(\Delta t(m+\frac{1}{2}))\}_{m=0}^{\mathbb{p}-1}) = \\
&\qquad F^{s,\pm}_{\mathrm{LC,E}}(q^{\mathrm{s}}(0), q^{\mathrm{s}}(\Delta T), q^{\mathrm{f}}(0), q^{\mathrm{f}}(\Delta T), u|_{[0,\Delta T]}) + \mathcal{O}((\Delta T)^{r+1}) \\
&F^{f,\pm}_{\mathrm{LC,d}}(q^{\mathrm{s}}(0), q^{\mathrm{s}}(\Delta T), q^{\mathrm{f}}(0), q^{\mathrm{f}}(\Delta T), \{u(\Delta t(m+\frac{1}{2}))\}_{m=0}^{\mathbb{p}-1}) = \\
&\qquad F^{f,\pm}_{\mathrm{LC,E}}(q^{\mathrm{s}}(0), q^{\mathrm{s}}(\Delta T), q^{\mathrm{f}}(0), q^{\mathrm{f}}(\Delta T), u|_{[0,\Delta T]}) + \mathcal{O}((\Delta T)^{r+1})
\end{aligned}$$

has to be satisfied where for simplicity we assume that the forces only depend on macro configurations. Here the exact discrete forces are defined as

$$\begin{aligned}
F^{s,-}_{\mathrm{E},k} &:= F^{\mathrm{s},-}_{\mathrm{LC,E}}(q^{\mathrm{s}}(0), q^{\mathrm{s}}(\Delta T), q^{\mathrm{f}}(0), q^{\mathrm{f}}(\Delta T), u|_{[0,\Delta T]}) \\
&= \int_0^{\Delta T} f^{\mathrm{s}}_{\mathrm{LC}}(q^{\mathrm{s}}(t), q^{\mathrm{f}}(t), \dot{q}^{\mathrm{s}}(t), \dot{q}^{\mathrm{f}}(t), u(t)) \frac{\partial q^{\mathrm{s}}(t)}{\partial q^{\mathrm{s}}_0} dt && \text{(3.45a)} \\
F^{s,+}_{\mathrm{E},k} &:= F^{\mathrm{s},+}_{\mathrm{LC,E}}(q^{\mathrm{s}}(0), q^{\mathrm{s}}(\Delta T), q^{\mathrm{f}}(0), q^{\mathrm{f}}(\Delta T), u|_{[0,\Delta T]}) \\
&= \int_0^{\Delta T} f^{\mathrm{s}}_{\mathrm{LC}}(q^{\mathrm{s}}(t), q^{\mathrm{f}}(t), \dot{q}^{\mathrm{s}}(t), \dot{q}^{\mathrm{f}}(t), u(t)) \frac{\partial q^{\mathrm{s}}(t)}{\partial q^{\mathrm{s}}_1} dt && \text{(3.45b)} \\
F^{f,-}_{\mathrm{E},k} &:= F^{\mathrm{f},-}_{\mathrm{LC,E}}(q^{\mathrm{s}}(0), q^{\mathrm{s}}(\Delta T), q^{\mathrm{f}}(0), q^{\mathrm{f}}(\Delta T), u|_{[0,\Delta T]}) \\
&= \int_0^{\Delta T} f^{\mathrm{f}}_{\mathrm{LC}}(q^{\mathrm{s}}(t), q^{\mathrm{f}}(t), \dot{q}^{\mathrm{s}}(t), \dot{q}^{\mathrm{f}}(t), u(t)) \frac{\partial q^{\mathrm{f}}(t)}{\partial q^{\mathrm{f},0}_0} dt && \text{(3.45c)} \\
F^{f,+}_{\mathrm{E},k} &:= F^{\mathrm{f},+}_{\mathrm{LC,E}}(q^{\mathrm{s}}(0), q^{\mathrm{s}}(\Delta T), q^{\mathrm{f}}(0), q^{\mathrm{f}}(\Delta T), u|_{[0,\Delta T]}) \\
&= \int_0^{\Delta T} f^{\mathrm{f}}_{\mathrm{LC}}(q^{\mathrm{s}}(t), q^{\mathrm{f}}(t), \dot{q}^{\mathrm{s}}(t), \dot{q}^{\mathrm{f}}(t), u(t)) \frac{\partial q^{\mathrm{f}}(t)}{\partial q^{\mathrm{f},\mathbb{p}}_0} dt && \text{(3.45d)}
\end{aligned}$$

with $q^{\mathrm{s}}_0 = q^{\mathrm{s}}(0), q^{\mathrm{s}}_1 = q^{\mathrm{s}}(\Delta T)$ and $q^{\mathrm{f},0}_0 = q^{\mathrm{f}}(0), q^{\mathrm{f},\mathbb{p}}_0 = q^{\mathrm{f}}(\Delta T)$.

To determine the approximation order of the multirate variational integrators, we thus have to compute the error between exact and discrete Lagrangians and forces. For the force estimate we use classical Taylor expansion as shown in the proof of Theorem 3.4.4. For the estimate of the Lagrangian, we make use of the variational error analysis for Galerkin variational integrators [110] but adapt several steps for the multirate case and extend it to forced systems. In the following, we give a detailed proof along the lines of [110] with particular emphasis on the needed modifications.

Let us introduce the space of polynomials

$$\mathcal{P}^l([0,\Delta T],Q) = \{q \in C^\infty([0,\Delta T],Q) \,|\, q \text{ a polynomial of degree at most } l\}.$$

We fix $l+1$ control points $\Delta T d_0 < \Delta T d_1 < \ldots < \Delta T d_l$, where $d_0 = 0$ and $d_l = 1$. If for each of these control points a value $q(\Delta T d_j) = q_j$ is prescribed, then the polynomial $q \in \mathcal{P}^l([0,\Delta T],Q)$ is uniquely determined. We denote by $\hat{q}(\,\cdot\,; q_0,\ldots,q_l,\Delta T)$ the polynomial obtained in this way. To analyse the multirate case, we also introduce the space of piecewise polynomials

$$\mathcal{P}^l_{\mathbb{p}}([0,\Delta T],Q) = \{q \in PC^\infty([0,\Delta T],Q) \,|\, q|_{[m\Delta t,(m+1)\Delta t)} \in \mathcal{P}^l([m\Delta t,(m+1)\Delta t),Q),$$
$$m=0,\ldots,\mathbb{p}-1 \text{ and } q \text{ is continuous at } m\Delta t,\ m=1,\ldots,\mathbb{p}-1\}.$$

where PC^∞ is the space of piecewise smooth functions. Similar as before we denote by $\check{q}(\,\cdot\,;\{q_0^m,\ldots,q_l^m\}_{m=0}^{\mathbb{p}-1},\Delta T)$ the piecewise polynomial designed by $\check{q}(m\Delta t + \Delta t d_j) = q_j^m$, $m = 0,\ldots,\mathbb{p}-1$. For the construction of the multirate integrator, we approximate the slow variable q^{s} by a polynomial $\hat{q}^{\mathrm{s}}$ defined on the macro interval $[0,\Delta T]$ and the fast variable q^{f} by a polynomial on the micro interval $[m\Delta t,(m+1)\Delta t]$ which corresponds to piecewise polynomial $\check{q}^{\mathrm{f}}$ on $[0,\Delta T]$.

Lemma 3.4.1. *Let q be a smooth curve and $\hat{q}$ a family of polynomials of degree l, parametrised by ΔT, which equals q at the control points $0 = \Delta T d_0 < \Delta T d_1 < \ldots < \Delta T d_l = \Delta T$. Then for any $k \le l$ there holds*

$$\left\| q^{(k)} - \hat{q}^{(k)} \right\|_\infty = \mathcal{O}(\Delta T^{l+1-k}),$$

where $\|\cdot\|_\infty$ denotes the maximum norm on $[0,\Delta T]$ and $[\cdot]^{(k)}$- the k-th derivative.

This lemma is needed for obtaining the error estimate (for a proof see [110]). For the approximation of the action we introduce a quadrature rule. We fix quadrature points $c_i \in [0,1]$ and weights $b_i \in \mathbb{R}$, with $\sum_i b_i = 1$ and denote by w the order of the corresponding quadrature rule. Then for any smooth function z it holds

$$\int_0^{\Delta T} z(t)\,dt - \Delta T \sum_i b_i z(\Delta T c_i) = \mathcal{O}(\Delta T^{w+1}).$$

Based on the polynomial spaces and this quadrature rule we investigate the multirate discrete Lagrangian defined as

$$\hat{L}_d(q_0^{\mathrm{s}}, q_0^{f,0}, q_1^{\mathrm{s}}, q_0^{f,\mathbb{p}}) = \operatorname*{ext}_{\substack{\hat{q}^{\mathrm{s}} \in \mathcal{P}^l([0,\Delta T], Q^{\mathrm{s}}),\\ \check{q}^{\mathrm{f}} \in \mathcal{P}^l_{\mathbb{p}}([0,\Delta T], Q^{\mathrm{f}})\\ \hat{q}^{\mathrm{s}}(0)=q_0^{\mathrm{s}},\, \hat{q}^{\mathrm{s}}(\Delta T)=q_1^{\mathrm{s}},\\ \check{q}^{\mathrm{f}}(0)=q_0^{f,0},\, \check{q}^{\mathrm{f}}(\Delta T)=q_0^{f,\mathbb{p}}}} \Delta t \sum_{m=0}^{\mathbb{p}-1} \sum_{i=1}^{r} b_i \mathcal{L}(\hat{q}^{\mathrm{s}}(t_i^m), \check{q}^{\mathrm{f}}(t_i^m), \dot{\hat{q}}^{\mathrm{s}}(t_m^i), \dot{\check{q}}^{\mathrm{f}}(t_i^m)). \tag{3.46}$$

with $t_i^m = m\Delta t + c_i \Delta t$. Note that the choice of $l = 1$, $r = 1$, $b_1 = 1$, $c_1 = \frac{1}{2}$ corresponds to the midpoint rule, the choice of $l = 1$, $r = 2$, $b_1 = b_2 = \frac{1}{2}$, $c_1 = 0, c_2 = 1$ corresponds to the trapezoidal rule and the choice of $l = 1$, $r = 1$, $b_1 = 1$, $c_1 \in \{0, 1\}$ corresponds to the rectangle rule as defined in equations (3.42).

One essential assumption to prove convergence rates of Galerkin variational integrators is that the discrete and continuous solutions of the discrete and continuous Euler-Lagrange equations, respectively, minimise the respective discrete and continuous actions. Considering general external forces, the action is not extremised anymore but changes according to the virtual work acting on the system (see equation (2.6)). Thus, a (discrete) solution of the (discrete) forced Euler-Lagrange equation can only minimise the (discrete) action if this change is zero along the solution. We thus formulate the following assumption.

Assumption 3.4.1. *The external forces act orthogonal to the motion of the forced Lagrangian system, i.e. the virtual work vanishes along the solution of the forced Euler-Lagrange equations:*

$$\int_0^T f_{\mathrm{LC}}(q, \dot{q}, u) \cdot \delta q \, dt = 0 \tag{3.47}$$

for $(q, \dot{q}, u)$ *satisfying*

$$\frac{d}{dt}\frac{\partial \mathfrak{L}}{\partial \dot{q}} - \frac{\partial \mathfrak{L}}{\partial q} = f_{\mathrm{LC}}(q, \dot{q}, u).$$

The approximation error of the discrete Lagrangian can now be determined.

Theorem 3.4.3. *Let* $\hat{L}_d$ *as given in* (3.46) *be a multirate discretisation of a regular Lagrangian* $\mathcal{L}$ *based on polynomials of degree* l *and a quadrature rule of degree* w*. Assume that under Assumption 3.4.1 all discrete and continuous critical curves minimize their respective actions. Then the difference between the discrete and the exact discrete Lagrangian is*

$$\begin{aligned}&\hat{L}_{\mathrm{d}}^{k}(q^{\mathrm{s}}(0), q^{\mathrm{s}}(\Delta T), q^{\mathrm{f}}(0), q^{\mathrm{f}}(\Delta T)) = \\ &L_{\mathrm{d}}^{\mathrm{E}}(q^{\mathrm{s}}(0), q^{\mathrm{s}}(\Delta T), q^{\mathrm{f}}(0), q^{\mathrm{f}}(\Delta T)) + \mathcal{O}((\Delta T)^{l+2}) + \mathcal{O}(\mathbb{p}(\Delta t)^{w+1})\end{aligned} \tag{3.48}$$

Proof. The proof strategy goes along the lines of [110]. Let q_{EL} denote the solution of the continuous forced Euler-Lagrange equations with $q_{\mathrm{EL}}(0) = q(0)$ and $q_{\mathrm{EL}}(\Delta T) = q(\Delta T)$. Let $\hat{q}^{\mathrm{s}} \in \mathcal{P}^{l}([0, \Delta T], Q^{\mathrm{s}})$ be the polynomial that agrees with $q_{\mathrm{EL}}^{\mathrm{s}}$ at the control points $0 = \Delta T d_0 < \Delta T d_1 < \ldots < \Delta T d_s = \Delta T$ and $\check{q}^{\mathrm{f}} \in \mathcal{P}_{\mathbb{p}}^{l}([0, \Delta T], Q^{\mathrm{f}})$ be the piecewise polynomial that agrees with $q_{\mathrm{EL}}^{\mathrm{f}}$ at the control points $0 = m\Delta t + \Delta t d_0 < m\Delta t + \Delta t d_1 < \ldots < m\Delta t + \Delta t d_s = \Delta T$ for $m = 0, \ldots, \mathbb{p} - 1$. Furthermore, let $\tilde{q}^{\mathrm{s}} \in \mathcal{P}^{l}([0, \Delta T], Q^{\mathrm{s}})$ and $\tilde{q}^{\mathrm{f}} \in \mathcal{P}_{\mathbb{p}}^{l}([0, \Delta T], Q^{\mathrm{f}})$ be the (piecewise) polynomials that minimise discrete action

$$\Delta t \sum_{m=0}^{p-1} \sum_{i=1}^{r} b_i \mathcal{L}(\tilde{q}^{\mathrm{s}}(m\Delta t + c_i \Delta t), \tilde{q}^{\mathrm{f}}(m\Delta t + c_i \Delta t), \dot{\tilde{q}}^{\mathrm{s}}(m\Delta t + c_i \Delta t), \dot{\tilde{q}}^{\mathrm{f}}(m\Delta t + c_i \Delta t))$$

in $\mathcal{P}^{l}([0, \Delta T], Q^{\mathrm{s}}) \times \mathcal{P}_{\mathbb{p}}^{l}([0, \Delta T], Q^{\mathrm{f}})$. With (3.43) we have to estimate the relation

$$\int_0^{\Delta T} \mathcal{L}(q_{\mathrm{EL}}^{\mathrm{s}}, q_{\mathrm{EL}}^{\mathrm{f}}, \dot{q}_{\mathrm{EL}}^{\mathrm{s}}, \dot{q}_{\mathrm{EL}}^{\mathrm{f}})\, dt - \Delta t \sum_{m=0}^{p-1} \sum_{i=1}^{r} b_i \mathcal{L}(\tilde{q}^{\mathrm{s}}(t_i^m), \dot{\tilde{q}}^{\mathrm{s}}(t_i^m), \tilde{q}^{\mathrm{f}}(t_i^m), \dot{\tilde{q}}^{\mathrm{f}}(t_i^m)). \tag{3.49a}$$

We expand this difference as

$$\begin{aligned}&\left(\int_0^{\Delta T} \mathcal{L}(q_{\mathrm{EL}}^{\mathrm{s}}, q_{\mathrm{EL}}^{\mathrm{f}}, \dot{q}_{\mathrm{EL}}^{\mathrm{s}}, \dot{q}_{\mathrm{EL}}^{\mathrm{f}})\, dt - \int_0^{\Delta T} \mathcal{L}(\hat{q}^{\mathrm{s}}, \check{q}^{\mathrm{f}}, \dot{\hat{q}}^{\mathrm{s}}, \dot{\check{q}}^{\mathrm{f}})\, dt\right) + \Big(\int_0^{\Delta T} \mathcal{L}(\hat{q}^{\mathrm{s}}, \check{q}^{\mathrm{f}}, \dot{\hat{q}}^{\mathrm{s}}, \dot{\check{q}}^{\mathrm{f}})\, dt - \\ &\Delta t \sum_{m=0}^{p-1} \sum_{i=1}^{r} b_i \mathcal{L}(\tilde{q}^{\mathrm{s}}(t_i^m), \dot{\tilde{q}}^{\mathrm{s}}(t_i^m), \tilde{q}^{\mathrm{f}}(t_i^m), \dot{\tilde{q}}^{\mathrm{f}}(t_i^m))\Big).\end{aligned} \tag{3.50}$$

We start with the first term of (3.50). From Lemma 3.4.1 we know that $q^{\mathrm{s}} - \hat{q}^{\mathrm{s}} = \mathcal{O}(\Delta T^{l+1})$ and $\dot{q}^{\mathrm{s}} - \dot{\hat{q}}^{\mathrm{s}} = \mathcal{O}(\Delta T^{l})$ on $[0, \Delta T]$ and $q^{\mathrm{f}} - \breve{q}^{\mathrm{f}} = \mathcal{O}(\Delta t^{l+1})$ and $\dot{q}^{\mathrm{f}} - \dot{\breve{q}}^{\mathrm{f}} = \mathcal{O}(\Delta t^{l})$ on $[m\Delta t, (m+1)\Delta t], m = 0, \ldots, \mathrm{p}-1$, hence

$$
\begin{aligned}
&\int_0^{\Delta T} \mathcal{L}(q^{\mathrm{s}}_{\mathrm{EL}}, q^{\mathrm{f}}_{\mathrm{EL}}, \dot{q}^{\mathrm{s}}_{\mathrm{EL}}, \dot{q}^{\mathrm{f}}_{\mathrm{EL}})\, dt - \int_0^{\Delta T} \mathcal{L}(\hat{q}^{\mathrm{s}}, \breve{q}^{\mathrm{f}}, \dot{\hat{q}}^{\mathrm{s}}, \dot{\breve{q}}^{\mathrm{f}})\, dt \\
&= \int_0^{\Delta T} \left(\frac{\partial \mathcal{L}(x_{\mathrm{EL}})}{\partial q^{\mathrm{s}}} (q^{\mathrm{s}}_{\mathrm{EL}} - \hat{q}^{\mathrm{s}}) + \frac{\partial \mathcal{L}(x_{\mathrm{EL}})}{\partial \dot{q}^{\mathrm{s}}} (\dot{q}^{\mathrm{s}}_{\mathrm{EL}} - \dot{\hat{q}}^{\mathrm{s}}) + \mathcal{O}(\Delta T^{2l}) \right) dt \\
&\quad + \sum_{m=0}^{\mathrm{p}-1} \int_{m\Delta t}^{(m+1)\Delta t} \left(\frac{\partial \mathcal{L}(x_{\mathrm{EL}})}{\partial q^{\mathrm{f}}} (q^{\mathrm{f}}_{\mathrm{EL}} - \breve{q}^{\mathrm{f}}) + \frac{\partial \mathcal{L}(x_{\mathrm{EL}})}{\partial \dot{q}^{\mathrm{f}}} (\dot{q}^{\mathrm{f}}_{\mathrm{EL}} - \dot{\breve{q}}^{\mathrm{f}}) + \mathcal{O}(\Delta t^{2l}) \right) dt \\
&= \int_0^{\Delta T} \left(\left(\frac{\partial \mathcal{L}(x_{\mathrm{EL}})}{\partial q^{\mathrm{s}}} - \frac{d}{dt} \frac{\mathcal{L}(x_{\mathrm{EL}})}{\partial \dot{q}^{\mathrm{s}}} \right) (q^{\mathrm{s}}_{\mathrm{EL}} - \hat{q}^{\mathrm{s}}) + \mathcal{O}(\Delta T^{2l}) \right) dt + \left(\frac{\partial \mathcal{L}(x_{\mathrm{EL}})}{\partial \dot{q}^{\mathrm{s}}} (q^{\mathrm{s}}_{\mathrm{EL}} - \hat{q}^{\mathrm{s}}) \right) \Bigg|_0^{\Delta T} \\
&\quad + \sum_{m=0}^{\mathrm{p}-1} \int_{m\Delta t}^{(m+1)\Delta t} \left(\left(\frac{\partial \mathcal{L}(x_{\mathrm{EL}})}{\partial q^{\mathrm{f}}} - \frac{d}{dt} \frac{\mathcal{L}(x_{\mathrm{EL}})}{\partial \dot{q}^{\mathrm{f}}} \right) (q^{\mathrm{f}}_{\mathrm{EL}} - \breve{q}^{\mathrm{f}}) + \mathcal{O}(\Delta t^{2l}) \right) dt \\
&\quad + \sum_{m=0}^{\mathrm{p}-1} \left(\frac{\partial \mathcal{L}(x_{\mathrm{EL}})}{\partial \dot{q}^{\mathrm{f}}} (q^{\mathrm{f}}_{\mathrm{EL}} - \breve{q}^{\mathrm{f}}) \right) \Bigg|_{m\Delta t}^{(m+1)\Delta t} \\
&= \int_0^{\Delta T} \left(- f^{\mathrm{s}}_{\mathrm{LC}}(x_{\mathrm{EL}}, u)(q^{\mathrm{s}}_{\mathrm{EL}} - \hat{q}^{\mathrm{s}}) + \mathcal{O}(\Delta T^{2l}) \right) dt \\
&\quad + \sum_{m=0}^{\mathrm{p}-1} \int_{m\Delta t}^{(m+1)\Delta t} \left(- f^{\mathrm{f}}_{\mathrm{LC}}(x_{\mathrm{EL}}, u)(q^{\mathrm{f}}_{\mathrm{EL}} - \breve{q}^{\mathrm{f}}) + \mathcal{O}(\Delta t^{2l}) \right) dt.
\end{aligned}
$$

For brevity we have used the following notation $x_{\mathrm{EL}} = (q^{\mathrm{s}}_{\mathrm{EL}}, q^{\mathrm{f}}_{\mathrm{EL}}, \dot{q}^{\mathrm{s}}_{\mathrm{EL}}, \dot{q}^{\mathrm{f}}_{\mathrm{EL}})$. For the first equality we have used Taylor expansion for the second integrand around $(q^{\mathrm{s}}_{\mathrm{EL}}, q^{\mathrm{f}}_{\mathrm{EL}})$ and the estimates for the polynomial interpolation (Lemma 3.4.1) where we have rewritten the integral involving fast derivatives as sum of integrals defined on the micro intervals. The second equality follows from applying integration by parts. The last equality follows since the boundary terms vanish because $\hat{q}^{\mathrm{s}}(0) = q^{\mathrm{s}}_{\mathrm{EL}}(0)$ and $\hat{q}^{\mathrm{s}}(\Delta T) = q^{\mathrm{s}}_{\mathrm{EL}}(\Delta T)$ as well as $\breve{q}^{\mathrm{f}}(m\Delta t) = q^{\mathrm{f}}_{\mathrm{EL}}(m\Delta t)$ for $m = 0, \ldots, \mathrm{p}$ and since $(q^{\mathrm{s}}_{\mathrm{EL}}, q^{\mathrm{f}}_{\mathrm{EL}})$ solves the forced Euler-Lagrange equation. For generic forces we have $f^{\mathrm{s/f}}_{\mathrm{LC}}(q_{\mathrm{EL}}, \dot{q}_{\mathrm{EL}}, u) = \mathcal{O}(1)$, $q^{\mathrm{s}}_{\mathrm{EL}} - \hat{q}^{\mathrm{s}} = \mathcal{O}\left(\Delta T^{l+1}\right)$ on $[0, \Delta T]$ and $q^{\mathrm{f}}_{\mathrm{EL}} - \breve{q}^{\mathrm{f}} = \mathcal{O}\left(\Delta t^{l+1}\right)$ on $[m\Delta t, (m+1)\Delta t], m = 0, \ldots, \mathrm{p}-1$. So we can estimate the first terms in the integrals only by $\mathcal{O}\left(\Delta T^{l+1}\right)$ and $\mathcal{O}\left(\Delta t^{l+1}\right)$, respectively. Thus, we find

$$
\begin{aligned}
&\int_0^{\Delta T} \mathcal{L}(q^{\mathrm{s}}_{\mathrm{EL}}, q^{\mathrm{f}}_{\mathrm{EL}}, \dot{q}^{\mathrm{s}}_{\mathrm{EL}}, \dot{q}^{\mathrm{f}}_{\mathrm{EL}})\, dt - \int_0^{\Delta T} \mathcal{L}(\hat{q}^{\mathrm{s}}, \breve{q}^{\mathrm{f}}, \dot{\hat{q}}^{\mathrm{s}}, \dot{\breve{q}}^{\mathrm{f}})\, dt \\
&\quad = \int_0^{\Delta T} \mathcal{O}\left(\Delta T^{l+1}\right)\, dt + \sum_{m=0}^{\mathrm{p}-1} \int_{m\Delta t}^{(m+1)\Delta t} \mathcal{O}\left(\Delta t^{l+1}\right)\, dt
\end{aligned}
$$

$$=\mathcal{O}\left(\Delta T^{l+2}\right)+\sum_{m=0}^{\mathrm{p}-1}\mathcal{O}\left((m+1)^{l+2}-m^{l+2})\Delta t^{l+2}\right)=\mathcal{O}\left(\Delta T^{l+2}\right) \tag{3.51}$$

since $\sum_{m=0}^{\mathrm{p}-1}\left((m+1)^{l+2}-m^{l+2})\right)=\mathrm{p}^{l+2}$ and $\mathrm{p}\Delta t=\Delta T$. To bound the second term of (3.50) we follow the arguments of [111, Theorem 3.3]. Since $(\tilde{q}^{\mathrm{s}},\tilde{q}^{\mathrm{f}})$ is the minimising element of $\mathcal{P}^l([0,\Delta T],Q^{\mathrm{s}})\times\mathcal{P}^l_{\mathrm{p}}([0,\Delta T],Q^{\mathrm{f}})$, we have

$$\Delta t\sum_{m=0}^{\mathrm{p}-1}\sum_{i=1}^{r}b_i\mathcal{L}(\tilde{q}^{\mathrm{s}}(t_i^m),\dot{\tilde{q}}^{\mathrm{s}}(t_i^m),\tilde{q}^{\mathrm{f}}(t_i^m),\dot{\tilde{q}}^{\mathrm{f}}(t_i^m))\leq\Delta t\sum_{m=0}^{\mathrm{p}-1}\sum_{i=1}^{\mathrm{s}}b_i\mathcal{L}(\hat{q}^{\mathrm{s}}(t_i^m),\check{q}^{\mathrm{f}}(t_i^m),\dot{\hat{q}}^{\mathrm{s}}(t_i^m),\dot{\check{q}}^{\mathrm{f}}(t_i^m))$$
$$=\sum_{m=0}^{\mathrm{p}-1}\int_{m\Delta t}^{(m+1)\Delta t}\mathcal{L}(\hat{q}^{\mathrm{s}},\check{q}^{\mathrm{f}},\dot{\hat{q}}^{\mathrm{s}},\dot{\check{q}}^{\mathrm{f}})\,dt+\mathcal{O}(\Delta t^{w+1})=\int_0^{\Delta T}\mathcal{L}(\hat{q}^{\mathrm{s}},\check{q}^{\mathrm{f}},\dot{\hat{q}}^{\mathrm{s}},\dot{\check{q}}^{\mathrm{f}})\,dt+\mathrm{p}\,\mathcal{O}(\Delta t^{w+1}).$$

On the other hand, since q_{EL} minimises the continuous action, there holds

$$\begin{aligned}
&\Delta t\sum_{m=0}^{\mathrm{p}-1}\sum_{i=1}^{r}b_i\mathcal{L}(\tilde{q}^{\mathrm{s}}(t_i^m),\dot{\tilde{q}}^{\mathrm{s}}(t_i^m),\tilde{q}^{\mathrm{f}}(t_i^m),\dot{\tilde{q}}^{\mathrm{f}}(t_i^m))\\
&=\int_0^{\Delta T}\mathcal{L}(\tilde{q}^{\mathrm{s}},\tilde{q}^{\mathrm{f}},\dot{\tilde{q}}^{\mathrm{s}},\dot{\tilde{q}}^{\mathrm{f}})\,dt+\mathrm{p}\,\mathcal{O}(\Delta t^{w+1})\\
&\geq\int_0^{\Delta T}\mathcal{L}(q_{\mathrm{EL}}^{\mathrm{s}},q_{\mathrm{EL}}^{\mathrm{f}},\dot{q}_{\mathrm{EL}}^{\mathrm{s}},\dot{q}_{\mathrm{EL}}^{\mathrm{f}})\,dt+\mathrm{p}\,\mathcal{O}(\Delta t^{w+1})\\
&=\int_0^{\Delta T}\mathcal{L}(\hat{q}^{\mathrm{s}},\check{q}^{\mathrm{f}},\dot{\hat{q}}^{\mathrm{s}},\dot{\check{q}}^{\mathrm{f}})\,dt+\mathcal{O}\left(\Delta T^{l+2}\right)+\mathrm{p}\,\mathcal{O}(\Delta t^{w+1}),
\end{aligned}$$

where the last line follows from (3.51). Combining both inequalities we find

$$\begin{aligned}
&\int_0^{\Delta T}\mathcal{L}(\hat{q}^{\mathrm{s}},\check{q}^{\mathrm{f}},\dot{\hat{q}}^{\mathrm{s}},\dot{\check{q}}^{\mathrm{f}})\,dt-\Delta t\sum_{m=0}^{\mathrm{p}-1}\sum_{i=1}^{r}b_i\mathcal{L}(\tilde{q}^{\mathrm{s}}(t_i^m),\dot{\tilde{q}}^{\mathrm{s}}(t_i^m),\tilde{q}^{\mathrm{f}}(t_i^m),\dot{\tilde{q}}^{\mathrm{f}}(t_i^m))\\
&=\mathcal{O}\left(\Delta T^{l+2}\right)+\mathrm{p}\,\mathcal{O}(\Delta t^{w+1})
\end{aligned}\tag{3.52}$$

Equations (3.51) and (3.52) together imply the desired result (3.48). □

For $\mathrm{p}=1$, the order of the discrete Lagrangian defined on a macro step is $\min(l+1,w)$. Keeping the micro time step the same, for $\mathrm{p}>1$, the error term corresponding to the quadrature error $\mathrm{p}\,\mathcal{O}(\Delta t^{w+1})$ is increased, nevertheless the order stays the same for constant p.

Lemma 3.4.2. *Let $\hat{L}_d^k$ be a multirate discrete Lagrangian according to* (3.36)*, then under the same assumptions as in Theorem 3.4.3 the discrete Lagrangian $\hat{L}_d^k$ approximates the regular continuous Lagrangian $\mathcal{L}$ with*

- *order* 2 *for the midpoint rule ($(\alpha,\gamma)=(\beta,\mu)=(1,\frac{1}{2})$)*

- *order* 2 *for the trapezoidal rule* $((\alpha, \gamma) = (\beta, \mu) = (\frac{1}{2}, 1))$
- *order* 1 *for the left and right rectangular rule* $((\alpha, \beta \in \{0, 1\}, \gamma = \mu = 1)$

Proof. The statement follows directly from Theorem 3.4.3 and the orders of the used quadrature rules. The discrete Lagrangian given in (3.36) can be written as the multirate discrete Lagrangian (3.46) with $l = 1$, $r = 1, (b_1, c_1) = (1, \frac{1}{2})$ for midpoint rule and with $l = 1$, $r = 2, b_1 = b_2 = \frac{1}{2}, c_1 = 0, c_2 = 1$ for trapezoidal rule which are both second order quadrature rules ($w = 2$). The rectangle rules correspond to the multirate discrete Lagrangian (3.46) with $r = 1, b_1 = 1, c_1 \in \{0, 1\}$ being a first order quadrature rule ($w = 1$). □

Remark 3.4.5. *The discrete approximation of the external forces has no influence on the order of the discrete Lagrangian as long as the external forces act orthogonal.*

Remark 3.4.6. *In contrast to the conservative case (no external forces), here, due to the consideration of forced systems, we obtain no superconvergence as a theoretical result (i.e. a convergence rate of* $\min(2l, w)$ *[26]). Nevertheless, for the considered approximation rules (midpoint, trapezoidal and rectangle rule) we obtain the correct orders as also demonstrated numerically for the midpoint rule in Chapter 4.*

Assumption 3.4.2. *We assume that the slow forces depend only on the control and the slow varying configuration variables. Additionally, we assume that the fast forces act only on the macro time nodes and thus based on the discrete Lagrange-d'Alembert principle* (3.23)*, they only appear in equation* (3.24b) *but not in* (3.24c)*.In Hamiltonian formulation that translates to forces in equation* (3.30c)*,* (3.30d) *only for* $m = 0, \mathbb{p}$.

From this assumption and (3.45), the exact slow forces become

$$F^{\mathrm{s},-}_{\mathrm{E},0} := F^{\mathrm{s},-}_{\mathrm{LC,E}}(q^{\mathrm{s}}(0), q^{\mathrm{s}}(\Delta T), u|_{[0,\Delta T]}) = \int_0^{\Delta T} f^{\mathrm{s}}_{\mathrm{LC}}(q^{\mathrm{s}}(t), \dot{q}^{\mathrm{s}}(t), u(t)) \frac{\partial q^{\mathrm{s}}(t)}{\partial q^{\mathrm{s}}_0} dt, \quad (3.53a)$$

$$F^{\mathrm{s},+}_{\mathrm{E},0} := F^{\mathrm{s},+}_{\mathrm{LC,E}}(q^{\mathrm{s}}(0), q^{\mathrm{s}}(\Delta T), u|_{[0,\Delta T]}) = \int_0^{\Delta T} f^{\mathrm{s}}_{\mathrm{LC}}(q^{\mathrm{s}}(t), \dot{q}^{\mathrm{s}}(t), u(t)) \frac{\partial q^{\mathrm{s}}(t)}{\partial q^{\mathrm{s}}_1} dt. \quad (3.53b)$$

To approximate them on the discrete time grids consider the discrete forces

$$
\begin{aligned}
&F^{\mathrm{s},+}_{\mathrm{LC,d}}(q^{\mathrm{s}}_0, q^{\mathrm{s}}_1, u_0) = \\
&\quad \sum_{m=0}^{\mathrm{p}-1} \Delta t \Bigg(\eta f^{\mathrm{s}}_{\mathrm{LC}} \Big(\nu q_0^{\mathrm{s},m} + (1-\nu) q_0^{\mathrm{s},m+1}, \frac{q_0^{\mathrm{s},m+1} - q_0^{\mathrm{s},m}}{\Delta t}, u(\nu \Delta t) \Big) \frac{\partial (\nu q_0^{\mathrm{s},m} + (1-\nu) q_0^{\mathrm{s},m+1})}{\partial q_0^{\mathrm{s,m+1}}} \\
&\quad + (1-\eta) f^{\mathrm{s}}_{\mathrm{LC}} \Big((1-\nu) q_0^{\mathrm{s},m} + \nu q_0^{\mathrm{s},m+1}, \frac{q_0^{\mathrm{s},m+1} - q_0^{\mathrm{s},m}}{\Delta t}, u((1-\nu)\Delta t) \Big) \frac{\partial ((1-\nu) q_0^{\mathrm{s},m} + \nu q_0^{\mathrm{s},m+1})}{\partial q_0^{\mathrm{s,m+1}}} \Bigg), \\
&F^{\mathrm{s},-}_{\mathrm{LC,d}}(q^{\mathrm{s}}_0, q^{\mathrm{s}}_1, u_0) = \\
&\quad \sum_{m=0}^{\mathrm{p}-1} \Delta t \Bigg(\eta f^{\mathrm{s}}_{\mathrm{LC}} \Big(\nu q_0^{\mathrm{s},m} + (1-\nu) q_0^{\mathrm{s},m+1}, \frac{q_0^{\mathrm{s},m+1} - q_0^{\mathrm{s},m}}{\Delta t}, u(\nu \Delta t) \Big) \frac{\partial (\nu q_0^{\mathrm{s},m} + (1-\nu) q_0^{\mathrm{s},m+1})}{\partial q_0^{\mathrm{s,m}}} \\
&\quad + (1-\eta) f^{\mathrm{s}}_{\mathrm{LC}} \Big((1-\nu) q_0^{\mathrm{s},m} + \nu q_0^{\mathrm{s},m+1}, \frac{q_0^{\mathrm{s},m+1} - q_0^{\mathrm{s},m}}{\Delta t}, u((1-\nu)\Delta t) \Big) \frac{\partial ((1-\nu) q_0^{\mathrm{s},m} + \nu q_0^{\mathrm{s},m+1})}{\partial q_0^{\mathrm{s,m}}} \Bigg).
\end{aligned}
$$

Theorem 3.4.4. *Let Assumption 3.4.2 hold and let $F^{s,\pm}_{\mathrm{LC,d}}$ defined as in* (3.54) *be a multirate discretisation of the forces $f^{\mathrm{s}}_{\mathrm{LC}}(q^{\mathrm{s}}(t), \dot{q}^{\mathrm{s}}(t), u(t))$. Then the local error for the discrete force approximation is*

$$
\begin{aligned}
&F^{s,\pm}_{\mathrm{LC,d}}(q^{\mathrm{s}}(0), q^{\mathrm{s}}(\Delta T), \{u(\nu \Delta T), u((1-\nu)\Delta T)\}) \qquad (3.54) \\
&= F^{s,\pm}_{\mathrm{LC,E}}(q^{\mathrm{s}}(0), q^{\mathrm{s}}(\Delta T), u|_{[0,\Delta T]}) + \begin{cases} \mathcal{O}((\Delta T)^3) \text{ for } \eta = 1, \nu = \frac{1}{2} \text{ (midpoint rule)} \\ \mathcal{O}((\Delta T)^3) \text{ for } \eta = \frac{1}{2}, \nu = 1 \text{ (trapezoidal rule)} \\ \mathcal{O}((\Delta T)^2) \text{ for } \eta \in \{0,1\}, \nu = 1 \text{ (rectangle rule)} \end{cases}
\end{aligned}
$$

Proof. Using Taylor expansion we have

$$
\begin{aligned}
F^{\mathrm{s},-}_{E,0}(q^{\mathrm{s}}(0), q^{\mathrm{s}}(\Delta T), u|_{[0,\Delta T]}) &= \Delta T f^{\mathrm{s}}_{\mathrm{LC}}\Big|_{t=0} \frac{\partial q^{\mathrm{s}}}{\partial q^{\mathrm{s}}_0}\Big|_{t=0} + \frac{(\Delta T)^2}{2} f^{\mathrm{s}}_{\mathrm{LC}}\Big|_{t=0} \frac{\partial \dot{q}^{\mathrm{s}}(0)}{\partial q^{\mathrm{s}}_0} \\
+ \frac{(\Delta T)^2}{2} \frac{\partial q^{\mathrm{s}}}{\partial q^{\mathrm{s}}_0}\Big|_{t=0} \Big(\frac{\partial f^{\mathrm{s}}}{\partial q^{\mathrm{s}}}\Big|_{t=0} \dot{q}^{\mathrm{s}}(0) + \frac{\partial f^{\mathrm{s}}}{\partial \dot{q}^{\mathrm{s}}}\Big|_{t=0} \ddot{q}^{\mathrm{s}}(0) + \frac{\partial f^{\mathrm{s}}}{\partial u}\Big|_{t=0} \dot{u}(0) \Big) &+ \mathcal{O}((\Delta T)^3). \qquad (3.55)
\end{aligned}
$$

From the boundary conditions $q^{\mathrm{s}}(0) = q^{\mathrm{s}}_0, \dot{q}^{\mathrm{s}}(0) = \dot{q}^{\mathrm{s}}_0$ it follows $\frac{\partial q^{\mathrm{s}}(0)}{\partial q^{\mathrm{s}}_0} = 1$, $\frac{\partial \dot{q}^{\mathrm{s}}(0)}{\partial q^{\mathrm{s}}_0} = 0$ and thus (3.55) simplifies to

$$
\begin{aligned}
&F^{\mathrm{s},-}_{E,0}(q^{\mathrm{s}}(0), q^{\mathrm{s}}(\Delta T), u|_{[0,\Delta T]}) = \qquad (3.56) \\
&\quad \Delta T f^{\mathrm{s}}_{\mathrm{LC}}\Big|_{t=0} + \frac{\Delta T^2}{2} \Big(\frac{\partial f^{\mathrm{s}}}{\partial q^{\mathrm{s}}}\Big|_{t=0} \dot{q}^{\mathrm{s}}(0) + \frac{\partial f^{\mathrm{s}}}{\partial \dot{q}^{\mathrm{s}}}\Big|_{t=0} \ddot{q}^{\mathrm{s}}(0) + \frac{\partial f^{\mathrm{s}}}{\partial u}\Big|_{t=0} \dot{u}(0) \Big) + \mathcal{O}((\Delta T)^3).
\end{aligned}
$$

The order of a given discrete forces can be calculated by expanding the expression for $F^{\mathrm{s},\pm}_{\mathrm{d},0}$ in a Taylor series and comparing this to the same expansion for the exact

discrete forces $F^{\mathrm{s},\pm}_{\mathrm{E},0}$, a technique similar to what was used for the order of Lagrangian in the singlerate case by [20]. If the series agrees up to r terms, then the discrete force approximation is of order r.

To begin, we note that $u^{\mathrm{s}}((1-\nu)t_0+\nu t_1) = u^{\mathrm{s}}(\nu\Delta t)$, $u^{\mathrm{s}}(\nu t_0+(1-\nu)t_1) = u^{\mathrm{s}}((1-\nu)\Delta t)$ for $t_0=0, t_1=\Delta t$. Using the following expansion

$$q_1^{\mathrm{s}} = q_0^{\mathrm{s}} + \Delta T\dot{q}_0^{\mathrm{s}} + \frac{(\Delta T)^2}{2}\ddot{q}_0^{\mathrm{s}} + \mathcal{O}(\Delta T)^3$$

and Equation (3.16) we have:

$$\nu q_0^{\mathrm{s},m}+(1-\nu)q_0^{\mathrm{s},m+1} = q_0^{\mathrm{s}}+(\nu b^m+(1-\nu)b^{m+1})(\Delta T\dot{q}_0^{\mathrm{s}}+\frac{(\Delta T)^2}{2}\dot{q}_0^{\mathrm{s}}+\mathcal{O}((\Delta T)^3) \tag{3.57a}$$

$$(1-\nu)q_0^{\mathrm{s},m}+\nu q_0^{\mathrm{s},m+1} = q_0^{\mathrm{s}}+((1-\nu)b^m+\nu b^{m+1})(\Delta T\dot{q}_0^{\mathrm{s}}+\frac{(\Delta T)^2}{2}\dot{q}_0^{\mathrm{s}}+\mathcal{O}((\Delta T)^3) \tag{3.57b}$$

$$\frac{q_0^{\mathrm{s},m+1}-q_0^{\mathrm{s},m}}{\Delta t} = q_0^{\mathrm{s}}+\Delta T\dot{q}_0^{\mathrm{s}}+\frac{(\Delta T)^2}{2}\ddot{q}_0^{\mathrm{s}}+\mathcal{O}((\Delta T)^3) \tag{3.57c}$$

$$\frac{\partial(\nu q_0^{\mathrm{s},m}+(1-\nu)q_0^{\mathrm{s},m+1})}{\partial q_0^{\mathrm{s},m}} = \frac{\partial((1-\nu)q_0^{\mathrm{s},m}+\nu q_0^{\mathrm{s},m+1})}{\partial q_0^{\mathrm{s},m}} = 1. \tag{3.57d}$$

Now coming back to (3.54) and using (3.57d), (3.57c) we have

$$F^{\mathrm{s},-}_{\mathrm{LC,d}}(q_0^{\mathrm{s}},q_1^{\mathrm{s}},u_0) = \sum_{m=0}^{\mathbb{p}-1}\Delta t\Bigg(\eta f^{\mathrm{s}}_{\mathrm{LC}}\Big(\nu q_0^{\mathrm{s},m}+(1-\nu)q_0^{\mathrm{s},m+1}, \tfrac{q_0^{\mathrm{s},m+1}-q_0^{\mathrm{s},m}}{\Delta t}, u(\nu\Delta t)\Big)+$$
$$+(1-\eta)f^{\mathrm{s}}_{\mathrm{LC}}\Big((1-\nu)q_0^{\mathrm{s},m}+\nu q_0^{\mathrm{s},m+1}, \tfrac{q_0^{\mathrm{s},m+1}-q_0^{\mathrm{s},m}}{\Delta t}, u((1-\nu)\Delta t)\Big)\Bigg).$$

We can expand this expression using a multi-variable Taylor expansion. For the readability of the presentation, we will do so variable by variable and combine the results for a final approximation. First, on the micro time scale we have:

$$\begin{aligned}
&f^{\mathrm{s}}_{\mathrm{LC}}\Big(\nu q_0^{\mathrm{s},m}+(1-\nu)q_0^{\mathrm{s},m+1}, \dot{q}_0^{\mathrm{s}}, u_0\Big)\\
&\quad= f_{\mathrm{LC}}\Big(q_0^{\mathrm{s}}+(\nu b^m+(1-\nu)b^{m+1})(\Delta T\dot{q}_0^{\mathrm{s}}+\frac{(\Delta T)^2}{2}\ddot{q}_0^{\mathrm{s}}+\mathcal{O}((\Delta T)^3), \dot{q}_0^{\mathrm{s}}, u_0\Big)\\
&\quad= f^{\mathrm{s}}_{\mathrm{LC}}\Big|_{x_0}+\Big(\frac{m+1-\nu}{\mathbb{p}}\Big)\Delta T\dot{q}_0^{\mathrm{s}}\frac{\partial f_{\mathrm{LC}}}{\partial q_0^{\mathrm{s}}}\Big|_{x_0}+\mathcal{O}((\Delta T)^2)\\
&f^{\mathrm{s}}_{\mathrm{LC}}\Big(q_0^{\mathrm{s}}, \frac{q_0^{\mathrm{s},m+1}-q_0^{\mathrm{s},m}}{\Delta t}, u_0\Big) = f_{\mathrm{LC}}\Big(q_0^{\mathrm{s}}, \dot{q}_0^{\mathrm{s}}+\frac{\Delta T}{2}\ddot{q}_0^{\mathrm{s}}+\mathcal{O}(\Delta T)^2, q_0^{\mathrm{f},0}, u_0\Big)\\
&\quad= f^{\mathrm{s}}_{\mathrm{LC}}\Big|_{x_0}+\frac{\Delta T}{2}\dot{q}_0^{\mathrm{s}}\frac{\partial f_{\mathrm{LC}}}{\partial \dot{q}_0^{\mathrm{s}}}\Big|_{x_0}+\mathcal{O}((\Delta T)^2)
\end{aligned}$$

$$f^{\mathrm{s}}_{\mathrm{LC}}\Big(q^{\mathrm{s}}_0, \dot{q}^{\mathrm{s}}_0, \dot{q}^{\mathrm{f}}_0, u(\nu m\Delta t + (1-\nu)m\Delta t)\Big) = f^{\mathrm{s}}_{\mathrm{LC}}\Big(q^{\mathrm{s}}_0, \dot{q}^{\mathrm{s}}_0, \dot{q}^{\mathrm{f}}_0, u^{\mathrm{s}}(0)+\nu\Delta t\dot{u}(0)+\mathcal{O}((\Delta t)^2)\Big)$$
$$= f^{\mathrm{s}}_{\mathrm{LC}}\Big|_{x_0} + (m+1-\nu)\Delta t \frac{\partial f^{\mathrm{s}}_{\mathrm{LC}}}{\partial u^{\mathrm{s}}_0}\Big|_{x_0} \dot{u}(0) + \mathcal{O}((\Delta t)^2)$$

where $(q^{\mathrm{s}}_0, \dot{q}^{\mathrm{f}}_0, u_0) = x_0$. Similarly

$$f^{\mathrm{s}}_{\mathrm{LC}}((1-\nu)q^{\mathrm{s},m}_0 + \nu q^{\mathrm{s},m+1}_0, \dot{q}^{\mathrm{s}}_0, u_0) = f^{\mathrm{s}}_{\mathrm{LC}}\Big|_{x_0} + \Big(\frac{m+\nu}{\mathbb{p}}\Big)\Delta T \dot{q}^{\mathrm{s}}_0 \frac{\partial f_{\mathrm{LC}}}{\partial q^{\mathrm{s}}_0}\Big|_{x_0} + \mathcal{O}((\Delta T)^2),$$
$$f^{\mathrm{s}}_{\mathrm{LC}}\Big(q^{\mathrm{s}}_0, \dot{q}^{\mathrm{s}}_0, \dot{q}^{\mathrm{f}}_0, u((1-\nu)m\Delta t + \nu m\Delta t)\Big) = f^{\mathrm{s}}_{\mathrm{LC}}\Big|_{x_0} + (m+\nu)\Delta t \frac{\partial f^{\mathrm{s}}_{\mathrm{LC}}}{\partial u_0}\Big|_{x_0} \dot{u}(0) + \mathcal{O}((\Delta t)^2)$$

Using these results, we can sum over the first macro time step

$$\sum_{m=0}^{\mathbb{p}-1} \Delta t\Big(\eta f^{\mathrm{s}}_{\mathrm{LC}}(q^{\mathrm{s}}_0, \tfrac{q^{\mathrm{s},m+1}_0 - q^{\mathrm{s},m}_0}{\Delta t}, u_0) + (1-\eta)\eta f^{\mathrm{s}}_{\mathrm{LC}}(q^{\mathrm{s}}_0, \tfrac{q^{\mathrm{s},m+1}_0 - q^{\mathrm{s},m}_0}{\Delta t}, u_0)\Big)$$
$$= \Delta T f^{\mathrm{s}}_{\mathrm{LC}}\Big|_{x_0} + \frac{(\Delta T)^2}{2}\dot{q}^{\mathrm{s}}_0 \frac{\partial f^{\mathrm{s}}_{\mathrm{LC}}}{\partial q^{\mathrm{s}}_0}\Big|_{x_0} + \mathcal{O}((\Delta T)^3), \tag{3.58a}$$

$$\sum_{m=0}^{\mathbb{p}-1} \Delta t\Big(\eta f^{\mathrm{s}}_{\mathrm{LC}}(q^{\mathrm{s}}_0, \dot{q}^{\mathrm{s}}_0, u(\nu\Delta t)) + (1-\eta) f^{\mathrm{s}}_{\mathrm{LC}}(q^{\mathrm{s}}_0, \dot{q}^{\mathrm{s}}_0, u((1-\nu)\Delta t))\Big)$$
$$= \Delta T f^{\mathrm{s}}_{\mathrm{LC}}\Big|_{x_0} + (\Delta t)^2(\eta+\nu+m-2\eta\nu)\dot{u}(0)\frac{\partial f^{\mathrm{s}}_{\mathrm{LC}}}{\partial u_0}\Big|_{x_0} + \mathcal{O}((\Delta T)^3), \tag{3.58b}$$

$$\sum_{m=0}^{\mathbb{p}-1} \Delta t\Big(\eta f^{\mathrm{s}}_{\mathrm{LC}}\Big(\nu q^{\mathrm{s},m}_0 + (1-\nu)q^{\mathrm{s},m+1}_0, \dot{q}^{\mathrm{s}}_0, u_0\Big) + (1-\eta) f^{\mathrm{s}}_{\mathrm{LC}}((1-\nu)q^{\mathrm{s},m}_0 + \nu q^{\mathrm{s},m+1}_0, \dot{q}^{\mathrm{s}}_0, u_0)\Big)$$
$$= \Delta T f^{\mathrm{s}}_{\mathrm{LC}}\Big|_{x_0} + \sum_{m=0}^{\mathbb{p}-1}\Big(\frac{\eta+\nu+m-2\eta\nu}{\mathbb{p}}\Big)\Delta t\Delta T \dot{q}^{\mathrm{s}}_0 \frac{\partial f_{\mathrm{LC}}}{\partial q^{\mathrm{s}}_0}\Big|_{x_0} + \mathcal{O}((\Delta T)^3), \tag{3.58c}$$

Combining these results Equation (3.54) becomes

$$F^{\mathrm{s},-}_{\mathrm{LC,d}}(q^{\mathrm{s}}_0, q^{\mathrm{s}}_1, u_0) = \Delta T f^{\mathrm{s}}_{\mathrm{LC}}\Big|_{x_0} + \tag{3.59}$$
$$\frac{(\Delta T)^2}{2}\sum_{m=0}^{\mathbb{p}-1}\frac{2(\eta+\nu+m-2\eta\nu)}{\mathbb{p}^2}\Big(\dot{q}^{\mathrm{s}}_0\frac{\partial f_{\mathrm{LC}}}{\partial q^{\mathrm{s}}_0}\Big|_{x_0} + \dot{q}^{\mathrm{s}}_0\frac{\partial f^{\mathrm{s}}_{\mathrm{LC}}}{\partial q^{\mathrm{s}}_0}\Big|_{x_0} + \dot{u}(0)\frac{\partial f^{\mathrm{s}}_{\mathrm{LC}}}{\partial u_0}\Big|_{x_0}\Big) + \mathcal{O}((\Delta T)^3).$$

Comparing Equation (3.59) with Equation (3.56) the order of the discrete force approximation on the macro scale is:

- of order 2 for $\eta = 1, \nu = \frac{1}{2}$ as $\sum_{m=0}^{\mathbb{p}-1}\frac{2(\eta+\nu+m-2\eta\nu)}{\mathbb{p}^2} = 1$
- of order 2 for $\eta = \frac{1}{2}, \nu = 1$ as $\sum_{m=0}^{\mathbb{p}-1}\frac{2(\eta+\nu+m-2\eta\nu)}{\mathbb{p}^2} = 1$
- of order 1 for $\eta \in \{0,1\}, \nu = 1$ as $\sum_{m=0}^{\mathbb{p}-1}\frac{\eta+\nu+m-2\eta\nu}{\mathbb{p}^2} = \frac{\mathbb{p}+1}{2\mathbb{p}}$

The same order can analogously be shown for $F^{\mathrm{s},+}_{\mathrm{LC,d}}$ as defined in (3.20), (3.38). □

Remark 3.4.7. *Following Assumption 3.4.2 the exact fast forces* $F_{\mathrm{E},0}^{\mathrm{f},\pm}$ *and their discretisation* $F_{\mathrm{LC,d}}^{\mathrm{f},\pm}$ *can be defined in a similar way to the slow forces* (3.53), (3.54) *depending only on the fast values at the macro time node* $q_k^{f,0}$, *for* $k = 0, \dots, N-1$ *with linear interpolation in between for the approximation of* $q_k^{f,m}$, *for* $k = 0, \dots, N-1$, $m = 1, \dots, \mathbb{p}-1$. *Analogously to Theorem 3.4.4 a new theorem can be formulated to show that the fast forces respecting Assumptions 3.4.1 and 3.4.2 are approximated with the same order as the slow forces if the same quadrature rules are being used.*

Lemma 3.4.3. *Consider a system described by a regular Lagrangian* $\mathcal{L}$ *of the form* (5.7) *and the Lagrangian control forces* $f_{\mathrm{LC}}^{\mathrm{s}}, f_{\mathrm{LC}}^{\mathrm{f}}$. *Consider the discrete approximation of these expressions* $L_{\mathrm{d},k} = \mathbb{T}_{\mathrm{d},k} - \mathbb{U}_{\mathrm{d},k} - \mathbb{P}_{\mathrm{d},k}$ *based on the approximation in* (3.42) *and* $F_{\mathrm{LC,d}}^{\mathrm{s},\pm}$, $F_{\mathrm{LC,d}}^{\mathrm{f},\pm}$ *as expressed in* (3.54) *and Remark 3.4.7. Under Assumption 3.4.1, Assumption 3.4.2 and the assumptions of Theorem 3.4.3, the resulting multirate variational model* (3.24) *or* (3.30) *is of order* 2 *when only midpoint or trapezoidal quadrature is chosen within* $L_{\mathrm{d},k}$, $F_{\mathrm{LC,d}}^{\mathrm{s},\pm}$ *and* $F_{\mathrm{LC,d}}^{\mathrm{f},\pm}$. *The order reduces to* 1 *if rectangular quadrature is used anywhere within these discrete approximations.*

Proof. Consider $\hat{L}_{\mathrm{d},k}$ based on (3.36) as the discrete approximation of $\mathcal{L}$. The order of approximation of the Lagrangian and the forces then follows from Lemma 3.4.2, Theorem 3.4.4 and Remark 3.4.7. The order of the resulting variational model then follows from Statement 3.4.1. The same order of accuracy is achieved from the variational model derived from the considered $L_{\mathrm{d},k}$ due to Proposition 3.4.1. □

Remark 3.4.8. *Assumption 3.4.1 on the orthogonality of forces is the same as the condition in the forced Noether's theorem 3.3.1 leading to conservation of momentum maps in presence of a symmetry actions. While we would expect the same order result for general forced systems, a proof would have to rely on other (not action minimiser) techniques which is still an open research question. In practice, orthogonal forces are such forces which change only the direction of the motion but not the kinetic energy of the system. Roughly speaking such a force would only steer the system but not (de-)accelerating the system.*

3.5 Discrete variational mechanics for forced constrained systems

Consider the continuous constrained system presented in Section 2.2.3. In the absence of constraints, its multirate formulation was presented in Section 3.4. We now describe how constraints can be accounted for in the discrete model.

First, changing coordinate systems let $g(q^{\mathrm{s}}, q^{\mathrm{f}}) = \mathfrak{g}(q(t)) = 0$ and $h(q^{\mathrm{s}}, q^{\mathrm{f}}, \lambda) = \lambda(t)^T \mathfrak{g}(q^{\mathrm{s}}, q^{\mathrm{f}})$. To discretise the constrained system, one can formulate a discrete augmented Lagrangian analogously to the continuous case in Section 2.2.3 and then reuse the multirate discrete virtual work description, the multirate discrete Lagrange-d'Alembert principle and the multirate forced discrete Legendre transforms defined in the unconstrained case in Section 3.4.1. As suggested by [3], in the multirate discrete setting, the trajectory of the Lagrangian multipliers can be described as

$$\lambda_{\mathrm{d}} := \{\lambda_k\}_{k=0}^{N-1}, \;\; \lambda_k := \{\lambda_k^m\}_{m=0}^{\mathbb{p}} \quad \text{where} \;\; \lambda_k^m \approx \lambda(t_k^m), \;\; \lambda_{k-1}^{\mathbb{p}} = \lambda_k^0.$$

We define the discrete constraints $h_{\mathrm{d}} : Q^{\mathrm{s}} \times Q^{\mathrm{s}} \times (Q^{\mathrm{f}})^{\mathbb{p}+1} \times \mathbb{R}^m \mapsto \mathbb{R}$ as

$$h_{\mathrm{d}}^k = h_{\mathrm{d}}(q_k^{\mathrm{s}}, q_{k+1}^{\mathrm{s}}, q_k^{\mathrm{f}}, \lambda_k) \approx \int_{t_k}^{t_{k+1}} h(q_{\mathrm{s}}, q^{\mathrm{f}}, \lambda) dt.$$

Thus the discrete augmented Lagrangian on the macro grid can be written as

$$L_{\mathrm{d}}^{\mathrm{c},k} = L_{\mathrm{d}}^{\mathrm{c}}(q_k^{\mathrm{s}}, q_{k+1}^{\mathrm{s}}, q_k^{\mathrm{f}}, \lambda_k) = L_{\mathrm{d}}^k - h_{\mathrm{d}}^k \approx \int_{t_k}^{t_{k+1}} \Big(\mathcal{L}(q^{\mathrm{s}}, \dot{q}^{\mathrm{s}}, q^{\mathrm{f}}, \dot{q}^{\mathrm{f}}) - h(q^{\mathrm{s}}, q^{\mathrm{f}}, \lambda) \Big) dt.$$

Applying the discrete Lagrange-d'Alembert principle and taking independent variations of $\{\delta q_k^{\mathrm{s}}\}_{k=0}^N$, $\{\{\delta q_k^{\mathrm{f},m}\}_{m=0}^{\mathbb{p}}\}_{k=0}^{N-1}$, $\{\{\delta \lambda_k^{\mathrm{f},m}\}_{m=0}^{\mathbb{p}}\}_{k=0}^N$ with $\delta q_0^{\mathrm{s}} = \delta q_N^{\mathrm{s}} = \delta q_0^{\mathrm{f},0} = \delta q_{N-1}^{\mathrm{f},\mathbb{p}}$ we obtain for $k = 1, \ldots, N-1, m = 1, \ldots, \mathbb{p}-1$:

$$0 = D_{q_k^{\mathrm{s}}} \Big(L_{\mathrm{d}}^{k-1} + L_{\mathrm{d}}^k + h_{\mathrm{d}}^{k-1} + h_{\mathrm{d}}^k \Big) + F_k^{s,-} + F_{k-1}^{s,+} \tag{3.60a}$$

$$0 = D_{q_k^{\mathrm{f},0}} \Big(L_{\mathrm{d}}^{k-1} + L_{\mathrm{d}}^k + h_{\mathrm{d}}^{k-1} + h_{\mathrm{d}}^k \Big) + f_k^{\mathrm{f},0,-} + f_{k-1}^{\mathrm{f},\mathbb{p}-1,+} \tag{3.60b}$$

$$0 = D_{q_k^{\mathrm{f},m}} \Big(L_{\mathrm{d}}^k + h_{\mathrm{d}}^k \Big) + f_k^{\mathrm{f},m,-} + f_k^{\mathrm{f},\mathrm{m}-1,+} \tag{3.60c}$$

$$0 = D_{\lambda_k^1} h_{\mathrm{d}}^k \tag{3.60d}$$

$$0 = D_{\lambda_k^{m+1}} h_{\mathrm{d}}^k + \delta_{m,\mathbb{p}-1}(1 - \delta_{k,N-1}) D_{\lambda_{k+1}^0} h_{\mathrm{d}}^{k+1} \tag{3.60e}$$

where $\delta_{m,\mathbb{p}-1}$ is the Kronecker delta equal to 0 for all m except $m = \mathbb{p} - 1$ where $\delta_{m,\mathbb{p}-1} = 1$. This is a straightforward extension of the model derived for constrained unforced multirate systems by [3, 112]. Comparing to the unconstrained model (3.24), the effect of constraints in (3.60a)- (3.60c) can be interpreted as a force exerted on the system by the constraints.

Equations (3.60) provide a time-stepping scheme in the Lagrange formalism for $k > 1$. For $k = 0$, to match the initial conditions on both the configuration and the velocity, one can use again the forced multirate Legendre transform (3.25) with the augmented discrete Lagrangian $L_{\mathrm{d}}^{\mathrm{c},k}$ resulting in:

$$0 = p_0^{\mathrm{s}} + D_{q_0^{\mathrm{s}}}(L_{\mathrm{d}}^0 + h_{\mathrm{d}}^0) + F_0^{s,-} \tag{3.61a}$$

$$0 = p_0^{\mathrm{f},0} + D_{q_0^{\mathrm{f},0}}(L_{\mathrm{d}}^0 + h_{\mathrm{d}}^0) + f_0^{\mathrm{f},0,-} \tag{3.61b}$$

$$0 = D_{q_0^{\mathrm{f},m}}(L_{\mathrm{d}}^0 + h_{\mathrm{d}}^0) + f_k^{\mathrm{f},m,-} + f_k^{\mathrm{f},m-1,+} \tag{3.61c}$$

$$0 = D_{\lambda_0^1} h_{\mathrm{d}}^0 \tag{3.61d}$$

$$0 = D_{\lambda_0^{m+1}} h_{\mathrm{d}}^0 + \delta_{m,\mathbb{p}-1} D_{\lambda_1^0} h_{\mathrm{d}}^1 \tag{3.61e}$$

for (3.61c) for $m = 1, \ldots, \mathbb{p} - 1$ and (3.61e) for $m = 1, \ldots, \mathbb{p}$. Equations (3.61) can be extended for $k > 0$ and represent the Hamiltonian form of MVI for forced constrained multirate systems approximating the trajectory of the system in the phase space.

Remark 3.5.1. *Following [112], one can consider slow and fast constraints, and consequently slow and fast Lagrange multipliers discretised on the macro and micro grid respectively similarly to* (3.14), (3.15). *This will lead to additional reductions in the number of variables being computed in simulations and optimal control schemes.*

Demonstration problem 3. *Choosing a quadrature of the form*

$$h_d(q_k^{\mathrm{s}}, q_{k+1}^{\mathrm{s}}, q_k^{\mathrm{f}}, \lambda_k) = \sum_{m=0}^{\mathbb{p}-1} [\tfrac{\Delta t}{2} \lambda_k^m g(q_k^{\mathrm{s},m}, q_k^{\mathrm{f},m}) + \tfrac{\Delta t}{2} \lambda_k^{m+1} g(q_k^{\mathrm{s},m+1}, q_k^{\mathrm{f},m+1})]$$

in Appendix C, it is shown that the Hamiltonian formulation can be simplified to:

$$0 = D_{q_k^{\mathrm{s}}} \Big(L_{\mathrm{d}}^{k-1} + L_{\mathrm{d}}^k + \sum_{m=1}^{\mathbb{p}-1} (\Delta t \lambda_{k-1}^m g_{\mathrm{d},k-1}^m) + \sum_{m=0}^{\mathbb{p}-1} (\Delta t \lambda_k^m g_{\mathrm{d},k}^m) \Big) + F_k^{s-} + F_{k-1}^{s,+} \tag{3.62a}$$

$$0 = D_{q_k^{\mathrm{f},0}}\Big(L_{\mathrm{d}}^{k-1} + L_{\mathrm{d}}^{k} + \Delta t \lambda_k^0 g_{\mathrm{d},k}^0\Big) + f_k^{\mathrm{f},0,-} + f_k^{f,\mathbb{p}-1,+} \tag{3.62b}$$

$$0 = D_{q_k^{\mathrm{f},m}}\Big(L_{\mathrm{d}}^{k} + \Delta t \lambda_k^m g_{\mathrm{d},k}^m\Big) + f_k^{\mathrm{f},m,-} + f_k^{\mathrm{f},m-1,+} \tag{3.62c}$$

$$0 = g(q_k^{\mathrm{s},m}, q_k^{\mathrm{f},m}) \tag{3.62d}$$

for $k = 1, \ldots, N-1$ *in all equations,* (3.62c) *for* $m = 1, \ldots, \mathbb{p}-1$ *and* (3.62d) *for* $m = 1, \ldots, \mathbb{p}$. *Here* $g_{\mathrm{d},k}^m := g(q_k^{\mathrm{s},m}, q_k^{\mathrm{f},m})$. *To begin the integration in simulations for* $k = 0$ *in Appendix C we have shown Equations* (3.62) *simplify to:*

$$0 = p_0^{\mathrm{s}} + D_{q_0^{\mathrm{s}}}\Big(L_{\mathrm{d}}^0 + \tfrac{\Delta t}{2}\lambda_0^0 g_0^0 + \sum_{m=1}^{\mathbb{p}-1}(\Delta t \lambda_0^m g_0^m)\Big) + F_0^{s,-} \tag{3.63a}$$

$$0 = p_0^{\mathrm{f},0} + D_{q_0^{\mathrm{f},0}}\Big(L_{\mathrm{d}}^0 + \tfrac{\Delta t}{2}\lambda_0^0 g_0^0\Big) + f_0^{\mathrm{f},0,-} \tag{3.63b}$$

$$0 = D_{q_0^{\mathrm{f},m}}\Big(L_{\mathrm{d}}^0 + \Delta t \lambda_0^m g_0^m\Big) + f_0^{\mathrm{f},m,-} + f_0^{\mathrm{f},m-1,+} \tag{3.63c}$$

$$0 = g(q_0^{\mathrm{s},m}, q_0^{\mathrm{f},m}) \tag{3.63d}$$

with (3.63c) *for* $m = 1, \ldots, \mathbb{p}-1$ *and* (3.63d) *for* $m = 1, \ldots, \mathbb{p}$.

Both sets of equations can be compared to their unconstrained counterparts, demonstrating how the additional terms in the constrained version represent forces exerted by the constraints on the system. Additionally, incorporating the discrete constraint into the model ensures that the resulting discrete trajectory respects it.

Remark: Going back to the singlerate variational formulation presented in Section 2.3.3 for forced unconstrained systems, a constrained version can be formulated by simply simplifying Equations (3.61), (3.60) for $\mathbb{p} = 1$. This leads to the following SVI model for constrained forced Lagrangian systems:

$$\begin{aligned}
\text{for } k = 0 \qquad -p(0) &= D_{q_0} L_d(q_0, q_1) + \tfrac{\Delta t}{2}\lambda_0 D_{q_0} g(q_0) + f_0^- \\
0 &= g(q_1) \\
\text{for } k > 0 \qquad 0 &= D_2 L_d(q_{k-1}, q_k) + D_1 L_d(q_k, q_{k+1}) + \Delta t \lambda_k D_{q_k} g(q_k) + f_{k-1}^+ + f_k^- \\
0 &= g(q_{k+1}).
\end{aligned}$$

This result agrees with the unforced SVI models developed by [1, 113].

4

Examples of multirate variational modelling and simulation

Contents

4.1 Introduction 74
4.1.1 Choice of approximation rules 74
4.1.2 Experimental set-up 76
4.2 Example 1: Fermi–Pasta–Ulam–Tsingou system with quadratic potentials 76
4.2.1 Mathematical model 76
4.2.2 Computational results 79
4.3 Example 2: Fermi–Pasta–Ulam–Tsingou system with quartic potential 85
4.3.1 Computational results 86
4.4 Example 3: Flexible spacecraft dynamics 87
4.4.1 Background 87
4.4.2 Mathematical model 88
4.4.3 Multirate configuration description and discretisation . 92
4.4.4 Computational results 93
4.5 Example 4: Electrodynamic tether motion 96
4.5.1 Introduction 97
4.5.2 Variational model of 6DOF tethered spacecraft dynamics 98
4.5.3 Numerical results 103

4.1 Introduction

This chapter introduces examples aimed at showcasing the capabilities of the methods introduced in Chapters 3, 5, 6,and 7. The examples are selected as follows:

- **Example 1**: linear unconstrained system
- **Example 2**: nonlinear unconstrained system
- **Example 3**: linear unconstrained system model for an aerospace application
- **Example 4**: nonlinear constrained system model for an aerospace application

Example 1 and 3 concentrate on linear systems, allowing for a direct comparison to an analytic solution and thus providing a clear demonstration of the capabilities of the multirate variational approach, as discussed and proved in Chapter 3. These examples aim to highlight the accuracy and structure-preserving properties of the approach, and demonstrate the computational savings achievable using this method. Additionally, Examples 2 and 4 demonstrate the application of MVIs to both unconstrained and constrained nonlinear systems, without the need to decouple the equations of motion.

Examples 3 and 4 hold particular significance as they develop variational models tailored to two practical aerospace applications, underscoring the real-world relevance and applicability of the proposed methods.

4.1.1 Choice of approximation rules

As outlined in Section 3.4.1, we establish two time grids within the discrete-time setting: a macro time grid characterised by the macro time step ΔT and a micro time grid obtained by subdividing each macro step into $\mathbb{p}$ equally spaced micro time steps of size Δt, as illustrated in Figure 3.1. We discretise the slow subsystem on the macro time grid, while the fast dynamics are discretised on the micro time grid. For this purpose, we define again the discrete paths $q_{\mathrm{d}}^{\mathrm{s}}, q_{\mathrm{d}}^{\mathrm{f}}$ as described in (3.14), (3.15) and the discrete control path u_{d} from (3.17). As in Section 3.4.4, we choose

piecewise-constant polynomial with $u^{\text{slow}} = u^{\text{s}}$, $u^{\text{fast}} = u^{\text{f}}$ for the approximation of the control variables (see Remark 3.4.1) and piecewise-linear polynomials for the the slow and fast configuration variables as follows:

$$q_{\text{d}}^{\text{s}}(t) = q_k^{\text{s}} + \frac{q_{k+1}^{\text{s}} - q_k^{\text{s}}}{\Delta T}\,(t - t_k), \qquad \dot{q}_{\text{d}}^{\text{s}}(t) = \frac{q_{k+1}^{\text{s}} - q_k^{\text{s}}}{\Delta T}, \qquad \text{for } \; t \in [t_k, t_{k+1}]$$

$$q_{\text{d}}^{\text{f}}(t) = q_k^{\text{f},m} + \frac{q_k^{\text{f},m+1} - q_k^{\text{f},m}}{\Delta t}\,(t - t_k^m), \quad \dot{q}_{\text{d}}^{\text{f}}(t) = \frac{q_k^{\text{f},m+1} - q_k^{\text{f},m}}{\Delta t}, \;\; \text{for } \; t \in [t_k^m, t_k^{m+1}]$$

for $k = 0, \ldots, N-1$, $m = 0, \ldots, \mathbb{p} - 1$. For all experiments, linear interpolation is employed to approximate the slow dynamics on the micro time grid, as detailed in (3.16) with $a^m = \frac{\mathbb{p}-m}{\mathbb{p}}$, $b^m = \frac{m}{\mathbb{p}}$, while the midpoint quadrature is utilised for the Lagrangian:

$$L_{\text{d}}^{k,m}(q_k^{\text{s},m}, q_k^{\text{s},m+1}, q_k^{\text{f},m}, q_k^{\text{f},m+1}) = \Delta t \mathcal{L}\Big(\tfrac{q_k^{\text{s},m}+q_k^{\text{s},m+1}}{2}, \tfrac{q_k^{\text{s},m+1}-q_k^{\text{s},m}}{\Delta t}, \tfrac{q_k^{\text{f},m}+q_k^{\text{f},m+1}}{2}, \tfrac{q_k^{\text{f},m+1}-q_k^{\text{f},m}}{\Delta t}\Big).$$

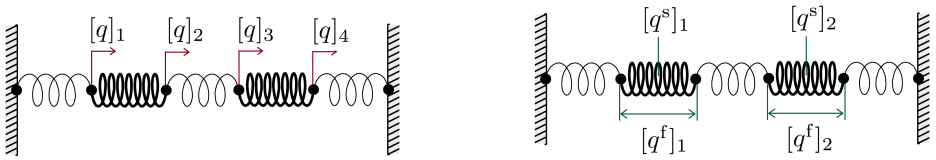
The same quadrature is chosen for the approximation of the virtual work. Thus, the discrete virtual work associated with the fast generalised forces becomes

$$\begin{aligned}
&W_{\text{d},k}^{\text{f}}(q_k^{\text{s}}, q_{k+1}^{\text{s}}, q_k^{\text{f}}, u_k) = \\
&\quad = \sum_{m=0}^{\mathbb{p}-1} \Delta t f_{\text{LC}}^{\text{f}}\Big(\tfrac{q_k^{\text{s},m}+q_k^{\text{s},m+1}}{2}, \tfrac{q_k^{\text{s},m+1}-q_k^{\text{s},m}}{\Delta t}, \tfrac{q_k^{\text{f},m}+q_k^{\text{f},m+1}}{2}, \tfrac{q_k^{\text{f},m+1}-q_k^{\text{f},m}}{\Delta t}, u_{k+1/2}\Big) \cdot \tfrac{\delta q_k^{\text{f},m}+\delta q_k^{\text{f},m+1}}{2} \\
&= \sum_{m=0}^{\mathbb{p}-1} \tfrac{\Delta t}{2} f_{\text{LC}}^{\text{f}}\Big(\tfrac{q_k^{\text{s},m}+q_k^{\text{s},m+1}}{2}, \tfrac{q_k^{\text{s},m+1}-q_k^{\text{s},m}}{\Delta t}, \tfrac{q_k^{\text{f},m}+q_k^{\text{f},m+1}}{2}, \tfrac{q_k^{\text{f},m+1}-q_k^{\text{f},m}}{\Delta t}, u_{k+1/2}\Big) \cdot \delta q_k^{\text{f},m} + \\
&\quad \sum_{m=0}^{\mathbb{p}-1} \tfrac{\Delta t}{2} f_{\text{LC}}^{\text{f}}\Big(\tfrac{q_k^{\text{s},m}+q_k^{\text{s},m+1}}{2}, \tfrac{q_k^{\text{s},m+1}-q_k^{\text{s},m}}{\Delta t}, \tfrac{q_k^{\text{f},m}+q_k^{\text{f},m+1}}{2}, \tfrac{q_k^{\text{f},m+1}-q_k^{\text{f},m}}{\Delta t}, u_{k+1/2}\Big) \cdot \delta q_k^{\text{f},m+1}
\end{aligned}$$

with $u_{k+1/2} = u(\frac{t_k+t_{k+1}}{2})$. This leads to an approximation of the left and right discrete-time fast generalised forces of the form:

$$f_k^{\text{f},m,+} = f_k^{\text{f},m,-} = \tfrac{\Delta t}{2} f_{\text{LC}}^{\text{f}}\Big(\tfrac{q_k^{\text{s},m}+q_k^{\text{s},m+1}}{2}, \tfrac{q_k^{\text{s},m+1}-q_k^{\text{s},m}}{\Delta t}, \tfrac{q_k^{\text{f},m}+q_k^{\text{f},m+1}}{2}, \tfrac{q_k^{\text{f},m+1}-q_k^{\text{f},m}}{\Delta t}, u_{k+1/2}\Big)$$

The approximation of the slow forces $f^{\text{s},m,\pm}$ can be analogously derived and used to formulate $F_k^{\text{s},\pm}$ based on (3.20). Overall, for all the considered examples, these choices are expected to lead to an approximation of the system dynamics of order 2 as stated in Lemma 3.4.3, although not all assumptions required for the formal proof are met in every example.



(a) With generalised coordinates q **(b)** With generalised coordinates $q^{\mathrm{s}}, q^{\mathrm{F}}$

Figure 4.1: Examples 1 and 2: An FPUT system with $n = 4$

4.1.2 Experimental set-up

The computational tests for all examples were carried out in either MATLAB or Python, utilising an Intel Core i7-10700 CPU @2.90GHz with 32GB RAM. For the MATLAB implementation, the necessary derivatives for the MVI approach were derived by hand and then implemented. In Python, the JAX library facilitated automatic differentiation for handling derivatives, with further optimisation achieved through just-in-time (JIT) compilation. Our primary focus in the implementation was on ensuring flexibility for multiple use cases rather than optimising for speed. Therefore, the purpose of our runtime experiments is to compare the computational costs of different approaches, not to showcase their fastest possible implementation.

4.2 Example 1: Fermi–Pasta–Ulam–Tsingou system with quadratic potentials

To demonstrate the advantages of MVI, we first explore a linear example, which allows us to demonstrate the main results derived in this paper using a direct comparison of the MVI simulation against the analytic solution. The system analysed is a modified version of the Fermi–Pasta–Ulam–Tsingou (FPUT) system, a common benchmark for multirate schemes [3, 26].

4.2.1 Mathematical model

The system comprises of a chain of n unit masses, connected with alternating stiff and soft springs of stiffness $\frac{w^2}{2}$ and k, respectively, as shown in Figure 4.1. The displacement of each mass is represented by a coordinate q_i, and for $n = 4$, the

system's Lagrangian takes the form:

$$\mathfrak{L}(q,\dot{q}) = \frac{1}{2}\dot{q}^\intercal M\dot{q} - \frac{1}{2}q^\intercal Kq,\ M = \begin{bmatrix}1&0&0&0\\0&1&0&0\\0&0&1&0\\0&0&0&1\end{bmatrix},\ K = \begin{bmatrix}k+\frac{w^2}{2} & -\frac{w^2}{2} & 0 & 0\\ -\frac{w^2}{2} & k+\frac{w^2}{2} & -k & 0\\ 0 & -k & k+\frac{w^2}{2} & -\frac{w^2}{2}\\ 0 & 0 & -\frac{w^2}{2} & k+\frac{w^2}{2}\end{bmatrix}$$

where the time dependence has been omitted to simplify the notation. If we consider viscous damping and external control acting on the system, then the virtual work can be expressed as

$$\delta W(q,u) = u\cdot\delta q - C\dot{q}\cdot\delta q, \quad C = \begin{bmatrix}\lambda_\mathrm{k}+\lambda_w & -\lambda_w & 0 & 0\\ -\lambda_w & \lambda_\mathrm{k}+\lambda_w & -\lambda_\mathrm{k} & 0\\ 0 & -\lambda_w & \lambda_\mathrm{k}+\lambda_w & -\lambda_\mathrm{k}\\ 0 & 0 & -\lambda_w & \lambda_\mathrm{k}+\lambda_w\end{bmatrix}$$

Here $\lambda_\mathrm{k}, \lambda_w$ are the damping coefficients for the soft and stiff spring, respectively, and the control vector entry u_i represents control applied to the i-th point mass along the q_i coordinate as portrayed in Figure 4.1a

As noted by [26], the system exhibits multirate behaviour: vibration of stiff springs operates on a time scale of w^{-1}, while soft spring motion occurs at w^0. A third-time scale of w is observed for oscillation energy exchange among stiff springs. An alternative description of the dynamics using the length of each stiff spring and its centre's position (Figure 4.1b) illustrates the system's multirate nature. Employing a coordinate change of the form

$$\begin{bmatrix}q^\mathrm{s}\\q^\mathrm{f}\end{bmatrix} = Eq,\ \ E = \begin{bmatrix}E^\mathrm{s}\\E^\mathrm{f}\end{bmatrix},\quad E^\mathrm{s} = \begin{bmatrix}\frac{1}{\sqrt{2}} & \frac{1}{\sqrt{2}} & 0 & 0\\ 0 & 0 & \frac{1}{\sqrt{2}} & \frac{1}{\sqrt{2}}\end{bmatrix},\ E^\mathrm{f} = \begin{bmatrix}-\frac{1}{\sqrt{2}} & \frac{1}{\sqrt{2}} & 0 & 0\\ 0 & 0 & -\frac{1}{\sqrt{2}} & \frac{1}{\sqrt{2}}\end{bmatrix}$$

we describe the system in slow coordinates $[q^\mathrm{s}]_i$, representing the location of the the center of the i-th stiff spring, and fast coordinates $[q^\mathrm{f}]_i$ representing its length for $i = 1,\ldots,n/2$. In this multirate coordinate system, the Lagrangian becomes

$$\mathcal{L}(q^\mathrm{s},q^\mathrm{f},\dot{q}^\mathrm{s},\dot{q}^\mathrm{f}) = \frac{1}{2}\left[(\dot{q}^\mathrm{s})^\intercal M^\mathrm{s}\dot{q}^\mathrm{s} + (\dot{q}^\mathrm{f})^\intercal M^\mathrm{f}\dot{q}^\mathrm{f} - (q^\mathrm{s})^\intercal K^\mathrm{s}q^\mathrm{s} - (q^\mathrm{f})^\intercal K^\mathrm{f}q^\mathrm{f} - 2(q^\mathrm{s})^\intercal K^\mathrm{sf}q^\mathrm{f}\right] \quad (4.1)$$

where $\mathcal{M} = (E^{-1})^\intercal\, M\, E^{-1} = \begin{bmatrix} M^\mathrm{s} & 0\\ 0 & M_\mathrm{f}\end{bmatrix},\ \mathcal{K} = (E^{-1})^\intercal\, K\, E^{-1} = \begin{bmatrix} K^\mathrm{s} & K^\mathrm{sf}\\ (K^\mathrm{sf})^\intercal & K^\mathrm{f}\end{bmatrix}$

which for $k = 2$ is often simplified to the following form:

$$\mathcal{L}(q^\mathrm{s},q^\mathrm{f},\dot{q}^\mathrm{s},\dot{q}^\mathrm{f}) = \frac{1}{2}\sum_{i=1}^{2}(([\dot{q}^\mathrm{s}]_i)^2 + ([\dot{q}^\mathrm{f}]_i)^2) \quad (4.2)$$

$$-\frac{1}{4}\Big[([q^{\mathrm{s}}]_1-[q^{\mathrm{f}}]_1)^2+([q^{\mathrm{s}}]_2-[q^{\mathrm{f}}]_2-[q^{\mathrm{s}}]_1-[q^{\mathrm{f}}]_1)^2+([q^{\mathrm{s}}]_2-[q^{\mathrm{f}}]_2)^2\Big]-\frac{w^2}{2}\sum_{i=1}^{2}([q^{\mathrm{f}}]_i)^2$$

In fact this Lagrangian is of the form considered in Demonstration problem 1 as w is assumed to take large values, thus introducing a very stiff potential.

Transforming the control and damping matrix as

$$\begin{bmatrix}u^{\mathrm{s}}\\u^{\mathrm{f}}\end{bmatrix}=((u)^{\intercal}E^{-1})^{\intercal}=Eu,\quad EC^{\intercal}E^{-1}=\begin{bmatrix}C^{\mathrm{s}} & C^{\mathrm{sf}}\\(C^{\mathrm{sf}})^{\intercal} & C^{\mathrm{f}}\end{bmatrix}$$

and noting that E is an orthogonal matrix, the virtual work can also be expressed in this coordinate system as

$$\begin{aligned}\delta W(q,u)&=u\cdot\delta q-C\dot{q}\cdot\delta q\\&=u^{\mathrm{s}}\cdot\delta q^{\mathrm{s}}+u^{\mathrm{f}}\cdot\delta q^{\mathrm{f}}-(C^{\mathrm{s}})^{\intercal}\dot{q}^{\mathrm{s}}\cdot\delta q^{\mathrm{s}}-(C^{\mathrm{f}})^{\intercal}\dot{q}^{\mathrm{f}}\cdot\delta q^{\mathrm{f}}-(C^{\mathrm{sf}})\dot{q}^{\mathrm{f}}\cdot\delta q^{\mathrm{s}}-(C^{\mathrm{sf}})^{\intercal}\dot{q}^{\mathrm{s}}\cdot\delta q^{\mathrm{f}}\end{aligned}$$

and thus the generalised forces can be expressed as :

$$f^{\mathrm{s}}_{\mathrm{LC}}=u^{\mathrm{s}}-(C^{\mathrm{s}})^{\intercal}\dot{q}^{\mathrm{s}}-(C^{\mathrm{sf}})\dot{q}^{\mathrm{f}} \tag{4.3a}$$

$$f^{\mathrm{f}}_{\mathrm{LC}}=u^{\mathrm{f}}-(C^{\mathrm{f}})^{\intercal}\dot{q}^{\mathrm{f}}-(C^{\mathrm{sf}})^{\intercal}\dot{q}^{\mathrm{s}} \tag{4.3b}$$

Using the Lagrangian viewpoint and applying the Lagrange-d'Alembert principle (Equation (3.2), (3.3)) leads us to the following equations of motion for the system

$$M^{\mathrm{s}}\ddot{q}^{\mathrm{s}}+(C^{\mathrm{s}})^{\intercal}\dot{q}^{\mathrm{s}}+(C^{\mathrm{sf}})\dot{q}^{\mathrm{f}}+K^{\mathrm{s}}q^{\mathrm{s}}+K^{\mathrm{sf}}q^{\mathrm{f}}=u^{\mathrm{s}} \tag{4.4a}$$

$$M^{\mathrm{f}}\ddot{q}^{\mathrm{f}}+(C^{\mathrm{f}})^{\intercal}\dot{q}^{\mathrm{f}}+(C^{\mathrm{sf}})^{\intercal}\dot{q}^{\mathrm{s}}+K^{\mathrm{f}}q^{\mathrm{f}}+K^{\mathrm{sf}}q^{\mathrm{s}}=u^{\mathrm{f}} \tag{4.4b}$$

The Hamiltonian control forces can be obtained by applying Equations (3.6) as:

$$\begin{aligned}f^{\mathrm{s}}_{\mathrm{HC}}&=u^{\mathrm{s}}-(C^{\mathrm{s}})^{\intercal}(M^{\mathrm{s}})^{-1}p^{\mathrm{s}}-(C^{\mathrm{sf}})(M^{\mathrm{f}})^{-1}p^{\mathrm{f}}\\f^{\mathrm{f}}_{\mathrm{HC}}&=u^{\mathrm{f}}-(C^{\mathrm{f}})^{\intercal}(M^{\mathrm{f}})^{-1}p^{\mathrm{f}}-(C^{\mathrm{sf}})^{\intercal}(M^{\mathrm{s}})^{-1}p^{\mathrm{s}}\end{aligned}$$

and thus the equations of motion in phase space (2.9) become

$$\dot{q}^{\mathrm{s}}=(M^{\mathrm{s}})^{-1}p^{\mathrm{s}},\qquad \dot{p}^{\mathrm{s}}=-K^{\mathrm{s}}q^{\mathrm{s}}+u^{\mathrm{s}}-(C^{\mathrm{s}})^{\intercal}(M^{\mathrm{s}})^{-1}p^{\mathrm{s}}-(C^{\mathrm{sf}})(M^{\mathrm{f}})^{-1}p^{\mathrm{f}} \tag{4.5a}$$

$$\dot{q}^{\mathrm{f}}=(M^{\mathrm{f}})^{-1}p^{\mathrm{f}},\qquad \dot{p}^{\mathrm{f}}=-K^{\mathrm{f}}q^{\mathrm{f}}+u^{\mathrm{f}}-(C^{\mathrm{f}})^{\intercal}(M^{\mathrm{f}})^{-1}p^{\mathrm{f}}-(C^{\mathrm{sf}})^{\intercal}(M^{\mathrm{s}})^{-1}p^{\mathrm{s}} \tag{4.5b}$$

4.2.2 Computational results

To simulate the system, we implement the analytic solution, the MVI approach and several alternative integrators:

- 2^{nd} order explicit Runge-Kutta method (RK2e)
- 2^{nd} order implicit Runge-Kutta method (RK2i, Crank-Nicholson)
- 2^{nd} order implicit symplectic Runge-Kutta method (RK2is, implicit midpoint)
- 4^{th} order Runge-Kutta method (RK4)
- the ode45 routine by MATLAB

All RK approaches directly discretise the equations of motion (4.4) or (4.5), approximating both the configuration and the velocity/momentum. On the other hand, the MVI approach discretises the Lagrangian (4.2) and Lagrangian control forces (4.3), as described in Sections 3.4.1, 3.4.2, and 4.1.1, and uses those discretisations in the discrete Lagrange-d'Alembert principle (3.23) to derive a multirate discrete-time structure-preserving model either in Lagrangian (Equation (3.24)) or Hamiltonian form (Equation (3.30)), approximating only the configuration or both the configuration and the momentum, respectively. In all experiments we set $w = 50$, the initial conditions as $q^{\text{f},0} = [1/w, 0]$, $q^{\text{s},0} = \dot{q}^{\text{s},0} = \dot{q}^{\text{f},0} = [1, 0]^\intercal$, and consider dissipative damping forces, but no external control forces ($u^{\text{s}} = u^{\text{f}} = 0$). A Newton-Raphson root-finding method is implemented for the implicit schemes with tolerances of 10^{-11}, and ode45 is run with *RelTol* of 10^{-10}. All listed schemes, apart from the MVI, integrate all variables on the micro time scale with step Δt while the MVI integrates the fast variables on the micro time scale and the slow variables on the macro time grid with $\Delta T = \mathbb{p}\Delta t$. In the following figures, the Lagrangian formulation of the MVI is denoted as LF, while the Hamiltonian formulation as HF.

Energy simulation for a linear conservative system

First, to investigate how well the MVI and the alternative integrators preserve the energy of a conservative system in simulations, we set the damping coefficients to

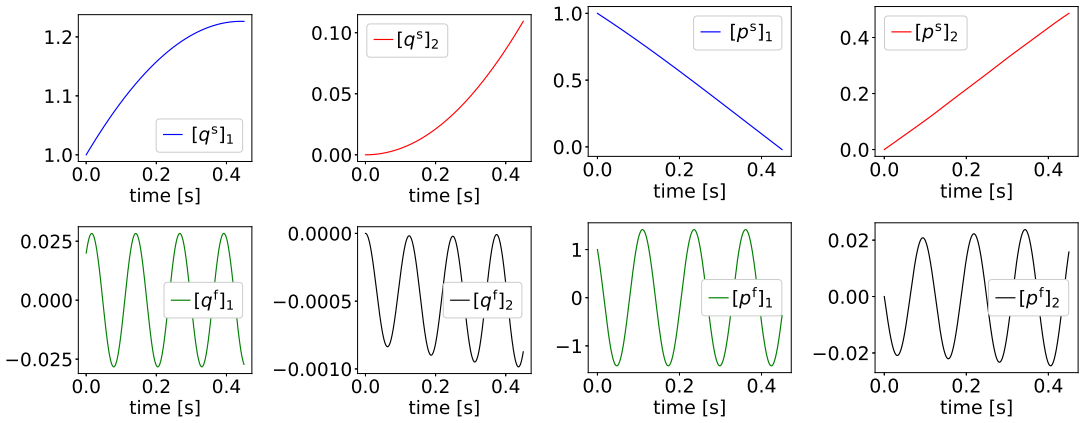
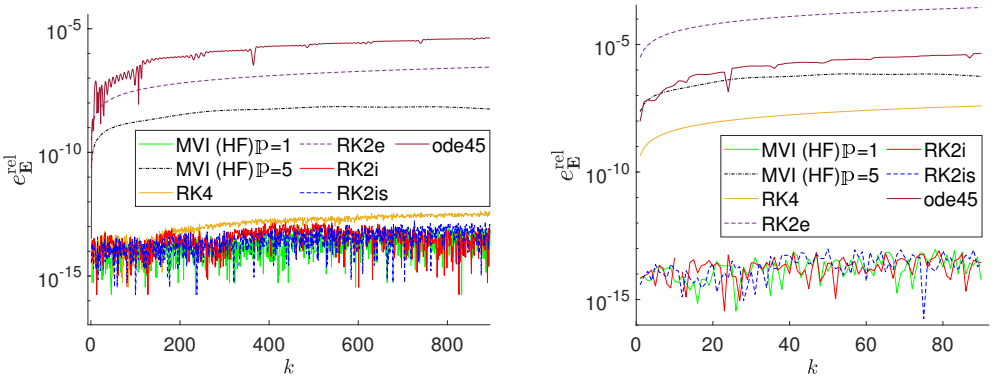


Figure 4.2: Example 1: Trajectory simulation in the absence of dissipative forces using the HF MVI with $T = 0.45$s, $\Delta t = 10^{-3}$s, and $\mathbb{p} = 5$



(a) $\Delta t = 10^{-4}$ **(b)** $\Delta t = 10^{-3}$

Figure 4.3: Example 1: Relative error of the system's energy simulation for $k > 1$ in the absence of dissipative forces for $T = 0.45$s (please note the y-axis is in a log scale)

zero ($\lambda_w = \lambda_k = 0$). The multirate nature of the resulting system is demonstrated in Figure 4.2 using the MVI approach in HF, with length of the simulation $T = 0.45$s, micro time step $\Delta t = 10^{-3}$s, and macro-micro proportionality $\mathbb{p} = 5$. The relative error of the energy simulation is then computed for simulations of all implemented integrators with $T = 0.45$s and $\Delta t = 10^{-4}$s or $\Delta t = 10^{-3}$s using:

$$e^{\mathrm{rel}}_{\mathbb{E}}(q_d, \dot{q}_d) = \max_{k=0,\dots,n^{\mathrm{s}}} \frac{\mathbb{E}^k_{\mathrm{d}} - \mathbb{E}(q(t_k), \dot{q}(t_k))}{\mathbb{E}(q(t_k), \dot{q}(t_k))} \tag{4.6}$$

where $\mathbb{E}(q(t), \dot{q}(t)) = \frac{1}{2}\dot{q}(t)^{\intercal} M \dot{q}(t) + \frac{1}{2} q(t)^{\intercal} K q(t)$

$$\mathbb{E}_{\mathrm{d}}^{k} = \mathbb{E}(q_k, \dot{q}_k) = \frac{1}{2}\dot{q}_k^{\intercal} M \dot{q}_k + \frac{1}{2} q_k^{\intercal} K q_k, \quad \dot{q}_d = \{\dot{q}_k\}_{k=0}^{N}, \quad , \dot{q}_k = E^{-1} \begin{bmatrix} (\mathbb{F}L^{\mathrm{s}})^{-1}(p_k^{\mathrm{s}}) \\ (\mathbb{F}L^{\mathrm{f}})^{-1}(p_k^{\mathrm{f},0}) \end{bmatrix}.$$

Here $\mathbb{E}(q(t_k), \dot{q}(t_k))$ is the system's total energy based on the analytic solution at a given macro time node $t_k = k\Delta T$ and $\mathbb{E}_{\mathrm{d}}^{k}$ is its value computed from the discrete trajectory simulation q_{d} from the integrator being tested. In the case of a conservative system ($\lambda_w = \lambda_k = 0$) the analytic energy remains constant, i.e $\mathbb{E}(q(t_k), \dot{q}(t_k)) = \mathbb{E}(q(0), \dot{q}(0))$ for $\forall k$. For the MVI, the test is done for its Hamiltonian formulation as values for the momentum at all macro time nodes are needed to compute the total energy.

The results of this test for $T = 0.45$ and micro time steps $\Delta t = 10^{-4}$ or $\Delta t = 10^{-3}$ are presented in Figure 4.3. For $\mathbb{p} = 1$ (corresponding to a singlerate variational solution), the MVI matches or outperforms other schemes in preserving the conservation law of the system with both micro step choices.[1] Moreover, for both micro step choices for $\mathbb{p} = 5$, the MVI outperforms the ode45 routine and does comparably well to the other RK schemes given that it calculates the slow system dynamics at five times fewer time nodes.

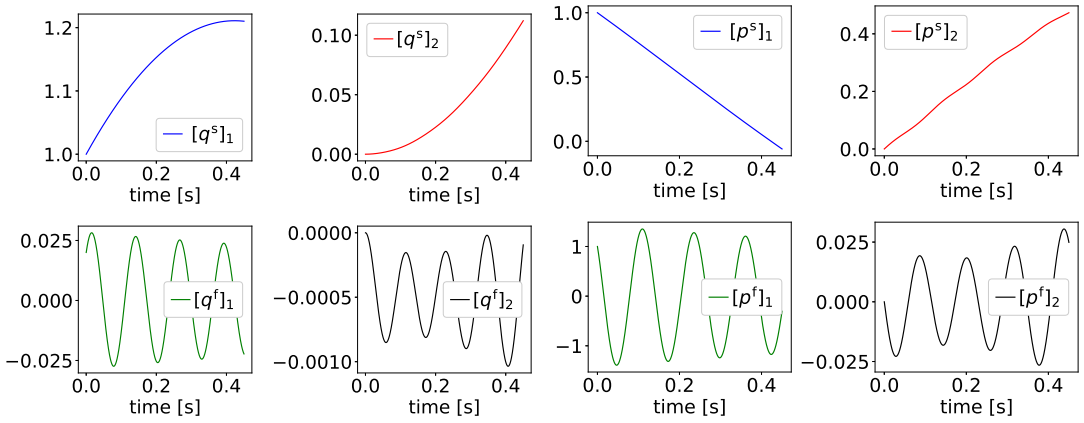
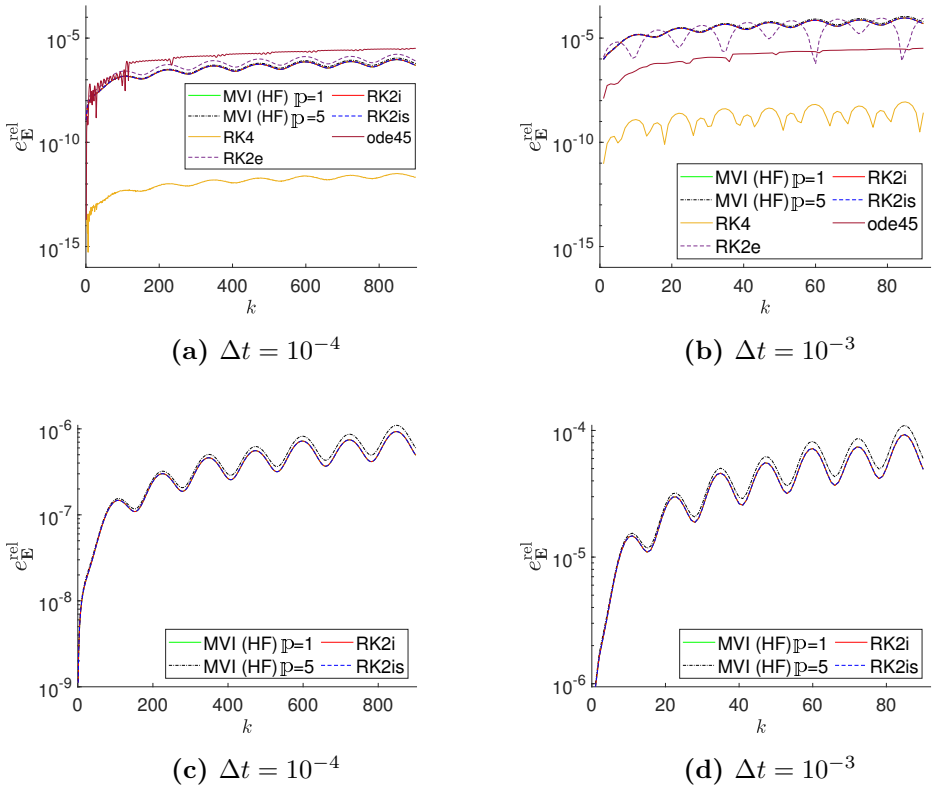


Figure 4.4: Example 1: Trajectory simulation in the presence of dissipative forces using the HF MVI with $T = 0.45$, $\Delta t = 10^{-3}$, and $\mathbb{p} = 5$

Energy simulation for a linear dissipative system

Next, we introduce damping by setting the damping coefficients as $\lambda_w = \lambda_k = 0.3$.

[1] Note that for $\mathbb{p} = 1$ the MVI is the midpoint integrator which preserves quadratic invariants and thus preserves the energy of the linear system up to numerical accuracy.



(a) $\Delta t = 10^{-4}$ **(b)** $\Delta t = 10^{-3}$

(c) $\Delta t = 10^{-4}$ **(d)** $\Delta t = 10^{-3}$

Figure 4.5: Example 1: Relative error of the system's energy simulation for $k > 1$ in the presence of dissipative forces for $T = 0.45$ (please note the y-axis is in a log scale)

The multirate nature of the resulting system is demonstrated in Figure 4.4 using a HF MVI simulation with $T = 0.45$, $\Delta t = 10^{-3}$, and $\mathbb{p} = 5$. In this case, the energy is not preserved. However, it is interesting to see how well the dissipation is modelled. Setting again $T = 0.45$s and $\Delta t = 10^{-4}$ or $\Delta t = 10^{-3}$, we perform simulations with all integrators and compare the result to the analytic solution using Equation (4.6). From Figure 4.5, it is clear that for both $\Delta t = 10^{-4}$s and $\Delta t = 10^{-3}$, the MVI is capable of obtaining the same error levels in the energy simulation as the other tested 2^{nd} order implicit integrators, despite performing the integration of the slow variables at approximately one fifth as many time nodes. Moreover, for $\Delta t = 10^{-3}$ the MVI performs better than the ode45 routine. Of course, the 4^{th} order method demonstrates smaller errors in almost all cases. However, it is inherently higher-order and computes both the slow and fast dynamics at more time nodes without the option to avoid the integration of the momentum. In comparison, the

MVI LF formulation leads to 10 times fewer variables computed on the macro time scale and two times fewer variables computed on the micro time scale.

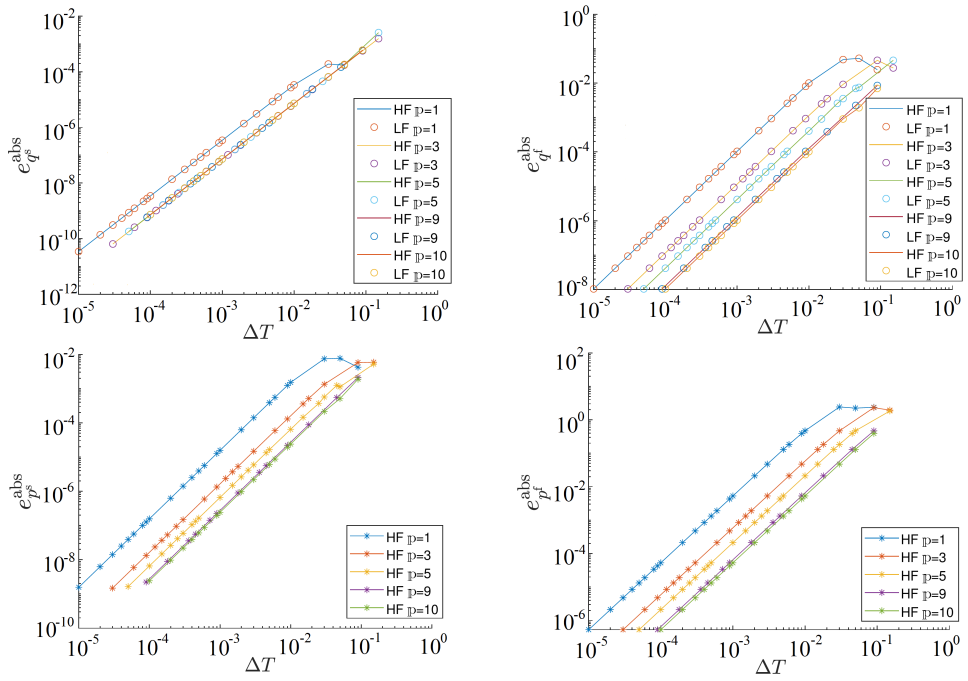


Figure 4.6: Example 1: Log-log plot demonstrating the order of convergence for the MVI based on simulations in the presence of damping for a constant length of simulation $T = 0.45$

Order of convergence for a linear dissipative system

Next, in a set of experiments, we demonstrate numerically the validity of Lemma 3.4.3 on the order of accuracy of the forced MVI. In fact, this lemma is limited to the investigation of the local error for a simplified case, while the following tests go a few steps further and demonstrate the global error of the simulations for a more complicated system, thus demonstrating the order of convergence of the chosen approach. This is achieved through an order test, which consists of a calculation of the error of the MVI simulation with respect to the analytical solution for a given base micro time step Δt and a variety of values for $\mathbb{p}$. The error is computed in the following manner:

$$e_x^{\text{abs}}(x_d, x) = \max_{k=0,\dots,N}(\|x_k - x(t_k)\|_\infty) \tag{4.7}$$

effectively comparing the trajectory solutions on the macro time grid.

Figure 4.6 presents the results for $\lambda_w = \lambda_k = 0.3$, $T = 0.45$ and macro-micro proportionalities of $\mathbb{p} = 1, 3, 5, 9, 10$. These figures demonstrate the order of convergence of approximately order 2, as expected from the chosen quadrature, thus validating the expected behaviour of the numerical integration scheme in the presence of forces. We also note that at the largest considered timesteps a plateau is observed indicating order reduction, which is expected for stiff systems (see [114]).

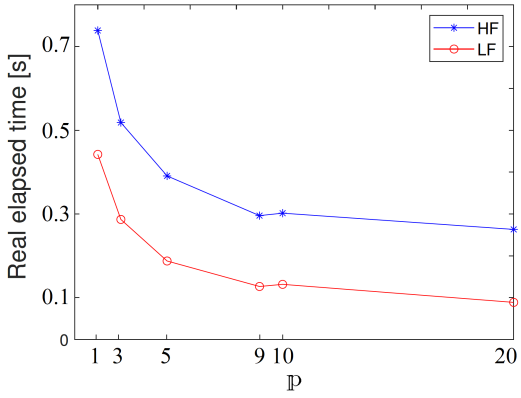


Figure 4.7: Example 1: Mean computational with standard deviation time for the MVI versus $\mathbb{p}$ for a constant micro time step of $\Delta t = 10^{-4}$ and length of simulation $T = 0.45$ (the standard deviation values are too small to be visible)

Computational efficiency of the MVI approach

We conduct a series of simulations for various macro-to-micro time step ratios $\mathbb{p}$ while maintaining the micro step at a constant 10^{-4} to illustrate the computational savings achievable with MVI for multirate system simulation. Figure 4.14 depicts the mean real elapsed time for each simulation derived from 10 measurements utilising the *tic-toc* MATLAB routine. As expected, avoiding the integration of the momentum with the Lagrangian formulation has introduced substantial runtime savings compared to the Hamiltonian formulation. Furthermore, it is clear that for both formulations, the computational time reduces significantly as $\mathbb{p}$ increases. It is important to note that $\mathbb{p}$ cannot be increased indefinitely, as doing so would progressively degrade the accuracy of the slow dynamics. A trade-off point can thus be chosen for the practitioner depending on the level of accuracy and efficiency required for a given application.

4.3 Example 2: Fermi–Pasta–Ulam–Tsingou system with quartic potential

The second example considers again the Fermi–Pasta–Ulam–Tsingou system, this time modifying the Lagrangian (4.2) to include quartic terms:

$$\mathcal{L}(q^{\mathrm{s}}, q^{\mathrm{f}}, \dot{q}^{\mathrm{s}}, \dot{q}^{\mathrm{f}}) = \frac{1}{2}\sum_{i=1}^{2}(([\dot{q}^{\mathrm{s}}]_i)^2 + ([\dot{q}^{\mathrm{f}}]_i)^2)$$
$$- \frac{1}{4}\Big[([q^{\mathrm{s}}]_1 - [q^{\mathrm{f}}]_1)^4 + ([q^{\mathrm{s}}]_2 - [q^{\mathrm{f}}]_2 - [q^{\mathrm{s}}]_1 - [q^{\mathrm{f}}]_1)^4 + ([q^{\mathrm{s}}]_2 - [q^{\mathrm{f}}]_2)^4\Big] - \frac{w^2}{2}\sum_{i=1}^{2}([q^{\mathrm{f}}]_i)^2$$

but considering the same damping and external forces (4.3) as in Example 1. This Lagrangian corresponds to an FPUT system comprising of alternating stiff harmonic and soft nonlinear springs [26]. In this case, both the continuous and discrete Lagrange-d'Alembert principles lead to nonlinear equations of motion. Using the quadrature rules selected in Section 4.1.1, we again derive discrete-time approximations of the Lagrangian and the virtual work. Consequently, using Equations (3.24) and (3.30), we develop a multirate variational discrete-time model for the system in Lagrangian and Hamiltonian formulation, respectively. The set-up is chosen to match Example 1 with $w = 50$, initial conditions $q^{\mathrm{f},0} = [1/w, 0]$, $q^{\mathrm{s},0} = \dot{q}^{\mathrm{s},0} = \dot{q}^{\mathrm{f},0} = [1, 0]^\intercal$, and the consideration of dissipative damping forces, but no external control forces ($u^{\mathrm{s}} = u^{\mathrm{f}} = 0$).

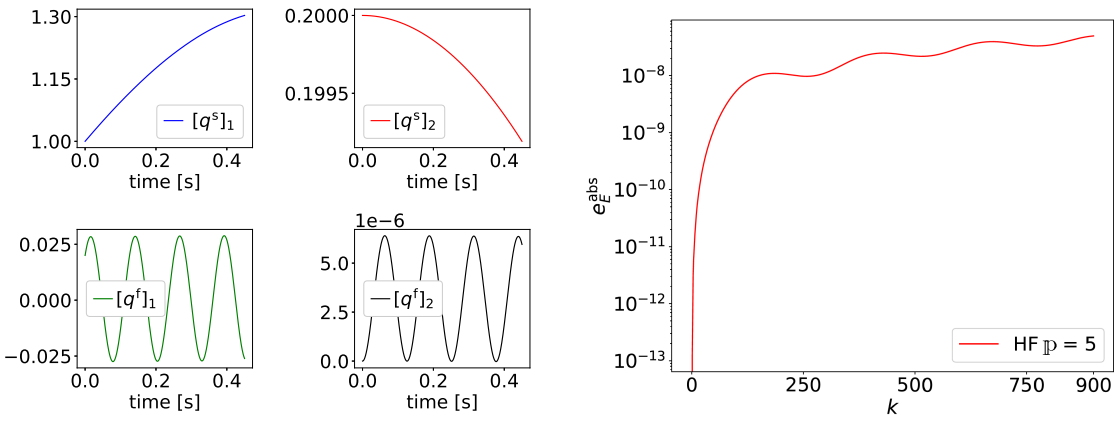


Figure 4.8: Example 3: Trajectory simulation in the absence of dissipative forces using the HF MVI with $T = 0.45$, $\Delta t = 10^{-4}$, and $\mathbb{p} = 5$

4.3.1 Computational results

To simulate the motion of the nonlinear system from Example 3, we implement the MVI and also, for comparison, the singlerate variational integrator (SVI) discussed in Section 2.3.3. All simulations in this example are performed in Python using automatic differentiation with *JAX* [115] for all derivatives in the SVI and MVI models. In Figure 4.8, we demonstrate an example simulation with the Lagrangian formulation (LF) of the MVI for macro-micro proportionality $\mathbb{p} = 5$, discrete micro time step $\Delta t = 10^{-4}$, length of the simulation $T = 1$, and damping coefficients $\lambda_w = \lambda_k = 0$. The figure demonstrates the multirate behaviour of the system and the conservation properties of the MVI, as energy should be preserved in the absence of dissipative forces and external controls. The bounded oscillations around the true energy value are typical for simulations with variational integrators, as mentioned in Chapter 2. Next, adding damping $\lambda_w = \lambda_k = 0.3$, we perform an order

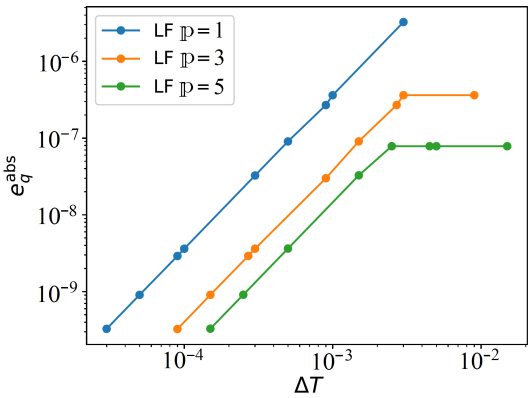


Figure 4.9: Example 3: Log-log plot demonstrating the order of convergence for the MVI based on simulations in the presence of damping for a length of simulation $T = 0.003$

test to demonstrate the accuracy of the MVI approach for forced nonlinear systems. The test is conducted for a simulation length of $T = 0.003$ and the macro-micro proportionalities $\mathbb{p} = 1$(effectively a singlerate solution), 3, and 5. The error of the multirate simulation is computed using Equation (4.7) with respect to a very fine SVI simulation with discrete time step $\Delta t = 10^{-7}$. From Figure 4.9 we can see an order of convergence two, as expected from Theorem 3.4.2 and the chosen quadratures and approximation rules.

4.4 Example 3: Flexible spacecraft dynamics

4.4.1 Background

The next example we consider comes from a practical application in the aerospace domain aiming to safely and accurately simulate and control flexible satellites. To provide a wide range of services worldwide, satellites are often equipped with various flexible appendages such as solar panels, antennas, and mechanical manipulators. In recent years, the demand for improvements in satellite functionality and efficiency has led to more lightweight and flexible structure designs operating under stringent performance, positioning, and energy usage requirements. Unfortunately, even the simplest attitude manoeuvres are capable of exciting vibrations in the flexible structures, causing loss of pointing accuracy, decreased performance or even structural damage [116, 117]. Thus, there is a need for a computationally efficient control method capable of maximising the system's performance while complying with hard safety and operational constraints.

A control methodology capable of guaranteeing efficient operation while respecting such constraints is optimal control. Its first application to the problem of flexible satellite control can be traced back as early as the 1970s. Initial developments included Markley's work on performance index selection, which considered a single flexible mode [118]. The work of Breakwell attempted the control of several modes using feedback control and verified the results experimentally [117]. Turner and Junkins also presented work including several modes of vibration and explored the difference in results obtained using a nonlinear model or its linearisation [119]. This research was later extended by Turner and Chun for a distributed control system [120]. In all these works and many subsequent ones, the satellite was modelled as a distributed parameter system and approximated using a spatial discretisation technique. This leads to the formulation of coupled ordinary and partial differential equations of motion. Two of the most common spatial discretisation techniques are the Assumed Modes Method (AMM) and the Finite Element Method (FEM). A detailed review of both and their implementation for flexible spacecraft models can

be found in Junkins, and Kim [121]. However, it must be noted that in both of these techniques, a more accurate representation of the flexible dynamics requires the construction of higher-dimensional models, which can lead to computationally intensive implementations.

This issue can be addressed through the use of a multirate variational formulation of the system model proposed in Chapter 3. To demonstrate the advantages of this approach, we formulate a general linear model of the spacecraft and derive its discrete structure-preserving form using the multirate variational approach (in both Lagrangian and Hamiltonian formulations). In a series of tests, we validate the MVI simulation against the analytical solution and demonstrate the superiority of the multirate approach compared to a singlerate solution in providing a high-fidelity solution at a reduced computational cost.

4.4.2 Mathematical model

To represent a wide range of flexible spacecraft, we model the system as a rigid hub, representing the main body, with two rigidly attached flexible appendages as shown in Figure 4.10. A single-axis rotation manoeuvre is considered under the action of torque control input $\tau(t)$ at the hub. It is assumed to excite the flexible appendages antisymmetrically, thus causing no shift in the centre-of-mass of the spacecraft and resulting in the same deflection profiles in both appendages. These elastic transverse deformations are restricted to the plane X-Y that is perpendicular to the axis of rotation as shown in Figure 4.10. The appendages are modelled as cantilever Euler-Bernoulli beams with attached tip masses. Thus, the effects of shear deformation and sectional rotary inertia are neglected. The appendages are assumed to be identical in geometry and material properties, and no structural damping is considered.

Spatial discretisation

To obtain a finite-dimensional model of the system, we employ the Assumed Modes spatial Method (AMM) [121]. This method expresses the transverse elastic deflection

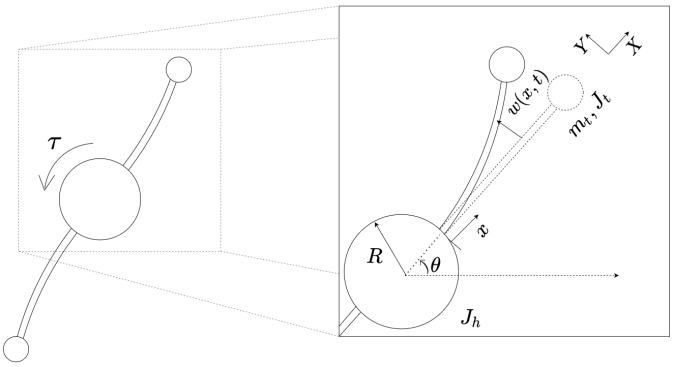


Figure 4.10: Example 3: Spacecraft model during single-axis rotation with antisymmetric deformation

of the beam $w(x,t)$ as a truncated series of products of assumed spatial mode shapes ϕ_j and time-varying modal amplitudes η_j as follows

$$w(x,t) = \sum_{j=1}^{n_{\text{vibr}}} \phi_j(x)\, \eta_j(t).$$

Here, n_{vibr} is the number of modes retained in the approximation, l is the length of the beam, and for this example only, $x \in [0, l]$ denotes the position along the beam. Together with the angle of hub rotation θ, the amplitudes $(\eta_1(t), \ldots, \eta_{n_{\text{vibr}}}(t))$ become the set of the generalised coordinates describing the configuration of the system in time [121]. For the context of rigid-flexible satellites, a widely used set of mode shapes is

$$\phi_j(x) = 1 - \cos\Big(\frac{j\pi x}{l}\Big) + \frac{1}{2}(-1)^{(j+1)}\Big(\frac{j\pi x}{l}\Big)^2.$$

This set of functions satisfies the physical and geometrical boundary conditions for a clamped-free beam but has been shown to produce satisfactory results for models which include tip masses [121].

The Lagrangian

Detailed formulation of the linearised equations of motions can be found in [120, 121]. Based on these derivations, the Lagrangian of the system can be expressed as:

$$\mathfrak{L}(\xi,\, \dot{\xi}) = \frac{1}{2}\, \dot{\xi}^{\intercal}\, \mathbf{M}\, \dot{\xi} - \frac{1}{2}\, \xi^{\intercal}\, \mathbf{K}\, \xi \tag{4.8}$$

where

$$\xi = \begin{bmatrix} \theta \\ \eta \end{bmatrix}, \quad \mathbf{M} = \begin{bmatrix} M_{\theta\theta} & M_{\theta\eta}^{\intercal} \\ M_{\theta\eta} & M_{\eta\eta} \end{bmatrix}, \quad \mathbf{K} = \begin{bmatrix} 0 & 0 \\ 0 & K_{\eta\eta} \end{bmatrix},$$

and the time dependence has been dropped to simplify the notation. Here $\eta \in \mathbb{R}^{n_{\text{vibr}} \times 1}$ is a vector of generalized coordinates defined as $\eta = [\eta_1,\, \eta_2,\, \ldots,\, \eta_{n_{\text{vibr}}}]^{\intercal}$ and ξ represents the configuration vector of the entire system. The elements of the mass and stiffness matrices are defined as

$$M_{\theta\theta} = J_{\text{h}} + 2\left[J_{\text{t}} + m_{\text{t}}(r+l)^2 + \int_0^l \rho A(r+x)^2 dx\right]$$

$$[M_{\theta\eta}]_i = 2\, m_{\text{t}}\, (r+l)\phi_i(L) + 2\, J_{\text{t}}\, \phi_i'(l) + 2\int_0^l \rho A(r+x)\phi_i(x) dx$$

$$[M_{\eta\eta}]_{i,j} = 2\, m_{\text{t}}\, \phi_i(L)\phi_j(l) + 2\, J_{\text{t}}\, \phi_i'(l)\phi_j'(l) + 2\int_0^l \rho A \phi_i(x)\phi_j(x) dx$$

$$[K_{\eta\eta}]_{i,j} = 2\int_0^l EI\phi_i''(x)\phi_j''(x) dx$$

for $M_{\theta\theta} \in \mathbb{R}^{1\times 1}$, $M_{\theta\eta} \in \mathbb{R}^{n_{\text{vibr}}\times 1}$, $M_{\eta\eta} \in \mathbb{R}^{n_{\text{vibr}}\times n_{\text{vibr}}}$, $K_{\eta\eta} \in \mathbb{R}^{n_{\text{vibr}}\times n_{\text{vibr}}}$. Here $[\cdot]'$ and $[.]''$ denote the first and second derivative with respect to x, $[\cdot]_i$ denotes the i-th element of the respective vector, and $[\cdot]_{i,j}$ the (i,j)-th element of the respective matrix. Additionally, J_{h} and r denote the rotary inertia and radius of the hub, while m_{t} and J_{t} represent the mass and the rotary inertia of each of the tip masses, and ρ, A, EI are, respectively, the density, the cross-sectional area and the flexural rigidity of the beams.

The virtual work in this example can be shown to be $\delta W = \mathfrak{f} \cdot \delta\xi = \tau\, \delta\theta$ where $\mathfrak{f}$ is the vector of generalized forces. Using the Lagrange-d'Alembert Principle (2.6), one can then obtain the following equations of motion for this example spacecraft

$$\mathbf{M}\,\ddot{\xi} + \mathbf{K}\,\xi = \mathbf{D}\,\tau \tag{4.9}$$

where $\mathbf{D} = [1, 0, ..., 0]^{\intercal}$ [19, 121].

Transformation to modal coordinates

Equation (4.9) represents a set of $n_{\text{vibr}} + 1$ coupled differential equations, and to decouple them, we introduce the Modal Coordinate Transformation [121, 122]. Solving for the eigenvalue problem for $\mathbf{M}$ and $\mathbf{K}$, we obtain a set of eigenvalues λ_j and normalized eigenvectors e_j as follows

$$|\mathbf{K} - \lambda_j \mathbf{M}| = 0, \;\; \mathbf{K}\, e_j = \lambda_j \mathbf{M}\, e_j, \quad \lambda_j \leq \lambda_{j+1} \quad \text{for} \quad j = 1, 2, \; \ldots, n_{\text{vibr}} + 1$$

such that

$$\mathbf{E}^{\intercal}\mathbf{M}\mathbf{E} = \mathbf{I}, \quad \mathbf{E}^{\intercal}\mathbf{K}\mathbf{E} = \mathbf{\Lambda}$$

$$\text{where} \quad \mathbf{E} = [e_1, \, e_2, \, \ldots, \, e_{n_{\text{vibr}}+1}], \quad \mathbf{\Lambda} = \begin{bmatrix} \lambda_1 & \cdots & 0 \\ \vdots & \ddots & \vdots \\ 0 & \cdots & \lambda_{n_{\text{vibr}}+1} \end{bmatrix}$$

and $\mathbf{I}$ is the identity matrix. Physically, each λ_j corresponds to the square of the natural frequency w_j (rad/s) of the system under consideration, and the corresponding eigenvector describes the corresponding mode shape. Such transformation is possible for real square positive definite matrices M, K (as proved for the more general hermitian matrices in [123, Theorem 2, p.106]). Thus introducing the linear transformation

$$\xi = \mathbf{E}\, q, \quad \dot{\xi} = \mathbf{E}\, \dot{q} \tag{4.10}$$

the Lagrangian and the generalised force vector (the Lagrangian control force) can be rewritten as

$$\mathcal{L} = \frac{1}{2}(\, \dot{q}^{\intercal}\dot{q} - q^{\intercal}\mathbf{\Lambda}\, q\,), \qquad f_{\text{LC}} = \mathbf{E}^{\intercal}\mathbf{D}\, \tau$$

Applying the Lagrange-d'Alembert Principle as before, the equations of motion can be rewritten as

$$\ddot{q} + \mathbf{\Lambda}\, q = \mathbf{E}^{\intercal}\mathbf{D}\, \tau$$

This is a system of $n_{\text{vibr}} + 1$ decoupled differential equations, each describing a motion with natural frequency w_j.

4.4.3 Multirate configuration description and discretisation

In this new coordinate system, depending on the natural frequency of each motion, the satellite's representation can be separated into slow and fast subsystems as

$$q = \begin{bmatrix} q^{\mathrm{s}} \\ q^{\mathrm{f}} \end{bmatrix}, \qquad f_{\mathrm{LC}} = \begin{bmatrix} f_{\mathrm{LC}}^{\mathrm{s}} \\ f_{\mathrm{LC}}^{\mathrm{f}} \end{bmatrix} = \mathbf{E}^{\intercal}\mathbf{D}\,\tau = \begin{bmatrix} Z^{\mathrm{s}} \\ Z^{\mathrm{f}} \end{bmatrix} \tau$$

$$\mathcal{L} = \frac{1}{2}\Big((\dot{q}^{\mathrm{s}})^{\intercal}\dot{q}^{\mathrm{s}} - (q^{\mathrm{s}})^{\intercal}\mathbf{\Lambda}^{\mathrm{s}}\, q^{\mathrm{s}} \Big) + \frac{1}{2}\Big((\dot{q}^{\mathrm{f}})^{\intercal}\dot{q}^{\mathrm{f}} - (q^{\mathrm{f}})^{\intercal}\mathbf{\Lambda}^{\mathrm{f}}\, q^{\mathrm{f}} \Big)$$

where $\mathbf{\Lambda}^{\mathrm{s}} = \mathrm{diag}(\lambda_1,\ \dots\ , \lambda_{n^{\mathrm{s}}})$, $\mathbf{\Lambda}^{\mathrm{f}} = \mathrm{diag}(\lambda_{n^{\mathrm{s}}+1},\ \dots\ , \lambda_{n_{\mathrm{vibr}}+1})$, $q^{\mathrm{s}}, \dot{q}^{\mathrm{s}}, f_{\mathrm{LC}}^{\mathrm{s}}, Z^{\mathrm{s}} \in \mathbb{R}^{\,n^{\mathrm{s}}\times 1}$, $q^{\mathrm{f}}, \dot{q}^{\mathrm{f}}, f_{\mathrm{LC}}^{\mathrm{f}}, Z^{\mathrm{f}} \in \mathbb{R}^{\,(n_{\mathrm{vibr}}+1-n^{\mathrm{s}})\times 1}$ and the time dependence has been dropped to simplify the notation. The size of the slow subsystem n^{s} is a free variable and expresses the number of modal coordinates, which will be treated as slow dynamics and thus discretised on a coarser time grid in the multirate approach.

Based on this multirate configuration description and formulation of the Lagrangian, one can discretise the trajectory on the micro and macro time grid and derive a discrete-time approximation of the Lagrangian work, as discussed in Sections 3.4.1, 3.4.2, and 4.1. On the other hand, the Lagrangian control forces $f_{\mathrm{LC}}^{\mathrm{f}}$ and $f_{\mathrm{LC}}^{\mathrm{s}}$ can be approximated by discrete left and right forces as follows

$$f_k^{\mathrm{s}\pm} = Z^{\mathrm{s}}\Big(\frac{\Delta t}{2} \sum_{m=0}^{\mathbb{p}-1} \tau_k^{m+1/2} \Big) \quad \text{for} \quad k = 0, \dots, N-1$$

$$f_k^{\mathrm{f},m\pm} = Z^{\mathrm{f}}\Big(\frac{\Delta t}{2}\, \tau_k^{m+1/2} \Big) \qquad \text{for} \quad k = 0, \dots, N-1,\ m = 0, \dots, \mathbb{p}-1$$

where the control path $u = \tau$ is approximated by piecewise-constant values in $u_{\mathrm{d}} = \tau_{\mathrm{d}}$ which are defined at the midpoints of the micro time grid as

$$\tau_{\mathrm{d}} = \{\{\tau_k^{m+1/2}\}_{m=0}^{\mathbb{p}-1}\}_{k=0}^{N-1} \quad \text{where} \quad \tau_k^{m+1/2} \approx \tau(t_k^{m+1/2}). \tag{4.11}$$

Additionally, we define $\tau_k = \{\tau_k^{m+1/2}\}_{m=0}^{\mathbb{p}-1}$. Applying these approximations in Equations (3.24) and (3.28), one can derive the multrate discrete-time variational model of the system in Lagrangian formulation. Equivalently, one can use the discrete Lagrangian and forces expressions to derive the Hamiltonian formulation of the system's multirate discrete-time model using Equation (3.30). In the next section, we will compare the capabilities of both formulations, demonstrating the advantages of the variational approach in both cases.

4.4.4 Computational results

The two multirate variational discrete-time models were implemented using MATLAB. An example system was used for all simulations with the key geometrical and material parameters presented in Table 4.1 as suggested by [121]. The model is constructed with five terms in the AMM approximation ($n_{\text{vibr}} = 5$) and three degrees of freedom were treated as slow dynamics in the multirate formulation ($n^{\text{s}} = 3$). Based on these specifications, the natural frequencies of the system were obtained as $w_1 = 0$ rad/s, $w_2 = 6.454$ rad/s, $w_3 = 52.41$, rad/s, $w_4 = 1.607 \times 10^2$ rad/s, $w_5 = 3.381 \times 10^2$ rad/s and $w_{n_{\text{vibr}}+1} = 5.78 \times 10^2$ rad/s resulting in dynamics on significantly different time-scales and allowing for thorough investigation of the advantages of the proposed multirate scheme.

Table 4.1: Structural parameters used for the simulations

Hub radius	r	1.0	ft
Hub rotary inertia	J_{h}	8.0	slug-ft^2
Tip mass	m_{t}	0.156941	slug
Tip mass rotary inertia	J_{t}	0.0018	slug-ft^2
Beam length	l	4.0	ft
Beam height	h	6.0	in.
Beam thickness	t	0.125	in.
Beam linear density	ρA	0.0271875	slug/ft
Beam elastic modulus	E	0.1584×10^{10}	lb/ft^2

System simulation

The proposed numerical integration scheme was validated against a reference analytic solution, and its advantages were thoroughly investigated. This was achieved through a series of forward simulations in the absence of control for a time period of $t \in [0, T]$ starting from a rest position with an initial deflection in the appendages of $\eta(t_0) = [0.05, 0.001, 0.001, 0.0001, 0.0001]^{\intercal}$.

First, the numerical convergence of the method was investigated by computing the global error of the HF MVI simulated configuration with respect to the analytical continuous solution. The comparison was conducted on the macro time nodes for both the slow and fast variables $(q^{\text{s}}, q^{\text{f}})$ using the following error definition

$$e_x(x_d, x) = \max_{k=0,\dots,N} (\|x_k - x(t_k)\|_\infty) \tag{4.12}$$

Figure 4.11 presents the results for $T = 1.2$s and macro-micro proportionalities of $\mathbb{p} = 1, 3, 5, 6$, where $\mathbb{p} = 1$ corresponds to a singlerate solution. These figures demonstrate error convergence of approximately order 2, as expected from the order of the chosen quadrature, thus validating the correct behaviour of the numerical integration scheme and demonstrating numerically its order of convergence. We also note that an order reduction is observed in both figures for a small region of time-steps, indicated by the presence of plateau. This behaviour is not surprising for stiff systems (see [114]). Figures 4.12 and 4.13 present the evolution of the

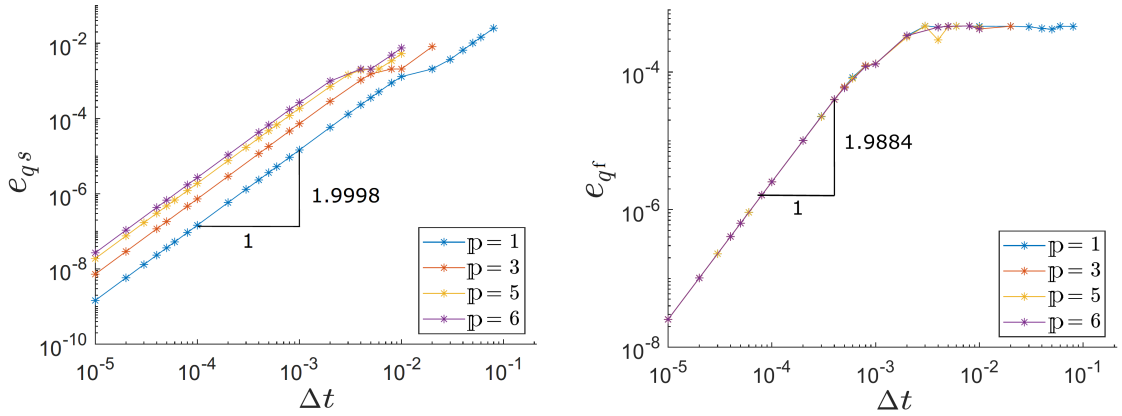


Figure 4.11: Example 3: Log-log plot demonstrating the order of convergence for the HF MVI based on simulations for a constant length of simulation $T = 1.2$s

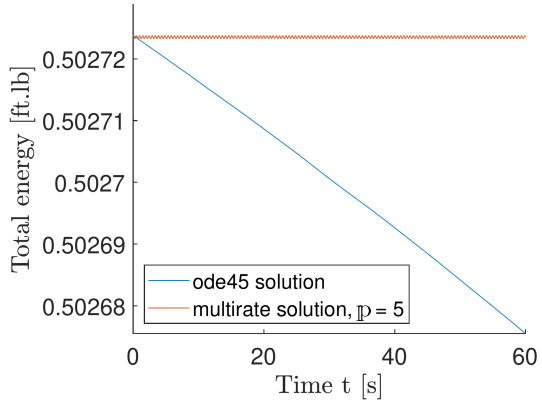


Figure 4.12: Example 3: Numerical dissipation of total energy for simulations of ode45 and HF MVI with $\Delta t = 10^{-4}$s and $T = 60$s

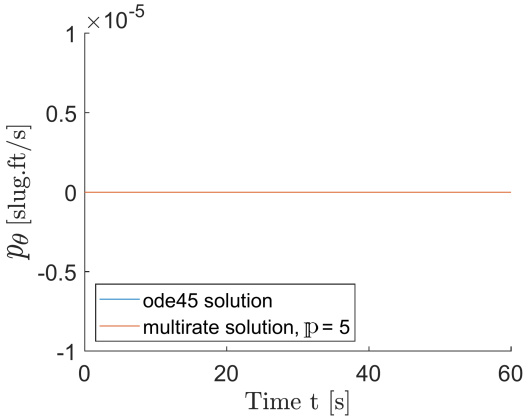


Figure 4.13: Example 3: Momentum preservation for simulations of ode45 and HF MVI with $\Delta t = 10^{-4}$s and $T = 60$s

total energy and the generalised momentum for θ defined as:

$$p_\theta = \frac{\partial \mathcal{L}}{\partial \dot{\theta}} = M_{\theta\theta}\,\dot{\theta} + (M_{\theta\eta})^\intercal\,\dot{\eta} \tag{4.13}$$

The results are obtained from simulations with step size of $\Delta t = 10^{-4}$ using both the Hamiltonian formulation of the variational scheme with $\mathbb{p} = 5$ and the ode45 MATLAB numerical solver with *RelTol* of 10^{-10}. As the Lagrangian (Equation (4.8)) is not explicitly dependent on t and θ and no damping and external forces are considered in this test case, both the total energy and p_θ should remain constant in time according to Noether's theorem [1]. Figure 4.13 demonstrates that both the ode45 implementation and the multirate solution successfully preserve p_θ. In Figure 4.12, however, it can be observed that the ode45 implementation introduces numerical dissipation, while the variational scheme successfully preserves the total energy of the system up to small bounded fluctuations known to be present for variational integrators (see [20]). Together, the two tests demonstrate the structure-preserving properties of the variational scheme.

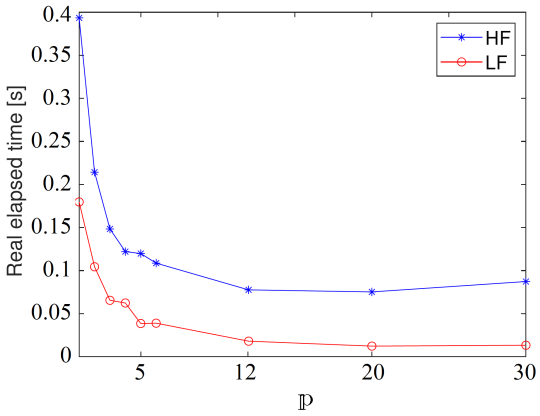


Figure 4.14: Example 3: Mean computational time with standard deviation versus $\mathbb{p}$ for a constant micro time step of $\Delta t = 10^{-4}$s and $T = 1.2$s

Returning to Figure 4.11, we can further observe that making the macro grid coarser by increasing $\mathbb{p}$ increases the error in the computation of the slow variables slightly but maintains the same accuracy in the approximation of the fast ones. This small sacrifice in the accuracy, however, enables great computational savings. To demonstrate the reduction in computational cost for of the multirate approach we performed a series of simulations for a number of macro-to-micro time step

proportionalities $\mathbb{p}$ while keeping the micro step constant at 10^{-4}. Figure 4.14 presents the mean of the real elapsed time for the respective simulation obtained from 10 measurements using the *tic-toc* MATLAB routine. Focusing first on the Hamiltonian formulation, a clear reduction in the required computational time can be seen by increasing $\mathbb{p}$ up to an optimal value ($\mathbb{p} = 6$ in this instance). The existence of an optimum $\mathbb{p}$-value is due to the specific implementation of the numerical integrator, which uses the Newton-Raphson method to resolve the system one macro time step at a time. As discussed previously, increasing the number of micro time steps within a macro time step increases the number of variables being obtained at each iteration of the Newton-Rhapson method and thus results in slower computations. While this effect might also occur with the LF of the MVI, it does not appear in this test for the given values of $\mathbb{p}$. Aside from this, the LF MVI formulation behaves similarly to the HF with the required computational runtime reducing as $\mathbb{p}$ increases. Notably, the computational runtime required by LF is roughly half that of the HF for all considered values of $\mathbb{p}$, since the momentum computation is excluded.

4.5 Example 4: Electrodynamic tether motion

In our fourth example, we aim to demonstrate the capabilities of the MVI for constrained nonlinear systems and its application to another real-world application. We develop a novel variational model for six-dimensional spacecraft motion in a three-body gravitational environment influenced by external forces, such as electrodynamic tethers, solar sails, external torque, and thrust controls. This model allows us to achieve high-fidelity simulations with reduced computational cost using both singlerate and multirate variational integrators. We caution the reader that for this section only, there is a change of notation, with the quaternion position of the satellite being denoted as $q \in \mathbb{R}^4$ and the orbital position coordinates as $x, y, z \in \mathbb{R}$ to honour the standard notation used in the field this application example belongs to.

4.5.1 Introduction

In recent years, the need for high-fidelity models in the simulation and control of spacecraft motion has increased. With the exploration of Jupiter's moons and the growing interest in exploring cis-lunar space as evidenced by the Global Exploration Roadmap [124], more stress has been placed on the accurate modelling of spacecraft dynamics in a three-body gravitational environment in order to enable safe execution of close-proximity manoeuvres such as docking, maintenance and others. With this in mind some works have shifted their focus from modelling spacecraft operations within a two-body gravitational environment to within a three-body gravitational environment ([125–128] among others). Recent publications have extended these models further, from 3DOF (3 degrees of freedom) to 6DOF models by considering simultaneously the orbital and attitude motion of the vehicle [104, 129]. When external configuration-dependent forces are considered, such 6DOF models allow for coupling effects to be considered in the simulation. Despite these advances, there is still considerable room for improvement in the model fidelity and computational cost, especially for spacecraft systems, where the available hardware capacity is limited due to the effect of harsh environments on the hardware and the limited weight/space onboard. The use of such models for optimal control problems is also in early stages with only a few tasks investigated so far [130].

To this problem, we apply the singlerate and multirate variational approach in order to exploit the resulting smaller dimensionality models and the system's multirate behaviour to obtain high-fidelity solutions at a reduced computational cost. The main drawback of using SVI and MVI, however, is the need to provide them with expressions for the Lagrangian of the system and the forces acting on it– a task that is not trivial for many applications. For this reason, in this section, we aim to propose a novel variational model for 6DOF spacecraft dynamics in the three-body gravitational environment considering both the orbital and attitude motion of the vehicle. As many other works, we consider the circular restricted three-body problem (CR3BP) in which the mass of the spacecraft is considered infinitesimal

to that of the two larger bodies whose motion is constrained to circular orbits about their barycenter. We describe the attitude motion of the spacecraft using a unit quaternion representation. Such formulation introduces a constraint in the dynamics in terms of the unit size of the quaternion vectors but does not present singularities and is often preferred for the description of large-angle manoeuvres [131]. Additionally, we consider the effect of a general force acting on the system, which could be used to model the effect of electrodynamic tethers, solar sails, thrust or torque controls and others on the system. When the chosen force is configuration-dependent, it introduces additional coupling between the orbital and attitude motion, allowing for the control of one of the motions through the other.

As an example, we choose electrodynamic tether force and, based on the resulting Lagrangian and and virtual work formulation, apply the singlerate and multirate variational approach. This allows us to demonstrate the capabilities of SVI and MVI for forced nonlinear constrained systems and the advantages of using them for the 6DOF control of a spacecraft in the CR3BP.

4.5.2 Variational model of 6DOF tethered spacecraft dynamics

To derive a variational model for the attitude and orbital motion of a spacecraft equipped with a tether in the gravitational field of two planers, we need to first find an expression for the system's Lagrangian and the external forcing in generalised coordinates. We describe the translational motion of the system in the inertial frame of reference $(\hat{X}, \hat{Y}, \hat{Z})$ whose origin coincides with the barycenter of the two large primary bodies with masses M_1 and M_2. The rotational frame $(\hat{x}, \hat{y}, \hat{z})$ coincides with the inertial frame initially and then rotates around $\hat{Z}$ with its origin remaining at the barycenter and the $\hat{z}$ aligned with $\hat{Z}$ at all times as depicted on Figure 4.15. A third body-fixed frame $(\hat{b}_1, \hat{b}_2, \hat{b}_3)$ is also introduced and aligned with the principle inertial axis of the small third body.

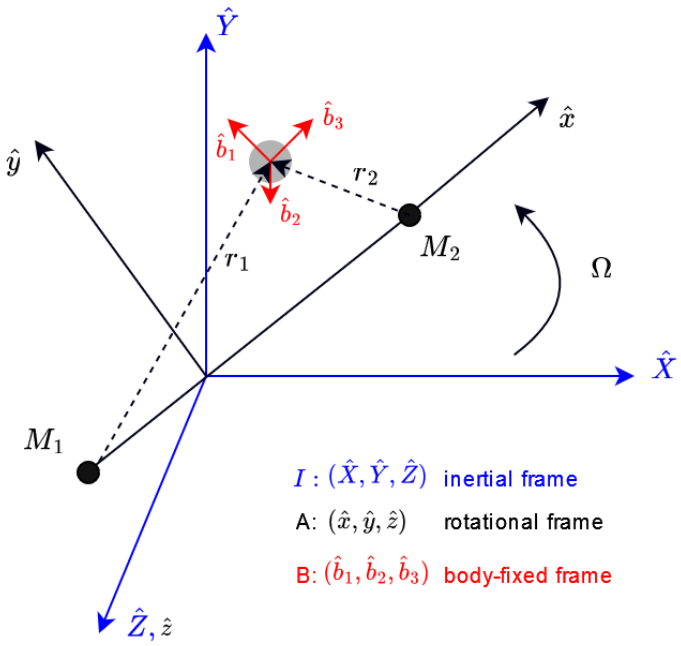


Figure 4.15: Example 4: Illustration of the chosen coordinate frames for a satellite in the CR3BP

Orbital dynamics

We consider the circular restricted three-body problem in which the mass of the spacecraft is considered infinitesimal to that of the two larger bodies, whose motion is constrained to circular orbits around their barycenter [104, 132]. The Lagrangian for this system system we express as:

$$L^{\text{orbit}}(x, y, z, \dot{x}, \dot{y}, \dot{z}) = \frac{1}{2}(\dot{x}^2 + \dot{y}^2 + \dot{z}^2 + 2\dot{y}x - 2y\dot{x}) + \frac{1}{2}(x^2 + y^2) + \frac{\mu - 1}{r_1} + \frac{-\mu}{r_2}$$
$$r_1 = \sqrt{(x+\mu)^2 + y^2 + z^2}, \quad r_2 = \sqrt{(x+\mu-1)^2 + y^2 + z^2}$$

where x, y, z are the position coordinates in the rotating frame, and μ is the mass ratio $\mu = M_2/(M_1 + M_2)$, allowing for a non-dimensional form of the resulting equations of motion with unitary gravitational constant and angular frequency Ω.

Attitude dynamics

The attitude motion of the body can be modelled using unit quaternions, describing the instantaneous relative orientation of the body-fixed frame with respect to the inertial frame as it evolves on the special orthogonal group SO(3) [113]. Such

parametrisation of the motion does not present singularities and is often preferred for describing large-angle manoeuvres [131]. Quaternions can be described as a four-dimensional object containing a three-dimensional vector part q_v and a scalar part q_s. They can also be described in terms of an axis of rotation $\hat{r} = [r_X, r_Y, r_Z]^\intercal$ and an angle of rotation θ around this axis as follows:

$$q = \begin{bmatrix} q_\mathrm{v} \\ q_\mathrm{s} \end{bmatrix} = \begin{bmatrix} \sin\left(\frac{\theta}{2}\right)\hat{r} \\ \cos\left(\frac{\theta}{2}\right) \end{bmatrix} \quad \text{with} \quad \|q_\mathrm{v}\|^2 + q_\mathrm{s}^2 = 1$$

The conjugate quaternion and the quaternion product are defined as

$$q^* = \begin{bmatrix} -q_\mathrm{v} \\ q_\mathrm{s} \end{bmatrix}, \quad q_1 \otimes q_2 = \begin{bmatrix} q_{\mathrm{v},1} \\ q_{\mathrm{s},1} \end{bmatrix} \otimes \begin{bmatrix} q_{\mathrm{v},2} \\ q_{\mathrm{s},2} \end{bmatrix} = \begin{bmatrix} q_{\mathrm{v},1} \times q_{\mathrm{v},2} + q_{\mathrm{s},1} q_{\mathrm{v},2} + q_{\mathrm{s},2} q_{\mathrm{v},1} \\ q_{\mathrm{s},1} q_{\mathrm{s},2} - q_{\mathrm{v},1} \cdot q_{\mathrm{v},2} \end{bmatrix}$$

The angular velocity of the body and the generalised forces corresponding to torques on the body can be expressed as:

$$\hat{w} = 2q^* \otimes \dot{q}, \quad F = 2q \otimes \hat{\tau}.$$

The Lagrangian describing the attitude dynamics can thus be expressed as [113]:

$$L^{\mathrm{attit}}(q, \dot{q}) = \frac{1}{2}(2q^* \otimes \dot{q}) \cdot J(2q^* \otimes \dot{q}), \quad J = diag\{I_1, I_2, I_3, 0\}$$

where I_1, I_2, I_3 denote the principal central moments of inertia. Furthermore, the gravity torque exerted by the primaries can be modelled as external forces as

$$f^{\mathrm{attit}} = 2q \otimes \begin{bmatrix} (I_3 - I_2)\left(\frac{3(1-\mu)}{r_1^5}[\mathfrak{f}]_2[\mathfrak{f}]_3 + \frac{3\mu}{r_2^5}[h]_2[h]_3\right) \\ (I_1 - I_3)\left(\frac{3(1-\mu)}{r_1^5}[\mathfrak{f}]_1[\mathfrak{f}]_3 + \frac{3\mu}{r_2^5}[h]_1[h]_3\right) \\ (I_2 - I_1)\left(\frac{3(1-\mu)}{r_1^5}[\mathfrak{f}]_1[\mathfrak{f}]_2 + \frac{3\mu}{r_2^5}[h]_1[h]_2\right) \\ 0 \end{bmatrix} \tag{4.14}$$

$$\mathfrak{f} = C^{B/A}[x + \mu, y, z]^\intercal, \quad h = C^{B/A}[x + \mu - 1, y, z]^\intercal$$

where $[\cdot]_i$ denotes the ith element of a vector, $u = [u_1, u_2, u_3]$ are external controls,

$$C^{B/A} = C^{B/I} C^{I/A} = (C^{A/B})^\intercal, \quad C^{I/A} = \begin{bmatrix} \cos(\Omega t) & -\sin(\Omega t) & 0 \\ \sin(\Omega t) & \cos(\Omega t) & 0 \\ 0 & 0 & 1 \end{bmatrix}$$

$$C^{B/I} = \begin{bmatrix} 1 - 2([q]_2^2 + [q]_3^2), & 2([q]_1[q]_2 + [q]_3[q]_4), & 2([q]_1[q]_3 - [q]_2[q]_4) \\ 2([q]_1[q]_2 - [q]_3[q]_4), & 1 - 2([q]_1^2 + [q]_3^2), & 2([q]_2[q]_3 + [q]_1[q]_4) \\ 2([q]_1[q]_3 + [q]_2[q]_4), & 2([q]_2[q]_3 - [q]_1[q]_4), & 1 - 2([q]_1^2 + [q]_2^2) \end{bmatrix}$$

It is important to note that this force introduces coupling between the orbital and attitude motion of the system.

External forcing

Additional coupling between the orbital and attitude dynamics can result from the presence of external forcing from devices such as electrodynamic tethers and solar sales. To demonstrate, we consider the tether and model it as an external force expressed in generalised coordinates. As in most of the literature (see, for example, [133]), we assume a non-tilted dipole magnetic field and a self-balanced tether [134] modelled as a rigid dumbbell in direction $\hat{b_3}$. Thus the Lorentz torque about the system centre of mass is assumed to be zero and does not affect the orientation of the system, only its orbital position. With those assumptions, the Lorentz force can be written as

$$f^{\text{ex}} = \int_0^l I(z) d\hat{u} \times B dz = I_{\text{avg}} L \hat{u} \times B \tag{4.15}$$

where $\hat{u} = \hat{b_3}$ is the unit vector along the tether line, $I(z)$ is the current profile along the tether with z measured from the anodic tip, l is the tether length and I_{avg} is the length-averaged electric current [127, 133, 135]. The generalised force corresponding to L^{orbit} and the generalised coordinates $[x, y, z]^\intercal$ can then be expressed as

$$f^{\text{ex}} = \frac{I_{\text{avg}} l B_0}{m_{\text{s/c}} r_1^5} C^{A/B} \begin{bmatrix} 0 \\ 0 \\ 1 \end{bmatrix} \times \begin{bmatrix} 3(x+\mu)z \\ 3yz \\ 2z^2 - (x+\mu)^2 - y^2 \end{bmatrix}, \tag{4.16}$$

normalised analogously to the orbital equations. Here B_0 is the local value of the magnetic field, and $m_{\text{s/c}}$ is the total mass of the tethered system. Details on how to calculate I_{avg} can be found in [127, 133, 135]. Within the full model, such force introduces additional coupling between the attitude and orbital dynamics, and by controlling the attitude motion, we control the force in the tether and thus the orbital dynamics indirectly (this is clear in the continuous model (A.2d) -(A.2b)).

Similarly, one could consider low-thrust dynamics instead. In this case

$$f^{\text{ex}} = C^{A/B} u, \quad \|u\|_2 \leq u^{\max} \tag{4.17}$$

for $u \in \mathbb{R}^3$ and a given maximum magnitude of the available thrust $u^{\max}$. The

attitude dynamics can also be prescribed using torque control, leading to

$$f^{\text{attit}} = 2q \otimes \begin{bmatrix} (I_3 - I_2)\left(\frac{3(1-\mu)}{r_1^5}[g]_2[g]_3 + \frac{3\mu}{r_2^5}[h]_2[h]_3\right) + \tau_1 \\ (I_1 - I_3)\left(\frac{3(1-\mu)}{r_1^5}[g]_1[g]_3 + \frac{3\mu}{r_2^5}[h]_1[h]_3\right) + \tau_2 \\ (I_2 - I_1)\left(\frac{3(1-\mu)}{r_1^5}[g]_1[g]_2 + \frac{3\mu}{r_2^5}[h]_1[h]_2\right) + \tau_3 \end{bmatrix} \tag{4.18}$$

Finalised 6DOF model

Taking sections 4.5.2-4.5.2 into account, we express the system's generalised coordinate vector s, Lagrangian, external Lagrangian control forces and constraints as:

$$s = [x, y, z, q_{\text{v}}^{\intercal}, q_{\text{s}}]^{\intercal} \tag{4.19a}$$

$$\mathcal{L}(s, \dot{s}) = \frac{1}{2}(\dot{x}^2 + \dot{y}^2 + \dot{z}^2 + 2\dot{y}x - 2y\dot{x} + x^2 + y^2) + \frac{\mu - 1}{r_1} + \frac{-\mu}{r_2} + \frac{1}{2}(2q^* \otimes \dot{q}) \cdot J(2q^* \otimes \dot{q}) \tag{4.19b}$$

$$f_{\text{LC}}(s, \dot{s}, u, \tau) = [(f^{\text{ex}})^{\intercal}, (f^{\text{attit}})^{\intercal}]^{\intercal} \tag{4.19c}$$

$$g(s) = \|q_{\text{v}}\|^2 + q_{\text{s}}^2 - 1 = 0 \tag{4.19d}$$

These equations can be used in Equations (A.2d)-(A.2b) to obtain a continuous model, which can then be discretised.

Alternative model

For comparison reasons in our numerical results, we note that one could also discretise the state-space singlerate model proposed by [104, 129]:

$$\ddot{x} = x + 2\dot{y} - \frac{(1-\mu)(x+\mu)}{r_1^3} - \frac{(\mu)(x-1+\mu)}{r_2^3} + [f^{\text{ex}}]_1 \tag{4.20a}$$

$$\ddot{y} = y - 2\dot{x} - \frac{(1-\mu)(y}{r_1^3} - \frac{(\mu)y}{r_2^3} + [f^{\text{ex}}]_2 \tag{4.20b}$$

$$\ddot{z} = -\frac{(1-\mu)z}{r_1^3} - \frac{(\mu)z}{r_2^3} + [f^{\text{ex}}]_3 \tag{4.20c}$$

$$[\dot{w}]_1 = \frac{I_3 - I_2}{I_1}\left(\frac{3(1-\mu)}{r_1^5}[g]_2[g]_3 - \frac{3(\mu)}{r_2^5}[h]_2[h]_3 - [w]_2[w]_3 + \tau_1\right) \tag{4.20d}$$

$$[\dot{w}]_2 = \frac{I_1 - I_3}{I_2}\left(\frac{3(1-\mu)}{r_1^5}[g]_1[g]_3 - \frac{3(\mu)}{r_2^5}[h]_1[h]_3 - [w]_1[w]_3 + \tau_2\right) \tag{4.20e}$$

$$[\dot{w}]_3 = \frac{I_2 - I_1}{I_3}\left(\frac{3(1-\mu)}{r_1^5}[g]_1[g]_2 - \frac{3(\mu)}{r_2^5}[h]_2[h]_2 - [w]_1[w]_2 + \tau_3\right) \tag{4.20f}$$

$$[\dot{q}]_1 = \frac{1}{2}([w]_3[q]_2 - [w]_2[q]_3 + [w]_1[q]_4) \tag{4.20g}$$

$$[\dot{q}]_2 = \frac{1}{2}(-[w]_3[q]_1 + [w]_1[q]_3 + [w]_2[q]_4) \tag{4.20h}$$

$$[\dot{q}]_3 = \frac{1}{2}([w]_2[q]_1 - [w]_1[q]_2 + [w]_3[q]_4) \tag{4.20i}$$

$$[\dot{q}]_4 = \frac{1}{2}(-[w]_1[q]_1 - [w]_2[q]_2 - [w]_3[q]_3) \tag{4.20j}$$

$$0 = [q]_1^2 + [q]_2^2 + [q]_3^2 + [q]_4^2 - 1 \tag{4.20k}$$

where $w \in \mathbb{R}^{n_q}$ denotes the angular velocity vector. The purpose of deriving Lagrangian forces and constraint expressions, however, is to allow us to employ the proposed variational approach instead, which allows for a reduction in the dimensionality of the model and computational savings in its simulation, as we will now demonstrate.

4.5.3 Numerical results

To demonstrate the developed variational models, we consider the Earth-Moon-spacecraft three-body environment with Earth as M_1, the moon as M_2. We perform simulations for a Near Rectilinear Halo Orbit as this family of orbits has been highlighted by many works as a good choice to host the Gateway Project. Although the Earth-Moon system does not provide a very strong magnetic field for the use of tethers, the chosen orbit is known as a challenging task for many integrators due to the sensitive nonlinear dynamics. It is thus a good choice for demonstrating the capabilities of the proposed variational models. The singlerate and multirate variational models for this constrained forced system are implemented based on the system description in (4.19) and the methodology described in Sections 3.5 and 4.1.1. These models are implemented using Python and the automatic differentiation library *JAX* [115]. A Runge-Kutta 4 (RK4) discretisation of the previously proposed singlerate state-space model (4.20) was also implemented as described in [129] and used as a comparison for the proposed variational formulation.

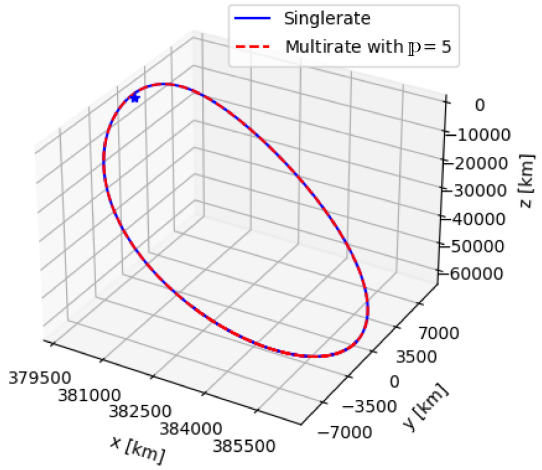


Figure 4.16: Example 4: Discrete-time simulation of the orbital dynamics with $\Delta t = 10^{-5}$ in the absence of forcing

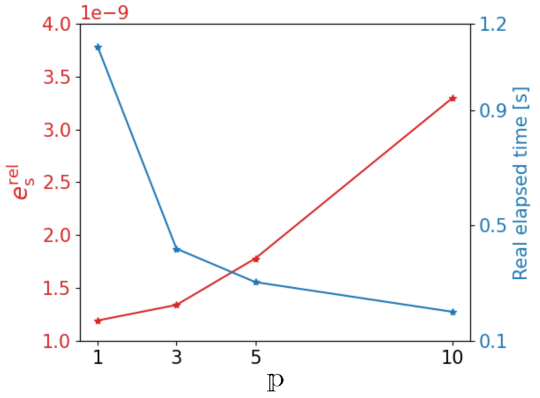


Figure 4.17: Example 4: Trade-off be between computational efficiency and accuracy penalty for a constant micro time step $\Delta t = 0.00012$ and length of simulation $T = 0.012$, but varying macro-micro proportionality $\mathbb{p}$

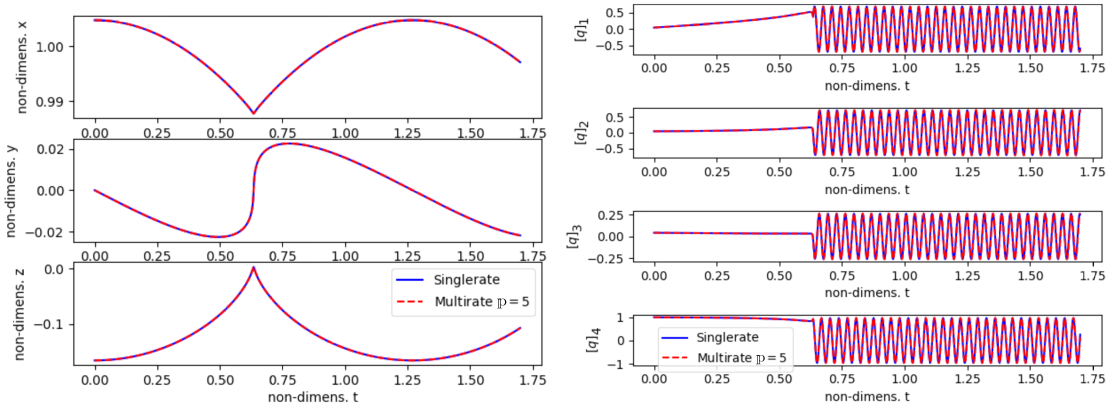


Figure 4.18: Example 4: Discrete-time trajectory simulations with $\Delta t = 0.00001$ in the absence of forcing

Simulations in the absence of external forcing

First, we performed simulations in the absence of thrust control, torque controls, and external forcing from tethers ($f^{\text{ex}} = u = \tau = 0$) in order to validate the proposed models against a standard approach such as the RK4 discretisation of the continuous model (4.20). Simulations were performed with $\Delta t = 10^{-5}$ for the RK4 and singlerate variational approaches. The same step was chosen for the micro time grid in the multirate approach with only the x-coordinate chosen as slow (thus $n^{\text{s}} = 1$). A series of tests were performed, keeping the micro step constant but increasing the macro-micro proportionality $\mathbb{p}$. As we can see from Figures 4.16

and 4.18, both the singlerate and the multirate integrators accurately captured the orbital dynamics for all choices of macro-micro proportionality.

Fundamentally, increasing $\mathbb{p}$ reduces the number of time nodes on which the slow variables are computed, introducing computational savings. Of course, as with our previous examples, $\mathbb{p}$ cannot be increased limitlessly as that will progressively degrade the resolution of the slow dynamics, leading to erroneous solutiona. Figure 4.17 shows the trade-off between computational efficiency and accuracy. Here, the norm is computed between the multirate solution and a very fine Runge-Kutta 4 solution of (4.20) as:

$$e_{\mathrm{s}}^{\mathrm{rel}} = \frac{\max_{k=0,\dots,N} \|s_k - s_k^{\mathrm{RK4}}\|_\infty}{\max_{k=0,\dots,N} \|s_k^{\mathrm{RK4}}\|_\infty} \tag{4.21}$$

The simulation is done using $\Delta t = 10^{-4}, T = 0.012, \mathbb{p} = 1, 3, 5, 10$. These values were chosen to ensure that an integer number of the macro steps fit within the simulation length T. Even with just a single coordinate discretised on the macro time grid, the figure demonstrates that from $\mathbb{p} = 1$ to $\mathbb{p} = 5$, the computational time has decreased more than four times for negligible penalty in accuracy. This result cannot be fully explained by the reduced size of the slow system alone. It is also influenced by the implementation details, such as the Newton-Raphson root-finding method and the use of an if-statement in the code to differentiate between the SVI and MVI implementations, which were kept as similar as possible. Therefore, a more meaningful comparison can be made between $\mathbb{p} = 3$ and 5, where the speed-up is a factor of 1.4. Further savings (accompanied by further small penalties in accuracy) are expected if the size of the slow system is increased. In practice, the trade-off can be tuned by the problem at hand and the available computational resources.

Simulations in the presence of external forcing

Next, we perform a test with the same simulation parameters but with the addition of external force from a tether as described in Equation (4.16) with $\frac{I_{\mathrm{avg}} L B_0}{m_{\mathrm{s/c}} r_1^5} = 1$. Figure 4.19 demonstrates the agreement between a Runge-Kutta 4 (RK4) integration of the alternative singlerate model (4.20) and the proposed variational model in both singlerate and multirate formulation. Additionally, Figure 4.20 demonstrates

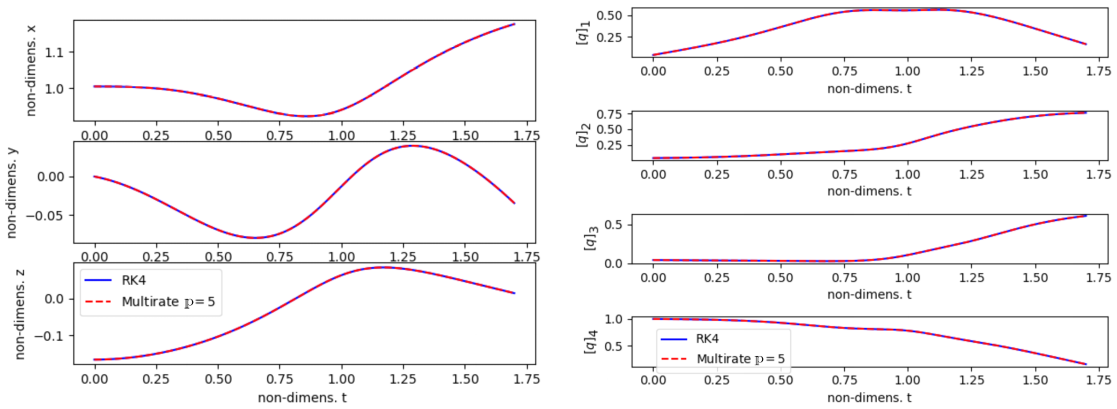


Figure 4.19: Example 4: Discrete-time trajectory simulation with $\Delta t = 0.00001$ in the presence of tether force

that both the RK4, the singlerate, and the multirate variational models obey the constraint placed on the system in terms of the unit quaternion norm. With this magnitude of the external force, we can see that the time scales of the problem are very similar. Thus, for this specific orbit and force magnitude, not much can be gained from the use of the multirate formulation. The variational formulation itself, however, reduces the dimensionality of the model without visible loss of accuracy in both singlerate and multirate Lagrangian form by avoiding the integration of the momentum and thus reduces the computational burden of the simulation compared to the alternative state-space models proposed by [104, 129].

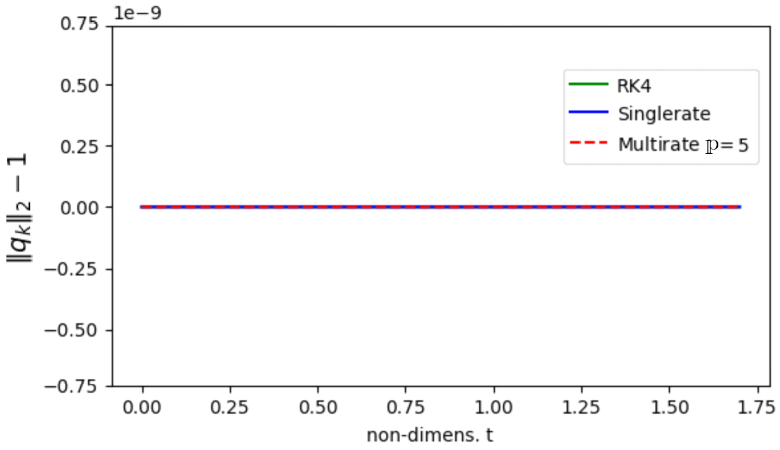


Figure 4.20: Example 4: Demonstration of the constraint satisfaction during discrete-time simulations with $\Delta t = 0.00001$

5

Open-Loop Control

5.1 Introduction

This chapter introduces a structure-preserving direct method for solving optimal control problems for systems exhibiting dynamics on different time scales. The approach, which we will refer to as Multirate DMOC, was originally proposed by [4] as a multirate reformulation of the DMOC method described in Chapter 2.

In this chapter, we provide a thorough mathematical analysis of Multirate DMOC. For a broad class of systems, we formulate a generic optimal control problem and derive the necessary conditions for optimality in both continuous and discrete time. Under certain assumptions, we prove the structure-preserving properties and accuracy order of the resulting solutions. Additionally, we demonstrate these properties numerically through two examples, a theoretical problem and a practical example from the aerospace domain.

5.2 Background

In Chapter 2 we discussed the existence of numerous techniques for approximating the behaviour of systems in discrete-time. One technique we specifically focused on was the variational integrator, particularly its formulation as presented by [1].

This scheme offers a qualitatively superior system representation by preserving the mathematical structures of the model in its discrete approximation, specifically its symplecticity and any symmetries present within the Lagrangian. Consequently, the method ensures accurate representation of the system's energy and momenta during simulations, where many non-geometric schemes introduce numerical dissipation [26]. Notably, as we presented in Chapter 2, this approach can also be integrated within a direct optimal control solution method to provide structure-preserving system and adjoint discrete-time models with well understood accuracy. The resulting scheme has been tested extensively in literature and found multiple practical applications.

In Chapter 3 we focused on the simulation of systems with dynamics on different time scales, i.e. multirate systems. We provided a detailed description of the formulation and properties of a multirate variational integrator (MVI) designed to deliver high-fidelity simulations for these systems at reduced computational cost. The approach achieves this by discretising the slow and fast dynamics on two different time scales, each with the appropriate time step, without the need to decouple the equations of motion. The model can be formulated either as a standard phase-space scheme, integrating both configuration and momentum over time, or as a multistep scheme integrating only the configuration variables over time theoretically without loss of accuracy. Notably, we proved that in both formulations, the resulting multirate scheme is structure-preserving and established its order of accuracy for a broad class of systems. In practice, the difference in accuracy between the two formulations depends on the accuracy of the methods used to solve the resulting discrete equations of motion.

In [4], Gail et al. successfully implemented MVI in the context of optimal control, developing a method known as Multirate Discrete Mechanics and Optimal Control (Multirate DMOC). This approach allows for a unified control of both the slow and fast dynamics without the need to decouple the equations of motion. Compared to its singlerate counterpart, when optimising the behaviour of systems with dynamics on different time scales, this multirate formulation allows for great reductions in

the number of unknowns and constraints. It is further expected and validated with examples that the method inherits the structure-preserving properties of variational integrators. Unlike many alternative techniques that divide the system into slow and fast components and apply different control strategies to each (e.g., [103]), Multirate DMOC offers a unified control approach that can potentially enhance the optimality of the solution. This method is also distinct from envelope-based techniques (e.g., [136]), as it is not limited to highly oscillatory systems where trajectories oscillate rapidly but follow a slowly changing envelope. Multirate DMOC, however, is not applicable to systems without a Lagrangian representation. These representations are challenging to formulate for some problems, but remain an active area of research as they can potentially allow better understanding of the system.

Since its introduction, Multirate DMOC has been successfully extended to systems with constraints [11] and, as we will present in the following chapter, used to create a new receding horizon technique [13, 112]. Despite its potential, the Multirate DMOC method itself has only been briefly introduced [4] and tested for a spring pendulum but was never further analysed or extended. Very recently, the method was described in more detail by [112]. However, limited new insight was presented.

In this chapter, we present a detailed mathematical description and analysis of the Multirate DMOC method. We expand on the previous works by deriving the continuous- and discrete-time necessary optimality conditions for a generic optimal control problem and thus under certain assumptions proving the structure-preserving properties and order of the Multirate DMOC solution. These theoretical investigations are suported with numerical tests for the control of two of the example systems presented in Chapter 4 - the FPUT system and the flexible satellite model. These numerical studies also demonstrate the computational efficiency of the approach highlighting a flavourable trade-off between accuracy and computational cost. The computational efficiency can further be improved when the multistep integrator formulation is used, removing the need to encode the velocity (or momentum) of the system for a negligible accuracy loss in practice.

5.3 Optimal control of multirate mechanics

Having examined the system's dynamics from both the Lagrangian (state space) and Hamiltonian (phase space) perspectives, we can now extend these frameworks to formulate an optimal control problem (OCP) in each space. While the two formulations are theoretically equivalent, in practice, their numerical solvers may converge to different local optima when dealing with nonconvex problems. The choice between these approaches depends on the specific problem, objectives, and available optimisation resources, as each offers distinct advantages and disadvantages that will be discussed shortly.

As before, we will consider a mechanical system which exhibits dynamics on different time scales and can be represented through a configuration vector $q(t) \in Q$ with all possible paths belonging to $\mathcal{C}([0,T],Q)$ (see (2.1)). We assume that through a change in the coordinate system, we can represent the evolution of the system on the configuration submanifolds Q^{s}, Q^{f} such that $Q^{\mathrm{s}} \times Q^{\mathrm{f}} = Q$ with associated tangent and cotangent bundles TQ^{s}, TQ^{f} and T^*Q^{s}, T^*Q^{f}, respectively. We also assume that the system can be described by a regular Lagrangian $\mathcal{L}: TQ^{\mathrm{s}} \times TQ^{\mathrm{f}} \to \mathbb{R}$ and is under the action of a Lagrangian control force $f_{\mathrm{LC}}(q(t), \dot{q}(t), u(t))$ which can be resolved into slow and fast components $f_{\mathrm{LC}}^{\mathrm{s/f}}(q^{\mathrm{s}}(t), q^{\mathrm{f}}(t), \dot{q}^{\mathrm{s}}(t), \dot{q}^{\mathrm{f}}(t), u(t))$ along the multirate configuration vectors $q^{\mathrm{s}}(t) \in Q^{\mathrm{s}}$ and $q^{\mathrm{f}}(t) \in Q^{\mathrm{f}}$ respectively as discussed in Section 3.3. We remind the reader that, as defined previously, these forces can represent time-independent forces such as friction and dissipation forces, but also forces involving time-dependent controls $u \in \mathcal{C}([0,T],U)$ as defined in (2.3).

5.3.1 Lagrangian viewpoint

Our objective is to move the system from a given initial state $(q^{\mathrm{s},0}, q^{\mathrm{f},0}, \dot{q}^{\mathrm{s},0}, \dot{q}^{\mathrm{f},0}) \in TQ$ to a given final state $(q^{\mathrm{s},T}, q^{\mathrm{f},T}, \dot{q}^{\mathrm{s},T}, \dot{q}^{\mathrm{f},T}) \in TQ$ during the time interval $t \in [0,T]$ under the influence of a control $u(t)$. In achieving this task, we aim to find such a trajectory in the state space $x = (q(t), \dot{q}(t)) = \left(\begin{bmatrix} q^{\mathrm{s}} \\ q^{\mathrm{f}} \end{bmatrix}, \begin{bmatrix} \dot{q}^{\mathrm{s}} \\ \dot{q}^{\mathrm{f}} \end{bmatrix} \right)$ and control $u(t)$ such

that the cost functional

$$J(q^{\mathrm{s}}, q^{\mathrm{f}}, u) = \int_0^T C(q^{\mathrm{s}}(t), q^{\mathrm{f}}(t), \dot{q}^{\mathrm{s}}(t), \dot{q}^{\mathrm{f}}(t), u(t))dt + \Phi(q^{\mathrm{s}}(T), q^{\mathrm{f}}(T), \dot{q}^{\mathrm{s}}(T), \dot{q}^{\mathrm{f}}(T))$$

is minimised, and any constraints placed on the system or the controls are satisfied. Additionally, both $C : TQ \times U \to \mathbb{R}$, representing the running cost, and $\Phi : TQ \to \mathbb{R}$, the terminal cost term, are assumed to be continuously differentiable. The constraints placed on the system include the initial and final positions defined as

$$(q^{\mathrm{s}}(0), q^{\mathrm{f}}(0), \dot{q}^{\mathrm{s}}(0), \dot{q}^{\mathrm{f}}(0)) = (q^{\mathrm{s},0}, q^{\mathrm{f},0}, \dot{q}^{\mathrm{s},0}, \dot{q}^{\mathrm{f},0})$$
$$(q^{\mathrm{s}}(T), q^{\mathrm{f}}(T), \dot{q}^{\mathrm{s}}(T), \dot{q}^{\mathrm{f}}(T)) = (q^{\mathrm{s},T}, q^{\mathrm{f},T}, \dot{q}^{\mathrm{s},T}, \dot{q}^{\mathrm{f},T})$$

as well as the equations of motion which the system obeys. These equations come from the need of the system to satisfy the Lagrange-d'Alembert principle given in Equation (3.2) and thus are equivalent to the equations of motion (3.3) presented in Section 3.3. Additionally, to represent a broader range of optimal control problems we include the possibility of an alternative terminal state constraint

$$r(q^{\mathrm{s}}(T), q^{\mathrm{f}}(T), \dot{q}^{\mathrm{s}}(T), \dot{q}^{\mathrm{f}}(T), q^{\mathrm{s},T}, q^{\mathrm{f},T}, \dot{q}^{\mathrm{s},T}, \dot{q}^{\mathrm{f},T}) = 0$$

with $r : TQ \times TQ \to \mathbb{R}^{n^r}$ and additional constraints on the states and controls

$$h(q^{\mathrm{s}}(t), q^{\mathrm{f}}(t), \dot{q}^{\mathrm{s}}(t), \dot{q}^{\mathrm{f}}(t), u(t)) \geq 0 \text{ for } t \in [0, T]$$

with $h : TQ \times U \to \mathbb{R}^{n^h}$, where both h and r assumed to be continuously differentiable. Overall the problem can be summarised in Lagrangian formulation in the following optimal control problem (OCP):

Problem 4. ***Lagrangian OCP formulation***

$$\min_{\begin{bmatrix} q^{\mathrm{s}} \\ q^{\mathrm{f}} \end{bmatrix} = q \in \mathcal{C}([0,T],Q), u \in \mathcal{C}([0,T],\mathcal{U})} J(q^{\mathrm{s}}, q^{\mathrm{f}}, u) =$$
$$= \int_0^T C(q^{\mathrm{s}}(t), q^{\mathrm{f}}(t), \dot{q}^{\mathrm{s}}(t), \dot{q}^{\mathrm{f}}(t), u)\, dt \; + \; \Phi(q^{\mathrm{s}}(T), q^{\mathrm{f}}(T), \dot{q}^{\mathrm{s}}(T), \dot{q}^{\mathrm{f}}(T))$$

subject to:

$$(q^{\mathrm{s}}(0), \dot{q}^{\mathrm{s}}(0)) = (q^{\mathrm{s},0}, \dot{q}^{\mathrm{s},0}), \quad (q^{\mathrm{f}}(0), \dot{q}^{\mathrm{f}}(0)) = (q^{\mathrm{f},0}, \dot{q}^{\mathrm{f},0})$$

$$\frac{\partial \mathcal{L}(q^{\mathrm{s}}, q^{\mathrm{f}}, \dot{q}^{\mathrm{s}}, \dot{q}^{\mathrm{f}})}{\partial q^{\mathrm{s}}} - \frac{d}{dt}\left(\frac{\partial \mathcal{L}(q^{\mathrm{s}}, q^{\mathrm{f}}, \dot{q}^{\mathrm{s}}, \dot{q}^{\mathrm{f}})}{\partial \dot{q}^{\mathrm{s}}}\right) + f_{\mathrm{LC}}^{\mathrm{s}}(q^{\mathrm{s}}, q^{\mathrm{f}}, \dot{q}^{\mathrm{s}}, \dot{q}^{\mathrm{f}}, u) = 0$$
$$\frac{\partial \mathcal{L}(q^{\mathrm{s}}, q^{\mathrm{f}}, \dot{q}^{\mathrm{s}}, \dot{q}^{\mathrm{f}})}{\partial q^{\mathrm{f}}} - \frac{d}{dt}\left(\frac{\partial \mathcal{L}(q^{\mathrm{s}}, q^{\mathrm{f}}, \dot{q}^{\mathrm{s}}, \dot{q}^{\mathrm{f}})}{\partial \dot{q}^{\mathrm{f}}}\right) + f_{\mathrm{LC}}^{\mathrm{f}}(q^{\mathrm{s}}, q^{\mathrm{f}}, \dot{q}^{\mathrm{s}}, \dot{q}^{\mathrm{f}}, u) = 0$$

$$r(q^{\mathrm{s}}(T), q^{\mathrm{f}}(T), \dot{q}^{\mathrm{s}}(T), \dot{q}^{\mathrm{f}}(T), q^{\mathrm{s},T}, q^{\mathrm{f},T}, \dot{q}^{\mathrm{s},T}, \dot{q}^{\mathrm{f},T}) = 0$$

$$h(q^{\mathrm{s}}(t), q^{\mathrm{f}}(t), \dot{q}^{\mathrm{s}}(t), \dot{q}^{\mathrm{f}}(t), u(t)) \geq 0 \textit{ for } t \in [0, T]$$

5.3.2 Hamiltonian viewpoint

The OCP can also be formulated in the phase space. For this purpose, we use the Hamiltonian equations of motion to describe the system dynamics and serve as path constraints. Additionally, we need to transform the cost and constraints in order to constrain the trajectory in phase space in a manner equivalent to that in the state space. For this purpose, we consider a general constraint placed on the system

$$h(q^{\mathrm{s}}(t), q^{\mathrm{f}}(t), \dot{q}^{\mathrm{s}}(t), \dot{q}^{\mathrm{f}}(t), u(t)) \geq 0 \text{ for } t \in [0, T] \tag{5.1}$$

with $h : TQ^{\mathrm{s}} \times TQ^{\mathrm{f}} \times U \to \mathbb{R}^{n^h}$ which restricts the choice of solutions in the state space to the set

$$\mathfrak{R} = \{(q^{\mathrm{s}}, q^{\mathrm{f}}, \dot{q}^{\mathrm{s}}, \dot{q}^{\mathrm{f}}, u) \in TQ^{\mathrm{s}} \times TQ^{\mathrm{f}} \times \mathcal{U} \mid h(q^{\mathrm{s}}, q^{\mathrm{f}}, \dot{q}^{\mathrm{s}}, \dot{q}^{\mathrm{f}}, u) \geq 0\}.$$

The corresponding set of feasible solutions in the phase space

$$\tilde{\mathfrak{R}} = \{(q^{\mathrm{s}}, q^{\mathrm{f}}, p^{\mathrm{s}}, p^{\mathrm{f}}, u) \in T^*Q^{\mathrm{s}} \times T^*Q^{\mathrm{f}} \times \mathcal{U} \mid \tilde{h}(q^{\mathrm{s}}, q^{\mathrm{f}}, p^{\mathrm{s}}, p^{\mathrm{f}}, u) \geq 0\} \tag{5.2}$$

is then obtained by transforming

$$\tilde{h} = h \circ ((\mathbb{F}^{\mathrm{s}}L)^{-1}, (\mathbb{F}^{\mathrm{f}}L)^{-1}, \mathrm{Id}) \text{ for } t \in [0, T] \tag{5.3}$$

with $\tilde{h} : T^*Q^{\mathrm{s}} \times T^*Q^{\mathrm{f}} \times \mathcal{U} \to \mathbb{R}^{n^h}$ and Id is the identity acting on the variable $u(t)$. Overall, the multirate Hamiltonian formulation of the OCP can be written as

Problem 5. ***Hamiltonian OCP formulation***

$$\min_{(q,p)\in T^*_q\mathcal{C}([0,T],T^*Q),u\in\mathcal{C}([0,T],\mathcal{U})} \tilde{J}(q^{\mathrm{s}},q^{\mathrm{f}},p^{\mathrm{s}},p^{\mathrm{f}},u) =$$
$$= \int_0^T \tilde{C}(q^{\mathrm{s}}(t),q^{\mathrm{f}}(t),p^{\mathrm{s}}(t),p^{\mathrm{f}}(t),u(t))dt + \tilde{\Phi}(q^{\mathrm{s}}(T),q^{\mathrm{f}}(T),p^{\mathrm{s}}(T),p^{\mathrm{f}}(T))$$

subject to:

$$(q^{\mathrm{s}}(0),p^{\mathrm{s}}(0)) = (q^{\mathrm{s},0},\mathbb{F}L^{\mathrm{s}}(\dot{q}^{\mathrm{s},0})), \qquad (q^{\mathrm{f}}(0),p^{\mathrm{f}}(0)) = (q^{\mathrm{f},0},\mathbb{F}L^{\mathrm{f}}(\dot{q}^{\mathrm{f},0}))$$

$$\dot{q}^{\mathrm{s}} = \frac{\partial H(q^{\mathrm{s}},q^{\mathrm{f}},p^{\mathrm{s}},p^{\mathrm{f}})}{\partial p^{\mathrm{s}}}, \qquad \dot{p}^{\mathrm{s}} = -\frac{\partial H(q^{\mathrm{s}},q^{\mathrm{f}},p^{\mathrm{s}},p^{\mathrm{f}})}{\partial q^{\mathrm{s}}} + f^{\mathrm{s}}_{\mathrm{HC}}(q,p,u)$$
$$\dot{q}^{\mathrm{f}} = \frac{\partial H(q^{\mathrm{s}},q^{\mathrm{f}},p^{\mathrm{s}},p^{\mathrm{f}})}{\partial p^{\mathrm{f}}}, \qquad \dot{p}^{\mathrm{f}} = -\frac{\partial H(q^{\mathrm{s}},q^{\mathrm{f}},p^{\mathrm{s}},p^{\mathrm{f}})}{\partial q^{\mathrm{f}}} + f^{\mathrm{f}}_{\mathrm{HC}}(q,p,u)$$
$$\tilde{r}(q^{\mathrm{s}}(T),q^{\mathrm{f}}(T),p^{\mathrm{s}}(T),p^{\mathrm{f}}(T),q^{\mathrm{s},T},q^{\mathrm{f},T},p^{\mathrm{s},T},p^{\mathrm{f},T}) = 0$$
$$\tilde{h}(q^{\mathrm{s}}(t),q^{\mathrm{f}}(t),p^{\mathrm{s}}(t),p^{\mathrm{f}}(t),u(t)) \geq 0 \text{ for } t\in[0,T]$$

where

$$(q^{\mathrm{s},T},p^{\mathrm{s},T}) = \mathbb{F}^{\mathrm{s}}L(q^{\mathrm{s},T},\dot{q}^{\mathrm{s},T}), \qquad (q^{\mathrm{f},T},p^{\mathrm{f},T}) = \mathbb{F}^{\mathrm{f}}L(q^{\mathrm{f},T},\dot{q}^{\mathrm{f},T}) \tag{5.5a}$$

and the running cost C, the terminal cost Φ, the equality r and inequality constraints h have been transformed using Equation (5.3) to $\tilde{C}$, $\tilde{\Phi}$, $\tilde{r}$ and $\tilde{h}$, respectively. Additionally, the space $T^*_q\mathcal{C}([0,T],T^*Q)$ represents the cotangent tangent space to the path space $\mathcal{C}([0,T],Q)$ (Equation (2.1)) at point q.

Definition 5.3.1. *A curve $(q,p,u)\in\mathcal{C}([0,T],T^*Q)\times\mathcal{C}([0,T],\mathcal{U})$ with $q=\begin{bmatrix}q^{\mathrm{s}}\\q^{\mathrm{f}}\end{bmatrix}, p=\begin{bmatrix}p^{\mathrm{s}}\\p^{\mathrm{f}}\end{bmatrix}$ is said to be admissible (or feasible) if it fulfils the constraints of Problem 5. The set of all admissible curves, which we will denote S, constitutes the admissible set of Problem 5. A curve $(q^*,p^*,u^*)\in S$ with $q^*=\begin{bmatrix}q^{\mathrm{s},*}\\q^{\mathrm{f},*}\end{bmatrix}, p^*=\begin{bmatrix}p^{\mathrm{s},*}\\p^{\mathrm{f},*}\end{bmatrix}$ is a (global) optimal solution to Problem 5 if $J(q^{\mathrm{s},*},q^{\mathrm{f},*},p^{\mathrm{s},*},p^{\mathrm{f},*},u^*) \leq J(q^{\mathrm{s}},q^{\mathrm{f}},p^{\mathrm{s}},p^{\mathrm{f}},u)$ for $\forall(q,p,u)\in S$. In this case, q^*,p^* and u^*, themselves, are called the optimal trajectory and control. Alternatively, if $J(q^{\mathrm{s},*},q^{\mathrm{f},*},p^{\mathrm{s},*},p^{\mathrm{f},*},u^*) \leq J(q^{\mathrm{s}},q^{\mathrm{f}},p^{\mathrm{s}},p^{\mathrm{f}},u)$ holds only in the neighbourhood of (q^*,p^*,u^*), then (q^*,p^*,u^*) is a local optimal solution for Problem 5, with q^*, p^* and u^* representing the locally optimal trajectory and control.*

5.3.3 Necessary optimality conditions

The necessary optimality conditions for Problem 5 can be derived using Pontryagin's maximum principle [137, 138]. To allow for concise and clear exposition, in the following sections, we restrict the discussion to a simplified version of this problem:

Problem 6.

$$\min_{q^{\mathrm{s}},p^{\mathrm{s}},q^{\mathrm{f}},p^{\mathrm{f}},u} \tilde{J}(q^{\mathrm{s}},p^{\mathrm{s}},q^{\mathrm{f}},p^{\mathrm{f}},u) =$$
$$\int_0^T \tilde{C}(q^{\mathrm{s}}(t),q^{\mathrm{f}}(t),p^{\mathrm{s}}(t),p^{\mathrm{f}}(t),u(t))dt + \tilde{\Phi}(q^{\mathrm{s}}(T),q^{\mathrm{f}}(T),p^{\mathrm{s}}(T),p^{\mathrm{f}}(T))$$

subject to:

$$\begin{array}{ll} q^{\mathrm{s}},q^{\mathrm{f}} \in W^{2,\infty}([0,T],Q) & u(t) \in \mathcal{U},\ t \in [0,T] \\ p^{\mathrm{s}},p^{\mathrm{f}} \in W^{1,\infty}([0,T],T_q^*Q) & u \in L^\infty([0,T],\mathcal{U}) \end{array}$$

$$\begin{bmatrix} q^{\mathrm{s}}(0) \\ p^{\mathrm{s}}(0) \end{bmatrix} = \begin{bmatrix} q^{\mathrm{s},0} \\ \mathbb{F}L^{\mathrm{s}}(\dot{q}^{\mathrm{s},0}) \end{bmatrix}, \quad \begin{bmatrix} \dot{q}^{\mathrm{s}} \\ \dot{p}^{\mathrm{s}} \end{bmatrix} = \begin{bmatrix} \nabla_{p^{\mathrm{s}}} H(q^{\mathrm{s}},q^{\mathrm{f}},p^{\mathrm{s}},p^{\mathrm{f}}) \\ -\nabla_{q^{\mathrm{s}}} H(q^{\mathrm{s}},q^{\mathrm{f}},p^{\mathrm{s}},p^{\mathrm{f}}) + f_{\mathrm{HC}}^{\mathrm{s}}(q,p,u) \end{bmatrix}$$
$$\begin{bmatrix} q^{\mathrm{f}}(0) \\ p^{\mathrm{f}}(0) \end{bmatrix} = \begin{bmatrix} q^{\mathrm{f},0} \\ \mathbb{F}L^{\mathrm{f}}(\dot{q}^{\mathrm{f},0}) \end{bmatrix}, \quad \begin{bmatrix} \dot{q}^{\mathrm{s}} \\ \dot{p}^{\mathrm{s}} \end{bmatrix} = \begin{bmatrix} \nabla_{p^{\mathrm{f}}} H(q^{\mathrm{s}},q^{\mathrm{f}},p^{\mathrm{s}},p^{\mathrm{f}}) \\ -\nabla_{q^{\mathrm{f}}} H(q^{\mathrm{s}},q^{\mathrm{f}},p^{\mathrm{s}},p^{\mathrm{f}}) + f_{\mathrm{HC}}^{\mathrm{f}}(q,p,u) \end{bmatrix}$$

where $p = [(p^{\mathrm{s}})^\intercal, (p^{\mathrm{f}})^\intercal]^\intercal$. Here the controls are constrained to the point-wise control set $\mathcal{U} = \{u(t) \in \mathbb{R}^{n_u}\}$ and $q^{\mathrm{s}}, q^{\mathrm{f}} \in W^{2,\infty}([0,T],Q)$, $p^{\mathrm{s}}, p^{\mathrm{f}} \in W^{1,\infty}([0,T],T_q^*Q)$ where $W^{j,\infty}(\mathbb{R}^{\mathrm{n}})$ is the defined as the Sobolev space of *vector-valued measurable functions* $q : [0,T] \to \mathbb{R}^n$ *whose j-th derivative lies in* L^p *for all* $0 \leq j \leq m$ *with the norm* $\|q\|_{W^{m,p}} = \sum_{j=0}^m \|q^{(j)}\|_{L^p}$ [139].

Let $x^{\mathrm{s}} = [(q^{\mathrm{s}})^\intercal, (p^{\mathrm{s}})^\intercal]^\intercal$, $x^{\mathrm{f}} = [(q^{\mathrm{f}})^\intercal, (p^{\mathrm{f}})^\intercal]^\intercal$ and $\mathbb{x} = [(x^{\mathrm{s}})^\intercal, (x^{\mathrm{f}})^\intercal]^\intercal$.

Theorem 5.3.1. ***Pontryagin maximum principle for the multirate system (first-order optimality conditions):*** *Let* $\left(\begin{bmatrix} x^{\mathrm{s},*} \\ x^{\mathrm{f},*} \end{bmatrix}, u^* \right) \in W^{2,\infty}([0,T],T*Q) \times W^{1,\infty}([0,T],\mathcal{U})$ *be an optimal solution to Problem 5 as defined in Definition 5.3.1. Then there exist* $\beta^{\mathrm{s}} \in W^{2,\infty}([0,T],\mathbb{R}^{n^{\mathrm{s}}})$, $\beta^{\mathrm{f}} \in W^{2,\infty}([0,T],\mathbb{R}^{n^{\mathrm{f}}})$ *such that:*

$$\mathcal{H}_C(x^{\mathrm{s},*}(t),x^{\mathrm{f},*}(t),u^*(t),\beta^{\mathrm{s}}(t),\beta^{\mathrm{f}}(t)) = \max_{u \in U} \mathcal{H}_C(x^{\mathrm{s}}(t),x^{\mathrm{f}}(t),u(t),\beta(t)) \quad t \in [0,T] \tag{5.6a}$$

$$\tilde{\dot{x}}^{\mathrm{s}} = \nabla_{\beta^{\mathrm{s}}} \mathcal{H}_C(x^{\mathrm{s},*}(t),x^{\mathrm{f},*}(t),u^*(t),\beta(t)), \qquad x^{\mathrm{s},*}(0) = x_0^{\mathrm{s}} \tag{5.6b}$$

$$\tilde{\dot{x}}^{\mathrm{f}} = \nabla_{\beta^{\mathrm{f}}} \mathcal{H}_C(x^{\mathrm{s},*}(t), x^{\mathrm{f},*}(t), u^*(t), \beta(t)), \qquad x^{\mathrm{f},*}(0) = x_0^{\mathrm{f}} \tag{5.6c}$$

$$\dot{\beta}^{\mathrm{s}} = -\nabla_{x^{\mathrm{s}}} \mathcal{H}_C(x^{\mathrm{s},*}(t), x^{\mathrm{f},*}(t), u^*(t), \beta(t)), \quad \beta^{\mathrm{s}}(T) = -\nabla_{x^{\mathrm{s}}} \tilde{\Phi}(x^{\mathrm{s}}(T), x^{\mathrm{f}}(T)) \tag{5.6d}$$

$$\dot{\beta}^{\mathrm{f}} = -\nabla_{x^{\mathrm{f}}} \mathcal{H}_C(x^{\mathrm{s},*}(t), x^{\mathrm{f},*}(t), u^*(t), \beta(t)), \quad \beta^{\mathrm{f}}(T) = -\nabla_{x^{\mathrm{f}}} \tilde{\Phi}(x^{\mathrm{s}}(T), x^{\mathrm{f}}(T)) \tag{5.6e}$$

where

$$\mathcal{H}_C(x^{\mathrm{s}}, x^{\mathrm{f}}, u, \beta^{\mathrm{s}}, \beta^{\mathrm{f}}) := -\tilde{C}(q^{\mathrm{s}}, q^{\mathrm{f}}, p^{\mathrm{s}}, p^{\mathrm{f}}, u) + \left\langle \beta^{\mathrm{s}}, \begin{bmatrix} \nabla_{p^{\mathrm{s}}} H(q^{\mathrm{s}}, q^{\mathrm{f}}, p^{\mathrm{s}}, p^{\mathrm{f}}) \\ -\nabla_{q^{\mathrm{s}}} H(q^{\mathrm{s}}, q^{\mathrm{f}}, p^{\mathrm{s}}, p^{\mathrm{f}}) + f_{\mathrm{HC}}^{\mathrm{s}}(q, p, u) \end{bmatrix} \right\rangle + \left\langle \beta^{\mathrm{f}}, \begin{bmatrix} \nabla_{p^{\mathrm{f}}} H(q^{\mathrm{s}}, q^{\mathrm{f}}, p^{\mathrm{s}}, p^{\mathrm{f}}) \\ -\nabla_{q^{\mathrm{f}}} H(q^{\mathrm{s}}, q^{\mathrm{f}}, p^{\mathrm{s}}, p^{\mathrm{f}}) + f_{\mathrm{HC}}^{\mathrm{f}}(q, p, u) \end{bmatrix} \right\rangle$$

is the optimal control Hamiltonian, $\beta(t) = \begin{bmatrix} \beta^{\mathrm{s}}(t) \\ \beta^{\mathrm{f}}(t) \end{bmatrix}$ *are the the adjoint variables (also known as the costates), and* $\mathbb{x}_0 = \begin{bmatrix} x_0^{\mathrm{s}} \\ x_0^{\mathrm{f}} \end{bmatrix}$ *are the given initial conditions with* $x_0^{\mathrm{s}} = \begin{bmatrix} q^{\mathrm{s},0} \\ \mathbb{F}L^{\mathrm{s}}(\dot{q}^{\mathrm{s},0}) \end{bmatrix}$, $x_0^{\mathrm{f}} = \begin{bmatrix} q^{\mathrm{f},0} \\ \mathbb{F}L^{\mathrm{f}}(\dot{q}^{\mathrm{f},0}) \end{bmatrix}$. *The optimal control is given by given by pointwise optimisation of the Hamiltonian*

$$u^*(t) = \arg \max_{u \in U} \mathcal{H}_C(\mathbb{x}^*(t), u^*(t), \beta(t)).$$

If $\mathcal{H}_C$ has a locally unique minimiser (u^*, β^*), then the control can be written as a function of the state and the adjoint $u^* = u(\mathbb{x}(t), \beta(t))$ and thus used to rewrite the necessary equality conditions (Equations (5.6b)-(5.6e)) in a standard boundary-value problem [19, 140].

Demonstration problem 4.

We now consider the problem of optimally controlling the system described in Demonstration problem 1 with Lagrangian

$$\mathcal{L}(q^{\mathrm{s}}, q^{\mathrm{f}}, \dot{q}^{\mathrm{s}}, \dot{q}^{\mathrm{f}}) = \frac{1}{2}(\dot{q}^{\mathrm{s}})^{\intercal} M^{\mathrm{s}} \dot{q}^{\mathrm{s}} + \frac{1}{2}(\dot{q}^{\mathrm{f}})^{\intercal} M^{\mathrm{f}} \dot{q}^{\mathrm{f}} - U(q^{\mathrm{s}}, q^{\mathrm{f}}) - P(q^{\mathrm{f}}) \tag{5.7}$$

and cost functional

$$\tilde{C}(q^{\mathrm{s}}, q^{\mathrm{f}}, p^{\mathrm{s}}, p^{\mathrm{f}}) = \frac{1}{2} \int_0^T \Big((u^{\mathrm{s}})^{\intercal} u^{\mathrm{s}} + (u^{\mathrm{f}})^{\intercal} u^{\mathrm{f}} \Big) dt + \tilde{\Phi}(q^{\mathrm{s}}(T), q^{\mathrm{f}}(T), p^{\mathrm{s}}(T), p^{\mathrm{f}}(T)) \tag{5.8}$$

in the presence of a Lagrangian control force such that $f_{\mathrm{HC}}^{\mathrm{s}}(u(t)) = u^{\mathrm{s}}(t)$ *and* $f_{\mathrm{HC}}^{\mathrm{f}}(u(t)) = u^{\mathrm{f}}(t)$ *as discussed in Remark 3.3.1. Here* $M^{\mathrm{s}} \in \mathbb{R}^{n^{\mathrm{s}}} \times \mathbb{R}^{n^{\mathrm{s}}}$, $M^{\mathrm{f}} \in \mathbb{R}^{n^{\mathrm{f}}} \times \mathbb{R}^{n^{\mathrm{f}}}$

are symmetric. To solve this optimal control problem, we formulate Problem 6 with $\tilde{\Phi}(q^{\mathrm{s}}(T), q^{\mathrm{f}}(T), p^{\mathrm{s}}(T), p^{\mathrm{f}}(T)) = 0$ *and the assumption that the control force can be resolved in slow and fast components* $f^{\mathrm{s}}_{\mathrm{HC}} = u^{\mathrm{s}}(t), f^{\mathrm{f}}_{\mathrm{HC}} = u^{\mathrm{f}}(t)$ *acting on the multirate configurations* $q^{\mathrm{s}}, q^{\mathrm{f}}$*, respectively. Based on the Pontryagin maximum principle above (Theorem 5.3.1) and splitting* $\beta^{\mathrm{s}} = [(\lambda^{\mathrm{s}})^{\intercal}, (\mu^{\mathrm{s}})^{\intercal}]^{\intercal}, \beta^{\mathrm{f}} = [(\lambda^{\mathrm{f}})^{\intercal}, (\mu^{\mathrm{f}})^{\intercal}]^{\intercal}$ *with* $\lambda^{\mathrm{s}}, \mu^{\mathrm{s}}, \lambda^{\mathrm{f}}, \mu^{\mathrm{f}} \in \mathbb{R}^{n/2}$*, the system of necessary optimality conditions becomes:*

$$\begin{aligned}\mathcal{H}_C(q^{\mathrm{s}}, q^{\mathrm{f}}, p^{\mathrm{s}}, p^{\mathrm{f}}, \lambda^{\mathrm{s}}, \mu^{\mathrm{s}}, \lambda^{\mathrm{f}}, \mu^{\mathrm{f}}) = &-\frac{(u^{\mathrm{s}})^{\intercal}u^{\mathrm{s}}}{2} - \frac{(u^{\mathrm{f}})^{\intercal}u^{\mathrm{f}}}{2} + (\lambda^{\mathrm{s}})^{\intercal}(M^{\mathrm{s}})^{-1}p^{\mathrm{s}} + (\lambda^{\mathrm{f}})^{\intercal}(M^{\mathrm{f}})^{-1}p^{\mathrm{f}} \\ &+ (\mu^{\mathrm{s}})^{\intercal}\Big[\Big(-\frac{\partial U(q^{\mathrm{s}}, q^{\mathrm{f}})}{\partial q^{\mathrm{s}}}\Big) + u^{\mathrm{s}}\Big] + (\mu^{\mathrm{f}})^{\intercal}\Big[\Big(-\frac{\partial U(q^{\mathrm{s}}, q^{\mathrm{f}})}{\partial q^{\mathrm{f}}} - \frac{\partial P(q^{\mathrm{f}})}{\partial q^{\mathrm{f}}}\Big) + u^{\mathrm{f}}\Big]\end{aligned}$$

$$\begin{aligned}
u^{\mathrm{s}}(t) &= \mu^{\mathrm{s}}(t), & u^{\mathrm{f}}(t) &= \mu^{\mathrm{f}}(t), \\
\dot{q}^{\mathrm{s}}(t) &= (M^{\mathrm{s}})^{-1}p^{\mathrm{s}}(t), & \dot{p}^{\mathrm{s}}(t) &= -\frac{\partial U(q^{\mathrm{s}}, q^{\mathrm{f}})}{\partial q^{\mathrm{s}}} + u^{\mathrm{s}}(t) \\
\dot{q}^{\mathrm{f}}(t) &= (M^{\mathrm{f}})^{-1}p^{\mathrm{f}}(t), & \dot{p}^{\mathrm{f}}(t) &= -\frac{\partial (U(q^{\mathrm{s}}, q^{\mathrm{f}}) + P(q^{\mathrm{f}}))}{\partial q^{\mathrm{f}}} + u^{\mathrm{f}}(t) \\
\dot{\mu}^{\mathrm{s}}(t) &= -(M^{\mathrm{s}})^{-1}\lambda^{\mathrm{s}}(t), & \dot{\lambda}^{\mathrm{s}}(t) &= \frac{\partial^2 U(q^{\mathrm{s}}, q^{\mathrm{f}})}{\partial^2 q^{\mathrm{s}}}\mu^{\mathrm{s}} + \frac{\partial^2 (U(q^{\mathrm{s}}, q^{\mathrm{f}}))}{\partial q^{\mathrm{s}}\partial q^{\mathrm{f}}}\mu^{\mathrm{f}} \\
\dot{\mu}^{\mathrm{f}}(t) &= -(M^{\mathrm{f}})^{-1}\lambda^{\mathrm{f}}(t), & \dot{\lambda}^{\mathrm{f}}(t) &= \frac{\partial^2 (U(q^{\mathrm{s}}, q^{\mathrm{f}}))}{\partial q^{\mathrm{s}}\partial q^{\mathrm{f}}}\mu^{\mathrm{s}} + \frac{\partial^2 (U(q^{\mathrm{s}}, q^{\mathrm{f}}) + P(q^{\mathrm{f}}))}{\partial^2 q^{\mathrm{f}}}\mu^{\mathrm{f}}
\end{aligned}$$

with boundary conditions

$$\begin{aligned}
q^{\mathrm{s}}(0) &= q^{\mathrm{s},0}, & \lambda^{\mathrm{s}}(T) &= -\nabla_{q^{\mathrm{s}}}\tilde{\Phi}(q^{\mathrm{s}}(T), q^{\mathrm{f}}(T), p^{\mathrm{s}}(T), p^{\mathrm{f}}(T)), \\
q^{\mathrm{f}}(0) &= q^{\mathrm{f},0}, & \lambda^{\mathrm{f}}(T) &= -\nabla_{q^{\mathrm{f}}}\tilde{\Phi}(q^{\mathrm{s}}(T), q^{\mathrm{f}}(T), p^{\mathrm{s}}(T), p^{\mathrm{f}}(T)), \\
p^{\mathrm{s}}(0) &= \mathbb{F}L^{\mathrm{s}}(\dot{q}^{\mathrm{s},0}), & \mu^{\mathrm{s}}(T) &= -\nabla_{p^{\mathrm{s}}}\tilde{\Phi}(q^{\mathrm{s}}(T), q^{\mathrm{f}}(T), p^{\mathrm{s}}(T), p^{\mathrm{f}}(T)), \\
p^{\mathrm{f}}(0) &= \mathbb{F}L^{\mathrm{f}}(\dot{q}^{\mathrm{f},0}), & \mu^{\mathrm{f}}(T) &= -\nabla_{p^{\mathrm{f}}}\tilde{\Phi}(q^{\mathrm{s}}(T), q^{\mathrm{f}}(T), p^{\mathrm{s}}(T), p^{\mathrm{f}}(T)).
\end{aligned} \tag{5.9}$$

If we additionally assume the potential energy is of the form

$$U(q^{\mathrm{s}}, q^{\mathrm{f}}) = \frac{1}{2}(q^{\mathrm{s}})^{\intercal}K^{\mathrm{s}}q^{\mathrm{s}}, \quad P(q^{\mathrm{f}}) = \frac{1}{2}(q^{\mathrm{f}})^{\intercal}K^{\mathrm{f}}q^{\mathrm{f}}$$

with symmetric matrices $K^{\mathrm{s}} \in \mathbb{R}^{n^{\mathrm{s}}} \times \mathbb{R}^{n^{\mathrm{s}}}$*,* $K^{\mathrm{f}} \in \mathbb{R}^{n^{\mathrm{f}}} \times \mathbb{R}^{n^{\mathrm{f}}}$ *and plug in the equations for the optimal control into the state equations, then the state and adjoint dynamics*

can further be simplified to

$$\begin{aligned}
\dot{q}^{\mathrm{s}}(t) &= (M^{\mathrm{s}})^{-1}p^{\mathrm{s}}(t), & \dot{p}^{\mathrm{s}}(t) &= -K^{\mathrm{s}}q^{\mathrm{s}}(t) + \mu^{\mathrm{s}}(t),\\
\dot{q}^{\mathrm{f}}(t) &= (M^{\mathrm{f}})^{-1}p^{\mathrm{f}}(t), & \dot{p}^{\mathrm{f}}(t) &= -K^{\mathrm{f}}q^{\mathrm{f}}(t) + \mu^{\mathrm{f}}(t),\\
\dot{\mu}^{\mathrm{s}}(t) &= -(M^{\mathrm{s}})^{-1}\lambda^{\mathrm{s}}(t), & \dot{\lambda}^{\mathrm{s}}(t) &= K^{\mathrm{s}}\mu^{\mathrm{s}}(t),\\
\dot{\mu}^{\mathrm{f}}(t) &= -(M^{\mathrm{f}})^{-1}\lambda^{\mathrm{f}}(t), & \dot{\lambda}^{\mathrm{f}}(t) &= K^{\mathrm{f}}\mu^{\mathrm{f}}(t).
\end{aligned} \tag{5.10}$$

Together with the boundary conditions above, the resulting optimality system is reduced to a boundary value problem.

Remark 5.3.1. *Differentiating the equations for $\dot{q}^{\mathrm{s}}(t), \dot{q}^{\mathrm{f}}(t)$ and substituting the expressions for $\dot{p}^{\mathrm{s}}(t), \dot{p}^{\mathrm{f}}(t)$, we obtain Euler-Lagrange equations*

$$\ddot{q}^{\mathrm{s}}(t) = -(M^{\mathrm{s}})^{-1}\Big(\frac{\partial U(q^{\mathrm{s}}, q^{\mathrm{f}})}{\partial q^{\mathrm{s}}}\Big) + u^{\mathrm{s}}(t), \tag{5.11a}$$

$$\ddot{q}^{\mathrm{f}}(t) = -(M^{\mathrm{f}})^{-1}\Big(\frac{\partial (U(q^{\mathrm{s}}, q^{\mathrm{f}}) + P(q^{\mathrm{f}}))}{\partial q^{\mathrm{f}}}\Big) + u^{\mathrm{f}}(t). \tag{5.11b}$$

Similar manipulation of the adjoint equations leads to:

$$\ddot{\mu}^{\mathrm{s}}(t) = -(M^{\mathrm{s}})^{-1}\Big(\frac{\partial^2 U(q^{\mathrm{s}}, q^{\mathrm{f}})}{\partial^2 q^{\mathrm{s}}}\Big)\mu^{\mathrm{s}} + \Big(\frac{\partial^2 (U(q^{\mathrm{s}}, q^{\mathrm{f}}))}{\partial q^{\mathrm{s}}\partial q^{\mathrm{f}}}\Big)\mu^{\mathrm{f}}, \tag{5.12a}$$

$$\ddot{\mu}^{\mathrm{f}}(t) = -(M^{\mathrm{f}})^{-1}\Big(\frac{\partial^2 (U(q^{\mathrm{s}}, q^{\mathrm{f}}))}{\partial q^{\mathrm{s}}\partial q^{\mathrm{f}}}\Big)\mu^{\mathrm{s}} + \Big(\frac{\partial^2 (U(q^{\mathrm{s}}, q^{\mathrm{f}}) + P(q^{\mathrm{f}}))}{\partial^2 q^{\mathrm{f}}}\Big)\mu^{\mathrm{f}}. \tag{5.12b}$$

These second order differential equations will help to assess the order of discretisation schemes in Section 5.4.3.

5.4 Multirate Discrete Mechanics and Optimal Control (Multirate DMOC)

Based on the Lagrangian and Hamiltonian formulation of the system representation, we can derive a multirate discrete mechanics and optimal control formulation. To provide a general formulation, we demonstrate how the problem can be formulated when controls on different time scales are present, and thus $u(t)$ can be discretised as described in Remark 3.4.1.

Discrete path constraints

In the continuous case, the system's equations of motion can be interpreted as equality constraints in the optimal control problem. In the discrete case, these equality constraints take the form of the *discrete forced multirate equations of motion* as stated in Equation (3.30). Additionally, any path constraints are approximated on each macro $[t_k, t_{k+1}]$ or micro time interval $[t_k^m, t_k^{m+1}]$ depending on the problem at hand. Thus, to approximate h we define

$$h_\mathrm{d}\colon (q_k^{\mathrm{s},m}, q_k^{\mathrm{s},m+1}, q_k^{\mathrm{f},m}, q_k^{\mathrm{f},m+1}, u_k^{m+\frac{1}{2}}) \mapsto h_\mathrm{d}(q_k^{\mathrm{s},m}, q_k^{\mathrm{s},m+1}, q_k^{\mathrm{f},m}, q_k^{\mathrm{f},m+1}, u_{k+1/2}^{\mathrm{slow}}, u_k^{\mathrm{fast},m+\frac{1}{2}})$$

such that

$$h_\mathrm{d}(q_k^{\mathrm{s,m}}, q_k^{\mathrm{s},m+1}, q_k^{\mathrm{f,m}}, q_k^{\mathrm{f},m+1}, u_{k+1/2}^{\mathrm{slow}}, u_k^{\mathrm{fast},m+1/2}) \geq 0 \quad \text{for } k=0,\ldots,N\text{–}1,\ m=0,\ldots,\mathbb{p}\text{–}1.$$

This way, we retain a formulation on the velocity level and replace the continuous path constraint $h(q^\mathrm{s}(t), q^\mathrm{f}(t), \dot{q}^\mathrm{s}(t), \dot{q}^\mathrm{f}(t), u(t)) \geq 0$ by a discrete path constraint $h_\mathrm{d} : Q \times Q \times U \to R^{n^h}$. If needed the discrete path constraint can be redefined on a macro time interval as

$$\mathbf{h}_\mathrm{d}(q_k^\mathrm{s}, q_{k+1}^\mathrm{s}, q_k^\mathrm{f}, u_k) \geq 0 \quad \text{for } k = 0,\ldots,N-1,$$

similarly to the definition of the discrete forces in Section 3.4.

If we wish to formulate the constraint equivalently on the momentum level we can do so either applying the Legendre transform to $\mathbf{h}_\mathrm{d}$ or h_d or by directly discretising $\tilde{h}(q^\mathrm{s}(t), q^\mathrm{f}(t), p^\mathrm{s}(t), p^\mathrm{f}(t), u(t)) \geq 0$ to obtain:

$$\tilde{h}_\mathrm{d}(q_k^{\mathrm{s},m}, q_k^{\mathrm{f},m}, p_k^{\mathrm{s},m}, p_k^{\mathrm{f},m}, u_{k+1/2}^{\mathrm{slow}}, u_k^{\mathrm{fast},m+1/2}) \geq 0 \quad \text{for } k=0,\ldots,N\text{–}1, m=0,\ldots,\mathbb{p}\text{–}1$$

on the micro time grid or

$$\tilde{\mathbf{h}}_\mathrm{d}(q_k^\mathrm{s}, q_k^\mathrm{f}, p_k^\mathrm{s}, p_k^\mathrm{f}, u_k) \geq 0 \quad \text{for } k=0,\ldots,N-1$$

on the macro time grid. Here $p_k^\mathrm{f} = \{p_k^{\mathrm{f},m}\}_{m=0}^{\mathbb{p}}$.

Boundary values and constraints

In contrast to the continuous case, we must use the *discrete multirate Legendre transform* not only for the Hamiltonian formulation, but for the Lagrangian one as well. This is needed as the discrete LF of the variational method encodes boundary conditions on the velocity on the configuration level using the Legendre transform, as demonstrated in (3.28) for the initial conditions. Analogously, we can use the *discrete multirate Legendre transform* to place constraints on the terminal states in discrete time. We assume the presence of a terminal state constraint r in the state space or its equivalent formulation $\tilde{r}$ in the phase space, as defined in Problem 4 and 5, respectively, and related as described in Section 5.3.2. These constraints can be approximated in discrete time as r_d and $\tilde{r}_\mathrm{d}$ as

$$\begin{aligned}0 &= r_\mathrm{d}(q^\mathrm{s}_{N-1}, q^\mathrm{s}_N, q^{\mathrm{f},\mathbb{p}-1}_{N-1}, q^{\mathrm{f},\mathbb{p}}_{N-1}, u^\mathrm{slow}_{N-1}, u^{\mathrm{fast},\mathbb{p}-1/2}_{N-1}, q^{\mathrm{s},T}, q^{\mathrm{f},T}, \dot{q}^{\mathrm{s},T}, \dot{q}^{\mathrm{f},T})\\ 0 &= \tilde{r}_\mathrm{d}(q^\mathrm{s}_N, q^{\mathrm{f},\mathbb{p}}_{N-1}, p^\mathrm{s}_N, p^{\mathrm{f},\mathbb{p}}_{N-1}, q^{\mathrm{s},T}, q^{\mathrm{f},T}, p^{\mathrm{s},T}, p^{\mathrm{f},T})\end{aligned}$$

where $p^{\mathrm{s},T}, p^{\mathrm{f},T}$ are defined in (5.5) and

$$(q^\mathrm{s}_N, p^\mathrm{s}_N) = \mathbb{F}^{F^{\mathrm{s},+}} L_\mathrm{d}(u_{N-1})(q^\mathrm{s}_{N-1}, q^\mathrm{s}_N) = (q^\mathrm{s}_N, D_{q^\mathrm{s}_N} L_\mathrm{d}^{N-1} + F^{\mathrm{s},+}_{N-1}) \tag{5.13a}$$

$$(q^{\mathrm{f},\mathbb{p}}_{N-1}, p^{\mathrm{f},\mathbb{p}}_{N-1}) = \mathbb{F}^{F^{\mathrm{f},+}} L_\mathrm{d}(u^{\mathbb{p}-\mathbb{1}/2}_{N-1})(q^{\mathrm{f},\mathbb{p}-1}_{N-1}, q^{\mathrm{f},\mathbb{p}}_{N-1}) = (q^{\mathrm{f},\mathbb{p}}_{N-1}, D_{q^{\mathrm{f},\mathbb{p}}_{N-1}} L_\mathrm{d}^{N-1,\mathbb{p}-1} + f^{\mathrm{f},\mathbb{p}-1,+}_{N-1}) \tag{5.13b}$$

Mayer term

Similarly for the Mayer term in the cost in the Lagrangian and the Hamiltonian formalism we use the discretisations $\Phi_\mathrm{d}(q^\mathrm{s}_{N-1}, q^\mathrm{s}_N, q^{\mathrm{f},\mathbb{p}-1}_{N-1}, q^{\mathrm{f},\mathbb{p}}_{N-1}, u^\mathrm{slow}_{N-1}, u^{\mathrm{fast},\mathbb{p}-1/2}_{N-1})$ and $\tilde{\Phi}_\mathrm{d}(q^\mathrm{s}_N, q^{\mathrm{f},\mathbb{p}}_{N-1}, p^\mathrm{s}_N, p^{\mathrm{f},\mathbb{p}}_{N-1})$ respectively.

Cost functional

For the running cost term, we approximate the discrete cost functional

$$C^k_\mathrm{d}(q^\mathrm{s}_k, q^\mathrm{s}_{k+1}, q^\mathrm{f}_k, u^\mathrm{slow}_{k+1/2}, u^\mathrm{fast}_k) \approx \int_{t_k}^{t_{k+1}} C(q^\mathrm{s}, \dot{q}^\mathrm{s}, q^\mathrm{f}, \dot{q}^\mathrm{f}, u)dt. \tag{5.14}$$

This formulation yields the multirate discrete cost functional

$$J_\mathrm{d}(q^\mathrm{s}_\mathrm{d}, q^\mathrm{f}_\mathrm{d}, u^\mathrm{slow}_\mathrm{d}, u^\mathrm{fast}_\mathrm{d}) = \sum_{k=0}^{N-1} C^k_\mathrm{d}(q^\mathrm{s}_k, q^\mathrm{s}_{k+1}, q^\mathrm{f}_k, u_k) + \Phi_\mathrm{d}(q^\mathrm{s}_{N-1}, q^\mathrm{s}_N, q^{\mathrm{f},\mathbb{p}-1}_{N-1}, q^{\mathrm{f},\mathbb{p}}_{N-1}, u^\mathrm{slow}_{N-1}, u^{\mathrm{fast},\mathbb{p}-\frac{1}{2}}_{N-1})$$

Similarly to the Lagrangian and the virtual work, the approximation of the cost functional can be further refined and approximated on a micro time scale if needed.

5.4.1 Lagrangian viewpoint

Based on these definitions, the general Lagrangian optimal control problem– Problem 4, can be discretised as follows

$$\min_{q_{\mathrm{d}}^{\mathrm{s}},q_{\mathrm{d}}^{\mathrm{f}},u_{\mathrm{d}}^{\mathrm{slow}},u_{\mathrm{d}}^{\mathrm{fast}}} J_{\mathrm{d}}(q_{\mathrm{d}}^{\mathrm{s}},q_{\mathrm{d}}^{\mathrm{f}},u_{\mathrm{d}}^{\mathrm{slow}},u_{\mathrm{d}}^{\mathrm{fast}}) = \tag{5.15a}$$

$$\sum_{k=0}^{N-1} C_{\mathrm{d}}^{k}(q_k^{\mathrm{s}},q_{k+1}^{\mathrm{s}},q_k^{\mathrm{f}},u_{k+1/2}^{\mathrm{slow}},u_k^{\mathrm{fast}}) + \Phi_{\mathrm{d}}(q_{N-1}^{\mathrm{s}},q_N^{\mathrm{s}},q_{N-1}^{\mathrm{f},\mathbb{p}-1},q_{N-1}^{\mathrm{f},\mathbb{p}},u_{N-1}^{\mathrm{slow}},u_{N-1}^{\mathrm{fast},\mathbb{p}-1/2})$$

subject to:

$$q_0^{\mathrm{s}} = q^{\mathrm{s},0}, \qquad p^{\mathrm{s},0} = -D_{q_0^{\mathrm{s}}} L_{\mathrm{d}}^{0}(q_0^{\mathrm{s}},q_1^{\mathrm{s}},q_0^{\mathrm{f}}) - F_0^{\mathrm{s},-} \tag{5.15b}$$

$$q_0^{\mathrm{f},0} = q^{\mathrm{f},0}, \quad p^{\mathrm{f},0} = -D_{q_0^{\mathrm{f},0}} L_{\mathrm{d}}^{0,0}(q_0^{\mathrm{s},0},q_1^{\mathrm{s}},q_0^{\mathrm{f},1}) - f_0^{\mathrm{f},0,-} \tag{5.15c}$$

$$D_{q_k^{\mathrm{s}}}(L_{\mathrm{d}}^{k} + L_{\mathrm{d}}^{k-1}) + F_k^{\mathrm{s}-} + F_{k-1}^{\mathrm{s},+} = 0 \qquad \text{for } k = 1,\dots,N-1 \tag{5.15d}$$

$$D_{q_k^{\mathrm{f},0}}(L_{\mathrm{d}}^{k} - L_{\mathrm{d}}^{k-1}) + f_k^{\mathrm{f},0,-} + f_k^{\mathrm{f},\mathbb{p}-1,+} = 0 \qquad \text{for } k = 1,\dots,N-1 \tag{5.15e}$$

$$D_{q_k^{\mathrm{f},m}} L_{\mathrm{d}}^{k} + f_k^{\mathrm{f},m,-} + f_k^{\mathrm{f},\mathrm{m}-1,+} = 0 \qquad \text{for } k = 0,\dots,N-1,\ m = 1,\dots,\mathbb{p}-1 \tag{5.15f}$$

$$\mathbf{h}_{\mathrm{d}}(q_k^{\mathrm{s}},q_{k+1}^{\mathrm{s}},q_k^{\mathrm{f}},u_{k+1/2}^{\mathrm{slow}},u_k^{\mathrm{fast}}) \geq 0 \qquad \text{for } k = 1,\dots,N-1 \tag{5.15g}$$

$$r_{\mathrm{d}}(q_{N-1}^{\mathrm{s}},q_N^{\mathrm{s}},q_{N-1}^{\mathrm{f},\mathbb{p}-1},q_{N-1}^{\mathrm{f},\mathbb{p}},u_{N-1}^{\mathrm{slow}},u_{N-1}^{\mathrm{fast},\mathbb{p}-1/2},q^{\mathrm{s},T},q^{\mathrm{f},T},\dot{q}^{\mathrm{s},T},\dot{q}^{\mathrm{f},T}) = 0 \tag{5.15h}$$

where $(q^{\mathrm{s},0},p^{\mathrm{s},0}) = \mathbb{F}^{\mathrm{s}}L(q^{\mathrm{s},0},\dot{q}^{\mathrm{s},0})$, $(q^{\mathrm{f},0},p^{\mathrm{f},0}) = \mathbb{F}^{\mathrm{f}}L(q^{\mathrm{f},0},\dot{q}^{\mathrm{f},0})$

5.4.2 Hamiltonian viewpoint

In the phase space, the optimal control problem takes the form

$$\min_{\substack{q_{\mathrm{d}}^{\mathrm{s}},q_{\mathrm{d}}^{\mathrm{f}},p_{\mathrm{d}}^{\mathrm{s}},p_{\mathrm{d}}^{\mathrm{f}},\\ u_{\mathrm{d}}^{\mathrm{slow}},u_{\mathrm{d}}^{\mathrm{fast}}}} \tilde{J}_{\mathrm{d}}(q_{\mathrm{d}}^{\mathrm{s}},q_{\mathrm{d}}^{\mathrm{f}},u_{\mathrm{d}}^{\mathrm{slow}},u_{\mathrm{d}}^{\mathrm{fast}}) = \tag{5.16a}$$

$$\sum_{k=0}^{N-1} \tilde{C}_{\mathrm{d}}^{k}(q_k^{\mathrm{s}},q_{k+1}^{\mathrm{s}},q_k^{\mathrm{f}},u_{k+1/2}^{\mathrm{slow}},u_k^{\mathrm{fast}}) + \tilde{\Phi}_{\mathrm{d}}(q_N^{\mathrm{s}},q_{N-1}^{\mathrm{f},\mathbb{p}},p_N^{\mathrm{s}},p_{N-1}^{\mathrm{f},\mathbb{p}}) \tag{5.16b}$$

subject to:

$$q_0^{\mathrm{s}} = q^{\mathrm{s}}(0), \quad q_0^{\mathrm{f},0} = q^{\mathrm{f}}(0), \qquad p_0^{\mathrm{s}} = p^{\mathrm{s},0}, \quad p_0^{\mathrm{f},0} = p^{\mathrm{f},0}, \tag{5.16c}$$

$$p_k^{\mathrm{s},-} = -D_{q_k^{\mathrm{s}}} L_{\mathrm{d}}^k - F_k^{\mathrm{s},-} \qquad \text{for } k = 0, \ldots, N-1 \tag{5.16d}$$

$$p_k^{\mathrm{s},+} = D_{q_k^{\mathrm{s}}} L_{\mathrm{d}}^{k-1} + F_k^{\mathrm{s},+} \qquad \text{for } k = 1, \ldots, N-1 \tag{5.16e}$$

$$p_k^{\mathrm{f},m,-} = -D_{q_k^{\mathrm{f},m}} L_{\mathrm{d}}^{k,m} - f_k^{\mathrm{f},m,-} \qquad \text{for } k = 0, \ldots, N-1,\ m = 0, \ldots, \mathbb{p}-1 \tag{5.16f}$$

$$p_k^{\mathrm{f},m,+} = D_{q_k^{\mathrm{f},m}} L_{\mathrm{d}}^{k,m-1} + f_k^{\mathrm{f},\mathrm{m}-1,+} \qquad \text{for } k = 0, \ldots, N-1,\ m = 1, \ldots, \mathbb{p} \tag{5.16g}$$

$$\tilde{\mathbf{h}}_{\mathrm{d}}(q_k^{\mathrm{s}}, q_k^{\mathrm{f}}, p_k^{\mathrm{s}}, p_k^{\mathrm{f}}, u_{k+1/2}^{\mathrm{slow}}, u_k^{\mathrm{fast}}) \geq 0 \qquad \text{for } k = 1, \ldots, N-1 \tag{5.16h}$$

$$\tilde{r}_{\mathrm{d}}(q_N^{\mathrm{s}}, q_{N-1}^{\mathrm{f},\mathbb{p}}, p_N^{\mathrm{s}}, p_{N-1}^{\mathrm{f},\mathbb{p}}, q^{\mathrm{s},T}, q^{\mathrm{f},T}, p^{\mathrm{s},T}, p^{\mathrm{f},T}) = 0 \tag{5.16i}$$

where $p_{\mathrm{d}}^{\mathrm{s}} = \{p_k^{\mathrm{s}}\}_{k=0}^{N}$, $p_{\mathrm{d}}^{\mathrm{f}} = \{\{p_k^{\mathrm{f},m}\}_{m=0}^{\mathbb{p}-1}\}_{k=0}^{N-1}$, and $\tilde{C}_{\mathrm{d}} = C_{\mathrm{d}} \circ ((\mathbb{F}^{F^{\mathrm{s},\pm}} L_{\mathrm{d}})^{-1}, (\mathbb{F}^{F^{\mathrm{f},\pm}} L_{\mathrm{d}})^{-1})$ analogously to the continuous Section 5.3.2.

Remark 5.4.1. *As we have discussed in Section 3.4.3, both the Lagrangian and Hamiltonian discrete forced system formulations maintain certain qualitative properties. However, one can note that the size of the problem in the Lagrangian formulation is smaller in both the number of optimisation variables and constraints due to the avoidance of integration of the momenta in the equations of motion. This could potentially make the Lagrangian formulation more computationally efficient than the Hamiltonian formulation while maintaining the conservation properties that provide qualitative better system representation. This is investigated for two example systems in Section 5.5.*

5.4.3 Necessary optimality conditions

In previous sections, we introduced the Pontryagin maximum principle to derive the adjoint system description through the necessary optimality conditions for an optimal control problem. Once derived, these conditions can be discretised and solved to obtain a trajectory in time for both the state and the adjoint. As we discussed in Chapter 2, such OCP solution methods are known as indirect. The resulting system of necessary optimality condition can be solved using gradient methods (see for example [141, 142]) or multiple shooting methods (see for an introduction [143], [144]). Alternatively, using the multirate discrete formulation, the optimal control problem can be rewritten in a finite-dimensional constrained NLP, as demonstrated in Problems 5.15 and 5.16, and as such belongs to the group

of direct solution methods [145, 146]. For these methods, the Karush-Kuhn-Tucker (KKT) equations have been shown to provide the discrete necessary optimality conditions directly, thereby encoding a discrete adjoint representation (for details see Chapter 2 and [23]). In [19] it was shown that this adjoint representation corresponds to a discretisation of the continuous adjoint system with the same variational integrator. Thus with the DMOC approach, the adjoint approximation is of the same order as the approximation of the state. In this section, we investigate whether this is also true in the multirate setting. We do so for the particular example of optimally controlling the system presented in Demonstration problem 2. Using the midpoint quadrature and finite difference approximation for the approximations within the variational approach, we derive the discrete adjoint equations and compare them to the continuous ones, to determine the corresponding order of approximation with Multirate DMOC.

Demonstration problem 5. *We take the system model from Demonstration problem 2 and rearrange the equations as:*

$$0 = \mathbb{f}_k^{\mathrm{s}} = -M^{\mathrm{s}}\frac{q_{k+1}^{\mathrm{s}} - q_k^{\mathrm{s}}}{\Delta T} + M^{\mathrm{s}}\frac{q_k^{\mathrm{s}} - q_{k-1}^{\mathrm{s}}}{\Delta T} - \frac{\Delta t}{2}\sum_{m=0}^{\mathbb{p}-1}\left(\alpha_m \partial_{\mathrm{s}} U_k^m + \beta_m \partial_{\mathrm{s}} U_{k-1}^m\right) + F_k^{\mathrm{s}} + F_{k-1}^{\mathrm{s},+} \tag{5.17a}$$

$$\begin{aligned} 0 = \mathbb{f}_k^{\mathrm{f},0} = &-M^{\mathrm{f}}\frac{q_k^{\mathrm{f},1} - q_k^{\mathrm{f},0}}{\Delta t} + M^{\mathrm{f}}\frac{q_{k-1}^{\mathrm{f},\mathbb{p}} - q_{k-1}^{\mathrm{f},\mathbb{p}-1}}{\Delta t} \\ &- \frac{\Delta t}{2}\left(\partial_{\mathrm{f}} U_{k-1}^{\mathbb{p}} + \partial_{\mathrm{f}} U_{k-1}^{\mathbb{p}-1} + \nabla P_k^{m+1} + \nabla P_k^m\right) + f_k^{\mathrm{f},0,-} + f_{k-1}^{\mathrm{f},\mathbb{p}-1,+} \end{aligned} \tag{5.17b}$$

$$\begin{aligned} 0 = \mathbb{f}_k^{\mathrm{f},m} = &-M^{\mathrm{f}}\frac{q_k^{\mathrm{f},m+1} - q_k^{\mathrm{f},m}}{\Delta t} + M^{\mathrm{f}}\frac{q_k^{\mathrm{f},m} - q_k^{\mathrm{f},m-1}}{\Delta t} \\ &- \frac{\Delta t}{2}\left(\partial_{\mathrm{f}} U_{k-1}^{\mathbb{p}} + \partial_{\mathrm{f}} U_{k-1}^{\mathbb{p}-1} + \nabla P_k^0 + \nabla P_{k-1}^{\mathbb{p}-1}\right) + f_k^{\mathrm{f},m,-} + f_k^{\mathrm{f},m-1,+}. \end{aligned} \tag{5.17c}$$

Here (D.14*a*) *for* $k = 1, \ldots, N-1$ *and* (D.14*b*) *for* $k = 0, \ldots, N-1$ *and* (D.14*c*) $k = 0, \ldots, N-1$,$m = 1, \ldots, \mathbb{p}-1$. *Based on equations* (3.30a), (3.30c) *the initial conditions for this model take the form:*

$$0 = \mathbb{f}_0^{\mathrm{s}} = p_0^{\mathrm{s}} - M^{\mathrm{s}}\frac{q_1^{\mathrm{s}} - q_0^{\mathrm{s}}}{\Delta T} - \frac{\Delta t}{2}\sum_{m=0}^{\mathbb{p}-1}\left(\alpha_m \partial_{\mathrm{s}} U_{\mathrm{d},0}^m\right) + F_k^{\mathrm{s},-} \tag{5.18a}$$

$$0 = \mathbb{f}_0^{\mathrm{f},0} = p_0^{\mathrm{f},0} - M^{\mathrm{f}}\frac{q_0^{\mathrm{f},1} - q_0^{\mathrm{f},0}}{\Delta t} - \frac{\Delta t}{2}\nabla P_{\mathrm{d},0}^0 + f_k^{\mathrm{f},-} \tag{5.18b}$$

For a separable potential $V(q^{\mathrm{s}}(t), q^{\mathrm{f}}(t)) = Y(q^{\mathrm{s}}(t)) + P(q^{\mathrm{f}}(t))$ *these simplify to*

$$\mathbb{f}_k^{\mathrm{s}} = -M^{\mathrm{s}} \frac{q_{k+1}^{\mathrm{s}} - q_k^{\mathrm{s}}}{\Delta T} + M^{\mathrm{s}} \frac{q_k^{\mathrm{s}} - q_{k-1}^{\mathrm{s}}}{\Delta T} - \frac{\Delta t}{2} \sum_{m=0}^{\mathbb{p}-1} \Big(\alpha_m \nabla Y_k^m + \beta_m \nabla Y_{k-1}^m \Big) + F_k^{\mathrm{s}} + F_{k-1}^{\mathrm{s},+} \tag{5.19a}$$

$$\mathbb{f}_k^{\mathrm{f},0} = -M^{\mathrm{f}} \frac{q_k^{\mathrm{f},1} - q_k^{\mathrm{f},0}}{\Delta t} + M^{\mathrm{f}} \frac{q_{k-1}^{\mathrm{f},\mathbb{p}} - q_{k-1}^{\mathrm{f},\mathbb{p}-1}}{\Delta t} - \frac{\Delta t}{2} \Big(\nabla P_k^0 + \nabla P_{k-1}^{\mathbb{p}-1} \Big) + f_k^{\mathrm{f},m,-} + f_k^{\mathrm{f},m-1,+} \tag{5.19b}$$

$$\mathbb{f}_k^{\mathrm{f},m} = -M^{\mathrm{f}} \frac{q_k^{\mathrm{f},m+1} - q_k^{\mathrm{f},m}}{\Delta t} + M^{\mathrm{f}} \frac{q_k^{\mathrm{f},m} - q_k^{\mathrm{f},m-1}}{\Delta t} - \frac{\Delta t}{2} \Big(\nabla P_k^{m+1} + \nabla P_k^m \Big) + f_k^{\mathrm{f},0,-} + f_{k-1}^{\mathrm{f},\mathbb{p}-1,+} \tag{5.19c}$$

$$0 = \mathbb{f}_0^{\mathrm{s}} = p_0^{\mathrm{s}} - M^{\mathrm{s}} \frac{q_1^{\mathrm{s}} - q_0^{\mathrm{s}}}{\Delta T} - \frac{\Delta t}{2} \sum_{m=0}^{\mathbb{p}-1} \Big(\alpha_m \nabla Y_{\mathrm{d},0}^m \Big) + F_k^{\mathrm{s},-} \tag{5.20a}$$

$$0 = \mathbb{f}_0^{\mathrm{f},0} = p_0^{\mathrm{f},0} - M^{\mathrm{f}} \frac{q_0^{\mathrm{f},1} - q_0^{\mathrm{f},0}}{\Delta t} - \frac{\Delta t}{2} \nabla P_{\mathrm{d},0}^0 + f_k^{\mathrm{f},m,-} \tag{5.20b}$$

with $Y_k^m = Y(\bar{q}_k^{\mathrm{s},m}) = Y(\frac{\alpha_m q_k^{\mathrm{s}} + \beta_m q_{k+1}^{\mathrm{s}}}{2})$ *and* $\mathbb{f}_k^{\mathrm{s}} = \mathbb{f}_k^{\mathrm{f},0} = \mathbb{f}_k^{\mathrm{f},m} = 0$. *Here* (5.19a) *is for* $k = 1, \ldots, N-1$, (5.19b) *for* $k = 0, \ldots, N-1$, (5.19c) $k = 0, \ldots, N-1$, $m = 1, \ldots, \mathbb{p}-1$.

Using this system model, the continuous OCP problem in Problem 6, can be discretiwed using Multirate DMOC as follows:

Problem 7.

$$\min_{\substack{q_{\mathrm{d}}^{\mathrm{s}}, q_{\mathrm{d}}^{\mathrm{f}}, \\ u_{\mathrm{d}}^{\mathrm{slow}}, u_{\mathrm{d}}^{\mathrm{fast}}}} J_{\mathrm{d}}(q_{\mathrm{d}}^{\mathrm{s}}, q_{\mathrm{d}}^{\mathrm{f}}, u_{\mathrm{d}}^{\mathrm{slow}}, u_{\mathrm{d}}^{\mathrm{fast}}) = \sum_{k=0}^{N-1} C_{\mathrm{d}}^k(u_{\mathrm{d}}^{\mathrm{s}}, u_{\mathrm{d}}^{\mathrm{f}}) + \Phi_{\mathrm{d}}(q_{N-1}^{\mathrm{s}}, q_N^{\mathrm{s}}, q_{N-1}^{\mathrm{f},\mathbb{p}-1}, q_{N-1}^{\mathrm{f},\mathbb{p}}, u_{N-1}^{\mathrm{slow}}, u_{N-1}^{fast,\mathbb{p}-1/2})$$

$$\text{subject to}: q_0^{\mathrm{s}} = q^{\mathrm{s},0},\ q_0^{\mathrm{f},0} = q^{\mathrm{f},0}, \tag{5.18}$$

$$(\mathrm{D}.14a) \quad \text{for } k = 1, \ldots, N-1,$$

$$(\mathrm{D}.14b) \quad \text{for } k = 0, \ldots, N-1,$$

$$(\mathrm{D}.14c) \quad \text{for } k = 1, \ldots, N-1,\ m = 1, \ldots, \mathbb{p}-1$$

Assumption 5.4.1. *For simplicity we assume* $u_{\mathrm{d}}^{\mathrm{slow}}$ *and* $u_{\mathrm{d}}^{\mathrm{fast}}$ *are the discrete approximations of* $u^{\mathrm{s}}(t)$ *and* $u^{\mathrm{f}}(t)$, *respectively, thus defining* $u_{\mathrm{d}}^{\mathrm{s}} = u_{\mathrm{d}}^{\mathrm{slow}}$, $u_{\mathrm{d}}^{\mathrm{f}} = u_{\mathrm{d}}^{\mathrm{fast}}$, *and* $F_k^{\mathrm{s}} = u_{k+1/2}^{\mathrm{slow}} = u_{k+1/2}^{\mathrm{s}}$, $f_k^{\mathrm{f},m} = u_k^{fast,m+1/2} = u_k^{\mathrm{f,m+1/2}}$ *for* $\forall k, m$.

Theorem 5.4.1. *Let Demonstration problem 4 be formulated with a regular multirate Lagrangian* $\mathcal{L}$ *and Lagrangian control forces* $f_{\mathrm{LC}}^{\mathrm{s}} = u^{\mathrm{s}}(t)$, $f_{\mathrm{LC}}^{\mathrm{f}} = u^{\mathrm{f}}(t)$ *which satisfy*

Assumption 5.4.1. Let this problem be discretised as proposed in Problem 7. Then the necessary optimality conditions provide the same structure-preserving discretization scheme for the adjoint system as for the state system.

Proof. We discretise the the running cost as

$$C_{\mathrm{d}}(u_{\mathrm{d}}^{\mathrm{s}}, u_{\mathrm{d}}^{\mathrm{f}}) = \frac{1}{2}\sum_{k=0}^{N-1}\left((u_{k+1/2}^{\mathrm{s}})^T u_{k+1/2}^{\mathrm{s}} + \sum_{m=0}^{\mathbb{p}-1}(u_k^{f,m+1/2})^T u_k^{f,m+1/2}\right).$$

For this OCP we can define the augmented discrete cost functional as

$$\begin{aligned}\mathcal{L}_{C,d}(q_{\mathrm{d}}^{\mathrm{s}}, q_{\mathrm{d}}^{\mathrm{f}}, u_{\mathrm{d}}^{\mathrm{slow}}, u_{\mathrm{d}}^{\mathrm{fast}}, \lambda_{\mathrm{d}}^{\mathrm{s}}, \lambda_{\mathrm{d}}^{\mathrm{f}}) &= \frac{1}{2}\sum_{k=0}^{N-1}\left((u_{k+1/2}^{\mathrm{s}})^T u_{k+1/2}^{\mathrm{s}} + \sum_{m=0}^{\mathbb{p}-1}(u_k^{f,m+1/2})^T u_k^{f,m+1/2}\right)\\ &+ \begin{bmatrix}\mu_0^{\mathrm{s}}\\ \mu_0^{\mathrm{f},0}\end{bmatrix}\cdot\begin{bmatrix}q_0^{\mathrm{s}} - q^{\mathrm{s},0}\\ q_0^{\mathrm{f},0} - q^{\mathrm{f},0}\end{bmatrix} + \begin{bmatrix}\lambda_0^{\mathrm{s}}\\ \lambda_0^{\mathrm{f},0}\end{bmatrix}\cdot\begin{bmatrix}\mathbb{f}_0^{\mathrm{s}}\\ \mathbb{f}_0^{\mathrm{f},0}\end{bmatrix} + \sum_{k=0}^{N-1}\left\{\begin{bmatrix}\lambda_k^{\mathrm{s}}\\ \lambda_0^{\mathrm{f},k}\end{bmatrix}\cdot\begin{bmatrix}\mathbb{f}_k^{\mathrm{s}}\\ \mathbb{f}_k^{\mathrm{f},0}\end{bmatrix} + \sum_{m=0}^{\mathbb{p}-1}\lambda_m^{\mathrm{f},k}\cdot\mathbb{f}_k^{\mathrm{f},m}\right\}\end{aligned}$$

where $\lambda_{\mathrm{d}}^{\mathrm{s}} = \{\lambda_k^{\mathrm{s}}\}_{k=0}^{N} \in \mathbb{R}^{n_{\mathrm{s}}}$ and $\lambda_{\mathrm{d}}^{\mathrm{f}} = \{\{\lambda_k^{\mathrm{f},m}\}_{m=0}^{\mathbb{p}-1}\}_{k=0}^{N} \in \mathbb{R}^{n_f}$ are the adjoint vectors. Using the KKT conditions, this leads to the same system representation as (5.20), (5.19), $q_0^{\mathrm{s}} = q^{\mathrm{s}}(0)$, $q_0^{\mathrm{f},0} = q^{\mathrm{f}}(0)$ and the following system for the adjoint equations:

$$\begin{aligned}0 =& -M^{\mathrm{s}}\frac{\lambda_{k+1}^{\mathrm{s}} - \lambda_k^{\mathrm{s}}}{\Delta T} + M^{\mathrm{s}}\frac{\lambda_k^{\mathrm{s}} - \lambda_{k-1}^{\mathrm{s}}}{\Delta T} - \frac{\Delta t}{2}\sum_{m=0}^{\mathbb{p}}\left(\alpha_m\partial_{\mathrm{sf}}U_k^m\lambda_k^{\mathrm{f},m} + \beta_m\partial_{\mathrm{sf}}U_{k-1}^m\lambda_{k-1}^{\mathrm{f},m}\right)\\ &- \frac{\Delta t}{2}\sum_{m=0}^{\mathbb{p}-1}\left(\alpha_m\partial_{\mathrm{ss}}^2U_k^m\frac{\alpha_m\lambda_k^{\mathrm{s}} + \beta_m\lambda_{k+1}^{\mathrm{s}}}{2} + \beta_m\partial_{\mathrm{ss}}^2U_{k-1}^m\frac{\alpha_m\lambda_{k-1}^{\mathrm{s}} + \beta_m\lambda_k^{\mathrm{s}}}{2}\right) \qquad (5.21a)\\ 0 =& -M^{\mathrm{f}}\frac{\lambda_k^{\mathrm{f},1} - \lambda_k^{\mathrm{f},0}}{\Delta t} + M^{\mathrm{f}}\frac{\lambda_k^{\mathrm{f},0} - \lambda_{k-1}^{\mathrm{f},\mathbb{p}-1}}{\Delta t} - \Delta t\,\partial_{\mathrm{fs}}^2U_k^{\mathbb{p}-1}\frac{\alpha_{\mathbb{p}-1}\lambda_k^{\mathrm{s}} + \beta_{\mathbb{p}-1}\lambda_{k+1}^{\mathrm{s}}}{2}\\ &- \frac{\Delta t}{2}\left(\nabla^2P_k^0\frac{\lambda_k^{\mathrm{f},0} + \lambda_k^{\mathrm{f},1}}{2} + \nabla^2P_{k-1}^{\mathbb{p}-1}\frac{\lambda_{k-1}^{\mathrm{f},0} + \lambda_k^{\mathrm{f},0}}{2}\right) \qquad (5.21b)\\ 0 =& -M^{\mathrm{f}}\frac{\lambda_k^{\mathrm{f},m+1} - \lambda_k^{\mathrm{f},m}}{\Delta t} + M^{\mathrm{f}}\frac{\lambda_k^{\mathrm{f},m} - \lambda_k^{\mathrm{f},m-1}}{\Delta t} - \Delta t\,\partial_{\mathrm{fs}}^2U_k^m\frac{\alpha_m\lambda_k^{\mathrm{s}} + \beta_m\lambda_{k+1}^{\mathrm{s}}}{2}\\ &- \frac{\Delta t}{2}\left(\nabla^2P_k^m\frac{\lambda_k^{\mathrm{f},m} + \lambda_k^{\mathrm{f},m+1}}{2} + \nabla^2P_k^{m-1}\frac{\lambda_k^{\mathrm{f},m-1} + \lambda_k^{\mathrm{f},m}}{2}\right) \qquad (5.21c)\end{aligned}$$

for $k = 1, \ldots, N-1$, $m = 1, \ldots, \mathbb{p}-1$ and $\lambda_{k-1}^{\mathrm{f},\mathbb{p}} = \lambda_k^{\mathrm{f},0}$ for $k = 1, \ldots, N$ with boundary conditions

$$\begin{aligned}0 =& \mu_0^{\mathrm{s}} - M^{\mathrm{s}}\frac{\lambda_1^{\mathrm{s}} - \lambda_0^{\mathrm{s}}}{\Delta T} - \frac{\Delta t}{2}\sum_{m=0}^{\mathbb{p}-1}\alpha_m\partial_{\mathrm{ss}}^2U_0^m\left(\frac{\alpha_m\lambda_0^{\mathrm{s}} + \beta_m\lambda_1^{\mathrm{s}}}{2}\right) - \frac{\Delta t}{2}\sum_{m=0}^{\mathbb{p}}\left(\alpha_m\partial_{\mathrm{sf}}U_{\mathrm{d},0}^m\lambda_0^{\mathrm{f},m}\right), \qquad (5.22a)\\ 0 =& \mu_0^{\mathrm{f},0} - M^{\mathrm{f}}\frac{\lambda_0^{\mathrm{f},1} - \lambda_0^{\mathrm{f},0}}{\Delta t} - \frac{\Delta t}{2}\partial_{\mathrm{fs}}^2U_{\mathrm{d},0}^0\frac{\alpha_0\lambda_0^{\mathrm{s}} + \beta_0\lambda_1^{\mathrm{s}}}{2} - \frac{\Delta t}{2}\nabla^2P_{\mathrm{d},0}^0\frac{\lambda_0^{\mathrm{f},0} + \lambda_0^{\mathrm{f},1}}{2}, \qquad (5.22b)\end{aligned}$$

$$0 = \lambda_{N-1}^{\mathrm{f},\mathbb{p}} + \nabla_{q_{N-1}^{\mathrm{f},\mathbb{p}}} \tilde{\Phi}_{\mathrm{d}}(q_N^{\mathrm{s}}, q_{N-1}^{\mathrm{f},\mathbb{p}}, p_N^{\mathrm{s}}, p_{N-1}^{\mathrm{f},\mathbb{p}}), \tag{5.22c}$$

$$0 = \lambda_N^{\mathrm{s}} + \nabla_{q_N^{\mathrm{s}}} \tilde{\Phi}_{\mathrm{d}}(q_N^{\mathrm{s}}, q_{N-1}^{\mathrm{f},\mathbb{p}}, p_N^{\mathrm{s}}, p_{N-1}^{\mathrm{f},\mathbb{p}}). \tag{5.22d}$$

Here the notation used is:

$$\partial_{\mathrm{ss}}^2 U_k^m = \frac{\partial^2 U(\bar{q}_k^{\mathrm{s},m}, \bar{q}_k^{\mathrm{f},m})}{\partial^2 \bar{q}_k^{\mathrm{s},m}}, \quad \partial_{\mathrm{ff}}^2 U_k^m = \frac{\partial^2 U(\bar{q}_k^{\mathrm{s},m}, \bar{q}_k^{\mathrm{f},m})}{\partial^2 \bar{q}_k^{\mathrm{f},m}}, \quad \nabla^2 P_k^m = \frac{\partial \nabla P_k^m}{\partial \bar{q}_k^{\mathrm{f},m}},$$
$$\partial_{\mathrm{sf}}^2 U_k^m = \frac{\partial^2 U(\bar{q}_k^{\mathrm{s},m}, \bar{q}_k^{\mathrm{f},m})}{\partial \bar{q}_k^{\mathrm{s},m} \partial \bar{q}_k^{\mathrm{f},m}}, \quad \partial_{\mathrm{fs}}^2 U_k^m = \frac{\partial^2 U(\bar{q}_k^{\mathrm{s},m}, \bar{q}_k^{\mathrm{f},m})}{\partial \bar{q}_k^{\mathrm{f},m} \partial \bar{q}_k^{\mathrm{s},m}}$$

For a separable potential $V(q^{\mathrm{s}}, q^{\mathrm{f}}) = Y(q_k^{\mathrm{s}}) + P(q^{\mathrm{f}})$ the equations simplify to:

$$0 = -M^{\mathrm{s}} \frac{\lambda_{k+1}^{\mathrm{s}} - \lambda_k^{\mathrm{s}}}{\Delta T} + M^{\mathrm{s}} \frac{\lambda_k^{\mathrm{s}} - \lambda_{k-1}^{\mathrm{s}}}{\Delta T} \tag{5.23a}$$

$$- \frac{\Delta t}{2} \sum_{m=0}^{\mathbb{p}-1} \left(\alpha_m \nabla^2 Y_k^m \frac{\alpha_m \lambda_k^{\mathrm{s}} + \beta_m \lambda_{k+1}^{\mathrm{s}}}{2} + \beta_m \nabla^2 Y_{k-1}^m \frac{\alpha_m \lambda_{k-1}^{\mathrm{s}} + \beta_m \lambda_k^{\mathrm{s}}}{2} \right) \tag{5.23b}$$

$$0 = -M^{\mathrm{f}} \frac{\lambda_k^{\mathrm{f},1} - \lambda_k^{\mathrm{f},0}}{\Delta t} + M^{\mathrm{f}} \frac{\lambda_k^{\mathrm{f},0} - \lambda_{k-1}^{\mathrm{f},\mathbb{p}-1}}{\Delta t} \tag{5.23c}$$

$$- \frac{\Delta t}{2} \left(\nabla^2 P_k^0 \frac{\lambda_k^{\mathrm{f},0} + \lambda_k^{\mathrm{f},1}}{2} + \nabla^2 P_{k-1}^{\mathbb{p}-1} \frac{\lambda_{k-1}^{\mathrm{f},0} + \lambda_k^{\mathrm{f},0}}{2} \right) \tag{5.23d}$$

$$0 = -M^{\mathrm{f}} \frac{\lambda_k^{\mathrm{f},m+1} - \lambda_k^{\mathrm{f},m}}{\Delta t} + M^{\mathrm{f}} \frac{\lambda_k^{\mathrm{f},m} - \lambda_k^{\mathrm{f},m-1}}{\Delta t} \tag{5.23e}$$

$$- \frac{\Delta t}{2} \left(\nabla^2 P_k^{m-1} \frac{\lambda_k^{\mathrm{f},m-1} + \lambda_k^{\mathrm{f},m}}{2} + \nabla^2 P_k^m \frac{\lambda_k^{\mathrm{f},m} + \lambda_k^{\mathrm{f},m+1}}{2} \right) \tag{5.23f}$$

for $k = 1, \ldots, N-1$, $m = 1, \ldots, \mathbb{p}-1$ and $\lambda_{k-1}^{\mathrm{f},\mathbb{p}} = \lambda_k^{\mathrm{f},0}$ for $k = 1, \ldots, N$ with boundary conditions

$$0 = \mu_0^{\mathrm{s}} - M^{\mathrm{s}} \frac{\lambda_1^{\mathrm{s}} - \lambda_0^{\mathrm{s}}}{\Delta T} - \frac{\Delta t}{2} \sum_{m=0}^{\mathbb{p}-1} \alpha_m \nabla^2 Y_{\mathrm{d},0}^m \left(\frac{\alpha_m \lambda_0^{\mathrm{s}} + \beta_m \lambda_1^{\mathrm{s}}}{2} \right), \tag{5.24a}$$

$$0 = \mu_0^{\mathrm{f},0} - M^{\mathrm{f}} \frac{\lambda_0^{\mathrm{f},1} - \lambda_0^{\mathrm{f},0}}{\Delta t} - \frac{\Delta t}{2} \nabla^2 P_0^0 \frac{\lambda_0^{\mathrm{f},0} + \lambda_0^{\mathrm{f},1}}{2}, \tag{5.24b}$$

$$0 = \lambda_{N-1}^{\mathrm{f},\mathbb{p}} + \nabla_{q_{N-1}^{\mathrm{f},\mathbb{p}}} \tilde{\Phi}_{\mathrm{d}}(q_N^{\mathrm{s}}, q_{N-1}^{\mathrm{f},\mathbb{p}}, p_N^{\mathrm{s}}, p_{N-1}^{\mathrm{f},\mathbb{p}}), \tag{5.24c}$$

$$0 = \lambda_N^{\mathrm{s}} + \nabla_{q_N^{\mathrm{s}}} \tilde{\Phi}_{\mathrm{d}}(q_N^{\mathrm{s}}, q_{N-1}^{\mathrm{f},\mathbb{p}}, p_N^{\mathrm{s}}, p_{N-1}^{\mathrm{f},\mathbb{p}}). \tag{5.24d}$$

Here $\nabla^2 Y_k^m = \nabla^2 Y(\bar{q}_k^{\mathrm{f},m})$. For $Y(q^{\mathrm{s}}) = (q^{\mathrm{s}})^\intercal K^{\mathrm{s}} q^{\mathrm{s}}$, $P(q^{\mathrm{f}}) = (q^{\mathrm{f}})^\intercal K^{\mathrm{f}} q^{\mathrm{f}}$ the adjoint model (5.23) can be simplified using $\nabla^2 Y_k^m = K^{\mathrm{s}}$ and $\nabla^2 P_k^m = K^{\mathrm{f}}$ and the initial conditions become:

$$0 = p_0^{\mathrm{s}} - M^{\mathrm{s}} \frac{q_1^{\mathrm{s}} - q_0^{\mathrm{s}}}{\Delta T} - \frac{\Delta t}{2} K^{\mathrm{s}} \sum_{m=0}^{\mathbb{p}-1} \left(\alpha_m \frac{\alpha_m q_0^{\mathrm{s}} + \beta_m q_1^{\mathrm{s}}}{2} \right) + F_k^{\mathrm{s},-}, \tag{5.25a}$$

$$0 = p_0^{\mathrm{f},0} - M^{\mathrm{f}}\frac{q_1^{\mathrm{s}} - q_0^{\mathrm{s}}}{\Delta t} - \frac{\Delta t}{2}K^{\mathrm{f}}\Big(\frac{q_0^{\mathrm{f},0} + q_0^{\mathrm{f},1}}{2}\Big) + f_k^{\mathrm{f},m,-}. \tag{5.25b}$$

Comparing the two dicretisation schemes for the state (5.18), (5.17) and the adjoint (5.21), (5.22) with the continuous state and adjoint expressions (5.11), (5.12), we see that the discretisation of the adjoint is the same as the that of the state system. □

Theorem 5.4.2. *Let Demonstration problem 4 be formulated with a regular multirate Lagrangian $\mathcal{L}$ and Lagrangian control forces $f_{\mathrm{LC}}^{\mathrm{s}} = u^{\mathrm{s}}(t), f_{\mathrm{LC}}^{\mathrm{f}} = u^{\mathrm{f}}(t)$ which satisfy Assumptions 3.4.1, 3.4.2, and 5.4.1. Let this problem be discretised as proposed in Problem 7. If L_{d}^k, $F_k^{\mathrm{s},\pm}$, $F_E^{\mathrm{s},\pm}$ approximate respectively $L_{\mathrm{d}}^{\mathrm{E}}$, $F_k^{\mathrm{f},\pm}$ and $F_E^{\mathrm{f},\pm}$ to an order $r \in \{1, 2\}$, the resulting discrete adjoint scheme approximates the continuous adjoint with the same order r in a structure-preserving manner (as defined by Theorem 3.4.2).*

Proof. Based on the regularity of the Lagrangian, the equivalence of the Hamiltonian and Lagrangian discrete variational formulations holds. Based on this equivalence and Assumptions 3.4.1, 3.4.2, it follows from Lemma 3.4.3 and Theorem 3.4.2 that the system models (5.17), (5.18) (or (3.35), (5.25)) are structure-preserving and of order two. Based on Theorem 5.4.1, it follows that the adjoint system is also approximated using a second-order symplectic scheme. Thus the solution of the Lagrangian formulation OCP (5.15) inherits the second-order accuracy and structure-preservation properties of the variational system model. As the Lagrangian formulation of the problem is equivalent to the Hamiltonian formulation, it thus follows that the Hamiltonian formulation (5.16) also provides second order symplectic approximation of the system and adjoint dynamics. Order one can be trivially achieved in the same manner using rectangular quadrature in any of the discrete configuration, velocity, energy or force approximations. □

Remark 5.4.2. *A quick check with $\mathbb{p} = 1$ simplifies the state* (5.17), (5.18) *and adjoint models* (5.21), (5.22) *to the singlerate second-order symplectic state and adjoint approximations by [19].*

5.5 Examples

In this section we present numerical tests on the application of Multirate DMOC to two example problems. First, we demonstrate its applicability to the control of nonlinear systems without the need to decouple the equations of motion. Afterwards, we focus on the control of a system with a linear model in order validate the Multirate DMOC solution against an analytic solution, and thus demonstrate the structure-preserving properties and the order of accuracy of the variational solution.

The approximation rules used for the Multirate DMOC formulation in both examples are the same as defined in Section 4.1.1, using picewise-linear polynomias to approximate the slow and fast configuration variables, and piecewise-constant polynomials to approximate the controls. Midpoint quadrature and finite difference approximations are again used for the formulation of the discrete Lagrangian and virtual work, as well as for the approximation of the cost functional $C(x^{\mathrm{s}}(t), x^{\mathrm{f}}(t), u^{\mathrm{s}}(t), u^{\mathrm{f}}(t))$ where $x^{\mathrm{s}} = [(q^{\mathrm{s}})^{\intercal}, (p^{\mathrm{s}})^{\intercal})]^{\intercal}$, $x^{\mathrm{f}} = [(q^{\mathrm{f}})^{\intercal}, (p^{\mathrm{f}})^{\intercal})]^{\intercal}$. In several figures, $\mathbb{p}$ is represented as p or $\mathbf{p}$ due to software limitations, with clarification provided in the captions. The runtime results in the following tests are recorded using the same setup as detailed in Section 4.1.2. These experiments aim to provide a comparative analysis across various $\mathbb{p}$ values and formulations, rather than to demonstrate the lowest runtime achievable with this method using an optimised code implementation.

5.5.1 Example 2: FPUT system with quartic potential

Problem formulation

The FPUT system and the considered external controls acting on the system were presented in detail in Section 4.2 for a quadratic potential and extended to a quartic potential (and thus a nonlinear model) in Section 4.3. In this section we focus on the latter, considering two point masses ($n = 2$) and applying Multirate DMOC to stabilise the system to its equilibrium from an initial displacement. The Hamiltonian formulation of the approach is chosen to derive the model of the system, while the

cost is selected as a quadratic function of the form:

$$C(x^{\mathrm{s}}(t), x^{\mathrm{f}}(t), u^{\mathrm{s}}(t), u^{\mathrm{f}}(t)) = \int_0^T \Big((x^{\mathrm{s}})^\intercal x^{\mathrm{s}} + (u^{\mathrm{s}})^\intercal u^{\mathrm{s}} + (x^{\mathrm{f}})^\intercal x^{\mathrm{f}} + (u^{\mathrm{f}})^\intercal u^{\mathrm{f}} \Big) dt$$

Computational results

The tests are carried out in Python, using the SLSQP optimisation solver from *scipy.optimize.minimize* [147]. The multirate DMOC approach is implemented without the need to decouple the equations of motion and the system's parameters chosen for testing match those used for uncontrolled simulations in Section with $w = 50$, initial displacement $q^{\mathrm{f},0} = [1/w, 2/w]^\intercal$, $q^{\mathrm{s},0} = [1, 0.2]^\intercal$, $\dot{q}^{\mathrm{s},0} = \dot{q}^{\mathrm{f},0} = [1, 0]^\intercal$ and damping coefficients $\lambda_w = \lambda_k = 0.3$. The results are presented in Figure 5.1, demonstrating that the Multirate DMOC formulation indeed obtains a solution which brings the system to the origin for a solution with $T = 0.99$, $\Delta t = 10^{-3}$, $\mathbb{p} = 3$.

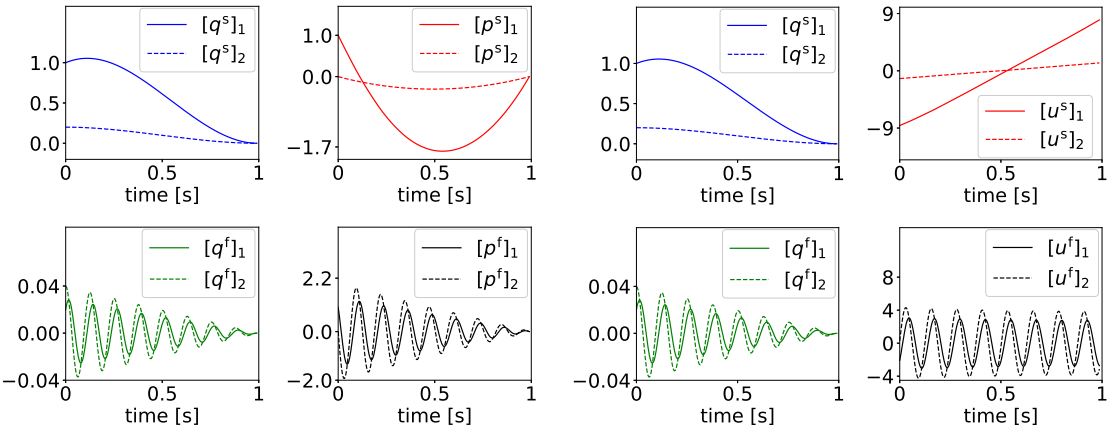


Figure 5.1: Example 2: OCP solution with Multirate DMOC in LF (first two columns) and in HF (last two columns) for $T = 0.99, \Delta t = 10^{-3}, \mathbb{p} = 3$

5.5.2 Example 3: Flexible spacecraft control

Our next example looks at the simultaneous vibration and manoeuvre control of the flexible satellite system, presented in Chapter 4. The system parameters and the selection of slow and fast coordinates used to define the discrete model are the same as those chosen for the uncontrolled simulations described in Section 4.4. Thus, the natural frequencies of the system span between 0 and 5.78×10^2 rad/s

resulting in dynamics on significantly different time scales and allowing for thorough investigation of the advantages of the proposed multirate scheme.

Problem formulation

Based on this model formulation, an optimal control problem is defined with the objective of achieving a rest-to-rest single-axis rotation with n_{vibr} quiescent modes at the end of the manoeuvre. The cost function is formulated as a sum of weighted quadratic functions of the modal amplitudes, the modal amplitude rates, and the applied control. Thus, the overall OCP can be expressed as follows

$$\min_{x,u} J(\,x,u) = \min_{x,u} \int_{t_0}^{T} C(\,x(t),u(t)\,)\,dt = \min_{x,u} \frac{1}{2}\int_{t_0}^{T} [\,x(t)^T \mathbf{W} x(t) + u(t)^2\,]dt \tag{5.26a}$$

$$\text{subject to} \qquad \dot{x}(t) = \mathbf{A}x(t) + \mathbf{B}\tau(t) \tag{5.26b}$$

$$q(t_0) = \mathbf{E}^{-1}\,\xi_{t_0}, \quad \xi_{t_0} = [0,...,0]^\intercal \tag{5.26c}$$

$$q(T) = \mathbf{E}^{-1}\,\xi_{T}, \quad \xi_{T} = [\theta_T,0,...,0]^\intercal \tag{5.26d}$$

$$\underline{\dot{q}}(t_0) = \dot{q}(T) = [0,...,0]^T \tag{5.26e}$$

$$\text{where} \qquad \underline{x}(t) = \begin{bmatrix} q(t) \\ \dot{q}(t) \end{bmatrix}, \quad u(t) = \tau(t), \quad \mathbf{A} = \begin{bmatrix} 0 & \mathbf{I} \\ -\mathbf{\Lambda} & 0 \end{bmatrix}, \quad \mathbf{B} = \begin{bmatrix} 0 \\ \mathbf{E}^T\mathbf{D} \end{bmatrix} \tag{5.26f}$$

and $\mathbf{W}$ is taken to be the identity matrix for this example. This formulation of the cost function allows for the minimisation of control effort, while penalising trajectories with large modal deformations, which could lead to potential loss of pointing accuracy, degradation of performance or even structural damage [116, 117].

Numerical results

Next, the full Multirate DMOC scheme (in Hamiltonian formulation) was applied for the solution of the optimal control problem detailed in Equation (5.26). The optimisation was implemented using the *interior-point-convex* method included in the MATLAB *quadprog* routine and validated against the analytical solution outlined by Turner and Junkins [119]. For this purpose, a numerical convergence test was performed analogously to the previous section, for simulations of length $T = 0.12$s and $\theta_T = 20°$. The test was performed using an absolute error computation for the optimal cost C and error estimation following the definition in Equation (4.12)

for the trajectory ξ and the control force τ. The results presented in Figure 5.2 are reasonable, as performing the manoeuvre in such short time interval results in values for the cost function and the control input of order as high as 10^{11}s and 10^{6}s, respectively. The figures show convergence of order 2 for all considered variables, as expected from the use of midpoint quadrature, thus validating the correct behaviour of the numerical scheme.

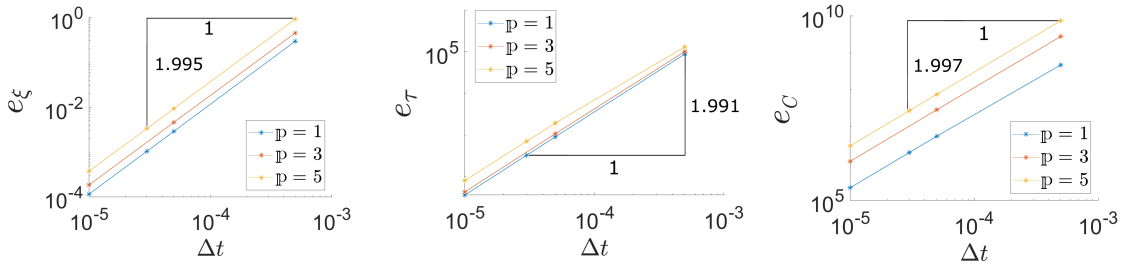


Figure 5.2: Example 3: Numerical convergence study for the OCP formulation using macro-node error computation for $T = 0.12$s

An example solution of the multirate OCP is presented in Figure 5.3 for a rest-to-rest manoeuvre with $\theta_T = 20°$, $T = 4.5$s, $\mathbb{p} = 5$ and $\Delta t = 10^{-3}$s. The results demonstrate the successful execution of the maneuver and vibration suppression in all modes included in the model. This example solution is also used to demonstrate the structure-preserving properties of the Multirate DMOC scheme. In the presence of control forces, the difference in total energy and external work is now conserved, and the momentum map evolves according to the Forced Multirate Discrete Noether's theorem 3.4.2 proved in Section 3.4.3. For the current multirate example, the theorem can be shown to be equivalent to the following discrete conservation law

$$\Psi_d^k = p_k^\theta - p_0^\theta - \sum_{i=0}^{k} \sum_{m=0}^{\mathbb{p}-1} \Delta t \tau_i^{m+1/2} = 0 \quad \text{for } k = 0, \ldots, N-1 \text{ and } \mathbf{E}^T \begin{bmatrix} p_k^\theta \\ p_k^\eta \end{bmatrix} = \begin{bmatrix} p_k^{rms} \\ p_k^{rmf} \end{bmatrix} \tag{5.27}$$

Next, the advantages of the multirate OCP scheme were demonstrated in a series of tests comparing the single rate ($\mathbb{p} = 1$) and the multirate ($\mathbb{p} > 1$) solutions. Fundamentally, increasing the proportionality $\mathbb{p}$ leads to a coarser macro time grid on which the slow variables are resolved, lowering the accuracy of their computation. On the other hand, using a coarser macro time grid reduces the number of time

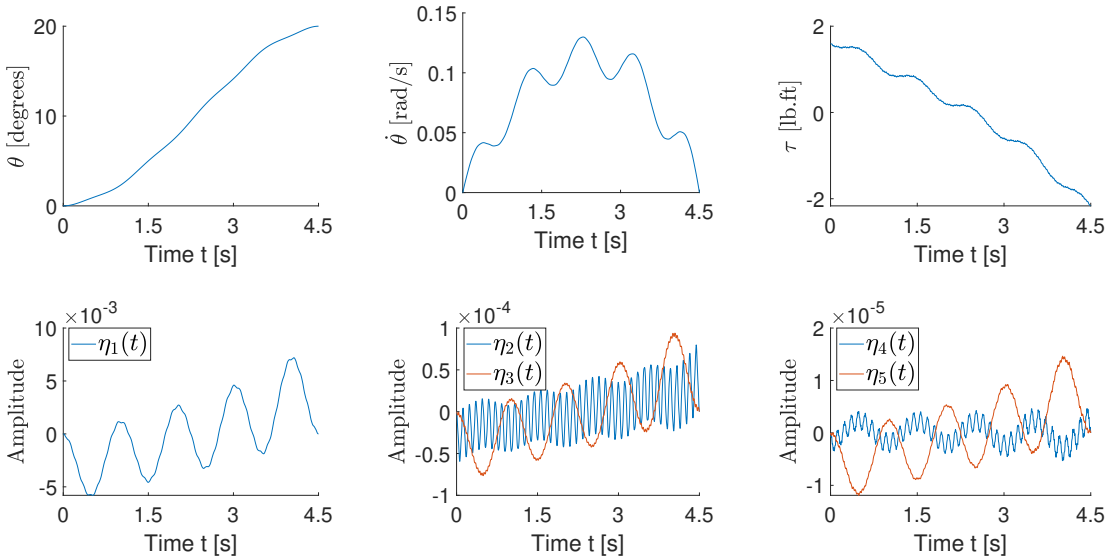


Figure 5.3: Example 3: OCP solution with Multirate DMOC for $\theta_T = 20°$, $T = 4.5$s, $\Delta t = 10^{-3}$ and $\mathbb{p} = 5$

nodes on which the slow variables are computed, and results in overall reduction in the number of optimisation variables $n_{\text{total var}}$ and equality constraints $n_{\text{eq con}}$ used to define the optimisation problem. This effect is demonstrated in Figure 5.4 for simulations with $\Delta t = 10^{-3}$s and $T = 4.5$s, where $n_{\text{total var}} = n_{\text{slow var}} + n_{\text{fast var}}$, where $n_{\text{slow var}}$ and $n_{\text{fast var}}$ denote the number of optimisation variables resulting from discretisation on the macro and micro grid, respectively.

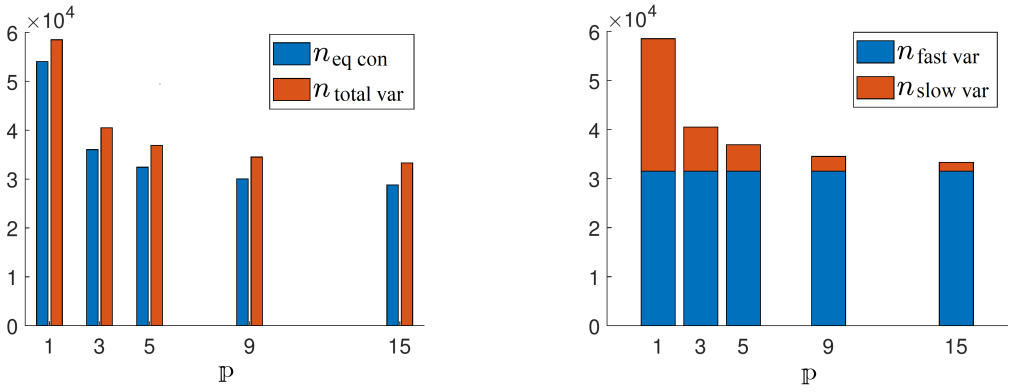


Figure 5.4: Example 3: Size of OCP based on Multirate DMOC (HF) versus $\mathbb{p}$ for a simulations with $\Delta t = 10^{-3}$ and $T = 4.5$s

A more detailed look at the trade-off between accuracy of the simulation and computational cost of the problem is presented in Figure 5.5. In this test a series of

simulations is performed keeping the micro time step constant at 10^{-3}s while varying the macro-micro time step proportionality and recording the resulting variations in both accuracy and real elapsed time for the optimisation. For this test, the relative error is computed using the following definition

$$e_{\xi}^{\text{rel}}(\xi_d, \xi) = \frac{\max_{k=0,\dots,N}(\|\xi_k - \xi(t_k)\|_\infty)}{\max_{k=0,\dots,N}(\|\xi(t_k)\|_\infty)} \tag{5.28}$$

The computation time in Figure 5.5 denotes the mean real elapsed time for the execution of *quadprog* obtained from 10 measurements using the MATLAB *tic-toc* routine. From the figure it can be seen that by adopting the proposed method it is possible to reduce computational costs significantly for small sacrifices in accuracy. For example, in our case the elapsed runtime is more than halved between $\mathbb{p} = 1$ to $\mathbb{p} = 5$ for a negligible increase in the relative error e_{ξ}^{rel} from 9.632×10^{-6} to 1.514×10^{-5}. Furthermore, unlike the real elapsed time curve for the numerical integrator, the real elapsed time for the *quadprog* function monotonically decreases. However, at greater values of $\mathbb{p}$ we observe diminishing returns as the error increases rapidly for smaller computational time reductions. Thus the multirate scheme allows for great flexibility, allowing the designer to decide upon the trade-off between computational cost and simulation fidelity.

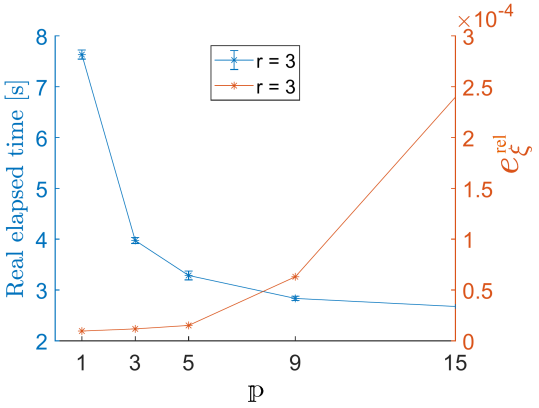


Figure 5.5: Example 3: Mean computational time with standard deviation and relative error in ξ versus $\mathbb{p}$ for HF with a constant $\Delta t = 10^{-3}$s, $T = 4.5$s and $\theta_T = 20°$

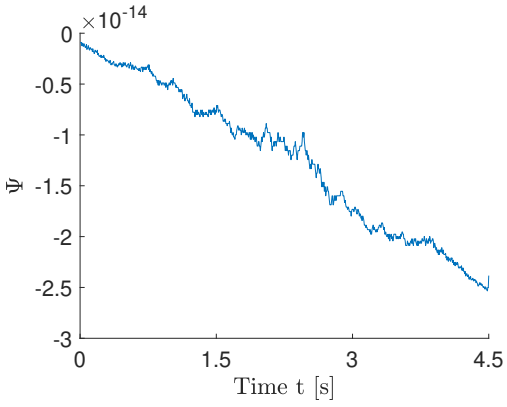


Figure 5.6: Example 3: Demonstration of the conservation properties of Multirate DMOC (HF) for a simulation with $\Delta t = 10^{-3}$s, $\mathbb{p} = 5$, $T = 4.5$s and $\theta_T = 20°$

The trade-off can further be optimised by investigation of the optimal combination of proportionality $\mathbb{p}$ and number of variables r discretised on the macro grid as slow

variables. For this implementation of multirate DMOC the dependence of the size of the number of optimisation variables can be expressed as follows

$$n_{\text{total var}} = n_{\text{slow var}} + n_{\text{fast var}} \tag{5.29a}$$

$$n_{\text{slow var}}(\mathbb{p}, r, n_{\text{vibr}}, T, \Delta t) = 2\, r \left(\frac{T}{\mathbb{p}\, \Delta t} + 1 \right) \tag{5.29b}$$

$$n_{\text{fast var}}(r, n_{\text{vibr}}, T, \Delta t) = 2\, (n_{\text{vibr}} + 1 - r) \left(\frac{T}{\Delta t} + 1 \right) + \frac{T}{\Delta t} \tag{5.29c}$$

As presented in Figures 5.7 and 5.8, increasing r, and thus reducing the variables discretised on the micro grid, allows for even larger reductions in computational cost. The choices in $\mathbb{p}$ and r provide freedom to the practitioner to tailor the method to the time scales present in the problem and allow one to obtain a high-fidelity solutions at reduced computational cost.

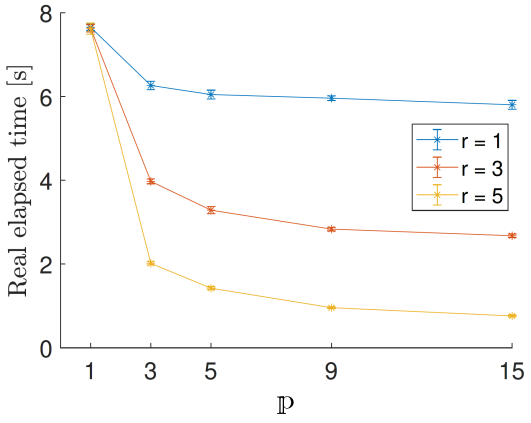


Figure 5.7: Example 3: Mean computational time with standard deviation versus $\mathbb{p}$ with HF for a constant micro time step of 10^{-3}s, $T = 4.5$s and $\theta_T = 20°$

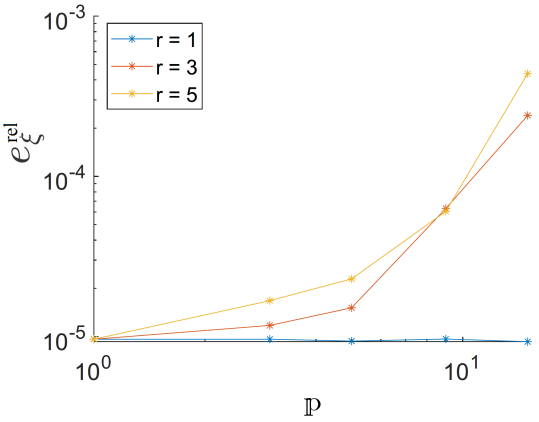


Figure 5.8: Example 3: Relative error in ξ versus $\mathbb{p}$ with HF for a constant micro time step of 10^{-3}s, $T = 4.5$s and $\theta_T = 20°$

Thus far the tests were performed using the Hamiltonian formulation of Multirate DMOC. Discretising the problem using the Lagrangian formulism results in additional savings by removing the need to obtain the conjugate momentum values in time. To demonstrate this, we perform a series of test solving the OCP using both the Hamiltonian and Lagrangian formalism with the quadratic momentum term in the cost function being zeroed. This is based on our preference, rather than necessity, as the momentum term in LF can be equivalently represented in terms of

a finite difference approximation of the system's velocity (without increasing the number of optimisation variables in the LF formulation). The tests were performed for a constant micro time step $\Delta t = 10^{-4}$s and $T = 0.45$s. As we can see in Figure 5.9, compared to the HF, the LF reduces the number of optimisation variables and constraints significantly for all values of $\mathbb{p}$. As shown in Figure 5.10, this results in a better solution approximation and significantly reduced computational runtime for the solution of the OCP for all values of $\mathbb{p}$. Theoretically, the accuracy for both formulations should be equivalent, but as in the uncontrolled simulations of Chapter 4, it varies slightly in experiments due to numerics.

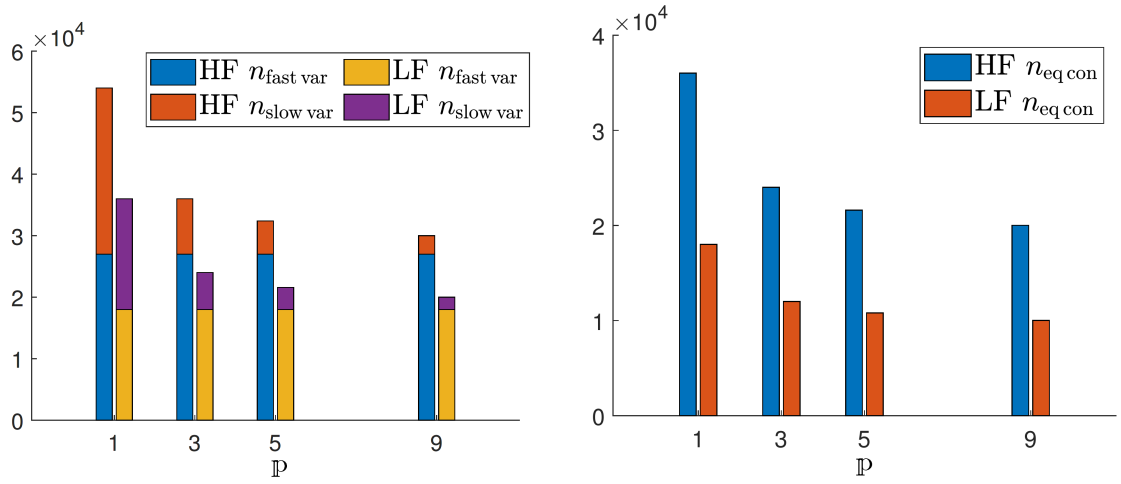


Figure 5.9: Example 3: Size of the OCP using Multirate DMOC HF and LF with varying $\mathbb{p}$ and $T = 0.45$, $\Delta t = 10^{-4}$

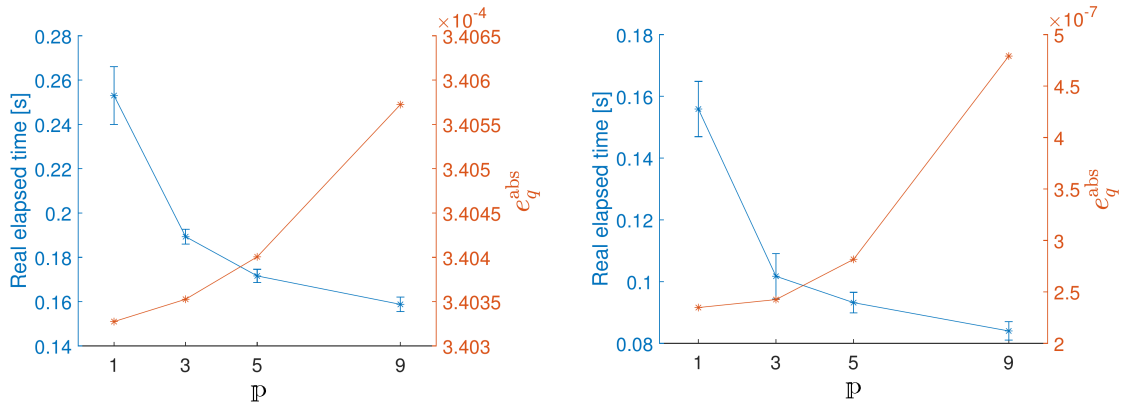


Figure 5.10: Example 3: Accuracy vs. efficiency using Multirate DMOC HF (left) and LF (right) with varying $\mathbb{p}$ and $T = 0.45$, $\Delta t = 10^{-4}$

6

Variational linearisation and multirate MPC

Contents

6.1 Introduction 135
6.2 Background 136
6.3 System representation 139
6.3.1 Singlerate variational linearisation and error bounds . . 140
6.3.2 Multirate variational linearisation and error bounds . . 144
6.4 Receding horizon control strategy 146
6.5 Multirate receding horizon control 149
6.6 Examples 150

6.1 Introduction

In this chapter, we continue our work on control schemes for multirate systems, focusing on the formulation of a closed-loop approach. We propose a multirate nonlinear model predictive control (NMPC) scheme based on a tube-based formulation and the multirate variational approach presented in Chapters 2 - 5. To maintain the structure-preservation of the variation model during the successive linearisation steps and provide a new means for computing the linearisation error bounds, we propose model linearisation using quadratic and linear Taylor series

approximations of the Lagrangian and generalised forces, respectively. The resulting linear multirate variational model allows for the optimisation to be performed less frequently than standard singlerate MPC schemes and also reduces the size of the OCP being solved. Moreover, we prove that the formulation guarantees recursive feasibility and stability. Numerical examples are provided to illustrate the multirate approach, its conservation properties, and computational savings.

6.2 Background

As discussed in Chapter 2, Model Predictive Control (MPC) is an optimisation-based control strategy for systems with state and input constraints, and model and measurement uncertainty. A key requirement for robust stability is the existence of a feasible trajectory each time the receding horizon optimal control problem (RHOCP) is solved [2]. However, for multirate systems, which exhibit dynamics and potentially controls on different time scales, a small discrete step is needed to allow accurate resolution of the dynamics and account for fast-changing controls. Small discrete steps, however, increase the computational burden of the RHOCP solved online and reduce the available time for its solution.

In this context, specialised MPC approaches for multirate systems have also been developed in the past. Many of these schemes rely on decoupling the overall dynamics into slow and fast subsystems and using a composite or hierarchical structure for their control [148–153]. For linear systems with both separable and non-separable dynamics, or systems with multiple agents or interconnected subsystems, a two-layered approach is considered by [154–157]. The commonality of these schemes is the use of higher-level, slower-rate long-term planning (often with reduced state models) and a lower-level local regulation on different time rates (with full model consideration). Another two-layered approach has been devised by [158], in which fast dynamics considered in the lower layer provide control inputs to the upper layer of slow subsystems. The works [159, 160] also use a two-layered approach and refer to their methods as multi-rate control. In these two works, however, the focus

is not on systems with multirate dynamics but on the provision of multirate control to achieve computational efficiency for real-time implementation while providing safety guarantees.

In all the aforementioned multirate MPC formulations, it is assumed that measurements of the state/output can be obtained exactly at the selected sampling instances for both the fast and the slow subsystems. Other works, such as [161], focus on developing an estimation of slow sampled variables at intermediate time nodes on which their measurements are not available, but a control action is required. Related work extending to multirate sampled linear systems in the context of model predictive control was carried out by [162] and [163]. Interesting work, again for linear systems, is presented by [164] and combines MPC with an optimal multirate filtering method used to reconstruct the slowly sampled variables. [165], on the other hand, focuses on identifying from irregularly sampled and corrupted multirate data a nonlinear fast rate model and a nonlinear multirate time-varying state observer for both current estimates and inter-sample predictions to develop an inferential multirate NMPC formulation. A hierarchical approach for systems with partially observable environments is provided by [166]. Other related works include application specific multirate methods such as [167–171] and multirate MPC schemes for distributed systems [172]. An extensive literature is also present based around the theory of wavelet transforms [173–176].

Tangentially related to the idea and method presented in this chapter is the work by Terezi et al. [177], which again does not focus on multirate systems but solves the RHOCP at a coarser time grid while calculating and applying the control on a finer time grid to provide more robust stability and feasibility guarantees with reduced conservativeness for systems affected by disturbances. Direct competitors to the approach proposed in this chapter are nonuniform grid approaches and move-blocking schemes. With nonuniform grid schemes, the dynamics are discretised on different time grids for different parts of the horizon, reducing the degrees of freedom in the optimal control problem and thus allowing for computational savings.

However, these schemes often lead to difficulty in quantifying the solution's accuracy. Move-blocking schemes, on the other hand, attempt to reduce the size of the optimal control problem by setting the value of the control or its derivative constant over several discrete time steps rather than computing it at each time node. These schemes can often lead to recursive feasibility and stability issues. [6–8, 178] provide a short overview of the relative merits of these two groups of schemes and present ideas of how their disadvantages can be overcome.

To address the issues of previous approaches and provide an alternative solution, we aim to design a scheme which accounts for both the slow and fast dynamics without estimation or averaging techniques and provides uniform receding horizon control of both the slow and fast dynamics with recursive feasibility and stability guarantees and well-understood solution accuracy. To achieve this, we propose a new multirate receding horizon strategy based on the singlerate and multirate variational optimal control discussed in Chapters 2 and 5. As we have highlighted, both approaches result in structure-preserving solutions for the system and adjoints, and allow for a reduction in the dimensionality of the state as they can represent the system's dynamics fully without the need to integrate the velocity in time. Furthermore, the multirate formulation allows for the resolution of slow- and fast-changing states on separate macro and micro time grids without the need to decouple the equations of motion. This further reduces the optimisation problem's size by reducing the number of optimisation variables and constraints.

Both the singlerate and multirate variational schemes were originally implemented via nonlinear programming (NLP), and as such, singlerate DMOC has previously been used in MPC. A naive multirate extension would solve the RHOCP using multirate DMOC at each micro time step. However, depending on the RHOCP size, the optimisation problem might not be solvable within this step, despite the savings multirate DMOC provides. Instead, we propose a multirate receding horizon strategy in which the RHOCP is formulated and solved only at the macro time

nodes. This allows larger prediction time steps than singlerate methods, providing computational savings while retaining high-fidelity resolutions of the fast dynamics.

Despite these advantages, the resulting problem remains nonconvex for nonconvex models. Thus, there is no guarantee for its successful solution within the available time, causing issues with the feasibility and stability of the MPC scheme. For this reason, we choose to use the convex approximation techniques discussed in Section 2.4.2 and incorporate multirate DMOC within the successive linearisation NMPC scheme of [9]. This provides stability and recursive feasibility guarantees by bounding the effect of linearisation errors using robust tubes. The resulting RHOCP is solved as a sequence of convex programs, providing significant computational savings and guarantees of required runtime. Moreover, if needed, the iteration of convex programs can be terminated before it converges to a single trajectory without loss of feasibility or stability guarantees.

To retain the structure-preserving properties of the variational system model, we explore linearisation using quadratic and linear approximations of the Lagrangian and generalised forces, respectively. We show that this approach is equivalent to Jacobian linearisation of the discrete variational model for particular choices of approximation points and derive corresponding error bounds. To our knowledge, this approach has not been used with variational models before.

6.3 System representation

To design this novel receding horizon scheme, we consider the optimal control of a nonlinear system with a discrete-time model representation of the form:

$$g(x_{k+1}, x_k, u_k) = 0 \tag{6.1}$$

where $x \in \mathbb{R}^{n^x}$ and $u \in \mathbb{R}^{n^u}$ denote the state and control input, $(x_k, u_k) = (0, 0)$ is an equilibrium point and we assume g is differentiable. The proposed NMPC approach relies on repeatedly linearising this model. Thus we consider its linear

model approximation around a seed trajectory $(x^0_{k+1}x^0_k, u^0_k)$ written in the form

$$0 = g(x_{k+1}, x_k, u_k) = M_k x^\delta_{k+1} + D_k x^\delta_k + J_k u^\delta_k + e(x_{k+1}, x_k, u_k) \tag{6.2}$$

where $x^\delta_k = x_k - x^0_k$, $u^\delta = u_k - u^0_k$, $g(x^0_{k+1}, x^0_k, u^0_k) = 0$. Here $M_k, D_k \in \mathbb{R}^{n^x \times n^x}$, $J_k \in \mathbb{R}^{n^x \times n^u}$ define the linearisation about x^0_{k+1}, x^0_k, u^0_k and $e(x_{k+1}, x_k, u_k)$ is the approximation error.

6.3.1 Singlerate variational linearisation and error bounds

To formulate the discrete model of the system (6.1), we first consider a singlerate variational approach. This would be achieved by providing an expression for the Lagrangian and external forces on the system, discretising these expressions as discussed in Section 2.3.3 and plugging them in the final model - (2.18) for LF or (2.19) for HF. For now we will focus on the HF defining $x_k = [q_k^\intercal, p_k^\intercal]^\intercal$ and $n^x = 2n^q$ to rewrite the equations in the state space form (6.1). A linear system approximation of the resulting model (6.2) can be derived using Jacobian linearisation of (6.1). Alternatively, we show in this section that a variational discrete approximation of the system can be obtained alternatively using (2.19) with a quadratic approximation of the Lagrangian $\mathfrak{L}(q, \dot{q})$ and a linear approximation of the generalised forces $f(q, \dot{q}, u)$ of the form

$$\begin{aligned}\tilde{\mathfrak{L}}(q, \dot{q}, q^0, \dot{q}^0) \approx & \mathfrak{L}(q^0, \dot{q}^0) + \nabla_q \mathfrak{L}|_{(q^0, \dot{q}^0)} \delta q + \nabla_{\dot{q}} \mathfrak{L}|_{(q^0, \dot{q}^0)} \delta \dot{q} \\ & + \tfrac{1}{2} \delta q^\top \nabla^2_q \mathfrak{L}|_{(q^0, \dot{q}^0)} \delta q + \tfrac{1}{2} \delta \dot{q}^\top \nabla^2_{\dot{q}} \mathfrak{L}|_{(q^0, \dot{q}^0)} \delta \dot{q}, \end{aligned} \tag{6.3}$$

$$\tilde{f}(q, \dot{q}, u, a) \approx f(a) + \nabla_q f|_a \delta q + \nabla_{\dot{q}} f|_a \delta \dot{q} + \nabla_u f|_a \delta u. \tag{6.4}$$

Here $a = (q^0, \dot{q}^0, u^0)$ is the approximation point, $\delta q = q - q^0$, $\delta \dot{q} = \dot{q} - \dot{q}^0$, $\delta u = u - u^0$. To simplify presentation we assume that $\mathfrak{L}$ and f are separable: $\mathfrak{L}(\dot{q}, q) = V(\dot{q}) + W(q)$, $f(q, \dot{q}, u) = z(q) + y(\dot{q}) + r(u)$.

Lemma 6.3.1. *If $\tilde{\mathfrak{L}}(q, \dot{q}, q^0, \dot{q}^0)$ is quadratic in $q, \dot{q}$ and $\tilde{f}(q, \dot{q}, u, a)$ is linear in $q, \dot{q}, u$, with discrete approximations*

$$\tilde{\mathfrak{L}}_{\mathrm{d},k} = \tilde{\mathfrak{L}}_{\mathrm{d}}(q_k, q_{k+1}, q^0, \dot{q}^0) = \Delta t \, \tilde{\mathfrak{L}}(b q_k + c q_{k+1}, \tfrac{q_{k+1} - q_k}{\Delta t}, q^0, \dot{q}^0) \tag{6.5}$$

$$\tilde{f}_k^{\pm} = \tfrac{\Delta t}{2}\tilde{f}(bq_k + cq_{k+1}, \tfrac{q_{k+1}-q_k}{\Delta t}, u_{k+1/2}, a) \tag{6.6}$$

for some constants b, c then the discrete model (2.19)*, with $\mathfrak{L}_{\mathrm{d}}, f_k^{\pm}$ replaced by $\tilde{\mathfrak{L}}_{\mathrm{d},k}, \tilde{f}_k^{\pm}$, is linear in $q_k, q_{k+1}, p_k, p_{k+1}$ and $u_{k+1/2}$.*

Proof. The discrete approximation $\tilde{f}_k^{\pm}$ inherits the linearity of $\tilde{f}(q, \dot{q}, u, a)$. Similarly, since $\tilde{\mathfrak{L}}(q, \dot{q}, q^0, \dot{q}^0)$ is quadratic, the discrete approximation $\tilde{\mathfrak{L}}_{\mathrm{d},k}$ is also quadratic in q_k and q_{k+1}. Thus the gradients $D_1\tilde{\mathfrak{L}}_{\mathrm{d}}(q_k, q_{k+1}, q^0, \dot{q}^0)$, $D_2\tilde{\mathfrak{L}}_{\mathrm{d}}(q_k, q_{k+1}, q^0, \dot{q}^0)$ are linear in q_k, q_{k+1} leaving all terms in (2.19) linear in $q_k, q_{k+1}, p_k, p_{k+1}, u_{k+1/2}$. □

Other appropriate discrete approximations of $\tilde{\mathfrak{L}}$, $\tilde{f}$ can also be used: for example, different integration schemes based on the choice of b, c or backward or central differences for the approximation of the velocity.

Theorem 6.3.1. *The linear model obtained at point $a = (q^0, \dot{q}^0, u^0)$ using* (6.3)- (6.6) *with $\mathfrak{L}_{\mathrm{d}}, f_k^{\pm}$ replaced by $\tilde{\mathfrak{L}}_{\mathrm{d}}, \tilde{f}_k^{\pm}$ in* (2.19) *is identical to the Jacobian linearisation of* (2.19) *with $\mathfrak{L}_{\mathrm{d},k}(q_k, q_{k+1}) = \Delta t\mathfrak{L}(bq_k + cq_{k+1}, \frac{q_{k+1}-q_k}{\Delta t})$, $f_k^{\pm}(q_k, q_{k+1}, u_{k+1/2}) = \frac{\Delta t}{2}f(bq_k + cq_{k+1}, \frac{q_{k+1}-q_k}{\Delta t}, u_{k+1/2})$ around the point $q_k^0, q_{k+1}^0, u_{k+1/2}^0$ such that $bq_k^0 + cq_{k+1}^0 = q^0$, $\frac{q_{k+1}^0-q_k^0}{\Delta t} = \dot{q}^0$, $u_{k+1/2}^0 = u^0$ for all k.*

Proof. To simplify the notation, we assume $n^q = n^u = 1$. From (6.3), $\mathfrak{L}$ and $\tilde{\mathfrak{L}}$ satisfy

$$\begin{aligned}\mathfrak{L}(q, \dot{q}) &= \tilde{\mathfrak{L}}(q, \dot{q}, q^0, \dot{q}^0) + e_{\tilde{\mathfrak{L}}}(q, \dot{q}, q^0, \dot{q}^0)\\ e_{\tilde{\mathfrak{L}}}(q, \dot{q}, q^0, \dot{q}^0) &= \sum_{n=3}^{\infty}\frac{1}{n!}\Big[\frac{\partial^n\mathfrak{L}}{\partial q^n}|_{(q^0,\dot{q}^0)}(\delta q)^n + \frac{\partial^n\mathfrak{L}}{\partial \dot{q}^n}|_{(q^0,\dot{q}^0)}(\delta \dot{q})^n\Big]\end{aligned}$$

based on Taylor series expansion. Using (6.5) and $\mathfrak{L}_{\mathrm{d},k} = \mathfrak{L}_{\mathrm{d}}(q_k, q_{k+1}) = \Delta t\mathfrak{L}(\bar{q}_k, \bar{\dot{q}}_k)$ with $\bar{q}_k = bq_k + cq_{k+1}$, $\bar{\dot{q}}_k = \frac{q_{k+1}-q_k}{\Delta t}$, the discrete approximation $\mathfrak{L}_{\mathrm{d},k}$ can be defined as

$$\begin{aligned}\mathfrak{L}_{\mathrm{d},k} &= \Delta t\tilde{\mathfrak{L}}(\bar{q}_k, \bar{\dot{q}}_k) + e_{\tilde{\mathfrak{L}}_{\mathrm{d},k}}(\bar{q}_k, \bar{\dot{q}}_k, q^0, \dot{q}^0) = \tilde{\mathfrak{L}}_{\mathrm{d},k} + e_{\tilde{\mathfrak{L}}_{\mathrm{d},k}}\\ e_{\tilde{\mathfrak{L}}_{\mathrm{d},k}} &= e_{\tilde{\mathfrak{L}}_{\mathrm{d},k}}(\bar{q}_k, \bar{\dot{q}}_k, q^0, \dot{q}^0) = \Delta t e_{\tilde{\mathfrak{L}}}(\bar{q}_k, \bar{\dot{q}}_k, q^0, \dot{q}^0)\\ &= \sum_{n=3}^{\infty}\frac{\Delta t}{n!}\Big[\frac{\partial^n\mathfrak{L}}{\partial \bar{q}_k^n}|_{(q^0,\dot{q}^0)}(\delta\bar{q}_k)^n + \frac{\partial^n\mathfrak{L}}{\partial \bar{\dot{q}}_k^n}|_{(q^0,\dot{q}^0)}(\delta\bar{\dot{q}}_k)^n\Big].\end{aligned}$$

Similarly, using $f_k^{\pm} = \frac{\Delta t}{2}f(\bar{q}_k, \bar{\dot{q}}_k, u_{k+1/2}, a)$ and (6.6)

$$f(q, \dot{q}, u) = \tilde{f}(q, \dot{q}, u, a) + e_{\tilde{f}}(q, \dot{q}, u, a)$$

$$
\begin{aligned}
f_k^{\pm} &= \tilde{f}_k^{\pm} + e_{\tilde{f}_k^{\pm}} \\
e_{\tilde{f}_k^{\pm}} &= e_{\tilde{f}_k^{\pm}}(\bar{q}_k, \bar{\dot{q}}_k, u_{k+1/2}, a) = \frac{\Delta t}{2} e_{\tilde{f}}(\bar{q}_k, \bar{\dot{q}}_k, u_{k+1/2}, a) \\
&= \sum_{n=2}^{\infty} \frac{\Delta t}{2} \frac{1}{n!} \Big[\frac{\partial^n f}{\partial \bar{q}_k^n}|_a (\delta \bar{q}_k)^n + \frac{\partial^n f}{\partial \bar{\dot{q}}_k^n}|_a (\delta \bar{\dot{q}}_k)^n + \frac{\partial^n f}{\partial u_{k+1/2}^n}|_a (\delta u_{k+\frac{1}{2}})^n \Big].
\end{aligned}
$$

Based on the definitions, we can rewrite (2.19) as

$$
\begin{aligned}
p_k + D_1(\tilde{\mathfrak{L}}_{\mathrm{d},k} + e_{\tilde{\mathfrak{L}}_{\mathrm{d},k}}) + \tilde{f}_k^- + e_{\tilde{f}_k^-} &= 0, \\
p_{k+1} - D_2(\tilde{\mathfrak{L}}_{\mathrm{d},k} + e_{\tilde{\mathfrak{L}}_{\mathrm{d},k}}) - f_k^+ - e_{\tilde{f}_k^+} &= 0.
\end{aligned}
$$

Thus, when using the approximations (6.3), (6.4) in (2.19), the approximation error $\tilde{e}$ can be expressed as

$$
\tilde{e}(q_k, q_{k+1}, u_{k+1/2}, a) = \begin{bmatrix} D_{q_k} e_{\tilde{\mathfrak{L}}_{\mathrm{d},k}} + e_{\tilde{f}^-} \\ -D_{q_{k+1}} e_{\tilde{\mathfrak{L}}_{\mathrm{d},k}} - e_{\tilde{f}^+} \end{bmatrix}.
$$

On the other hand, the error of the Jacobian linearisation of (2.19) around the point $q_k^0, q_{k+1}^0, u_{k+1/2}^0$, such that $u_{k+1/2}^0 = u^0$, $bq_k^0 + cq_{k+1}^0 = q^0$, and $\frac{q_{k+1}^0 - q_k^0}{\Delta t} = \dot{q}^0$ for all k, takes the form

$$
\sum_{j=2}^{\infty} \frac{\Delta t}{j!} \Big[b \frac{\partial^j}{\partial q^j} \frac{\partial \mathfrak{L}}{\partial q}|_{x^0} (\delta \bar{q}_k)^j - \frac{1}{\Delta t} \frac{\partial^j}{\partial \dot{q}^j} \frac{\partial \mathfrak{L}}{\partial \dot{q}}|_{x^0} (\delta \bar{q}_k)^j \Big] + e_{\tilde{f}^-}
$$

since $D_1 \mathfrak{L}_{\mathrm{d},k} = \Delta t \Big[b \frac{\partial \mathfrak{L}}{\partial q}|_{(q^0, \dot{q}^0)} - \frac{1}{\Delta t} \frac{\partial \mathfrak{L}}{\partial q}|_{(q^0, \dot{q}^0)} \Big]$ and $x^0 = (q^0, \dot{q}^0)$. Comparing this with

$$
D_{q_k} e_{\tilde{\mathfrak{L}}_{\mathrm{d},k}} + e_{\tilde{f}^-} = \sum_{n=3}^{\infty} \frac{\Delta t}{(n-1)!} \Big[b \frac{\partial^n \mathfrak{L}}{\partial \bar{q}_k^n}|_{(q^0, \dot{q}^0)} (\delta \bar{q}_k)^{n-1} - \frac{1}{\Delta t} \frac{\partial^n \mathfrak{L}}{\partial \dot{q}^n}|_{(q^0, \dot{q}^0)} (\delta \bar{\dot{q}})^{n-1} \Big] + e_{\tilde{f}^-} \tag{6.7}
$$

it can be seen that the Jacobian linearisation is equivalent to the approximation (6.7). Similar expansions of (2.19b) and $-D_{q_{k+1}} e_{\tilde{\mathfrak{L}}_{\mathrm{d},k}} - e_{\tilde{f}^+}$ show that they are also equivalent, thus completing the proof of this Theorem. □

The variational linearisation defined by Lemma 6.3.1 allows us to gain significant insights into linearised variational models. The equivalence established by Theorem 6.3.1 ensures that the characteristics we investigate hold true regardless of which of the two linearisation methods is employed.

Theorem 6.3.2. *If* $\mathfrak{L}$ *and* f *are nonlinear, then the use of a quadratic Lagrangian approximation and a linear force approximation of the form* (6.3)- (6.6) *in* (2.19) *results in a structure-preserving linear discrete model if the same quadratic Lagrangian approximation is used at each discrete time step, i.e. if the approximations* (6.3) *and* (6.5) *are computed at the same point a at all times.*

Proof. In the absence of forcing, the scheme (2.19) is symplectic and guarantees the preservation of the discrete momentum map [1]. In the presence of forcing, the preservation of discrete momentum is likewise guaranteed by the Discrete Noether Theorem with Forcing [19]. These properties are maintained by (2.19) for any continuous force and regular Lagrangian expression and their appropriate discrete approximations [1, 19]. Thus, the use of (6.4), (6.6) and the same Lagrangian function (6.3), (6.5) throughout the horizon guarantees the resulting model will inherit these properties (2.19) and its linearity follows from Lemma 6.3.1. □

Remark 6.3.1. *In the numerical experiments presented in Section 6.4 it is also observed that simulations using successive linearisation of the variational model computed around a seed trajectory, with a different Lagrangian approximation at each discrete time step, provide better numerical behaviour than standard non-geometric approaches. In such cases, Theorem 6.3.1 can be rewritten to state the equivalence of the successive linearisation schemes obtained from the variational model using either Jacobian linearisation of* (2.19) *around the points* $(q_k^0, q_{k+1}^0, u_k^0)$ *for* $k = 0, ...N$ *or the method proposed by Theorem 6.3.1 at* $a_k = (\bar{q}_k^0, \bar{\dot{q}}_k^0, u_k^0)$ *for* $k = 0, ...N$ *where* $\{q_k^0\}_{k=0}^N$, $\{u_k^0\}_{k=0}^{N-1}$ *denotes the chosen discrete seed trajectory and* $\bar{q}_k^0 = bq_k^0 + cq_{k+1}^0$, $\bar{\dot{q}}_k^0 = \frac{q_{k+1}^0 - q_k^0}{\Delta t}$.

Proposition 6.3.1. *Lemma 6.3.1 and Theorems 6.3.1 and 6.3.2 hold for non-separable expressions for* $\mathfrak{L}$ *and* f*. This results in mixed derivative terms in the approximations* (6.3), (6.4)*, and the proof of Theorem 6.3.1 is then analogous to the separable case.*

In summary, regardless of whether the linearisation method of Lemma 6.3.1 or Jacobian linearisation at the specifically chosen linearisation points is used, the variational model (2.19) retains its structure-preserving properties in its linearised form. Moreover, from the equivalence of the two linearisation approaches, the error e in the Jacobian linearisation of (2.19) can be related directly to the error in the approximation of the Lagrangian $e_{\tilde{\mathcal{L}}}$ and the generalised force $e_{\tilde{f}}$ as

$$e(q_k, q_{k+1}, u_{k+1/2}, a) = \Delta t \begin{bmatrix} \nabla_{q_k} e_{\tilde{\mathfrak{L}}}(\bar{q}_k, \bar{\dot{q}}_k, a) + \frac{1}{2} e_{\tilde{f}^-}(\bar{\bar{q}}_k, \bar{\dot{q}}_k, u_{k+1/2}, a) \\ \nabla_{q_{k+1}} e_{\tilde{\mathfrak{L}}}(\bar{q}_k, \bar{\dot{q}}_k, a) - \frac{1}{2} e_{\tilde{f}^+}(\bar{\bar{q}}_k, \bar{\dot{q}}_k, u_{k+1/2}, a) \end{bmatrix}.$$

Thus, bounds on $e_{\tilde{\mathfrak{L}}}$ and $e_{\tilde{f}}$ allow the derivation of bounds for e. Hence, the proposed linearisation approach provides a method of deriving the error bounds required for the tube NMPC approach proposed in Section 6.4. The approach is simplified if either the Lagrangian is quadratic and only the force needs to be approximated, or if the force is linear and only the Lagrangian needs to be approximated.

6.3.2 Multirate variational linearisation and error bounds

The variational models considered so far are singlerate, i.e. they discretise the system on a single time grid. To formulate a multirate receding horizon strategy for systems exhibiting dynamics on different time scales, we can use the multirate variational formulation. Based on the developments of Chapter 3, the multirate model (3.30) can be written in the form:

$$p_k^{\mathrm{s}} + D_{q_k^{\mathrm{s}}} L_{\mathrm{d}}^k + F_k^{\mathrm{s},-} = 0 \tag{6.8a}$$

$$p_{k+1}^{\mathrm{s}} - D_{q_{k+1}^{\mathrm{s}}} L_{\mathrm{d}}^k - F_k^{\mathrm{s},+} = 0 \tag{6.8b}$$

$$p_k^{\mathrm{f},0} + D_{q_k^{\mathrm{f},0}} L_{\mathrm{d}}^{k,0} + f_k^{\mathrm{f},0,-} = 0 \tag{6.8c}$$

$$p_{k+1}^{\mathrm{f},0} - D_{q_i^{\mathrm{f},\mathbb{p}}} L_{\mathrm{d}}^{k,\mathbb{p}-1} - f_k^{\mathrm{f},\mathbb{p}-1,+} = 0 \tag{6.8d}$$

$$D_{q_k^{\mathrm{f},m}} L_{\mathrm{d}}^k + f_k^{\mathrm{f},m,-} + f_k^{\mathrm{f},m-1,+} = 0 \tag{6.8e}$$

where (6.8a)-(6.8d) apply for $k = 0, \ldots, N-1$ and (6.8e) for $k = 0, \ldots, N-1$, $m = 1, \ldots, \mathbb{p}$. Here $p_{\mathrm{d}}^{\mathrm{s}} = \{p_k^{\mathrm{s}}\}_{k=0}^N$, $p_{\mathrm{d}}^{\mathrm{f}} = \{\{p_k^{\mathrm{f},m}\}_{m=0}^{\mathbb{p}}\}_{k=0}^{N-1}$ and the slow and fast control paths are approximated using piecewise-constant functions on the macro and micro

time grids respectively as $\{u^{\mathrm{s}}_{k+1/2}\}_{k=0}^{N-1}$, $u^{\mathrm{s}}_{k+1/2} \approx u^{\mathrm{s}}(t_{k+1/2})$ and $\{\{u_k^{\mathrm{f},m+1/2}\}_{m=0}^{\mathbb{p}-1}\}_{k=0}^{N-1}$, $u_k^{\mathrm{f},m+1/2} \approx u^{\mathrm{f}}(t_k^{m+1/2})$.

Equations (6.8) can be expressed in the form of (6.1) with

$$x_k = \begin{bmatrix} q^{\mathrm{s}}_k \\ q^{\mathrm{f},0}_k \\ p^{\mathrm{s}}_k \\ p^{\mathrm{f},0}_k \end{bmatrix}, \quad u_k = \begin{bmatrix} u^{\mathrm{s}}_{k+1/2} \\ u^{\mathrm{f}}_k \end{bmatrix}, \tag{6.9}$$

$n^x = 2n^{\mathrm{s}} + 2n^{\mathrm{f}}$, $n^u = 2n^{u,\mathrm{s}} + 2n^{u,\mathrm{f}}$ for $u^{\mathrm{s}} \in \mathbb{R}^{n^{u,\mathrm{s}}}$, $u^{\mathrm{f}} \in \mathbb{R}^{n^{u,\mathrm{f}}}$ and $u^{\mathrm{f}}_k = \{u_k^{\mathrm{f},m+1/2}\}_{m=0}^{\mathbb{p}-1}$. This model formulation is derived by using (6.8e) to determine an expression for q^{f}_k, and then eliminating this variable from (6.8a)-(6.8d). Thus, the state vector retains the values of the slow and fast variables only on the macro time grid. If the fast configuration variables q^{f}_k need to be evaluated on the micro time grid, these can be obtained using (6.8e) or its equivalent formulation, for $k = 0, \ldots, N-1$, $m = 1, \ldots, \mathbb{p}-1$,

$$\begin{aligned} p_k^{\mathrm{f},m} + D_{q_k^{\mathrm{f},m}} L_{\mathrm{d}}^{k,m} + f_k^{\mathrm{f},m,-} = 0, \\ p_k^{\mathrm{f},m+1} - D_{q_k^{f,m+1}} L_{\mathrm{d}}^{k,m} - f_k^{f,m,+} = 0, \end{aligned} \tag{6.10}$$

resulting in the Hamiltonian formulation of the model.

Analogously to the singlerate case, for the multirate approach, the linearisation of the model can again be achieved using two different techniques and bounds on the error of the approximation of (6.8)-(6.10) can be obtained based on bounds on the approximation of $\mathfrak{L}$ and f made at each macro time step. Linearisation of equation (6.8e) or its equivalent (6.10) provides expressions for q^{f}_k and p^{f}_k that are linear in x_k and u_k. Thus, although the proposed state (6.9) does not contain discrete instances of the configuration and momenta at all micro time nodes, penalties on these variables can be included via a quadratic cost function. Similarly, the linear expressions for q^{f}_k and p^{f}_k allow linear constraints to be imposed on the configuration and momentum variables at all micro and macro time steps using sets of linear constraints.

6.4 Receding horizon control strategy

Having outlined the formulation of the multirate linear system model and its error bounds, we now continue with the formulation of the control problem and the proposed multirate NMPC law. We consider optimal regulation of the system (6.1) subject to a quadratic cost and linear constraints of the form

$$\sum_{k=0}^{\infty} \left(\|x_k\|_Q^2 + \|u_k\|_R^2 \right) \tag{6.11}$$

$$Fx_k + Gu_k \leq h, \quad \forall k \geq 0 \tag{6.12}$$

where $\|x\|_Q^2 = x^\top Q x$, $F \in \mathbb{R}^{n^c \times n^x}$ and $G \in \mathbb{R}^{n^c \times n^u}$. A measurement of the state x_k is assumed to be available at each discrete time step k, $R \succ 0$ is a positive definite matrix and $Q \succeq 0$. The NMPC strategy is based on [9], which linearises the system model about predicted trajectories and uses tubes to bound the effects of approximation errors.

We consider two predicted state and input trajectories of the system (6.1): $(\mathbf{x}_i^0, \mathbf{u}_i^0) = \{x_{k|i}^0, u_{k|i}^0\}_{k=0}^N$ (the 'seed' trajectory), and $(\mathbf{x}_i, \mathbf{u}_i) = \{x_{k|i}, u_{k|i}\}_{k\geq 0}$, with $x_{0|i}^0 = x_{0|i} = x_k$. Here $(\cdot)_{k|i}$ indicates the prediction at time i of the value of $(\cdot)$ at time $k+i$ and N is the prediction horizon. The seed trajectory $(\mathbf{x}_i^0, \mathbf{u}_i^0)$ is exactly known but $(\mathbf{x}_i, \mathbf{u}_i)$ lies in a sequence of sets (i.e. a tube) determined by the linearisation of (6.1) around $(\mathbf{x}_i^0, \mathbf{u}_i^0)$ and its associated linearisation error bounds.

Assumption 6.4.1. *We assume g is differentiable and the seed trajectory $(\mathbf{x}_i^0, \mathbf{u}_i^0)$ obeys the constraints* (6.12).

Let the difference between these two trajectories be

$$x_{k|i}^\delta = x_{k|i} - x_{k|i}^0, \quad u_{k|i}^\delta = u_{k|i} - u_{k|i}^0, \tag{6.13}$$

then, from (6.2), the linearisation of (6.1) around $(\mathbf{x}_k^0, \mathbf{u}_k^0)$ gives

$$M_{k|i} x_{k+1|i}^\delta + D_{k|i} x_{k|i}^\delta + J_{k|i} u_{k|i}^\delta + e(x_{k+1|i}, x_{k|i}, u_{k|i}) = 0$$

which (assuming that $M_{k|i}$ is invertible) can be expressed as

$$x_{k+1|i}^\delta = A_{k|i} x_{k|i}^\delta + B_{k|i} u_{k|i}^\delta + w_{k|i}, \quad x_{0|i}^\delta = 0 \tag{6.14}$$

where $M_{k|i}A_{k|i} = -D_{k|i}$, $M_{k|i}B_{k|i} = -J_{k|i}$ and $w_{k|i}$ accounts for linearisation error. We parametrise u^δ in terms of a feedback law and a feedforward control sequence $\{\nu_{k|i}\}_{k=0}^{N-1}$, where each $\nu_{k|i}$ is an optimisation variable, as

$$\left.\begin{aligned} u^\delta_{k|i} &= K_{k|i}x^\delta_{k|i} + \nu_{k|i} \\ x^\delta_{k+1|i} &= \Phi_{k|i}x^\delta_{k|i} + B_{k|i}\nu_{k|i} + w_{k|i} \end{aligned}\right\} \quad k = 0, \dots, N-1 \tag{6.15}$$

Here $\Phi_{k|i} = A_{k|i} + B_{k|i}K_{k|i}$, and $K_{k|i}$ is chosen to stabilise the time-varying linear system (6.14) in order to improve the feasibility and numerical conditioning of the NMPC scheme (see e.g. [83]).

For prediction time steps $k \geq N$, a fixed, locally stabilising feedback law is assumed for the linearisation of (6.1) around the target point $(x^0, u^0) = (0, 0)$:

$$\left.\begin{aligned} u_{k|i} &= \hat{K}x_{k|i} \\ x_{k+1|i} &= \hat{\Phi}x_{k|i} + \hat{w}_{k|i} \end{aligned}\right\} \quad k \geq N \tag{6.16}$$

where $\hat{\Phi} = \hat{A} + \hat{B}\hat{K}$ and $\hat{w}_{k|i}$ represents linearisation error.

Based on the assumption that g is differentiable (Assumption 6.4.1), [9] describes convex polytopic sets bounding $\{w_{k|i}\}_{k=0}^{N-1}$ and $\{\hat{w}_{k|i}\}_{i\geq N}$ of the form

$$w_{k|i} \in \mathrm{Co}\Big(\{C^j_{k|i}x^\delta_{k|i} + D^j_{k|i}u^\delta_{k|i}\}_{j=1}^{n^j}\Big) \tag{6.17}$$

$$\hat{w}_{k|i} \in \mathrm{Co}\Big(\{\hat{C}^j x_{k|i} + \hat{D}^j u_{k|i}\}_{j=1}^{n^j}\Big) \tag{6.18}$$

where the matrices $\{\hat{C}^j, \hat{D}^j\}_{j=1}^{n^j}$ are fixed and the matrices $\{\{C^j_{k|i}, D^j_{k|i}\}_{j=1}^{n^j}\}_{k=0}^{N-1}$ depend on $(\mathbf{x}^0_i, \mathbf{u}^0_i)$. For convenience, we decompose x^δ into nominal and disturbed components,

$$x^\delta_{k|i} = z_{k|i} + \varepsilon_{k|i} \quad \begin{cases} z_{k+1|i} = \Phi_{k|i}z_{k|i} + B_{k|i}\nu_{k|i}, & z_{0|i} = 0 \\ \varepsilon_{k+1|i} = \Phi_{k|i}\varepsilon_{k|i} + w_{k|i}, & \varepsilon_{0|i} = 0 \end{cases}$$

Then the linearisation error bounds (6.17), (6.18) allow a tube to be constructed containing the uncertain sequence $\{\varepsilon_{k|i}\}_{k=0}^{N-1}$. The tube cross-sections are chosen to be ellipsoidal:

$$\varepsilon_{k|i} \in \mathcal{E}(V_{k|i}, \beta^2_{k|i}), \qquad k = 1, \dots, N \tag{6.19a}$$

$$x_{k|i} \in \mathcal{E}(\hat{V}, 1), \qquad k \geq N, \tag{6.19b}$$

where $\mathcal{E}(X, \eta^2) = \{y : y^\top X y \leq \eta^2\}$ for $X \succ 0$, is an ellipsoid, $\{V_{k|i}\}_{k=0}^{N-1}$ and $\{\beta_{k|i}\}_{k=0}^{N-1}$ are optimisation variables, and $\hat{V}$ is chosen so that $\mathcal{E}(\hat{V}, 1)$ is positively invariant under (6.16).

The preceding representation of predicted state and input trajectories enables a dual mode MPC strategy [2] to determine optimal perturbations $(\mathbf{x}_i^\delta, \mathbf{u}_i^\delta) = \{x_{k|i}^\delta, u_{k|i}^\delta\}_{k\geq 0}$ on a feasible seed trajectory $(\mathbf{x}_i^0, \mathbf{u}_i^0)$, then update the seed trajectory via $(\mathbf{x}_i^0, \mathbf{u}_i^0) \leftarrow (\mathbf{x}_i^0, \mathbf{u}_i^0) + (\mathbf{x}_i^\delta, \mathbf{u}_i^\delta)$ and repeat this process iteratively until convergence as outlined in [9]. To define a computationally tractable RHOCP, ensure convergence of the iteration, and closed loop stability, a min-max problem is solved at each iteration:

$$\min_{\substack{\nu_{k|i}, \beta_{k|i} \\ k=0,\ldots,N-1}} \max_{\substack{x_{N|i} \in \mathcal{E}(\hat{V},1) \\ \varepsilon_{k|i} \in \mathcal{E}(V_{k|i}, \beta_{k|i}^2) \\ k=0,\ldots,N-1}} \|x_{N|i}\|_P^2 + \sum_{k=0}^{N-1} (\|x_{k|i}\|_Q^2 + \|u_{k|i}\|_R^2) \tag{6.20}$$

subject to (6.13), (6.15), (6.18), additional constraints ensuring (6.12) (see [9]) and the recursive membership condition $\varepsilon_{k|i} \in \mathcal{E}(V_{k|i}, \beta_{k|i}^2)$ for $k = 1, \ldots, N$. This problem can be formulated as a (convex) second-order cone program (SOCP) as described in [9]. In this formulation, the maximization is encoded by recognizing that the maximization of a quadratic function over a quadratic set can be rewritten as an induced matrix norm, which is subsequently expressed in an epigraph form.

A semidefinite program (SDP) can be formulated and solved offline to obtain the terminal feedback gain $\hat{K}$, and corresponding $\hat{V}$ such that the volume of $\mathcal{E}(\hat{V}, 1)$ is maximised subject to a bound on of the form $\max_{x \in \mathcal{E}(\hat{V},1)} \|x\|_P^2 \leq \rho$ [2]. Similarly, the terminal weight P can be computed offline by minimising $\mathrm{tr}(P)$ subject to

$$P - (\hat{\Phi} + \hat{C}^j + \hat{D}^j \hat{K})^\top P (\hat{\Phi} + \hat{C}^j + \hat{D}^j \hat{K}) \succeq Q + \hat{K}^\top R \hat{K} \quad \text{for } j = 1, \ldots, n^j$$

requiring the solution of a SDP. The sequences $\{K_{k|i}\}_{k=0}^{N-1}$, $\{V_{k|i}\}_{k=0}^{N-1}$ can be computed online by solving a SDP for each $k = N-1, \ldots, 0$ (or set equal to $\hat{K}$ and $\hat{V}$ to reduce the computation burden).

Detailed analysis of the scheme and an algorithm for its implementation can be found in [9]. In this chapter, we focus on the choice and accuracy of the model (6.14) and propose the use of a variational integrator. As we will demonstrate in the NMPC context, this representation allows for more accurate long-term simulations, presenting new possibilities for error-bound computation and, most importantly, allowing for a multirate formulation, which reduces the computational cost of the overall MPC approach.

6.5 Multirate receding horizon control

Using the multirate model presented in Chapter 3, we propose a novel receding horizon strategy executed on the macro time grid. Namely, linearisation of the model and calculation of finite horizon prediction is performed only at the macro time steps with the RHOCP formulated based on Multirate DMOC using a linearised variational model. This approach allows for an increase in the prediction horizon time step by a factor $\mathbb{p}$ for negligible sacrifices in accuracy in the resolution of the fast dynamics, while allowing for fast control changes [10]. Furthermore, for a given horizon length N in the RHOCP, the number of degrees of freedom in control variables reduces from $n^{u,\mathrm{f}} + n^{u,\mathrm{f}}$ to $n^{u,\mathrm{f}}/\mathbb{p} + n^{u,\mathrm{f}}$. Similar reductions are seen in the number of state constraints and the sparse structure of their Jacobian is maintained. Overall, this provides significant computational savings compared to a singlerate approach, as demonstrated in Section 6.6. Additional advantages of the variational structure-preserving representation are the improved qualitative system representation and the option to develop linearisation error bounds on the equations of motion using quadratic and linear approximations of the Lagrangian and generalised forces, respectively.

Remark 6.5.1. *The choice of multirate state space representation in* (6.1) *is not unique. For the specific choice* (6.9)*, the error in the approximation of* (6.8a)-(6.8d) *depends on* $\{\delta q_k^{\mathrm{f},m}\}_{m=1}^{\mathbb{p}-1}$*, which are not included in the state perturbation vector* x_k^δ*. Thus, the bounds for this error cannot straightforwardly be expressed in the*

form of (6.17) *or* (6.18) *but rather in the form* $w_{k|i} \in \mathrm{Co}(\{W^j_{k|i}x^\delta_{k|i} + O^j_{k|i}u^\delta_{k|i} + \sum_{m=1}^{\mathbb{p}-1} X^{j,m}_{k|i}\delta q^{\mathrm{f},m}_{k|i}\}_{j=1}^{n^j})$. *However, a bound on* $\delta q^{\mathrm{f},m}_{k|i}$ *can be obtained in the form* $\delta q^{\mathrm{f},m}_{k|i} \in \mathrm{Co}(\{Y^j_{k|i}x^\delta_{k|i} + Z^j_{k|i}u^\delta_{k|i}\}_{j=1}^{n^j})$ *using* (6.8e). *Combinations of each vertex of this set with each vertex of the set* $\{W^j_{k|i}\delta x^M_{k|i} + O^j_{k|i}\delta u^M_{k|i}\}_{j=1}^{n^j}$ *therefore provide a new bounding set definition for* w *and* $\hat{w}$ *of the desired form* (6.17) *or* (6.18)*, but with the number of vertices increased from* n^j *to* $(n^j)^2$. *On the other hand, including* q^{f}_{i-1} *in the definition of the model state increases the state dimension* n^x *from* $2(n^{q,\mathrm{s}} + n^{q,\mathrm{f}})$ *to* $2n^{q,\mathrm{s}} + (\mathbb{p}+1)n^{q,\mathrm{f}}$*, leading again to an increased number of constraints in both offline computations and the online RHOCP. Thus, the preferred definition of the discrete state variable* $x_{k|i}$ *is strongly problem-dependent.*

6.6 Examples

The results in this section are obtained using Python, with the scipy.optimize trust-constr method solver for the NLP formulations and the MOSEK solver in combination with the CVXPY library for the solution of the SDP and SOCP problems [147, 179, 180]. In all NLP, SDP, and SOCP problems, the equations of motion were implemented using automatic differentiation with JAX [115] rather than analytically derived and implemented. The focus during implementation is the ability of the code to be applied to multiple examples rather than to obtain the lowest possible runtime. Thus, these runtime tests are used only as comparison between the methods implemented with the current code version.

Example 5: We first consider a planar model of a quadcopter in order to validate the resulting optimal control sequences to those obtained in [9]. For this system

$$\begin{aligned} \mathfrak{L}(q,\dot{q}) &= \tfrac{1}{2}\dot{q}^\top\dot{q} - [0,g,0]^\top \cdot q, \\ f_{\mathrm{LC}} &= [(u_1+g)\sin\alpha, (u_1+g)\cos\alpha, u_2]^\top \end{aligned} \tag{6.21}$$

where $q = [y,z,\alpha]^\top$ and $u = [u_1,u_2]^\top$. Here y,z,α represent the horizontal, vertical and angular displacement, u_1 and u_2 are controls proportional to the net thrust and moment acting on the quadcopter and g is the gravitational acceleration. To this problem, we apply singlerate variational modelling and implement the proposed

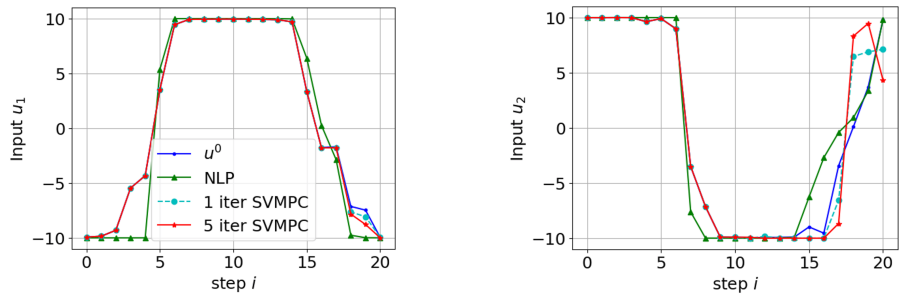


Figure 6.1: Example 5: Example control path solution with $\Delta t = 0.05$s, $N = 21$

MPC scheme with a singlerate variational integrator (SVMPC) using either constant ($V_{k|i} = \hat{V}$) or varying ($V_{k|i}$ computed online) parameters defining MPC tube cross-sections. We refer to these variants as Algorithms 1 and 2, respectively. Figure 6.1 presents the predicted control paths for $\Delta t = 0.05$s, $N = 21$ and initial condition $x_0 = (0, -1, -1, 0, 0, 0)$. The cost weights are $Q = \text{diag}\{0.1, 0.1, 10, 1, 1, 1\}$ and $R = \text{diag}\{10^{-4}, 10^{-3}\}$, and input constraints: $|u_{1,i}| \leq 10$, $|u_{2,i}| \leq 10$. The bounds in (6.18) are computed using (6.4) and $|u_{1,k|i}| \leq 2.5$, $|u_{2,k|i}| \leq 5$, $|\alpha_{k|i}| \leq 0.3$, $|\dot{\alpha}_{k|i}| \leq 1$, the bounds (6.17) are computed online with $|u^{\delta}_{1,k|i}|$,$|u^{\delta}_{2,k|i}|$, $|\alpha^{\delta}_{k|i}|$ and $|\dot{\alpha}^{\delta}_{k|i}|$ restricted to 15% of these bounds. The terminal cost is restricted with $\rho = 10$ as in the setting of the original investigation in [9].

This example also demonstrates the structure-preserving properties of the variational scheme. As the Lagrangian does not explicitly depend on time, y or α, the total energy and the momentum associated with y (p^1) and α (p^3) should remain constant in the absence of external forces according to Noether's theorem (Theorem 2.3.1). In the discrete setting and in the presence of control forces, the momentum map evolves according to the Discrete Noether's theorem with forcing [1, 19]. For Example 5, this result is equivalent to the following discrete conservation laws:

$$\Psi_{y,k|i} = [p_{k|i}]_1 - [p_{0|i}]_1 - \Delta t \sum_{n=0}^{k-1} [f_{n|i}]_1 = 0$$
$$\Psi_{\alpha,k|i} = [p_{k|i}]_3 - [p_{0|i}]_3 - \Delta t \sum_{n=0}^{k-1} [f_{n|i}]_3 = 0$$

Figure 6.2 illustrates these are preserved for the proposed variational approach.

Example 2:

To investigate the advantages of the multirate approach, we look again at the

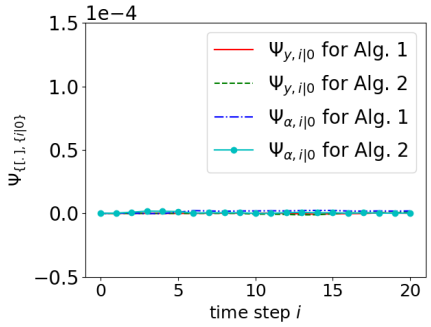


Figure 6.2: Example 5: Demonstration of the conservation properties of the proposed approach

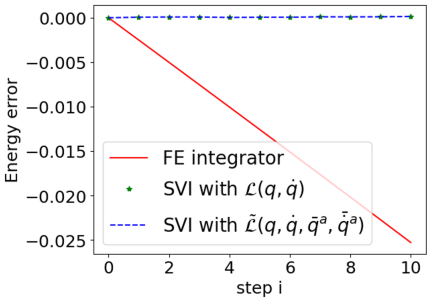


Figure 6.3: Example 2: Demonstration of the qualitative properties of the linearised variational scheme

nonlinear Fermi-Pasta-Ulam-Tsingou problem from Section 4.3 with two unit masses ($n = 2$) and Lagrangian of the form

$$\mathcal{L}(q^{\mathrm{s}}, q^{\mathrm{f}}, \dot{q}^{\mathrm{s}}, \dot{q}^{\mathrm{f}}) = \frac{(\dot{q}^{\mathrm{s}})^2+(\dot{q}^{\mathrm{f}})^2-(\eta q^{\mathrm{f}})^2}{2} - \frac{(q^{\mathrm{s}}+q^{\mathrm{f}})^4+(q^{\mathrm{s}}-q^{\mathrm{f}})^4}{4}$$

with $f^{\mathrm{s}} = u^{\mathrm{s}}$, $f^{\mathrm{f}} = u^{\mathrm{f}}$, where u^{s} and u^{f} represent the resolution of the control applied to the ith mass along q^{s} and q^{f} respectively. All tests are performed with $\eta = 50$ and initial conditions $q_0^{\mathrm{s}} = \dot{q}_0^{\mathrm{s}} = \dot{q}_0^{\mathrm{f}} = 1$ and $q_0^{\mathrm{f}} = \frac{1}{\eta}$.

To investigate the effect of the proposed linearisation scheme on the qualitative properties of the model, simulations were performed in the absence of controls using a Forward Euler (FE) scheme and the singlerate variational scheme (SVI) (2.19) using $\mathfrak{L}$ and its approximation $\tilde{\mathfrak{L}}$ around a seed trajectory as discussed in Remark 6.3.1. Results for $T = 0.01$ sand $\Delta t = 10^{-3}$ are shown in Figure 6.3. As in Example 5, the total energy of the system is expected to remain constant in the absence of external forces. The proposed linearisation scheme demonstrates more accurate conservation properties than the FE integrator despite the use of a different Lagrangian approximation at each discrete time step k (Figure 6.3).

We next consider the proposed multirate variational strategy in an optimal regulation problem starting from the same initial condition with $Q^M = \Delta T \mathrm{diag}\{1,1,1,1\}$, $R^M = \mathrm{diag}\{\Delta T, \Delta t, \Delta t, \ldots, \Delta t\}$ and constraints $E[q^{\mathrm{s}}, q^{\mathrm{f}}]^\top \leq [10,10]^\top$, $E[\dot{q}^{\mathrm{s}}, \dot{q}^{\mathrm{f}}]^\top \leq [10,10]^\top$, $E[u^{\mathrm{s}}, u^{\mathrm{f}}]^\top \leq [20,20]^\top$ with $E = [1/\sqrt{2}, -1/\sqrt{2}; 1/\sqrt{2}, 1/\sqrt{2}]$. For this example with $\rho = 1000$, the bounds (6.18) are based on $E[q^{\mathrm{s}}, q^{\mathrm{f}}]^\top \leq [0.8, 0.8]^\top$ and

Table 6.1: Example 2: Online computational runtime in seconds

	Algorithm 1			Algorithm 2	
$\mathbb{p}$	1	3	5	1	3
CPU time per iter at $k=0$	**3.18** ±0.03	**2.57** ±0.48	**1.49** ±0.02	**5.52** ±0.17	**4.46** ±0.01
n_{RHOCP}	30	10	6	30	10
CPU time to reach t_{target}	**96.3** ±0.24	**27.47** ±0.43	**11.14** ±0.89	**173.79** ±1.59	**51.17** ±0.08

(6.17) are computed using 5% of these bounds. The computational advantages of the multirate approach are investigated experimentally in a series of tests with a fixed micro time step, $\Delta t = 0.01$, and with $T = 0.6$ and a progressively increasing the micro-macro proportionality $\mathbb{p}$. Optimal control paths are obtained using the proposed singlerate and multirate NMPC scheme with an approximation of the Lagrangian around a pre-computed seed trajectory for both constant (Algorithm 1) and varying tube cross sections (Algorithm 2), each with *maxiter* = 1. The runtime of the online computation is recorded until discrete time $t_{\text{target}} = 30\Delta t$. The number of RHOCP steps performed is denoted n_{RHOCP}. This test is designed to measure the effect of performing the RHOCP less frequently in the multirate approach compared to the singlerate variational scheme.

The results in Table 6.1 demonstrate that increasing $\mathbb{p}$ reduces the computational load for both approaches. For comparison, the required times for a single NLP solution with $\mathbb{p} = 1, 3, 5$ are $43.57, 31.76, 29.55$. Thus, the proposed singlerate and multirate NMPC schemes outperform the NLP implementation in computation time per discrete time step, with the multirate NMPC approach achieving the greatest savings for both Algorithms. For our implementation of Algorithm 1, the elapsed iteration runtime has a percentage decrease of 53.14% between $\mathbb{p} = 1$ and $\mathbb{p} = 5$ and the time to reach t_{target} has reduced by a factor of 8.6. For Algorithm 2, the SDP to compute $V_{k|i}$, $K_{k|i}$ was not feasible for $\mathbb{p} = 5$ for this example. However, $\mathbb{p} = 3$ provides a percentage decrease in computation runtime of 19.2% per iteration, requiring only a third of the time to reach t_{target} compared to the singlerate case. Of course, as discussed in previous chapters, in general, $\mathbb{p}$ cannot be increased indefinitely as this will reduce the resolution of the slow dynamics and a trade-off, therefore, exists between computational complexity and accuracy [10].

7

A successive convexification approach for robust receding horizon control

Contents

7.1 Introduction 154
7.2 Background 155
7.3 Technique for explicit system models 162
7.3.1 Problem formulation 162
7.3.2 Proposed nominal control law 164
7.3.3 Nominal feasibility and stability guarantees 170
7.3.4 Problem formulation with additive disturbances 173
7.3.5 Proposed robust control law 174
7.3.6 Robust feasibility and stability guarantees 177
7.3.7 Numerical examples 181
7.4 Technique for implicit system models 186
7.4.1 Problem formulation 187
7.4.2 Proposed nominal control law 188
7.4.3 Nominal feasibility and stability guarantees 191
7.4.4 Proposed variational reformulation 194
7.4.5 Numerical examples 198

7.1 Introduction

In this chapter, we explore the challenges of implementing Model Predictive Control (MPC) for real-time systems, without limiting the discussion to multirate systems.

The objective is to introduce a novel method for optimisation-based trajectory design and receding horizon control of nonlinear systems subject to external disturbances or model inaccuracies. The proposed method guarantees non-conservative nominal solutions while significantly reducing computational costs compared to solving the original nonlinear problem, making it advantageous for real-time control.

The approach is applicable to nonlinear systems with convex state and control constraints. It employs a sequential convex approximation and a difference of convex functions representation of the system model to construct tubes that encompass all possible predicted model trajectories, accounting for linearisation errors and disturbances to ensure constraint satisfaction. Initially, we develop the scheme for the nominal case, where external disturbances are absent, and demonstrate that the proposed method is non-conservative, with solutions from successive convex programs converging to a locally optimal solution for the original nonconvex OCP. We then extend the method to handle additive disturbances (robust case) using a novel strategy for linearisation points selection. In both cases, stability and recursive feasibility are guaranteed and tested with computational examples, even when the sequence of convex programs is terminated before convergence.

These methods are first presented for systems with explicit discrete-time models, and then extended in the nominal case to systems with implicit discrete-time models, which may result from implicit continuous-time models or the use of implicit discretisation schemes for explicit continuous-time models. Special attention is given to the integration of variational models within the nominal approach, enhancing the representation of the system qualitatively and achieving significant additional runtime savings, as illustrated by numerical examples.

7.2 Background

Optimisation-based control techniques allow for a task to be completed optimally with respect to a given performance index while respecting both system and environment constraints [2, 181]. As such, they have often been implemented

for online trajectory design or receding horizon control of systems subject to stringent or safety-critical constraints such as, for example, autonomous vehicles [182, 183], spacecraft systems [184, 185], and robotics [186]. In its simplest form, optimisation-based control entails the single solution of an optimal control problem (OCP), resulting in an optimal trajectory and open-loop control sequence for the entire time period of interest. To allow for feedback, a receding horizon strategy (also known as model predictive control or MPC) can be implemented as discussed in Chapters 2 and 6. In this method, at each discrete time step, an OCP is solved, the first control of the resulting optimal control sequence is applied, and the new state of the system is measured. Based on this measurement, a new OCP is solved, and the procedure is repeated [2]. Thus, for open-loop autonomous trajectory generation or receding horizon implementation for real-time systems, it is critical that the OCP can be solved successfully and reliably within the available time. The nonlinear nature of most systems, however, implies that the resulting OCP is a nonlinear program (NLP), and thus has high computation complexity with no guarantees for a successful solution within the available time, for both singlerate and multirate systems.

Various approaches have been developed to address this problem. For example, dynamic programming can determine globally optimal control policies, however it requires heavy computation, which restricts its implementation in real-time applications [2]. Another method, known as sequential quadratic programming (SQP) [187], focuses on iterative approximation approaches that approximate NLPs using sequences of quadratic programming (QP) problems. Despite the existence of efficient methods for solving QPs, these schemes can lead to high computational demand and present difficulties when accounting for approximation errors and determining the appropriate step sizes for each iteration to ensure convergence.

An alternative approach replaces the system model with a sequence of models obtained from linear approximations around trajectories of the controlled system (e.g. [9, 188–190]). The seminal work [188] relaxes the nonlinear model dynamics into

a set of inequalities, which are subsequently linearised to obtain a sequence of convex optimisation problems. Under convexity assumptions on the nonlinear dynamics and the state and input constraints, the solutions of this sequence are shown to converge to a local optimum of the original NLP provided a set of parameters (which are introduced into the objective function to enforce satisfaction of the original model dynamics) are chosen appropriately. However, the required values of cost parameters are not usually known, and the method converges only asymptotically to a feasible solution of the NLP.

More recently, [189] proposed using Jacobian model linearisation to construct a sequence of convex optimisation problems. The authors use trust regions to account for the effects of linearisation errors and are thus able to demonstrate convergence to a locally optimal solution of the NLP. The disadvantages of the approach are that it relies on heuristics for determining whether model approximations are sufficiently accurate, and that the iterates are not guaranteed to be feasible for the NLP, so the iteration cannot be terminated prior to convergence.

In [9], a tube (or sequence of sets) containing all possible trajectories of the nonlinear system is constructed by linearising the model around trajectories and bounding linearisation errors, and all trajectories within the tube are required to respect the system state and control constraints. Using successive linearisation, the NLP is replaced by a sequence of second-order cone programs (SOCPs) [9, 190], each generating a feasible solution for the original NLP. The implementation of the approach is complicated by the need to provide bounds on the linearisation errors, which can be a computationally challenging task that relies on heuristics. Conservative linearisation error bounds can cause slow convergence or infeasibility of the sequence of optimisation problems even if the NLP itself is feasible. Furthermore, the available schemes can introduce suboptimality and do not account for external disturbances. The tube-based approach in [191] can ensure convergence to a locally optimal solution of the NLP. However, it is computationally costly and does not account for external disturbances. In Chapter 6, we discussed multirate techniques

for enabling the implementation of MPC for systems with both slow and fast dynamics. Moreover, we built upon the work of [9] to develop an MPC approach for multirate systems which increases the available time for solving the receding horizon optimal control problem (RHOCP) and reduces its size, allowing for its implementation for systems with fast dynamics while maintaining stability and feasibility guarantees. However, the approach still exhibits the remaining limitations of [9].

Despite the disadvantages of SQP and successive convexification approaches based on linearising nonlinear dynamic models, the efficiency and practicality of convex NLP approximations are well-known in the context of receding horizon control. Therefore, many real-time MPC applications employ convex descriptions of the model dynamics and constraints (for example in aerospace applications [192–194], among many others). Moreover, successive convexification incorporating robust tube MPC methods provides new opportunities for computationally efficient receding horizon control, particularly when the model is affected by unknown disturbances. Approaches such as [195–198], provide a varying level of efficiency, complexity and conservativeness for a wide range of disturbance realisations as discussed in detail in [196]. For instance, [196] uses homothetic tubes and discusses efficiency in terms of the size of the optimisation problem and the offline computations, but retains an nonlinear RHOCP formulation. [199], on the other hand, develops an approach for continuous-time nonlinear systems affected by bounded disturbances with guaranteed feasibility and input-to-state stability that does not require a quadratic cost but again retains the nonlinear RHOCP formulation. In contrast, [195] replaces the dynamics with a robust feed-forward invariant tube for the disturbance-free system and optimises the feedback policy, but restricts the discussion to nonlinear input-affine systems.

The works of [197, 198] provide alternative robust MPC formulations, which employ constraint tightening using Lipschitz constants based on input-to-state stability considerations. These bounds, however, rely on the nominal model and are not

optimised online, which can cause greatly conservative performance. Leveraging these insights, a two-tier approach is proposed by [200] using an ancillary controller, which tracks the solution of a tightened-constrained nominal MPC formulation. The amount of tightening, however, is determined by heuristics, which, together with the rigid shape of the tubes, can be expected to result in conservativeness and suboptimality. More recent work by [201] addresses these issues with another two-tier approach that simultaneously optimises tubes and trajectories online for feedback linearisable or minimum phase systems. In contrast, [202] does not optimise for a nominal trajectory but rather propagates ellipsoidal uncertainty tubes using linear feedback gains as optimisation variables. The optimisation is performed by a mixture of Ricatti recursion and nominal RHOCP solution with only approximate robustness due to unaccounted linearisation errors in the nonlinear constraints. This work, and its successor [203], develop tailored solution methods for the optimisation problem to ensure convergence to a KKT point of the original nonlinear OCP.

To address these limitations, the approach presented in this chapter exploits the convexity properties of systems with continuous dynamics, as well as convex state, control, and disturbance constraints, to develop a robust approach with stability and feasibility guarantees. The effects of model approximations and disturbances are bounded by tubes, which do not rely on heuristics and their cross-sections are optimised online alongside the calculation of a feasible control sequence in a sequence of convex programs. Feasibility and stability guarantees are maintained even if the sequence of convex programs is terminated early. For the disturbance-free case, the resulting tight bounds on linearisation errors can be used to obtain non-conservative solutions. Despite the convex formulation, the resulting min-max approach relies on enumerating polytopic tube vertices, which can be computationally costly for high-order systems; therefore we discuss strategies to ensure linear growth in the number of variables and constraints with the state dimension.

We assume that the system discrete model has a convex difference (DC) form, i.e. it can be represented as the difference of a pair of convex functions. This is

not necessarily restrictive, as any continuous function can be approximated to any desired precision as the difference of two convex functions [204]. Differences of convex functions have been used to develop techniques such as DC programming [204], the convex-concave procedure [205, 206], and novel control invariant set computation methods for nonlinear systems [207], which have proven numerical advantages when applied to nonconvex problems ([208, 209]). Using DC decomposition, we derive a tube-based receding horizon controller with robustness to disturbances and guarantees of recursive feasibility and stability.

To this end, in the first part of this chapter, we present a formulation of the proposed approach for systems with explicit models in the absence of disturbance, similar to [210]. Our contributions include a novel initialisation strategy and a proof that the sequence of convex programs proposed to approximate the NLP converges to one of the NLP local optima, and thus removes the degree of suboptimality that other such approaches introduce. We also present proof that the iteration can be terminated early without loss of feasibility or stability.

In this disturbance-free case, feasibility is guaranteed if at least one system trajectory satisfies the constraints of the problem. However, when unknown disturbances are present, both a nominal trajectory and all its potential alternative realisations must respect the constraints. This presents additional non-trivial difficulties when choosing linearisation points and guaranteeing recursive feasibility. Thus, we extend previous works by proposing a new formulation to address these issues. As in the disturbance-free case, the proposed approach approximates the NLP with a sequence of convex programs, and a tube containing all possible trajectories is optimised online. Based on the implementation of a novel linearisation technique, we prove recursive feasibility and a form of quadratic stability for the resulting closed-loop system.

With both the nominal and robust approach described so far, the existence of an explicit discrete-time system model with certain convexity properties is assumed. When provided with an explicit continuous model, this prevents the use of many

higher-order or structure-preserving model discretisation techniques, limiting the choice to lower accuracy discrete-time model approximation. Such restriction might not be problematic for a receding horizon implementation, which relies on feedback to deal with model inaccuracies, but can be detrimental when used for trajectory generation. The assumption also prevents the approach from being applied to a wide range of systems with implicit continuous models, such as many multibody systems and other constrained systems.

For this purpose, in the second part of this chapter, we provide a reformulation of the proposed approach for implicit convex system models in the absence of disturbances. We present the approach for a receding horizon implementation, which can trivially be simplified for single trajectory design use. We prove the recursive feasibility and stability of the proposed approach and provide a proof that it also converges to a point which is a local optimum of the original NLP. As such, the approach for explicit models can be seen as a specific case of the one proposed here with a simpler formulation.

In addition, we focus on a specific use of the proposed approach for structure-preserving discrete models [26] and, more specifically, for variational models [1]. As discussed in the previous chapters, by preserving certain mathematical structures and conservation laws from the continuous into the discrete domain, such discretisation schemes allow for better qualitative representation of the system and accurate energy and momentum simulation, even for larger discrete time steps [26, 211]. For this reason, they have been used to reduce the computational cost of simulations and optimal control strategies and could be of great benefit for fuel and energy optimisation problems ([10, 13, 212, 213]). In this chapter, we present how such models can readily be used in the proposed optimisation-based scheme and show that their characteristics can be employed to simultaneously reduce the number of constraints and guarantee structure-preserving properties of the resulting solution. The advantages of the proposed approach are then demonstrated for two example

systems, showing convergence of the sequence of convex programs and the effect of the structure-preservation model on the resulting solution.

This chapter is organised as follows:

1. Part I: Focuses on systems with explicit models, developing first an approach in the absence of disturbances and then extending the formulation to handle the effect of additive disturbances. For both the nominal and robust formulation, feasibility and stability properties are proved theoretically and demonstrated through numerical examples.

2. Part II: Discusses the reformulation for implicit models in the absence of disturbances. Feasibility and stability guarantees are proved theoretically and again demonstrated using numerical examples. The approach is then extended for the implementation of variational models.

7.3 Technique for explicit system models

We first focus on developing a technique for explicit discrete-time system models.

7.3.1 Problem formulation

Consider a discrete-time nonlinear system with state $x_i \in \mathbb{R}^{n_x}$ and control input $u_i \in \mathbb{R}^{n_u}$ at the ith time step, where

$$x_{i+1} = f(x_i, u_i), \quad i = 0, 1, \dots \tag{7.1}$$

and f is differentiable for all (x_i, u_i) in the operating region $\mathcal{X} \times \mathcal{U}$. We pose the problem of optimally controlling the system trajectories $\mathbf{x} : \{x_0, x_1, ...\}$, $\mathbf{u} : \{u_0, u_1, ...\}$ to track a given state and input reference trajectory $\mathbf{x^r} : \{x_0^r, x_1^r, ...\}$, $\mathbf{u^r} : \{u_0^r, u_1^r, ...\}$ where $x_{i+1}^r = f(x_i^r, u_i^r)$ for all $i \geq 0$ subject to a quadratic objective

$$\sum_{i=0}^{\infty} \Big(\|x_i - x_i^r\|_Q^2 + \|u_i - u_i^r\|_R^2 \Big) \tag{7.3}$$

and initial constraints $x_0 = x_{\text{init}}$ and inequality constraints of the form

$$x_i \in \mathcal{X} \subset \mathbb{R}^{n_x}, \;\; u_i \in \mathcal{U} \subset \mathbb{R}^{n_u}. \tag{7.5}$$

Here $\mathcal{X}, \mathcal{U}$ are compact convex sets and x_{init} is a known initial condition.

An MPC strategy can be employed to solve this problem. For this purpose, a receding horizon optimal control problem can be formulated as

$$\text{EnMPC:} \quad (\mathbf{u}_i^*, \mathbf{x}_i^*) \coloneqq \underset{\mathbf{u}_i, \mathbf{x}_i}{\operatorname{argmin}} J_{\text{EnMPC}}(\mathbf{u}_i, \mathbf{x}_i) \tag{7.6a}$$

subject to, for $k = 0, \ldots, N-1$:

$$x_{k|i} \in \mathcal{X}, \quad u_{k|i} \in \mathcal{U} \tag{7.6b}$$

$$x_{k+1|i} = f(x_{k|i}, u_{k|i}) \tag{7.6c}$$

$$x_{0|i} = x_i \tag{7.6d}$$

$$x_{N|i} \in \mathcal{X}_N \subseteq \mathcal{X} \tag{7.6e}$$

with $\mathbf{u}_i \coloneqq \{u_{0|i}, \ldots, u_{N-1|i}\}$, $\mathbf{x}_i \coloneqq \{x_{0|i}, \ldots, x_{N|i}\}$ and

$$J_{\text{EnMPC}}(\mathbf{u}_i, \mathbf{x}_i) \coloneqq \|x_{N|i} - x_{N+i}^r\|_{Q_N}^2 + \sum_{k=0}^{N-1} \Big(\|x_{k|i} - x_{k+i}^r\|_Q^2 + \|u_{k|i} - u_{k+i}^r\|_R^2 \Big). \tag{7.6f}$$

Here $x_{k|i}$, $u_{k|i}$ denote the state and control input at time $k+i$ predicted at time i. The matrices Q, R, Q_N and the terminal set $\mathcal{X}_N$ are subject to the following assumptions:

Assumption 7.3.1.

(a) x_i is known at each time i.

(b) $x_i^r \in \mathcal{X}_N \subseteq \mathcal{X}$ and $u_i^r \in \mathcal{U}$, $\forall i \geq N$.

(c) $f(x, \kappa_i(x)) \in \mathcal{X}_N$, $\forall x \in \mathcal{X}_N$, $\forall i \geq N$, where $\kappa_i(x) \coloneqq K(x - x_i^r) + u_i^r$ satisfies $\kappa_i(x) \in \mathcal{U}$, $\forall x \in \mathcal{X}_N$, $\forall i \geq N$.

(d) Q, R, Q_N are positive definite matrices, and (7.1) with $u_i = K(x_i - x_i^r) + u_i^r$ satisfies, $\forall x_i \in \mathcal{X}_N$, $\forall i \geq N$,

$$\|x_i - x_i^r\|_{Q_N}^2 - \|x_{i+1} - x_{i+1}^r\|_{Q_N}^2 \geq \|x_i - x_i^r\|_Q^2 + \|u_i - u_i^r\|_R^2.$$

In receding horizon control, at each discrete time step i, the EnMPC RHOCP is solved to obtain an optimal control sequence $\mathbf{u}_i^* : \{u_{0|i}^*, u_{1|i}^*, \ldots, u_{N-1|i}^*\}$, and the first element of this sequence is used to define a receding control law $u_i = u_{0|i}^*$. At the next time step, a new RHOCP is formulated using the measurement (or

estimate) of x_{i+1} and the process is repeated. To guarantee stability of the control strategy, it is essential that a feasible solution can be obtained within each discrete time step.

In its form in (7.6a)-(7.6f), the EnMPC RHOCP is a nonlinear program, and thus, in general, no guarantees can be given that either the optimal solution or a suboptimal feasible point is determinable within one discrete time step. To address these problems, Section 7.3.2 proposes a successive linearisation approach to reformulate the problem as a sequence of convex programs. Compared to other such approaches, the proposed method bounds linearisation errors as functions of the predicted state tube that is optimised online. This removes the need to compute linearisation error bounds prior to solving the RHOCP and ensures that a fixed point of the successive approximation scheme corresponds to an optimal point of the EnMPC RHOCP. As shown in Section 7.3.3, it also provides guarantees of convergence to a fixed point, recursive feasibility and stability of the resulting MPC law.

7.3.2 Proposed nominal control law

To simplify the explanation, we first strengthen the assumptions on the system model.

Assumption 7.3.2. *The function $f : \mathcal{X} \times \mathcal{U} \to \mathbb{R}^{n_x}$ in (7.1) is differentiable and componentwise convex.*

Although few real systems satisfy this convexity assumption, we later discuss how it can be relaxed to accommodate models with a DC form, enabling the application of the proposed scheme to systems with neither convex nor concave dynamics.

Given state and control sequences $\mathbf{x}_i^0 = \{x_{0|i}^0, \dots, x_{N|i}^0\}$, $\mathbf{u}_i^0 = \{u_{0|i}^0, \dots, u_{N-1|i}^0\}$, which we refer to as a seed trajectory, the model (7.1) can be equivalently expressed as

$$x_{k+1|i} = x_{k+1|i}^0 + A_{k|i} s_{k|i} + B_{k|i} v_{k|i} + e(x_{k|i}, u_{k|i}) \tag{7.7a}$$

$$s_{k|i} = x_{k|i} - x_{k|i}^0, \quad v_{k|i} = u_{k|i} - u_{k|i}^0 \tag{7.7b}$$

$$A_{k|i} = \frac{\partial f}{\partial x_{k|i}}|_{(x_{k|i}^0, u_{k|i}^0)}, B_{k|i} = \frac{\partial f}{\partial u_{k|i}}|_{(x_{k|i}^0, u_{k|i}^0)} \tag{7.7c}$$

and $e_{k|i}$ is the Jacobian linearization error

$$e_{k|i} = f(x_{k|i},u_{k|i}) - f(x^0_{k|i},u^0_{k|i}) - A_{k|i}s_{k|i} - B_{k|i}v_{k|i}. \tag{7.8}$$

Assumption 7.3.3. *The initial seed trajectory* $(\mathbf{x}^0, \mathbf{u}^0)$ *is feasible (but potentially suboptimal) for constraints* (7.6b)-(7.6e).

Anticipating the explicit treatment of disturbances in Section 7.3.4, we assume a feedback control law:

$$u_{k|i} = u^0_{k|i} + v_{k|i} = u^0_{k|i} + Ks_{k|i} + c_{k|i}, \tag{7.9}$$

for a given feedback gain K, and consider the sequence $\mathbf{c}_i \coloneqq \{c_{0|i}, \dots, c_{N-1|i}\}$ as an optimisation variable instead of $\mathbf{u}_i$.

Assumption 7.3.2 requires the components of f to be convex and hence the components of the linearisation error $e_{k|i}$ in (7.8), denoted $e_{k|i,j}(x_{k|i}, u_{k|i})$, $j = 1, \dots, n_x$, are convex functions of $(x_{k|i}, u_{k|i}) \in (\mathcal{X}, \mathcal{U})$. Since $e_{k|i,j}(x_{k|i}, u_{k|i})$ is convex and the linearization point $(x^0_{k|i}, u^0_{k|i})$ lies in $(\mathcal{X}, \mathcal{U})$ we have

$$\min_{(x_{k|i},u_{k|i})\in(\mathcal{X},\mathcal{U})} e_{k|i,j}(x_{k|i}, u_{k|i}) = 0, \tag{7.10}$$

and moreover, a constraint of the form

$$e_{k|i,j}(s_{k|i} + x^0_{k|i}, Ks_{k|i} + c_{k|i} + u^0_{k|i}) \leq r$$

is convex in $s_{k|i}$, $c_{i|k}$ and r. Figure 7.1 visualises the validity of (7.10) for a simple 1-dimensional example.

Let $\mathbf{S}_i = \{S_{0|i}, \dots, S_{N|i}\}$ denote a tube bounding the state perturbations $s_{k|i}$ in (7.7a)-(7.31c), where each set $S_{k|i}$ is a hyperrectangle defined in terms of optimisation variables $\underline{s}_{k|i}$, $\bar{s}_{k|i} \in \mathbb{R}^{n_x}$ as

$$S_{k|i} = \{s : \underline{s}_{k|i} \leq s \leq \bar{s}_{k|i}\}. \tag{7.11}$$

Then, at time i, a convex RHOCP can be formulated as

$$\text{EcMPC: } (\mathbf{c}^*_i, \mathbf{S}^*_i) \coloneqq \underset{\mathbf{c}_i, \mathbf{S}_i}{\operatorname{argmin}} \; J_{\text{EcMPC}}(\mathbf{c}_i, \mathbf{S}_i, \mathbf{x}^0_i, \mathbf{u}^0_i)$$

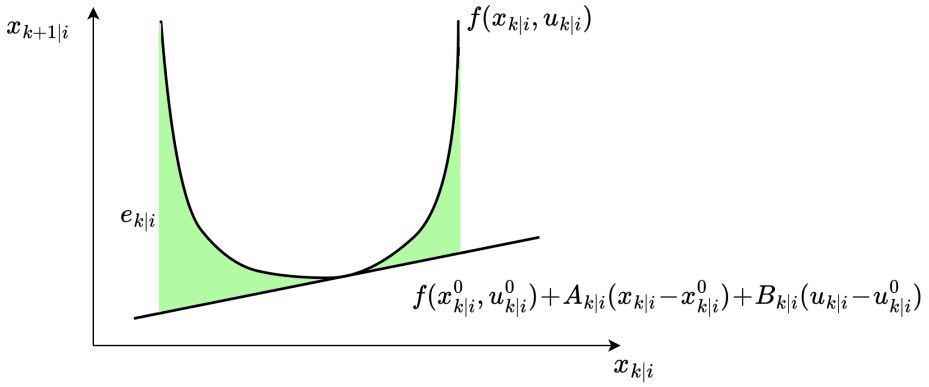


Figure 7.1: A simple 1-dimensional example, which illustrates how the error (in green) between the convex function f and its linearisation at a given point is always positive with a minimum value of zero at the point where the tangent touches the convex curve.

subject to, for $k = 0, \dots, N-1$:

$$S_{k|i} \oplus \{x^0_{k|i}\} \subseteq \mathcal{X} \tag{7.12a}$$

$$KS_{k|i} \oplus \{c_{k|i} + u^0_{k|i}\} \subseteq \mathcal{U} \tag{7.12b}$$

$$\begin{aligned} [\bar{s}_{k+1|i}]_j &\geq [A_{k|i} + B_{k|i}K]_j s + [B_{k|i}]_j c_{k|i} + e_{k|i,j}(s + x^0_{k|i}, Ks + c_{k|i} + u^0_{k|i}) \\ [\underline{s}_{k+1|i}]_j &\leq [A_{k|i} + B_{k|i}K]_j s + [B_{k|i}]_j c_{k|i} \quad \text{for } \forall s \in S_{k|i},\ j = 1, \dots, n_x \end{aligned} \tag{7.12c}$$

$$S_{0|i} = \{0\} \tag{7.12d}$$

$$S_{N|i} \oplus \{x^0_{N|i}\} \subseteq \mathcal{X}_N \tag{7.12e}$$

$$\begin{aligned} \text{with } J_{\text{EcMPC}}(\mathbf{c}_i, \mathbf{S}_i, \mathbf{x}^0_i, \mathbf{u}^0_i) \coloneqq & \max_{s_{N|i} \in S_{N|i}} \|x^0_{N|i} + s_{N|i} - x^r_{N+i}\|^2_{Q_N} \\ & + \sum_{k=0}^{N-1} \max_{s_{k|i} \in S_{k|i}} \left[\|x^0_{k|i} + s_{k|i} - x^r_{k+i}\|^2_Q + \|u^0_{k|i} + Ks_{k|i} + c_{k|i} - u^r_{k+i}\|^2_R \right]. \end{aligned} \tag{7.12f}$$

The inequalities in (7.12c) can be imposed for all $s \in S_{k|i}$ by replacing s with the 2^{n_x} vertices of $S_{k|i}$, which depend linearly on $\underline{s}_{k|i}$, $\bar{s}_{k|i}$. The minimisation of the cost (7.12f) can be performed via an equivalent epigraph form with a linear objective subject to convex (second order cone) constraints on $\mathbf{c}_i$ and $\{\underline{s}_{k|i}, \bar{s}_{k|i},\ k = 0, \dots, N\}$ the vertices of $S_{k|i}$. The EcMPC RHOCP is convex and can be solved using, for example, interior-point methods or large-scale first order solvers such as the alternating direction method of multipliers (ADMM) [23, 214–216].

The EcMPC strategy is summarised in Algorithm 2. At each discrete time step i, the algorithm first solves the EcMPC RHOCP to obtain $\mathbf{c}^*_i$ given a feasible seed

$(\mathbf{x}_i^0, \mathbf{u}_i^0)$ (lines 3-4). The predicted state and control sequences $(\mathbf{x}_i^*, \mathbf{u}_i^*)$ are then computed using the model dynamics (7.1) with $\mathbf{c}_i = \mathbf{c}_i^*$ and $x_{0|i}^* = x_i$ (lines 5-6). The seed trajectory $(\mathbf{x}_i^0, \mathbf{u}_i^0)$ is then updated (line 7) and this iteration is repeated until either $\|\mathbf{c}_i^*\| < tol$, where tol is a specified threshold, or the limit $maxiters$ on the number of iterations is reached.

Algorithm 2: EcMPC

Offline: Determine K, Q_N, $\mathcal{X}_N$, and an initial seed trajectory $(\mathbf{x}_0^0, \mathbf{u}_0^0)$ satisfying (7.6b)-(7.6e) with $x_0 = x_{\text{init}}$

Online: At each discrete time step $i = 0, 1, \ldots$:

1 Obtain x_i and set the iteration counter $n \leftarrow 1$;
2 **while** $n \leq maxiters$ *and* $\|\mathbf{c}_i^*\| \geq tol$ **do**
3 Compute $A_{k|i}$, $B_{k|i}$ for $k = 0, \ldots, N-1$ using (7.31c) and $(\mathbf{x}_i^0, \mathbf{u}_i^0)$;
4 Solve EcMPC RHOCP to obtain $(\mathbf{c}_i^*, \mathbf{S}_i^*)$;
5 **for** $k = 0, \ldots, N-1$ **do**
6 Compute $u_{k|i}^* = u_{k|i}^0 + c_{k|i}^* + K(x_{k|i}^* - x_{k|i}^0)$ and $x_{k+1|i}^* = f(x_{k|i}^*, u_{k|i}^*)$ with $x_{0|i}^* = x_i$;
7 Update the seed trajectory: $(\mathbf{x}_i^0, \mathbf{u}_i^0) \leftarrow (\mathbf{x}_i^*, \mathbf{u}_i^*)$;
8 $n \leftarrow n + 1$;
9 Implement $u_i \leftarrow u_{0|i}^*$;
10 Set $u_{N|i}^* = K(x_{N|i}^* - x_{N+i}^r) + u_{N+i}^r$ and $\mathbf{u}_{i+1}^0 \leftarrow \{u_{1|i}^*, \ldots, u_{N-1|i}^*, u_{N|i}^*\}$ $\mathbf{x}_{i+1}^0 \leftarrow \{x_{1|i}^*, \ldots, x_{N|i}^*, f(x_{N|i}^*, u_{N|i}^*)\}$;

Compared to other successive linearisation approaches [9, 189, 190], the EcMPC strategy does not require prior knowledge or online calculation of sets bounding linearisation errors, and it avoids conservative approximate linear constraints by using tight bounds on the approximation error in (7.12c). In particular, the first inequality in (7.12c) is equivalent to

$$\bar{s}_{k+1|i,j} \geq [f(s_{k|i} + x_{k|i}^0, Ks_{k|i} + c_{k|i} + u_{k|i}^0)]_j - [f(x_{k|i}^0, u_{k|i}^0)]_j,$$

and the second is a tight bound due to (7.10). As shown in Section 7.3.3, this ensures that the tube computed by the EcMPC iteration converges to a single trajectory, and hence, a fixed point of the EcMPC iteration is a local minimum for the EnMPC RHOCP. In addition, the maximum number of iterations can be chosen as any value satisfying $maxiters \geq 1$ without affecting the recursive feasibility and stability guarantees discussed in Section 7.3.3.

The feedback gain K can be chosen as the terminal feedback gain K in Assumption 7.3.1, which is stabilising for $k \geq N$ due to Assumption 7.3.1 (d). The computation of K, the terminal set $\mathcal{X}_N$ and Q_N is nontrivial for nonlinear systems. A scheme to compute them while maximising the volume of the terminal set can be found in [2, 13] using semidefinite programming.

Remark 7.3.1. *A time-varying feedback gain (such as the linear-quadratic optimal controller for the linear time-varying model computed on line 3 of Algorithm 1) may be used instead of a fixed feedback gain K in* (7.9)*. This is likely to give better numerical conditioning and disturbance rejection as the fixed gain K is only required by Assumption 7.3.1 to be locally stabilising within the terminal set $\mathcal{X}_N$.*

A procedure for obtaining an initial seed trajectory is suggested in [210]. This assumes knowledge of an initial trajectory satisfying constraints (7.6b)-(7.6c) and the initial condition (7.6d), but not necessarily the terminal constraint (7.6e). The method updates this seed via a sequence of convex optimisations to obtain a feasible trajectory for the EcMPC RHOCP.

We propose an alternative method of finding a feasible initial seed trajectory $(\mathbf{x}_0^0, \mathbf{u}_0^0)$ for Algorithm 2 that does not require knowledge of a feasible trajectory with initial condition x_{init}. We define an offline optimisation of $(\mathbf{c}_0, \mathbf{S}_0)$ subject to the constraints (7.12a)-(7.12c), (7.12e), and $S_{0|0} = \{s\}$, where s is an additional optimisation variable, and we minimise the distance of $x_{0|0}^0 + s$ from x_{init} by setting the objective to $\|x_{\text{init}} - x_{0|0}^0 - s\|$. Initially we set $\mathbf{x}_0^0 \coloneqq \{x_N^r, \ldots, x_{2N}^r\}$ and $\mathbf{u}_0^0 \coloneqq \{u_N^r, \ldots, u_{2N-1}^r\}$, since by Assumption 7.3.1 this choice ensures that constraints (7.12a)-(7.12c), (7.12e) and $S_{0|0} = \{s\}$ are feasible with $s = 0$. To obtain a feasible initial seed for Algorithm 2, we iteratively solve this optimisation and update $(\mathbf{x}_0^0, \mathbf{u}_0^0)$ as in lines 2-8 of Algorithm 2, with $x_{0|0}^* = x_0$ in line 6 replaced by $x_{0|0}^* = x_{0|0}^0 + s^*$, until either the optimal objective is equal to zero, or the optimal objective converges to a non-zero value, in which case the constraints should (if possible) be relaxed, for example by increasing N or enlarging $\mathcal{X}_N$.

Remark 7.3.2. *Assumption 7.3.2 can be relaxed to allow functions f which are DC, i.e. they can be written as the difference of convex functions: $f(x,u) = g(x,u) - h(x,u)$ where $g, h : \mathcal{X} \times \mathcal{U} \to \mathbb{R}^{n_x}$ are differentiable and componentwise convex and the sets $\mathcal{X}$,$\mathcal{U}$ are convex. In this case, the error function has the following properties*

$$
\begin{aligned}
&e_{k|i} = e^g_{k|i} - e^h_{k|i} \\
&e^g_{k|i} = g(x_{k|i}, u_{k|i}) - g(x^0_{k|i}, u^0_{k|i}) - A^g_{k|i} s_{k|i} - B^g_{k|i} v_{k|i}, \\
&e^h_{k|i} = h(x_{k|i}, u_{k|i}) - h(x^0_{k|i}, u^0_{k|i}) - A^h_{k|i} s_{k|i} - B^h_{k|i} v_{k|i}, \\
&\min_{(x_{k|i}, u_{k|i}) \in (\mathcal{X}, \mathcal{U})} e^g_{k|i,j}(x_{k|i}, u_{k|i}) = 0 \\
&\max_{(x_{k|i}, u_{k|i}) \in (\mathcal{X}, \mathcal{U})} -e^h_{k|i,j}(x_{k|i}, u_{k|i}) = 0
\end{aligned}
$$

where $e^g_{k|i}, e^h_{k|i}$ are componentwise convex and

$$
\begin{aligned}
A^g_{k|i} &= \frac{\partial g}{\partial x_{k|i}}|_{(x^0_{k|i}, u^0_{k|i})}, \quad B^g_{k|i} = \frac{\partial g}{\partial u_{k|i}}|_{(x^0_{k|i}, u^0_{k|i})}, \\
A^h_{k|i} &= \frac{\partial h}{\partial x_{k|i}}|_{(x^0_{k|i}, u^0_{k|i})}, \quad B^h_{k|i} = \frac{\partial h}{\partial u_{k|i}}|_{(x^0_{k|i}, u^0_{k|i})}.
\end{aligned}
$$

Thus Algorithm 2 can be used with constraints (7.12c) *in step 4 replaced, for all $s \in S_{k|i}$, $j = 1, \ldots, n_x$, by*

$$
\begin{aligned}
[\bar{s}_{k+1|i}]_j &\geq [A_{k|i} + B_{k|i}K]_j s + [B_{k|i}]_j c_{k|i} + e^g_{k|i,j}(s + x^0_{k|i}, Ks + c_{k|i} + u^0_{k|i}), \\
[\underline{s}_{k+1|i}]_j &\leq [A_{k|i} + B_{k|i}K]_j s + [B_{k|i}]_j c_{k|i} - e^h_{k|i,j}(s + x^0_{k|i}, Ks + c_{k|i} + u^0_{k|i}).
\end{aligned}
$$

Remark 7.3.3. *If the EcMPC RHOCP* (7.12) *is implemented by replacing s with the 2^{n_x} vertices of $S_{k|i}$ (which depend linearly on $\underline{s}_{k|i}$, $\bar{s}_{k|i}$), then the number of constraints in* (7.12c) *will grow exponentially with the state dimension n_x. However, this exponential growth can be avoided by using homothetic tubes (see e.g. [2]) to bound the state perturbations $s_{k|i}$. In this formulation, the tube description in* (7.11) *is replaced with $S_{k|i} = \{z^0_{k|i}\} \oplus \alpha_{k|i}\mathrm{co}\{z^1, ..., z^m\}$, where* co *denotes the convex hull. Here $z^0_{k|i} \in \mathbb{R}^{n_x}$ and the scaling $\alpha_{k|i} \in \mathbb{R}$ are optimisation variables in the RHOCP and the vertices $\{z^1, ..., z^m\}$ are fixed by the designer. This reduces the number of optimisation variables at each time step from $2n_x$ to n_x+1 and reduces the number of*

constraints in (7.12c) *to* $2mn_x$. *Here* m *can be as small as* n_x+1 *if* $S_{k|i}$ *is chosen to be a simplex, allowing the number of constraints in the EcMPC RHOCP to depend quadratically on the state dimension* n_x.

7.3.3 Nominal feasibility and stability guarantees

In this section, we demonstrate that Algorithm 2 is recursively feasible and that it provides a feasible solution for the EnMPC RHOCP. We further show that the optimal EcMPC RHOCP objective value is an upper bound on the cost of the EnMPC RHOCP and that the optimal cost is non-increasing at successive iterations (lines 2-8 of Algorithm 2) and at successive time steps. Using these properties, we show that the iteration converges (if the iteration limit *maxiters* is sufficiently large) to a solution satisfying the first-order optimality conditions of the EnMPC RHOCP and that (for any value of *maxiters*) the control law of Algorithm 2 is asymptotically stable.

Theorem 7.3.1 (Recursive feasibility)**.** *If Assumptions 7.3.1 and 7.3.2 hold and the initial seed trajectory* $(\mathbf{x}_0^0, \mathbf{u}_0^0)$ *satisfies* (7.6b)-(7.6e)*, then the EcMPC RHOCP is feasible at each iteration of Algorithm 2, at all times* $i \geq 0$.

Proof. Let $\mathbf{c}_i = 0$ and $\mathbf{S}_i = \{\{0\}, \ldots, \{0\}\}$, then the constraints of EcMPC RHOCP in line 4 of Algorithm 2 reduce to $\{x_{k|i}^0\} \subseteq \mathcal{X}$, $u_{k|i}^0 \in \mathcal{U}$ and $\{x_{N|i}^0\} \subseteq \mathcal{X}_N$. These conditions are satisfied if $(\mathbf{x}_i, \mathbf{u}_i) = (\mathbf{x}_i^0, \mathbf{u}_i^0)$ satisfies (7.6b)-(7.6e), which is true by assumption for the initial seed trajectory $(\mathbf{x}_0^0, \mathbf{u}_0^0)$, and is true for the seed trajectories $(\mathbf{x}_i^0, \mathbf{u}_i^0)$ and $(\mathbf{x}_{i+1}^0, \mathbf{u}_{i+1}^0)$ in lines 7 and 10 of Algorithm 2 due to constraints (7.12a)-(7.12e) and the properties of $\mathcal{X}_N$ (Assumptions 7.3.1 (b), (c)). □

We next consider how the optimal EcMPC RHOCP cost relates to the cost associated with the seed trajectory at successive iterations of Algorithm 2, and hence prove that the iteration converges to a solution that is at least locally optimal for the EnMPC RHOCP. At the i-th time step and n-th iteration of Algorithm 2, let $(\mathbf{x}_i^{0,n}, \mathbf{u}_i^{0,n})$ denote the seed trajectory in line 3, let $(\mathbf{c}_i^{*,n}, \mathbf{S}_i^{*,n})$ denote the optimal solution of the EcMPC RHOCP in line 4 and define $J_{\text{EcMPC},i}^{*,n} := J_{\text{EcMPC}}(\mathbf{c}_i^{*,n}, \mathbf{S}_i^{*,n}, \mathbf{x}_i^{0,n}, \mathbf{u}_i^{0,n})$.

Lemma 7.3.1. *For all $i \geq 0$ and for all $n \geq 1$, we have $J_{EnMPC}(\mathbf{x}_i^{0,n+1}, \mathbf{u}_i^{0,n+1}) \leq J_{EcMPC,i}^{*,n} \leq J_{EnMPC}(\mathbf{x}_i^{0,n}, \mathbf{u}_i^{0,n})$.*

Proof. Let $\mathbf{c}_i = 0$ and $\mathbf{S}_i = \{\{0\}, \ldots, \{0\}\}$, then

$$J_{\text{EcMPC}}(0, \{\{0\}, \ldots, \{0\}\}, \mathbf{x}_i^{0,n}, \mathbf{u}_i^{0,n}) = J_{\text{EnMPC}}(\mathbf{x}_i^{0,n}, \mathbf{u}_i^{0,n}),$$

and since this is a feasible (possibly suboptimal) choice, the optimal EcMPC cost in line 4 of Algorithm 2 satisfies

$$J_{\text{EcMPC}}(\mathbf{c}_i^*, \mathbf{S}_i^*, \mathbf{x}_i^{0,n}, \mathbf{u}_i^{0,n}) \leq J_{\text{EnMPC}}(\mathbf{x}_i^{0,n}, \mathbf{u}_i^{0,n}).$$

Furthermore, the updated seed in lines 5-7 satisfies

$$J_{\text{EnMPC}}(\mathbf{x}_i^{0,n+1}, \mathbf{u}_i^{0,n+1}) \leq J_{\text{EcMPC}}(\mathbf{c}_i^*, \mathbf{S}_i^*, \mathbf{x}_i^{0,n}, \mathbf{u}_i^{0,n})$$

since the tube $\mathbf{S}_i^*$ necessarily contains $\mathbf{x}_i^{0,n+1}$. □

Theorem 7.3.2. *For all $i \geq 0$, the iteration on lines 2-8 of Algorithm 2 converges to a seed trajectory $(\mathbf{x}_i^{0,n}, \mathbf{u}_i^{0,n})$ such that $\mathbf{c}_i^{*,n} = 0$ and $\mathbf{S}_i^{*,n} = \{\{0\}, \ldots, \{0\}\}$ is an optimal solution of the EcMPC RHOCP in the limit as $n \to \infty$.*

Proof. From Lemma 7.3.1 we have $J_{\text{EcMPC},i}^{*,n+1} \leq J_{\text{EcMPC},i}^{*,n}$ for all n, so $J_{\text{EcMPC},i}^{*,n} \geq 0$ (based on Assumption 7.3.1) implies $J_{\text{EcMPC},i}^{*,n} - J_{\text{EcMPC},i}^{*,n+1} \to 0$ and hence $J_{\text{EcMPC},i}^{*,n} - J_{\text{EnMPC}}(\mathbf{x}_i^{0,n}, \mathbf{u}_i^{0,n}) \to 0$ as $n \to \infty$. Therefore $(\mathbf{c}_i^{*,n}, \mathbf{S}_i^{*,n}) = (0, \{\{0\}, \ldots, \{0\}\})$ is an optimal solution of the EcMPC RHOCP in the limit as $n \to \infty$. □

Remark 7.3.4. *The optimal solution of the EcMPC RHOCP for $\mathbf{c}_i^*$ is unique since R is positive definite. Therefore Theorem 7.3.2 implies $\mathbf{c}_i^{*,n} \to 0$ as $n \to \infty$, justifying the termination criterion in line 2 of Algorithm 2. Moreover, even if the optimal $\mathbf{S}_i^*$ is non-unique, we can choose $\mathbf{S}_i^{*,n} = 0$ if $\mathbf{c}_i^{*,n} = 0$ and thus ensure that the iteration converges to a tube containing a single trajectory.*

Theorem 7.3.3. *The iteration of Algorithm 1 converges to a local minimum of the EnMPC RHOCP* (7.6b)-(7.6f).

Proof. A proof of Theorem 7.3.3 can be found in Appendix D.

Remark 7.3.5. *The converse of Theorem 7.3.3 is also true: a local minimum of the EnMPC problem is a local minimum of the EcMPC RHOCP* (7.12a)-(7.12f) *due to Theorem 7.3.2.*

Theorem 7.3.4. *Given Assumptions 7.3.1 and 7.3.2, the control law of Algorithm 1 ensures that* $x-x^r=0$ *is an asymptotically stable equilibrium of the system* (7.1)[1]*, with region of attraction consisting of the initial conditions* x_0 *of* (7.1) *for which there exists a control sequence such that* $u_k \in \mathcal{U}$ *and* $x_k \in \mathcal{X}$ *for* $k = 0, \ldots, N-1$*, and* $x_N \in \mathcal{X}_N$*.*

Proof. Assumption 7.3.1(d) and the update policy in line 10 of Algorithm 2 imply that the cost associated with the seed trajectory at the first iteration at time $i+1$ satisfies

$$J_{\text{EnMPC}}(\mathbf{x}_{i+1}^{0,1}, \mathbf{u}_{i+1}^{0,1}) \leq J_{\text{EnMPC}}(\mathbf{x}_i^{0,n_i}, \mathbf{u}_i^{0,n_i}) - (\|x_i - x_i^r\|_Q^2 + \|u_i - u_i^r\|_R^2),$$

where n_i is the final iteration count at time i. Hence

$$J_{\text{EnMPC}}(\mathbf{x}_{i+1}^{0,n_{i+1}}, \mathbf{u}_{i+1}^{0,n_{i+1}}) \leq J_{\text{EnMPC}}(\mathbf{x}_i^{0,n_i}, \mathbf{u}_i^{0,n_i}) - (\|x_i - x_i^r\|_Q^2 + \|u_i - u_i^r\|_R^2)$$

due to Lemma 7.3.1, and, since Q, R, Q_N are positive definite, $J_{\text{EnMPC}}(\mathbf{x}_{i+1}^{0,n_i}, \mathbf{u}_{i+1}^{0,n_i})$ is therefore a Lyapunov function demonstrating stability of $x - x^r = 0$. Summing both sides of this inequality over $i = 0, \ldots, t$ we obtain

$$\sum_{i=0}^{\infty}(\|x_i - x_i^r\|_Q^2 + \|u_i - u_i^r\|_R^2) \leq J_{\text{EnMPC}}(\mathbf{x}_0^{0,n_1}, \mathbf{u}_0^{0,n_1})$$

and it follows that $(x_i, u_i) \to (x_i^r, u_i^r)$ as $i \to \infty$. □

From Theorem 7.3.3 and Remark 7.3.5, it can be seen that the explicit consideration of the nonlinear dynamics in the constraints of the EcMPC RHOCP allows Algorithm 2 to approximate the optimal control law while formulating the control problem as a sequence of convex programs.

[1]More precisely, $x^\delta = x - x^r = 0$ is an asymptotically stable equilibrium of the system $x_{i+1}^\delta = f(x_i^\delta + x_i^r, u_i) - f(x_i^r, u_i^r)$.

7.3.4 Problem formulation with additive disturbances

Next, we consider the formulation of the proposed successive convexification approach to accommodate model inaccuracies or external disturbances. For this purpose we consider uncertain systems of the form

$$x_{i+1} = f(x_i, u_i) + w_i, \qquad w_i \in \mathcal{W}, \tag{7.13}$$

where w_i is an unknown disturbance input and $\mathcal{W} \subset \mathbb{R}^{n_x}$ is a known compact set. We consider an optimal tracking control problem similar to (7.6), with the model (7.13) replacing (7.1).

In this setting, we retain Assumption 7.3.2 (we discuss later how this can be relaxed to allow nonlinear functions that are neither convex nor concave), and we replace Assumption 7.3.1 with the following assumption:

Assumption 7.3.4.

(a) x_i is known at each time i.

(b) $x_i^r \in X(\underline{x}_N, \bar{x}_N) := \{x : \underline{x}_N \leq x \leq \bar{x}_N\} \subseteq \mathcal{X}$ and $u_i^r \in \mathcal{U}$ $\forall i \geq N$, for some $(\underline{x}_N, \bar{x}_N) \in \mathcal{X}_N$.

(c) for all $(\underline{x}_N, \bar{x}_N) \in \mathcal{X}_N$ we have: (i) $(\underline{x}_N^+, \bar{x}_N^+) \in \mathcal{X}_N$ where

$$[\bar{x}_N^+]_j \geq [f(x, \kappa_i(x))]_j + [\bar{w}]_j, \quad [\underline{x}_N^+]_j \leq [f(x, \kappa_i(x))]_j + [\underline{w}]_j, \quad j = 1, \ldots, n_x$$

$\forall x \in X(\underline{x}_N, \bar{x}_N)$, $\forall i \geq N$, and (ii) $x \in \mathcal{X}$ and $\kappa_i(x) := K(x - x_i^r) + u_i^r \in \mathcal{U}$, $\forall x \in X(\underline{x}_N, \bar{x}_N)$, $\forall i \geq N$.

(d) $Q, R, Q_N \succ 0$ and (7.13) with $u_i = K(x_i - x_i^r) + u_i^r$ satisfies, for all $i \geq N$, for some $\beta \geq 0$ and some $(\underline{x}_N, \bar{x}_N) \in \mathcal{X}_N$,

$$\|x_i - x_i^r\|_{Q_N}^2 - \|x_{i+1} - x_{i+1}^r\|_{Q_N}^2 \geq \|x_i - x_i^r\|_Q^2 + \|u_i - u_i^r\|_R^2 - \beta, \quad \forall x_i \in X(\underline{x}_N, \bar{x}_N).$$

The uncertainty in the future disturbance sequence implies that future state trajectories generated by (7.13) for a given control sequence or control law are uncertain. Therefore, although a convex successive optimisation approach can again be used to define an MPC law, the optimal tube bounding the predicted model

states cannot converge to a single trajectory as in the nominal case considered in Section 7.3.3. In addition, the seed trajectory used to define a linear model approximation in the disturbance-free case must be replaced by a tube.

7.3.5 Proposed robust control law

Recursive feasibility requires that a feasible seed tube be constructed at each iteration, guaranteeing that the state and control constraints are satisfied under all possible realisations of the disturbance input in (7.13). Given an initial state $x_{0|i}$ and perturbation sequence $\mathbf{c}_i^0$, we propose the method summarised in Algorithm 3 for constructing a linear model approximation and a seed tube

$$\mathbf{X}_i^0 \coloneqq \{X_{0|i}^0, \dots, X_{N|i}^0\} \quad \text{where } X_{k|i}^0 = \{x : \underline{x}_{k|i} \leq x \leq \bar{x}_{k|i}\}. \tag{7.14}$$

The linearisation points, denoted $(x_{k|i,j}^0, u_{k|i,j}^0)$, are computed for each component, $[f]_j$, $j = 1, \dots, n_x$, of f, via

$$x_{k|i,j}^0 = \arg \min_{x \in X_{k|i}^0} [f(x, Kx + c_{k|i}^0)]_j \tag{7.15}$$

and $u_{k|i,j}^0 = Kx_{k|i,j}^0 + c_{k|i}^0$. We show in Section 7.3.6 that this choice ensures recursive feasibility. The seed tube is computed using elementwise bounds, for $j = 1, \dots, n_x$,

$$[\bar{x}_{k+1|i}]_j = \max_{x \in X_{k|i}^0} [f(x, Kx + c_{k|i}^0)]_j + [\bar{w}]_j \tag{7.16}$$

$$[\underline{x}_{k+1|i}]_j = [f(x_{k|i,j}^0, u_{k|i,j}^0)]_j + [\underline{w}]_j \tag{7.17}$$

$$\text{where } [\bar{w}]_j = \max_{w \in \mathcal{W}} [w]_j, \qquad [\underline{w}]_j = \min_{w \in \mathcal{W}} [w]_j.$$

Note that the minimisation in (7.15) is a convex problem, and the maximisation in (7.16) can be performed as a maximisation over the vertices of $X_{k|i}^0$, each of which is a known linear function of $\underline{x}_{k|i}, \bar{x}_{k|i}$.

The linear model approximation computed using Algorithm 3 can be used to formulate the following robust RHOCP.

$$\text{REcMPC}: \ (\mathbf{c}_i^*, \mathbf{X}_i^*) \coloneqq \operatorname*{argmin}_{\mathbf{c}_i, \mathbf{X}_i} J_{\text{REcMPC}}(\mathbf{c}_i, \mathbf{X}_i, \mathbf{c}_i^0)$$

$$\text{subject to, for } k = 0, \dots, N-1:$$

$$X_{k|i} \subseteq \mathcal{X} \tag{7.18a}$$

$$KX_{k|i} \oplus \{c_{k|i} + c^0_{k|i}\} \subseteq \mathcal{U}, \tag{7.18b}$$

$$[\bar{x}_{k+1|i}]_j \geq [f(x, Kx + c_{k|i} + c^0_{k|i})]_j + [\bar{w}]_j$$

$$[\underline{x}_{k+1|i}]_j \leq [f(x^0_{k|i,j}, u^0_{k|i,j})]_j + [A_{k|i} + B_{k|i}K]_j(x - x^0_{k|i,j}) + [B_{k|i}]_j c_{k|i} + [\underline{w}]_j$$

$$\text{for all } x \in X_{k|i},\ j = 1, \ldots, n_x \tag{7.18c}$$

$$X_{0|i} = \{x_i\} \tag{7.18d}$$

$$X_{N|i} \subseteq \mathcal{X}_N \tag{7.18e}$$

$$\begin{aligned} \text{with } J_{\text{REcMPC}}(\mathbf{c}_i, \mathbf{X}_i, \mathbf{c}^0_i) \coloneqq & \max_{x_{N|i} \in X_{N|i}} \|x_{N|i} - x^r_{N+i}\|^2_{Q_N} \\ & + \sum_{k=0}^{N-1} \max_{x_{k|i} \in X_{k|i}} \Big[\|x_{k|i} - x^r_{k+i}\|^2_Q + \|Kx_{k|i} + c_{k|i} + c^0_{k|i} - u^r_{k+i}\|^2_R \Big]. \end{aligned} \tag{7.18f}$$

The constraints in (7.18c) can be imposed for all $x \in X_{k|i}$ by replacing x with the 2^{n_x} vertices of $X_{k|i}$, which are linear functions of the optimisation variables $\underline{x}_{k|i}$, $\bar{x}_{k|i}$. Hence, the REcMPC RHOCP can be expressed as a convex program similar to the cMPC RHOCP for the nominal case.

Algorithm 3: Seed tube and linearisation for the REcMPC approach

Require: Initial state x_i and seed $\mathbf{c}^0_i$

Set $\bar{x}_{0|i} = \underline{x}_{0|i} = x_i$ so that $X^0_{0|i} \leftarrow \{x_i\}$;
for $k = 0, \ldots, N-1$ **do**
  for $j = 1, \ldots, n_x$ **do**
    Solve problem (7.15) for $x^0_{k|i,j}$ and $u^0_{k|i,j} = Kx^0_{k|i,j} + c^0_{k|i}$;
    Compute $[A_{k|i}]_j = \dfrac{\partial [f]_j}{\partial x}\Big|_{(x^0_{k|i,j}, u^0_{k|i,j})}$ and $[B_{k|i}]_j = \dfrac{\partial [f]_j}{\partial u}\Big|_{(x^0_{k|i,j}, u^0_{k|i,j})}$;
    Solve (7.16)-(7.17) for $[\bar{x}_{k+1|i}]_j$, $[\underline{x}_{k+1|i}]_j$;
  Set $X^0_{k+1|i} \leftarrow \{x : \underline{x}_{k+1|i} \leq x \leq \bar{x}_{k+1|i}\}$;

Remark 7.3.6. *The feedback law $Kx_{k|i} + c_{k|i} + c^0_{k|i}$ can be interpreted as a controller of the form $Ks_{k|i} + c_{k|i} + v^0_{k|i}$, where $s_{k|i} = x_{k|i} - \hat{x}_{k|i}$, $v^0_{k|i} = K\hat{x}_{k|i} + c^0_{k|i}$, and $\hat{x}_{k|i}$ is a point in $X^0_{k|i}$ such as the Chebyshev centre of $X^0_{k|i}$, for example. However, this equivalent formulation would require the additional unnecessary computation of $\hat{x}_{k|i}$ for $k = 0, \ldots, N$.*

The robust EcMPC strategy is presented in Algorithm 4. The initial seed $\mathbf{c}^0_0$ can be computed similarly to the initialisation of Algorithm 2. Starting with $x_0 \coloneqq x^r_N$ and

$\mathbf{c}_0^0 \coloneqq \{u_N^r - Kx_N^r, \ldots, u_{2N-1}^r - Kx_{2N-1}^r\}$, the tube $\mathbf{X}_0^0$ generated by Algorithm 3 satisfies $X_{k|i}^0 \subseteq \mathcal{X}_N$ for all k (by Assumption 7.3.4), and hence (7.18a)-(7.18c) and (7.18e) are feasible with this choice and $(\mathbf{c}_0, \mathbf{X}_0) = (0, \mathbf{X}_0^0)$. To generate a feasible initial seed for Algorithm 4, we perform the iteration in lines 2-5 of Algorithm 4, with line 4 replaced by the minimisation of $\|x_{\text{init}} - x_0\|$ over variables $(\mathbf{c}_0, \mathbf{X}_0)$ and x_0 subject to (7.18a)-(7.18c), $X_{0|0}^0 = \{x_0\}$ and (7.18e), with $x_0 \leftarrow x_0^*$, $\mathbf{c}_0^0 \leftarrow \mathbf{c}_0^* + \mathbf{c}_0^0$ in line 5. This converges either to a feasible $\mathbf{c}_0^0$ with $x_0^* = x_{\text{init}}$, or to a non-zero value of $\|x_{\text{init}} - x_0^*\|$ (in which case the constraints should be relaxed, e.g. by increasing N or enlarging $\mathcal{X}_N$).

Algorithm 4: REcMPC

Offline: Determine K, Q_N, $\mathcal{X}_N$, and initial seed $\mathbf{c}_0^0$ with which Algorithm 3 generates a tube $\mathbf{X}_0^0$ such that $(\mathbf{c}_0, \mathbf{X}_0) = (0, \mathbf{X}_0^0)$ satisfies (7.18a)-(7.18e) with $x_0 = x_{\text{init}}$

Online: At each discrete time step $i = 0, 1, \ldots$:

1 Obtain x_i and set the iteration counter $n \leftarrow 1$;
2 **while** $n \leq$ *maxiters and* $\|\mathbf{c}_i^*\| \geq$ *tol* **do**
3 Compute $(x_{k|i,j}^0, u_{k|i,j}^0)$, $j = 1, \ldots, n_x$ and $A_{k|i}$, $B_{k|i}$ for $k = 0, \ldots, N-1$ using Algorithm 3;
4 Solve REcMPC RHOCP to obtain $(\mathbf{c}_i^*, \mathbf{X}_i^*)$;
5 Update the seed: $\mathbf{c}_i^0 \leftarrow \mathbf{c}_i^* + \mathbf{c}_i^0$, $n \leftarrow n + 1$;
6 Implement $u_i \leftarrow Kx_i + c_{0|i}^0$ and set $\mathbf{c}_{i+1}^0 \leftarrow \{c_{1|i}^0, \ldots, c_{N-1|i}^0, u_{N+i}^r - Kx_{N+i}^r\}$

Remark 7.3.7. *If $\mathcal{W} = \{0\}$, then $(x_{k|i,j}^0, u_{k|i,j}^0) = (x_{k|i,1}^0, u_{k|i,1}^0)$ for all $j = 2, \ldots, n_x$, so at each time step k all linearisation points are identical. In this case, the tube $\mathbf{X}_i^*$ generated by Algorithm 4 contains a single trajectory, which is identical to $\mathbf{x}_i^*$ at each iteration of Algorithm 2. Thus, Algorithm 2 is a special case of Algorithm 4 when disturbances are absent.*

Various methods are available for computing a robustly invariant terminal set $\mathcal{X}_N$ and a terminal weighting matrix Q_N satisfying the conditions of Assumption 7.3.4. We refer the reader to [2, 217] for example.

Remark 7.3.8. *Analogously to the disturbance-free case in Remark 7.3.2, Assumption 7.3.2 can be relaxed to consider DC functions $f(x, u) = g(x, u) - h(x, u)$, where $g, h : \mathcal{X} \times \mathcal{U} \to \mathbb{R}^{n_x}$ are differentiable and componentwise convex on the convex sets*

$\mathcal{X}$,$\mathcal{U}$. *In this case Algorithms 3 and 4 can still be used, with* (7.16), (7.17) *in step 4 of Algorithm 3 replaced by:*

$$\begin{aligned}[\bar{x}_{k+1|i}]_j = \max_{x\in X^0_{k|i}} \Big(&[f(x^0_{k|i,j}, u^0_{k|i,j})]_j + [A_{k|i}+B_{k|i}K]_j(x- x^0_{k|i,j}) + [B_{k|i}]_j c_{k|i} \\ &+ [e^g_{k|i}(x_{k|i,j}, u_{k|i,j})]_j \Big) + [\bar{w}]_j \\ [\underline{x}_{k+1|i}]_j = \min_{x\in X^0_{k|i}} \Big(&[f(x^0_{k|i,j}, u^0_{k|i,j})]_j + [A_{k|i}+B_{k|i}K]_j(x- x^0_{k|i,j}) + [B_{k|i}]_j c_{k|i} \\ &- [e^h_{k|i}(x_{k|i,j}, u_{k|i,j})]_j \Big) + [\underline{w}]_j \end{aligned}$$

and with constraints (7.18c) *in the REcMPC RHOCP replaced by*

$$\begin{aligned}[\bar{x}_{k+1|i}]_j \geq &[f(x^0_{k|i,j}, u^0_{k|i,j})]_j + [A_{k|i}+B_{k|i}K]_j(x- x^0_{k|i,j}) + \\ &[B_{k|i}]_j c_{k|i} + [\bar{w}]_j + [e^g_{k|i}(x_{k|i,j}, u_{k|i,j})]_j, \end{aligned} \tag{7.19}$$

$$\begin{aligned}[\underline{x}_{k+1|i}]_j \leq &[f(x^0_{k|i,j}, u^0_{k|i,j})]_j + [A_{k|i}+B_{k|i}K]_j(x- x^0_{k|i,j}) + \\ &[B_{k|i}]_j c_{k|i} + [\underline{w}]_j - [e^h_{k|i}(x_{k|i,j}, u_{k|i,j})]_j. \end{aligned} \tag{7.20}$$

Remark 7.3.9. *Similarly to the nominal approach, the REcMPC RHOCP can be implemented by replacing x in* (7.18c) *by each of the vertices of the set $X_{k|i}$. If $X_{k|i}$ is defined by the elementwise bounds in* (7.14)*, then the number of constraints will grow exponentially with the state dimension n_x. However, this exponential growth can be avoided if $\mathbf{X}_i$ is defined instead as a homothetic tube, as discussed in Remark 7.4.4.*

7.3.6 Robust feasibility and stability guarantees

This section shows that, given an initial perturbation sequence $\mathbf{c}_0^0$ such that Algorithm 3 with $x_0 = x_{\text{init}}$ generates a feasible tube, the REcMPC RHOCP remains feasible at each iteration of Algorithm 4 and each discrete time step. We also show that the optimal objective of the REcMPC RHOCP is non-increasing, and therefore, the iteration of Algorithm 4 converges, and the MPC law provides a robust quadratic stability guarantee for any chosen limit on the number of iterations satisfying *maxiters* ≥ 1.

To make notation more precise, at the ith time step and nth iteration of Algorithm 4 we denote the seed trajectory as $\mathbf{c}_i^{0,n}$ and the tube generated by Algorithm 3 with $\mathbf{c}_i^0 = \mathbf{c}_i^{0,n}$ as $\mathbf{X}_i^{0,n}$. Similarly, we denote the solution of the REcMPC RHOCP in line 4 as $(\mathbf{c}_i^{*,n}, \mathbf{X}_i^{*,n})$, and the optimal objective as $J^{*,n}_{\text{REcMPC},i} = J_{\text{REcMPC}}(\mathbf{c}_i^{*,n}, \mathbf{X}_i^{*,n}, \mathbf{c}_i^{0,n})$.

First note that the tubes $\mathbf{X}_i^{0,n}$ and $\mathbf{X}_i^{*,n}$ generated by Algorithms 3 and 4 necessarily contain all trajectories of (7.13) with initial condition $x_{0|i} = x_i$ under the control laws $u_{k|i} = Kx_{k|i} + c^{0,n}_{k|i}$ and $u_{k|i} = Kx_{k|i} + c^{*,n}_{k|i}$ respectively. This follows from the convexity of f (Assumption 7.3.2), and from the definition of $X^{0,n}_{k+1|i}$ in (7.16)-(7.17), and the constraints on $X^{*,n}_{i+1|k}$ in (7.18c), which imply

$$f(x, Kx + c^{0,n}_{k|i}) + w \in X^{0,n}_{k+1|i} \quad \forall x \in X^{0,n}_{k|i}, \tag{7.21}$$

$$f(x, Kx + c^{*,n}_{k|i}) + w \in X^{*,n}_{k+1|i} \quad \forall x \in X^{*,n}_{k|i}, \tag{7.22}$$

for all $w \in \mathcal{W}$, $k = 0, \dots, N-1$ and $i \geq 0$, where $\mathbf{c}_i^{0,n} = \{c^{0,n}_{0|i}, \dots, c^{0,n}_{N-1|i}\}$ and $\mathbf{c}_i^{*,n} = \{c^{*,n}_{0|i}, \dots, c^{*,n}_{N-1|i}\}$. The recursive feasibility of Algorithm 4 is a consequence of the following properties of the sets $X^{0,n}_{i|k}$, $X^{*,n}_{i|k}$.

Lemma 7.3.2. *For all $i \geq 0$ and $n = 1, \dots n_i$ we have*

$$\text{if } X^{0,n+1}_{k|i} \subseteq X^{*,n}_{k|i} \qquad \text{then } X^{0,n+1}_{k+1|i} \subseteq X^{*,n}_{k+1|i}, \tag{7.23a}$$

$$\text{if } X^{0,1}_{k|i+1} \subseteq X^{*,n_i}_{k+1|i} \qquad \text{then } X^{0,1}_{k+1|i+1} \subseteq X^{*,n_i}_{k+2|i}, \tag{7.23b}$$

$$\text{if } X^{0,1}_{N-1|i+1} \subseteq X^{*,n_i}_{N|i} \qquad \text{then } X^{0,1}_{N|i+1} \subseteq \mathcal{X}_N, \tag{7.23c}$$

where (7.23a) *holds for $k = 0, \dots, N-1$,* (7.23b) *holds for $k = 0, \dots, N-2$, and n_i is the final iteration at time i.*

Proof. Condition (7.23a) follows from the definition of the linearisation points in (7.15), which implies

$$[f(x^{0,n+1}_{k|i,j}, u^{0,n+1}_{k|i,j})]_j = \min_{x \in X^{0,n+1}_{k|i}} [f(x, Kx + c^{0,n+1}_{k|i})]_j \tag{7.24a}$$

$$\geq \min_{x \in X^{*,n}_{k|i}} [f(x, Kx + c^{0,n+1}_{k|i})]_j \tag{7.24b}$$

$$\geq \min_{x \in X^{*,n}_{k|i}} \left\{ [f(x^{0,n}_{k|i,j}, u^{0,n}_{k|i,j}]_j + [A^n_{k|i}]_j (x - x^{0,n}_{k|i,j}) + [B^n_{k|i}]_j (Kx + c^{0,n+1}_{k|i} - u^{0,n}_{k|i}) \right\} \tag{7.24c}$$

$$= \min_{x \in X^{*,n}_{k|i}} \left\{ [f(x^{0,n}_{k|i,j}, u^{0,n}_{k|i,j}]_j + [A^n_{k|i} + B^n_{k|i} K]_j (x - x^{0,n}_{k|i,j}) + [B^n_{k|i}]_j c^{*,n}_{k|i} \right\} \tag{7.24d}$$

where (7.24b) holds if $X^{0,n+1}_{k|i} \subseteq X^{*,n}_{k|i}$, (7.24c) is due to the convexity of f, and (7.24d) follows from $u^{0,n}_{k|i} = K x^{0,n}_{k|i} + c^{0,n}_{k|i}$ and $c^{0,n+1}_{k|i} = c^{*,n}_{k|i} + c^{0,n}_{k|i}$. Therefore, from (7.18c) we obtain

$$\underline{x}^{0,n+1}_{k+1|i} \geq \underline{x}^{*,n}_{k+1|i}.$$

Similarly, if $X^{0,n+1}_{k|i} \subseteq X^{*,n}_{k|i}$, then

$$\max_{x \in X^{0,n+1}_{k|i}} [f(x, Kx + c^{0,n+1}_{k|i}]_j \leq \max_{x \in X^{*,n}_{k|i}} [f(x, Kx + c^{0,n+1}_{k|i}]_j = \max_{x \in X^{*,n}_{k|i}} [f(x, Kx + c^{*,n}_{k|i} + c^{0,n}_{k|i}]_j$$

and hence

$$\bar{x}^{0,n+1}_{k+1|i} \leq \bar{x}^{*,n}_{k+1|i}$$

by (7.16) and (7.18c), which demonstrates (7.23a). Conditions (7.23b) and (7.23c) follow from the $\mathbf{c}^0_{i+1}$ update in line 6 of Algorithm 4, which implies $c^{0,1}_{k|i+1} = c^{*,n_i}_{k+1|i} + c^{0,n_i}_{k+1|i}$, $k = 0, \ldots, N-2$, and $c^{0,1}_{N-1|i+1} = u^r_{N+i} - K x^r_{N+i}$. Hence (7.23b) can be shown analogously to (7.23a), and (7.23c) holds because $X^{*,n_i}_{N|i} \subseteq \mathcal{X}_N$ by (7.18e) and $\mathcal{X}_N$ satisfies Assumption 7.3.4. □

Theorem 7.3.5 (Recursive feasibility)**.** *If Assumptions 7.3.2 and 7.3.4 hold, and if* $\mathbf{c}_0, \mathbf{X}_0$ *exist satisfying* (7.18a)-(7.18e) *with the initial seed* $\mathbf{c}^0_0$*, then the REcMPC RHOCP is feasible at each iteration of Algorithm 4, for all times* $i \geq 0$*.*

Proof. If, at time i and iteration n the REcMPC RHOCP in line 4 of Algorithm 4 has solution $(\mathbf{c}^{*,n}_i, \mathbf{X}^{*,n}_i)$, then $(\mathbf{c}_i, \mathbf{X}_i) = (0, \mathbf{X}^{0,n+1}_i)$ is a feasible solution at iteration $n+1$ by Lemma 7.3.2 since $X^{0,n+1}_{0|i} = \{x_i\} = X^{*,n}_{0|i}$. Similarly, Lemma 7.3.2 implies that if $(\mathbf{c}^{*,n_i}_i, \mathbf{X}^{*,n_i}_i)$ is the solution of the REcMPC RHOCP at the final iteration performed at time i, then $(\mathbf{c}_{i+1}, \mathbf{X}_{i+1}) = (0, \mathbf{X}^{0,1}_{i+1})$ is a feasible solution at the first iteration at time $i+1$ since $X^{0,1}_{0|i+1} = \{x_{i+1}\} \subseteq X^{*,n_i}_{0|i}$. Furthermore, feasibility of (7.18a)-(7.18e) with the initial seed $\mathbf{c}^0_0$ ensures feasibility of REcMPC RHOCP at the first iteration at $i = 0$, thus ensuring feasibility at all iterations and all time steps. □

Lemma 7.3.3. *For all $i \geq 0$ and $n \geq 1$ the optimal cost satisfies $J^{*,n+1}_{\mathrm{REcMPC},i} \leq J^{*,n}_{\mathrm{REcMPC},i}$.*

Proof. Lemma 7.3.2 implies that $(\mathbf{c}_i, \mathbf{X}_i) = (0, \mathbf{X}_i^{0,n+1})$ is a feasible solution of the REcMPC RHOCP at iteration $n+1$. Therefore, the optimal solution at iteration $n+1$ satisfies $J^{*,n+1}_{\mathrm{REcMPC},i} \leq J_{\mathrm{REcMPC}}(0, \mathbf{X}_i^{0,n+1}, \mathbf{c}_i^{0,n+1})$. But from Lemma 7.3.2 we also have $X^{0,n+1}_{k|i} \subseteq X^{*,n}_{k|i}$ for $k = 0, \ldots, N$, and the definition of the cost in (7.18f) therefore implies $J_{\mathrm{REcMPC}}(0, \mathbf{X}_i^{0,n+1}, \mathbf{c}_i^{*,n}) \leq J^{*,n}_{\mathrm{REcMPC},i}$. □

Remark 7.3.10. *Since $J^{*,n}_{REcMPC,i} \geq 0$, Lemma 7.3.3 implies that, in the ideal case of unlimited iterations, the optimal REcMPC cost in line 4 of Algorithm 4 converges to a finite limit as $n \to \infty$. As in the nominal case, it follows that $\mathbf{c}_i^{*,n} \to 0$ as $n \to \infty$. In this case, however, the seed tube $\mathbf{X}_i^{0,n}$ generated by Algorithm 3 will in general contain more than a single trajectory at all iterations $n \geq 1$, and hence $\mathbf{X}_i^{0,n}$ does not converge to a single trajectory.*

Theorem 7.3.6. *If Assumptions 7.3.2 and 7.3.4 hold and the offline computation of Algorithm 4 is feasible, then the closed loop system formed by* (7.13) *and Algorithm 4 satisfies the state and input constraints* (7.5) *and the quadratic stability condition:*

$$\lim_{t\to\infty} \frac{1}{t} \sum_{i=0}^{t-1} (\|x_i - x_i^r\|_Q^2 + \|u_i - u_i^r\|_R^2) \leq \beta \tag{7.25}$$

where β satisfies Assumption 7.3.4(d).

Proof. By Lemma 7.3.2 and Theorem 7.3.5, $(\mathbf{c}_{i+1}, \mathbf{X}_{i+1}) = (0, \mathbf{X}_{i+1}^{0,1})$ is a feasible solution for REcMPC RHOCP at iteration one of Algorithm 4 at time $i+1$, thus

$$\begin{aligned} J^{*,1}_{\mathrm{REcMPC},i+1} &\leq J_{\mathrm{REcMPC}}(0, \mathbf{X}_{i+1}^{0,1}, \mathbf{c}_{i+1}^{0,1}) \\ &\leq J_{\mathrm{REcMPC}}(\mathbf{c}_i^{*,n_i}, \mathbf{X}_i^{*,n_i}, \mathbf{c}_i^{0,n_i}) - \|x_i - x_i^r\|_Q^2 - \|u_i - u_i^r\|_i^2 + \beta, \end{aligned}$$

where the definition of $\mathbf{c}_{i+1}^{0,1}$ in line 6 and the inequality in Assumption 7.3.4(d) have been used. But Lemma 7.3.3 implies $J^{*,n_{i+1}}_{\mathrm{REcMPC},i+1} \leq J^{*,1}_{\mathrm{REcMPC},i+1}$ and hence

$$J^{*,n_{i+1}}_{\mathrm{REcMPC},i+1} \leq J^{*,n_i}_{\mathrm{REcMPC},i} - \|x_i - x_i^r\|_Q^2 - \|u_i - u_i^r\|_i^2 + \beta. \tag{7.26}$$

The bound (7.25) follows by summing both sides of (7.26) over $i = 0, \ldots, t-1$ and noting that $J^{*,n_i}_{\mathrm{RcMPC},i}$ is finite for all i since $\mathcal{X}$, $\mathcal{U}$ are compact and the REcMPC RHOCP is feasible. □

Remark 7.3.11. *If Assumption 7.3.4 reduces to Assumption 7.3.1 in the absence of disturbances (i.e. if $\beta \to 0$ as $\mathcal{W} \to \{0\}$), then the origin ($x - x^r = 0$) of the closed loop system of* (7.13) *with Algorithm 4 is input-to-state stable (ISS) [218], since* (7.26) *and Assumption 7.3.4(d) imply $J^{*,n_i}_{\mathrm{RcMPC},i}$ is an ISS Lyapunov function.*

7.3.7 Numerical examples

This section presents numerical results obtained by applying the nominal EcMPC (Algorithm 2) and robust REcMPC (Algorithm 4) strategies to two example problems. In each case, the algorithms are implemented in Python, using *CVXPY* [179] and MOSEK [180] for convex optimisation problems, and using the SciPy SLSQP algorithm [147] for comparisons with a general nonlinear programming solver. Unless stated otherwise *maxiters* = 3, $tol = 10^{-6}$ and MPC simulations are terminated when $\|x_{N|i}\|_2$ reaches 10^{-4} (Example 6) or 10^{-6} (Example 2).

Example 6: First we consider a system with model

$$\begin{aligned}\dot{x}_1(t) &= x_2(t) + w_1(t)\\ \dot{x}_2(t) &= 0.2e^{-x_1(t)} - x_2(t) + u_1(t) - 0.2 + w_2(t).\end{aligned}$$

and cost weights $Q = \mathrm{diag}\{1, 1\}$, $R = 1$, and initial condition $x_1(0) = 5$, $x_2(0) = 10$. Forward Euler discretisation is used with discrete time step $\Delta t = 8 \times 10^{-3}$s, and the prediction horizon is $N = 25$. The reference trajectory is chosen as $x^r_i = 0, u^r_i = 0$ for all i, and the system constraints are $|x_1(t)| \leq 10$, $|x_2(t)| \leq 10$, $|u_1(t)| \leq 150$ at all discrete times $t = i\Delta t$, $i = 0, 1, \ldots$.

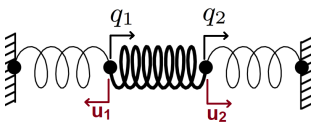


Figure 7.2: Example 2: FPUT system with two unit masses with coordinates q_1, q_2, and control forces u_1, u_2 applied directly to each mass.

Example 2: Applying a change of coordinates to the FPUT system from Section 4.3 with two point masses (Figure 7.2), we obtain a convex model formulation:

$$\begin{aligned}
\dot{x}_1(t) &= x_3(t) + w_1(t) \\
\dot{x}_2(t) &= x_4(t) + w_2(t) \\
\dot{x}_3(t) &= -\tfrac{\eta^2}{2}\Big(x_2(t) + x_1(t)\Big) + 3x_1(t)^2 + u_1(t) + w_3(t) \\
\dot{x}_4(t) &= -\tfrac{\eta^2}{2}\Big(x_2(t) + x_1(t)\Big) + 3x_2(t)^2 + u_2(t) + w_4(t).
\end{aligned}$$

Forward Euler discretisation with $\Delta t = 10^{-2}$s and a prediction horizon $N = 25$ are used. The model and optimisation parameters are $\eta = 50$, $x_i^r = 0$, $u_i^r = 0$ for all i, $Q = \text{diag}\{0.01, 0.01, 0.01, 0.01\}$, $R = \text{diag}\{0.01, 0.01\}$, $|x_1(t)| \leq 10$, $|x_2(t)| \leq 10$, $|x_3(t)| \leq 10$, $|x_4(t)| \leq 10$, $|u_1(t)| \leq 33$, $|u_2(t)| \leq 33$ for $t = i\Delta t$, for all $i = 0, 1, \ldots,$

$$\begin{bmatrix} x_1(0) \\ x_2(0) \end{bmatrix} = E \begin{bmatrix} 1 \\ 1 \end{bmatrix}, \begin{bmatrix} x_3(0) \\ x_4(0) \end{bmatrix} = E \begin{bmatrix} 1/\eta \\ 1 \end{bmatrix}, E = \tfrac{1}{\sqrt{2}} \begin{bmatrix} -1 & 1 \\ 1 & 1 \end{bmatrix}.$$

Nominal EcMPC

The performance of the nominal EcMPC strategy (Algorithm 2) described in Section 7.3.2 was investigated by setting $w_1(t) = w_2(t) = 0$ and $w_3(t) = w_4(t) = 0$ for all t in Examples 6 and 2. The initial seed was obtained using the initialisation strategy described in Section 7.3.2. Figure 7.3 shows the predicted trajectories obtained by applying Algorithm 2 to both example problems. As expected from Lemma 7.3.1 and Theorem 7.3.2, the optimal predicted cost is non-increasing at successive iterations and discrete time steps, and $\mathbf{c}_i^*$ converges to 0. This is shown in Figure 7.4 for Example 2. The convergence of the tube to a single trajectory (Theorem 7.3.2 and Remark 7.3.4) is illustrated in Figure 7.5 for Example 6. The iteration clearly converges rapidly ($\mathbf{S}_0^*$ is already difficult to see at the second iteration), and the tube at iteration n contains the seed trajectory updated for iteration $n + 1$ via line 6 of Algorithm 2, as expected from Theorem 7.3.1.

Timing tests were conducted by comparing the $CVXPY$ implementation of Algorithm 2 to a receding horizon strategy that solves the EnMPC RHOCP at each time step using the scipy.optimize library and its SLSQP solver. The EcMPC

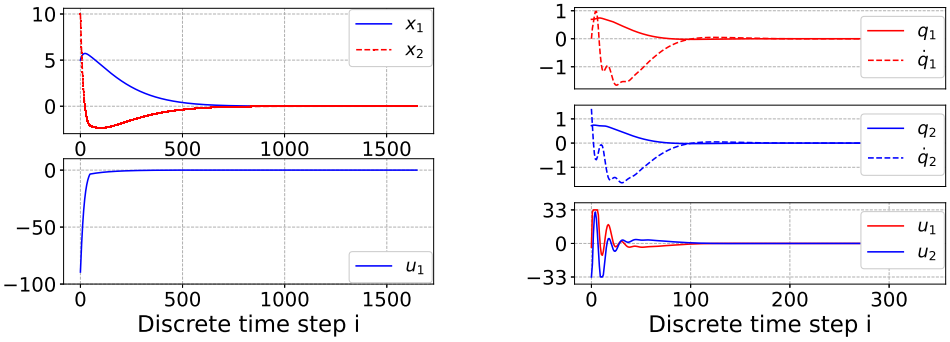


Figure 7.3: Closed loop trajectories with EcMPC (Algorithm 2) for Example 6 (left plot) and Example 2 (right plot)

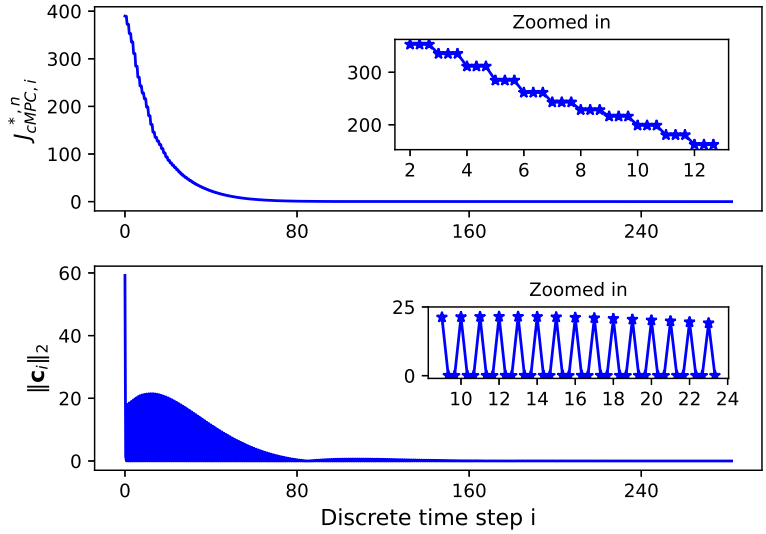


Figure 7.4: Example 2: Convergence of the optimal const (upper plot) and $\|\mathbf{c}_i^*\|$ (lower plot) for EcMPC at successive iterations and time steps

RHOCP in line 4 of Algorithm 2 is implemented using the *parameters* functionality of the *CVXPY* library and is thus pre-compiled offline. The solver timings were tested both with and without pre-compilation using the jit functionality of the *JAX* library [219]. For the *CVXPY* algorithm *jit* is used to speed up lines 3 and 6, whereas for scipy.optimize it is used to pre-compile the constraints, constraint Jacobians, cost function and cost gradient. Results obtained using a i7-10700 CPU at 2.90GHz are shown in Table 7.1, where n_v, n_c, n_p are the number of variables, constraints and parameters respectively, J_0^* is the optimal cost at $i = 0$ and J_{cl} is the cost evaluated using closed loop system responses. For Example 6 with standard implementation at $i = 0$ Algorithm 2 requires only 1.71% and 3.69%. of

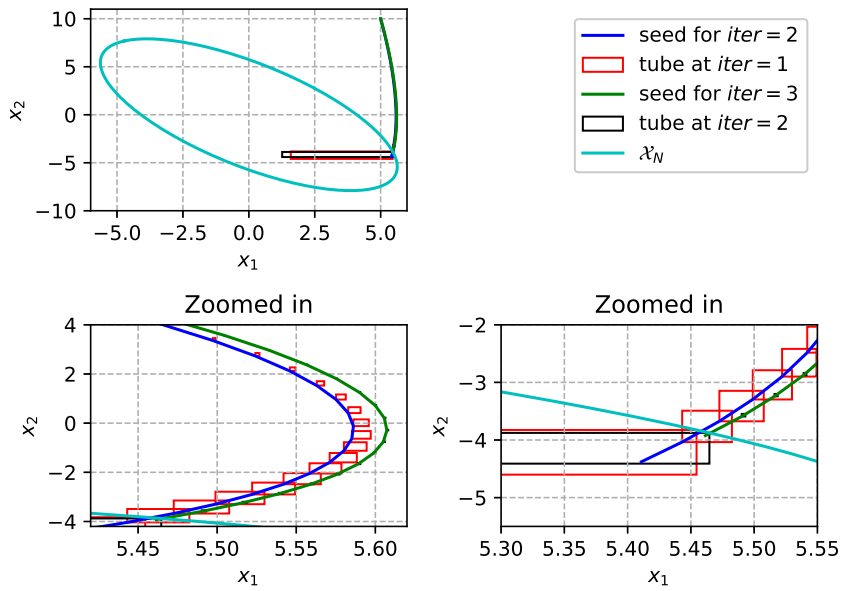


Figure 7.5: Example 6: Seed trajectories and tubes ($x^0_{i|k}$ and $x^0_{i|k} \oplus S^*_{i|k}$) for EcMPC at iterations $n = 1, 2, 3$ at time $i = 0$.

	solver	maxiters	n_v	n_c	n_p	time for iter 1 $i=0$	**total time at** $i=0$	total time at $i=1$	total time at $i=2$	J_0^*	J_{cl}
Example 6	*CVXPY*	1	180	510	277	0.038	0.229	0.053	0.055	132297	80588
	CVXPY	3				0.039	0.331	0.168	0.154	121999	80152
	CVXPY	5				0.040	0.494	0.258	0.262	121932	80138
	CVXPY + *jit*	1				0.040	**0.255**	**0.039**	**0.057**	132297	80588
	CVXPY + *jit*	3				0.039	0.292	0.124	0.122	121999	80152
	CVXPY + *jit*	5				0.041	**0.391**	**0.204**	**0.191**	121932	80137
	NLP	-	77	355	-	-	13.401	17.881	12.828	121782	77340
	NLP+*jit*	-				-	**1.547**	**1.562**	**1.507**	121782	77340
Example 2	*CVXPY*	1	309	2034	854	0.970	1.284	0.192	0.192	386.77	198.85
	CVXPY	3				0.902	2.056	0.634	0.629	389.27	198.80
	CVXPY + *jit*	1				0.992	**1.259**	**0.167**	**0.152**	389.77	198.85
	CVXPY + *jit*	3				0.974	**1.608**	**0.447**	**0.459**	389.27	198.80
	NLP	-	154	709	-	-	31.602	34.365	37.811	389.27	198.80
	NLP+jit	-				-	**2.375**	**2.099**	**2.060**	389.27	198.80

Table 7.1: Comparison of solution times and optimal costs.

the EnMPC solution time for *maxiters* = 1 and 5 respectively. Even when special just-in-time compilation with jit is used to speed up both EcMPC and EnMPC, Algorithm 2 still presents great improvement requiring 16.48% and 25.27% of the EnMPC solution time for *maxiters* = 1 and 5 respectively. This percentage reduces to 2.50% and 13.06% at $i = 1$. For Example 2, we have a larger state space and hence more constraints in the EcMPC RHOCP. Despite this, we see that for $i = 0$

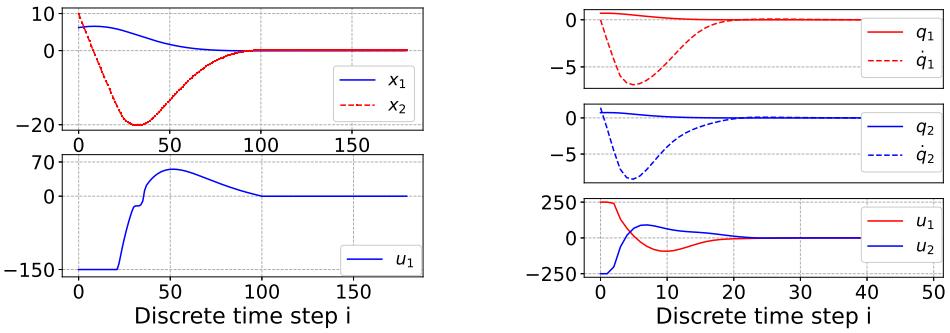


Figure 7.6: Closed-loop state trajectories with REcMPC for Example 6 (left plot) and Example 2 (right plot)

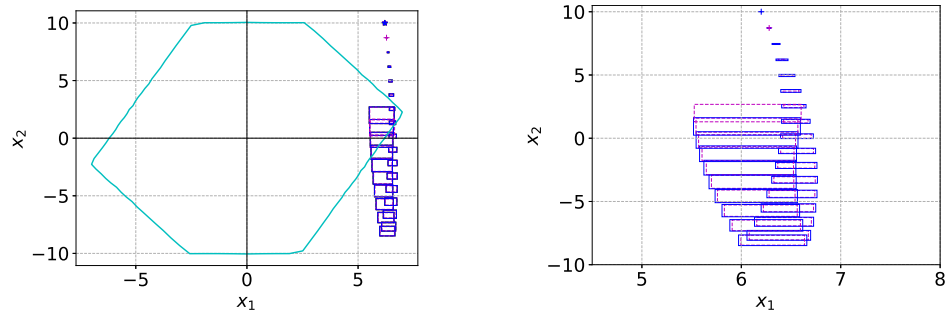


Figure 7.7: Example 6: Optimal and seed tubes for REcMPC: $\mathbf{X}_0^{*,3}$ (blue, solid lines), $\mathbf{X}_1^{0,1}$ (pink dashed). Left: Tube cross-sections for $k = 0, \ldots, N$ and terminal set $\mathcal{X}_N$ (cyan polytope). Right: Tube cross-sections for prediction times $k = 0, \ldots, N-1$.

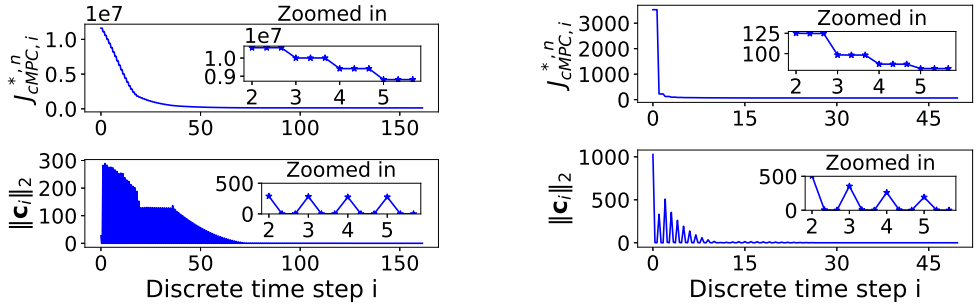


Figure 7.8: Convergence of the REcMPC optimal cost and control perturbation sequence norm $\|\mathbf{c}_i^*\|$ for Example 6 (left plot) and Example 2 (right plot)

Algorithm 2 requires 53.01% and 67.71% of the NLP solution time with jit for both approaches and 4.06% and 6.51% without jit, for *maxiters* $= 1$ and 3 respectively. Again, for $i > 0$, these percentages reduce significantly further. Furthermore, as *maxiters* increases the optimal EcMPC RHOCP cost decreases and converges to the optimal EnMPC RHOCP cost, which is consistent with Theorem 7.3.3.

Robust EcMPC (REcMPC)

The performance of RcMPC (Algorithm 4) presented in Section 7.3.4 was investigated using Examples 1 and 2 with non-zero disturbance bounds of $|w_j(t)| \leq 0.02$, $j = 1, 2$, and $|w_j(t)| \leq 10^{-4}$, $j = 1, 2, 3, 4$ respectively, for all t. All other RHOCP parameters remain the same for Example 6 and Example 2 except in the former $|x_1(t)| \leq 20$, $j = 1, 2$, $x(0) = [6.2, 10]^\intercal$ and in the latter the horizon is shortened to $N = 10$, $Q = 10^{-4}\text{diag}\{1, 1, 1, 1\}$, $R = 10^{-4}\text{diag}\{1, 1\}$ and the constraints are relaxed to $|x_j(t)| \leq 20$, $j = 1, 2, 3, 4$ and $|u_j(t)| \leq 250$, $j = 1, 2$, for all t. The initial seed in both examples was obtained using the initialization strategy described in Section 7.3.4.

Figure 7.6 (left) shows the closed loop trajectories for RcMPC applied to Example 6 with state x_2 reaching a minimum value of -19.980, thus robustly satisfying the constraints. Figure 7.7 shows that, in agreement with Theorem 7.3.5, the seed tube $\mathbf{X}_1^{0,1}$ computed at the first iteration at time $i = 1$ is contained within the optimal tube $\mathbf{X}_0^{*,3}$ computed at the final iteration for $i = 0$. Figure 7.8 demonstrates that, for any time step i, the optimal cost decreases at successive iterations and the perturbation sequence $\mathbf{c}_i^*$ converges to a value close to zero, as expected from Lemma 7.3.3 and Remark 7.3.10. Note that, although this control perturbation converges to zero during the convex program iteration at each horizon time step, there is no guarantee that this perturbation will be smaller at the start of the iteration with each horizon time step i. Thus, $\|\mathbf{c}_i^*\| \not\to 0$ as $i \to \infty$ in Figure 7.8.

7.4 Technique for implicit system models

In this section, we aim to formulate the proposed successive convexification approach for a more generalised systems' description with implicit models. This enables the use of more complex discretisation schemes, as well as the application of the approach to examples with equations of motion in differential-algebraic form (such as multibody systems with kinematic constraints, for example).

7.4.1 Problem formulation

Consider a nonlinear system with state $x(t) \in \mathbb{R}^{n_x}$, control input $u(t) \in \mathbb{R}^{n_u}$ and continuous model of the form

$$f(\dot{x}, x, u) = 0 \tag{7.27}$$

where f is differentiable for all $(\dot{x}, x, u)$ in the operating region $\mathbb{R}^{n_x} \times \mathcal{X} \times \mathcal{U}$ and componentwise convex with respect to $\dot{x}$, x and u.

Assumption 7.4.1. *We assume a discrete-time model can be created of the form*

$$g(x_{i+1}, x_i, u_i) = 0 \tag{7.28}$$

such that g is differentiable for all (x_{i+1}, x_i, u_i) in the operating region $\mathcal{X} \times \mathcal{X} \times \mathcal{U}$ and convexity is preserved, i.e. the elements of $g(\cdot)$ are convex with respect to all $x_{i+1} \in \mathcal{X}$, $x_i \in \mathcal{X}$ and $u_i \in \mathcal{U}$. We further assume the discrete time step is chosen to guarantee $g(\cdot)$ is locally Lipshitz.

We again pose the problem of optimally controlling this system's trajectory $\mathbf{x} : \{x_0, x_1, ...\}$, $\mathbf{u} : \{u_0, u_1, ...\}$ to track a given state and input reference trajectory $\mathbf{x^r} : \{x_0^r, x_1^r, ...\}$, $\mathbf{u^r} : \{u_0^r, u_1^r, ...\}$ where $g(x_{i+1}^r, x_i^r, u_i^r) = 0$ for all $i \geq 0$ subject to a quadratic objective (7.3) and additional initial and polytopic constraints of the form $x_0 = x_{init}$ and (7.5). To solve this problem, we again propose an MPC approach for which a standard RHOCP can take the form

$$\text{InMPC RHOCP: } \mathbf{u}_i^* = \arg\min_{\mathbf{x}_i, \mathbf{u}_i} J_{\text{InMPC}}(\mathbf{x}_i, \mathbf{u}_i) \tag{7.29b}$$

subject to:

$$x_{0|i} = x_i \tag{7.29c}$$

$$x_{k|i} \in \mathcal{X}, \qquad u_{k|i} \in \mathcal{U} \qquad \text{for } k = 0, ..., N-1 \tag{7.29d}$$

$$g(x_{k+1|i}, x_{k|i}, u_{k|i}) = 0 \qquad \text{for } k = 0, ..., N-1 \tag{7.29e}$$

$$x_{N|i} \in \mathcal{X}_N \subseteq \mathcal{X} \tag{7.29f}$$

where $J_{\text{InMPC}}(\mathbf{x}_i, \mathbf{u}_i) = \sum_{k=0}^{N-1} \Big(\|x_{k|i} - x_{k|i}^r\|_Q^2 + \|u_{k|i} - u_{k|i}^r\|_R^2 \Big) + \|x_{N|i} - x_{N|i}^r\|_{Q_N}^2$.

We also make similar assumptions to the explicit nominal case:

Assumption 7.4.2. *We assume the state x_i can be measured at each discrete time step i, the reference trajectory (x_i^r, u_i^r) satisfies* (7.29c)-(7.29f) *for all i, and Q and R are positive definite. We further assume the prediction horizon N, the terminal weight matrix Q_N and the terminal set $\mathcal{X}_N$ are chosen such that there exists a feedback gain K for which the set $\mathcal{X}_N$ is positively invariant for the system* (7.28) *under the control law $u_i = K(x_i - x_i^r) + u_i^r \in \mathcal{U}$, and for all $x_N \in \mathcal{X}_N$*

$$\sum_{i=N}^{\infty} (\|x_i - x_i^r\|_Q^2 + \|u_i - u_i^r\|_R^2) \leq \|x_N - x_N^r\|_{Q_N}^2. \tag{7.30}$$

At each discrete time step i, the implicit model nonlinear MPC (InMPC) RHOCP could be solved online to obtain an optimal control sequence $\mathbf{u}_i^* : \{u_{0|i}, u_{1|i}, \ldots, u_{N-1|i}\}$ and the first element of the sequence $u_i = u_{0|i}$ can be applied. At the next step, the current state x_{i+1} could be measured or estimated. Based on this updated state, a new InMPC RHOCP could be formulated, and the process repeated. However, in this form (7.29), the InMPC RHOCP is a nonlinear program. Thus, one cannot guarantee that it will indeed be solved within a single discrete time step, leading to loss of feasibility and stability guarantees. To address this problem, we again propose to reformulate the RHOCP using a successive linearisation approach. The proposed approach is an extension of REcMPC, now applicable for implicit system models and thus a wider variety of systems. In fact, REcMPC can be seen as a special case of the approach proposed in this section.

7.4.2 Proposed nominal control law

Given a prior pair of state and control trajectories $\mathbf{x}_i^0 : \{x_{0|i}^0, x_{1|i}^0, \ldots, x_{N|i}^0\}$ and $\mathbf{u}_i^0 : \{u_{0|i}^0, u_{1|i}^0, \ldots, u_{N-1|i}^0\}$ using Taylor series the discrete-time dynamics of the system can be linearised as follows :

$$g(x_{k+1|i}, x_{k|i}, u_{k|i}) = g(x_{k+1|i}^0, x_{k|i}^0, u_{k|i}^0) + C_{k|i} s_{k+1|i} + D_{k|i} s_{k|i} + E_{k|i} v_{k|i} + e(x_{k+1|i}, x_{k|i}, u_{k|i}) \tag{7.31a}$$

$$\text{where} \qquad s_{k|i} = x_{k|i} - x_{k|i}^0, \qquad v_{k|i} = u_{k|i} - u_{k|i}^0, \tag{7.31b}$$

$$C_{k|i} = \frac{\partial g}{\partial x_{k+1|i}}\Big|_{(x_{k+1|i}^0, x_{k|i}^0, u_{k|i}^0)}, \quad D_{k|i} = \frac{\partial g}{\partial x_{k|i}}\Big|_{(x_{k+1|i}^0, x_{k|i}^0, u_{k|i}^0)} \quad E_{k|i} = \frac{\partial g}{\partial u_{k|i}}\Big|_{(x_{k+1|i}^0, x_{k|i}^0, u_{k|i}^0)}. \tag{7.31c}$$

Assumption 7.4.3. *The initial seed trajectory* $(\mathbf{x}^0, \mathbf{u}^0)$ *is a feasible (but potentially suboptimal) for constraints* (7.29c)-(7.29f).

Remark 7.4.1. *Due to the convexity of* g *it is known that* $e(x_{k+1|i}, x_{k|i}, u_{k|i})$ *is also componentwise convex in* $x_{k+1|i}$, $x_{k|i}$, $u_{k|i}$ *and* $e(x_{k+1|i}, x_k, u_k) \geq 0$. *Therefore Assumption 7.4.3 (*$g(x^0_{k+1}, x^0_k, u^0_k) = 0$*) and Equation* (7.31a) *imply*

$$C_k s_{k+1|i} + D_{k|i} s_{k|i} + E_{k|i} v_{k|i} \geq 0 \Rightarrow g(x_{k+1|i}, x_{k|i}, u_{k|i}) \geq 0.$$

Based on this linearisation, we can define perturbation sets based on their vertices $S_{k|i} = Co\{s^m_{k|i}, m = 1, ..., n_v\}$, $S^-_{k|i} = Co\{s^{-,m}_{k|i}, m = 1, ..., n_v\}$, $S^+_{k|i} = Co\{s^{+,m}_{k|i}, m = 1, ..., n_v\}$ and formulate a convex program:

$$\text{IcMPC RHOCP} : (\mathbf{c}^*_i, \mathbf{S}^*_i, \mathbf{S}^{+,*}_i, \mathbf{S}^{-,*}_i) = \arg \min_{\mathbf{c}_i,\, \mathbf{S}^+_i,\, \mathbf{S}^-_i, \mathbf{S}_i} J_{\text{IcMPC}}(\mathbf{c}_i, \mathbf{S}_i, \mathbf{x}^0_i, \mathbf{u}^0_i)$$

subject to:

$$S_{0|i} = \{0\} \tag{7.32a}$$

$$S_{k|i} \oplus \{x^0_{k|i}\} \subseteq \mathcal{X}, \text{ for } k = 1, ...N-1 \tag{7.32b}$$

$$S^+_{k|i} \subseteq S_{k|i}, \;\; S^-_{k|i} \subseteq S_{k|i}, \text{ for } k = 1, ..., N \tag{7.32d}$$

$$S_{N|i} \oplus \{x^0_{N|i}\} \subseteq \mathcal{X}_N \tag{7.32e}$$

$$K s_{k|i} + c_{k|i} + u^0_{k|i} \in \mathcal{U} \; \forall s_{k|i} \in S_{k|i}, k = 0, ..., N-1 \tag{7.32f}$$

$$g(x^0_{k+1|i} + s^-_{k+1|i}, \; x^0_{k|i} + s_{k|i}, \; K s_{k|i} + c_{k|i} + u^0_{k|i}) \leq 0$$

$$C_{k|i} s^+_{k+1|i} + (D_{k|i} + E_{k|i} K) s_{k|i} + E_{k|i} c_{k|i} \geq 0$$

$$\text{for } \forall s_{k|i} \in S_{k|i}, \forall s^+_{k+1|i} \in S^+_{k+1|i}, \forall s^-_{k+1|i} \in S^-_{k+1|i} \text{ and } k = 0, ...N-1 \tag{7.32g}$$

where $\oplus$ is the Minkowski sum, $\mathbf{S}^+_i = \{S^+_{1|i}, \ldots, S^+_{N|i}\}$, $\mathbf{S}^-_i = \{S^-_{1|i}, \ldots, S^-_{N|i}\}$, $\mathbf{S}_i = \{S_{0|i}, \ldots, S_{N|i}\} \in S^{N+1}$,

$$J_{\text{IcMPC}}(\mathbf{c}_i, \mathbf{S}_i, \mathbf{x}^0_i, \mathbf{u}^0_i) = \sum_{k=0}^{N-1} \Big(\max_{s_{k|i} \in S_{k|i}} \|x^0_{k|i} + s_{k|i} - x^r_{k|i}\|^2_Q + \max_{s_{k|i} \in S_{k|i}} \|u_{k|i} - u^r_{k|i}\|^2_R \Big) + \max_{s_{N|i} \in S_{N|i}} \|x^0_{N|i} + s_{N|i} - x^r_{N|i}\|^2_{Q_N}$$

and a dual mode prediction strategy of the form

$$u_{k|i} = u^0_{k|i} + v_{k|i} = u^0_{k|i} + K s_{k|i} + c_{k|i} \quad \text{for } k = 0, ...N-1$$

has been used shifting the optimisation from the sequence $\mathbf{u}_i$ to the sequence $\mathbf{c}_i : \{c_{0|i}, ..., c_{N-1|i}\}$. In Equation (7.31c) s_k and v_k can be viewed as perturbations from the original trajectory $\mathbf{x}^0$ and control sequence $\mathbf{u}^0$, respectively. Thus the sets sequence $\mathbf{S}_i \oplus \mathbf{x}_i = \{S_{0|i} \oplus \{x^0_{0|i}\}, \ldots, S_{N|i} \oplus \{x^0_{N|i}\}\}$ can be viewed as a tube containing all possible system trajectories corresponding to the sequence $\mathbf{c}_i$.

Remark 7.4.2. *In comparison to the explicit model formulation in Section 7.3, the use of implicit models dictates that additional sets $S^+_{k|i}, S^-_{k|i}$ have to be defined because implementing both constraints in (7.32g) for a single set $S_{k|i}$ would only be satisfied for a single-trajectory tube ($S_{k|i} = \{0\}$ for all k). In Section 7.4.3 we guarantee that the tube obtained with the proposed formulation ($S_{k|i} \supseteq Co\{s^{-,m}_{k|i}, s^{+,m}_{k|i}, m = 1, ..., n_v\}$) contains the feasible solutions of the original NLP* (7.29b)-(7.29f).

Using the convex RHOCP formulation for implicit models (IcMPC RHOCP), a receding horizon strategy can be formulated as described in Algorithm 5, which optimises both the tube cross sections and control sequences online. As we will prove in the next section, the iterations performed at each discrete time step i converge to a local minimum of the original InMPC RHOCP, eliminating the conservativeness and suboptimality presented by other tube-based approaches. We also show that the iteration can be terminated early without loss of recursive feasibility and stability.

Remark 7.4.3. *The initial seed trajectory can be obtained by reformulating the IcMPC RHOCP in a strategy analogous to the one outlined in Section 7.3. Similarly to EcMPC, the constraints and cost can be expressed as a maximisation over the vertices of $\mathbf{S}_i, \mathbf{S}^+_i, \mathbf{S}^-_i$, allowing the cost to be reformulated to a linear objective with an additional second-order cone constraint on the vertices of $\mathbf{S}_i$. The resulting problem is convex and can thus be solved efficiently using a variety of solvers (see for example [23]).*

Remark 7.4.4. *The representation of $\mathbf{S}_i, \mathbf{S}^+_i, \mathbf{S}^-_i$ causes exponential growth in the number of variables and constraints in IcMPC RHOCP with the state dimension n_x. Alternatively, the use of homothetic sets, as described for EcMPC in Remark 7.4.4, allows the numbers of variables and constraints to depend linearly on n_x and*

Algorithm 5: IcMPC

Offline: Determine K, Q_N, $\mathcal{X}_N$, and an initial seed trajectory $(\mathbf{x}_0^0, \mathbf{u}_0^0)$ satisfying (7.29c)-(7.29f) with $x_0 = x_{\text{init}}$

Online: At each discrete time step $i = 0, 1, \ldots$:

Obtain x_i and set the iteration counter $n \leftarrow 1$;
while $n \leq$ *maxiters and* $\|\mathbf{c}_i^*\| \geq$ *tol* **do**
  Compute $C_{k|i}$, $D_{k|i}$, $E_{k|i}$ for $k = 0, \ldots, N-1$ using (7.31c) and $(\mathbf{x}_i^0, \mathbf{u}_i^0)$;
  Solve nominal RHOCP to obtain $(\mathbf{c}_i^*, \mathbf{S}_i^*, \mathbf{S}_i^{+,*}, \mathbf{S}_i^{-,*})$;
  for $k = 0, \ldots, N-1$ **do**
    Compute $u_{k|i}^* = u_{k|i}^0 + c_{k|i}^* + K(x_{k|i}^* - x_{k|i}^0)$ and $g(x_{k+1|i}^*, x_{k|i}^*, u_{k|i}^*) = 0$ with $x_{0|i}^* = x_i$;
  Update the seed: $(\mathbf{x}_i^0, \mathbf{u}_i^0) \leftarrow (\mathbf{x}_i^*, \mathbf{u}_i^*)$;
  $n \leftarrow n + 1$;
Implement $u_i \leftarrow u_{0|i}^*$;
Set $u_{N|i}^* = K(x_{N|i}^* - x_{N+i}^r) + u_{N+i}^r$ and solve $g(x_{N+1|i}^*, x_{N|i}^*, u_{N|i}^*) = 0$ for $x_{N+1|i}^*$;
Set $\mathbf{u}_{i+1}^0 \leftarrow \{u_{1|i}^*, \ldots, u_{N-1|i}^*, u_{N|i}^*\}$ $\mathbf{x}_{i+1}^0 \leftarrow \{x_{1|i}^*, \ldots, x_{N|i}^*, x_{N+1|i}^*\}$;

the chosen number of vertices of $\mathbf{S_i}$*, respectively. In either case, a reduction in* n_x *allows for computational savings, and a method for achieving this is proposed in Section 7.4.4.*

Remark 7.4.5. *In principle, the approach could be extended to include multirate integrators, providing a scheme similar to the multirate variational MPC scheme discussed in Chapter 6. Compared to that approach, this new multirate IcMPC scheme would offer guarantees of non-conservativeness and allow for a later extension to a robust formulation. However, while such a formulation would reduce the number of constraints and optimisation variables in the RHOCP, it would also increase the size of the state vector. As noted in Remark 7.4.4, the anticipated exponential growth may thus render the multirate approach less computationally efficient than the singlerate version, even for multirate systems. Nevertheless, the suggested improvements in Remark 7.4.4 could address this issue and facilitate the development of such multirate IcMPC formulation, as we plan to explore in future work.*

7.4.3 Nominal feasibility and stability guarantees

In this section we demonstrate the recursive feasibility and stability of the proposed approach. Additionally we prove that the iteration at each horizon time step i

converges to a locally optimal solution of the original InMPC RHOCP.

First, we prove that for non-zero perturbations, the tube contains the original nonlinear system trajectory and converges to it when the iterations are not terminated early. Let

$$X_{k|i} = Co\{x^m_{k|i}, m = 1, ..., n_v\} = \{x^0_{k|i}\} \oplus S_{k|i},$$
$$X^-_{k|i} = Co\{x^{-,m}_{k|i}, m = 1, ..., n_v\} = \{x^0_{k|i}\} \oplus S^-_{k|i},$$
$$X^+_{k|i} = Co\{x^{+,m}_{k|i}, m = 1, ..., n_v\} = \{x^0_{k|i}\} \oplus S^+_{k|i}.$$

Lemma 7.4.1. *If $S_{k+1|i}$ satisfies (7.32d) and $s^{-,m}_{k+1|i}$, $s^{+,m}_{k+1|i}$ satisfy (7.32g) for $m = 1, ..., n_v$ then there exists a $x_{k+1|i} \in X_{k+1|i}$ satisfying $g(x_{k+1|i}, x_{k|i}, u_{k|i}) = 0$ for $\forall x_{k|i} \in X_{k|i}$ with $u_{k|i} = K(x_{k|i} - x^0_{k|i}) + c_{k|i} + c^0_{k|i}$.*

Proof. Constraints (7.32d) imply $S_{k|i} \supseteq Co\{s^{-,m}_{k|i}, s^{+,m}_{k|i}, m = 1, ..., n_v\}$. Furthermore let $z^\lambda = \lambda z^m + (1-\lambda)z^v$ for $\lambda \in [0,1]$, $m, v \in \{1, ..., n_v\}$. Then from Remark 7.4.1

$$\left.\begin{aligned} g(x^{-,m}_{k+1|i}, x^m_{k|i}, u^m_{k|i}) \le 0 \\ g(x^{-,v}_{k+1|i}, x^v_{k|i}, u^v_{k|i}) \le 0 \end{aligned}\right\} \Rightarrow \quad g(x^{-,\lambda}_{k+1|i}, x^\lambda_{k|i}, u^\lambda_{k|i}) \le 0 \quad \text{for any } \lambda \in [0,1]$$
$$\left.\begin{aligned} C_{k|i}s^{+,m}_{k+1|i} + D_{k|i}s^m_{k|i} + E_{k|i}(u^m_{k|i} - u^0_{k|i}) \ge 0 \\ C_{k|i}s^{+,v}_{k+1|i} + D_{k|i}s^v_{k|i} + E_{k|i}(u^v_{k|i} - u^0_{k|i}) \ge 0 \end{aligned}\right\} \Rightarrow g(x^{+,\lambda}_{k+1|i}, x^\lambda_{k|i}, u^\lambda_{k|i}) \ge 0 \text{ for any } \lambda \in [0,1]$$

where $u^m_{k|i} = K(x^m_{k|i} - x^0_{k|i}) + c_{k|i} + c^0_{k|i}$, $u^v_{k|i}$ are defined similarly and $x^\lambda_{k|i} = s^\lambda_{k|i} + x^0_{k|i}$. Based on this and from setting $S_{k+1|i}$ as the convex hull of its vertices it follows that there exists $s^\lambda_{k+1|i} \in Co\{s^{-,\lambda}_{k+1|i}, s^{+,\lambda}_{k+1|i}\} \subseteq S_{k+1|i}$ satisfying $g(x^\lambda_{k+1|i}, x^\lambda_{k|i}, u^\lambda_{k|i}) = 0$ for all $\lambda \in [0,1]$. □

To make notation more precise, at the ith time step and nth iteration of lines 3-8 of Algorithm 1 we denote the seed trajectory as $\mathbf{x}^{0,n}_i$, the seed control sequence as $\mathbf{u}^{0,n}_i$ and the tube as $\mathbf{S}^n_i$. Similarly, we denote the solution of the IcMPC RHOCP in line 4 as $(\mathbf{c}^{*,n}_i, \mathbf{S}^{*,n}_i, \mathbf{S}^{+,*,n}_i, \mathbf{S}^{-,*,n}_i)$, and the optimal objective as $J^{*,n}_{\text{IcMPC},i} = J_{\text{IcMPC}}(\mathbf{c}^{*,n}_i, \mathbf{S}^{*,n}_i, \mathbf{x}^{0,n}_i, \mathbf{u}^{0,n}_i)$.

Theorem 7.4.1 (Recursive feasibility)**.** *If the initial seed trajectory* $(\mathbf{x}_i^0, \mathbf{u}_i^0)$ *is feasible w.r.t. constraints* (7.29c)-(7.29f) *and the Assumptions 7.27, 7.4.2, 7.4.3 hold, then the nominal RHOCP in step 4) of Algorithm 5 is feasible at each iteration and for* $i \geq 0$.

Proof. Let $c_{k|i} = 0$, $k = 0, \ldots, N-1$ and $S_{k|i} = \{0\}$ for $k = 0, \ldots, N$ reducing the constraints in the nominal IcMPC RHOCP to $\{x_{k|i}^0\} \subseteq \mathcal{X}$,$u_{k|i}^0 \in \mathcal{U}$, $\{x_{N|i}^0\} \subseteq \mathcal{X}_N$. In this case, the trajectory takes the form $(\mathbf{x}_i, \mathbf{u}_i) = (\mathbf{x}_i^0, \mathbf{u}_i^0)$ and based on Assumption 7.4.3 is a feasible (but possibly suboptimal) solution of IcMPC RHOCP at $i = 0$. Feasibility of the trajectory $(\mathbf{x}_{i+1}^0, \mathbf{u}_{i+1}^0)$ at any subsequent horizon steps is then guaranteed by constraints $(7.32b)$-$(7.32e)$ and the conditions placed on the choice of set $\mathcal{X}_N$ in Assumption 7.4.2. □

Theorem 7.4.2. *For all* $i \geq 0$ *and for all* $n \geq 1$

$$J_{InMPC}(\mathbf{x}_i^{0,n+1}, \mathbf{u}_i^{0,n+1}) \leq J_{IcMPC}(\mathbf{c}_i, \mathbf{S}_i^n, \mathbf{x}_i^{0,n}, \mathbf{u}_i^{0,n}) \tag{7.33}$$

for $(\mathbf{x}_i^{0,n+1}, \mathbf{u}_i^{0,n+1})$ *obtained by steps 4-7 of Algorithm 5.*

Proof. It follows from the nominal IcMPC RHOCP formulation that $\mathbf{x}_i^{0,n+1}$ belongs to the tube $\mathbf{S}_i^n \oplus \{x_k^{0,n}\}$. The statement then follows from Equation (7.31b), steps 5-7 in Algorithm 5 and the maximisation formulation of the IcMPC cost returning the maximum cost over the tube $\mathbf{S}_i^n$. In more detail

$$\begin{aligned}
\|x_{k|i}^{0,n+1} - x_{k|i}^r\|_Q^2 &\leq \max_{s_{k|i} \in S_{k|i}} \|x_{k|i}^{0,n} + s_{k|i} - x_{k|i}^r\|_Q^2, \\
\|u_{k|i}^{0,n+1} - u_{k|i}^r\|_Q^2 &\leq \max_{s_{k|i} \in S_{k|i}} \|u_{k|i}^{0,n} + K s_{k|i} + c_{k|i} - u_{k|i}^r\|_R^2, \\
\|x_{N|i}^{0,n+1} - x_{N|i}^r\|_Q^2 &\leq \max_{s_{N|i} \in S_{N|i}} \|x_{N|i}^{0,n} + s_{N|i} - x_{N|i}^r\|_{Q_N}^2,
\end{aligned}$$

and Equation (7.33) follows from summing the terms before and after the inequality sign for all $k = 0, \ldots, N-1$ to obtain the expressions for $J_{\text{InMPC}}(\mathbf{x}_i^{0,n+1}, \mathbf{u}_i^{0,n+1})$ and $J_{\text{IcMPC}}(\mathbf{c}_i, \mathbf{S}_i^n, \mathbf{x}_i^{0,n}, \mathbf{u}_i^{0,n})$. □

Theorem 7.4.3. *For all* $i \geq 0$ *and for all* $n \geq 1$*, we have*

$$J_{IcMPC}^{*,n+1} \leq J_{IcMPC}^{*,n}. \tag{7.34}$$

Proof. From Theorem 7.4.1 and Theorem 7.4.2 it follows that a suboptimal solution exists $\mathbf{c}_i = 0$ and $\mathbf{S}_i = \{\{0\}, \ldots, \{0\}\}$ and thus

$$J_{\text{IcMPC}}(\{0\}, \{0\}, \mathbf{x}_i^{0,n+1}, \mathbf{u}_i^{0,n+1}) = J_{\text{InMPC}}(\mathbf{x}_i^{0,n+1}, \mathbf{u}_i^{0,n+1}) \tag{7.35}$$

$$J_{\text{InMPC}}(\mathbf{x}_i^{0,n+1}, \mathbf{u}_i^{0,n+1}) \leq J_{\text{IcMPC}}(\mathbf{c}_i^{*,n}, \mathbf{S}_i^{*,n}, \mathbf{x}_i^{0,n}, \mathbf{u}_i^{0,n}). \tag{7.36}$$

From Theorem 7.4.1, optimality and (7.35) it follows that

$$J_{\text{IcMPC}}(\mathbf{c}_i^{*,n}, \mathbf{S}_i^{*,n}, \mathbf{x}_i^{0,n}, \mathbf{u}_i^{0,n}) \leq J_{\text{InMPC}}(\mathbf{x}_i^{0,n}, \mathbf{u}_i^{0,n}). \tag{7.37}$$

(7.34) follows from the combination of (7.35), (7.36), (7.37). □

Theorem 7.4.4. *For all $i \geq 0$, the iteration on lines 2-8 of Algorithm 5 converges to a seed trajectory $(\mathbf{x}_i^{0,n}, \mathbf{u}_i^{0,n})$ such that $\mathbf{c}_i^{*,n} = 0$ and $\mathbf{S}_i^{*,n} = \{\{0\}, \ldots, \{0\}\}$ is an optimal solution of the IcMPC RHOCP in the limit as $n \to \infty$.*

Proof. Based on Assumption 7.4.2 and Lemma 7.4.3, the proof is analogous to the proof of Theorem 7.3.2.

Theorem 7.4.5. *The iteration defined in steps 2-9 of Algorithm 5 converges to a local minimum of InMPC RHOCP* (7.29b)-(7.29f).

Proof. The proof can be found in Appendix D.

Theorem 7.4.6. *Given Assumptions 7.27 and 7.4.2, the control law of Algorithm 5 ensures that $x_{i+1}^{\delta} = x_i^{\delta} = u_i^{\delta} = 0$ with $x_i^{\delta} = x_i - x_i^r$ and $u_i^{\delta} = u_i - u_i^r$ is an asymptotically stable equilibrium of the system* (7.28) *(i.e. $g(x_{i+1}^{\delta}, x_i^{\delta}, u_i^{\delta}) = 0$), with region of attraction consisting of the initial conditions x_0 of* (7.28) *for which there exists a control sequence such that $u_i \in \mathcal{U}$ and $x_i \in \mathcal{X}$ for $k = 0, \ldots, N-1$, and $x_N \in \mathcal{X}_N$.*

Proof. The proof is analogous to that of Theorem 7.3.4 in Section 7.3.3.

7.4.4 Proposed variational reformulation

In this section, we present how the proposed approach can accommodate a structure-preserving model and discuss how such a model can reduce the number of variables and constraints in the respective RHOCP. These developments are demonstrated

for a system with an explicit continuous model, but the extension to implicit models (such as for systems with constraints) is analogous.

Model formulation and terminal set calculation

We consider a general mechanical system with configuration $q(t) \in \mathbb{R}^{n_q}$ and Lagrangian of the form

$$\mathfrak{L}(q, \dot{q}) = \frac{1}{2}\dot{q}^T M \dot{q} - V(q) \tag{7.38}$$

Using the continuous forced Euler-Lagrange equations, the continuous model of the system motion under the influence of control forces $u(t) \in \mathbb{R}^{n_u}$ can be derived as

$$\ddot{q} = -M^{-1}\nabla_q V(q) + u \tag{7.39}$$

Assumption 7.4.4. *We assume a regular $\mathfrak{L}$, symmetric invertible M, polytopic configuration constraints $q \in \mathcal{Q}$ and assume the expression $M^{-1}\nabla_q V(q)$ is concave.*

To discretise the equations of motion, we formulate a discrete approximation of the Lagrangian and derive a discrete-time system model using the variational integrator presented in Section 2.3.3:

$$\begin{aligned} &g(q_{k+1}, q_k, q_{k-1}, u_k, u_{k-1}) = -q_{k+1} + 2q_k - q_{k-1} - \\ &\tfrac{\Delta t^2}{2}(M^{-1}\nabla_{\eta_k} V(\eta_k) + M^{-1}\nabla_{\eta_{k-1}} V(\eta_{k-1}) + \tfrac{\Delta t^2 M^{-1}}{2}(u_{k-1} + u_i)) \end{aligned} \tag{7.40}$$

for $\eta_k = \frac{q_{k+1}+q_k}{2}$. To implement initial and terminal conditions on the configuration and velocity (or momentum), the equivalent Hamiltonian formulation of the variational model can be used:

$$\begin{aligned} 0 = y(x_{k+1}, x_k, u_k) &= \begin{bmatrix} r(q_{k+1}, x_k, u_k) \\ f(x_{k+1}, q_k, u_k) \end{bmatrix} \\ &= \begin{bmatrix} -q_{i+1} + q_k - \frac{\Delta t^2}{2} M^{-1}\nabla_{\eta_k} V(\eta_k) + \Delta t M^{-1} p_i - \frac{\Delta t^2}{2} M^{-1} u_k \\ q_{k+1} - q_k - \frac{\Delta t^2}{2} M^{-1}\nabla_{\eta_i} V(\eta_k) - \Delta t M^{-1} p_{k+1} + \frac{\Delta t^2}{2} M^{-1} u_k \end{bmatrix} \end{aligned} \tag{7.41}$$

Here Δt denotes the discrete time step and $x_i = [q_i^T, p_i^T]$ where $p_i \in \mathbb{R}^{n_q}$ is the discrete conjugate momentum [1].

Remark 7.4.6. *Notably, the model* (7.40) *has reduced dimensionality* ($g \in \mathbb{R}^{n_q}$) *compared to its equivalent reformulation* (7.41) ($y \in \mathbb{R}^{2n_q}$) *and to other standard Euler or Runge-Kutta models used to discretise* (7.39) *in which both the configuration and the velocity are simulated in time.*

Remark 7.4.7. *Based on Assumption 7.4.4, the continuous model* (7.39) *can be rewritten as a convex implicit function. Using both* (7.40) *and* (7.41) *the discrete model remains a convex function, something that is not guaranteed with higher stage Runge-Kutta methods or other higher order standard methods. Thus the variational model provides a convex, second-order approximation of the system dynamics, which can simulate energy and momenta accurately even in long-term simulations larger time steps (in the presence of forcing, any momentum conservation laws from the continuous case are accurately preserved in the discrete simulation as guaranteed by the Discrete Noether Theorem with Forcing [19]). As we will discuss in Section 7.4.4, it also allows for a reduction in the number of optimisation variables and constraints of an OCP.*

Variational RHOCP formulation

A IcMPC RHOCP formulation can be created using only the implicit model (7.41) for $k = 0, ..., N-1$ as presented in (7.32a)-(7.32g) with a state vector comprising of both the configuration and the momentum instances $x_{k|i} = [q_{k|i}^T, p_{k|i}^T]$. Alternatively, in the cases where no cost weights are placed on the velocity/momentum, a second formulation can be made which reduces the number of constraints and variables based on the configuration-only model in (7.40) as follows:

VcMPC RHOCP :

$$(\mathbf{c}_i^*, \mathbf{S}_i^*, \mathbf{S}_i^{+,*}, \mathbf{S}_i^{-,*}, Z_{0|i}^*, Z_{N|i}^*, Z_{N|i}^{+,*}, Z_{N|i}^{-,*}) = \arg \min_{\substack{\mathbf{c}_i, \mathbf{S}_i^+, \mathbf{S}_i^-, \\ \mathbf{S}_i, Z_{0|i}, Z_{N|i}, \\ Z_{N|i}^+, Z_{N|i}^-}} J_{\text{IcMPC}}(\mathbf{v}_i, \mathbf{S}_i, Z_{N|i}, \mathbf{q}_i^0, x_N^0, \mathbf{u}_i^0)$$

subject to:

$$Z_{0|i} = \{0\} \tag{7.42a}$$

$$S_{k|i} \oplus \{q_{k|i}^0\} \subseteq \mathcal{Q}, \text{ for } k = 1, ...N-1 \tag{7.42b}$$

$$S^+_{k|i} \subseteq S_{k|i}, \;\; S^-_{k|i} \subseteq S_{k|i}, \text{ for } k = 1, ..., N-1 \tag{7.42c}$$

$$Z^+_{N|i} \oplus \{x^0_{N|i}\} \subseteq \mathcal{X}_N, \;\; Z^-_{N|i} \oplus \{x^0_{N|i}\} \subseteq \mathcal{X}_N \tag{7.42d}$$

$$Z^+_{N|i} \subseteq Z_{N|i}, \;\; Z^-_{N|i} \subseteq Z_{N|i} \tag{7.42e}$$

$$v_{k|i} + u^0_{k|i} \in \mathcal{U} \quad \text{for } k = 0, ..., N-1 \tag{7.42f}$$

$$\begin{aligned} &r(q^0_{1|i} + s^-_{1|i},\; x^0_{0|i} + z_{0|i},\; v_{0|i} + u^0_{0|i}) \leq 0 \\ &F_{0|i}s^+_{1|i} + G_{0|i}z_{0|i} + Y_{0|i}v_{0|i} \geq 0 \quad \text{for } \forall z_{0|i} \in Z_{0|i}, \forall s^+_{1|i} \in S^+_{1|i}, \forall s^-_{1|i} \in S^-_{1|i} \end{aligned} \tag{7.42g}$$

$$\begin{aligned} &g(q^0_{k+1|i} + s^-_{k+1|i},\; q^0_{k|i} + q_{k|i}, q^0_{k-1|i} + s^-_{k-1|i},\; v_{k|i} + u^0_{k|i},\; v_{k-1|i} + u^0_{k-1|i}) \leq 0 \\ &C_{k|i}s^+_{k+1|i} + D_{k|i}s_{k|i} + H_{k|i}s_{k-1|i} + E_{k|i}v_{k|i} + P_{k|i}v_{k-1|i} \geq 0 \\ &\text{for } \forall s_{k-1|i} \in S_{k-1|i},\; \forall s_{k|i} \in S_{k|i},\; \forall s^+_{k+1|i} \in S^+_{k+1|i},\; \forall s^-_{k+1|i} \in S^-_{k+1|i} \text{ and } k = 1, ...N-1 \end{aligned} \tag{7.42h}$$

$$\begin{aligned} &f(x^0_{N|i} + z^-_{N|i},\; q^0_{N-1|i} + s_{N-1|i},\; v_{N-1|i} + u^0_{N-1|i}) \leq 0 \\ &L_{N-1|i}z^+_{N|i} + P_{N-1|i}s_{N-1|i} + T_{N-1|i}v_{N-1|i} \geq 0 \\ &\qquad \text{for } \forall s_{N-1|i} \in S_{N-1|i}, \forall z^+_{N|i} \in Z^+_{N|i}, \forall z^-_{N|i} \in Z^-_{N|i} \end{aligned} \tag{7.42i}$$

where the variational convex RHOCP is denoted VcMPC RHOCP, $s_{k|i} = q_{k|i} - q^0_{k|i}$, $x_{k|i} = x_{k|i} - x^0_{k|i}$, $s_{0,i} = z_{0,i}[0 : n_q]$, $Z_{k,i} = Co\{z^m_{k,i} \in \mathbb{R}^{2n_q}, m = 0, ..., 2n_q\}$, $S_{k,i} = Co\{s^m_{k,i} \in \mathbb{R}^{n_q}, m = 0, ..., n_q\}$ and the plus and minus sets are defined similarly. Additionally the matrices $(F_{0|i}, G_{0|i}, Y_{0|i})$, $(C_{k|i}, D_{k|i}, H_{k|i}, E_{k|i}, P_{k|i})$, $(L_{N-1|i}, P_{N-1|i}, T_{N-1|i})$ are defined similarly to (7.31a) with respect to the elements of $r(\cdot)$, $g(\cdot)$, and $f(\cdot)$ respectively with the linearisation performed around the seed configuration trajectory $\mathbf{q}^0$ and the given initial state $x^0_i = [(q^0_i)^T, (p^0_i)^T]$. Here $\mathbf{q}^0_i : \{q^0_{0|i}, q^0_{1|i}, \ldots, q^0_{N-1|i}\}$ and

$$\begin{aligned} &J_{\text{VcMPC}}(\mathbf{v}_i, \mathbf{S}_i, Z_{N|i}, \mathbf{q}^0_i, x^0_N, \mathbf{u}^0_i) = \textstyle\sum_{k=0}^{N-1}(\|u^0_{k|i} + v_{0|i} - u^r_{k|i}\|^2_R \\ &+ \max_{s_{k|i} \in S_{k|i}} \|q^0_{k|i} + s_{k|i} - q^r_{k|i}\|^2_Q) + \max_{z_{N|i} \in Z_{N|i}} \|x^0_{N|i} + z_{N|i} - x^r_{N|i}\|^2_{Q_N} \end{aligned}$$

but constraints on the velocity can also be placed using forward, backward or central difference approximation. In this formulation, we have used (7.40) to define the model constraints for $k = 1, ..., N-1$ and Equations (7.41) to define the initial and terminal constraints. The terminal set and cost can, in this case, be computed based on (7.41), guaranteeing convergence of both the configuration and momentum to an equilibrium point. Such formulation maintains feasibility guarantees due to

the equivalence of the model (7.40) and (7.41). Steps 5-6 in Algorithm 5 must also be replaced with

$$\begin{aligned} &\text{At } k=0 && u^*_{0|i} = u^0_{0|i} + v^*_{0|i}, \quad r(q^*_{1|i}, x^*_{0|i}, u^*_{0|i}) = 0 \text{ with } x^*_{0|i} = x_i \\ &\text{For } k = 1, ..., N-1 && u^*_{k|i} = u^0_{k|i} + v^*_{k|i}, \quad g(q^*_{k+1|i}, q^*_{k|i}, q^*_{k-1|i}, u^*_{k|i}, u^*_{k-1|i}) = 0 \end{aligned}$$

Even though constraints (7.42g) have to be encoded for three sets rather than two in the standard formulation in (7.32g), as we will demonstrate in Section 7.4.5, due to the smaller dimensionality of the elements of the sets in the variational formulation, such formulation allows for the reduction in both the number of optimisation variables and constraints. Furthermore, due to Theorem 7.4.5, it is guaranteed that the sequence of convex problems will converge to a local optimum of the original nonlinear OCP with (7.29e) replaced by (7.40) for steps $1, .., N-1$ and (7.41) for steps $0, N$. As discussed in the previous chapters, such variational OCP formulations have been proved to demonstrate conservation properties in their solutions and thus the sequence of convex programs is guaranteed to converge to a structure-preserving solution.

7.4.5 Numerical examples

In this section the numerical results are obtained by applying the proposed approach with a variational RHOCP formulation using Python and the $CVXPY$ library [179]. The RHOCP constraints are implemented by solving each constraint for each of the vertices the perturbation sets. For all experiments $maxiter = 3$ and $tol = 10^{-6}$.

Example 6: First we consider the example system presented in Section 7.3.7 with

$$\mathfrak{L}(q, \dot{q}) = \tfrac{1}{2}(\dot{q})^T \dot{q} - 0.2e^{-q[1]}, \quad f(\dot{q}, u) = \begin{bmatrix} u[1] - \dot{q}[1] - 0.2 \\ u[2] \end{bmatrix}$$

where $n_q = 2$, $n_u = 2$ and f represents the generalisd forces acting on the system. The discrete model is obtained using the forced singlerate variational integrator from Chapter 2, Section 2.3.3, and discrete time step $\Delta t = 8 \times 10^{-3}$s. A VcMPC RHOCP with $N = 14$, $Q = 1$, $R = \text{diag}\{1, 1\}$, initial condition $q[0](0) = q[1](0) = 2$,

$\dot{q}[1](0) = \dot{q}[2](0) = 2$, constraints $|q[1](t)| \leq 10$, $|q[2](t)| \leq 10$, $|u[1](t)| \leq 150$, $|u[2](t)| \leq 150$ and reference solution $q_i^r = 0, u_i^r = 0$ for all i.

Example 7: We also consider the Fermi-Pasta-Ulam–Tsingou (FPUT) problem introduced in Chapter 4 with $n_q = 2$, $n_u = 2$,

$$\mathfrak{L}(q, \dot{q}) = \tfrac{1}{2}(\dot{q})^T\dot{q} - \tfrac{\eta^2(q[1]+q[2])^2}{4} - q[1]^3 - q[2]^3, \quad f(u) = u$$

with $\eta = 50$. The discrete model is again obtained using the forced variational integrator and $\Delta t = 10^{-2}$s. The VcMPC RHOCP is solved with $N = 10$, $Q = 0.1$, $R = \text{diag}\{0.1, 0.1\}$, reference solution $q_i^r = 0, u_i^r = 0$ for $\forall i$, constraints $|q[1](t)| \leq 10$, $|q[2](t)| \leq 10$, $|u[1](t)| \leq 33$, $|u[2](t)| \leq 33$ and initial conditions

$$\begin{bmatrix} q[1](0) \\ q[2](0) \end{bmatrix} = E\begin{bmatrix} 1 \\ 1 \end{bmatrix}, \ \begin{bmatrix} \dot{q}[1](0) \\ \dot{q}[2](0) \end{bmatrix} = E\begin{bmatrix} 1/\eta \\ 1 \end{bmatrix}, \ E = \tfrac{1}{\sqrt{2}}\begin{bmatrix} -1 & 1 \\ 1 & 1 \end{bmatrix}.$$

Nominal IcMPC:

Figure 7.9 demonstrates the closed-loop trajectories for both examples obtained using Algorithm 5 with the variational changes discussed in Section 7.4.4. In general the conjugate momentum and its change are defined as $p = \frac{\partial \mathcal{L}(q,\dot{q})}{\partial q}$, $\dot{p} = \frac{\partial \mathcal{L}(q,\dot{q})}{\partial \dot{q}}$, and thus for the system in Example 6 $p[1]$ is conserved. Based the Forced Noether's Theorem [1], this is equivalent to the following discrete conservation law

$$\Psi_{k|i} = p_{k|i} - p_{0|i} - h\sum_{k=0}^{k-1} f(\frac{q_{k+1|i} - q_{k|i}}{h}, u_{k|i}) = 0$$

Using the trajectory and control sequence result from the last iteration at $i = 0$, in Figure 7.10 it is demonstrated that the discrete conservation law is indeed preserved by the successive approach. In Table 7.2 it is also shown that the proposed variational formulation (7.42g)-(7.42i) reduces the number of model constraints and optimisation variables compared to an Euler formulation of (7.32g). The number of constraints will be higher with a multi-stage Runge-Kutta scheme.

Lastly, the performance of the receding horizon scheme itself is demonstrated. In Figure 7.12 it is shown that for both examples at successive iterations and discrete time steps the optimal predicted cost is non-increasing and $\|\mathbf{c}_i^*\| \to 0$ as expected from Theorems 7.4.3 and 7.4.4. In Figure 7.11 one can also see the rapid convergence of the tube to a single trajectory within a single iteration.

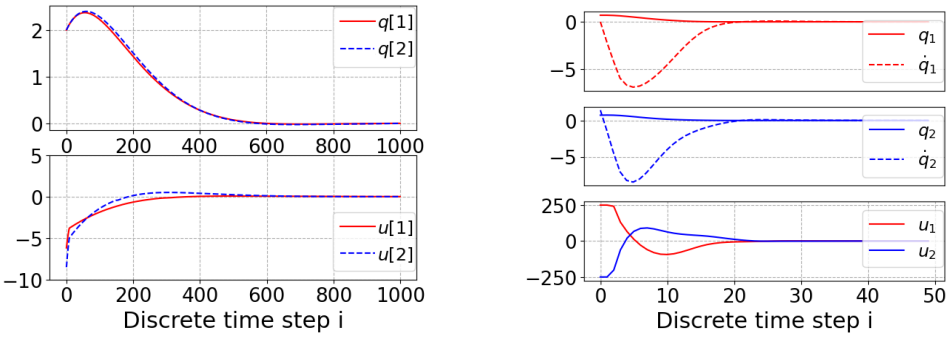


Figure 7.9: Closed-loop state trajectories for Example 6 (left) and Example 7 (right)

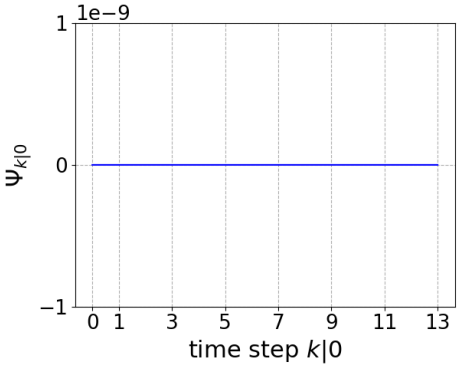


Figure 7.10: Example 6: Demonstration of the conservation properties of the variational cMPC approach

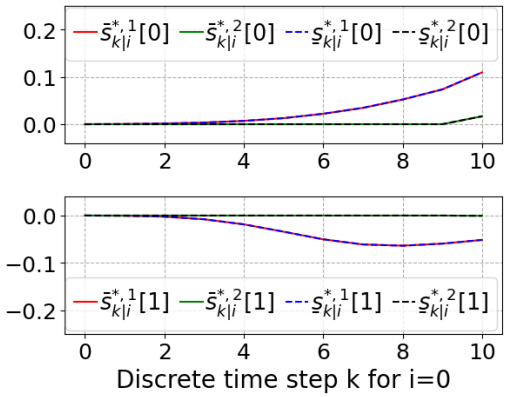


Figure 7.11: Example 7: Convergence of the tube shown through the size of the perturbations between iterations 1 and 2 at $i=0$

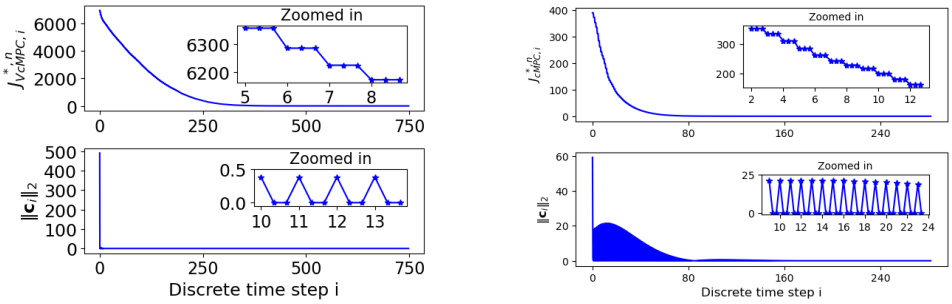


Figure 7.12: Convergence of the IcMPC optimal cost and control perturbation sequence norm $\|\mathbf{c}_i^*\|$ for Example 6 (left plot) and Example 7 (right plot)

Example	Number of model constraints		Number of optimisation variables	
	IcMPC RHOCP	VcMPC RHOCP	IcMPC RHOCP	VcMPC RHOCP
	$Nn_q 2^{4n_q+2}$	$\frac{N+1}{2} n_q 2^{3n_q+2}$	$Nn_u + n_q(12N+4)$	$Nn_u + n_q(6N+10)$
6	28672	3840	372	216
7	20480	2816	268	160

Table 7.2: Demonstration of the RHOCP Size for the IcMPC and VcMPC approaches.

8

Conclusion

8.1 Contributions of this dissertation

This dissertation is focused on the development of methods for simulation, optimisation and control of systems which exhibit dynamics on different time scales. The key contributions of this thesis to the field can be summarised as follows:

Extension of structure-preserving simulation schemes

Multirate variational integrators: In Chapter 3, we presented a detailed mathematical analysis of the multirate variational integrator proposed by [3]. We extended previous works by proving its structure-preserving properties and its order of accuracy when simulating a general class of forced systems. We also derived its formulation for constrained forced systems. The resulting schemes were applied to several examples, including some beyond the limits of our theoretical assumptions. In all cases, the simulation's order of accuracy matched theoretical expectations and demonstrated structure-preserving solutions. Furthermore, we showed that this approach is applicable to nonlinear systems without decoupling the equations of motion, offering significant computational savings for both singlerate and multirate systems.

Linearisation strategy for variational models: In Chapter 6, we proposed a linearisation strategy for singlerate and multirate variational models that retains the

structure-preserving properties of the discrete model. The strategy uses quadratic and linear Taylor series approximations of the Lagrangian and generalised forces, respectively, providing new means for computing linearisation error bounds and allowing for the formulation of structure-preserving Jacobian linearisation models. The conservation properties of the method and its usefulness for linearisation-based optimisation control schemes were demonstrated in Chapter 6.

Extension of structure-preserving optimal control schemes

We continued our study of the multirate variational approach by providing a detailed analysis of its use in an optimal control scheme. Building on previous literature, we formulated the resulting necessary optimality conditions in a continuous- and discrete-time setting. Consequently, we proved the order of accuracy and structure-preserving properties of the resulting discrete-time adjoint system under mild assumptions for a general system example. These findings were tested on the control of a common multirate benchmark system and on the first practical application of the approach- the simultaneous vibration and attitude control of a flexible satellite.

Novel multirate NMPC scheme

We proposed a novel tube-based NMPC strategy for discrete multirate systems. The proposed scheme utilises the variational approach to reduce the size of the RHOCP and allow a longer prediction horizon time step compared to the discretisation step used in the resolution of the fast dynamics. This enables great computational savings compared to singlerate schemes while ensuring recursive feasibility and stability. The nonlinear problems are approximated using a sequence of convex programs through successive linearisation around a seed trajectory. This is achieved using the proposed variational linearisation approach, maintaining the conservation properties of the model as well as providing alternative means for computing linearisation error bounds. Numerical examples are provided to illustrate the multirate approach, its conservation properties and computational savings.

Novel convex approach for robust trajectory optimisation and receding horizon control (cMPC and RcMPC)

We proposed a novel robust nonlinear model predictive control strategy for systems with nonlinear dynamics and convex state and control constraints. Using a sequential convex approximation approach and a difference of convex functions representation of the dynamics, the scheme constructs tubes that contain predicted model trajectories, accounting for approximation errors and disturbances and guaranteeing constraint satisfaction. Based on this formulation, the original nonlinear OCP is solved as a sequence of convex programs.

We develop the scheme initially in the absence of external disturbances and show that the proposed nominal approach is non-conservative, with the solutions of successive convex programs converging to a locally optimal solution for the original optimal control problem. We extend the approach to the case of additive disturbances using a novel strategy for selecting linearisation points. As a result, we formulate a robust receding horizon strategy with guarantees of recursive feasibility and closed-loop system stability, allowing termination of the convex program iteration after any number of iterations.

This theoretical analysis is carried out for systems with explicit models and findings are supported by numerical examples that demonstrate the non-conservativeness, convergence, and efficiency of the approach. The formulation, analysis and testing are then extended to systems with implicit models in the absence of disturbances. The use of variational models is considered in detail, providing structure-preserving solution and computational savings facilitated by the reduction in the number of constraints and optimisation variables.

Practical applications to the aerospace domain

This thesis has made advances in two control problems in the aerospace domain.

6DOF Spacecraft trajectory design in three-body gravitational environment: Firstly, we developed a novel variational model for 6DOF spacecraft motion in the three-

body gravitational environment under the influence of external forcing, for example, from electrodynamic tethers, solar sails, external torque or thrust controls. The model is developed based on the variational principle for constrained dynamics using a unit-norm quaternion constraint and generalised coordinates comprising the orbital coordinates and the attitude quaternions. The variational derivation guarantees structure-preserving properties of the scheme for both uncontrolled simulations and optimal control trajectory solutions, thus providing a qualitatively better and more computationally efficient discrete system simulation than previously available models using standard discretisation and integration schemes. Furthermore, a multirate formulation of the variational model is derived, and a study is performed to investigate to what extent the multirate approach can help improve the computational cost of simulating and optimally controlling spacecraft in the three-body environment.

Simultaneous manoeuvre and vibration control of flexible satellites: Secondly, we looked at the problem of simultaneous manoeuvre and vibration control of satellites equipped with flexible appendages. For this purpose, we implement the multirate variational approach for simultaneous slewing and vibration control of flexible spacecraft. Considering dynamics on different time scales, this formulation allows us to discretise the dynamics on different time scales without the need to decouple the equations of motion as other competitive approaches. The multirate formulation thus achieves great computational savings in the simulation and control of the system with well-understood accuracy. Simulation results for a single-axis rotational manoeuvre demonstrate vibration suppression and achieve the same accuracy as the singlerate method at a reduced computational cost.

8.2 Directions for future research

There are multiple possible directions to improve and extend this work.

Global error and stability analysis of MVIs and Multirate DMOC

This thesis provides a proof of the local error of approximation achieved for simulations and optimal control solutions using MVI and Multirate DMOC for a specific class of systems under mild assumptions. Despite numerical results supporting the validity of these proofs for a wider range of systems, a more general theoretical analysis, including stability and global error investigations, remains an open research topic.

Advancements in cMPC and RcMPC

The formulation and testing of RcMPC for implicit models are currently in progress. Furthermore, it is important to note that both cMPC and RcMPC approaches experience (for some tube formulations) exponential growth in the number of constraints as the state dimension increases, as highlighted in Chapter 7. Although strategies for addressing this challenge have been proposed, their implementation and comparative benchmarking against other robust tube MPC schemes are yet to be completed.

As mentioned in Section 7.4.2, such extension would potentially allow for the formulation of a multirate IcMPC scheme, which provides qualitative better models of the system behaviour, reduces the size of the RHOCP and increases the available time for its solution, while guaranteeing feasibility, stability and in the nominal case- non-conservativeness.

Formulation of a robust distributed control scheme based on RcMPC

Up to now, we have explored RcMPC as a trajectory design and receding horizon control tool for a single agents. Moving forward, our goal is to leverage it as a foundation for developing a novel approach to decentralised control of multiple heterogeneous agents in the presence of disturbances. We aim to test the resulting approach for both drone and spacecraft swarm control.

Learning-based control

Work has already began by colleagues on the use of system models learned from data in the context of cMPC and RcMPC [220, 221]. This is an exciting direction with multiple theoretical and practical opportunities for both single and multi-agent trajectory design and control.

Orbital transfer via attitude control

Finally, we aim to advance our work on modelling and simulating satellites in a three-body gravitational environment. Building on the example system from Chapter 4 and utilising the proposed multirate control schemes, we plan to perform an optimal point-to-point transfer using only attitude motion control. Preliminary tests suggest that this is feasible within strong electromagnetic fields, due to the effects of coupled electrodynamic forces.

Appendices

A

Appendix: MVI derivation for forced systems

In this appendix we include the proof for Theorem 3.4.1 deriving the discrete forced multirate equations of motion. We begin from the discrete Lagrange-d'Alembert principle stated in (3.23):

$$\begin{aligned} 0 =& \delta S_{\mathrm{d}}(q_{\mathrm{d}}^{\mathrm{s}}, q_{\mathrm{d}}^{\mathrm{f}}) \cdot (\delta q_{\mathrm{d}}^{\mathrm{s}}, \delta q_{\mathrm{d}}^{\mathrm{f}}) + W_{\mathrm{d}}(q_{\mathrm{d}}^{\mathrm{s}}, q_{\mathrm{d}}^{\mathrm{f}}, u_{\mathrm{d}}) = \delta \sum_{k=0}^{N-1} L_{\mathrm{d}}^{k}(q_k^{\mathrm{s}}, q_{k+1}^{\mathrm{s}}, q_k^{\mathrm{f}}) \\ &+ \sum_{k=0}^{N-1} \Big(F_k^{\mathrm{s}-} \cdot \delta q_k^{\mathrm{s}} + F_k^{\mathrm{s}+} \cdot \delta q_{k+1}^{\mathrm{s}} + \sum_{m=0}^{\mathbb{p}-1} (f_k^{\mathrm{f},m,-} \cdot \delta q_k^{\mathrm{f},m} + f_k^{\mathrm{f},m,+} \cdot \delta q_k^{\mathrm{f},m+1}) \Big). \end{aligned} \tag{A.1}$$

We consider variations of the variables q_k^{s} and $q_k^{\mathrm{f},m}$ for $k = 0, \ldots, N-1$, $m = 0, \ldots, \mathbb{p}$ taking $q_{k-1}^{\mathrm{f},\mathbb{p}} = q_k^{\mathrm{f},0}$ for $k = 1, \ldots, N$ into account. Addressing (A.1) in parts:

$$\delta S_{\mathrm{d}} \cdot (\delta q_{\mathrm{d}}^{\mathrm{s}}, \delta q_{\mathrm{d}}^{\mathrm{f}}) \tag{A.2a}$$

$$\begin{aligned} &= \sum_{k=0}^{N-1} \Big(D_{q_k^{\mathrm{s}}} L_{\mathrm{d}}^{k} \cdot \delta q_k^{\mathrm{s}} + D_{q_{k+1}^{\mathrm{s}}} L_{\mathrm{d}}^{k} \cdot \delta q_{k+1}^{\mathrm{s}} + \sum_{m=0}^{\mathbb{p}-1} (D_{q_k^{\mathrm{f},m}} L_{\mathrm{d}}^{k,m} \cdot \delta q_k^{\mathrm{f},m} + D_{q_k^{\mathrm{f},m+1}} L_{\mathrm{d}}^{k,m} \cdot \delta q_k^{\mathrm{f},m+1}) \Big) \\ &= \sum_{k=1}^{N-1} D_{q_k^{\mathrm{s}}} (L_{\mathrm{d}}^{k} + L_{\mathrm{d}}^{k-1}) \cdot \delta q_k^{\mathrm{s}} + \sum_{k=1}^{N-1} \Big(D_{q_k^{\mathrm{f},0}} (L_{\mathrm{d}}^{k} + L_{\mathrm{d}}^{k-1}) \cdot \delta q_k^{\mathrm{f},0} \Big) \\ &\quad + D_{q_0^{\mathrm{s}}} L_{\mathrm{d}}^{0} \cdot \delta q_0^{\mathrm{s}} + D_{q_N^{\mathrm{s}}} L_{\mathrm{d}}^{N-1} \cdot \delta q_N^{\mathrm{s}} + D_{q_0^{\mathrm{f},0}} L_{\mathrm{d}}^{0} \cdot \delta q_0^{\mathrm{f},0} + D_{q_{N-1}^{\mathrm{f},\mathbb{p}}} L_{\mathrm{d}}^{N-1} \cdot \delta q_{N-1}^{\mathrm{f},\mathbb{p}} \end{aligned} \tag{A.2b}$$

$$\begin{aligned} &\sum_{k=0}^{N-1} \Big(F_k^{\mathrm{s}-} \cdot \delta q_k^{\mathrm{s}} + F_k^{\mathrm{s}+} \cdot \delta q_{k+1}^{\mathrm{s}} \Big) = \\ &= \sum_{k=1}^{N-1} (F_k^{\mathrm{s}-} \cdot \delta q_k^{\mathrm{s}}) + F_0^{\mathrm{s}-} \cdot \delta q_0^{\mathrm{s}} + \sum_{k=1}^{N-1} (F_{k-1}^{\mathrm{s}+} \cdot \delta q_k^{\mathrm{s}}) + F_{N-1}^{\mathrm{s}+} \cdot \delta q_N^{\mathrm{s}} \end{aligned} \tag{A.2c}$$

$$\begin{aligned} &\sum_{k=0}^{N-1} \sum_{m=0}^{\mathbb{p}-1} (f_k^{\mathrm{f},m,-} \cdot \delta q_k^{\mathrm{f},m} + f_k^{\mathrm{f},m,+} \cdot \delta q_k^{\mathrm{f},m+1}) \\ &= \sum_{k=0}^{N-1} (f_k^{\mathrm{f},0,-} \cdot \delta q_k^{\mathrm{f},0} + f_k^{\mathrm{f},\mathbb{p}-1,+} \cdot \delta q_k^{\mathrm{f},\mathbb{p}}) + \sum_{k=0}^{N-1} \sum_{m=1}^{\mathbb{p}-1} (f_k^{\mathrm{f},m,-} + f_k^{\mathrm{f},\mathrm{m}-1,+}) \cdot \delta q_k^{\mathrm{f},m} \\ &= \sum_{k=1}^{N-1} (f_k^{\mathrm{f},0,-} + f_{k-1}^{\mathrm{f},\mathbb{p}-1,+}) \cdot \delta q_k^{\mathrm{f},0} + f_0^{\mathrm{f},0,-} \cdot \delta q_0^{\mathrm{f},0} + f_{N-1}^{\mathrm{f},\mathbb{p}-1,+} \cdot \delta q_{N-1}^{\mathrm{f},\mathbb{p}} \end{aligned}$$

$$+\sum_{k=0}^{N-1}\sum_{m=1}^{\mathbb{p}-1}(f_k^{\mathrm{f},m,-}+f_{k-1}^{\mathrm{f},\mathrm{m}-1,+})\cdot\delta q_k^{\mathrm{f},m}. \tag{A.2d}$$

Now plugging in Equations (A.2b) ,(A.2c), (A.2d) in Equation (A.1) and taking variations with zero boundaries $\delta q_0^{\mathrm{s}}=\delta q_N^{\mathrm{s}}=\delta q_0^{\mathrm{f},0}=\delta q_{N-1}^{\mathrm{f},\mathbb{p}}=0$ we obtain

$$0=\delta S_{\mathrm{d}}\cdot(\delta q_{\mathrm{d}}^{\mathrm{s}},\delta q_{\mathrm{d}}^{\mathrm{f}})+\delta W_{\mathrm{d}}\cdot(\delta q_{\mathrm{d}}^{\mathrm{s}},\delta q_{\mathrm{d}}^{\mathrm{f}})=$$
$$\sum_{k=1}^{N-1}\Big(D_{q_k^{\mathrm{s}}}(L_{\mathrm{d}}^k+L_{\mathrm{d}}^{k-1}+F_k^{\mathrm{s},-}+F_{k-1}^{\mathrm{s},+})\cdot\delta q_k^{\mathrm{s}}+\sum_{k=1}^{N-1}(D_{q_k^{\mathrm{f},0}}(L_{\mathrm{d}}^k+L_{\mathrm{d}}^{k-1})+f_k^{\mathrm{f},0,-}+f_k^{\mathrm{f},\mathbb{p}-1,+})\cdot\delta q_k^{\mathrm{f},0}$$
$$+\sum_{k=0}^{N-1}\sum_{m=1}^{\mathbb{p}-1}(D_{q_k^{\mathrm{f},m}}L_{\mathrm{d}}^k+f_k^{\mathrm{f},m,-}+f_k^{\mathrm{f},\mathrm{m}-1,+})\cdot\delta q_k^{\mathrm{f},m}.$$

Taking independent variations δq_k^{s} and $\delta q_k^{\mathrm{f},m}$ for $k=0,\ldots,N-1$, $m=0,\ldots,\mathbb{p}$ leads to the derivation of the following discrete multirate version of the forced Euler-Lagrange Equations

$$D_{q_k^{\mathrm{s}}}(L_{\mathrm{d}}^k+L_{\mathrm{d}}^{k-1})+F_k^{\mathrm{s},-}+F_{k-1}^{\mathrm{s},+}=0 \qquad \text{for } k=1,\ldots,N-1 \tag{A.3a}$$
$$D_{q_k^{\mathrm{f},0}}(L_{\mathrm{d}}^k+L_{\mathrm{d}}^{k-1})+f_k^{\mathrm{f},0,-}+f_{k-1}^{\mathrm{f},\mathbb{p}-1,+}=0 \qquad \text{for } k=1,\ldots,N-1 \tag{A.3a}b$$
$$D_{q_k^{\mathrm{f},m}}L_{\mathrm{d}}^k+f_k^{\mathrm{f},m,-}+f_k^{\mathrm{f},\mathrm{m}-1,+}=0 \quad \text{for } k=0,\ldots,N-1,\ m=1,\ldots,\mathbb{p}-1. \tag{A.3b}$$

□

B

Appendix: MVI formulation for Demonstration problem 2

In this appendix we provide a derivation of Equations (3.31) found in Demonstration problem 2. For this problem in the discrete-time setting we can approximate the kinetic and potential energy as

$$T_{\mathrm{d}}^{\mathrm{s}}(q_k^{\mathrm{s},m}, q_k^{\mathrm{s},m+1}) \approx \int_{t_k^m}^{t_k^{m+1}} \frac{1}{2}(\dot{q}^{\mathrm{s}})^{\intercal} M^{\mathrm{s}} \dot{q}^{\mathrm{s}}\, dt,$$

$$T_{\mathrm{d}}^{\mathrm{f}}(q_k^{\mathrm{f},m}, q_k^{\mathrm{f},m+1}) \approx \int_{t_k^m}^{t_k^{m+1}} \frac{1}{2}(\dot{q}^{\mathrm{f}})^{\intercal} M^{\mathrm{f}} \dot{q}^{\mathrm{f}}\, dt,$$

$$U_{\mathrm{d}}(q_k^{\mathrm{s},m}, q_k^{\mathrm{s},m+1}, q_k^{\mathrm{f},m}, q_k^{\mathrm{f},m+1}) \approx \int_{t_k^m}^{t_k^{m+1}} U(q^{\mathrm{s}}, q^{\mathrm{f}})\, dt,$$

$$P_{\mathrm{d}}(q_k^{\mathrm{f},m}, q_k^{\mathrm{f},m+1}) \approx \int_{t_k^m}^{t_k^{m+1}} P(q^{\mathrm{f}})\, dt.$$

Choosing the midpoint rule and linear interpolation for the values of $\{q^{\mathrm{s},m}\}_{m=0}^{p}$ as defined in (3.16) with $a^m = \frac{\mathbb{p}-m}{\mathbb{p}},\ b^m = \frac{m}{\mathbb{p}}$, these approximations take the form:

$$U_{\mathrm{d}}(q_k^{\mathrm{s},m}, q_k^{\mathrm{s},m+1}, q_k^{\mathrm{f},m}, q_k^{\mathrm{f},m+1}) = \Delta t\, U\Big(\frac{q_k^{\mathrm{s},m} + q_k^{\mathrm{s},m+1}}{2}, \frac{q_k^{\mathrm{f},m} + q_k^{\mathrm{f},m+1}}{2}\Big) = \Delta t U_k^m \quad \text{(B.1a)}$$

$$P_{\mathrm{d}}(q_k^{\mathrm{f},m}, q_k^{\mathrm{f},m+1}) = \Delta t\, P\Big(\frac{q_k^{\mathrm{f},m} + q_k^{\mathrm{f},m+1}}{2}\Big) = \Delta t P_k^m \quad \text{(B.1b)}$$

$$T_{\mathrm{d}}^{\mathrm{f}}(q_k^{\mathrm{f},m}, q_k^{\mathrm{f},m+1}) = \tfrac{\Delta t}{2}\Big(\frac{q_k^{\mathrm{f},m+1} - q_k^{\mathrm{f},m}}{\Delta t}\Big)^{\intercal} \cdot M^{\mathrm{f}} \cdot \Big(\tfrac{q_k^{\mathrm{f},m+1} - q_k^{\mathrm{f},m}}{\Delta t}\Big) = \Delta t T_k^{\mathrm{f},m} \quad \text{(B.1c)}$$

$$\begin{aligned} T_{\mathrm{d},k}^{\mathrm{s}} = T_{\mathrm{d}}^{\mathrm{s}}(q_k^{\mathrm{s}}, q_{k+1}^{\mathrm{s}}) &= \sum_{m=0}^{\mathbb{p}-1} \Big[\frac{\Delta t}{2}\Big(\frac{q_k^{\mathrm{s},m+1} - q_k^{\mathrm{s},m}}{\Delta t}\Big)^{\intercal} \cdot M^{\mathrm{s}} \cdot \Big(\frac{q_k^{\mathrm{s},m+1} - q_k^{\mathrm{s},m}}{\Delta t}\Big)\Big] \\ &= \Delta t \sum_{m=0}^{\mathbb{p}-1} T_k^{\mathrm{s},m} = \frac{\Delta T}{2}\Big(\frac{q_{k+1}^{\mathrm{s}} - q_k^{\mathrm{s}}}{\Delta T}\Big)^{\intercal} \cdot M^{\mathrm{s}} \cdot \Big(\frac{q_{k+1}^{\mathrm{s}} - q_k^{\mathrm{s}}}{\Delta T}\Big) \quad \text{(B.1d)} \end{aligned}$$

Thus the discrete Lagrangian can be written as

$$L_{\mathrm{d}}^{k,m} = \Delta t \sum_{m=0}^{\mathbb{p}-1} \Big(T_{\mathrm{d}}^{\mathrm{s},m} + T_{\mathrm{d}}^{\mathrm{f},m} - U_{\mathrm{d},k}^m - P_{\mathrm{d},k}^m\Big),$$

$$L_{\mathrm{d}}^{k}=\sum_{m=0}^{\mathbb{p}-1}L_{\mathrm{d}}^{k,m}=T_{\mathrm{d},k}^{\mathrm{s}}+\sum_{m=0}^{\mathbb{p}-1}(T_{\mathrm{d},k}^{\mathrm{f},m}-U_{\mathrm{d},k}^{m}-P_{\mathrm{d},k}^{m}) \tag{B.2}$$

The virtual work can similarly be approximated as using the same quadrature as

$$\begin{aligned}\int_{t_k^m}^{t_k^{m+1}} f_{\mathrm{LC}}^{\mathrm{s}}(q^{\mathrm{s}}q^{\mathrm{f}},\dot{q}^{\mathrm{s}},\dot{q}^{\mathrm{f}},u)\cdot\delta q^{\mathrm{s}}dt &\approx \Delta t f_{\mathrm{LC}}^{\mathrm{s}}\Big(\bar{q}_k^{\mathrm{s},m},\bar{q}_k^{\mathrm{f},m},\dot{q}_k^{\mathrm{s},m},\dot{q}_k^{\mathrm{f},m},u_k\Big)\cdot\tfrac{\delta q_k^{\mathrm{s},m+1}+\delta q_k^{\mathrm{s},m}}{2}\\ &= f_k^{\mathrm{s,m-}}\cdot\delta q_k^{m}+f_k^{\mathrm{s,m+}}\cdot\delta q_k^{m+1}\\ \int_{t_k^m}^{t_k^{m+1}} f_{\mathrm{LC}}^{\mathrm{f}}(q^{\mathrm{s}}q^{\mathrm{f}},\dot{q}^{\mathrm{s}},\dot{q}^{\mathrm{f}},u)\cdot\delta q^{\mathrm{f}}dt &\approx \Delta t f_{\mathrm{LC}}^{\mathrm{f}}\Big(\bar{q}_k^{\mathrm{s},m},\bar{q}_k^{\mathrm{f},m},\dot{q}_k^{\mathrm{s},m},\dot{q}_k^{\mathrm{f},m},u_k\Big)\cdot\tfrac{\delta q_k^{\mathrm{f},m+1}+\delta q_k^{\mathrm{f},m}}{2}\\ &= f_k^{\mathrm{f,m-}}\cdot\delta q_k^{m}+f_k^{\mathrm{f,m+}}\cdot\delta q_k^{m+1}\end{aligned}$$

with

$$\begin{aligned}f_k^{\mathrm{s},m,-}=f_k^{\mathrm{s},m,+}&=\frac{\Delta t}{2}f_{\mathrm{LC}}^{\mathrm{s}}\Big(\bar{q}_k^{\mathrm{s},m},\bar{q}_k^{\mathrm{f},m},\dot{q}_k^{\mathrm{s},m},\dot{q}_k^{\mathrm{f},m},u_k\Big),\\ f_k^{\mathrm{f},m,-}=f_k^{\mathrm{f},m,+}&=\frac{\Delta t}{2}f_{\mathrm{LC}}^{\mathrm{f}}\Big(\bar{q}_k^{\mathrm{s},m},\bar{q}_k^{\mathrm{f},m},\dot{q}_k^{\mathrm{s},m},\dot{q}_k^{\mathrm{f},m},u_k\Big),\end{aligned}$$

$$\bar{q}_k^{\mathrm{s},m}=\frac{q_k^{\mathrm{s},m}+q_k^{\mathrm{s},m+1}}{2},\quad \bar{q}_k^{\mathrm{f},m}=\frac{q_k^{\mathrm{f},m}+q_k^{\mathrm{f},m+1}}{2},\quad \dot{q}_k^{\mathrm{s},m}=\frac{q_k^{\mathrm{s},m}-q_k^{\mathrm{s},m+1}}{\Delta t},\quad \dot{q}_k^{\mathrm{f},m}=\frac{q_k^{\mathrm{f},m}-q_k^{\mathrm{f},m+1}}{\Delta t}.$$

as defined previously in (3.32) and $F_k^{\mathrm{s},\pm}$ defined by (3.20). Using discrete forced multirate Hamilton's equations (3.30)

$$\begin{aligned}p_k^{\mathrm{s},-}&=-D_{q_k^{\mathrm{s}}}L_{\mathrm{d}}^{k}-F_k^{\mathrm{s},-}=\frac{M^{\mathrm{s}}}{\Delta T}(q_{k+1}^{\mathrm{s}}-q_k^{\mathrm{s}})+\Delta t\sum_{m=0}^{\mathbb{p}-1}\Big(a^m\frac{\partial U_{\mathrm{d},k}^m}{\partial q_k^{\mathrm{s},m}}+a^{m+1}\frac{\partial U_{\mathrm{d},k}^m}{\partial q_k^{\mathrm{s},m+1}}\Big)-F_k^{\mathrm{s},-}\\ p_k^{\mathrm{s},+}&=D_{q_k^{\mathrm{s}}}L_{\mathrm{d}}^{k-1}+F_{k-1}^{\mathrm{s},+}=\frac{M^{\mathrm{s}}}{\Delta T}(q_k^{\mathrm{s}}-q_{k-1}^{\mathrm{s}})-\Delta t\sum_{m=0}^{\mathbb{p}-1}\Big(b^m\frac{\partial U_{k-1}^m}{\partial q_{k-1}^{\mathrm{s},m}}+b^{m+1}\frac{\partial U_{k-1}^m}{\partial q_{k-1}^{\mathrm{s},m+1}}\Big)+F_{k-1}^{\mathrm{s},+}\\ p_k^{\mathrm{f},m,-}&=-D_{q_k^{\mathrm{f},m}}L_{\mathrm{d}}^{k,m}-f_k^{\mathrm{f},m,-}=\frac{M^{\mathrm{f}}}{\Delta t}(q_k^{\mathrm{f},m+1}-q_k^{\mathrm{f},m})+\Delta t\sum_{m=0}^{\mathbb{p}-1}\frac{\partial(U_{\mathrm{d},k}^m+P_{\mathrm{d},k}^m)}{\partial q_k^{\mathrm{f},m}}-f_k^{\mathrm{f},m,-}\\ p_k^{\mathrm{f},m,+}&=D_{q_k^{\mathrm{f},m}}L_{\mathrm{d}}^{k,m-1}+f_k^{\mathrm{f,m-1,+}}=\frac{M^{\mathrm{f}}}{\Delta t}(q_k^{\mathrm{f},m}-q_k^{\mathrm{f,m-1}})-\Delta t\sum_{m=0}^{\mathbb{p}-1}\frac{\partial(U_{\mathrm{d},k}^{m-1}+P_{\mathrm{d},k}^{m-1})}{\partial q_k^{\mathrm{f},m}}+f_k^{\mathrm{f,m-1,+}}\end{aligned}$$

Based on these equations we derive the following relationships

$$\begin{aligned}\frac{p_k^{\mathrm{s},-}+p_{k+1}^{\mathrm{s},+}}{2}&=\frac{M^{\mathrm{s}}}{\Delta T}(q_{k+1}^{\mathrm{s}}-q_k^{\mathrm{s}})+\frac{\Delta t}{2}\sum_{m=0}^{\mathbb{p}-1}\Big(\tfrac{\mathbb{p}-2m}{\mathbb{p}}\frac{\partial U_{\mathrm{d},k}^m}{\partial q_k^{\mathrm{s},m}}+\tfrac{\mathbb{p}-2(m+1)}{\mathbb{p}}\frac{\partial U_{\mathrm{d},k}^m}{\partial q_k^{\mathrm{s},m+1}}\Big)-\frac{(F_k^{\mathrm{s},-}-F_k^{\mathrm{s},+})}{2}\\ p_k^{\mathrm{s},-}-p_{k+1}^{\mathrm{s},+}&=\Delta t\sum_{m=0}^{\mathbb{p}-1}\Big(\frac{\partial U_{\mathrm{d},k}^m}{\partial q_k^{\mathrm{s},m}}+\frac{\partial U_{\mathrm{d},k}^m}{\partial q_k^{\mathrm{s},m+1}}\Big)-\frac{(F_k^{\mathrm{s},-}+F_k^{\mathrm{s},+})}{2}\\ \frac{p_k^{\mathrm{f},m,-}+p_k^{\mathrm{f,m+1,+}}}{2}&=\frac{M^{\mathrm{f}}}{\Delta t}(q_k^{\mathrm{f},m+1}-q_k^{\mathrm{f},m})-\frac{(f_k^{\mathrm{f},m,-}-f_k^{\mathrm{f},m,+})}{2}\\ p_k^{\mathrm{f},m,-}-p_k^{\mathrm{f,m+1,+}}&=2\Delta t\frac{\partial(U_{\mathrm{d},k}^m+P_{\mathrm{d},k}^m)}{\partial q_k^{\mathrm{f},m}}-\frac{(f_k^{\mathrm{f},m,-}+f_k^{\mathrm{f},m,+})}{2}.\end{aligned}$$

Rearanging these equations and noting that $p_k^{\mathrm{s},+} = p_k^{\mathrm{s},-} = p_k^{\mathrm{s}}$ and $p_k^{\mathrm{f},m,+} = p_k^{\mathrm{f},m,-} = p_k^{\mathrm{f},m}$ we obtain

$$\begin{aligned}
q_{k+1}^{\mathrm{s}} =& q_k^{\mathrm{s}} + \frac{\Delta T}{2}(M^{\mathrm{s}})^{-1}\Big[p_k^{\mathrm{s}} + p_{k+1}^{\mathrm{s}} - \Delta t \sum_{m=0}^{\mathbb{p}-1}\Big(\tfrac{\mathbb{p}-(2m+1)}{\mathbb{p}}\frac{\partial U(\bar{q}_k^{\mathrm{s},m}, \bar{q}_k^{\mathrm{f},m})}{\partial \bar{q}_k^{\mathrm{s},m}}\Big) - F_k^{\mathrm{s},-} + F_k^{\mathrm{s},+}\Big] \\
p_{k+1}^{\mathrm{s}} =& p_k^{\mathrm{s}} - \Delta t \sum_{m=0}^{\mathbb{p}-1}\Big(\frac{\partial U(\bar{q}_k^{\mathrm{s},m}, \bar{q}_k^{\mathrm{f},m})}{\partial \bar{q}_k^{\mathrm{s},m}}\Big) + \frac{1}{2}(F_k^{\mathrm{s},-} + F_k^{\mathrm{s},+}) \\
q_k^{\mathrm{f},m+1} =& q_k^{\mathrm{f},m} + \frac{\Delta t (M^{\mathrm{f}})^{-1}}{2}\Big[p_k^{\mathrm{f},m} + p_k^{\mathrm{f},m+1} - f_k^{\mathrm{f},m,-} + f_k^{\mathrm{f},m,+}\Big] \\
p_k^{\mathrm{f},m+1} =& p_k^{\mathrm{f},m} - \Delta t \frac{\partial (U(\bar{q}_k^{\mathrm{s},m}, \bar{q}_k^{\mathrm{f},m}) + P(\bar{q}_k^{\mathrm{f},m}))}{\partial \bar{q}_k^{\mathrm{f},m}} + \frac{1}{2}(f_k^{\mathrm{f},m,-} + f_k^{\mathrm{f},m,+})
\end{aligned} \tag{B.3}$$

for $k = 0, \ldots, N-1$ in all equations and $m = 0, \ldots, \mathbb{p}-1$ in the last two because

$$\frac{\partial U_k^m}{\partial q_k^{\mathrm{s},m+1}} = \frac{\partial U_k^m}{\partial q_k^{\mathrm{s},m}} = \frac{1}{2}\frac{\partial U(\bar{q}_k^{\mathrm{s},m}, \bar{q}_k^{\mathrm{f},m})}{\partial \bar{q}_k^{\mathrm{s},m}}, \qquad \frac{\partial U_k^m}{\partial q_k^{\mathrm{f},m+1}} = \frac{\partial U_k^m}{\partial q_k^{\mathrm{f},m}} = \frac{1}{2}\frac{\partial U(\bar{q}_k^{\mathrm{s},m}, \bar{q}_k^{\mathrm{f},m})}{\partial \bar{q}_k^{\mathrm{f},m}}.$$

C

Appendix: Simplified MVI for constrained forced systems

In this appendix we simplify the MVI for constrained forced systems in both Lagrangian (3.60) and Hamiltonian formulations (3.61) for a specific quadrature used in the discrete constraint approximation:

$$h_d(q_k^{\mathrm{s}}, q_{k+1}^{\mathrm{s}}, q_k^{\mathrm{f}}, \lambda_k) = \sum_{m=0}^{\mathbb{p}-1} [\tfrac{\Delta t}{2} \lambda_k^m g(q_k^{\mathrm{s},m}, q_k^{\mathrm{f},m}) + \tfrac{\Delta t}{2} \lambda_k^{m+1} g(q_k^{\mathrm{s},m+1}, q_k^{\mathrm{f},m+1})] \tag{C.1}$$

Taking the initial conditions (3.61), rearranging their order and expanding we have:

$$-p_0^{\mathrm{s}} = D_{q_0^{\mathrm{s}}}\Big(L_d(q_0^{\mathrm{s}}, q_1^{\mathrm{s}}, q_0^{\mathrm{f}}) + h_d(q_0^{\mathrm{s}}, q_1^{\mathrm{s}}, q_0^{\mathrm{f}}, \lambda_0) \Big) + F_0^{s,-} \tag{C.2a}$$

$$-p_0^{\mathrm{f},0} = D_{q_0^{\mathrm{f},0}}\Big(L_d(q_0^{\mathrm{s}}, q_1^{\mathrm{s}}, q_0^{\mathrm{f}}) + h_d(q_0^{\mathrm{s}}, q_1^{\mathrm{s}}, q_0^{\mathrm{f}}, \lambda_0) \Big) + f_0^{\mathrm{f},0,-} \tag{C.2b}$$

$$0 = D_{q_0^{\mathrm{f},m}}\Big(L_d(q_0^{\mathrm{s}}, q_1^{\mathrm{s}}, q_0^{\mathrm{f}}) + h_d(q_0^{\mathrm{s}}, q_1^{\mathrm{s}}, q_0^{\mathrm{f}}, \lambda_0) \Big) + f_0^{\mathrm{f},m,-} + f_0^{\mathrm{f},m-1,+} \tag{C.2c}$$

$$0 = D_{\lambda_0^1} h_d(q_0^{\mathrm{s}}, q_1^{\mathrm{s}}, q_0^{\mathrm{f}}, \lambda_0) \tag{C.2d}$$

$$0 = D_{\lambda_0^{m+1}} h_d(q_0^{\mathrm{s}}, q_1^{\mathrm{s}}, q_0^{\mathrm{f}}, \lambda_0) + \delta_{m,\mathbb{p}-1} D_{\lambda_1^0} h_d(q_1^{\mathrm{s}}, q_2^{\mathrm{s}}, q_1^{\mathrm{f}}, \lambda_1) \tag{C.2e}$$

for $k = 1, \ldots, N-1, m = 1, \ldots, \mathbb{p}-1$. Considering the terms which would not be zeroed after the differentiation and simplifying, Equations (C.2a)-(C.2d) become

$$\begin{aligned} -p_0^{\mathrm{s}} &= D_{q_0^{\mathrm{s}}}\Big(L_d(q_0^{\mathrm{s}}, q_1^{\mathrm{s}}, q_0^{\mathrm{f}}) + \sum_{m=0}^{\mathbb{p}-1} [\tfrac{\Delta t}{2} \lambda_0^m g(q_0^{\mathrm{s},m}, q_0^{\mathrm{f},m}) + \\ &\quad \tfrac{\Delta t}{2} \lambda_0^{m+1} g(q_0^{\mathrm{s},m+1}, q_0^{\mathrm{f},m+1})] + \tfrac{\Delta t}{2} \lambda_0^{\mathbb{p}-1} g(q_0^{s,\mathbb{p}-1}, q_0^{f,\mathbb{p}-1}) \Big) + F_0^{s,-} \\ &= D_{q_0^{\mathrm{s}}}\Big(L_d(q_0^{\mathrm{s}}, q_1^{\mathrm{s}}, q_0^{\mathrm{f}}) + \tfrac{\Delta t}{2} \lambda_0^0 g(q_0^{s,0}, q_0^{\mathrm{f},0}) + \sum_{m=1}^{\mathbb{p}-1} [\Delta t \lambda_0^m g(q_0^{\mathrm{s},m}, q_0^{\mathrm{f},m})] \Big) + F_0^{s,-} \end{aligned} \tag{C.3a}$$

$$-p_0^{\mathrm{f},0} = D_{q_0^{\mathrm{f},0}}\Big(L_d(q_0^{\mathrm{s}}, q_1^{\mathrm{s}}, q_0^{\mathrm{f}}) + \tfrac{\Delta t}{2} \lambda_0^0 g(q_0^{s,0}, q_0^{\mathrm{f},0}) \Big) + f_0^{\mathrm{f},0,-} \tag{C.3b}$$

$$0 = D_{q_0^{\mathrm{f},m}}\Big(L_d(q_0^{\mathrm{s}}, q_1^{\mathrm{s}}, q_0^{\mathrm{f}}) + \Delta t \lambda_0^m g(q_0^{\mathrm{s},m}, q_0^{\mathrm{f},m}) \Big) + f_0^{\mathrm{f},m,-} + f_0^{\mathrm{f},m-1,+}, \ m = 1, \ldots, \mathbb{p}$$

$$0 = \Delta t g(q_0^{s,1}, q_0^{f,1}) \tag{C.3c}$$

For $m = 1, \ldots, \mathbb{p} - 2$ Equation (C.2e) can be simplified as

$$0 = D_{\lambda_0^{m+1}} h_d(q_0^{\mathrm{s}}, q_1^{\mathrm{s}}, q_0^{\mathrm{f}}, \lambda_0) = \Delta t g(q_0^{\mathrm{s},m+1}, q_0^{\mathrm{f},m+1}) \tag{C.4}$$

At $m = \mathbb{p} - 1$ we have $\delta_{m,\mathbb{p}-1} = 1$ and thus

$$\begin{aligned} 0 &= D_{\lambda_0^{\mathbb{p}}} h_d(q_0^{\mathrm{s}}, q_1^{\mathrm{s}}, q_0^{\mathrm{f}}, \lambda_0) + D_{\lambda_1^0} h_d(q_1^{\mathrm{s}}, q_2^{\mathrm{s}}, q_1^{\mathrm{f}}, \lambda_1) \\ &= \tfrac{\Delta t}{2} g(q_0^{s,\mathbb{p}}, q_0^{f,\mathbb{p}}) + \tfrac{\Delta t}{2} g(q_1^{s,0}, q_1^{\mathrm{f},0}) = \Delta t g(q_0^{s,\mathbb{p}}, q_0^{f,\mathbb{p}}) \end{aligned} \tag{C.5}$$

Combining (C.4) and (C.5), (C.2e) can be simplified and combined with (C.3c) as

$$0 = g(q_0^{\mathrm{s},m}, q_0^{\mathrm{f},m}) \text{ for } m = 1, \ldots, \mathbb{p} \tag{C.6}$$

and thus the final set of simplified initial conditions takes the form

$$-p_0^{\mathrm{s}} = D_{q_0^{\mathrm{s}}}\Big(L_d(q_0^{\mathrm{s}}, q_1^{\mathrm{s}}, q_0^{\mathrm{f}}) + \tfrac{\Delta t}{2}\lambda_0^0 g(q_0^{s,0}, q_0^{\mathrm{f},0}) + \sum_{m=1}^{\mathbb{p}-1} [\Delta t \lambda_0^m g(q_0^{\mathrm{s},m}, q_0^{\mathrm{f},m})] \Big) + F_0^{s,-} \tag{C.7a}$$

$$-p_0^{\mathrm{f},0} = D_{q_0^{\mathrm{f},0}}\Big(L_d(q_0^{\mathrm{s}}, q_1^{\mathrm{s}}, q_0^{\mathrm{f}}) + \tfrac{\Delta t}{2}\lambda_0^0 g(q_0^{s,0}, q_0^{\mathrm{f},0}) \Big) + f_0^{\mathrm{f},0,-} \tag{C.7b}$$

$$0 = D_{q_0^{\mathrm{f},m}}\Big(L_d(q_0^{\mathrm{s}}, q_1^{\mathrm{s}}, q_0^{\mathrm{f}}) + \Delta t \lambda_0^m g(q_0^{\mathrm{s},m}, q_0^{\mathrm{f},m}) \Big) + f_0^{\mathrm{f},m,-} + f_0^{\mathrm{f},m-1,+} \tag{C.7c}$$

$$0 = g(q_0^{\mathrm{s},m}, q_0^{\mathrm{f},m}) \tag{C.7d}$$

where (C.7c) is solved for $m = 1, \ldots, \mathbb{p}-1$ and (C.7d) for $m = 1, \ldots, \mathbb{p}$. As a check, in total we have $n^q(1+\mathbb{p})+\mathbb{p}$ equations and unknowns (i.e. $q_{k+1}^{\mathrm{s}}, \{q_k^{\mathrm{f},m}\}_1^{\mathbb{p}}, \{\lambda_k^{\mathrm{f},m}\}_0^{\mathbb{p}-1}$).

Next, we focus on the model for $k > 1$ in (3.60) and again expand the terms:

$$\begin{aligned} 0 = D_{q_k^{\mathrm{s}}}\Big(& L_d(q_{k-1}^{\mathrm{s}}, q_k^{\mathrm{s}}, q_{k-1}^{\mathrm{f}}) + L_d(q_k^{\mathrm{s}}, q_{k+1}^{\mathrm{s}}, q_k^{\mathrm{f}}) + h_d(q_{k-1}^{\mathrm{s}}, q_k^{\mathrm{s}}, q_{k-1}^{\mathrm{f}}, \lambda_{k-1}) + \\ & h_d(q_k^{\mathrm{s}}, q_{k+1}^{\mathrm{s}}, q_k^{\mathrm{f}}, \lambda_k) \Big) + F_k^{s,-} + F_{k-1}^{s,+} \end{aligned} \tag{C.8a}$$

$$\begin{aligned} 0 = D_{q_k^{\mathrm{f},0}}\Big(& L_d(q_{k-1}^{\mathrm{s}}, q_k^{\mathrm{s}}, q_{k-1}^{\mathrm{f}}) + L_d(q_k^{\mathrm{s}}, q_{k+1}^{\mathrm{s}}, q_k^{\mathrm{f}}) + h_d(q_{k-1}^{\mathrm{s}}, q_k^{\mathrm{s}}, q_{k-1}^{\mathrm{f}}, \lambda_{k-1}) + \\ & h_d(q_k^{\mathrm{s}}, q_{k+1}^{\mathrm{s}}, q_k^{\mathrm{f}}, \lambda_k) \Big) + f_k^{\mathrm{f},0,-} + f_{k-1}^{\mathrm{f},\mathbb{p}-1,+} \end{aligned} \tag{C.8b}$$

$$0 = D_{q_k^{\mathrm{f},m}}\Big(L_d(q_k^{\mathrm{s}}, q_{k+1}^{\mathrm{s}}, q_k^{\mathrm{f}}) + h_d(q_k^{\mathrm{s}}, q_{k+1}^{\mathrm{s}}, q_k^{\mathrm{f}}, \lambda_k) \Big) + f_k^{\mathrm{f},m,-} + f_k^{\mathrm{f},\mathrm{m}-1,+} \tag{C.8c}$$

$$0 = D_{\lambda_k^1} h_d(q_k^{\mathrm{s}}, q_{k+1}^{\mathrm{s}}, q_0^{\mathrm{f}}, \lambda_k) \tag{C.8d}$$

$$0 = D_{\lambda_k^{m+1}} h_d(q_k^{\mathrm{s}}, q_{k+1}^{\mathrm{s}}, q_k^{\mathrm{f}}, \lambda_k) + \delta_{m,\mathbb{p}-1}(1 - \delta_{k,N-1}) D_{\lambda_{k+1}^0} h_d(q_{k+1}^{\mathrm{s}}, q_{k+2}^{\mathrm{s}}, q_{k+1}^{\mathrm{f}}, \lambda_1) \tag{C.8e}$$

These equations can again be simplified. Equation (C.8a) can be expanded as:

$$
\begin{aligned}
0 = D_{q_k^{\mathrm{s}}}\Big(& L_d(q_{k-1}^{\mathrm{s}}, q_k^{\mathrm{s}}, q_{k+1}^{\mathrm{f}}) + L_d(q_k^{\mathrm{s}}, q_{k+1}^{\mathrm{s}}, q_k^{\mathrm{f}}) + \tfrac{\Delta t}{2}\lambda_{k-1}^{1} g(q_{k-1}^{s,1}, q_{k-1}^{f,1}) + \\
& \sum_{m=1}^{\mathbb{p}-1} [\tfrac{\Delta t}{2}\lambda_{k-1}^{m} g(q_{k-1}^{\mathrm{s},m}, q_{k-1}^{\mathrm{f},m}) + \tfrac{\Delta t}{2}\lambda_{k-1}^{m+1} g(q_{k-1}^{\mathrm{s},m+1}, q_{k-1}^{\mathrm{f},m+1})] + \\
& \sum_{m=0}^{\mathbb{p}-1} [\tfrac{\Delta t}{2}\lambda_{k}^{m} g(q_{k}^{\mathrm{s},m}, q_{k}^{\mathrm{f},m}) + \tfrac{\Delta t}{2}\lambda_{k}^{m+1} g(q_{k}^{\mathrm{s},m+1}, q_{k}^{\mathrm{f},m+1})] + \\
& \tfrac{\Delta t}{2}\lambda_{k}^{\mathbb{p}-1} g(q_{k}^{s,\mathbb{p}-1}, q_{k}^{f,\mathbb{p}-1})\Big) + F_k^{s,-} + F_{k-1}^{s,+} \\
= D_{q_k^{\mathrm{s}}}\Big(& L_d(q_{k-1}^{\mathrm{s}}, q_k^{\mathrm{s}}, q_{k+1}^{\mathrm{f}}) + L_d(q_k^{\mathrm{s}}, q_{k+1}^{\mathrm{s}}, q_k^{\mathrm{f}}) + \sum_{m=1}^{\mathbb{p}-1} [\Delta t \lambda_{k-1}^{m} g(q_{k-1}^{\mathrm{s},m}, q_{k-1}^{\mathrm{f},m})] + \\
& \tfrac{\Delta t}{2}\lambda_{k-1}^{\mathbb{p}} g(q_{k-1}^{s,\mathbb{p}}, q_{k-1}^{f,\mathbb{p}}) + \tfrac{\Delta t}{2}\lambda_{k}^{0} g(q_{k}^{s,0}, q_{k}^{\mathrm{f},0}) + \sum_{m=1}^{\mathbb{p}-1} [\Delta t \lambda_{k}^{m} g(q_{k}^{\mathrm{s},m}, q_{k}^{\mathrm{f},m})]\Big) + F_k^{s,-} + F_{k-1}^{s,+} \\
= D_{q_k^{\mathrm{s}}}\Big(& L_d(q_{k-1}^{\mathrm{s}}, q_k^{\mathrm{s}}, q_{k+1}^{\mathrm{f}}) + L_d(q_k^{\mathrm{s}}, q_{k+1}^{\mathrm{s}}, q_k^{\mathrm{f}}) + \sum_{m=1}^{\mathbb{p}-1} [\Delta t \lambda_{k-1}^{m} g(q_{k-1}^{\mathrm{s},m}, q_{k-1}^{\mathrm{f},m})] + \\
& \sum_{m=0}^{\mathbb{p}-1} [\Delta t \lambda_{k}^{m} g(q_{k}^{\mathrm{s},m}, q_{k}^{\mathrm{f},m})]\Big) + F_k^{s,-} + F_{k-1}^{s,+}
\end{aligned}
$$

as $\lambda_{k-1}^{\mathbb{p}} = \lambda_k^0$, $q_{k-1}^{\mathrm{s/f},\mathbb{p}} = q_k^{\mathrm{s/f},0}$. As $q_k^{\mathrm{f},0} = q_{k-1}^{\mathrm{f},\mathbb{p}}$ Equation (C.8b) becomes

$$
\begin{aligned}
0 = D_{q_k^{\mathrm{f},0}}\Big(& L_d(q_{k-1}^{\mathrm{s}}, q_k^{\mathrm{s}}, q_{k-1}^{\mathrm{f}}) + L_d(q_k^{\mathrm{s}}, q_{k+1}^{\mathrm{s}}, q_k^{\mathrm{f}}) + \\
& \tfrac{\Delta t}{2}\lambda_{k-1}^{\mathbb{p}} g(q_{k-1}^{s,\mathbb{p}}, q_{k-1}^{f,\mathbb{p}}) + \tfrac{\Delta t}{2}\lambda_{k}^{0} g(q_{k}^{s,0}, q_{k}^{\mathrm{f},0})\Big) + f_k^{\mathrm{f},0,-} + f_{k-1}^{\mathrm{f},\mathbb{p}-1,+} \\
= D_{q_k^{\mathrm{f},0}}\Big(& L_d(q_{k-1}^{\mathrm{s}}, q_k^{\mathrm{s}}, q_{k-1}^{\mathrm{f}}) + L_d(q_k^{\mathrm{s}}, q_{k+1}^{\mathrm{s}}, q_k^{\mathrm{f}}) + \Delta t \lambda_{k-1}^{\mathbb{p}} g(q_{k-1}^{s,\mathbb{p}}, q_{k-1}^{f,\mathbb{p}})\Big) + f_k^{\mathrm{f},0,-} + f_{k-1}^{\mathrm{f},\mathbb{p}-1,+}
\end{aligned}
$$

As in the initial conditions, Equations (C.8d) and (C.8e) can be expressed together as (C.6). This equation is still valid at $k = N-1$ due to the action of the Kronecker delta and the simplification of the resulting expression in a similar fashion to the one for the initial conditions. The final simplified form of model (3.60) for the constraint approximation (C.1) takes the form for $k = 1, \ldots, N-1$:

$$
\begin{aligned}
0 = D_{q_k^{\mathrm{s}}}\Big(& L_d(q_{k-1}^{\mathrm{s}}, q_k^{\mathrm{s}}, q_{k-1}^{\mathrm{f}}) + L_d(q_k^{\mathrm{s}}, q_{k+1}^{\mathrm{s}}, q_k^{\mathrm{f}}) + \sum_{m=1}^{\mathbb{p}-1} [\Delta t \lambda_{k-1}^{m} g(q_{k-1}^{\mathrm{s},m}, q_{k-1}^{\mathrm{f},m})] + \\
& \sum_{m=0}^{\mathbb{p}-1} [\Delta t \lambda_{k}^{m} g(q_{k}^{\mathrm{s},m}, q_{k}^{\mathrm{f},m})]\Big) + F_k^{s,-} + F_{k-1}^{s,+} \\
0 = D_{q_k^{\mathrm{f},0}}\Big(& L_d(q_{k-1}^{\mathrm{s}}, q_k^{\mathrm{s}}, q_{k-1}^{\mathrm{f}}) + L_d(q_k^{\mathrm{s}}, q_{k+1}^{\mathrm{s}}, q_k^{\mathrm{f}}) + \Delta t \lambda_{k}^{0} g(q_{k}^{s,0}, q_{k}^{\mathrm{f},0})\Big) + f_k^{\mathrm{f},0,-} + f_{k-1}^{\mathrm{f},\mathbb{p}-1,+} \\
0 = D_{q_k^{\mathrm{f},m}}\Big(& L_d(q_k^{\mathrm{s}}, q_{k+1}^{\mathrm{s}}, q_k^{\mathrm{f}}) + \Delta t \lambda_{k}^{m} g(q_{k}^{\mathrm{s},m}, q_{k}^{\mathrm{f},m})\Big) + f_k^{\mathrm{f},m,-} + f_k^{\mathrm{f},\mathrm{m}-1,+}, \quad m = 1, \ldots, \mathbb{p}-1 \\
0 = & g(q_k^{\mathrm{s},m}, q_k^{\mathrm{f},m}), \quad m = 1, \ldots, \mathbb{p}
\end{aligned}
$$

D

Appendix: Proofs of the non-conservativeness of cMPC

Contents

D.1 Proof of the non-conservativeness of EcMPC 216
D.2 Proof of the non-conservativeness of IcMPC 220

In this appendix we provide the proofs for Theorems 7.3.3 and 7.4.5, guaranteeing the non-conservativeness of the EcMPC and IcMPC approaches when the sequence of convex programs is not terminated early.

D.1 Proof of the non-conservativeness of EcMPC

Theorem 7.3.2 shows that the cMPC iteration converges to a fixed point. We now prove Theorem 7.3.3, stating that this point is a local optimum of the nMPC RHOCP. For readability we set $n_x = 1$, but the proof for $n_x > 1$ is analogous. We also assume that the EnMPC RHOCP (7.6) satisfies a suitable constraint qualification (e.g. linear independence constraint qualification, definition 2.4.2), so that a local minimizer satisfies the first order necessary conditions (Theorem 2.4.1).

From Theorem 7.3.2 it is known that the EcMPC iteration converges to $\{c_{0|i}, \ldots, c_{N-1|i}\} = \{0, \ldots, 0\}$, $S_{0|i} = \{0\}$, $\ldots$, $S_{N|i} = \{0\}$. At this point $(\mathbf{x}_i^*, \mathbf{u}_i^*) = (\mathbf{x}_i^{0,j}, \mathbf{u}_i^{0,j})$ due to (7.31b), (7.9). To prove this point coincides with a local optimum for both cMPC and nMPC RHOCPs, we consider the equivalence to first-order of the cMPC RHOCP at this point and the nMPC RHOCP at $(\mathbf{x}_i, \mathbf{u}_i) = (\mathbf{x}_i^{0,j}, \mathbf{u}_i^{0,j})$. By inspection of (7.6b)-(7.6f) and (7.12a)-(7.12f) it is clear that if only constraints (7.6b), (7.6d), (7.6e) and (7.12a)-(7.12d), (7.12e) were present in the EnMPC and EcMPC RHOCPs, then their first order optimality conditions would be identical

at $\mathbf{x}_i = \mathbf{x}_i^0$, $\mathbf{u}_i = \mathbf{u}_i^0$ and $\{c_{0|i}, \dots, c_{N-1|i}\} = \{0, \dots, 0\}$, $S_{0|i} = \{0\}$, $\dots$, $S_{N|i} = \{0\}$. Therefore, we prove the same is true when (7.6c) and (7.12c) are included, by showing the equivalence to first-order of the following two simplified problems:

$$\begin{aligned}&\text{EnMPC simplified: } \mathbf{c}_i^* \coloneqq \underset{\mathbf{x}_i, \mathbf{c}_i}{\operatorname{argmin}} J^c_{\text{EnMPC}}(\mathbf{x}_i, \mathbf{c}_i)\\ &\text{subject to, for } k = 0, \dots, N-1: \quad x_{k+1|i} - \phi(x_{k|i}, c_{k|i}) = 0\end{aligned}$$

where $f(x_{k|i}, u_{k|i}) = \phi(x_{k|i}, c_{k|i})$ for $u_{k|i} = Kx_{k|i} + c_{k|i}$, $J^c_{\text{nMPC}}(\cdot,\cdot) = J_{\text{nMPC}}(\cdot,\cdot)$, and

$$\begin{aligned}&\text{EcMPC simplified:} \quad (\mathbf{c}_i^*, \mathbf{S}_i^*) = \underset{\mathbf{c}_i, \mathbf{S}_i}{\operatorname{argmin}} J^c_{\text{EcMPC}}(\mathbf{c}_i, \mathbf{S}_i, \mathbf{x}_i^0, \mathbf{c}_i^0)\\ &\text{subject to, for } k = 0, \dots, N-1: \qquad\qquad (D.3)\\ &\bar{s}_{k+1|i} \geq \phi(\bar{s}_{k|i} + x^0_{k|i}, c_{k|i} + u^0_{k|i} - Kx^0_{k|i}) - \phi(x^0_{k|i}, c^0_{k|i}), \quad \underline{s}_{k+1|i} \leq \Phi_{k|i}\bar{s}_{k|i} + B_{k|i}c_{k|i}\\ &\bar{s}_{k+1|i} \geq \phi(\underline{s}_{k|i} + x^0_{k|i}, c_{k|i} + u^0_{k|i} - Kx^0_{k|i}) - \phi(x^0_{k|i}, c^0_{k|i}), \quad \underline{s}_{k+1|i} \leq \Phi_{k|i}\underline{s}_{k|i} + B_{k|i}c_{k|i}\end{aligned}$$

Here $u^0_{k|i} = Kx^0_{k|i} + c^0_{k|i}$, $J^c_{\text{EcMPC}}(\mathbf{c}_i, \mathbf{S}_i, \mathbf{x}_i^0, \mathbf{c}_i^0) = J_{\text{EcMPC}}(\mathbf{c}_i, \mathbf{S}_i, \mathbf{x}_i^0, \mathbf{u}_i^0)$, and

$$\phi(s + x^0, c + u^0 - Kx^0) = f(s + x^0, Ks + c + u^0) \tag{D.4a}$$
$$\frac{\partial \phi(x,c)}{\partial x} = \frac{\partial f(x, Kx+c)}{\partial x} = \frac{\partial f(x,u)}{\partial x} + \frac{\partial f(x,u)}{\partial u}\frac{\partial u}{\partial x} = A_k + B_k K = \Phi_k \tag{D.4b}$$
$$\frac{\partial \phi(x,c)}{\partial c} = \frac{\partial f(x, Kx+c)}{\partial c} = \frac{\partial f(x,u)}{\partial u}\frac{\partial u}{\partial c} = B_k \tag{D.4c}$$

where A_k and B_k are defined in (7.31c) and $\Phi_k = A_k + B_k K$.

For the simplified EnMPC RHOCP, the augumented Lagrangian and the Karush-Kuhn-Tucker (KKT) first-order necessary conditions [23] become

$$L_{\text{EnMPC}}(\mathbf{x}_i, \mathbf{c}_i, \lambda_\mathbf{i}) = J^c_{\text{EnMPC}}(\mathbf{x}_i, \mathbf{c}_i) - \sum_{k=0}^{N} \lambda_{k|i}(x_{k+1|i} - \phi(x_{k|i}, c_{k|i}))$$

KKT EnMPC simplified:

$$0 = \frac{\partial J^c_{\text{EnMPC}}(\mathbf{x}_i, \mathbf{c}_i)}{\partial x_{0|i}}|_{(\mathbf{x}_i^{*,n}, \mathbf{c}_i^{*,n})} + \lambda^{*,n}_{0|i}\frac{\partial \phi(x,c)}{\partial x}|_{(x^{*,n}_{0|i}, c^{*,n}_{0|i})} \tag{D.5a}$$

and for $k = 0, \dots, N-1$

$$0 = \frac{\partial J^c_{\text{EnMPC}}(\mathbf{x}_i, \mathbf{c}_i)}{\partial x_{k|i}}|_{(\mathbf{x}_i^{*,n}, \mathbf{c}_i^{*,n})} + \lambda^{*,n}_{k|i}\frac{\partial \phi(x,c)}{\partial x}|_{(x^{*,n}_{k|i}, c^{*,n}_{k|i})} - \lambda^{*,n}_{k-1|i} \tag{D.5b}$$

$$0 = \frac{\partial J^c_{\text{EnMPC}}(\mathbf{x}_i, \mathbf{u}_i)}{\partial u_{k|i}}|_{(\mathbf{x}_i^{*,n}, \mathbf{c}_i^{*,n})} + \lambda^{*,n}_{k|i}\frac{\partial \phi(x,c)}{\partial c}|_{(x^{*,n}_{k|i}, u^{*,n}_{k|i})} \tag{D.5c}$$

$$0 = x^{*,n}_{k+1|i} - \phi(x^{*,n}_{k|i}, c^{*,n}_{k|i}) \tag{D.5d}$$

where $(\cdot)^{*,n}$ denotes the value at the local optimum point for EnMPC simplified and $\mathbf{x}_i^{*,n}$ is obtained from $\mathbf{c}_i^{*,n}$ and $x_{k+1|i} = \phi(x_{k|i}, c_{k|i})$. On the other hand, for simplified EcMPC RHOCP we have

$$L_{\text{EcMPC}}(\mathbf{c}_i, \mathbf{S}_i, \mathbf{x}_i^0, \mathbf{u}_i^0, \alpha_{\mathbf{i}}, \beta_{\mathbf{i}}, \gamma_{\mathbf{i}}, \mu_{\mathbf{i}}) = J_{\text{EcMPC}}(\mathbf{c}_i, \mathbf{S}_i, \mathbf{x}_i^0, \mathbf{u}_i^0)$$
$$- \sum_{k=0}^{N-1} \alpha_{k|i}\Big(\bar{s}_{k+1|i} - \phi(\bar{z}_{k|i}) + \phi(x_{k|i}^0, c_{k|i}^0)\Big) - \sum_{k=0}^{N-1} \beta_{k|i}\Big(\bar{s}_{k+1|i} - \phi(\underline{z}_{k|i}) + \phi(x_{k|i}^0, c_{k|i}^0)\Big)$$
$$- \sum_{k=0}^{N-1} \gamma_{k|i}(\Phi_{k|i}\bar{s}_{k|i} + B_{k|i}c_{k|i} - \underline{s}_{k+1|i}) - \sum_{k=0}^{N-1} \mu_{k|i}(\Phi_{k|i}\underline{s}_{k|i} + B_{k|i}c_{k|i} - \underline{s}_{k+1|i})$$

KKT EcMPC simplified:

$$0 = \frac{\partial J_{\text{EcMPC}}}{\partial \bar{s}_{0|i}}|_{\mathbf{z}_{\mathbf{i}}^{*,\mathbf{c}}} + \alpha_{0|i}^{*,c}\frac{\partial \phi(x,c)}{\partial x}|_{\bar{z}_{0|i}^{*,c}} - \gamma_{0|i}^{*,c}\frac{\partial \phi(x_{0|i}^0, c_{0|i}^0)}{\partial x_{0|i}^0} \tag{D.6a}$$

$$0 = \frac{\partial J_{\text{EcMPC}}}{\partial \underline{s}_{0|i}}|_{\mathbf{z}_{\mathbf{i}}^{*,\mathbf{c}}} + \beta_{0|i}^{*,c}\frac{\partial \phi(x,c)}{\partial x}|_{\underline{z}_{0|i}^{*,c}} - \mu_{k|i}^{*,c}\frac{\partial \phi(x_{k|i}^0, c_{k|i}^0)}{\partial x_{k|i}^0} \tag{D.6b}$$

and for $k = 1, \ldots, N-1$

$$0 = \frac{\partial J_{\text{EcMPC}}}{\partial \bar{s}_{k|i}}|_{\mathbf{z}_{\mathbf{i}}^{*,\mathbf{c}}} - (\alpha_{k-1|i}^{*,c} + \beta_{k-1|i}^{*,c}) + \alpha_{k|i}^{*,c}\frac{\partial \phi(x,u)}{\partial x}|_{\bar{z}_{k|i}^{*,c}} - \gamma_{k|i}^{*,c}\frac{\partial \phi(x_{k|i}^0, c_{k|i}^0)}{\partial x_{k|i}^0} \tag{D.6c}$$

$$0 = \frac{\partial J_{\text{EcMPC}}}{\partial \underline{s}_{k|i}}|_{\mathbf{z}_{\mathbf{i}}^{*,\mathbf{c}}} + (\mu_{k-1|i}^{*,c} + \gamma_{k-1|i}^{*,c}) + \beta_{k|i}^{*,c}\frac{\partial \phi(x,c)}{\partial x}|_{\underline{z}_{k|i}^{*,c}} - \mu_{k|i}^{*,c}\frac{\partial \phi(x_{k|i}^0, c_{k|i}^0)}{\partial x_{k|i}^0} \tag{D.6d}$$

$$0 = \frac{\partial J_{\text{EcMPC}}}{\partial c_{k|i}}|_{\mathbf{z}_{\mathbf{i}}^{*,\mathbf{c}}} + \alpha_{k|i}^{*,c}\frac{\partial \phi(x,c)}{\partial c}|_{\bar{z}_{k|i}^{*,c}} + \beta_{k|i}^{*,c}\frac{\partial \phi(x,c)}{\partial c}|_{\underline{z}_{k|i}^{*,c}} - (\gamma_{k|i}^{*,c} + \mu_{k|i}^{*,c})\frac{\partial \phi(x_{k|i}^0, c_{k|i}^0)}{\partial c_{k|i}^0} \tag{D.6e}$$

$$0 = \alpha_{k|i}(\bar{s}_{k+1|i}^{*,c} - \phi(\bar{z}_{k|i}^{*,c}) + \phi(x_{k|i}^0, u_{k|i}^0)), \quad 0 = \gamma_{k|i}(\Phi_{k|i}\bar{s}_{k|i}^{*,c} + B_{k|i}c_{k|i}^{*,c} - \underline{s}_{k+1|i}^{*,c}) \tag{D.6f}$$

$$0 = \beta_{k|i}(\bar{s}_{k+1|i}^{*,c} - \phi(\underline{z}_{k|i}^{*,c}) + \phi(x_{k|i}^0, u_{k|i}^0)), \quad 0 = \mu_{k|i}(\Phi_{k|i}\underline{s}_{k|i}^{*,c} + B_{k|i}c_{k|i}^{*,c} - \underline{s}_{k+1|i}^{*,c}) \tag{D.6g}$$

$$\alpha_{k|i}^{*,c} \geq 0, \quad \beta_{k|i}^{*,c} \geq 0, \quad \gamma_{k|i}^{*,c} \geq 0, \quad \mu_{k|i}^{*,c} \geq 0 \tag{D.6h}$$

These expressions are based on (D.4), simplified using the chain rule

$$\nabla_{c_{k|i}}\phi(\underline{s}_{k|i} + x_{k|i}^0, c_{k|i} + u_{k|i}^0 - Kx_{k|i}^0) = \nabla_c \phi(x,c)|_{\underline{z}_{k|i}}$$
$$\nabla_{\underline{s}_{k|i}}\phi(\underline{s}_{k|i} + x_{k|i}^0, c_{k|i} + u_{k|i}^0 - Kx_{k|i}^0) = \nabla_x \phi(x,u)|_{\underline{z}_{k|i}}$$

and denoting: $\mathbf{z}_i^{*,c} = (\mathbf{c}_i^{*,c}, \mathbf{S}_i^{*,c}, \mathbf{x}_i^0, \mathbf{u}_i^0)$,

$$\bar{z}_{k|i} = (\bar{s}_{k|i} + x_{k|i}^0, c_{k|i} + u_{k|i}^0 - Kx_{k|i}^0), \quad \underline{z}_{k|i} = (\underline{s}_{k|i} + x_{k|i}^0, c_{k|i} + u_{k|i}^0 - Kx_{k|i}^0)$$
$$\bar{z}_{k|i}^{*,c} = (\bar{s}_{k|i}^{*,c} + x_{k|i}^0, c_{k|i}^{*,c} + u_{k|i}^0 - Kx_{k|i}^0), \quad \underline{z}_{k|i}^{*,c} = (\underline{s}_{k|i}^{*,c} + x_{k|i}^0, c_{k|i}^{*,c} + u_{k|i}^0 - Kx_{k|i}^0)$$

with $(\cdot)^{*,c}$ signifying the value at the local optimum point for EcMPC simplified and $\mathbf{x}_i^{*,c}$ is obtained from $\mathbf{c}_i^{*,c}$ and $x_{k+1|i} = \phi(x_{k|i}, c_{k|i})$. The complementarity conditions must be checked for several cases. By inspection due to the maximization formulation of the cost it is clear that at least one of the constraints in (D.3) will be active for each k. Furthermore all four constraints in (D.3) for a given k will simultaneously be active only for the case $S_{k|i} = \{0\}$ at which point $\bar{s}_{k|i} = \underline{s}_{k|i}$. Thus there will be a non-zero Lagrange multiplier at all times. It is important to note that in Equations (D.6c) and (D.6d) either $\frac{\partial J_{\text{EcMPC}}}{\partial \bar{s}_{k|i}}|_{\mathbf{z}_i^{*,c}}$ or $\frac{\partial J_{\text{EcMPC}}}{\partial \underline{s}_{k|i}}|_{\mathbf{z}_i^{*,c}}$ would be zero for each k due to the maximization defining J_{cMPC} in (7.12f). The nonzero gradient of those would be equal to $\frac{\partial J_{\text{EnMPC}}}{\partial x_{k|i}}|_{(\mathbf{x}_i^r, \mathbf{c}_i^r)}$ due to the formulation of the cost and the chain rule of differentiation with $c_{k|i}^r = c_{k|i}^{*,c} + c_{k|i}^0$ and $x_{k|i}^r$ equal to $\bar{s}_{k|i}^{*,c} + x_{k|i}^0$ or $\underline{s}_{k|i}^{*,c} + x_{k|i}^0$ depending on which one maximizes the cost. Summing conditions (D.6a), (D.6b) and (D.6c), (D.6d) therefore leads to

$$0 = \frac{\partial J_{\text{EnMPC}}}{\partial x_{0|i}}|_{(\mathbf{x}_i^r, \mathbf{c}_i^r)} + \alpha_{0|i}^{*,c} \frac{\partial \phi(x,c)}{\partial x}|_{\bar{z}_{0|i}^{*,c}} + \beta_{0|i}^{*,c} \frac{\partial \phi(x,c)}{\partial x}|_{\underline{z}_{0|i}^{*,c}} - (\gamma_{0|i}^{*,c} + \mu_{0|i}^{*,c}) \frac{\partial \phi(x_{0|i}^0, c_{0|i}^0)}{\partial x_{0|i}^0} \tag{D.7}$$

$$\begin{aligned} 0 = {} & \frac{\partial J_{\text{EnMPC}}}{\partial x_{k|i}}|_{(\mathbf{x}_i^r, \mathbf{c}_i^r)} + \alpha_{k|i}^{*,c} \frac{\partial \phi(x,c)}{\partial x}|_{\bar{z}_{k|i}^{*,c}} + \beta_{k|i}^{*,c} \frac{\partial \phi(x,c)}{\partial x}|_{\underline{z}_{k|i}^{*,c}} - (\gamma_{k|i}^{*,c} + \mu_{k|i}^{*,c}) \frac{\partial \phi(x_{k|i}^0, c_{k|i}^0)}{\partial x_{k|i}^0} \\ & - (\alpha_{k-1|i}^{*,c} + \beta_{k-1|i}^{*,c} - \mu_{k-1|i}^{*,c} - \gamma_{k-1|i}^{*,c}) \end{aligned} \tag{D.8}$$

From Theorem 7.3.2 we know the EcMPC iteration converges to a fixed point at which $c_{0|i} = 0, \ldots, c_{N-1|i} = 0, S_{0|i} = \{0\}, ..., S_{N|i} = \{0\}$, which we will denote $(\{0\}, \{0\}, \mathbf{x}_{k|i}^0, \mathbf{u}_{k|i}^0)$. As this point is an optimum of the EcMPC RHOCP, the simplified EcMPC KKT conditions must be satisfied. Noting that for $S_{k|i} = \{0\}$, $\mathbf{c}_{k|i} = \{0\}$, $\bar{z}_{k|i}^* = \underline{z}_{k|i}^* = (x_{k|i}^0, c_{k|i}^0)$, $(\mathbf{x}_i^r, \mathbf{c}_i^r) = (\mathbf{x}_i^0, \mathbf{c}_i^0)$ and comparing conditions (D.5a) with (D.7), (D.5b) with (D.8), and (D.5c) with (D.6e) for $(\mathbf{x}_{k|i}^{*,n}, \mathbf{c}_{k|i}^{*,n}) = (\mathbf{x}_{k|i}^0, \mathbf{c}_{k|i}^0)$ it can be seen that they are equivalent for $\lambda_{k|i}^{*,n} = \alpha_{k|i}^{*,c} + \beta_{k|i}^{*,c} - \gamma_{k|i}^{*,c} - \mu_{k|i}^{*,c}$ for $k = 0, \ldots, N$. Furthermore, Theorem 7.3.1 guarantees condition (D.5d) is satisfied by $(x_{k|i}^{*,n}, c_{k|i}^{*,n}) = (x_{k|i}^0, c_{k|i}^0)$. It follows that at the optimum of EcMPC RHOCP the KKT conditions for both problems are equivalent and thus both satisfied. It follows that the point $(\mathbf{x}_i^0, \mathbf{c}_i^0, \{\alpha_{k|i}^{*,c} + \beta_{k|i}^{*,c} - \gamma_{k|i}^{*,c} - \mu_{k|i}^{*,c}$ for $k = 0, \ldots, N\})$ satisfies the simplified KKT conditions for EnMPC RHOCP simplified and is thus a locally optimal solution. □

D.2 Proof of the non-conservativeness of IcMPC

Analogously to the proof of 7.3.3 in the previous section, here we present the proof for Theorem 7.4.5. We do so again for a system with $n_x = 1$ with the proof for proof for higher-dimensional systems being analogous. We omit the $\{\cdot|i\}$ notation to conserve space and focus on simplified problems which incorporate only the constraints which do not clearly lead to the same Karush-Kuhn-Tucker (KKT) first-order necessary conditions [23]. Thus we take consider

$$\begin{aligned}&\text{InMPC RHOCP simplified}: \quad \mathbf{c}^* = \arg\ \min J^c_{InMPC}(\mathbf{x}, \mathbf{c})\\ &\text{subject to:} \quad \phi(x_{k+1}, x_k, c_k) = 0 \ \text{ for } k = 0, \dots, N-1\end{aligned}$$

IcMPC RHOCP simplified :

$$(\mathbf{c}^*, \mathbf{S}^*, \mathbf{S}^{+,*}, \mathbf{S}^{-,*}) = \arg \min_{\substack{\mathbf{c},\, \mathbf{S}\in S^{N+1},\\ \mathbf{S}^+\in(S^+)^N, \mathbf{S}^-\in(S^-)^N}} J_{\text{IcMPC}}(\mathbf{c}, \mathbf{S}, \mathbf{x}^0, \mathbf{c}^0)$$

$$\text{subject to: for } \forall s^-_{k+1} \in S^-_{k+1}, \forall s^+_{k+1} \in S^+_{k+1}, \forall s_k \in S_k, k = 0, ..., N-1 \tag{D.11}$$

$$C_k\bar{s}^+_{k+1} + \Phi_k\bar{s}_k + E_kc_k \geq 0, \quad \phi(x^0_{k+1} + \bar{s}^-_{k+1},\ x^0_k + \bar{s}_{k|i},\ c_{k|i} + u^0_k - Kx^0_k) \leq 0$$

$$C_k\underline{s}^+_{k+1} + \Phi_k\bar{s}_k + E_kc_k \geq 0, \quad \phi(x^0_{k+1} + \underline{s}^-_{k+1},\ x^0_k + \bar{s}_{k|i},\ c_{k|i} + u^0_k - Kx^0_k) \leq 0$$

$$C_k\bar{s}^+_{k+1} + \Phi_k\underline{s}_k + E_kc_k \geq 0, \quad \phi(x^0_{k+1} + \bar{s}^-_{k+1},\ x^0_k + \underline{s}_{k|i},\ c_{k|i} + u^0_k - Kx^0_k) \leq 0$$

$$C_k\underline{s}^+_{k+1} + \Phi_k\underline{s}_k + E_kc_k \geq 0 \quad \phi(x^0_{k+1} + \underline{s}^-_{k+1},\ x^0_k + \underline{s}_{k|i},\ c_{k|i} + u^0_k - Kx^0_k) \leq 0$$

Here the InMPC problem has been reformulated using $u_k = Kx_k + c_k$, $\Phi_k = D_k + E_kK$, $J_{InMPC}(\mathbf{x}, \mathbf{u}) = J^c_{InMPC}(\mathbf{x}, \mathbf{c}) = \sum_{k=0}^{\infty}\Big(\ \|x_k - x^r_k\|^2_Q + \|Kx_k + c_k - u^r_k\|^2_R\ \Big)$, $g(x_{k+1}, x_k, u_k) = \phi(x_{k+1}, x_k, c_k)$. To simplify the IcMPC RHOCP, constraints $(7.32d)$ have been removed as at the cMPC convergence point $S^+_k = S_k = S^-_k . = \{0\}$ The sets have been implemented using their bounds $\underline{s}^+_{k|i}$, $\bar{s}^+_{k|i}$,$\underline{s}^-_{k|i}$, $\bar{s}^-_{k|i} \in \mathbb{R}^{n_x}$ as optimization variables where $S^+_{k|i} = \{s : \underline{s}^+_{k|i} \leq s^+ \leq \bar{s}^+_{k|i}\}$, $S^-_{k|i} = \{s : \underline{s}^-_{k|i} \leq s^- \leq \bar{s}^-_{k|i}\}$. The augumented Lagrangian and the KKT conditions for the simplified NLP are

$$L_{\text{InMPC}}(\mathbf{x}, \mathbf{c}, \lambda) = J^c_{\text{InMPC}}(\mathbf{x}, \mathbf{c}) - \sum_{k=0}^{N-1} \lambda_k \phi(x_{k+1}, x_k, c_k)$$

$$0 = \frac{\partial J^c_{\text{InMPC}}(\mathbf{x}_i, \mathbf{c}_i)}{\partial x_0}|_{(\mathbf{x}^{*,n}, \mathbf{c}^{*,n})} - \lambda^{*,n}_0 \frac{\partial \phi(r, y, c)}{\partial y}|_{(x^{*,n}_1, x^{*,n}_0, c^{*,n}_0)},$$

$$
\begin{aligned}
&\text{for } k = 1, \dots, N-1 \\
0 =& \frac{\partial J^c_{\text{InMPC}}(\mathbf{x}_i, \mathbf{c}_i)}{\partial x_k}|_{(\mathbf{x}^*, \mathbf{c}^{*,n})} - \lambda^{*,n}_k \frac{\partial \phi(r,y,c)}{\partial y}|_{(x^{*,n}_{k+1}, x^{*,n}_k, c^{*,n}_k)} - \lambda^{*,n}_{k-1} \frac{\partial \phi(r,y,c)}{\partial r}|_{(x^{*,n}_k, x^{*,n}_{k-1}, c^{*,n}_{k-1})} \\
&\text{and for } k = 0, \dots, N-1 \\
0 =& \frac{\partial J^c_{\text{InMPC}}(\mathbf{x}_i, \mathbf{c})}{\partial c_k}|_{(\mathbf{x}^{*,n}, \mathbf{c}^{*,n})} - \lambda^{*,n}_k \frac{\partial \phi(r,y,c)}{\partial c}|_{(x^{*,n}_{k+1}, x^{*,n}_k, u^{*,n}_k)} \\
0 =& \phi(x^{*,n}_{k+1}, x^{*,n}_k, c^{*,n}_k)
\end{aligned}
$$

where $(\cdot)^{*,n}$ denotes the value at the local optimum point for InMPC simplified and $\mathbf{x}^{*,n}_i$ is obtained from $\mathbf{c}^{*,n}_i$ and $\phi(x_{k+1}, x_k, c_k)$. The augumented Lagrangian and the KKT conditions for the simplified IcMPC RHOCP become

$$
\begin{aligned}
&L_{\text{IcMPC}}(\mathbf{c}, \mathbf{S}, \mathbf{x}^0, \mathbf{u}^0, \alpha, \beta, \gamma, \mu, \psi, \eta, \xi, \tau) = J_{\text{IcMPC}}(\mathbf{c}, \mathbf{S}, \mathbf{x}^0, \mathbf{u}^0) + \\
&+ \sum_{k=0}^{N-1} \Big(\alpha_k \phi(z^1_k) + \beta_k \phi(z^2_k) + \gamma_k \phi(z^3_k) + \mu_k \phi(z^4_k) \\
&- (\psi_k (C_k \bar{s}^-_{k+1} + \Phi_k \bar{s}_k + E_k c_k) + \eta_k (C_k \underline{s}^-_{k+1} + \Phi_k \bar{s}_k + E_k c_k) \\
&+ \xi_k (C_k \bar{s}^-_{k+1} + \Phi_k \underline{s}_k + E_k c_k) + \tau_k (C_k \underline{s}^-_{k+1} + \Phi_k \underline{s}_k + E_k c_k)) \Big) \\
&\text{for } k = 1, \dots, N-1 \\
0 =& \alpha^{*,c}_{k-1} \frac{\partial \phi(r,y,c)}{\partial r}|_{z^{1,*,c}_{k-1}} + \gamma^{*,c}_{k-1} \frac{\partial \phi(r,y,c)}{\partial r}|_{z^{3,*,c}_{k-1}} && \text{(D.14}a\text{)} \\
0 =& \beta^{*,c}_{k-1} \frac{\partial \phi(r,y,c)}{\partial r}|_{z^{2,*,c}_{k-1}} + \mu^{*,c}_{k-1} \frac{\partial \phi(r,y,c)}{\partial r}|_{z^{4,*,c}_{k-1}} && \text{(D.14}b\text{)} \\
0 =& -\psi^{*,c}_{k-1} \frac{\partial \phi(r,y,c)}{\partial r}|_{z^{5,*,c}_{k-1}} - \xi^{*,c}_{k-1} \frac{\partial \phi(r,y,c)}{\partial r}|_{z^{7,*,c}_{k-1}} && \text{(D.14}c\text{)} \\
0 =& -\eta^{*,c}_{k-1} \frac{\partial \phi(r,y,c)}{\partial r}|_{z^{6,*,c}_{k-1}} - \tau^{*,c}_{k-1} \frac{\partial \phi(r,y,c)}{\partial r}|_{z^{8,*,c}_{k-1}} && \text{(D.14}d\text{)} \\
&\text{and for } k = 0, \dots, N-1 \\
0 =& \frac{\partial J_{\text{IcMPC}}}{\partial \bar{s}_k}|_{\mathbf{z}^{*,\mathbf{c}}_\mathbf{i}} + \alpha^{*,c}_k \frac{\partial \phi(r,y,c)}{\partial y}|_{z^{1,*,c}_k} + \beta^{*,c}_k \frac{\partial \phi(r,y,c)}{\partial y}|_{z^{2,*,c}_k} \\
&- \psi^{*,c}_k \frac{\partial \phi(r,y,c)}{\partial y}|_{z^{5,*,c}_k} - \eta^{*,c}_k \frac{\partial \phi(r,y,c)}{\partial y}|_{z^{6,*,c}_k} && \text{(D.14}e\text{)} \\
0 =& \frac{\partial J_{\text{IcMPC}}}{\partial \underline{s}_k}|_{\mathbf{z}^{*,\mathbf{c}}_\mathbf{i}} + \gamma^{*,c}_k \frac{\partial \phi(r,y,c)}{\partial y}|_{z^{3,*,c}_k} + \mu^{*,c}_k \frac{\partial \phi(r,y,c)}{\partial y}|_{z^{4,*,c}_k} \\
&- \xi^{*,c}_k \frac{\partial \phi(r,y,c)}{\partial y}|_{z^{7,*,c}_k} - \tau^{*,c}_k \frac{\partial \phi(r,y,c)}{\partial y}|_{z^{8,*,c}_k} && \text{(D.14}f\text{)} \\
0 =& \frac{\partial J_{\text{IcMPC}}}{\partial c_k}|_{\mathbf{z}^{*,\mathbf{c}}_\mathbf{i}} + \alpha^{*,c}_k \frac{\partial \phi(r,y,c)}{\partial c}|_{z^{1,*,c}_k} + \beta^{*,c}_k \frac{\partial \phi(r,y,c)}{\partial c}|_{z^{2,*,c}_k} \\
&+ \gamma^{*,c}_k \frac{\partial \phi(r,y,c)}{\partial c}|_{z^{3,*,c}_k} + \mu^{*,c}_k \frac{\partial \phi(r,y,c)}{\partial c}|_{z^{4,*,c}_k} - \psi^{*,c}_k \frac{\partial \phi(r,y,c)}{\partial c}|_{z^{5,*,c}_k}
\end{aligned}
$$

$$- \eta_k^{*,c}\frac{\partial \phi(r,y,c)}{\partial c}|_{z_k^{6,*,c}} - \xi_k^{*,c}\frac{\partial \phi(r,y,c)}{\partial c}|_{z_k^{7,*,c}} - \tau_k^{*,c}\frac{\partial \phi(r,y,c)}{\partial c}|_{z_k^{8,*,c}} \quad \text{(D.14}g\text{)}$$

$$0 = \alpha_k^{c,*}\phi(z_k^{1,c,*}) = \beta_k^{c,*}\phi(z_k^{2,c,*}) = \gamma_k^{c,*}\phi(z_k^{3,c,*}) = \mu_k^{c,*}\phi(z_k^{4,c,*}) \quad \text{(D.14}h\text{)}$$

$$0 = \psi_k^{c,*}(C_k\bar{s}_{k+1}^{-,c,*} + \Phi_k\bar{s}_k^{c,*} + E_k c_k^{c,*}) = \eta_k^{c,*}(C_k\underline{s}_{k+1}^{-,c,*} + \Phi_k\bar{s}_k^{c,*} + E_k c_k^{c,*})$$

$$0 = \xi_k^{c,*}(C_k\bar{s}_{k+1}^{-,c,*} + \Phi_k\underline{s}_k^{c,*} + E_k c_k^{c,*}) = \tau_k^{c,*}(C_k\underline{s}_{k+1}^{-,c,*} + \Phi_k\underline{s}_k^{c,*} + E_k c_k^{c,*})$$

where: $\mathbf{z}_i^* = (\mathbf{c}^{c,*}, \mathbf{S}^{c,*}, \mathbf{S}^{+,c,*}, \mathbf{S}^{-,c,*}, \mathbf{x}_i^0, \mathbf{u}_i^*)$

$$z_k^1 = (x_{k+1}^0 + \bar{s}_{k+1}^-,\ x_k^0 + \bar{s}_k,\ \sigma_k),\quad z_k^2 = (x_{k+1}^0 + \underline{s}_{k+1}^-,\ x_k^0 + \bar{s}_k,\ \sigma_k)$$

$$z_k^3 = (x_{k+1}^0 + \bar{s}_{k+1}^-,\ x_k^0 + \underline{s}_k,\ \sigma_k),\quad z_k^4 = (x_{k+1}^0 + \underline{s}_{k+1}^-,\ x_k^0 + \underline{s}_k,\ \sigma_k)$$

$$z_k^5 = (x_{k+1}^0 + \bar{s}_{k+1}^+,\ x_k^0 + \bar{s}_k,\ \sigma_k),\quad z_k^6 = (x_{k+1}^0 + \underline{s}_{k+1}^+,\ x_k^0 + \bar{s}_k,\ \sigma_k)$$

$$z_k^7 = (x_{k+1}^0 + \bar{s}_{k+1}^+,\ x_k^0 + \underline{s}_k,\ \sigma_k),\quad z_k^8 = (x_{k+1}^0 + \underline{s}_{k+1}^+,\ x_k^0 + \underline{s}_k,\ \sigma_k)$$

and $z_k^{1,*,c} - z_k^{8,*,c}$ are analogously defined with $\sigma_k = c_k + u_k^0 - Kx_k^0$. Now at the convergence point $(\mathbf{c}_i^{*,n}, \mathbf{S}_i^{*,n}) = (0, \{\{0\}, \ldots, \{0\}\})$ summing (D.14a)-(D.14d) for $k = 0$ and (D.14a)-(D.14f) for $k > 1$ we obtain

$$0 = \frac{\partial J_{\text{IcMPC}}}{\partial x_0}|_{\mathbf{z_i}^{*,\mathbf{c}}} + (\alpha_0^{*,c} + \beta_0^{*,c} + \gamma_0^{*,c} + \mu_0^{*,c} - \psi_0^{*,c} - \eta_0^{*,c} - \xi_0^{*,c} - \tau_0^{*,c})\frac{\partial \phi(r,y,c)}{\partial y}|_{(x_1^0,\, x_0^0,\, c_0^0)} \quad \text{(D.15)}$$

$$0 = \frac{\partial J_{\text{IcMPC}}}{\partial x_k}|_{\mathbf{z_i}^{*,\mathbf{c}}} + (\alpha_k^{*,c} + \beta_k^{*,c} + \gamma_k^{*,c} + \mu_k^{*,c} - \psi_k^{*,c} - \eta_k^{*,c} - \xi_k^{*,c} - \tau_k^{*,c})\frac{\partial \phi(r,y,c)}{\partial y}|_{(x_{k+1}^0,\, x_k^0,\, c_k^0)}$$
$$+ (\alpha_{k-1}^{*,c} + \gamma_{k-1}^{*,c} + \beta_{k-1}^{*,c} + \mu_{k-1}^{*,c} - \psi_{k-1}^{*,c} - \eta_{k-1}^{*,c} - \xi_{k-1}^{*,c} - \tau_{k-1}^{*,c})\frac{\partial \phi(r,y,c)}{\partial r}|_{(x_k^0,\, x_{k-1}^0,\, c_{k-1}^0)} \quad \text{(D.16)}$$

for $k \geq 1$ with $c_k^0 = u_k^0 - Kx_k^0$ because at the point of interest $z_k^{1,*,c} = z_k^{2,*,c} = \ldots = z_k^{8,*,c}$ and the cost derivative for a given k is non-zero for either the bar or the underbar variable, but never both at the same time due to the min-max cost formulation. Similarly for $k \geq 0$ Equation (D.14g) becomes

$$0 = \frac{\partial J_{\text{IcMPC}}}{\partial c_k}|_{\mathbf{z_i}^{*,\mathbf{c}}} + (\alpha_k^{*,c} + \beta_k^{*,c} + \gamma_k^{*,c} + \mu_k^{*,c} - \psi_k^{*,c} - \eta_k^{*,c} - \xi_k^{*,c} - \tau_k^{*,c})\frac{\partial \phi(r,y,c)}{\partial c}|_{(x_{k+1}^0,\, x_k^0,\, c_k^0)} \quad \text{(D.17)}$$

Now using (D.15), (D.16), (D.17) together and comparing to the InMPC KKT for the simplified problem with $\mathbf{x} = \mathbf{x}^0, \mathbf{c} = \mathbf{c}^0$ it is clear that the point $(\mathbf{x}_i^0, \mathbf{c}_i^0, \{-\alpha_k^{*,c} - \beta_k^{*,c} - \gamma_k^{*,c} - \mu_k^{*,c} + \psi_k^{*,c} + \eta_k^{*,c} + \xi_k^{*,c} + \tau_k^{*,c}$ for $k = 0, \ldots, N\})$ satisfies the simplified KKT conditions for InMPC RHOCP simplified. This point, to which the successive convex programs converge, is also a local optimum for the original NLP.

References

[1] Jerrold E Marsden and Matthew West. "Discrete mechanics and variational integrators". In: *Acta Numerica* 10.1 (2001), pp. 357–514.

[2] Basil Kouvaritakis and Mark Cannon. *Model Predictive Control: Classical, Robust and Stochastic*. Advanced Textbooks in Control and Signal Processing. Springer International Publishing, 2016.

[3] Sigrid Leyendecker and Sina Ober-Blöbaum. "A Variational Approach to Multirate Integration for Constrained Systems". In: *Multibody Dynamics: Computational Methods and Applications*. Ed. by Jean-Claude Samin and Paul Fisette. Dordrecht: Springer Netherlands, 2013, pp. 97–121.

[4] T Gail, S Ober-Blöbaum, and S Leyendecker. "Variational multirate integration in discrete mechanics and optimal control". In: *Proceedings of ECCOMAS*. 2017, pp. 1–4.

[5] Tobias Gail. *Numerical studies on variational multirate integrators and their use in discrete mechanics and optimal control*. PhD thesis, University of Erlangen–Nuremberg, 2021.

[6] Raphael Cagienard et al. "Move blocking strategies in receding horizon control". In: *Journal of Process Control* 17.6 (2007), pp. 563–570.

[7] Mingzhao Yu and Lorenz T Biegler. "A Stable and Robust NMPC Strategy with Reduced Models and Nonuniform Grids". In: *IFAC-PapersOnLine* 49.7 (2016), pp. 31–36.

[8] Rohan C Shekhar and Chris Manzie. "Optimal move blocking strategies for model predictive control". In: *Automatica* 61 (2015), pp. 27–34.

[9] Mark Cannon et al. "Robust Tubes in Nonlinear Model Predictive Control". In: *IEEE Transactions on Automatic Control* 56.8 (2011), pp. 1942–1947.

[10] Yana Lishkova et al. "A Multirate Variational Approach to Simulation and Optimal Control for Flexible Spacecraft". In: *Advances in the Astronautical Sciences* 175 (2021).

[11] Yana Lishkova, Mai Bando, and Sina Ober-Blöbaum. "Variational approach for modelling and optimal control of electrodynamic tether motion". In: *International Astronautical Congress (IAC)*. 2023.

[12] Yana Lishkova, Sina Ober-Blöbaum, and Sigrid Leyendecker. "Multirate discrete mechanics and optimal control for a flexible satellite model". In: *GAMM Rundbrief 2023*.

[13] Yana Lishkova, Mark Cannon, and Sina Ober-Blöbaum. "A Multirate Variational Approach to Nonlinear MPC". In: *2022 European Control Conference (ECC)*. IEEE. 2022, pp. 729–735.

[14] Yana Lishkova and Mark Cannon. "Robust receding horizon control for convex dynamics and bounded disturbances". In: *arXiv preprint:2302.07744* (2023).

[15] Y. Lishkova and M.Cannon. "Optimization-based trajectory generation and receding horizon control for systems with convex dynamics". In: *Conference on Decision and Control (CDC) 2023* (2023).

[16] Yana Lishkova et al. "Discrete Lagrangian neural networks with automatic symmetry discovery". In: *IFAC-PapersOnLine* 56 (2023).

[17] Yana Lishkova et al. "Divert-feasible lunar landing under navigational uncertainty". In: *Conference on Decision and Control (CDC) 2024* (2024).

[18] Sina Ober-Blöbaum. "Discrete mechanics and optimal control". PhD thesis. University of Paderborn, 2008.

[19] Sina Ober-Blöbaum, Oliver Junge, and Jerrold E Marsden. "Discrete mechanics and optimal control: an analysis". In: *ESAIM: Control, Optimisation and Calculus of Variations* 17.2 (2011), pp. 322–352.

[20] Matthew West. "Variational integrators". PhD thesis. California Institute of Technology, 2004.

[21] Arieh Iserles. *A First Course in the Numerical Analysis of Differential Equations*. 2nd ed. Cambridge Texts in Applied Mathematics. Cambridge University Press, 2008.

[22] David F Griffiths and Desmond J Higham. *Numerical methods for ordinary differential equations: initial value problems*. Springer Science & Business Media, 2010.

[23] Jorge Nocedal and Stephen J Wright. *Numerical optimization*. Springer, 1999.

[24] Stephen P Boyd and Lieven Vandenberghe. *Convex optimization*. Cambridge university press, 2004.

[25] Dina Razafindralandy, Aziz Hamdouni, and Marx Chhay. "A review of some geometric integrators". In: *Advanced Modeling and Simulation in Engineering Sciences* 5 (2018), pp. 1–67.

[26] Ernst Hairer, Christian Lubich, and Gerhard Wanner. *Geometric Numerical Integration. Structure-Preserving Algorithms for Ordinary Differential Equations*. 2nd ed. Vol. 31. Springer Series in Computational Mathematics. Springer Science & Business Media, 2006.

[27] Robert I Mclachlan and G Reinout W Quispel. "Geometric integrators for ODEs". In: *Journal of Physics A, Mathematical and General* 39.19 (May 2006), pp. 5251–5285.

[28] Jerrold E Marsden and Tudor S Ratiu. *Introduction to mechanics and symmetry: a basic exposition of classical mechanical systems*. Vol. 17. Springer Science & Business Media, 2013.

[29] Jesus M Sanz-Serna. "Symplectic integrators for Hamiltonian problems: an overview". In: *Acta numerica* 1 (1992), pp. 243–286.

[30] Vladimir Igorevich Arnol'd. *Mathematical methods of classical mechanics*. Vol. 60. Springer Science & Business Media, 1989.

[31] Ge Zhong and Jerrold E Marsden. "Lie-poisson hamilton-jacobi theory and lie-poisson integrators". In: *Physics Letters A* 133.3 (1988), pp. 134–139.

[32] C. Kane et al. "Variational integrators and the Newmark algorithm for conservative and dissipative mechanical systems". In: *International Journal for Numerical Methods in Engineering* 49.10 (2000), pp. 1295–1325.

[33] Adrian Lew et al. "An overview of variational integrators". In: *Finite Element Methods: 1970's and Beyond* (2004).

[34] Oliver Junge, Jerrold E Marsden, and Sina Ober-Blöbaum. "Discrete mechanics and optimal control". In: *IFAC Proceedings Volumes* 38.1 (2005), pp. 538–543.

[35] Sigrid Leyendecker, Jerrold E Marsden, and Michael Ortiz. "Variational integrators for constrained dynamical systems". In: *ZAMM-Journal of Applied Mathematics and Mechanics/Zeitschrift für Angewandte Mathematik und Mechanik: Applied Mathematics and Mechanics* 88.9 (2008), pp. 677–708.

[36] Sigrid Leyendecker et al. "Discrete mechanics and optimal control for constrained systems". In: *Optimal Control Applications and Methods* 31.6 (2010), pp. 505–528.

[37] Peter Betsch et al. “Variational integrators and energy-momentum schemes for flexible multibody dynamics”. In: *Journal of Computational and Nonlinear Dynamics* 5.3 (2010).

[38] Marin Kobilarov, Jerrold Marsden, and Gaurav S Sukhatme. “Geometric Discretization of Nonholonomic Systems with Symmetries”. In: *Discrete and Continuous Dynamical Systems-Series S* 3.1 (2010), pp. 61–84.

[39] Nawaf Bou-Rabee and Houman Owhadi. “Stochastic variational integrators”. In: *IMA Journal of Numerical Analysis* 29.2 (2009), pp. 421–443.

[40] Sina Ober-Blöbaum et al. “Variational integrators for electric circuits”. In: *Journal of Computational Physics* 242 (2013), pp. 498–530.

[41] Jeongseok Lee et al. “A Linear-Time Variational Integrator for Multibody Systems”. In: *Algorithmic Foundations of Robotics XII: Proceedings of the Twelfth Workshop on the Algorithmic Foundations of Robotics*. Ed. by Ken Goldberg et al. Springer International Publishing, 2020, pp. 352–367.

[42] David JN Limebeer, Sina Ober-Blöbaum, and Farhang Haddad Farshi. “Variational Integrators for Dissipative Systems”. In: *IEEE Transactions on Automatic Control* 65.4 (2020), pp. 1381–1396.

[43] E Weinan et al. “Heterogeneous multiscale methods: a review”. In: *Communications in computational physics* 2.3 (2007), pp. 367–450.

[44] Bruce A Conway. “A survey of methods available for the numerical optimization of continuous dynamic systems”. In: *Journal of Optimization Theory and Applications* 152.2 (2012), pp. 271–306.

[45] Francesco Biral, Enrico Bertolazzi, and Paolo Bosetti. “Notes on numerical methods for solving optimal control problems”. In: *IEEJ Journal of Industry Applications* 5.2 (2016), pp. 154–166.

[46] Anil V Rao. “A survey of numerical methods for optimal control”. In: *Advances in the Astronautical Sciences* 135.1 (2009), pp. 497–528.

[47] Matthew Kelly. “An introduction to trajectory optimization: How to do your own direct collocation”. In: *SIAM Review* 59.4 (2017), pp. 849–904.

[48] Richard Bellman. *Dynamic Programming*. 1st ed. Princeton, NJ, USA: Princeton University Press, 1957.

[49] Dimitri P Bertsekas. *Dynamic programming and optimal control*. Athena scientific Belmont, MA, 1995.

[50] Rein Luus. *Iterative dynamic programming*. Chapman & Hall/CRC Press, 2000.

[51] David H Jacobson and David Q Mayne. *Differential dynamic programming*. Modern Analytic and Computational Methods in Science and Mathematics 24. New York: American Elsevier Pub. Co., 1970.

[52] Zhong Wang and Yan Li. “An indirect method for inequality constrained optimal control problems”. In: *IFAC-PapersOnLine* 50.1 (2017), pp. 4070–4075.

[53] Amin Nikoobin and M Moradi. “Indirect solution of optimal control problems with state variable inequality constraints: finite difference approximation”. In: *Robotica* 35.1 (2017), pp. 50–72.

[54] Francesco Topputo and C Zhang. “Survey of direct transcription for low-thrust space trajectory optimization with applications”. In: *Abstract and Applied Analysis*. Vol. 2014. Hindawi. 2014.

[55] Michael Dellnitz et al. “A multi-objective approach to the design of low thrust space trajectories using optimal control”. In: *Celestial Mechanics and Dynamical Astronomy* 105.1-3 (2009), p. 33.

[56] Ashley Moore, Sina Ober-Blöbaumy, and Jerrold E Marsden. "Optimization of Spacecraft Trajectories: A Method Combining Invariant Manifold Techniques and Discrete Mechanics and Optimal Control". In: (2009).

[57] Ashley Moore, Sina Ober-Blöbaum, and Jerrold E Marsden. "Trajectory design combining invariant manifolds with discrete mechanics and optimal control". In: *Journal of Guidance, Control, and Dynamics* 35.5 (2012), pp. 1507–1525.

[58] Sina Ober-Blöbaum, Maik Ringkamp, and Garlef zum Felde. "Solving multiobjective optimal control problems in space mission design using discrete mechanics and reference point techniques". In: *2012 IEEE 51st IEEE Conference on Decision and Control (CDC)*. IEEE. 2012, pp. 5711–5716.

[59] Oliver Junge and Sina Ober-Blobaum. "Optimal reconfiguration of formation flying satellites". In: *Proceedings of the 44th IEEE Conference on Decision and Control*. IEEE. 2005, pp. 66–71.

[60] Oliver Junge, Jerrold E Marsden, and Sina Ober-Blobaum. "Optimal Reconfiguration of Formation Flying Spacecraft—a Decentralized Approach". In: *Proceedings of the 45th IEEE Conference on Decision and Control*. IEEE. 2006, pp. 5210–5215.

[61] Jiawei Zhang, Weizhong Zhang, and Jiayuan Shan. "A new DMOC-based approach to solve Goddard rocket problem". In: *2012 IEEE International Conference on Mechatronics and Automation*. IEEE. 2012, pp. 2165–2169.

[62] Jiawei Zhang, Weizhong Zhang, and Jiayuan Shan. "DMOC approach to solve Goddard rocket problem in comparison with RPM". In: *Proceedings of the 32nd Chinese Control Conference*. IEEE. 2013, pp. 2185–2189.

[63] Zdravko Terze et al. "Discrete mechanics and optimal control optimization of flapping wing dynamics for Mars exploration". In: *Aerospace Science and Technology* 106 (2020), p. 106131.

[64] Marin Kobilarov. "Discrete geometric motion control of autonomous vehicles". PhD thesis. University of Southern California, 2008.

[65] Dan Wang and Weizhong Zhang. "Trajectory optimization and tracking control of mobile robots based on DMOC". In: *Proceedings of the 33rd Chinese Control Conference*. IEEE. 2014, pp. 2422–2427.

[66] Eva Kanso and Jerrold E Marsden. "Optimal motion of an articulated body in a perfect fluid". In: *Proceedings of the 44th IEEE Conference on Decision and Control*. IEEE. 2005, pp. 2511–2516.

[67] Sigrid Leyendecker et al. "Discrete mechanics and optimal control for constrained multibody dynamics". In: *International Design Engineering Technical Conferences and Computers and Information in Engineering Conference*. Vol. 4806. 2007, pp. 623–632.

[68] Sina Ober-Blöbaum and Julia Timmermann. "Optimal control for a pitcher's motion modeled as constrained mechanical system". In: *International Design Engineering Technical Conferences and Computers and Information in Engineering Conference*. Vol. 49019. 2009, pp. 597–606.

[69] MW Koch, M Ringkamp, and S Leyendecker. "Discrete mechanics and optimal control of walking gaits". In: *Journal of Computational and Nonlinear Dynamics* 12.2 (2017).

[70] Michael W Koch and Sigrid Leyendecker. "Structure preserving optimal control of a 3d-dimensional upright gait". In: *ECCOMAS Thematic Conference on Multibody Dynamics 2015, Barcelona, Spain* (2015).

[71] Sigrid Leyendecker, David Pekarek, and Jerrold E Marsden. "Structure preserving optimal control of three-dimensional compass gait". In: *Modeling, Simulation and Optimization of Bipedal Walking*. Springer, 2013, pp. 99–116.

[72] Ashley Moore. "Time Adaptive Discrete Mechanics and Optimal Control". PhD thesis. Keck Institute for Space Studies, California Institute of Technology, 2011.

[73] Maik Ringkamp, Sina Ober-Blöbaum, and Sigrid Leyendecker. "Discrete mechanics and mixed integer optimal control of dynamical systems". In: *PAMM* 14.1 (2014), pp. 919–920.

[74] Weizhong Zhang, Dan Wang, and Tamer Inanc. "A multiphase DMOC-based trajectory optimization method". In: *Optimal Control Applications and Methods* 39.1 (2018), pp. 114–129.

[75] Dan Wang, Weizhong Zhang, and Jiayuan Shan. "A multi-phase DMOC-based optimal trajectory generation methodology for a quadrotor". In: *Proceedings of the 33rd Chinese Control Conference*. IEEE. 2014, pp. 8984–8989.

[76] David Pekarek, Aaron D Ames, and Jerrold E Marsden. "Discrete mechanics and optimal control applied to the compass gait biped". In: *2007 46th IEEE Conference on Decision and Control*. IEEE. 2007, pp. 5376–5382.

[77] Sina Ober-Blöbaum, Maik Ringkamp, and Garlef zum Felde. "Solving multiobjective optimal control problems in space mission design using discrete mechanics and reference point techniques". In: *2012 IEEE 51st IEEE Conference on Decision and Control (CDC)*. IEEE. 2012, pp. 5711–5716.

[78] Weizhong Zhang, Tamer Inanc, and Jerrold E Marsden. "DMOC approach of real-time trajectory generation for mechanical systems". In: *2008 10th International Conference on Control, Automation, Robotics and Vision*. IEEE. 2008, pp. 2192–2195.

[79] Marin B Kobilarov and Jerrold E Marsden. "Discrete geometric optimal control on Lie groups". In: *IEEE Transactions on Robotics* 27.4 (2011), pp. 641–655.

[80] David Q Mayne et al. "Constrained model predictive control: Stability and optimality". In: *Automatica* 36.6 (2000), pp. 789–814.

[81] James Blake Rawlings, David Q Mayne, Moritz Diehl, et al. *Model predictive control: theory, computation, and design*. Vol. 2. Nob Hill Publishing Madison, WI, 2017.

[82] Mark Cannon. "C21 Model Predictive Control". In: *Lecture Notes, Oxford University, Oxford* (2016).

[83] J Anthony Rossiter. *Model-based predictive control: a practical approach*. CRC press, 2003.

[84] DM Raimondo et al. "Multirate sliding mode disturbance compensation for model predictive control". In: *International Journal of Robust and Nonlinear Control* 25.16 (2015), pp. 2984–3003.

[85] Gilberto Pin et al. "Robust model predictive control of nonlinear systems with bounded and state-dependent uncertainties". In: *IEEE Transactions on automatic control* 54.7 (2009), pp. 1681–1687.

[86] Dimitri P Bertsekas and Ian B Rhodes. "On the minimax reachability of target sets and target tubes". In: *Automatica* 7.2 (1971), pp. 233–247.

[87] David Q Mayne, María M Seron, and SV Raković. "Robust model predictive control of constrained linear systems with bounded disturbances". In: *Automatica* 41.2 (2005), pp. 219–224.

[88] David Q Mayne and Eric C Kerrigan. "Tube-based robust nonlinear model predictive control". In: *IFAC Proceedings Volumes* 40.12 (2007), pp. 36–41.

[89] Tor Aksel N. Heirung et al. "Stochastic model predictive control — how does it work?" In: *Computers & Chemical Engineering* 114 (2018). FOCAPO/CPC 2017, pp. 158–170.

[90] X. Lu and M. Cannon. "Robust Adaptive Tube Model Predictive Control". In: *2019 American Control Conference (ACC)*. 2019, pp. 3695–3701.

[91] Monimoy Bujarbaruah et al. "Adaptive MPC under time varying uncertainty: Robust and Stochastic". In: *arXiv preprint arXiv:1909.13473* (2019).

[92] Marko Tanaskovic et al. "Adaptive model predictive control for constrained linear systems". In: *2013 European Control Conference (ECC)*. IEEE. 2013, pp. 382–387.

[93] Ari Stern and Eitan Grinspun. "Implicit-Explicit Variational Integration of Highly Oscillatory Problems". In: *Multiscale Modeling & Simulation* 7.4 (2009), pp. 1779–1794.

[94] Ioannis G Kevrekidis et al. "Equation-free, coarse-grained multiscale computation: Enabling mocroscopic simulators to perform system-level analysis". In: *Communications in Mathematical Sciences* 1.4 (2003), pp. 715–762.

[95] Ioannis G. Kevrekidis and Giovanni Samaey. "Equation-Free Multiscale Computation: Algorithms and Applications". In: *Annual Review of Physical Chemistry* 60.1 (2009). PMID: 19335220, pp. 321–344.

[96] E Weinan and Bjorn Engquist. "The heterognous multiscale methods". In: *Communications in Mathematical Sciences* 1.1 (2003), pp. 87–132.

[97] Bjorn Engquist and Yen-Hsi Tsai. "Heterogeneous multiscale methods for stiff ordinary differential equations". In: *Mathematics of computation* 74.252 (2005), pp. 1707–1742.

[98] Michael Günther, Anne Kvaernø, and Peter Rentrop. "Multirate partitioned Runge-Kutta methods". In: *BIT Numerical Mathematics* 41 (2001), pp. 504–514.

[99] Michael Günther and Adrian Sandu. "Multirate generalized additive Runge Kutta methods". In: *Numerische Mathematik* 133 (2016), pp. 497–524.

[100] Bruno Seny et al. "Multirate time stepping for accelerating explicit discontinuous Galerkin computations with application to geophysical flows". In: *International Journal for Numerical Methods in Fluids* 71.1 (2013), pp. 41–64.

[101] Donald R Smith. *Singular-perturbation theory: an introduction with applications*. Cambridge University Press, 1985.

[102] Neil Fenichel. "Geometric singular perturbation theory for ordinary differential equations". In: *Journal of differential equations* 31.1 (1979), pp. 53–98.

[103] M Azadi et al. "Dynamics and control of a smart flexible satellite moving in an orbit". In: *Multibody System Dynamics* 35.1 (2015), pp. 1–23.

[104] Francesco Colombi, Andrea Colagrossi, and Michèle Lavagna. "Characterisation of 6DOF natural and controlled relative dynamics in cislunar space". In: *Acta Astronautica* 196 (2022), pp. 369–379.

[105] Tobias Gail, Sigrid Leyendecker, and Sina Ober-Blöbaum. "On the role of quadrature rules and system dimensions in variational multirate integrators". In: *The 3rd Joint International Conference on Multibody System Dynamics, The 7th Asian Conference on Multibody Dynamics, Busan, Korea* (2014).

[106] Tobias Gail, Sigrid Leyendecker, and Sina Ober-Blöbaum. "Computing time investigations for variational multirate integration". In: *PAMM* 13.1 (2013), pp. 43–44.

[107] Tobias Gail, Sigrid Leyendecker, and Sina Ober-Blöbaum. "Computing time investigations for variational multirate integration". In: *ECCOMAS Multibody Dynamics 2013, Zagreb, Croatia* 13.1 (2013), pp. 43–44.

[108] Tobias Gail, Sigrid Leyendecker, and Sina Ober-Blöbaum. "Limitations of computing time savings in variational multirate integrations". In: *PAMM* 14.1 (2014), pp. 45–46.

[109] Sina Ober-Blöbaum et al. "Variational multirate integrators". In: *Under review* (2023).

[110] Sina Ober-Blöbaum and Mats Vermeeren. "Superconvergence of Galerkin variational integrators". In: *IFAC-PapersOnLine* 54.19 (2021), pp. 327–333.

[111] James Hall and Melvin Leok. "Spectral variational integrators". In: *Numerische Mathematik* 130 (2015), pp. 681–740.

[112] Tobias Gail. "Numerical studies on variational multirate integrators and their use in discrete mechanics and optimal control". PhD thesis. Friedrich-Alexander-Universitaet Erlangen-Nuernberg (Germany), 2021.

[113] Jeffrey M Wendlandt and Jerrold E Marsden. "Mechanical integrators derived from a discrete variational principle". In: *Physica D: Nonlinear Phenomena* 106.3-4 (1997), pp. 223–246.

[114] Bernd Simeon. "Order reduction of stiff solvers at elastic multibody systems". In: *Applied Numerical Mathematics* 28.2-4 (1998), pp. 459–475.

[115] James Bradbury et al. "JAX: composable transformations of Python+NumPy programs". In: *Version 0.2.5* (2018).

[116] Qing-Lei Hu, Zidong Wang, and Huijun Gao. "Sliding mode and shaped input vibration control of flexible systems". In: *IEEE Transactions on Aerospace and Electronic systems* 44.2 (2008), pp. 503–519.

[117] John A Breakwell. "Optimal feedback slewing of flexible spacecraft". In: *Journal of Guidance and Control* 4.5 (1981), pp. 472–479.

[118] F.L. Markley. "Large angle maneuver strategies for flexible spacecraft". In: *AAS/AIAA Astrodynamics Specialist Conference* 40.2 (1979), pp. 625–647.

[119] James D Turner and John L Junkins. "Optimal large-angle single-axis rotational maneuvers of flexible spacecraft". In: *Journal of Guidance and Control* 3.6 (1980), pp. 578–585.

[120] James D Turner and Hon M Chun. "Optimal distributed control of a flexible spacecraft during a large-angle maneuver". In: *Journal of Guidance, Control, and Dynamics* 7.3 (1984), pp. 257–264.

[121] John L Junkins and Youdan Kim. *Introduction to dynamics and control of flexible structures*. American Institute of Aeronautics and Astronautics, 1993.

[122] Leonard Meirovitch. *Fundamentals of vibrations*. Waveland Press, 2010.

[123] Joel N Franklin. *Matrix theory*. Courier Corporation, 2012.

[124] Kathleen C Laurini et al. "The global exploration roadmap and expanding human/robotic exploration mission collaboration opportunities". In: *IAF 66th International Astronautical Congress*. 2015, pp. 1–9.

[125] J Peláez et al. "Dynamics and stability of tethered satellites at lagrangian points". In: *Ariadna Study* 7 (2008), p. 4201.

[126] Yuki Kayama, Mai Bando, and Shinji Hokamoto. "Sparse Optimal Control for Nonlinear Trajectory Design in Three-Body Problem". In: *Transactions of the Japan Society for Aeronautical and Space Sciences, Aerospace Technology Japan* 19.4 (2021), pp. 545–552.

[127] Davide Curreli et al. “Three-body dynamics and self-powering of an electrodynamic tether in a plasmasphere”. In: *Journal of propulsion and power* 26.3 (2010), pp. 385–393.

[128] Sergio Cuevas del Valle, Hodei Urrutxua, and Pablo Solano-López. “Optimal Floquet Stationkeeping under the Relative Dynamics of the Three-Body Problem”. In: *Aerospace* 10.5 (2023), p. 393.

[129] Andrea Colagrossi and Michèle Lavagna. “Preliminary results on the dynamics of large and flexible space structures in Halo orbits”. In: *Acta Astronautica* 134 (2017), pp. 355–367.

[130] Andrea Colagrossi et al. “Guidance, navigation and control for 6DOF rendezvous in Cislunar multi-body environment”. In: *Aerospace Science and Technology* 114 (2021), p. 106751.

[131] Suresh M Joshi, Atul G Kelkar, and JT-Y Wen. “Robust attitude stabilization of spacecraft using nonlinear quaternion feedback”. In: *IEEE Transactions on Automatic control* 40.10 (1995), pp. 1800–1803.

[132] Bong Wie. *Space vehicle dynamics and control*. Aiaa, 1998.

[133] Kevin A Bokelmann, Ryan P Russell, and Gregory Lantoine. “Periodic orbits and equilibria near jovian moons using an electrodynamic tether”. In: *Journal of Guidance, Control, and Dynamics* 38.1 (2015), pp. 15–29.

[134] Jesus Pelaez. “Self balanced electrodynamic tether”. In: *AIAA/AAS Astrodynamics Specialist Conference and Exhibit*. 2004, p. 5309.

[135] Denis Zanutto, Davide Curreli, and EC Lorenzini. “Stability of electrodynamic tethers in a three-body system”. In: *Journal of Guidance, Control, and Dynamics* 34.5 (2011), pp. 1441–1456.

[136] Jakob Harzer, Jochem De Schutter, and Moritz Diehl. “Efficient numerical optimal control for highly oscillatory systems”. In: *IEEE Control Systems Letters* 6 (2022), pp. 2719–2724.

[137] Lev Semenovich Pontryagin. *Mathematical theory of optimal processes*. CRC press, 1987.

[138] Richard F Hartl, Suresh P Sethi, and Raymond G Vickson. “A survey of the maximum principles for optimal control problems with state constraints”. In: *SIAM review* 37.2 (1995), pp. 181–218.

[139] William W Hager. “Runge-Kutta methods in optimal control and the transformed adjoint system”. In: *Numerische Mathematik* 87 (2000), pp. 247–282.

[140] William W Hager. “Convex control and dual approximations”. In: *Control Cybern* 8.522 (1979), p. 19.

[141] F. L. Chernousko and A. A. Lyubushin. “Method of successive approximations for solution of optimal control problems”. In: *Optimal Control Applications and Methods* 3.2 (1982), pp. 101–114.

[142] Arthur Earl Bryson. *Applied optimal control: optimization, estimation and control*. Routledge, 2018.

[143] Uri M Ascher, Robert MM Mattheij, and Robert D Russell. *Numerical solution of boundary value problems for ordinary differential equations*. SIAM, 1995.

[144] Josef Stoer et al. *Introduction to numerical analysis*. Vol. 1993. Springer, 1980.

[145] John T Betts. “Survey of numerical methods for trajectory optimization”. In: *Journal of guidance, control, and dynamics* 21.2 (1998), pp. 193–207.

[146] John T Betts. *Practical methods for optimal control and estimation using nonlinear programming*. SIAM, 2010.

[147] Pauli Virtanen et al. “SciPy 1.0: Fundamental Algorithms for Scientific Computing in Python”. In: *Nature Methods* 17 (2020), pp. 261–272.

[148] P Sanila and Jeevamma Jacob. “Simultaneous tracking and vibration control of flexible joint manipulator using Laguerre network based composite fast-slow MPC”. In: *2015 IEEE International Conference on Signal Processing, Informatics, Communication and Energy Systems (SPICES)*. IEEE. 2015, pp. 1–6.

[149] Melanie Wogrin and Luigi Glielmo. “An MPC scheme with guaranteed stability for linear singularly perturbed systems”. In: *49th IEEE Conference on Decision and Control (CDC)*. IEEE. 2010, pp. 5289–5295.

[150] Matthew Ellis, Mohsen Heidarinejad, and Panagiotis D Christofides. “Economic model predictive control of nonlinear singularly perturbed systems”. In: *Journal of Process Control* 23.5 (2013), pp. 743–754.

[151] Xianzhong Chen et al. “Composite fast-slow MPC design for nonlinear singularly perturbed systems”. In: *AIChE Journal* 58.6 (2012), pp. 1802–1811.

[152] Xianzhong Chen et al. “Composite fast-slow MPC design for nonlinear singularly perturbed systems: Stability analysis”. In: *2012 American Control Conference (ACC)*. IEEE. 2012, pp. 4136–4141.

[153] Xianzhong Chen et al. “Model predictive control of nonlinear singularly perturbed systems: Application to a reactor-separator process network”. In: *2011 50th IEEE Conference on Decision and Control and European Control Conference*. IEEE. 2011, pp. 8125–8132.

[154] Xinglong Zhang et al. “Multi-rate model predictive control algorithm for systems with fast-slow dynamics”. In: *IET Control Theory & Applications* 12.18 (2018), pp. 2468–2477.

[155] Xinglong Zhang et al. “A Dual-level Model Predictive Control Scheme for Multi-timescale Dynamical Systems”. In: *arXiv preprint arXiv:1906.07334* (2019).

[156] Marcello Farina, Xinglong Zhang, and Riccardo Scattolini. “A hierarchical multi-rate MPC scheme for interconnected systems”. In: *Automatica* 90 (2018), pp. 38–46.

[157] Felix Petzke, Marcello Farina, and Stefan Streif. “A multirate hierarchical MPC scheme for ensemble systems”. In: *2018 IEEE Conference on Decision and Control (CDC)*. IEEE. 2018, pp. 5874–5879.

[158] Bruno Picasso et al. “An MPC approach to the design of two-layer hierarchical control systems”. In: *Automatica* 46.5 (2010), pp. 823–831.

[159] Noel Csomay-Shanklin et al. “Multi-rate planning and control of uncertain nonlinear systems: Model predictive control and control lyapunov functions”. In: *2022 IEEE 61st Conference on Decision and Control (CDC)*. IEEE. 2022, pp. 3732–3739.

[160] Kunal Garg et al. “Multi-rate control design under input constraints via fixed-time barrier functions”. In: *IEEE Control Systems Letters* 6 (2021), pp. 608–613.

[161] Weiping Lu and D GRANT FISHER. “Output estimation with multi-rate sampling”. In: *International Journal of Control* 48.1 (1988), pp. 149–160.

[162] Masahiro Ohshima et al. “Multirate multivariable model predictive control and its application to a polymerization reactor”. In: *International Journal of Control* 59.3 (1994), pp. 731–742.

[163] Riccardo Scattolini and N Schiavoni. “A multirate model based predictive controller”. In: *Proceedings of 1994 33rd IEEE Conference on Decision and Control*. Vol. 1. IEEE. 1994, pp. 243–248.

[164] J H LEE, Marc S Gelormino, and Manfred Morarih. "Model predictive control of multi-rate sampled-data systems: a state-space approach". In: *International Journal of Control* 55.1 (1992), pp. 153–191.

[165] Meka Srinivasarao, Sachin C Patwardhan, and Ravindra D Gudi. "Nonlinear predictive control of irregularly sampled multirate systems using blackbox observers". In: *Journal of Process Control* 17.1 (2007), pp. 17–35.

[166] Ugo Rosolia, Andrew Singletary, and Aaron D Ames. "Unified multirate control: From low-level actuation to high-level planning". In: *IEEE Transactions on Automatic Control* 67.12 (2022), pp. 6627–6640.

[167] MA Brdys et al. "Hierarchical predictive control of integrated wastewater treatment systems". In: *Control Engineering Practice* 16.6 (2008), pp. 751–767.

[168] DW Yu and DL Yu. "Multi-rate model predictive control of a chemical reactor based on three neural models". In: *Biochemical engineering journal* 37.1 (2007), pp. 86–97.

[169] Yankai Cao et al. "Multiscale model predictive control of battery systems for frequency regulation markets using physics-based models". In: *Journal of Process Control* 90 (2020), pp. 46–55.

[170] Mudassir M Rashid, Prashant Mhaskar, and Christopher LE Swartz. "Multi-rate modeling and economic model predictive control of the electric arc furnace". In: *Journal of Process Control* 40 (2016), pp. 50–61.

[171] T Wang, H Gao, and J Qiu. "A Combined Adaptive Neural Network and Nonlinear Model Predictive Control for Multirate Networked Industrial Process Control". In: *IEEE transactions on neural networks and learning systems* 27.2 (2016), p. 416.

[172] Mohsen Heidarinejad et al. "Multirate distributed model predictive control of nonlinear systems". In: *Proceedings of the 2011 American Control Conference*. IEEE. 2011, pp. 5181–5188.

[173] Arun Krishnan and Karlene A Hoo. "A multiscale model predictive control strategy". In: *Industrial & engineering chemistry research* 38.5 (1999), pp. 1973–1986.

[174] Orhan Ismet Karsligil. "Multiscale modeling and model predictive control of processing systems". PhD thesis. Massachusetts Institute of Technology, 2000.

[175] George Stephanopoulos, Orhan Karsligil, and Matthew S Dyer. "Multiscale theory for linear dynamic processes: Part 1. Foundations". In: *Computers & Chemical Engineering* 32.4-5 (2008), pp. 857–884.

[176] George Stephanopoulos, Orhan Karsligil, and Matthew Dyer. "Multiscale theory for linear dynamic processes: Part 2. Multiscale model predictive control (MS-MPC)". In: *Computers & Chemical Engineering* 32.4-5 (2008), pp. 885–912.

[177] Enrico Terzi et al. "Robust multi-rate predictive control using multi-step prediction models learned from data". In: *Automatica* 136 (2022), p. 109852.

[178] Yutao Chen et al. "Efficient move blocking strategy for multiple shooting-based non-linear model predictive control". In: *IET Control Theory & Applications* 14.2 (2020), pp. 343–351.

[179] Steven Diamond and Stephen Boyd. "CVXPY: A Python-embedded modeling language for convex optimization". In: *Journal of Machine Learning Research* 17.83 (2016), pp. 1–5.

[180] MOSEK ApS. *The MOSEK optimization toolbox for MATLAB manual. Version 10.0.* 2022. URL: `http://docs.mosek.com/9.0/toolbox/index.html`.

[181] Danylo Malyuta et al. “Convex optimization for trajectory generation”. In: *arXiv preprint arXiv:2106.09125* (2021).

[182] Xuhui Feng, Stefano Di Cairano, and Rien Quirynen. “Inexact adjoint-based SQP algorithm for real-time stochastic nonlinear MPC”. In: *IFAC-PapersOnLine* 53.2 (2020), pp. 6529–6535.

[183] Jean Pierre Allamaa et al. “Real-time nonlinear mpc strategy with full vehicle validation for autonomous driving”. In: *2022 American Control Conference (ACC)*. IEEE. 2022, pp. 1982–1987.

[184] Charles E Oestreich, Richard Linares, and Ravi Gondhalekar. “Tube-Based Model Predictive Control with Uncertainty Identification for Autonomous Spacecraft Maneuvers”. In: *Journal of Guidance, Control, and Dynamics* 46.1 (2023), pp. 6–20.

[185] Lars Blackmore, Behçet Açikmeşe, and Daniel P Scharf. “Minimum-landing-error powered-descent guidance for Mars landing using convex optimization”. In: *Journal of guidance, control, and dynamics* 33.4 (2010), pp. 1161–1171.

[186] Jean-Pierre Sleiman et al. “A unified MPC framework for whole-body dynamic locomotion and manipulation”. In: *IEEE Robotics and Automation Letters* 6.3 (2021), pp. 4688–4695.

[187] H. G. Bock et al. “A Direct Multiple Shooting Method for Real-Time Optimization of Nonlinear DAE Processes”. In: *Nonlinear Model Predictive Control*. Ed. by Frank Allgöwer and Alex Zheng. Basel: Birkhäuser Basel, 2000, pp. 245–267.

[188] J. B. Rosen. “Iterative Solution of Nonlinear Optimal Control Problems”. In: *SIAM Journal on Control* 4.1 (1966), pp. 223–244.

[189] Yuanqi Mao, Michael Szmuk, and Behçet Açıkmeşe. “Successive convexification of non-convex optimal control problems and its convergence properties”. In: *2016 IEEE 55th Conference on Decision and Control (CDC)*. 2016, pp. 3636–3641.

[190] Y.I. Lee, B. Kouvaritakis, and M. Cannon. “Constrained receding horizon predictive control for nonlinear systems”. In: *Automatica* 38.12 (2002), pp. 2093–2102.

[191] Rebecca Foust, Soon-Jo Chung, and Fred Y Hadaegh. “Optimal guidance and control with nonlinear dynamics using sequential convex programming”. In: *Journal of Guidance, Control, and Dynamics* 43.4 (2020), pp. 633–644.

[192] Martin Doff-Sotta, Mark Cannon, and James Richard Forbes. “Spacecraft energy management using convex optimisation”. In: (2021).

[193] Costantinos Zagaris et al. “Model predictive control of spacecraft relative motion with convexified keep-out-zone constraints”. In: *Journal of Guidance, Control, and Dynamics* 41.9 (2018), pp. 2054–2062.

[194] Behcet Acikmese and Scott R Ploen. “Convex programming approach to powered descent guidance for mars landing”. In: *Journal of Guidance, Control, and Dynamics* 30.5 (2007), pp. 1353–1366.

[195] Mario E Villanueva et al. “Robust MPC via min–max differential inequalities”. In: *Automatica* 77 (2017), pp. 311–321.

[196] Johannes Köhler et al. “A computationally efficient robust model predictive control framework for uncertain nonlinear systems”. In: *IEEE Transactions on Automatic Control* 66.2 (2020), pp. 794–801.

[197] Gilberto Pin et al. “Robust model predictive control of nonlinear systems with bounded and state-dependent uncertainties”. In: *IEEE Transactions on automatic control* 54.7 (2009), pp. 1681–1687.

[198] Daniel Limón Marruedo, Teodoro Alamo, and Eduardo F Camacho. “Input-to-state stable MPC for constrained discrete-time nonlinear systems with bounded additive uncertainties”. In: *Proceedings of the 41st IEEE Conference on Decision and Control, 2002.* Vol. 4. IEEE. 2002, pp. 4619–4624.

[199] Shuyou Yu et al. “Tube MPC scheme based on robust control invariant set with application to Lipschitz nonlinear systems”. In: *Systems & Control Letters* 62.2 (2013), pp. 194–200.

[200] David Q Mayne et al. “Tube-based robust nonlinear model predictive control”. In: *International journal of robust and nonlinear control* 21.11 (2011), pp. 1341–1353.

[201] Brett T Lopez, Jean-Jacques E Slotine, and Jonathan P How. “Dynamic tube MPC for nonlinear systems”. In: *2019 American Control Conference (ACC)*. IEEE. 2019, pp. 1655–1662.

[202] Florian Messerer and Moritz Diehl. “An efficient algorithm for tube-based robust nonlinear optimal control with optimal linear feedback”. In: *2021 60th IEEE Conference on Decision and Control (CDC)*. IEEE. 2021, pp. 6714–6721.

[203] Antoine P Leeman et al. “Fast System Level Synthesis: Robust Model Predictive Control using Riccati Recursions”. In: *arXiv preprint arXiv:2401.13762* (2024).

[204] Reiner Horst and Nguyen V Thoai. “DC programming: overview”. In: *Journal of Optimization Theory and Applications* 103 (1999), pp. 1–43.

[205] Gert Lanckriet and Bharath K. Sriperumbudur. “On the Convergence of the Concave-Convex Procedure.” In: *Advances in Neural Information Processing Systems 22 (NIPS 2009)*. 2009, pp. 1759–1767.

[206] Thomas Lipp and Stephen Boyd. “Variations and extension of the convex–concave procedure”. In: *Optimization and Engineering* 17 (2016), pp. 263–287.

[207] Mirko Fiacchini, Teodoro Alamo, and Eduardo F Camacho. “On the computation of convex robust control invariant sets for nonlinear systems”. In: *Automatica* 46.8 (2010), pp. 1334–1338.

[208] A.A. Ahmadi and G. Hall. “DC decomposition of nonconvex polynomials with algebraic techniques”. In: *Math. Program.* 169 (2018), pp. 69–94.

[209] Gaurav Misra and Xiaoli Bai. “Iteratively feasible optimal spacecraft guidance with non-convex path constraints using convex optimization”. In: *AIAA Scitech 2020 Forum*. 2020, p. 1350.

[210] Martin Doff-Sotta and Mark Cannon. “Difference of convex functions in robust tube nonlinear MPC”. In: *2022 IEEE 61st Conference on Decision and Control (CDC)*. 2022, pp. 3044–3050.

[211] Silvia Manara et al. “On the integration of singularity-free representations of SO (3) SO (3) for direct optimal control”. In: *Nonlinear Dynamics* 90 (2017), pp. 1223–1241.

[212] Taeyoung Lee, Melvin Leok, and N Harris McClamroch. “Geometric numerical integration for complex dynamics of tethered spacecraft”. In: *2011 American Control Conference*. IEEE. 2011, pp. 1885–1891.

[213] Taeyoung Lee, Melvin Leok, and N McClamroch. “Lie group variational integrators for the full body problem in orbital mechanics”. In: *Celestial Mechanics and Dynamical Astronomy* 98 (2007), pp. 121–144.

[214] S. Boyd et al. "Distributed optimization and statistical learning via the alternating direction method of multipliers". In: *Foundations and Trends in Machine learning* 3.1 (2011), pp. 1–122.

[215] Yuwen Chen and Paul Goulart. "An Efficient IPM Implementation for A Class of Nonsymmetric Cones". In: *arXiv preprint arXiv:2305.12275* (2023).

[216] Yang Zheng et al. "Fast ADMM for semidefinite programs with chordal sparsity". In: *2017 American Control Conference (ACC)*. IEEE. 2017, pp. 3335–3340.

[217] Diego Muñoz-Carpintero, Mark Cannon, and Basil Kouvaritakis. "Robust MPC strategy with optimized polytopic dynamics for linear systems with additive and multiplicative uncertainty". In: *Systems & Control Letters* 81 (2015), pp. 34–41.

[218] D Limon et al. "Input-to-state stability: a unifying framework for robust model predictive control". In: *Nonlinear model predictive control*. Springer, 2009, pp. 1–26.

[219] J. Bradbury and et al. "JAX: composable transformations of Python+NumPy programs". Version 0.3.13. In: (2018). URL: `http://github.com/google/jax`.

[220] Martin Doff-Sotta, Mark Cannon, and Marko Bacic. "Data-driven robust MPC of tiltwing VTOL aircraft". In: *arXiv preprint:2308.03557* (2023).

[221] Johannes Buerger, Mark Cannon, and Martin Doff-Sotta. "Safe learning in nonlinear model predictive control". In: *6th Annual Learning for Dynamics & Control Conference*. PMLR. 2024, pp. 603–614.